NASA/TP–2009-215369

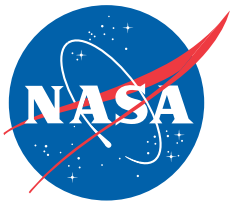

A Status of NASA Rotorcraft Research

Edited by:
Gloria K. Yamauchi and Larry A. Young
Ames Research Center, Moffett Field, California

September 2009

The NASA STI Program Office . . . in Profile

Since its founding, NASA has been dedicated to the advancement of aeronautics and space science. The NASA Scientific and Technical Information (STI) Program Office plays a key part in helping NASA maintain this important role.

The NASA STI Program Office is operated by Langley Research Center, the Lead Center for NASA's scientific and technical information. The NASA STI Program Office provides access to the NASA STI Database, the largest collection of aeronautical and space science STI in the world. The Program Office is also NASA's institutional mechanism for disseminating the results of its research and development activities. These results are published by NASA in the NASA STI Report Series, which includes the following report types:

- TECHNICAL PUBLICATION. Reports of completed research or a major significant phase of research that present the results of NASA programs and include extensive data or theoretical analysis. Includes compilations of significant scientific and technical data and information deemed to be of continuing reference value. NASA's counterpart of peer-reviewed formal professional papers but has less stringent limitations on manuscript length and extent of graphic presentations.

- TECHNICAL MEMORANDUM. Scientific and technical findings that are preliminary or of specialized interest, e.g., quick release reports, working papers, and bibliographies that contain minimal annotation. Does not contain extensive analysis.

- CONTRACTOR REPORT. Scientific and technical findings by NASA-sponsored contractors and grantees.

- CONFERENCE PUBLICATION. Collected papers from scientific and technical conferences, symposia, seminars, or other meetings sponsored or cosponsored by NASA.

- SPECIAL PUBLICATION. Scientific, technical, or historical information from NASA programs, projects, and missions, often concerned with subjects having substantial public interest.

- TECHNICAL TRANSLATION. English-language translations of foreign scientific and technical material pertinent to NASA's mission.

Specialized services that complement the STI Program Office's diverse offerings include creating custom thesauri, building customized databases, organizing and publishing research results . . . even providing videos.

For more information about the NASA STI Program Office, see the following:

- Access the NASA STI Program Home Page at *http://www.sti.nasa.gov*

- E-mail your question via the Internet to help@sti.nasa.gov

- Fax your question to the NASA Access Help Desk at (301) 621-0134

- Telephone the NASA Access Help Desk at (301) 621-0390

- Write to:
  NASA Access Help Desk
  NASA Center for AeroSpace Information
  7115 Standard Drive
  Hanover, MD 21076-1320

NASA/TP–2009-215369

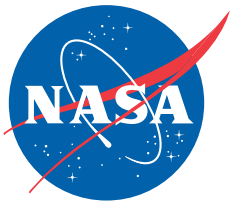

A Status of NASA Rotorcraft Research

Edited by:
Gloria K. Yamauchi and Larry A. Young
Ames Research Center, Moffett Field, California

National Aeronautics and
Space Administration

Ames Research Center
Moffett Field, California 94035-1000

September 2009

Acknowledgments

The many outstanding technical contributions of the rotorcraft community at NASA Ames, Glenn, and Langley Research Centers are gratefully acknowledged in preparing this document. Technical contributions and comments from the U.S. Army, Industry, and Academia researchers are also acknowledged. In particular, thanks are extended to the following individuals:

Bell Helicopter Textron: Ted Trept
Continuum Dynamics, Inc.: Daniel Wachspress
NASA: Paula Dempsey, Susan Gorton, Norman Schaeffler
SAIC: William Chung
Sukra Helitek, Inc.: Ganesh Rajagopalan
U.S. Army Aeroflightdynamics Directorate: Mahendra Bhagwat, Mark Fulton, Preston Martin, Kevin Noonan, Hyeonsoo Yeo
U.S. Army Research Laboratory: Matt Floros, Matt Wilbur
University of California, Davis: Ronald Hess

We also thank the following people for reviewing this document and providing valuable feedback:

Fenton Bartlett
John Coy
Troy Gaffey
Frank Harris
Danny Hoad
Wayne Johnson
Chee Tung

Finally, we are very grateful to Charlotte Barton (NASA) and Catherine Dow (PDI) for their careful preparation of this document.

This work will be instrumental in the conduct and oversight of rotorcraft research currently underway at NASA and will aid in defining the technology research investment portfolios of the future.

Gloria K. Yamauchi and Larry A. Young
Editors

Available from:

NASA Center for AeroSpace Information
7115 Standard Drive
Hanover, MD 21076-1320
(301) 621-0390

National Technical Information Service
5285 Port Royal Road
Springfield, VA 22161
(703) 487-4650

TABLE OF CONTENTS

Chapter 2 Aeromechanics (cont.)

Chapter 3 Acoustics

Chapter 4 Computational Fluid Dynamics (External Flow)

Chapter 4 Computational Fluid Dynamics (External Flow) (cont.)

Chapter 5 Experimental Capabilities

Chapter 6 Flight Dynamics and Control

Chapter 7 Propulsion

Chapter 8 Structures and Materials

Chapter 9 Multi-disciplinary Analysis and Technology Development

LIST OF FIGURES

Chapter 2 Aeromechanics

Chapter 2 Aeromechanics (cont.)

Chapter 2 Aeromechanics (cont.)

Chapter 3 Acoustics

Chapter 3 Acoustics (cont.)

Chapter 4 Computational Fluid Dynamics (External Flow)

Chapter 4 Computational Fluid Dynamics (External Flow) (cont.)

Chapter 4 Computational Fluid Dynamics (External Flow) (cont.)

Chapter 5 Experimental Capabilities

Chapter 5 Experimental Capabilities (cont.)

Chapter 6 Flight Dynamics and Control

Chapter 6 Flight Dynamics and Control (cont.)

Chapter 7 Propulsion

Chapter 7 Propulsion (cont.)

Chapter 8 Structures and Materials

Chapter 8 Structures and Materials (cont.)

Chapter 9 Multi-disciplinary Analysis and Technology Development

LIST OF TABLES

Chapter 1 Introduction

Chapter 2 Aeromechanics

Chapter 3 Acoustics

Chapter 4 Computational Fluid Dynamics (External Flow)

Chapter 5 Experimental Capabilities

Chapter 6 Flight Dynamics and Control

Chapter 7 Propulsion

CHAPTER 1

INTRODUCTION

Gloria K. Yamauchi[1]

ACRONYMS

ARMD	Aeronautics Research Mission Directorate
CFD	computational fluid dynamics
FAA	Federal Aviation Administration
ITR/FRR	Integrated Technology Rotor/Flight Research Rotor
JPDO	Joint Planning and Development Office
MDAO	Multi-Disciplinary Analysis and Optimization
MDATD	Multi-Disciplinary Analysis and Technology Development
RIA	Runway Independent Aircraft
SHCT	Short-Haul Civil Tiltrotor
SRW	Subsonic Rotary Wing
TRAC	Tiltrotor Aeroacoustic Code
VMS	Vertical Motion Simulator
VTOL	vertical takeoff and landling

OVERVIEW

In 2006, NASA rotorcraft research was refocused to emphasize high-fidelity "first-principles" predictive tool development and validation. As part of this new emphasis, documenting the status of NASA rotorcraft research and defining the state-of-the-art in rotorcraft predictive capability were undertaken. This report is the result of this two-year effort. Contributors to this work encompass a wide range of expertise covering the technical disciplines of aeromechanics, acoustics, computational fluid dynamics (CFD), flight dynamics and control, experimental capabilities, propulsion, structures and materials, and multi-disciplinary analysis.

This document highlights technical areas in which NASA has invested resources and therefore the document does not provide a comprehensive review of all areas of rotorcraft research, nor is there an attempt made to exhaustively review and reference the works of other organizations. Within the last 10 years, excellent surveys have been written on different disciplines and topics of rotorcraft research—they are referenced in the chapters to follow. Collectively, these surveys provide a

[1] NASA Ames Research Center.

comprehensive review of the progress and current state of rotorcraft research, and this document serves as a complementary assessment strictly from a NASA perspective. This document will serve as a reference against which NASA research progress beyond 2007 can be measured. In order to measure progress, however, metrics must be established, and that is not a straightforward exercise. Often, a predictive capability is mature for certain flight conditions or configurations, but not for others. For example, much effort has been expended in predicting rotor-blade airloads for hover and steady, level flight but not for unsteady, maneuvering flight conditions. A key challenge in preparing this document was to present measurements and predictions in a format that can be used for multiple conditions, configurations, and parameters so that in the future, improvements in predictive capability can be easily tracked.

A snapshot of current rotorcraft predictive capabilities is provided in table 1.1, which is reproduced from Johnson and Datta [2008]. In general, the goals listed in table 1.1 represent an order-of-magnitude improvement over SOA tools. NASA's research is geared toward enabling future rotorcraft to "fly as designed", rather than to "fly and fix", so first-principles predictive tools will need to approach the accuracy goals suggested by Johnson and Datta [2008].

In any research area, monitoring progress against established goals and frequently assessing the path ahead are critical for the research to remain relevant. For NASA, where the research is typically long-term and high-risk, this self-assessment process can be especially challenging. This document is hopefully the first of a series of periodic assessments of rotorcraft research within NASA.

A brief history of NASA rotorcraft research, the future direction of the research, and descriptions of each chapter complete this Introduction.

TABLE 1.1. ESTIMATE OF PREDICTIVE CAPABILITY FOR STATE-OF-THE-ART ROTORCRAFT AEROMECHANICS TOOLS (FROM TABLE 1 OF JOHNSON AND DATTA [2008]; PERCENTAGES ARE ACCURACY OF CALCULATION COMPARED TO MEASURED DATA)

	Goal	**SOA Engineering Tool**	**SOA Physics-Based Model**
Forward flight performance	1%	4%	20%
Hover performance	0.5%	2%	2% (but flow field not correct)
Airloads (c_n/c_m) without mean	1%	10/35%	6%/20%
Airloads (c_n/c_m) with mean	1%	10/35%	15%/40%
Blade loads (flap/chord/torsion)	3%	20%/35%/25%	20%/35%/25%
Vibration	10%	100%	Not available
Stability (fraction of critical damping)	0.002	0.02	Not available
Noise	3 dB	10 dB	15 dB

ROTORCRAFT RESEARCH AT NASA

The current NASA rotorcraft research effort is the proud beneficiary of a history beginning with the NACA in 1915. The first 70 years of this history (1915 to 1984) is summarized by Ward [1984]. Key events in this history are the establishment of Army research laboratories at Ames (1965), Glenn (1970), and Langley (1972) Research Centers. The genesis of the co-located Army labs at the NASA Centers and some of the major joint projects resulting from the NASA/Army partnership are described by Richard Carlson in Fischer [1983].

A comprehensive review of Army/NASA collaboration in key technical disciplines was showcased in several major conferences in the 1980's. In 1981, the Advanced Power Transmission Technology Symposium was held at NASA Glenn (then Lewis) Research Center [Fischer, 1983]. The symposium highlighted the work under the Helicopter Transmission System Technology Program, a program co-sponsored by NASA and the U.S. Army. In 1983, a methodology workshop on rotorcraft dynamics was convened as part of the Integrated Technology Rotor/Flight Research Rotor (ITR/FRR) program, another Army/NASA effort [McNulty and Bousman, 1988]. The workshop brought together Army, NASA, and industry to assess the capability of the rotorcraft community to predict aeromechanical stability. In 1987, another co-sponsored conference was held at NASA Ames Research Center: the NASA/Army Rotorcraft Technology Conference. The 3-volume conference proceedings [Department of the Army and the National Aeronautics and Space Administration, 1988a, 1988b, 1988c] document progress in rotorcraft technology from the mid-1970s to mid-1980s covering the disciplines of: Volume I - Aerodynamics, Dynamics and Aeroelasticity; Volume II – Materials and Structures, Propulsion and Drive Systems, Flight Dynamics and Control, and Acoustics; and Volume III – Systems Integration, Research Aircraft, and Industry.

The NASA/Army partnership remains effective to this day at all three Centers, though aspects of the partnership have evolved with the changing research focus of each partner. There can be no doubt that significant advances in technology resulted from this partnership, examples of which include the Rotor Systems Research Aircraft (RSRA), the XV-15 Tiltrotor Research Aircraft, the Rotorcraft-Aircrew Systems Concepts Airborne Laboratory (RASCAL), and development of full-scale rotorcraft crash testing. Another highlight of NASA/Army cooperation was the UH-60 Airloads Aircraft flight tests conducted during 1993-1994 [Kufeld et al., 1994]. This benchmark dataset has been used by the rotorcraft community to improve aeromechanic predictive methodologies. The lasting value of the UH-60 Airloads data is evidenced by the continuing bi-annual workshops held since 2001 and attended by government, industry, and academia. The workshops aim to identify key modeling issues of current capabilities by focusing on a few flight conditions and sharing lessons learned.

Up until the 1990s, funding for NASA rotorcraft research was primarily through "base" program funding that supported basic research covering the landscape of rotorcraft technical areas at the three Centers. Research funding came through two sources in the 1990s: base and focused. Base funding continued to fund basic research while "focused" funding was aimed at specific technologies, and for rotorcraft that technology was tiltrotor aircraft. The Short-Haul Civil Tiltrotor (SHCT) project was a 7-yr project initiated in 1994. The SHCT project, described by Giulianetti [2003], comprised several elements: efficient, low-noise proprotor, low-noise terminal area approaches, contingency power, and technology integration. All of these elements focused on enabling a safe, quiet, and efficient civil tiltrotor transport. The project consisted of major experimental efforts that included

wind tunnel tests of a 0.25-scale V-22 isolated rotor, advanced tiltrotor configurations developed by industry, and a full-scale XV-15 isolated rotor. Using the Vertical Motion Simulator (VMS) to evaluate potential low-noise approaches, three acoustic flight tests using the XV-15 were executed. On the analysis side, the Tiltrotor Aeroacoustic Code (TRAC) was developed and validated using the data from wind tunnel and flight tests conducted under SHCT. The primary rotorcraft manufacturers (Bell, Boeing, and Sikorsky) were heavily involved in the project.

The SHCT project provided a sound technical foundation for the follow-on program that was captured under the theme of Runway Independent Aircraft, or RIA. In the early 2000s, the NASA rotorcraft effort [Coy, 2000] sought to exploit the attributes of vertical takeoff and landing (VTOL) by promoting an alternative to conventional fixed-wing use of runways and the national airspace. Indeed, the concept of RIA and civil tiltrotors was not a new idea; the concept had been seriously studied under a Congressional mandate [Civil Tilt Rotor Development Advisory Committee, 1995]. With renewed emphasis on airport and airspace congestion, NASA sponsored industry studies and workshops during 2001–2004 that focused on the impact of RIA on reducing delays and increasing capacity [Stouffer et al., 2001 and Johnson et al., 2001]. Advanced rotorcraft configurations that could serve as RIA were studied by industry [Smith et al., 2003].

Between 2004 and 2005, rotorcraft research was executed within the Rotorcraft Sector of the Vehicle Systems Program of the Aeronautics Research Mission Directorate (ARMD). Primary goals of the Sector were to improve public mobility and access to air transportation. To this end, the Sector focused on technologies enabling a notional heavy-lift rotorcraft transport capable of carrying 120 passengers at a cruise speed of 350 knots at 30,000-ft altitude with a range of 1200 nm. Many of the vehicle technology goals (for example, noise) were based on the work from the RIA studies. An investigation [Johnson et al., 2005] of several heavy-lift rotorcraft configurations was a major product of the short-lived Sector.

ARMD research was refocused in late-2005 to concentrate more on foundational research and high-fidelity multi-disciplinary analysis rather than vehicle-centric technology goals. For rotorcraft research, reorganized under the auspices of the Subsonic Rotary Wing (SRW) Project of the Fundamental Aeronautics Program, emphasis was placed on first-principles tool development and validation. Milestones with quantitative metrics were developed for key activities in order to track progress in six technical disciplines: Propulsion, Flight Dynamics and Control, Aeromechanics, Acoustics, Structures and Materials, and Experimental Capabilities. In 2008, the project added the Multi-Disciplinary Analysis and Technology Development (MDATD) discipline in response to increasing emphasis on studies of advanced rotorcraft in the Next Generation Air Transportation System (NextGen), Multi-Disciplinary Analysis and Design Optimization (MDAO) tool development, and integrated system technology assessments.

FUTURE DIRECTIONS

Since 2004, several studies have been conducted on the state and future direction of U.S. aeronautics research, including a 10-year plan for rotorcraft research [H. R. 2115, 2004], a study on NASA Aeronautics [National Strategy Team, 2005], and a review of civil aeronautics [Steering Committee for the Decadal Survey of Civil Aeronautics, 2006]. The most recent and overriding document is the National Plan for Aeronautics Research and Development Infrastructure [Aeronautics Science and Technology Subcommittee (ASTS), 2007]. The National Plan responds to Executive Order 13419 and represents the nation's first policy on Federal Aeronautics research and development through the year 2020. The Plan is based on five key principles comprising specific goals. Rotorcraft research is particularly prominent in two of the principles: Mobility Through the Air Is Vital to Economic Stability, Growth, and Security as a Nation; and Aviation Is Vital to National Security and Homeland Defense. The Plan advocates the development of improved lift, range, and mission capability for rotorcraft as a goal. Not surprisingly, NASA rotorcraft research has supported and continues to support these principles since many of the technical challenges (e.g., drag reduction) have persisted for decades, and only through sustained efforts can they be overcome.

Developing rotorcraft predictive capability based on high-fidelity, physics-based tools is a key driver for making significant progress toward achieving the goals of the National Plan. Rotorcraft problems are very complex because of their multi-disciplinary nature, and hence problems were historically attacked piece-meal. With the increase in computational capability, coupled problems (e.g., aerodynamics/structural dynamics and noise propagation/structural dynamics) can now be addressed. Several enlightening papers, written from a rotorcraft technologist perspective, offer specific guidance on the future direction of rotorcraft research.

Using historical examples of military rotorcraft development efforts, Crawford [1990] provides a revealing look at the consequences of inadequate predictive tools and inadequate testing to validate these tools. Vibration, rotor loads, and aerodynamic performance are identified by Crawford as areas requiring improved predictive methodologies—and nearly 20 years later, these observations still hold true.

Leishman [2008] also encourages the rotorcraft community to aim for a true predictive capability based on physics in order to develop better rotorcraft. Cross-discipline research, model validation, correlation studies, and precision measurements from well-designed experiments are also advocated. Kunz [2005] offers recommendations on attributes (e.g., integration with CFD tools and implementation of an underlying mathematical engine) that future third-generation comprehensive rotorcraft analyses should feature. In this context, Kunz [2005] uses comprehensive analysis to describe codes such as CAMRAD II, RCAS, and DYMORE that are capable of modeling a rotorcraft using a combination of multibody dynamics, structural dynamics, and approximations for the rotor wake and blade aerodynamics.

Johnson and Datta [2008] and Datta and Johnson [2008] look further into the future and envision "comprehensive analysis" to represent a high-performance computing, modular, parallel, and scalable software tool executed on multiple processor cores. The comprehensive analysis tool of the future described by Johnson and Datta [2008] is multi-disciplinary and will calculate performance, blade loads, vibration, airframe and drive-train loads, aeroelastic stability, flight dynamics, handling

qualities, and noise for any operating condition of any rotorcraft configuration. This notional single tool will be based on first principles (i.e., physics). Though the projected required computing power will eventually become available for this single tool, the software framework, geometry engine, and the numerous subsystem requirements and how they interface are the key technical challenges facing the developers of the future comprehensive rotorcraft analysis.

While first-principles tool development and validation will continue to be a major focus of NASA rotorcraft research, emphasis on the role of advanced rotorcraft configurations in the NextGen will increase. In 2003, the NextGen concept was endorsed by law [H. R. 2115, 2003], and the Joint Planning and Development Office (JPDO) was formed to enable the long-term transformation of the national airspace. JPDO is supported by: NASA; the Federal Aviation Administration (FAA); the Departments of Transportation, Homeland Security, Defense, and Commerce; and the White House Office of Science and Technology Policy. The NASA-sponsored RIA studies provide a good foundation for more detailed investigations of advanced rotorcraft, such as a large civil tiltrotor, operating in the NextGen with other aircraft. The JPDO [2007] describes the NextGen Concept of Operations (ConOps) in the 2025 timeframe and beyond, where the approach to air transportation will be fundamentally different from that of the present. Studies focusing on the integration of civil transport rotorcraft in NextGen will generate a wide range of research topics for NASA, such as environmental constraints, safe operational procedures, and assessments of advanced technology.

The SRW project has established goals that address desired attributes of NextGen rotorcraft. These goals include:

- Capability for 50% main rotor speed reduction
- 100 kt speed increase over present-day rotorcraft
- Noise contained in landing area
- Cabin noise < 77dB with no weight penalty.

In a building-block approach, research and goals at the foundational level (e.g., Table 1.1) will be integrated into multi-disciplinary system demonstrations that are aimed at enabling the NextGen rotorcraft.

ORGANIZATION OF THIS REPORT

The chapters of this report cover the technical disciplines that comprise rotorcraft research within NASA: Aeromechanics, Acoustics, Computational Fluid Dynamics – External Flow, Experimental Capabilities, Flight Dynamics and Control, Propulsion, Structures and Materials, and Multi-Disciplinary Analysis and Technology Development. The chapters describe a NASA perspective and priority on research topics, which likely differ from those of the private sector, the military, and academia. Within each chapter, brief descriptions of the discipline and subdisciplines are followed by a discussion of the tools available or in development, examples (where available) of measured versus predicted results, plans for improving predictive capability, required validation data, and possible contributions to other technical areas. Predictive capability, available data, and measurement techniques are at different levels of maturity for each discipline. Hence, illustrative examples

vary in detail and quantity from chapter to chapter. In some cases, NASA's in-house predictive capability is emerging (interior noise) rather than established (rotor airloads).

For the purposes of this document, the Aeromechanics discipline is separated into non-CFD (Chapter 2) and CFD (Chapter 4) areas. Chapter 2 focuses primarily on obtaining datasets for validating analyses and the use of lower-fidelity, but highly integrated, comprehensive analyses. The chapter focuses on four primary areas: Rotor Aerodynamics and Interactions; Active Control for Loads, Vibration, and Noise Alleviation; Rotor Dynamics and Control; and Fluid Mechanics for Rotorcraft Applications.

Acoustics (Chapter 3) is organized to cover three key areas: External Noise Sources, Internal Noise Sources, and Noise Propagation Modeling and Optimized Flight Paths. The section on External Noise Sources includes a description of predictive capabilities of a system of interfaced non-CFD/CFD codes and a higher-fidelity modeling approach that is primarily CFD-based. Examples of noise predictions are provided for both predictive approaches. The section on Interior Noise Sources includes two main topics: interior noise modeling and gear noise modeling. Propagation of source noise through the atmosphere is discussed in the third major section of this chapter. Optimizing low-noise flight approaches is also discussed in this section.

The external flow CFD areas (Chapter 4) emphasize improvements in higher-fidelity analyses that have yet to be fully integrated with other disciplines, though much progress has been made coupling CFD with computational-structural-dynamics (CSD) analyses. Within the CFD chapter, structured and unstructured analyses are discussed and icing analyses are described. Applications to external flows are treated only in this chapter.

The Experimental Capabilities (Chapter 5) effort within NASA is highly integrated with the other technical disciplines. The work focuses on developing and applying measurement techniques that enable the acquisition of critical validation data. The primary areas of emphasis described in Chapter 5 include measurements of rotor wake, blade air loads, blade aeroelastic deflections, in-flight rotorcraft state, oscillatory hub loads, and improvements in test and measurement efficiency.

The Flight Dynamics and Control research (Chapter 6) emphasizes the integrated solution of handling qualities and dynamics problems. Topics that are explored include a variable-speed rotor, which has serious unexplored implications for dynamics and handling qualities that directly affect operational utility; control-mode transition modeling; and development of precision guidance, navigation, and control capabilities to enable data collection and evaluation for rotorcraft flight experiments, including studies of acoustic properties, vehicle dynamics modeling, noise reduction, and terminal-area operations.

The Propulsion work (Chapter 7) includes the engine and drive system as major topic areas. The engine part of the program focuses on ways of achieving high-power density and a wide operating range. Key development areas include: concepts to extend the stable operating range of highly loaded compressors; development of wide-speed-range power turbine concepts; and development of oil-free bearing technology to enable application of airfilm foil bearings to future turboshaft engines. The drive system work is concentrated in the areas of windage, variable-speed transmissions, and gear and bearing performance.

Chapter 8 describes the Structures and Materials discipline that is divided into the two general areas of propulsion materials and airframe structures and materials. Research on propulsion materials focuses on probabilistic life prediction methods for powder metallurgy turbine disk alloys, erosion-resistant thermal barrier coatings for turbine blades, and ceramic materials, including environmental barrier coatings for Si_3N_4 monolithic ceramics and fabrication methods for SiC/SiC CMCs. Airframe structures and materials research emphasize durability and damage tolerance of composite rotorcraft structure, crashworthiness, and cabin noise reduction.

Finally, Chapter 9 addresses the Multi-Disciplinary Analysis and Technology Development (MDATD) effort. In this context, MDATD includes rotorcraft system analysis, assessment of advanced configurations, integrated experimental efforts, and possible methods for determining research investments in the future.

REFERENCES

Aeronautics Science and Technology Subcommittee, Committee on Technology, National Science and Technology Council: National Plan for Aeronautics Research and Development and Related Infrastructure, Dec. 2007. (Ace. No. ADA492431.)

Department of the Army and the National Aeronautics and Space Administration: NASA/Army Rotorcraft Technology. Volume I: Aerodynamics, and Dynamics and Aeroelasticity. NASA CP 2495, Feb. 1, 1988a.

Department of the Army and the National Aeronautics and Space Administration: NASA/Army Rotorcraft Technology. Volume II: Materials and Structures, Propulsion and Drive Systems, Flight Dynamics and Control, and Acoustics. NASA CP 2495, Feb. 1, 1988b.

Department of the Army and the National Aeronautics and Space Administration: NASA/Army Rotorcraft Technology. Volume III: Systems Integration, Research Aircraft, and Industry. NASA CP 2495, Feb. 1, 1988c.

Coy, J. J.: Rotorcraft Vision. Presentation at the International Powered Lift Conference, Cosponsored by AHS, AIAA, SAE, RaeS, Arlington, Va., Oct. 30–Nov. 1, 2000.

Crawford, C. C.: Rotorcraft Analytical Improvement Needed to Reduce Development Risk – The 1989 Alexander A. Nikolsky Lecture. J. Amer. Hel. Soc., vol. 35, no. 1, Jan. 1990.

Datta, A.; and Johnson, W.: An Assessment of the State-of-the-Art in Multidisciplinary Aeromechanical Analyses. AHS Specialists' Conference on Aeromechanics, San Francisco, Calif., Jan. 23–25, 2008.

Fischer, G. K., Editor: Advanced Power Transmission Technology. NASA CP 2210, AVRADCOM Technical Report 82-C-16, Jan. 1, 1983.

Guilianetti, D.: Aviation System Capacity Program: Short Haul Civil Transport Project. Noise Reduction and Terminal Area Operations. NASA/TP-2003-212800, Nov. 2003.

H. R. 2115: Vision 100—Century of Aviation Reauthorization Act (P.L. 108-176). Dec. 12, 2003.

H. R. 2115: Vision 100—Century of Aviation Reauthorization Act (P.L. 108-176, Sec. 711, Rotorcraft Research and Development Initiative), Dec. 12, 2003.

Johnson, J; Stouffer, V.; Long, D.; and Gribko, J.: Evaluation of the National Throughput Benefits of the Civil Tiltrotor. NASA CR-2001-211055, Sept. 2001.

Johnson, W.; and Datta, A.: Requirements for Next Generation Comprehensive Analysis of Rotorcraft. AHS Specialists' Conference on Aeromechanics, San Francisco, Calif., Jan. 23–25, 2008.

Johnson, W.; Yamauchi, G. K.; and Watts, M. E.: NASA Heavy Lift Rotorcraft Systems Investigation. NASA/TP-2005-213467, Dec. 2005.

Joint Planning and Development Office: Concept of Operations for the Next Generation Air Transportation System, Version 2.0, Joint Planning and Development Office, Next Generation Air Transportation System, Wash., D.C., 13 June 2007.

Kufeld, R. M.; Balough, D. L,; Cross, J. L.; Studebaker, K. F.; Jennison, C. D.; and Bousman, W. G.: Flight Testing the UH-60A Airloads Aircraft. Proc. AHS 50th Annual Forum, May 1994.

Kunz, D. L.: Comprehensive Rotorcraft Analysis: Past, Present, and Future. AIAA Paper No. 2005-2244, 48th AIAA/ASME/ASCE/AHS/ASC Structural Dynamics and Materials Conf., Austin, Tex., Apr. 18–21, 2005.

Leishman, J. G.: Rotorcraft Aeromechanics—Getting Through the Dip. AHS Specialists' Conference on Aeromechanics, San Francisco, Calif., Jan. 23–25, 2008.

McNulty, M. J. and Bousman, W. G., Editors: Integrated Technology Rotor Methodology Assessment Workshop. NASA CP 10007, USAAVSCOM 88-A-001, June 1, 1988.

National Strategy Team: Responding to the Call: Aviation Plan for American Leadership. Recommendation to Congress to Augment NASA 2006 and Beyond Runout of the FY05 Aeronautics Research Budget, Press Release, May 3, 2005.

Wilkerson, J.; Montoro, J.; Smith, D. E.; Coy, J.; and Zuk, J.: Technology Development for Runway Independent Aircraft. 39th Annual Forum of the American Helicopter Society, Phoenix, Ariz., May 6–8, 2003.

Steering Committee for the Decadal Survey of Civil Aeronautics, National Research Council Report. Decadal Survey of Civil Aeronautics: Foundation for the Future, A Status Report. Washington, D.C., June 5, 2006.

Stouffer, V.; Johnson, J.; and Gribko, J.: Civil Tiltrotor Feasibility Study for the New York and Washington Terminal Areas; Final Report. NASA CR-2001-210659, Jan. 2001.

Ward, J.: An Updated History of NACA/NASA Rotary-Wing Aircraft Research 1915–1984. Vertiflight, vol. 30, May/June 1984, pp. 108–117.

CHAPTER 2

AEROMECHANICS

William G. Bousman[1] and Thomas R. Norman[2]

ACRONYMS

2GCHAS	Second Generation Comprehensive Helicopter Analysis System
AER	Active Elevon Rotor
AFC	active flow control
CAMRAD	Comprehensive Analytical Model of Rotorcraft Aerodynamics and Dynamics
CFD	computational fluid dynamics
CHARM	Comprehensive Hierarchical Aeromechanics Rotorcraft Model
CSD	computational structural dynamics
DNW	German-Dutch Wind Tunnel
EHPIC	Evaluation of Hover Performance using Influence Coefficients
FRF	frequency response function
FUN3D	Fully Unstructured Navier–Stokes 3D
HHC	higher harmonic control
IBC	individual blade control
IBL	interactive boundary layer
IRT	Icing Research Tunnel
IRTS	Isolated Rotor Test System
LRTA	Large Rotor Test Apparatus
LEWICE	Lewis Ice Accretion Prediction code
LV	laser velocimetry
M	Mach number
NFAC	National Full-Scale Aerodynamics Complex
OEI	one engine inoperative
OVERFLOW	OVERset grid FLOW solver
PIV	particle image velocimetry
RCAS	Rotorcraft Comprehensive Analysis System

[1] Retired, U. S. Army Aeroflightdynamics Directorate.
[2] NASA Ames Research Center.

ROBIN	ROtor-Body INteraction
SBMR	Sikorsky bearingless main rotor
SMART	Smart Material Actuated Rotor Technology
TRAM	Tilt Rotor Aeroacoustic Model
UMARC	University of Maryland Advanced Rotor Code
UTTAS	Utility Tactical Transport Aircraft System
VROC	vertical rate of climb
WCB	wide-chord blades

INTRODUCTION

Definition of Aeromechanics

Aeromechanics blends the disciplines of aerodynamics, dynamics, structures, and acoustics, since all are interrelated. Problems at an elementary level may be solved using fewer of these disciplines; for example, performance for preliminary design needs to consider only aerodynamics. But detail design requires that all or nearly all of these disciplines be incorporated in analysis.

The division of the aeromechanics area into "non-computational fluid dynamics" (non-CFD) aeromechanics (or classical aeromechanics) in this chapter and "CFD" aeromechanics in Chapter 4 is to some extent arbitrary. But there is utility in this division, first, in the relative maturity of the non-CFD methods with respect to CFD methods and, second, in the objectives of workers in the two fields. In the non-CFD areas, much of the focus is towards obtaining improved datasets that can guide analysis, whereas in the CFD area more of the focus is towards analytical improvements that must be obtained to use these techniques for rotorcraft detail design. But despite the division used here, the relationships between these two subdisciplines are close, and within NASA rotorcraft research, these relationships are enhanced. CFD aeromechanics is making considerable progress towards the accurate calculation of nonlinear aerodynamic loads based on first-principles analyses, and this calculation will replace the table lookup and empirical models of current comprehensive analyses in some cases. The comprehensive analyses, on the other hand, bring integrated models of structures and rotorcraft configurations that are absent in present CFD methods. These structural models, sometimes referred to as computational structural dynamics or CSD models, provide the basis for the newly coupled CFD/CSD predictions.

The harmonics of rotor frequency provide a useful way of looking at the various disciplines of aeromechanics and how they are related. Performance, to first order, is a steady or zero-harmonic discipline. Oscillatory loads are normally defined in the rotating system, and these loads extend from the first harmonic loads (1/rev) upwards. These rotor oscillatory loads are important in their own right, since they define the fatigue loading on rotating-system components, but also are a source of airframe vibratory loads. For fatigue loading, the oscillatory loads are normally important only over the harmonic range of from one to three or four harmonics (1/rev to 3 or 4/rev). In contrast to oscillatory loads, vibratory loads are those loads that will be passed to the fixed system and cause fatigue damage for fixed-system components as well as vibration that can be debilitating for passengers and

equipment. The vibratory loads depend upon blade number. For example, for a 4-bladed rotor, the dominant vibratory loads are 3–5/rev, and sometimes, 7–9/rev. In contrast to oscillatory and vibratory loads, aerodynamically generated noise, particularly that caused by blade vortex interactions (BVI), is usually dominated by harmonics above 10 or 15/rev, and is therefore beyond the regime of vibratory loads.

The interrelationship of the rotor physics between Acoustics (Chapter 3) and Aeromechanics (this chapter) can be illustrated with a low-speed example. At low speed in level flight, the rotor-blade tip vortices quickly roll up into disk vortices on either side of the rotor. The vorticity in these disk vortices (sometimes called vortex bundles) is distributed in space such that the change in peak velocities, negative to positive, is in the regime of 3 or 4/rev, and thus excite vibratory blade loads that are felt in the fuselage as severe vibration (transition vibration). If the aircraft now starts to descend, at some point the individual blade vortices no longer coalesce, but instead form a trail of individual vortices. The change in peak velocities, negative to positive, is in the regime of 10 to 20/rev (as the vortices never coalesce), and when these vortices intersect succeeding blades they cause severe acoustic radiation, but not vibration.

Interrelationships between aeromechanics and flight dynamics and control (Chapter 6) can also be understood in terms of frequency separation. Flight dynamics and control inputs typically are less than 1/rev, and thus are below the dynamics frequency range. But modern high-bandwidth controllers may result in input frequencies that couple with low-frequency blade structural frequencies and designers must consider the possibility of interactions. Moreover, although there is frequency separation between the two disciplines, the aerodynamic forces required for all flight path changes are based on the aeromechanics disciplines. As modern computers become more powerful, simulations in the disciplines of flight dynamics and control are more often based on direct calculations using classical aeromechanics approaches, rather than on simplified representations as have been used in the past.

Historically, the interrelationships between aeromechanics and propulsion, including transmission design (Chapter 7), have infrequently been addressed. The natural frequencies in the drive train, however, can couple with the rotor system and significantly affect the loads [Hansford, 1994]. These interrelationships will become very important for slowed rotor designs and not just for rotor underspeed conditions following power failures.

History of Developments in Aeromechanics

Useful histories of developments in aeromechanics are available in such classic texts as Johnson [1980] and Leishman [2000]. Surveys of research through the late 1980s are accessible in NASA Conference Publication 2495 [1988].

The “modern era” of rotary-wing aeromechanics follows the development of blade-element theory. Briefly, this theory combines the forces on an airfoil element, including lift, drag, and pitching moment, based on an angle of attack that includes the effects of induced flow. The airfoil forces and moments are obtained from table lookup and thereby include nonlinear viscous and compressibility effects. Unlike a fixed-wing aircraft, the induced-flow portion of the elemental airfoil angle of attack

is typically of the same order as the geometric angle of attack. The induced flow comprises many factors, but is generally dominated by the rotor wake; that is, the induced flows generated not only by the elemental airfoil rotor blade, but also by all other rotor blades. In a theoretical sense, the elemental airfoil forces and moments are an inner solution, whereas the wake is the outer solution, using the theory of matched asymptotic expansions [Johnson, 1986].

The determination of the elemental airfoil forces and moments is dependent upon accurate measurements of these characteristics in a wind tunnel. The technology for these measurements is generally satisfactory, except at higher Mach number ($M > 0.6$ or 0.7). The major advances in rotor aerodynamics in the last 40 to 50 years have been in the development of improved rotor-wake models. These models are computationally intensive, although this reality is now less of a concern with the power of modern computers.

On the structural side of developments in aeromechanics theory, the dominant approach has been beam theory using modal methods. In the last 20 years, finite-element methods have supplanted the modal approach, although because of the complexity of comprehensive methods, including both aerodynamics and elasticity, it has not always been apparent that the new finite-element methods offer significant improvements in accuracy [Hansford and Vorwald, 1998]. What is clear, however, is that the new finite-element methods coupled with multibody dynamics have allowed for more flexible and representative modeling of complicated rotorcraft structures.

Needs of the Designer

Before examining the state of the art, it is useful to review the needs of the designer of a helicopter or tiltrotor in the area of aeromechanics. By understanding these needs, one can focus on what the more important calculations are and how their accuracy is assessed. Seven aeromechanics design needs are considered of major importance: 1) hover and vertical rate-of-climb performance; 2) one-engine-inoperative (OEI) performance; 3) performance and loads at the maximum flight speed; 4) loads in maneuvers; 5) vibration in low-speed transition (vortex wake) and at high speed (transonic loading); and 6) noise in low-speed descents. Depending upon the mission of a rotorcraft, some of these design needs may be more or less important.

Hover performance is a basic measure of the utility of any rotorcraft. This performance is often guaranteed, and it is critical to the designer to have very accurate calculations, long before the aircraft is built and flown. For military aircraft there is sometimes a specification of additional power for maneuver at the critical hover point, and it is generally expressed as an additional vertical-rate-of-climb (VROC) capability.

OEI performance is specified near the minimum power speed for a rotorcraft. This design condition is critical for two-engine civilian rotorcraft as it determines the gross weight that can be used for operations from heliports. It can also be an important criterion for two-engine military aircraft operating at low speeds at night. Although an aerodynamically benign condition in the sense that there is no stall or transonic loading on the rotor, the performance must be accurately determined.

Performance at maximum-level speed is also critical for rotorcraft, and it may be a guarantee under a development contract. As with the other performance measures, it must be accurately calculated long before the aircraft is developed. At lower aircraft gross weights, this performance limit depends upon transonic loading on the rotor blades as well as fuselage drag, whereas at higher weights the limit may be more dependent on blade stall. In either case, the oscillatory loads must not exceed the endurance limit of any component, since it is essential that no fatigue damage occur in normal-level flight.

Vehicle maneuvers size many rotor components, both in the fixed and rotating systems. For example, the control loads in a maneuver may be 3 to 4 times higher than those at the maximum-level speed [Kufeld and Bousman, 1995]. These maneuver loads are important for both military and civilian rotorcraft. Currently, maneuver loads calculations are not considered trustworthy, so these loads are estimated from flight tests of similar rotorcraft.

For helicopters, the most severe vibration normally occurs either in transition (low speed), or at the maximum-level flight speed. The sources of vibration are different for these two cases. At low speed, the vibratory sources are from the vortex wake, whereas at high speed the vibratory sources are generally caused by periodic transonic loading on the blades. Currently, most helicopters use some sort of vibration isolation or suppression system, and it is important to know how severe these vibrations are going to be when designing the vibration suppression system.

Civilian aircraft must demonstrate that they meet specified noise limits in approaches to landing, in level flight, and in takeoff. The prediction of noise in descending flight depends upon an accurate model of the trailing vortex wake (see Chapter 3).

Design Continuum

Aeromechanics technology represents a continuum that stretches from the development of current-technology rotorcraft to innovative ideas to improve rotorcraft performance, loads, vibration, or noise characteristics. For current technology, the focus is on the accuracy of analysis and comprehensive methods, so that calculations are trustworthy for designer use. Thus, at this end of the continuum there is a need for highly accurate and unique measurements (see Chapter 5), and the careful validation of our best analytical methods using these data. At the other end of the continuum, innovative ideas tend to begin at a fairly simple level, but as they move closer to implementation they become more complex. In the early stages of an idea, aeromechanics efforts may focus on a mix of testing and exploratory calculations (to include CFD). Later, as the technology matures, experiments will become more sophisticated. Eventually efforts will focus on calculation methods and allow for incorporation of the innovative ideas into the comprehensive analysis codes and CFD/CSD computations.

Chapter Organization

This chapter begins by describing the technical approach we have taken towards the state-of-the-art assessment, and this description is followed by a discussion of the kinds of analyses and datasets that we used for the assessment. The four primary areas that are the focus of the chapter are then assessed: Rotor Aerodynamics and Interactions; Active Control for Loads, Vibration, and Noise Alleviation; Rotor Dynamics and Control; and Fluid Mechanics for Rotorcraft Applications. These technology areas roughly correspond to the design continuum discussed previously, although the boundaries can rarely be neatly drawn. Finally, at the conclusion of the chapter we attempt to describe what is needed to advance the technologies in these areas.

In the first primary area, on Rotor Aerodynamics and Interactions, we assess non-CFD aeromechanics for current technology rotors, paying particular attention to accurate and sometimes unique measurements that have been made in recent years. Using current comprehensive analyses, we evaluate the accuracy of these methods by comparing with multiple datasets (if possible). Our objective is to determine if these analytical methods are sufficiently accurate and trustworthy for design use.

In the second primary area, Active Control for Loads, Vibration, and Noise Alleviation, our focus is on future technology, that is, controls within the rotating system, sometimes referred to as individual blade control (IBC), which can be used to improve performance and decrease loads, vibration, and noise. IBC approaches may include active pitch links, as have already been tested with full-scale rotors [Jacklin et al., 2002; and Jacklin et al., 2003], or on-blade devices such as flaps, flow-control devices, or structural twist. In these cases, through careful measurements, we will attempt to demonstrate that the technology is sufficiently mature that testing can move to the next technology step of flight. As part of the demonstration that the technology is ready for flight, we must show that our comprehensive models are accurate and trustworthy, thus reducing the risk of moving this technology forward.

In the third primary area, we focus on two difficult areas in dynamics for current technology: rotor hub oscillatory loads and aeroelastic stability. Current predictions of hub loads are unsatisfactory for design use, a deficiency that is caused by a variety of factors that are examined through careful measurement and analysis. Aeroelastic stability remains a concern in the design of new rotorcraft.

Fluid mechanics, specifically two programs associated with dynamic stall and one with rotorcraft icing, are examined in the fourth primary area. At this level of the design continuum, we focus more on the experimental techniques than the analysis, although in all of these areas we wish to demonstrate improvements in predictive capability.

The chapter concludes with a discussion of future needs and challenges in all of the primary areas, some where we expect to make substantial headway, but also others where a path forward is still unclear.

TECHNICAL APPROACH FOR THE STATE-OF-THE-ART ASSESSMENT

In this study, we employ a standardized approach to the assessment of the predictive accuracy of analytical methods. This approach can be illustrated with a number of examples. Figure 2.1 compares flight-test data for a UH-60L aircraft, using standard blades, with the CAMRAD II analysis [Yeo et al., 2004].

A qualitative examination of this figure shows that there is fairly good agreement between analysis and data, but the power is underpredicted at low speeds and overpredicted for $0.25 \leq \mu \leq 0.35$. A more quantitative approach, and the one selected here, is to plot the calculated power coefficient, C_P as a function of the measured C_P for these same data, as shown in figure 2.2. If there was exact agreement, then the data points would lie on a 45° line (shown as a solid black line in the figure). We calculate a linear regression of the calculated and measured values, and this fit is shown as the solid red line. The scatter of the linear-regression fit is indicated by $\pm S_e$ (the standard error of estimate, which is equivalent to $\pm 1\sigma$) and is shown as bounding red dashed lines. The scatter in this case is a little more than 1% (based on the maximum ordinate scale), which is typical of better performance calculations. But the accuracy of the calculation is best assessed in this case by comparing the slope of the linear regression line with the 45° reference line (which has a slope, m, of 1). In this case, m = 1.093, indicating a 9.3% overprediction.

The utility of this approach requires that there be substantial variation in the dependent variables, in this case the calculated and measured C_P's. This variation is created in this example by the independent variable μ, and there is an approximate threefold range in the values of C_P. It has been found useful in many cases to include additional independent variables and group comparisons together. Thus, for the UH-60L flight-test data, power coefficient data at other weight coefficients (C_w) can be used, and grouping the data together perhaps provides a better test, as suggested by figure 2.3. In this example, data and calculations from four airspeed sweeps (four weight coefficients) are used, and the estimate of the calculation accuracy (+2.4%) is achieved for the combined calculations and data.

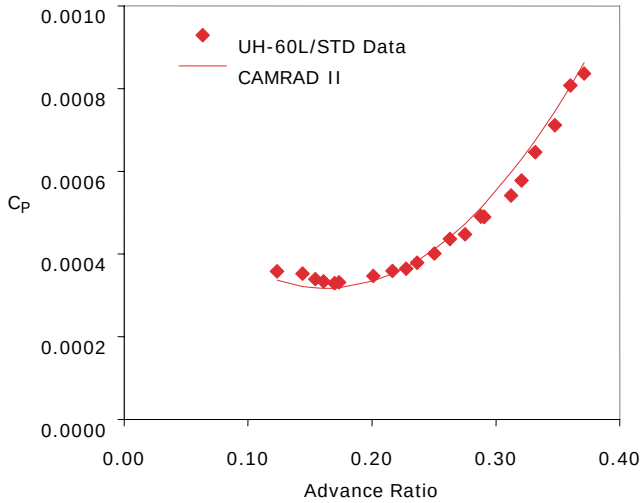

Figure 2.1. UH-60L with standard blades, power coefficient as a function of advance ratio; $C_w = 0.0065$ [Yeo et al., 2004].

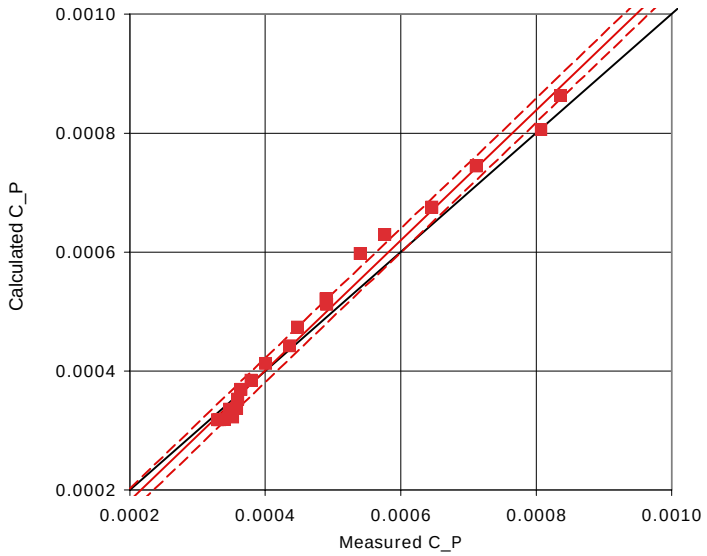

Figure 2.2. Predictive accuracy of CAMRAD II for UH-60L with standard blades for C_w = 0.0065; m = 1.093, S_e = ±1% [Yeo et al., 2004].

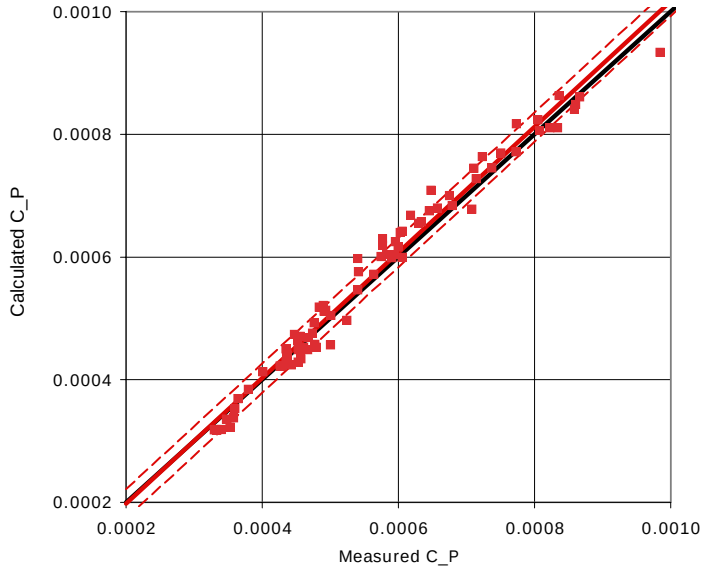

Figure 2.3. Predictive accuracy of CAMRAD II for UH-60L with standard blade for four weight coefficients; m = 1.024, S_e = ±2% [Yeo et al., 2004].

The performance examples here show relatively good predictive accuracy, as is expected. The prediction of rotor structural loads is more difficult and the accuracy is generally reduced. Figure 2.4a compares the measured and calculated nondimensional vibratory-flap bending moments (3/rev and above) for the SA 330 Puma [Yeo and Johnson, 2005a]. It is apparent in this time history that the CAMRAD II analysis underpredicts the peak-to-peak magnitude of the vibratory loads, but the phasing is closely matched. The data and calculations can be compared using the present technical approach by considering the nondimensional flap bending moments as the comparison variable and the blade azimuth angle as the independent variable, as shown in figure 2.4b. The slope of the

prediction is 0.65 or 35% low, but the scatter, as indicated by S_e, is about ±7%. In this case, the predictive-accuracy results (fig. 2.4b) appear straightforward and the 35% underprediction closely matches the ratio of the half peak-to-peak loads, which is 0.59 (fig. 2.4a).

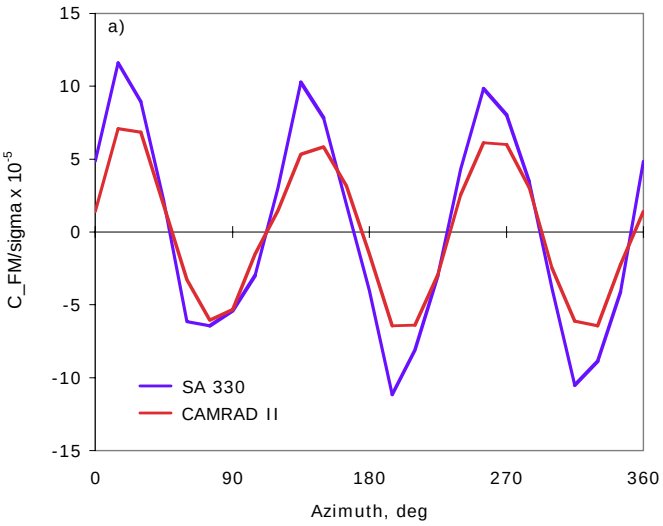

a) Flap bending moment as a function of azimuth

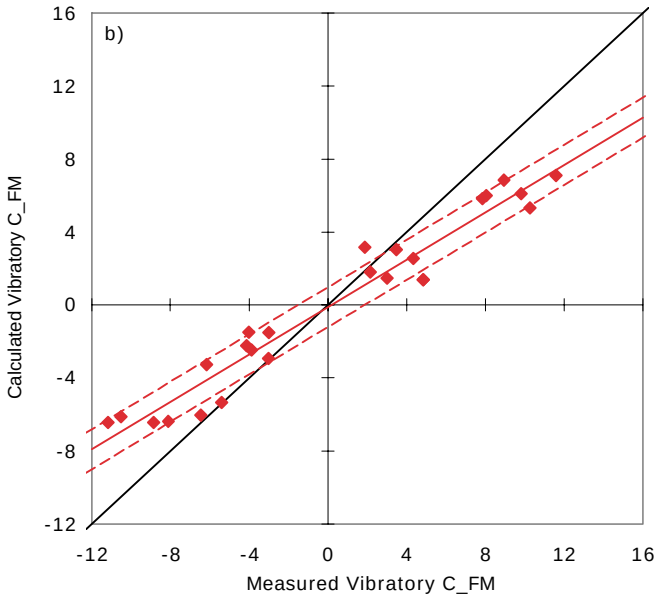

b) Linear regression: m = 0.649, S_e = ±7%

Figure 2.4. Comparison of SA 330 vibratory flap bending moments at 0.46R; μ = 0.362 [Yeo and Johnson, 2005a].

A second example of a vibratory loads calculation is shown in figure 2.5 for the UH-60A. In this example, although the calculations and data both show a dominant 3/rev loading, there is a phase difference that severely degrades the assessed predictive accuracy, as is shown in figure 2.5b. For structural loads, the UH-60A calculation can be considered an improvement over the SA 330 calculation, since the predicted half peak-to-peak load ratio in this case is 0.74, whereas for the SA 330 it was only 0.59. But using the present methodology, the UH-60A calculation predictive accuracy is judged to be poor.

We have shown here examples of the technical approach we will use for the present state-of-the-art assessment. Although we believe this approach offers significant advantages over qualitative judgments, the approach does have numerous deficiencies, and we offer the following cautions.

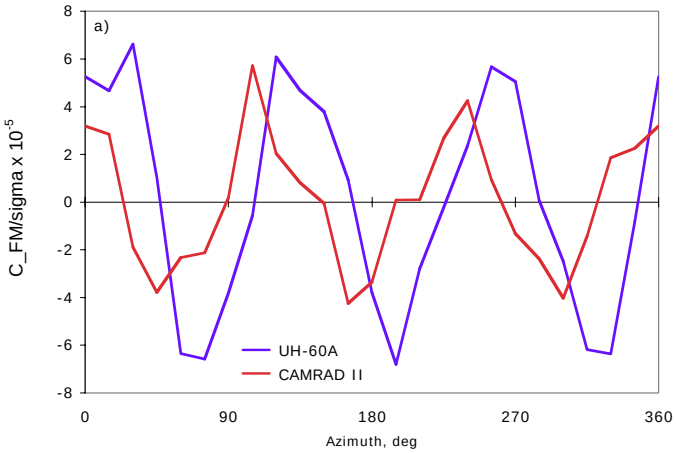

a) Flap bending moment as a function of azimuth

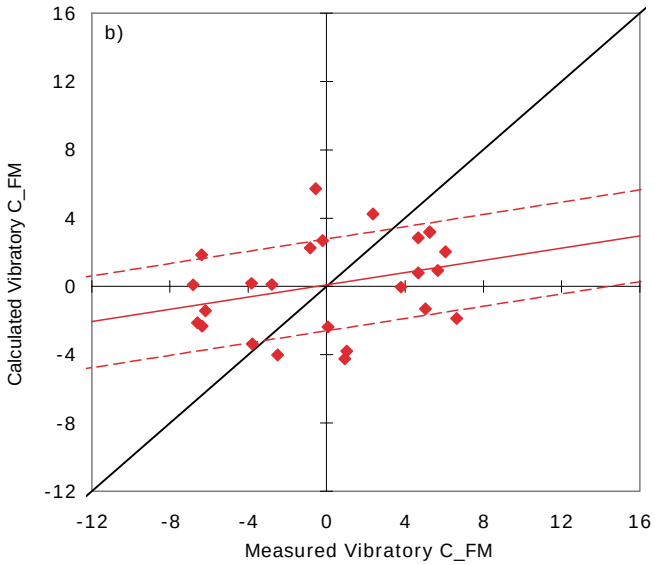

b) Linear regression: m = 0.180, S_e = ±17%

Figure 2.5. Comparison of UH-60A vibratory flap bending moments at 0.50R; μ = 0.368 [Yeo and Johnson, 2005a].

First, and perhaps most importantly, by showing calculated values as a function of measured values, we may imply that the measurements are exact and thereby deviations in calculated results represent prediction errors. Although we have selected results from the published literature where we believe that the experimental results are in most cases representative of the present measurement state of the art, this does not mean that these results are exact. In some cases we will directly identify potential measurement problems and suggest that technology advances may depend more upon improvements in measurement than in calculation. Moreover, we will use words such as error, difference, discrepancy, and so forth interchangeably on occasion and ask that the reader not place too much emphasis on the exact meaning of these words.

Second, using the present approach, no one number can be used to assess the predictive accuracy of calculations. Although the slope of the linear regression curve can provide a good estimate of accuracy in many cases, it can be confounded, particularly in cases with poor accuracy. For example, we have seen cases where phase errors in the calculation result in large scatter (large S_e values), but the slope is very close to one. Also when we state the S_e as a percent, we refer this value to the maximum absolute ordinate value, but understand that this value is somewhat arbitrary. Finally, there are cases where the slope may be close to one, the scatter may be low, but the calculations and measurements show substantial offset and the predictive accuracy is poor. Some of these deficiencies will be illustrated in this chapter.

The choice here of correlation sets for this assessment is based on the following guidelines. First, we used only correlation that had been published in the open literature. Second, we attempted to use correlation sets where we could obtain access to the actual data and could easily load them in a spreadsheet. We did, in some cases, scan figures from older papers, but this work was laborious. Finally, we sought out datasets that were wide-ranging in their coverage. These criteria often led us to use correlations studies from NASA or the U.S. Army.

ROTOR AERODYNAMICS AND INTERACTIONS

The primary comprehensive analysis tools used for the calculation of rotor aerodynamics and interactions in this assessment are CAMRAD II [Johnson, 1994], RCAS [Saberi et al., 2004], and CHARM [Quackenbush et al., 1999], but other codes used by industry and academia may well provide equivalent results. Both CAMRAD II and RCAS are based on multibody dynamics and finite-element models. All three codes are purposely designed to allow considerable flexibility in modeling various rotor configurations and to provide a sophisticated structural representation. The codes can also operate at different levels; that is, they can reduce the sophistication of the aerodynamic or structural models in order to make faster calculations, or they can increase the sophistication with a concomitant increase in solution time and cost.

CAMRAD II and RCAS have been designed to couple with CFD analyses, and in these circumstances, these two codes represent the CSD part of the coupled codes. By themselves, these codes use table lookup to determine the viscous nonlinear airfoil forces and moments, but when coupled, these forces are calculated by the CFD analysis. Similarly, by themselves, these codes represent the vortex wake with a model, whereas when coupled, the wake may be calculated within the CFD grid.

Hover Performance

Bell Helicopter Textron predictive capability

Most of the helicopter companies have tested their predictive capability for hover performance to some degree, but few have published their results. An exception is Bell Helicopter Textron, where Kocurek et al. [1980] evaluated their methodology for datasets from 4 isolated main rotors, 2 isolated tail rotors, and 13 helicopters. Rotor thrust and power were determined using a lifting surface method with an empirical-wake model. Blade aeroelasticity was not included in the analysis. For the helicopter datasets, the calculations of thrust and power included fuselage download, calculated tail-rotor power, accessory losses, and transmission losses. Kocurek et al. [1980] show their results as the error between predicted and measured power. These values range from about –3.2% to +3.2%.

EHPIC predictive capability

Continuum Dynamics, under NASA sponsorship, developed a hover-prediction method that used a free-wake relaxation scheme. The method is strictly an aerodynamic calculation with no allowance for the effects of blade flexibility. The aerodynamic model is based on lifting surface theory with a free wake, but uses table lookup for viscous drag. Felker et al. [1988] evaluated this method using data from 2 tail rotors, 4 main rotors, and 3 tiltrotors. They concluded that they could predict tail-rotor performance within 5–10%, main-rotor performance within 5%, and tiltrotor performance within 5%. Figure 2.6 shows the calculations for the 2 tail rotors, where the calculated power coefficient is shown as a function of the measured power coefficient for various thrust values and tip Mach numbers. Power coefficient as a function of thrust coefficient is shown in figure 2.6a as an example of the original comparison. There is little scatter in the individual tests of these two rotors, but the slope varies from 0.876 (Bell Model 214A at a tip Mach number of 0.73) to 1.123 (Model 222 tail rotor). For the combined assessment, the slope is 1.100 (10% overprediction).

Figure 2.7 shows the predictive accuracy for four main rotors [Felker et al., 1988]. The four datasets include a two-bladed rotor with significant taper that was tested about 1958 and is here referred to as the TN 4357 rotor (referring to the NACA technical note wherein the data were published). This rotor, 53.6 feet in diameter, was tested on a whirl tower with a height-to-diameter ratio of 0.78. Because of ground-plane effects, the data were corrected (about 5%). The second dataset was for a three-bladed rotor, obtained about 1951, referred to as the TN 2277 rotor. This rotor was untapered and had a 38-foot diameter. The third dataset was a CH-47B rotor tested on a whirl tower, also with three blades. The fourth dataset was for the four-bladed YUH-61A rotor, also tested on a whirl tower. Sample results for the YUH-61A are shown in figure 2.7a. The predictive accuracy of the individual datasets ranges from m = 0.927 for the CH-47B to m = 0.973 for the TN 4357 rotor. The combined predictive accuracy is quite good in this case at 0.985 (–1.5%) and the scatter is low.

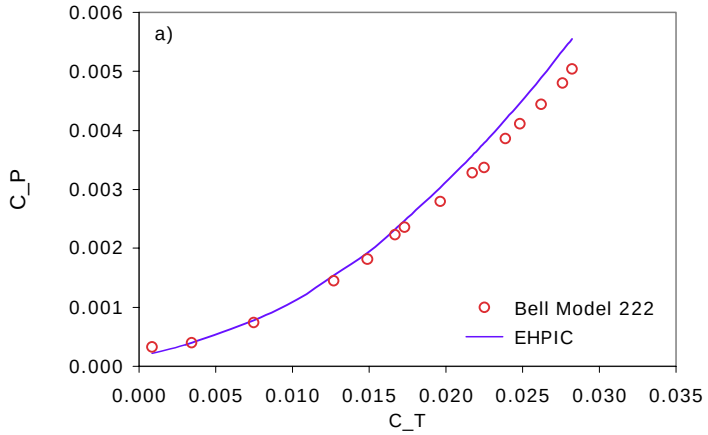

a) C_P as a function of C_T for Bell Model 222

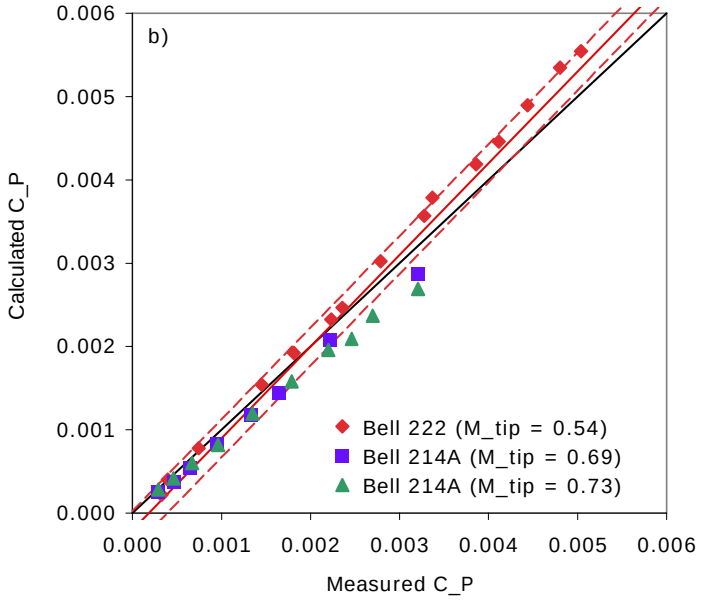

b) Linear regression for all datasets: m = 1.100, S_e = ±4%

Figure 2.6. Predictive accuracy of EHPIC hover prediction for two tail rotors [Felker et al., 1988].

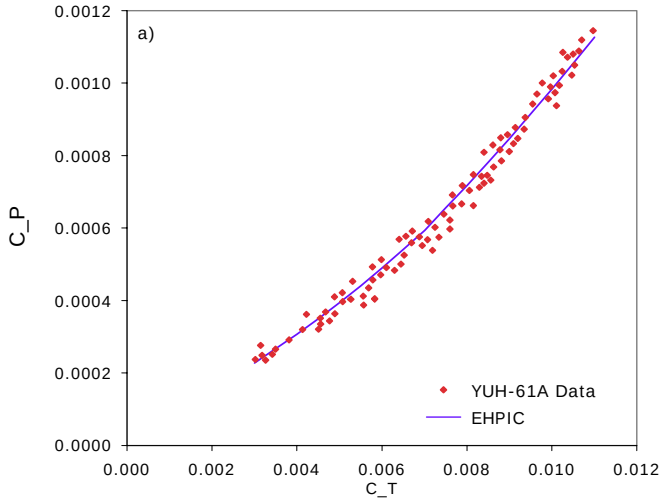

a) C_P as a function of C_T for Boeing YUH-61A

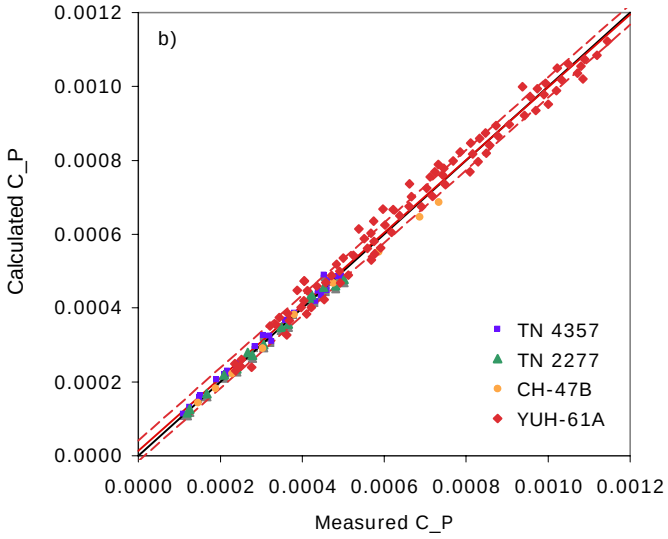

b) Linear regression for all datasets: m = 0.985, S_e = ±2%

Figure 2.7. Predictive accuracy of EHPIC hover prediction for four main rotors [Felker et al., 1988].

With the development of tiltrotor technology since the 1970s, there has been extensive hover testing of these rotors. Figure 2.8 shows the EHPIC predictive accuracy for three tiltrotors, all tested on a hover test stand at NASA Ames Research Center. For the individual tests, the accuracy varies from m = 1.067 for the XV-15 to m = 1.095 for the ATB blades. The combined results show an overprediction, m = 1.072 (+7.2%). The scatter in the regression is low for all of these datasets.

The comparisons shown in figures 2.6 through 2.8 extend from low-aspect-ratio, untwisted-tail rotor blades to higher aspect ratio, moderately twisted main rotors (one with taper), to highly twisted and variably tapered tiltrotors. The predictive accuracy of the EHPIC code varies from roughly –1.5 to +10% over this range. The code appears most accurate for conventional main rotors, less so for tail rotors and tiltrotors.

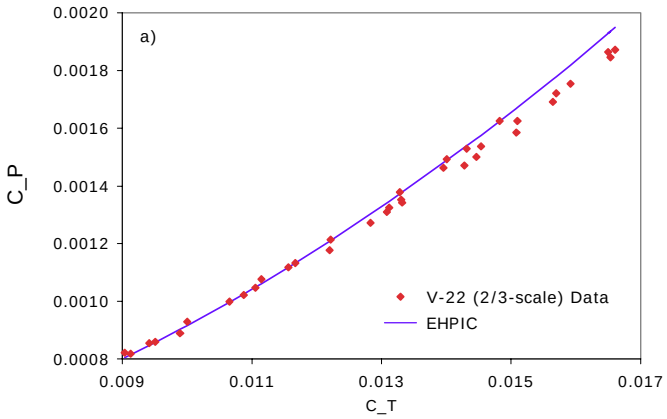

a) C_P as a function of C_T for V-22

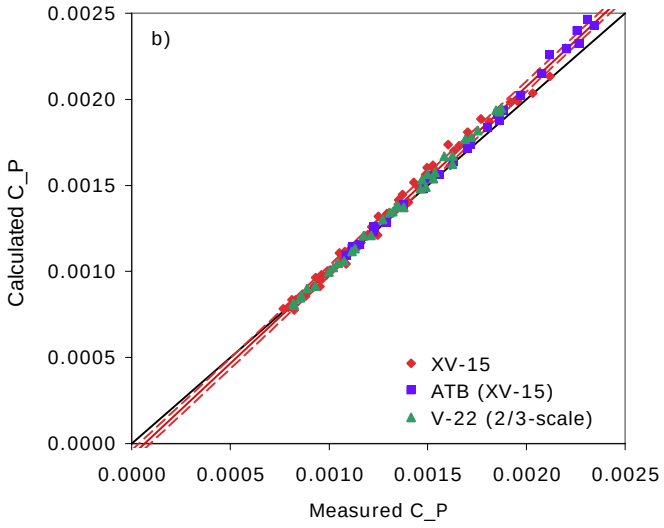

b) Linear regression for all datasets: m = 1.072, S_e = ±1%

Figure 2.8. Predictive accuracy of EHPIC hover prediction for three tiltrotors [Felker et al., 1988].

CHARM predictive capability

The CHARM comprehensive analysis, a successor to EHPIC, employs a lifting surface theory and a free wake. Wachspress et al. [2003] have applied this analysis to two isolated main rotors, a model-scale main rotor, and a tiltrotor, using Figure of Merit as their measure. Figure 2.9a shows an example of the Figure of Merit results for the 0.17-scale UH-60A rotor and figure 2.9b compares the calculations with measurements for the four rotor sets. For the individual tests, the accuracy varied from m = 0.794 for the full-scale CH-47B main rotor to m = 1.007 for the model-scale UH-60A main rotor. This scatter in predictive accuracy is greater than was seen in the EHPIC calculations. The combined analysis shows a slope of 0.978 (–2.2% accuracy), which is perhaps comparable to the previous results. The use of Figure of Merit as a comparison variable is believed to be a more stringent test than the use of C_P, since the range of calculation is so much less—the ratio of the minimum to maximum C_P in figure 2.7 is about 9, whereas it is about 2 in figure 2.9.

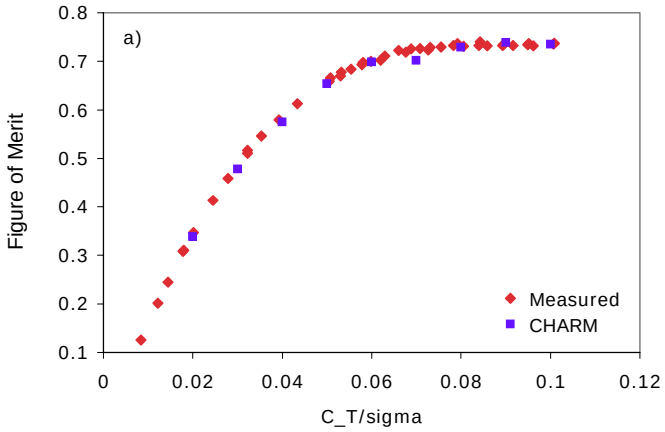

a) Figure of Merit as a function of C_T/σ for 0.17-scale UH-60A rotor

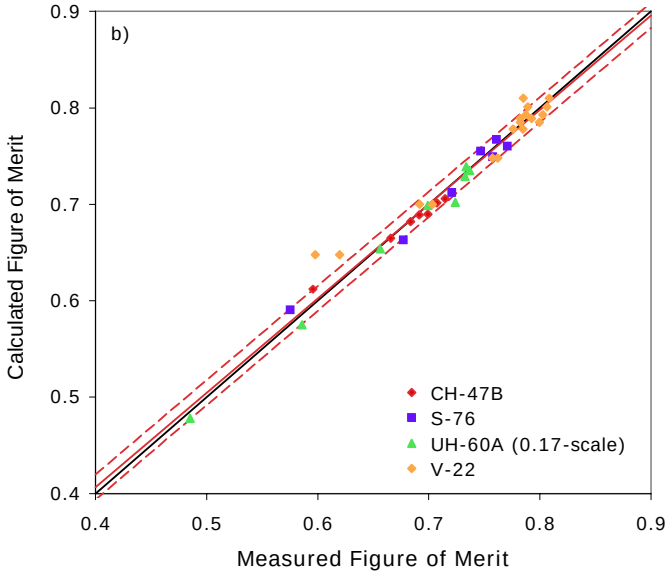

b) Linear regression for all datasets: m = 0.978, S_e = ±2%

Figure 2.9. Predictive accuracy of CHARM Figure of Merit for four rotors [Wachspress et al., 2003].

Felker et al. [1988] also assessed the accuracy of the EHPIC code for the prediction of vertical rate of climb (VROC). As mentioned previously, the VROC requirement is normally required for U.S. Army helicopters to provide a maneuver capability at the design hover condition. Using flight-test data from an OH-58D helicopter, Felker et al. compared the power ratio (normalized by hover power) for various nondimensional climb rates, as shown in figure 2.10a. The predictive accuracy is shown in figure 2.10b. The slope in this case, 0.862, shows an underprediction of the power required for climb. Although the scatter is low, the predicted power ratio is about 2.5% high.

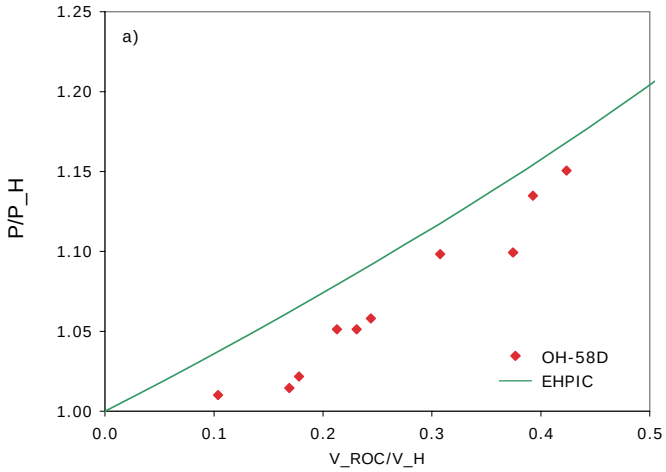

a) Power ratio in climb as a function of nondimensional climb rate

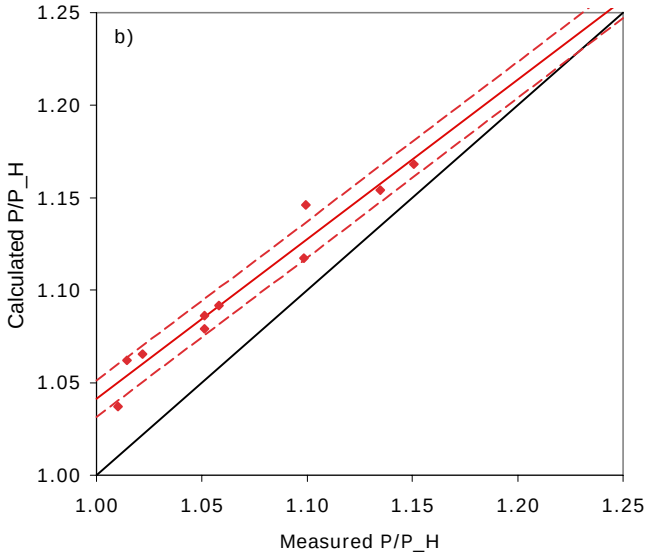

as

b) Linear regression: m = 0.862, S_e = ±1%

Figure 2.10. Predictive accuracy of EHPIC for power ratio in VROC [Felker et al., 1988].

Data limitations

The difficulty with hover prediction is caused in part by the inherent unsteadiness of the rotor wake, but other problems affect measurement accuracy, including controlling for disturbances such as winds or pilot inputs [see Bousman and Kufeld, 2005, for example], and the influence of nearby surfaces, whether of a wind tunnel or a whirl tower [Shinoda and Johnson, 1993]. The development of tethered hover flight testing, in which the tether guarantees the physical location of the rotorcraft and its thrust, has made flight testing perhaps more accurate than other methods. But serious errors can occur in flight-test aircraft calibrations that have not been properly addressed [Bousman, 2002].

Even with proper aircraft calibrations, it is still necessary to separate the main rotor thrust and power from the engine power and aircraft weight. This separation requires the identification of download on the aircraft, tail-rotor power, accessory power, and transmission losses. Although few of these factors exceed 10% of main rotor thrust and power for any one condition, more accurate measurements than are presently available cannot be obtained until improved accuracy is obtained for all of these features. Download, which is probably the most difficult of these effects to calculate, is currently estimated by decomposing the fuselage into appropriate shapes and assuming appropriate drag coefficients. Moreover, some aircraft fuselage configurations can have a significant "ground-plane" influence, and it must be incorporated in analysis. Fuselage and ground-plane effects may possibly be done more accurately with CFD analysis.

New experimental techniques may provide improved datasets [Caradonna et al., 1997]. Or new calculations can be made where external influences such as whirl towers or wind tunnel surfaces are modeled within the code. For outdoor testing, some success in compensating for wind has been obtained with neural network processing of the data [Kottapalli, 2000].

Summary

As shown here, numerous investigators have assessed the accuracy of current methods for hover prediction in the last 35 years. Calculation errors of the order of 5 to 10% have been obtained in some cases, although as Kocurek et al. [1980] have shown, a careful set of calculations over multiple datasets can achieve accuracies of ±3%. But it is unclear whether these accuracy limits depend more upon the accuracy of the calculation methods or inaccuracies in the multiple datasets that are used. To achieve accuracies beyond ±3%, it will be necessary to correct the deficiencies in available datasets or establish new datasets of improved accuracy. The prediction of VROC, although critical for some military aircraft, has received little attention. Limited comparisons show that the current methods are insufficiently accurate [Harris, 1986; and Wachspress et al., 2003].

The designer would probably be satisfied with an absolute accuracy for hover prediction of the order of 1 or 2%, but that is not achievable today. In some cases, it may be possible to show a delta change in thrust or power of this order, based on a rotor redesign, but this possibility is not clear. Moreover, rotor-wake and airframe interference in hover may have significant effects, whether they are ground-plane influences on performance or main rotor/tail rotor-wake interference in hover that are not properly calculated. Improvements are needed in both analysis and measurement.

OEI Performance

One-engine-inoperative (OEI) performance is evaluated near the minimum power speed, which for a typical rotorcraft is between 0.15 and 0.20 advance ratio.

Bell Helicopter Textron predictive capability

Harris et al. [1979] have evaluated their performance analyses using multiple datasets, with a particular focus on the minimum power speed and the power required at the best cruise speed. The datasets included 4 isolated rotor cases, 3 isolated model-scale cases, and 11 full-scale helicopter datasets. Including multiple thrust conditions, they examined 45 conditions and found that 29 conditions were within a ±3% band and 39 were within ±6%. They noted the importance of the accurate prediction of OEI performance in that a 3% error in power is magnified to an 11% error in the OEI service ceiling.

CHARM predictive capability

Wachspress et al. [2003] have calculated power for numerous rotors in wind tunnels near the minimum-power airspeed, including the UH–60A rotor in the 80- by 120-Foot Wind Tunnel and the Tilt Rotor Aeroacoustic Model (TRAM), a quarter-scale V-22 tiltrotor, in the German-Dutch Wind Tunnel (DNW).

The calculated power for the UH–60A is compared with test measurements in figure 2.11a, where the CHARM analysis models the Large Rotor Test Apparatus (LRTA) as a body of revolution and the wind tunnel walls are modeled as flat panels. The analysis captures the influence of the LRTA and the wind tunnel walls quite well down to $\mu \sim 0.04$ or 0.05, when the wake-induced flows on the wind tunnel walls probably separated, a feature not captured with the CHARM nonviscous panel method. The linear-regression analysis for this calculation shows good accuracy (+2.3%) and the scatter is slight (figure 2.11b). If modeling of the LRTA body and the wind tunnel walls are not included in the calculation, then m = 1.132 (+13.2% overprediction).

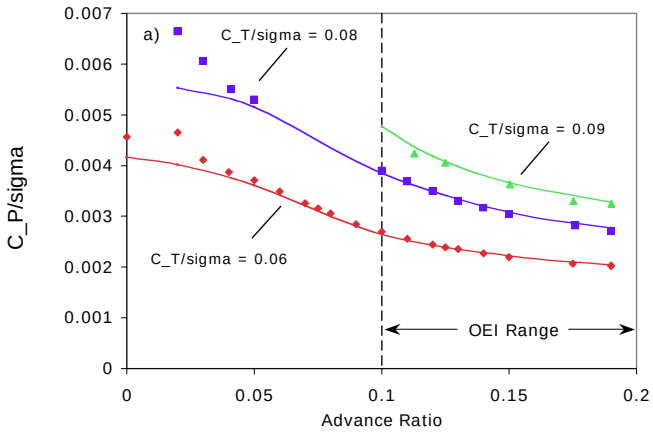

a) C_P/σ as a function of μ, data as symbols

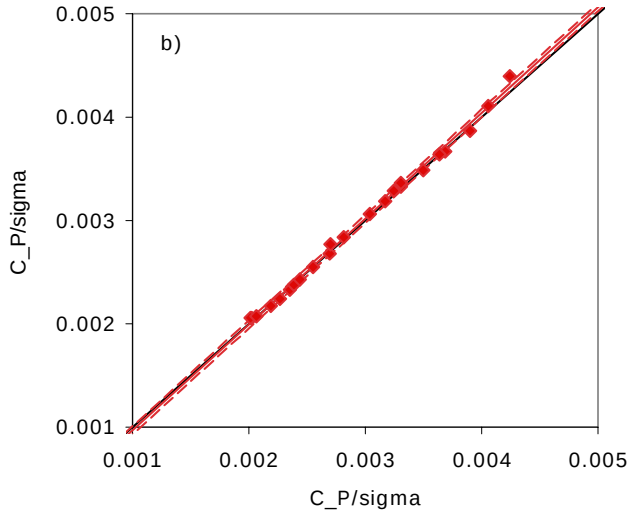

b) Linear regression for all C_T/σ: m = 1.023, $S_e = \pm 1\%$

Figure 2.11. Predictive accuracy of CHARM for UH-60A power coefficient in 80- by 120-Foot Wind Tunnel for $0.10 \le \mu \le 0.20$ and three thrust coefficients [Wachspress et al., 2003].

Calculations were also made for the TRAM at $\mu = 0.15$ in the DNW wind tunnel, as shown in figure 2.12a. The primary independent variable was shaft angle, and data were obtained at two thrust coefficients. The rotor was in the open jet section and the data were corrected using standard procedures. The CHARM calculations were made assuming the rotor was in free air. The calculation was made blind; that is, the data were not provided to CDI (the developers of the CHARM analysis) prior to doing the computation. The accuracy for this calculation is comparable to the UH-60A calculation shown previously (–1.4%).

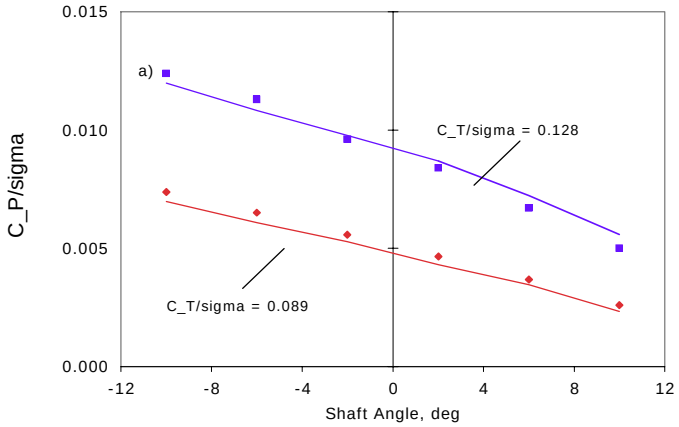

a) C_P/σ as a function of shaft angle, two thrust coefficients, data as symbols

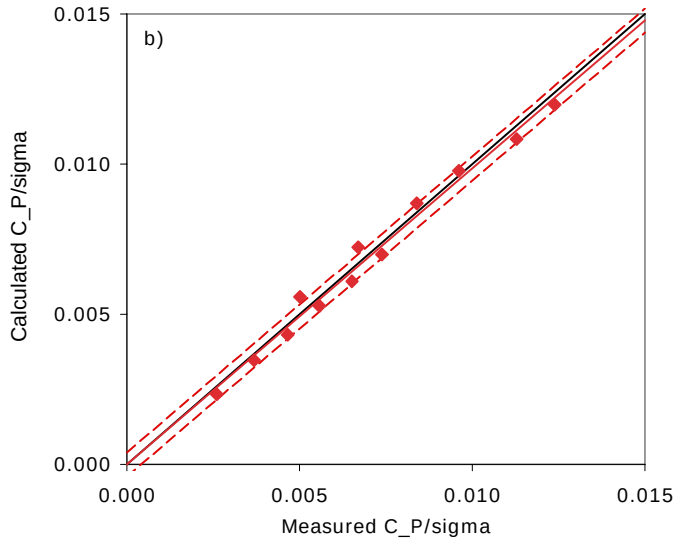

b) Linear regression for two C_T/σ: m = 0.986, $S_e = \pm 3\%$

Figure 2.12. Predictive accuracy of CHARM for TRAM power coefficient in DNW at $\mu = 0.15$ [Wachspress et al., 2003].

CAMRAD II predictive capability

Yeo et al. [2004] examined forward flight performance for three different UH-60 flight tests. These tests included the data obtained on the standard blades during the NASA/U.S. Army Airloads Program, a test of the standard blades on a UH-60L during development of the wide-chord blades (WCB), and a test of the WCB on a UH-60L. The Airloads Program data provided two datasets, one for aircraft power and the other for main rotor power. An evaluation of CAMRAD II predictions has been made using these four flight-test datasets. Since the minimum power speed occurs at about $\mu \sim 0.17$ for the UH-60, the comparison is examined over the range $0.12 \leq \mu \leq 0.22$. An example of these datasets, the UH-60L with the standard blades, is shown in figure 2.13a, Here, the power coefficient is shown as a function of advance ratio for four weight coefficients. The linear-regression analysis of all four datasets is shown in figure 2.13b. The slope for this combined analysis is 1.043, which is not as good as was seen using the wind tunnel test data previously. But the comparisons for each of the individual cases separately are less satisfactory, and these vary from m = 0.957 for main-rotor torque on the UH-60A to m = 1.131 for the UH-60A using the engine calibration. This range is excessive for performance testing.

Data limitations

For testing of isolated rotors in wind tunnels, it is necessary to correct for wind tunnel and model support interference effects that increase at lower speeds, but this correction probably cannot be done accurately for advance ratios below 0.05. The capability demonstrated using CHARM is encouraging over the range $0.10 < \mu < 0.20$ (see figure 2.11). For flight tests, airspeed systems become less accurate at lower speeds and an accurate calculation of induced power is more important.

Summary

The predictions of rotor power in wind tunnel tests are generally between 1 and 3%, and in some cases show very low scatter (see figure 2.11). A recent examination of UH-60A flight-test data is less satisfactory with predictions between –4 and +13% and with excessive scatter. Harris et al. [1979] have shown that in most cases Bell Helicopter Textron could predict the minimum power speed characteristics of most aircraft with ±3% at the end of the 1970s. Improvements in this area in the future mandate better test data.

Forward Flight Performance

The designer requires an accurate calculation of the maximum-level flight speed and the power and engine fuel flow at airspeeds for best range, as well as the minimum power condition discussed previously. An assessment of these calculations normally looks at all airspeeds above the aircraft transition speed.

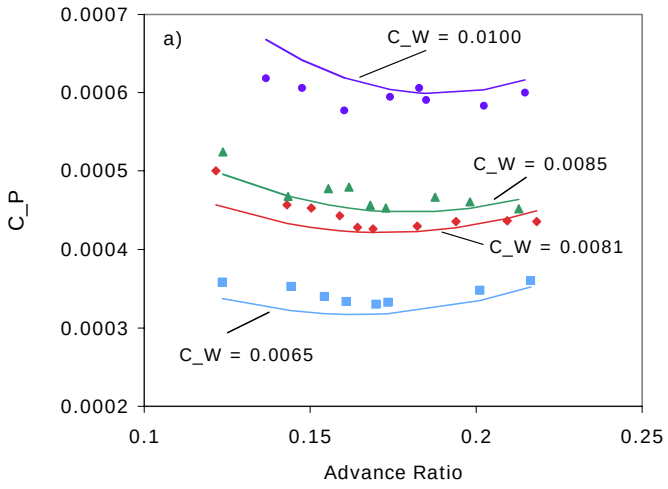

a) C_P as a function of μ, four weight coefficients

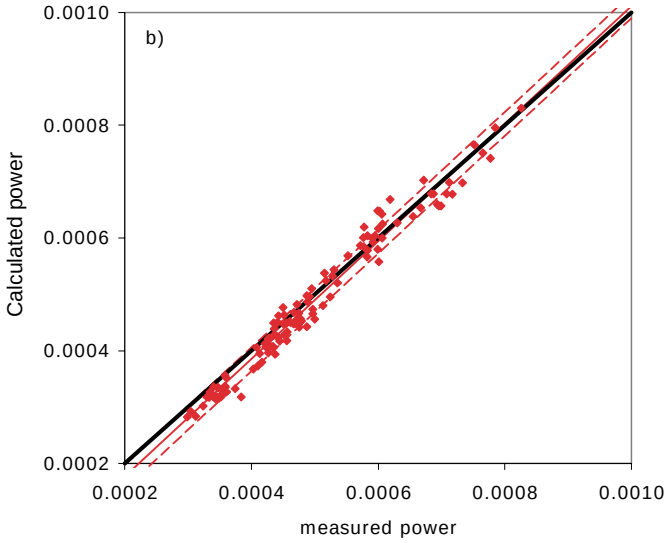

b) Linear regression for four datasets: m = 1.043, S_e = ±2%

Figure 2.13. Predictive accuracy of CAMRAD II for UH-60A in flight, 0.12 ≤ μ ≤ 0.22 [Yeo et al., 2004].

Bell Helicopter Textron predictive capability

In their evaluation of their performance methodology, Harris et al. [1979] examined cruise performance for 11 helicopters for various thrust values, resulting in 35 test conditions. Of these conditions, 18 were within a ±3% error band and 30 were within a ±6% band. The accuracy of these calculations depends not just on the calculation of the rotor power, but also on the calculation of fuselage drag and tail-rotor power, and the accurate determination of aircraft trim.

CAMRAD II predictive capability

As mentioned previously, Yeo et al. [2004] examined forward flight performance for three different UH-60 flight tests. These tests included the data obtained on the standard blades during the NASA/

U.S. Army Airloads Program, a test of the standard blades on a UH-60L during development of the WCB, and a test of these blades. The Airloads Program data provided two datasets, one for aircraft power and the other for main rotor power, thus providing four datasets in all. An example of the data for the UH-60A aircraft power is shown in figure 2.14a (where data from one of the airspeed sweeps, C_P = 0.0074, is not included to avoid excessive clutter). The airspeed-sweep data shown here are approximately a quarter of the data used for the combined analysis. For the combined analysis of all four datasets, m = 0.981, which is good for performance analysis. If the individual datasets are examined, however, the slopes range form m = 0.868 for the WCB to m = 1.076 for the UH-60A with the standard blades. The range in these inaccuracies appears excessive. If just the high-speed point is examined for the three lowest thrust values for each dataset, which is analogous to the Harris et al. [1979] approach, then the error ranges from –5 to +2% for the UH–60A with the standard blades, from –1 to +3% for the UH–60L with the standard blades, and from –6 to 0% for the UH–60L with the WCB.

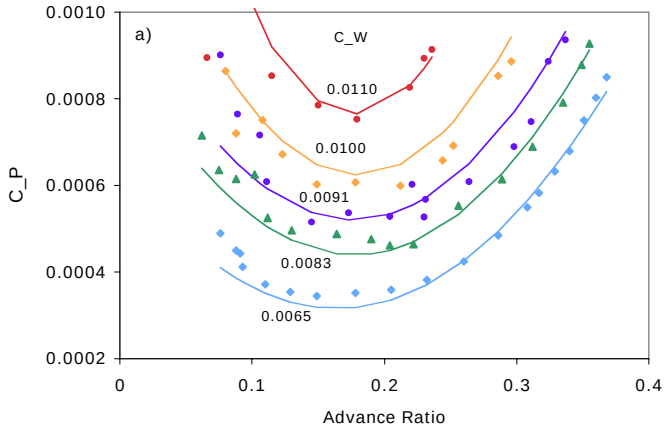

a) C_P as a function of μ for 5 weight coefficients for the UH-60A

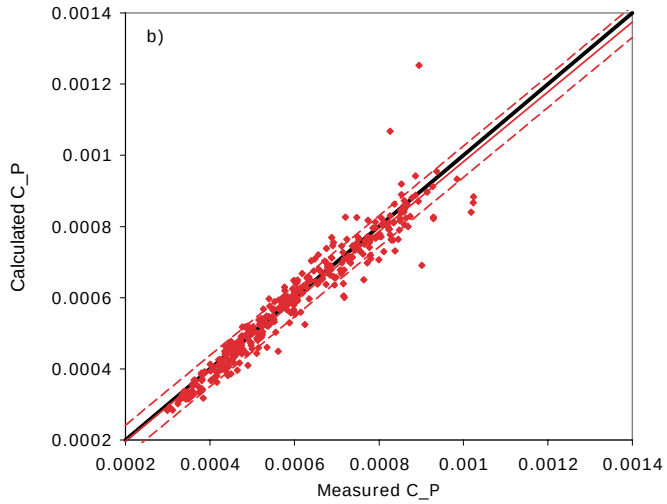

b) Linear regression for all data: m = 0.981, S_e = ±3%

Figure 2.14. Predictive accuracy of CAMRAD II for UH-60 flight performance for multiple aircraft and weight coefficients [Yeo et al., 2004].

Data limitations

To assess accuracy, it is necessary to examine multiple cases, but to achieve experimental accuracies of the order of ±1% or ±2%, which would be required to demonstrate improvement, may be beyond the state of the art. There is some optimism that wind tunnel performance tests of full-scale rotors may achieve close to this accuracy if appropriate wind tunnel corrections are made (although these corrections are quite small at high speed).

It is not possible to obtain equivalent accuracy with flight tests until serious inaccuracies in engine and drive-train calibrations are improved [Bousman, 2002]. Calibration errors in these cases may exceed 5%.

Summary

Predictive capability has been examined differently for the Bell Helicopter Textron and CAMRAD II methodologies. But when a similar approach is used, it appears that current comprehensive analyses are little different from performance methods of a generation ago. Thus, current accuracy appears to be on the order of ±3% to ±5%.

The variation in accuracy in the calculation of forward flight performance between various aircraft that is shown here may be discouraging to the rotorcraft designer. At higher speeds, the accurate calculation of performance is particularly dependent upon parasite drag, which is often estimated on the basis of small-scale model tests, and profile drag, particularly as dynamic stall becomes important. The inadequate accuracy at the present time seems more dependent upon experimental measurement limitations than it does on theoretical difficulties. The use of CFD analyses for these problems may eventually reduce or eliminate problems with parasite and profile drag calculations, but will not affect measurement inaccuracies.

Forward Flight Airloads

Rotor-blade airloads measurements require the installation of chordwise arrays of pressure transducers at multiple radial stations. Older experiments, using differential pressure transducers, are able to compute normal force and pitching moment, whereas more recent experiments, employing arrays of absolute pressure transducers, also obtain chord force. In general, better accuracy of normal-force measurements is achieved than for chord-force or pitching-moment measurements. Because of the cost and complexity, these types of experiments are few.

CAMRAD II predictive capability

Yeo and Johnson [2005b] have used CAMRAD II to compare calculated and measured airloads for five rotors at two airspeeds. Three of the five rotor datasets (SA 349/2, SA 330, and UH-60A) were obtained in flight test. One dataset (H-34) includes flight-test data at low speed and wind tunnel data at high speed. The final dataset (BO-105) is a 0.40-scale wind tunnel test at low speed (but there is no high-speed case for these tests). The low-speed cases selected for comparison were at $\mu \sim 0.14$, whereas high-speed cases were at $\mu \sim 0.37$. Calculations were made for one radial station near the blade tip ($r/R \sim 0.9$). For each set of data, the same modeling assumptions were used within the CAMRAD II analysis. The primary independent variable is blade azimuth. Figure 2.15a shows a

sample result for the Puma at $\mu = 0.141$ and $r/R = 0.92$, one of 18 cases. The calculated normal force (M^2c_n) is shown as a function of blade azimuth. Two CAMRAD II calculations are shown, using different wake models, and both overpredict the normal force. The regression analysis in figure 2.15b shows the low- and high-speed data separately. The slope for this combined analysis, $m = 0.834$, is an underprediction, but by combining so many different cases, the slopes or errors for the constituent test cases are obscured. These range from 0.138 for the low-speed BO 105 case to 1.403 for the low-speed Puma case (fig. 2.15a).

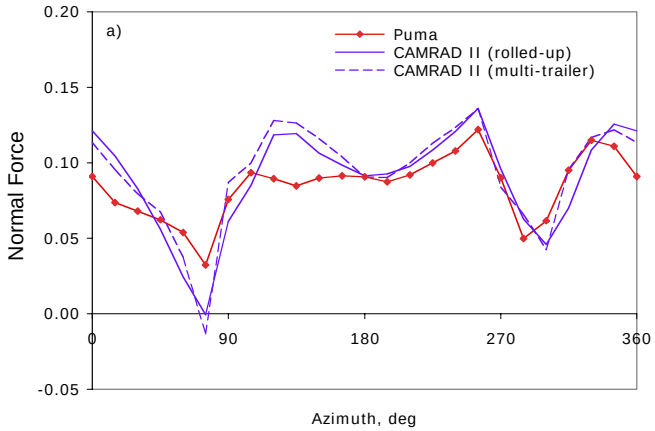

a) M^2c_n as a function of blade azimuth for Puma, low speed

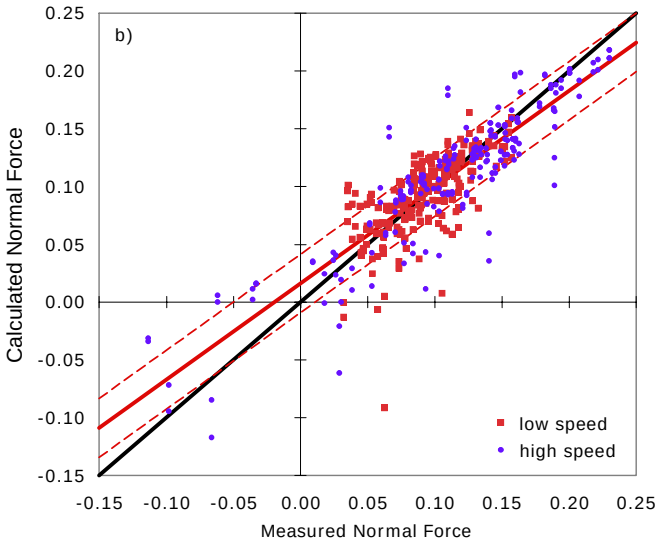

b) Linear regression for all cases: $m = 0.834$, $S_e = \pm 10\%$

Figure 2.15. Predictive accuracy of CAMRAD II for normal force, 5 tests, 2 airspeeds, 2 wake models [Yeo and Johnson, 2005b].

The pitching moment (M^2c_m) comparison is shown in figure 2.16. A sample calculation is shown in figure 2.16a for the SA 349/2, where $\mu = 0.14$ and $r/R = 0.88$. This case is one of 16 cases (there are no BO 105 data for pitching moment). The lifting model in CAMRAD II does not adequately represent the disk-vortex loading in this low-speed case. The slope for this combined analysis, $m = 0.747$, and is also an underprediction. Again, combining this many cases with such a variety of predictive accuracies may be misleading. For pitching moment, individual slopes varied from –0.040 for the SA 349/2 (fig. 2.16a) at low speed to 1.029 for the H-34 at high speed.

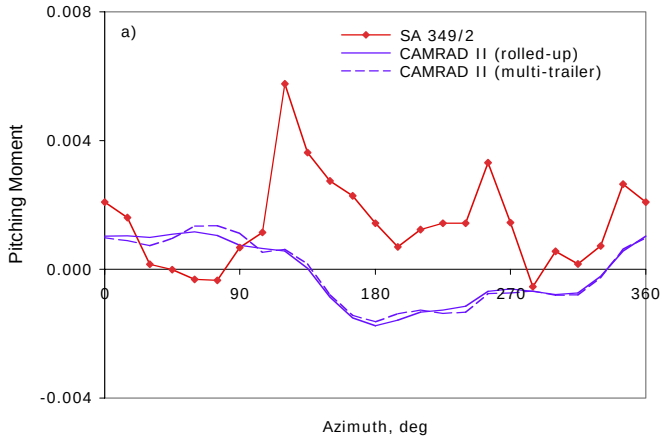

a) M^2c_m as a function of blade azimuth, SA 349/2, low airspeed

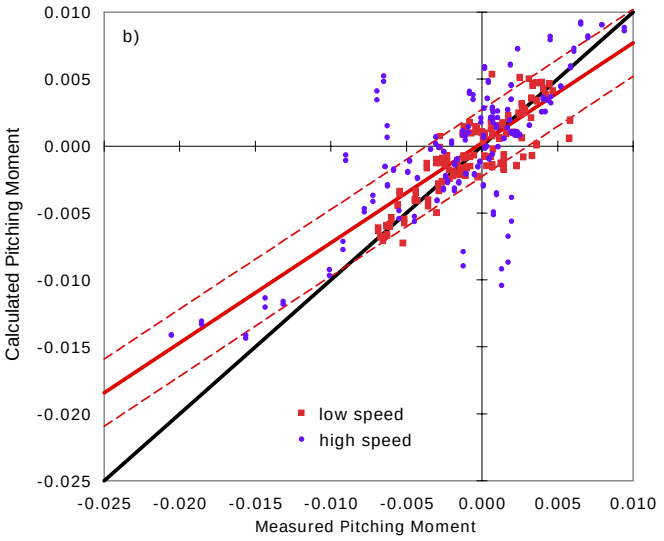

b) Linear regression for all cases: $m = 0.747$, $S_e = \pm 25\%$

Figure 2.16. Predictive accuracy of CAMRAD II for pitching moment, 4 tests, 2 airspeeds, 2 wake models [Yeo and Johnson, 2005b].

Data limitations

Airloads are computed by integrating measured pressures over the blade chord. Even if the pressure measurements are exact, integration errors are introduced because of the limited number of transducers. Each transducer, as with most other measurements, has scale and bias errors. Both types of errors are minimized by calibration procedures, but the bias error (offset) is the more difficult to correct. An overall check of bias errors and load integration is obtained for the UH–60A test data by comparing blade thrust with aircraft weight, after accounting for fuselage and stabilator download and tail-rotor lift. Kufeld et al. [1994] have shown that the integrated thrust is about 7% high and this may be representative of errors in steady load measurements at the present time.

Summary

The prediction of blade airloads in forward flight, based on the CAMRAD II calculations of Yeo and Johnson [2005b], is poor to fair. In a global sense, there is an underprediction of both the normal force and pitching moment. For individual cases, there is a wide variance in predictive accuracy and the causes are not immediately clear. It is useful to point out, however, that there are known limitations with lifting-line theory in both low- and high-speed cases. For example, in low-speed flight, the passage of the blade through the disk vortices causes vortical loading on the blades, which is responsible for substantial variations in the normal force and pitching moments as is evident in the experimental data. To some degree, the wake models in the comprehensive analysis properly account for the angle-of-attack variations for normal force, but little or no effect is observed for pitching moment (a consequence of the lifting-line representation). At high speed, there is substantial positive and negative loading on the advancing side for most of these rotors, and the modeling of the wake and the calculation of unsteady transonic loading is difficult. In comparing time histories of calculation and measurement, it is apparent that the analysis is capturing parts of these phenomena, but not accurately.

Blade Structural Loads in Forward Flight

Blade structural loads are important in forward flight in two respects. First, the oscillatory loads (first harmonic and above) determine the fatigue damage of rotating-system components. All loads must be below endurance levels at normal flight speeds. Second, the vibratory loads (third harmonic and above for a four-bladed rotor) may cause fatigue damage in fixed-system components and vibration that affects the pilot, crew, and equipment. The highest vibratory loads occur in transition (about $\mu = 0.10$) and at the maximum flight speed.

CAMRAD II structural loads predictive capability

Yeo and Johnson [2005a] have examined the oscillatory loads for five rotors: four full-scale rotors in flight and one model-scale rotor in the tunnel (the same cases as examined for the airloads in the previous section). The calculated and measured nondimensional flap bending moments near the midsection of the blade are compared for the five datasets in figure 2.17. The primary independent variable for the comparison is the blade azimuth angle (time history). As with the previous airloads comparisons, two wake models are used for the calculation: a rolled-up wake and a multitrailer wake. A sample result for the Puma at $\mu = 0.362$ and $r/R = 0.46$ is shown in figure 2.17a, one of 18 cases. Note that the steady value for flap bending moment has been removed for this assessment.

The slope for the combined analysis in figure 2.17b, m = 0.733, is similar to that computed previously for the normal force, and again the underprediction is about 25%. The scatter is about the same as for the normal force. Although the bending moments are greater for the high-speed cases, there is little difference in slopes between the two airspeeds. The predictive accuracy of the individual cases varies a great deal, ranging from a slope of 0.372 for the BO 105 to 1.080 for the UH-60A (both for $\mu = 0.15$ with a rolled-up wake model).

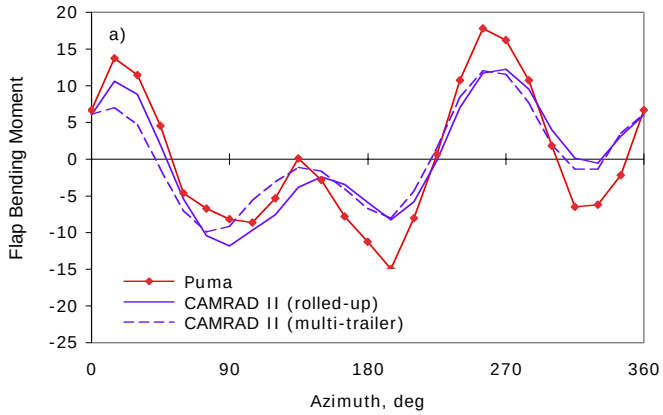

a) Nondimensional flap bending moment as a function of blade azimuth, Puma at high speed

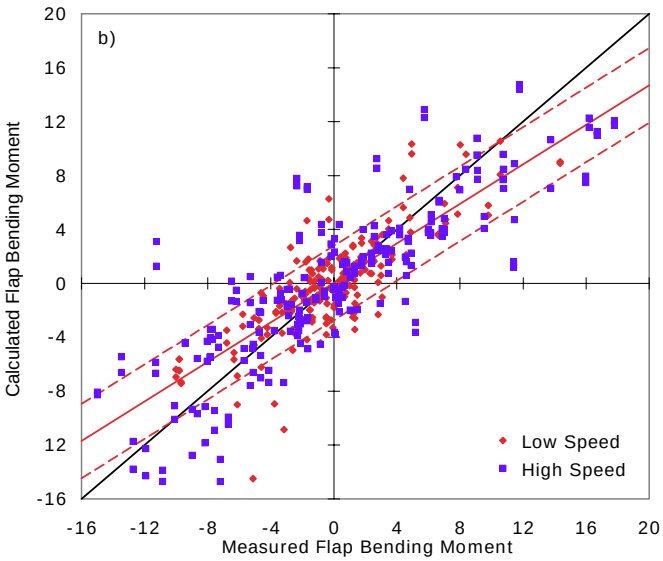

b) Linear regression for 18 datasets: m = 0.733, $S_e = \pm 14\%$

Figure 2.17. Predictive accuracy of CAMRAD II for flap bending moment, 5 tests, 2 airspeeds, 2 wake models [Yeo and Johnson, 2005b].

Figure 2.18 compares the calculations and data for the nondimensional chord bending moment at a midspan station for the five rotor tests. As with the flap bending moment, the mean value has been removed for the comparison. A sample result is shown in figure 2.18a for the SA 349/2 at $\mu = 0.361$ and $r/R = 0.54$. For this sample case, the prediction is fair, but for the combined analysis shown in figure 2.18b, the accuracy is very poor to poor with an underprediction of greater than 70%. This underprediction may be caused partly by the strong nonlinearities from the hydraulic lag damper for the H-34, SA 330, and UH-60A rotors. The SA 349/2 uses an elastomeric damper, with weaker nonlinearities, and the BO 105 has no damper (but probably does have some friction damping). The moments for the high-speed cases are considerably larger than for the low-speed cases, but the slopes are much the same (equally poor, for the most part). The slopes for individual rotor cases vary from 0.141 for the Puma to 0.754 for the SA 349/2 (both for $\mu = 0.36$ with a multitrailer wake model).

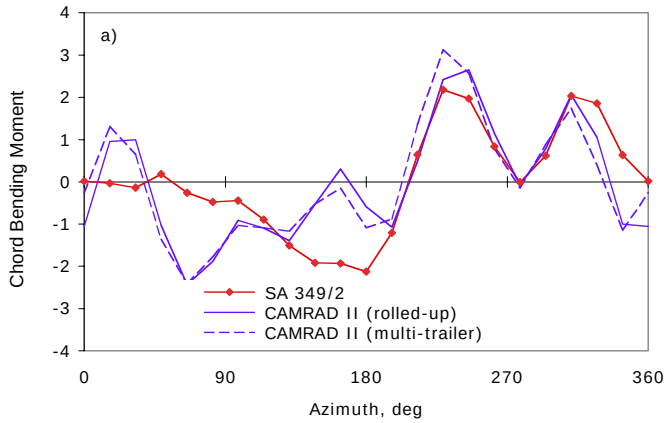

a) Nondimensional chord bending moment as a function of blade azimuth, SA 349/2 at high speed

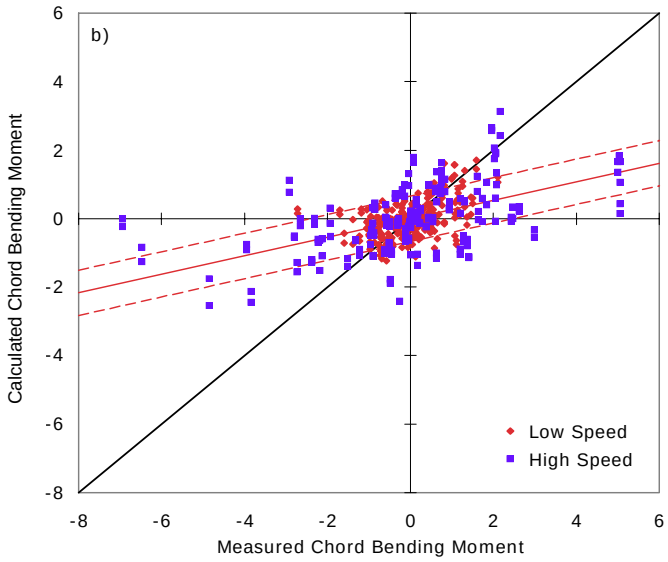

b) Llinear regression for 18 datasets: m = 0.271, $S_e = \pm 11\%$

Figure 2.18. Predictive accuracy of CAMRAD II for chord bending moment, 5 tests, 2 airspeeds, 2 wake models [Yeo and Johnson, 2005b].

A comparison of calculated and measured nondimensional torsion moments is shown in figure 2.19 for the 18 datasets. As before, the mean value has been removed. A sample dataset is shown for the UH-60A at high speed, $\mu = 0.368$ and $r/R = 0.30$, in figure 2.19a. The predictive accuracy for the combined datasets is similar to the flap bending moments, the underprediction here being about 33%. The scatter ($\pm S_e$) is similar to that of the other structural loads. The torsion moments at high speeds are significantly greater than at low speeds, as expected. Nonetheless, there is very little difference in the slopes at the two speeds. As with the other load components, there is variation in slopes for the individual cases, ranging from $m = 0.526$ for the Puma at $\mu = 0.362$ to $m = 0.879$ for the BO 105 at $\mu = 0.15$ (both with a multitrailer wake model).

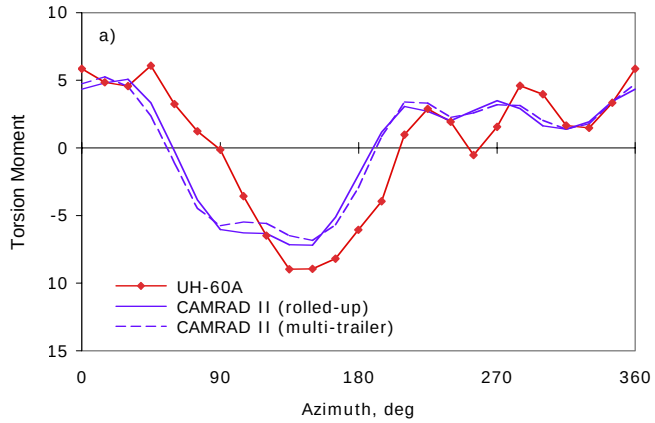

a) Nondimensional torsion moment as a function of blade azimuth, UH-60A at high speed,

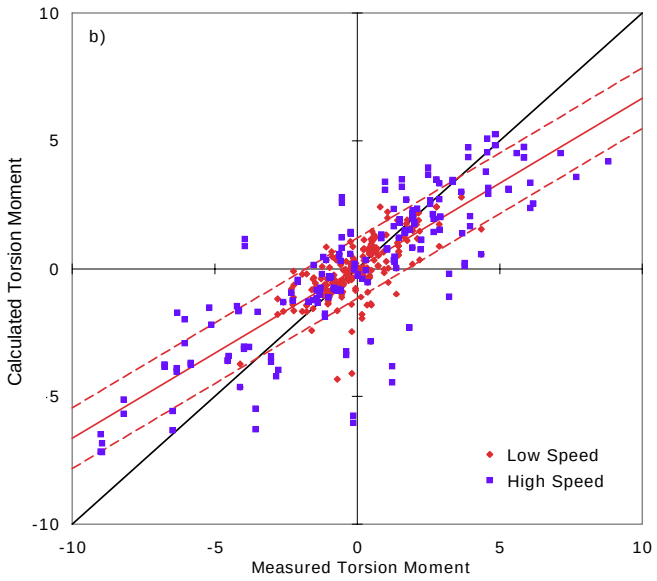

b) Linear regression for 18 datasets: $m = 0.665$, $S_e = \pm 12\%$

Figure 2.19. Predictive accuracy of CAMRAD II for torsion moment, 5 tests, 2 airspeeds, 2 wake models [Yeo and Johnson, 2005b].

TABLE 2.1. COMPARISON OF SLOPE AND STANDARD ERROR OF ESTIMATE FOR STANDARD AND PEAK-TO-PEAK APPROACHES

	Flap		Chord		Torsion	
	m	S_e	m	S_e	m	S_e
Standard	0.733	14%	0.271	11 %	0.665	12%
Peak-to-peak	0.756	11%	0.409	9%	0.674	7%

The approach to evaluating predictive accuracy, as employed here, uses the blade azimuth angle (time history) as the primary independent variable. For the design engineer who is interested in fatigue damage, small differences in time histories are not of concern. Rather, it is the peak-to-peak loading that occurs over a wide range of conditions that is most meaningful. Using the Yeo and Johnson [2005b] calculations and data it is possible to compute the peak-to-peak loads for these same cases and assess the predictive accuracy based only on these peak-to-peak loads. The results for slope and the standard error of estimate obtained from the analysis shown in figures 2.17 to 2.19 (referred to here as the standard approach) are compared with those obtained using the peak-to-peak data in table 2.1. The slopes for flap-bending and torsion-moment accuracy do not change significantly, but the scatter as indicated by S_e is less. The accuracy of the chord bending moment is improved, but it remains poor.

Data limitations

The use of strain-gauge bridges to measure blade moments is an established technique, although precise measurements of blade strain in a centrifugal force field can be difficult. Nonetheless, the inaccuracies in predictive accuracy shown in this section for blade internal loads are not believed to be significantly affected by limitations in measurement accuracy.

For those rotor tests with a full suite of chordwise pressure transducer arrays (e.g., the H-34 and UH-60A rotors), it is possible to compare the measured structural loads with structural loads calculated using measured airloads [Esculier and Bousman, 1988; and Ho et al., 2007]. When successful, this approach provides a case of self-validation of the data as both sets of measurements: (1) blade forces and moments and (2) structural measurements are independent. Nonetheless problems remain with this approach and are not completely understood.

Summary

The state of the art for the prediction of structural loads has been examined by comparing calculations and data for rotor-blade midspan locations for five rotors at two airspeeds. The modeling of the five rotors using CAMRAD II was done in a uniform fashion. Results were computed for two different wake models. In general, flap bending and torsion moments were underpredicted by 25 to 35% and the overall correlation at best was only fair. The prediction of chord bending moments, however, was significantly worse, and this result did not appear to depend upon the type of lag damper used. If the analysis was performed using peak-to-peak data instead of time histories, little change was seen in accuracy for the flap bending and torsion moments, whereas the chord bending moments improved slightly (but remained 60% underpredicted).

Maneuver Loads

Maneuver loads determine the size of many of the blade components, both in the rotating and fixed systems. Compared to a maximum-level flight condition, blade loads are often doubled during severe maneuvers, and the control loads may increase by a factor of 2.5 or 3.0 [Kufeld and Bousman, 1995]. Current analytical methods are not considered reliable for these calculations, so currently these design loads are determined from flight-test databases. Recent developments, however, offer optimism that some improvement can be achieved, even with comprehensive analyses.

RCAS predictive capability

Recently, Bhagwat et al. [2007] have applied RCAS to the maneuver loads problem as the CSD side of a CFD calculation. The primary results of the paper are very encouraging for the development of CSD/CFD prediction; the RCAS calculations provide an appropriate baseline as to the best that can be expected from current comprehensive analyses. Bhagwat et al. [2007] focused on the UTTAS maneuver for the UH-60A, where the aircraft enters the maneuver at its maximum-level flight speed, pulls up to achieve a 1.75-g load factor, and attempts to maintain that load factor for 3 seconds. This maneuver, in terms of loading, is one of the most severe encountered in the U.S. Army/NASA Airloads Program [Kufeld and Bousman, 1995]. Figure 2.20 shows the half peak-to-peak flap bending moments at the 0.50R radial station as computed by RCAS during the maneuver. The half peak-to-peak moments are computed for each revolution during the maneuver; hence the independent variable in this figure is the revolution number. Figure 2.20a shows the flap bending moments over the length of the maneuver (which also includes the coupled CSD/CFD calculation using RCAS and OVERFLOW2). In this case, RCAS overpredicts the loads, whereas RCAS/OVERFLOW2 underpredicts the loads over most of the maneuver. The accuracy in this case, m = 1.078, is good, particularly when compared to the systematic evaluation of accuracy shown previously for five rotor datasets level in flight in figure 2.17. The scatter in the data is less than ±10%. The half peak-to-peak chord bending moments at 0.50R for the same maneuver are shown in figure 2.21. Figure 2.21a shows how the loads change over the maneuver, and the RCAS predictions are close to the measured data over most of the maneuver. The predictive accuracy in this case, m = 1.012, is excellent, in contrast to the five level-flight cases examined previously in figure 2.18. The scatter in this case, ±8%, is moderate.

The RCAS and RCAS/OVERFLOW2 calculated pitch-link loads are compared with the measured loads in figure 2.22a. Unlike the blade flap and chord bending comparisons shown previously, the RCAS calculation is well below the measurements, whereas the RCAS/OVERFLOW2 result is quite close. The linear-regression analysis in figure 2.22b for RCAS shows that its predictive capability for these control loads is poor. The pitch-link loads in this maneuver are dominated by severe dynamic stall, and the semiempirical stall model in RCAS does not accurately account for these loads (as compared to the calculations using RCAS/OVERFLOW2.

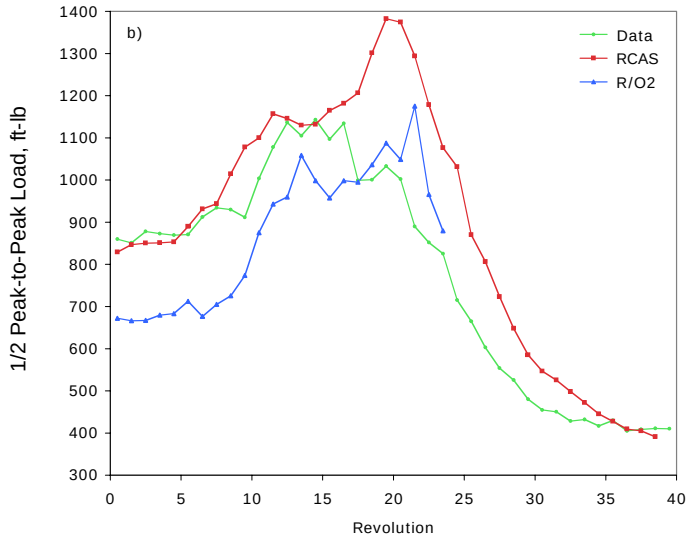

a) Half peak-to-peak flap bending moments during UTTAS maneuver on UH-60A

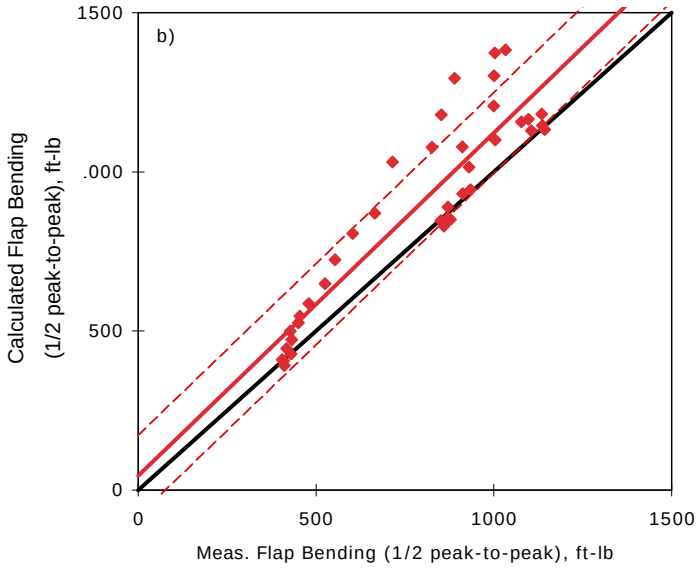

b) Linear regression: m = 1.078, S_e = ±9%

Figure 2.20. Predictive accuracy of RCAS for flap bending moment for UH-60A in UTTAS maneuver [Bhagwat et al., 2007].

As shown in figures 2.20a through 2.22a, the combined CSD/CFD predictions have been made for this same flight maneuver as for RCAS [Bhagwat et al., 2007]. The combined results show a substantial improvement for the prediction of the pitch-link loads (see table 2.2). For the flap bending computation, OVERFLOW/RCAS shows about the same accuracy as RCAS, whereas for chord bending, it is substantially less accurate. But for the pitch-link loads, the OVERFLOW/RCAS prediction is very good.

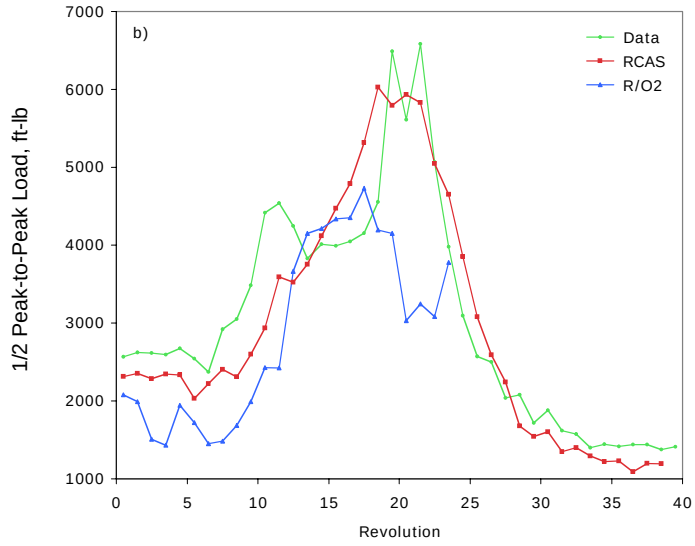

a) Half peak-to-peak chord bending moments during UTTAS maneuver on UH-60A

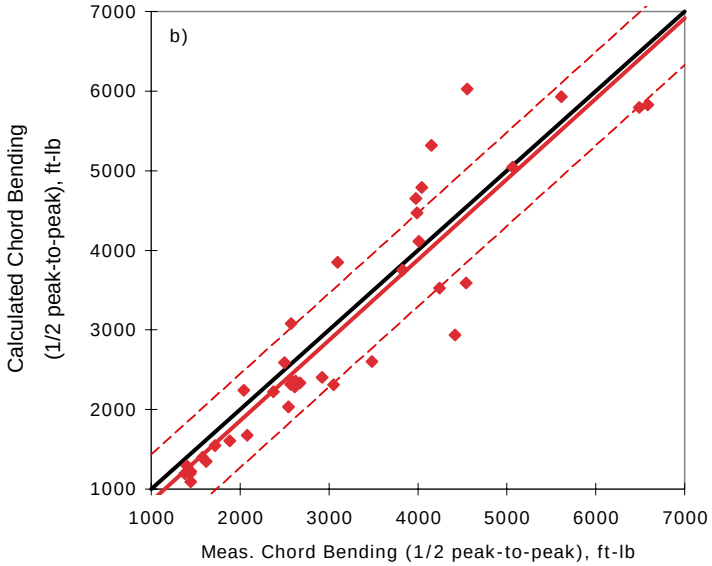

b) Linear regression: m = 1.012, S_e = ±8%

Figure 2.21. Predictive accuracy of RCAS for chord bending moment for UH-60A in UTTAS maneuver [Bhagwat et al., 2007].

Summary

The ability to predict maneuver loads has been examined only on occasion, as the industry experience has been that these analyses cannot provide reliably accurate answers. But the recent results, of which a few are summarized here, show mixed results in that in some cases, alternating loads can be well estimated by a comprehensive code such as RCAS, and even better results can be obtained with a CFD/CSD computation. Nonetheless, these capabilities have not yet been shown to be consistently reliable and must be applied across a broad spectrum of different aircraft and flight conditions.

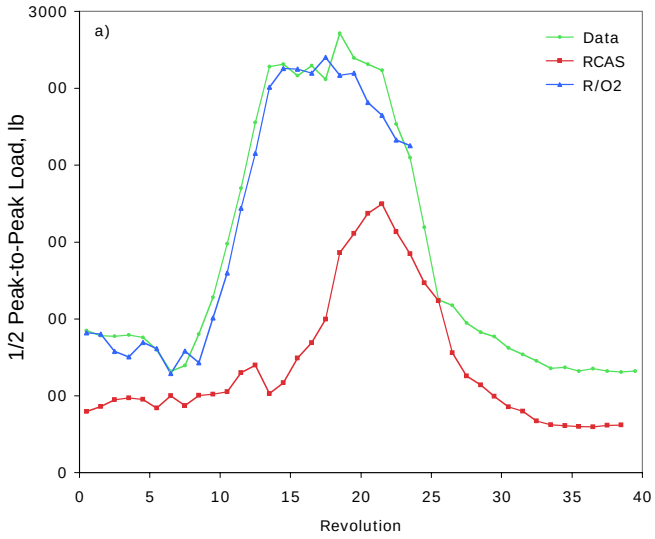

a) Half peak-to-peak pitch-link loads during UTTAS maneuver on UH-60A

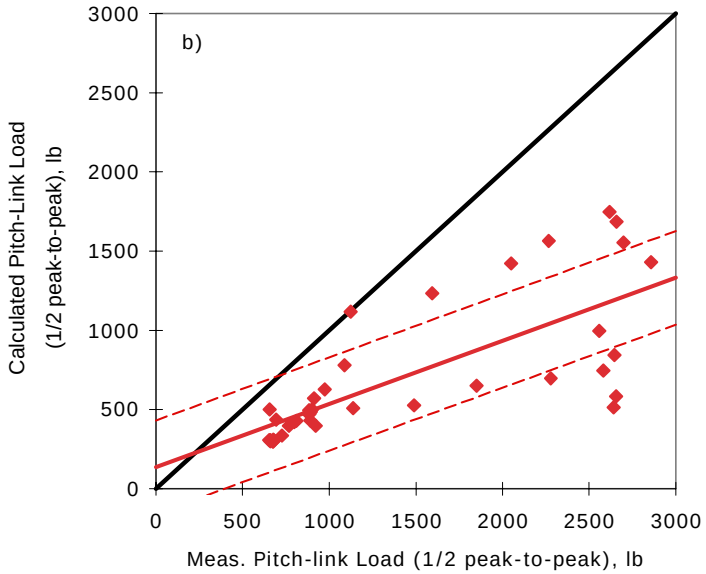

b) Linear regression: m = 0.398, S_e = ±10%

Figure 2.22. Predictive accuracy of RCAS for pitch-link loads for UH-60A in UTTAS maneuver [Bhagwat et al., 2007].

TABLE 2.2. COMPARISON OF SLOPES AND STANDARD ERRORS OF ESTIMATE FOR CSD (RCAS) AND CFD/CSD (RCAS/OVERFLOW2)

	Flap		**Chord**		**Pitch-link load**	
	m	**S_e**	**m**	**S_e**	**m**	**S_e**
RCAS	1.078	9%	1.012	18 %	0.398	10%
RCAS/OVERFLOW2	0.949	10%	0.586	13%	0.963	4%

Typically the designer uses previous flight-test databases to determine the maximum loading that may occur for rotating- and fixed-system components of a new or modified rotorcraft. This maximum loading determines the sizes of most of these components for the new design. Although this designer may be encouraged by the results shown here, it is unlikely that he will put much faith in these demonstrations until the same methods have been applied to many rotorcraft and many maneuvers, and the calculations compared to measurements. The first useful application of these new analytical approaches may not occur until the designer is faced with a new design whose parameters are well outside the range of current flight-test databases.

Vibratory Loads

The peak vibratory loads (resulting loads in the fixed system) occur at transition airspeeds (about $\mu = 0.10$) and at the maximum-level flight speed. The calculation problem involves the prediction of these vibratory loads in the rotating system, their transmission to the fuselage, and then their amplification or attenuation at various sites in the aircraft depending upon the airframe impedance. Such calculations have yet to be successfully demonstrated. A first step is to divide this problem into the separate components of the vibratory loads on the blade, the vibratory loads at the rotor hub, and the vibratory response in the fuselage. The vibratory loads on the blade are discussed here, and the vibratory loads at the hub are considered in the section on Oscillatory Loads.

CAMRAD II vibratory blade loads predictive capability

Yeo and Johnson [2005a] have examined the vibratory-flap bending moments for rotor datasets at low speed (five rotors) and high speed (four rotors). The calculations are compared with the measurements in figures 2.23 and 2.24 for low and high speed, respectively. The primary independent variable is blade azimuth (time history). A sample low-speed time history, one of 10, is shown for the Puma in figure 2.23a for $\mu = 0.141$ and $r/R = 0.46$. Here, it is clear that these vibratory loads are dominated by 3/rev. The linear-regression analysis of the combined datasets in figure 2.23b shows that the vibratory loads are underpredicted, by roughly 25%, and the scatter is about ±8%. These results are comparable to the predictive accuracy observed for the oscillatory flap bending moment loads (see figure 2.17). But the predictive accuracy for these cases shows wide variation, with the slopes ranging from –0.229 for the BO 105 with a multitrailer wake model to 1.572 for the UH-60A with a rolled-up wake model. Figure 2.24 shows the predictive accuracy for the vibratory flap bending moments at high speed. Again, an example case is shown for the Puma in figure 2.24a, this time for $\mu = 0.362$. The accuracy shown by the linear-regression analysis in figure 2.24b is $m = 0.494$, which is considerably less than the slope seen for the oscillatory flap bending moment prediction in figure 2.17. For the individual aircraft, the slope values range from 0.023 for the UH-60A to 0.763 for the SA 349/2 (both with multitrailer wake models). The phase of the calculations shown in the sample cases for the Puma in figures 2.23a and 2.23b is good, but the poor predictive capability shown in many other cases has been affected by differences in phase for the vibratory loads between calculation and test. These phase differences generally lead to large errors in the regression analysis.

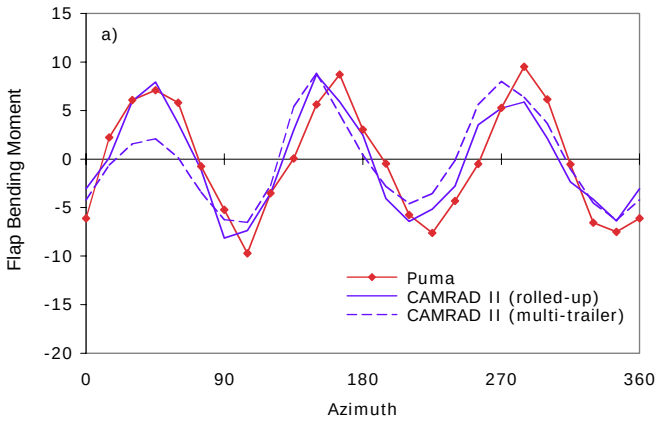

a) Vibratory flap bending moment as a function of blade azimuth, Puma at low speed

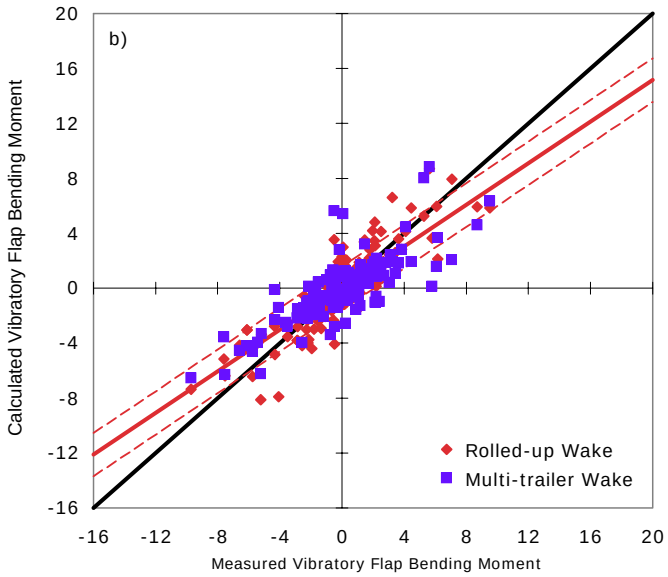

b) Linear regression for all cases: m = 0.758, S_e = ±8%

Figure 2.23. Predictive accuracy of CAMRAD II for flap vibratory loads at low speed, 5 rotors, 2 wake models [Yeo and Johnson, 2005a].

Summary

In general, the prediction of vibratory-flap bending moments is poor. As with the prediction of oscillatory-flap bending moments, as discussed previously, there is a general underprediction of the vibratory loads. But in many cases there are significant phase differences that degrade the accuracy.

Currently, designers deal with vibratory loads in new or modified rotorcraft by including provisions for vibration isolators or other control devices. The great difficulty of calculating vibratory loads, as evidenced here, makes it unlikely that design for vibration reduction will be successful in the near future.

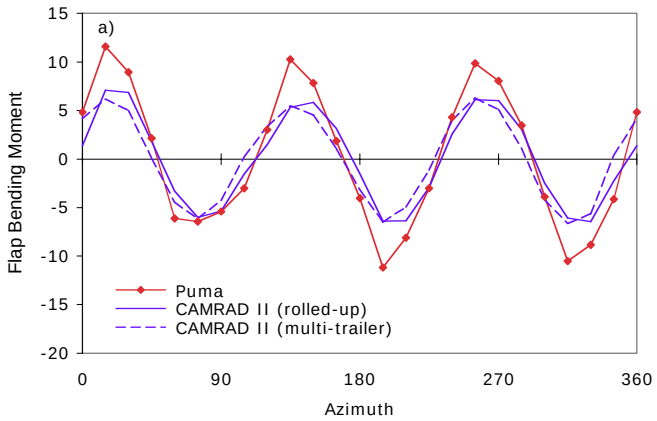

a) Vibratory-flap bending moment as a function of blade azimuth, Puma at high speed

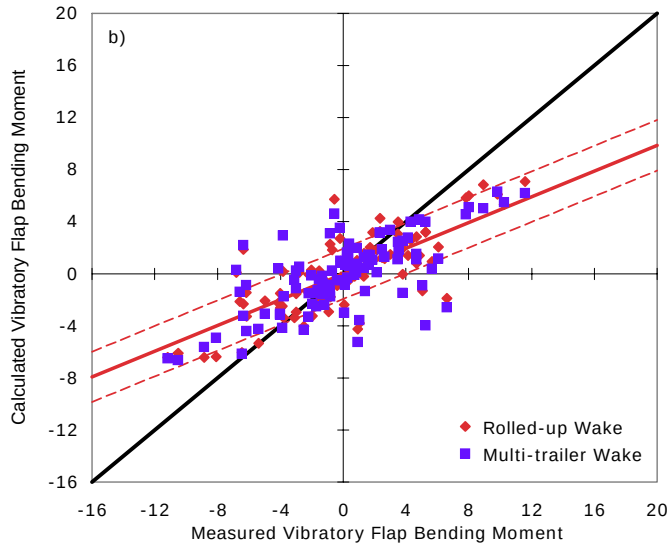

b) Linear regression for all cases: m = 0.494, S_e = ±10%

Figure 2.24. Predictive accuracy of CAMRAD II for flap vibratory loads at high speed, 4 rotors, 2 wake models [Yeo and Johnson, 2005a].

New Rotor Configurations

Slowed rotors

Conventional rotors in edgewise flight rarely exceed advance ratios of 0.4. Alternatives to these rotors already exist with the development of the tiltrotor, which avoids the edgewise flight limitations by tilting the rotor 90 deg and using the rotor as a propeller. Other means of achieving high-speed flight without the propulsive-force limitations of conventional rotors is to use either a compound helicopter or an autogyro; interest in both configurations has been shown in recent years [Floros and Johnson, 2004]. In such designs, some form of auxiliary propulsion provides the force to overcome airframe drag, and the rotor is slowed so as to further reduce the rotor drag. For such a design, the unloaded rotor advance ratio may exceed one.

CAMRAD II predictive capability

Floros and Johnson [2004] compared the predictions of CAMRAD II with data from a high-speed test of a two-bladed teetering rotor at the Langley Research Center in the 1960s. This untwisted rotor was tested at advance ratios from 0.65 to 1.45. They calculated C_T and C_Q as a function of collective pitch for a variety of shaft angles and advance ratios. Figure 2.25a shows an example of calculations and data for C_T as a function of collective pitch. The calculations show the same trend as the data but are offset. A linear-regression analysis of both C_T and C_Q has been made, where the primary independent variables are the rotor shaft angle and advance ratio. The results for C_T are shown in figure 2.25b. The analysis underpredicts the data, and the offset of the data is apparent. This offset is likely related to measurement problems [Floros and Johnson, 2004]. A similar analysis for the rotor torque for the two shaft angles shows a poor prediction; m = 0.373 and S_e = ±17%.

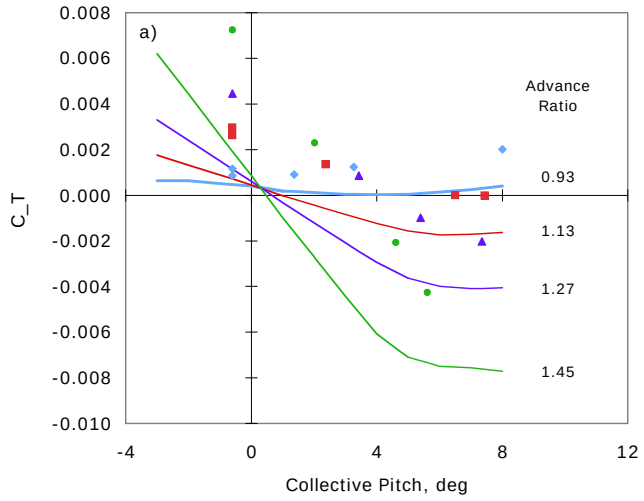

a) C_T as a function of collective pitch, where calculations are shown by solid line and data as symbols

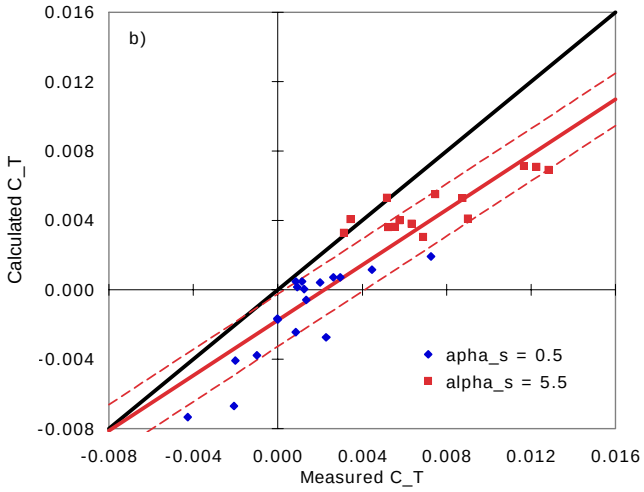

b) Linear regression: m = 0.796, S_e = ±9%

Figure 2.25. Predictive accuracy of CAMRAD II for C_T for two shaft angles and various advance ratios [Floros and Johnson, 2004].

Summary

The predictive capability of CAMRAD II for the limited data available for a slowed rotor is poor to fair. In particular, the utility of a slowed rotor is to obtain reduced vehicle drag and the inability to accurately predict the rotor power in this case places a limitation on the designer.

Rotor, Wake, and Fuselage Interactions

Rotor-wake interaction includes impulsive loading of nearby portions of the fuselage, excitation of empennage surfaces, and the creation of regular or irregular flow separation on the fuselage. Some of the wake-interaction calculation methods fall into non-CFD techniques, using wake models and panel methods to compute rotor-wake excitation of the fuselage or empennage. But CFD methods are also applied to these problems and are probably the only appropriate techniques to use when substantial separated flows exist and there is a need to compute the drag.

Numerous sets of measurements have been obtained to assess rotor aerodynamic interactions, both in the universities and in government laboratories. Tests at the Langley Research Center have used a generic fuselage, known as the Rotor Body Interaction (or ROBIN) fuselage, and both fuselage pressure and wake data have been obtained [Mineck and Gorton, 2000]. Correlation with these data using CFD methods has been made by Boyd et al. [2000]. Data from a test of a model Dauphin rotor and fuselage in the S2Ch tunnel at Chalais Meudon have also been used for correlation [Berry and Bettschart, 1997], including using non-CFD methods, as discussed in the following section.

CHARM predictive capability

Wachspress et al. [2000] have examined the interaction of the rotor wake with the fuselage by comparing calculations using CHARM with unsteady pressure measurements on a model Dauphin rotor and fuselage in a wind tunnel. The rotor loading is computed with a wake model and the fuselage is represented using a panel method. Figure 2.26 compares calculated unsteady pressures with measured values, where the primary independent variables are location of the pressure taps and rotor azimuth.

A sample time history of the unsteady pressure, comparing analysis and data, is shown in figure 2.26a for a pressure tap on the fuselage centerline forward of the rotor. Comparisons were made at pressure taps at five locations on the upper fuselage centerline and 10 locations on the sides of the fuselage at two different longitudinal stations. The regression analysis for these 15 locations is shown in figure 2.26b. The slopes for individual locations range from m = 0.677 (a centerline location just downstream of the rotor hub) to m = 1.080. Most of the individual location slopes are quite close to 0.9, and the overall accuracy of the method is good.

Summary

The predictive accuracy of the CHARM analysis for unsteady pressures on a fuselage is good. The accuracy of such methods on a horizontal or vertical stabilizer, particularly when flow separation is encountered, is uncertain.

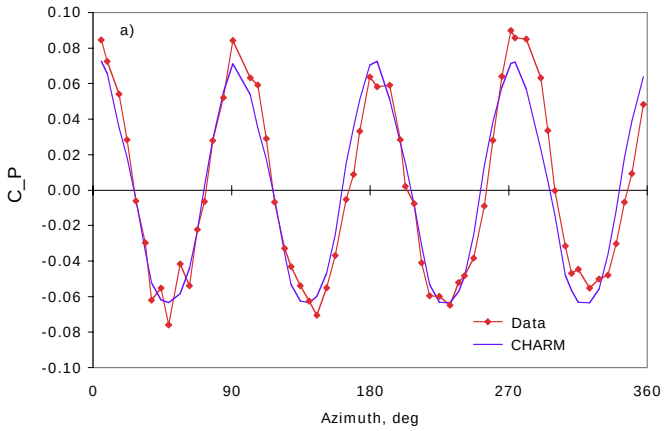

a) Unsteady C_P as a function of rotor azimuth

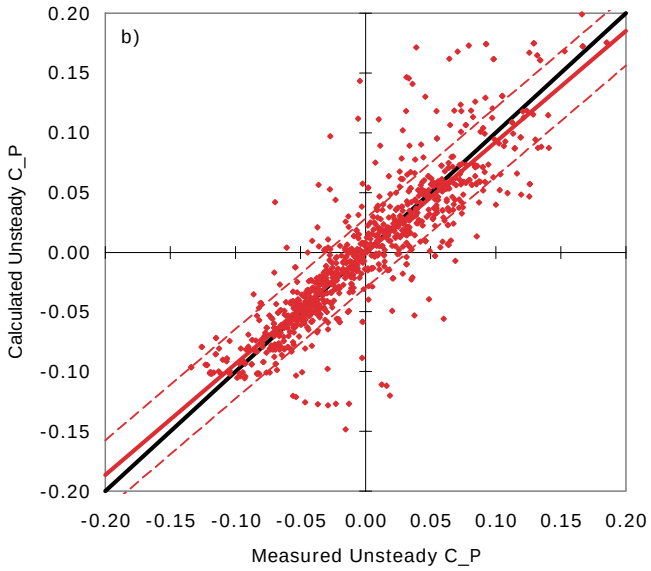

b) Linear regression for all locations: m = 0.929, S_e = ±15%

Figure 2.26. Predictive accuracy of CHARM for unsteady pressures on a Dauphine fuselage from a model rotor/fuselage test [Wachspress et al., 2000].

ACTIVE CONTROL FOR LOADS, VIBRATION, AND NOISE ALLEVIATION

The inherent drawbacks of helicopter technology—that is, limits on performance, and sometimes excessive loads, vibration, and noise—have for decades drawn inventors within the community to consider control schemes that could be implemented to increase the performance and decrease the loads, vibration, and noise of a helicopter. One approach, e.g., higher harmonic control (HHC), wherein the fixed-system swashplate is oscillated at higher harmonics of rotor speed, has been demonstrated at model scale in the wind tunnel, and at full scale in both the wind tunnel and in flight tests. These tests have shown the potential for a significant reduction in vibration and noise, but with increases in cost. Currently, research in active control technology focuses on mechanisms within the rotating system, generally called individual blade control (IBC). This research focus is partly based on the belief that IBC control schemes will be more capable than HHC schemes.

Numerous schemes for IBC active controls have been implemented in modern comprehensive analyses; for example, CAMRAD II, RCAS, and its predecessor 2GCHAS, as well as many of the academic codes (UMARC and others). These schemes include both active pitch links and some form of active flaps or elevons, and active twist. In some cases, the capability to model the geometry and characteristics of active control devices lacks the sophistication to adequately represent the main rotor, in part because so little data have been available for the development of these models.

Active Controls Predictive Capability

We know that active controls can reduce vibration and noise. But despite numerous model-scale and full-scale wind tunnel tests, there are no satisfactory demonstrations that existing analytical methods can accurately show these same improvements; much remains to be learned.

UMARC predictive capability (IBC using active pitch links)

The first test of an IBC system in the wind tunnel at full scale was a BO 105 rotor test performed in two phases [Jacklin et al., 2003]. The basic scheme in this test was an active pitch link (actuated hydraulically) installed between the rotating swashplate and hub. Torok [1996] used a Sikorsky version of the UMARC analysis to predict the effects of 2/rev and 3/rev input phase angles on 4/rev hub loads. Because there was no calibrated dynamic balance, Torok computed the percent change in load rather than the actual loads themselves. Figure 2.27a shows an example of one of these cases: the change in 4/rev shear with changes in the 2/rev input phase angle. Figure 2.27b shows a linear-regression analysis of the three measured responses (shear, moment, and lift) and two types of input (2/rev and 3/rev). In this case, it is not clear that a combined analysis is appropriate. The combined predictive accuracy in this case, judged by the slope 0.939, is good, but the combined analysis obscures the reality that the individual predictions are in almost all cases poor. These slopes range from 0.240 for a 4/rev lift change from a 3/rev pitch-link input to 1.251 for a 4/rev shear change from a 3/rev pitch-link input.

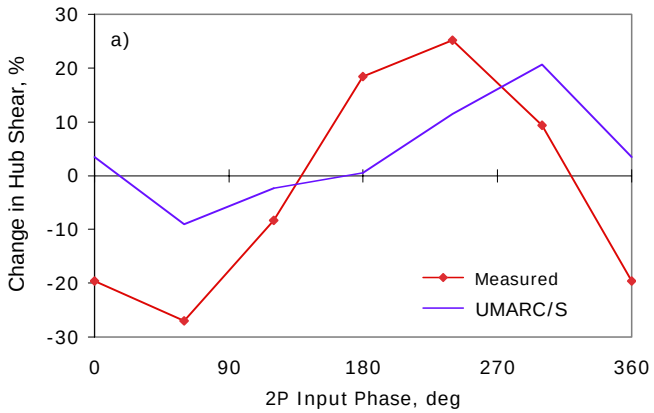

a) Change in 4/P hub shear as a function of 2P input phase angle

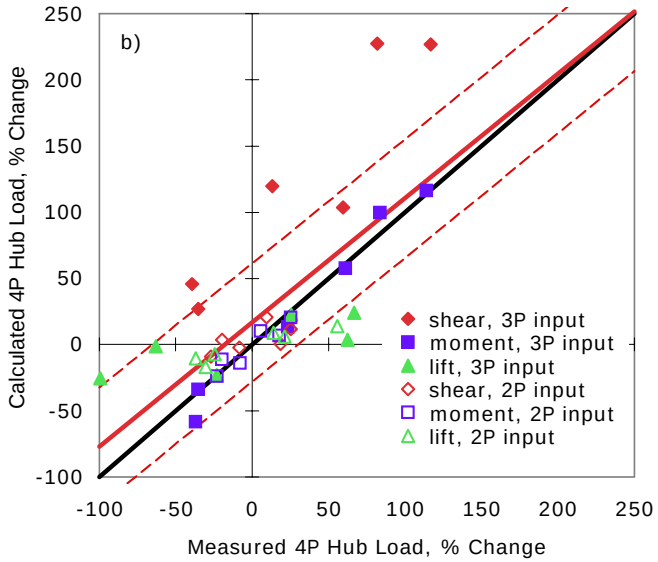

b) Linear regression of all hub component changes: m = 0.939, S_e = ±18%

Figure 2.27. Predictive accuracy of Sikorsky UMARC code for change in 4P hub loads with variable 2P and 3P inputs [Torok, 1996].

CAMRAD II predictive capability (IBC using active pitch links)

A UH-60A rotor with IBC controls was tested in the 80- by 120-Foot Wind Tunnel mounted on the LRTA in a preliminary investigation of IBC in low-speed flight in 2001 [Jacklin et al., 2002], and significant reductions in vibration and noise were demonstrated. Kottapalli [2007] has examined these IBC test results using CAMRAD II. Kottapalli has qualitatively compared the calculated and fixed-system loads, but since there has been no complete dynamic calibration of the LRTA balance, he was unable to compare the analysis with the known fixed-system loads. However, quantitative comparisons can be made of the rotating-system vibratory blade loads that are the major source of the fixed-system 4/rev vibrations; that is, the 3/rev and 5/rev chord bending moments and the 4/rev flap bending moments. Figure 2.28a provides a sample comparison of the calculated and measured

3/rev chord bending moment at r/R = 0.70 (one of 3 radial stations) as a function of the 3/rev input phase angle. A linear regression of the calculations and measurements for all three radial stations is shown in figure 2.28b. The primary variable is the phase of the 3/rev pitch-link input. The slope for the combined analysis, m = 0.937, indicates good predictive capability, but the slopes for the three stations, 1.219, 2.349, and 1.365, at 0.20R, 0.50R, and 0.70R, respectively, are poor to fair, so the combined slope is misleading.

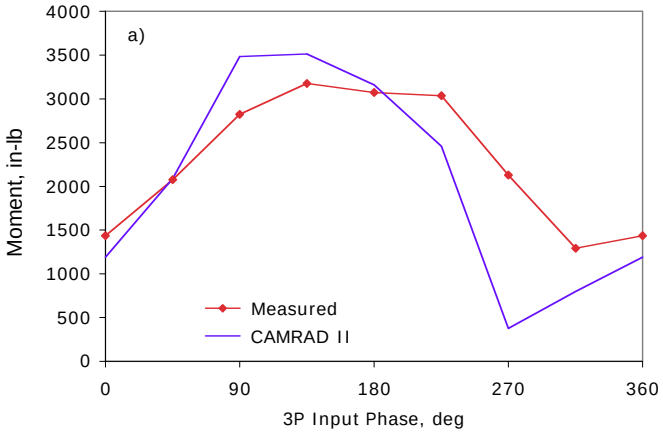

a) Chord bending moment as a function of 3P input phase angle, 0.70R

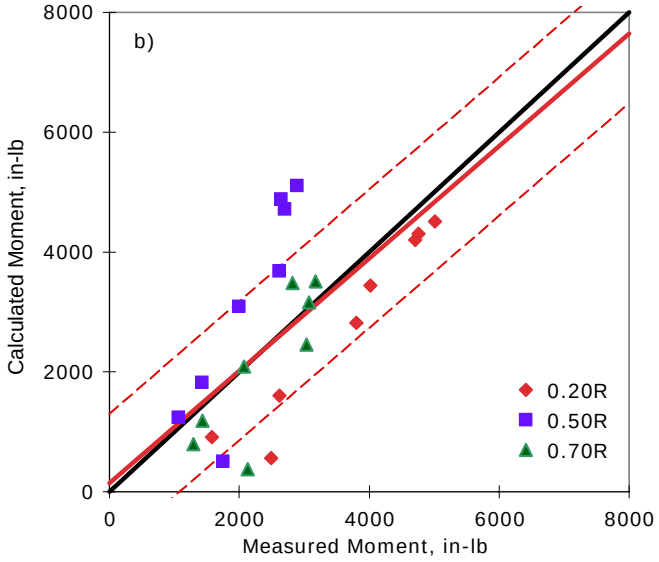

b) Linear regression for 3 radial stations: m = 0.937, S_e = ±14%

Figure 2.28. Predictive accuracy of CAMRAD II for 3/rev chord bending moments at three radial stations for UH-60A with IBC [Kottapalli, 2007].

The calculated and measured 5/rev chord bending moments are compared in figure 2.29 for three radial stations, where the primary independent variable is again the 3/rev input phase angle. An example of the 5/rev chord bending moment at r/R = 0.70 as a function of the 3/rev input change is shown in figure 2.28a (one of three radial stations). The combined slope in this case, m = –0.179, is poor. The slopes at the individual radial stations vary from –0.723 to –0.424, and they are poor.

The third contributor to 4/rev loads in the fixed system is the 4/rev flap bending moments. Figure 2.30a shows an example of the 4/rev flap bending moment at r/R = 0.70 as a function of the 3/rev input change (one of three radial stations). The combined slope in figure 2.30b is poor, m = 0.094, and the individual slopes range from 0.279 to 1.729.

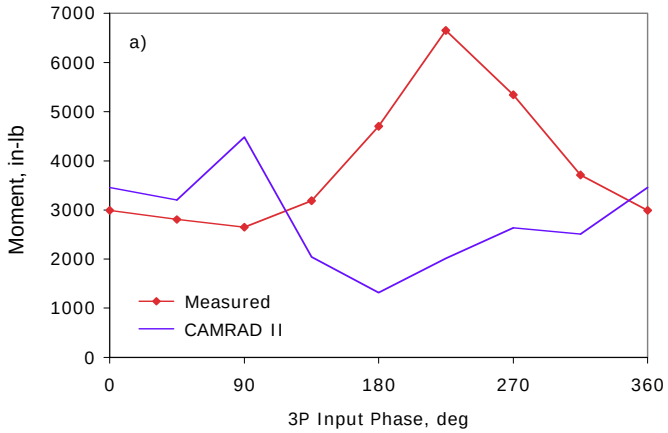

a) Chord bending moment as a function of 3P input phase angle, 0.70R

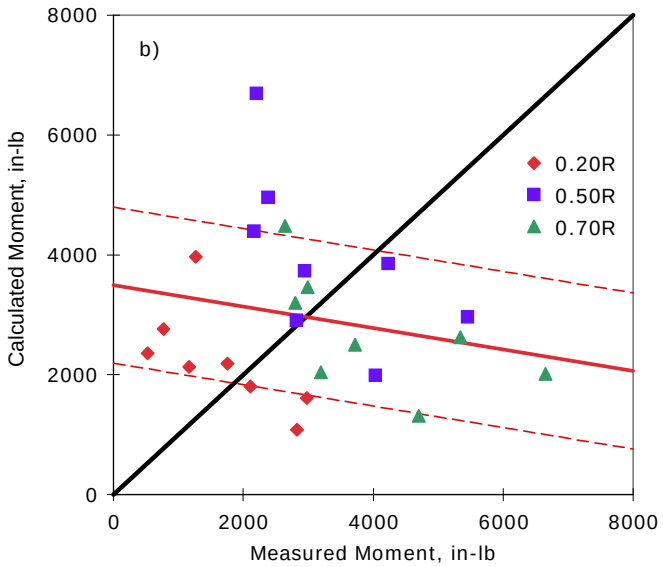

b) Linear regression for 3 radial stations: m = –0.179, S_e = ±16%

Figure 2.29. Predictive accuracy of CAMRAD II for 5/rev chord bending moments at three radial stations for UH-60A with IBC [Kottapalli, 2007].

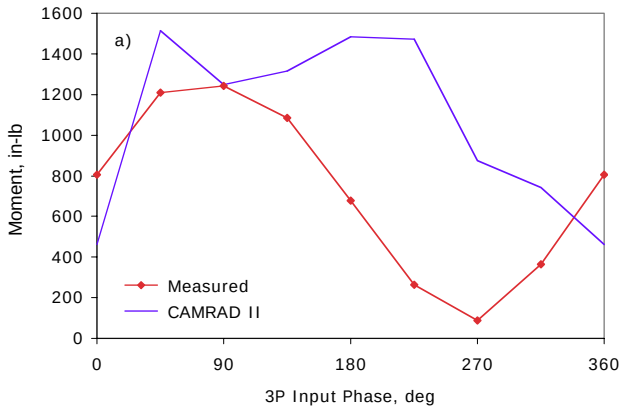

a) Flap bending moment as a function of 3P input phase angle, 0.70R

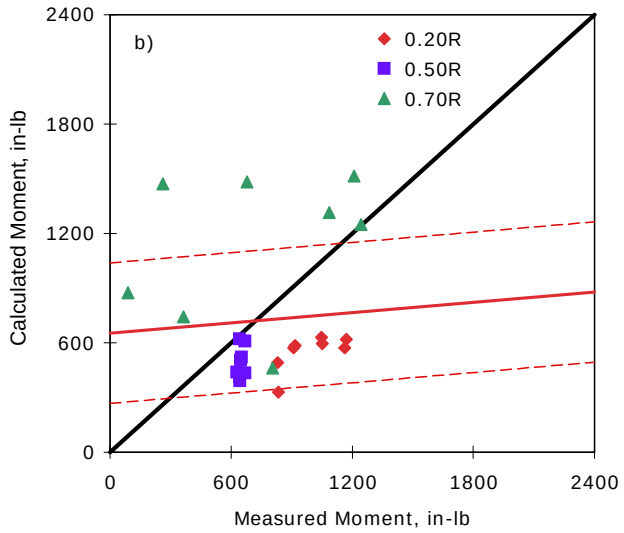

b) Linear regression for 3 radial stations: m = 0.094, S_e = ±16%

Figure 2.30. Predictive accuracy of CAMRAD II for 4/rev flap bending moments at three radial stations for UH-60A with IBC [Kottapalli, 2007].

2GCHAS predictive capability (using active elevon)

Another approach to IBC is to use on-blade active controls instead of active pitch links. Ormiston and Fulton [1998] have reported results from testing a two-bladed rotor in hover. For this very preliminary experiment, they compared calculations and measurements for the torsion moment frequency response functions (FRFs) using the comprehensive analysis 2GCHAS (a predecessor version of the current RCAS) at three rotor speeds. The FRF shows the blade response in terms of torsional deflection (twisting) as caused by the elevon excitation as it oscillates in pitch. Figure 2.31a shows the torsion response as a function of elevon frequency at three rotor speeds. The torsion response is the dependent variable and the elevon frequency is the primary independent variable. The linear regression analysis combining the results for the three rotor speeds is shown in figure 2.31b. The predictive accuracy, m = 0.732, is a 27% underprediction. At higher rotor speeds, the accuracy is improved (m = 0.892), whereas at the lowest rotor speed it is poor (m = 0.168). The results shown here are for an elastic-blade analysis, but a rigid-blade analysis provides similar FRFs. For the rigid blade, the combined analysis gives a slope of 0.779.

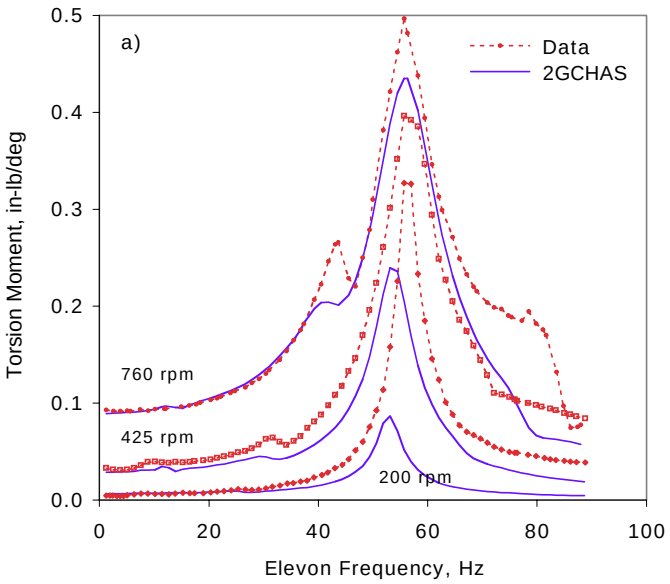

a) Torsion moment response to elevon frequency, 3 rotor speeds

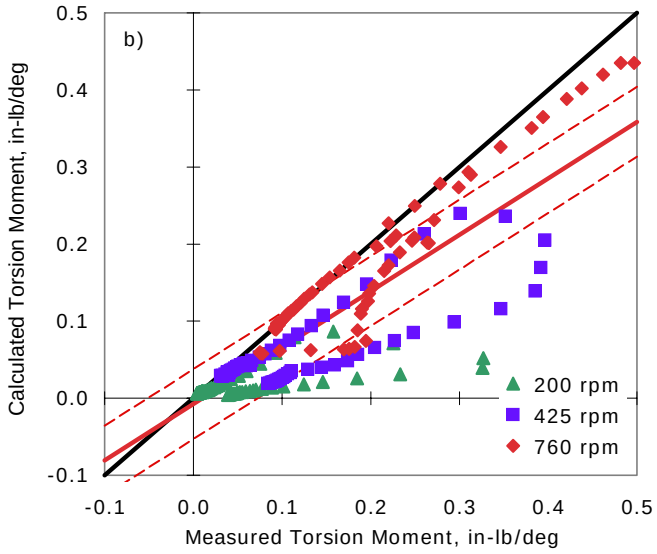

b) Linear regression: m = 0.732, S_e = ±9%

Figure 2.31. Predictive accuracy of 2GCHAS for frequency response function of active elevon rotor in hover [Ormiston and Fulton, 1998].

CAMRAD II predictive capability (using active twist)

Another design approach for on-blade active controls is to incorporate active twist in the blade design. A prototype active twist rotor was tested at Langley Research Center in hover [Wilbur et al., 2000]. During this testing, the blade was twisted at frequencies from 1 to 100 Hz, which excited the first two elastic flap bending modes and the first torsion mode. Response measurements were made at three radial stations for flap bending and four stations for torsion. Figure 2.32a shows the moment measured at the flap bending station at 0.287R. As is apparent, the blade responds at the two flap

elastic modes during the frequency sweep. The CAMRAD II analysis was used to predict the blade-moment response to active twist. This analysis generally underpredicted the moments. For a combined analysis of the moments at the three flap bending stations, m = 0.720. As shown in figure 2.32b, the underprediction was greater for the four torsion measurement stations, m = 0.359.

Data limitations

We know that the measurement of fixed-system loads requires an accurate dynamic calibration of a rotor balance, but these calibrations are difficult and it is hard to demonstrate the accuracy of the calibration. The equivalent rotating-system load-measurement problem is easier, but modeling of the experimental setup also requires an approximation of hub impedance—a difficult task. But there may also be aspects of the active controls operating within the rotating system that are not being correctly modeled.

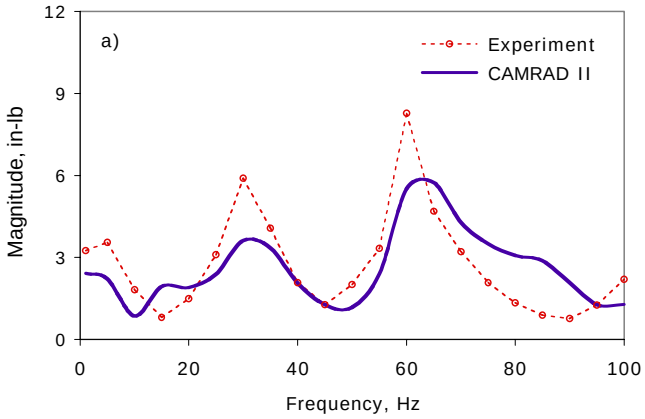

a) Flap bending moment at 0.287R as a function of excitation frequency

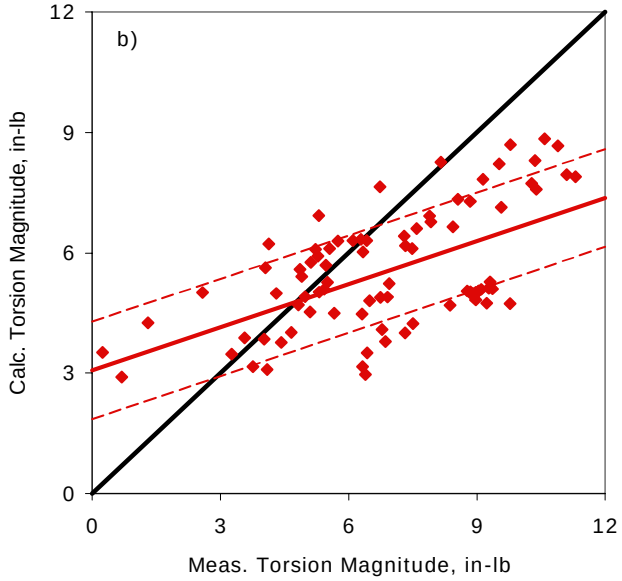

b) Four torsion radial stations: linear regression: m = 0.359, S_e = ±10%

Figure 2.32. Predictive accuracy of CAMRAD II for flap and torsion response in hover to active twist [Wilbur et al., 2000].

All of these problems work against obtaining a detailed and accurate set of data that can be used to drive analysis improvements.

Summary

From the limited comparisons shown here, the predictive capability for active controls technology is poor (and disappointing as well). We know from tests that these active control technologies can be effective in reducing vibration, but we cannot reproduce these results with analysis. We know that the prediction of oscillatory loads in the rotating system and vibratory loads in the fixed system is one of the most difficult calculation problems in the helicopter disciplines, so we have low expectations that we can accurately compute these loads with current analyses. But the fact that we cannot compute the effects of relatively small pitch-angle changes at higher harmonics suggests that there is much we do not understand about this problem.

ROTOR DYNAMICS AND CONTROL

Comprehensive analyses are designed to provide calculations of oscillatory loads at the rotor hub as well as aeroelastic stability, both objectives of this technology area.

Oscillatory Loads

Oscillatory loads, in the rotating system, generally refer to the unsteady loads at 1/rev and higher. For this section, the definition of oscillatory loads is restricted to the combined loads at the rotor hub from all blade oscillatory loads. The hub oscillatory loads are not all transmitted to the fixed system. In some cases there is load cancellation (for perfectly uniform blades) and the resulting loads in the fixed system, termed the vibratory loads, will not contain all harmonics.

Oscillatory load prediction on the blade was discussed previously. These loads combine at the hub, but their measurement is difficult and an alternative approach is to measure those loads that occur in the fixed system, where a dynamically calibrated balance can be installed. In this case, information on those oscillatory loads that are canceled in the rotating system is lost, but the fixed-system information is of primary importance.

Sikorsky Aircraft oscillatory loads predictive capability

Sikorsky Aircraft and NASA tested a 5-bladed Sikorsky bearingless main rotor (SBMR) in the 40- by 80-Foot Wind Tunnel in 1992. Fixed-system balance loads were measured and three different comprehensive analyses were used to predict these loads [Wang and van Aken, 1994]. The fixed-system measurements were obtained with a dynamically calibrated balance and were corrected using measured pitch-link loads that were not metric. Balance loads have five components (all forces and moments except torque), and the published results have been normalized by an arbitrary factor. Three Sikorsky Aircraft analyses have been compared with the measurement: two analyses developed by the company, KTRAN and RDYNE, and UMARC/S, a proprietary version of the University of Maryland comprehensive analysis. Figure 2.33a provides an example of the measurements of the 5/rev vertical force for the SBMR and includes the predictions of the three analyses. The combined analysis of all 5/rev vibratory loads is shown in figure 2.33b. Such an analysis has its limita-

tions. Even if these loads had not been arbitrarily scaled, a combined analysis can be misleading as it is difficult to equate, for example, the 5/rev drag force with the 5/rev rolling moment. Regardless, the combined analysis is poor and the scatter is excessive. More relevant are the individual slopes and standard errors for the three analyses and five balance components, and they are shown in table 2.3. A component of the balance load is predicted within ±25% in only a few cases; in most cases, the errors are much larger. But the scatter as measured by the standard error of estimate is good in most cases. Even for the best analysis, UMARC/S, the predictions are poor.

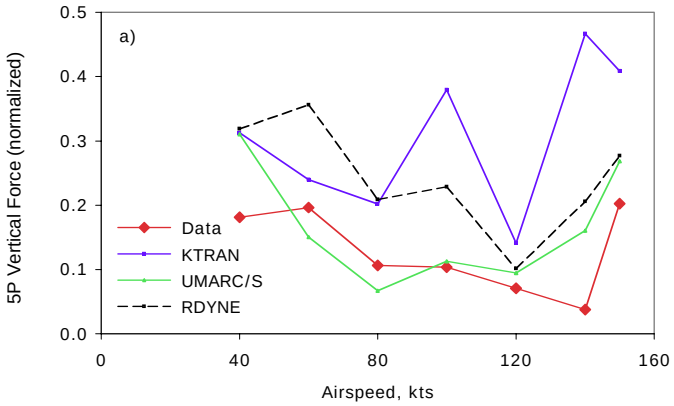

a) Normalized 5P vertical force as a function of airspeed

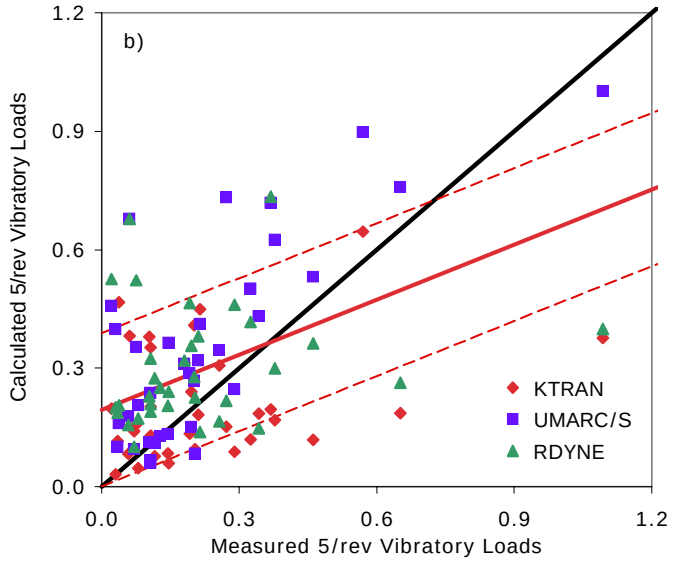

b) Linear-regression analysis of 5 normalized balance loads: m = 0.465, S_e = ±16%

Figure 2.33. Predictive accuracy of three Sikorsky Aircraft analyses for prediction of balance loads for SBMR test [Wang and van Aken, 1994].

TABLE 2.3. COMPARISON OF SLOPE AND STANDARD ERROR OF ESTIMATE FOR FIVE COMPONENTS OF BALANCE LOADS USING THREE SIKORSKY AIRCRAFT ANALYSES

Balance	KTRAN		UMARC/S		RDYNE	
Load	m	S_e	m	S_e	m	S_e
Drag force	0.331	2%	0.678	20%	0.614	7%
Side force	0.197	2%	1.557	6%	0.496	8%
Pitch moment	0.548	14%	1.243	9%	1.549	28%
Roll moment	0.073	10%	0.474	13%	–0.210	10%
Vertical force	–0.042	11%	0.872	6%	1.049	5%

Data limitations

Measurements of fixed-system loads with a balance require a dynamic calibration of that balance to determine the appropriate transfer function for all measurement frequencies. This calibration is affected by the balance natural frequencies, rotor speed, and steady loads and is one of the most difficult measurement tasks in rotor testing. Gabel et al. [1983] have addressed important aspects of these measurement problems.

Summary

Most researchers when examining oscillatory loads are content to measure changes in the loads with some independent parameter, such as a higher-harmonic control input, and compare the measured change with calculation (see Torok [1996] as an example). The Sikorsky Aircraft calculations shown here represent an important step in calculating the absolute value of the fixed-system vibratory loads, but the results are poor and it is clear that a great deal of effort is required to advance this technical capability.

Aeromechanical/Aeroelastic Stability

There is extensive literature about aeroelastic and aeromechanical stability, dating back to the earliest rotorcraft flight tests. For current rotorcraft designs, the major stability problems are those dealing with tiltrotor whirl stability and rotorcraft air and ground resonance.

Bell Helicopter Textron whirl stability predictive capability

Bell Helicopter Textron has used its stability analysis ASAP to predict whirl stability boundaries for two wing designs tested at model scale in NASA's Transonic Dynamics Tunnel [Corso et al., 1997]. Figure 2.34a shows the stability boundaries for the two wing designs, where for each rotor speed the boundary (in knots-equivalent airspeed) where the damping becomes neutral is shown. The linear regression for these boundary points, where rotor speed is the primary independent variable, is shown in figure 2.34b. The stability boundary is underpredicted by 12%, which is fair to good. The scatter as indicated by the standard error of estimate is low.

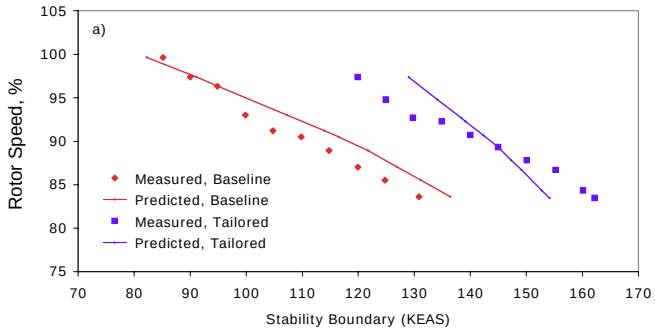

a) Whirl flutter stability boundaries for two wing designs

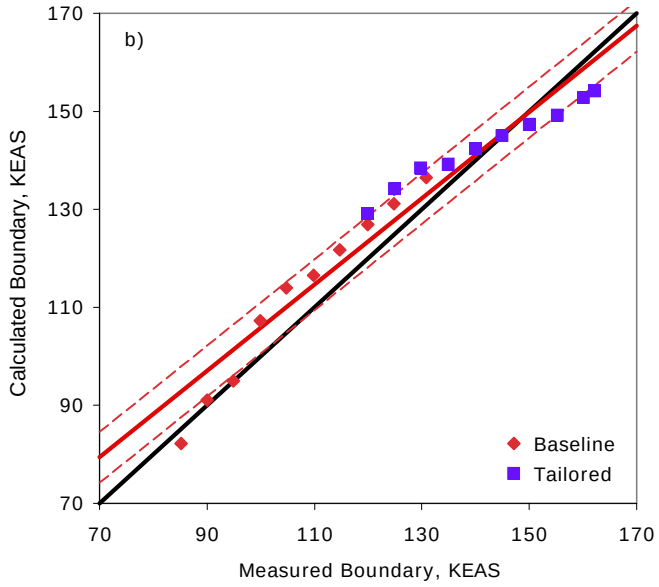

b) Linear regression for both designs: m = 0.880, S_e = ±3%

Figure 2.34. Predictive accuracy of Bell Helicopter Textron ASAP analysis for whirl stability boundaries for two model rotor designs [Corso et al., 1997].

CAMRAD/JA aeromechanical stability predictive capability

Peterson and Johnson [1991] have compared the stability predictions of the comprehensive analysis CAMRAD/JA (a predecessor to CAMRAD II) with measurements obtained in hover (in the 40- by 80-Foot Wind Tunnel) for a full-scale BO 105 rotor where the independent variable is rotor thrust (blade collective pitch). The damping as a function of thrust is shown in figure 2.35a. The linear-regression analysis of these data is shown in figure 2.35b. The damping is underpredicted and is poor, although the scatter in the results is low. To a degree, this result is typical for aeromechanical stability testing since the accuracy of damping measurements is degraded at higher damping values (all results in figure 2.33 were at the stability boundary or zero damping), but even if 50% of the higher damping points in figure 2.35 were removed, the damping prediction would still be poor.

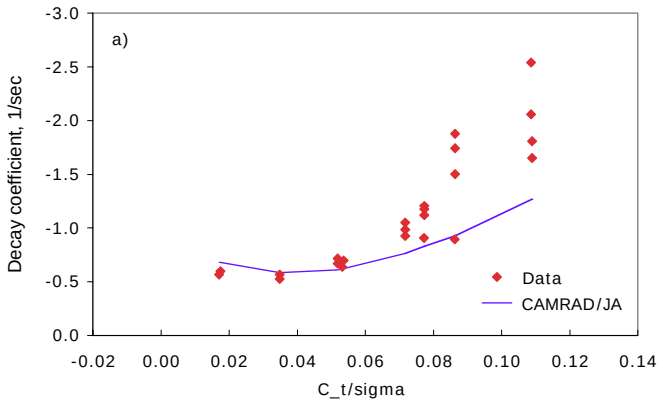

a) Lead-lag damping as a function of thrust coefficient

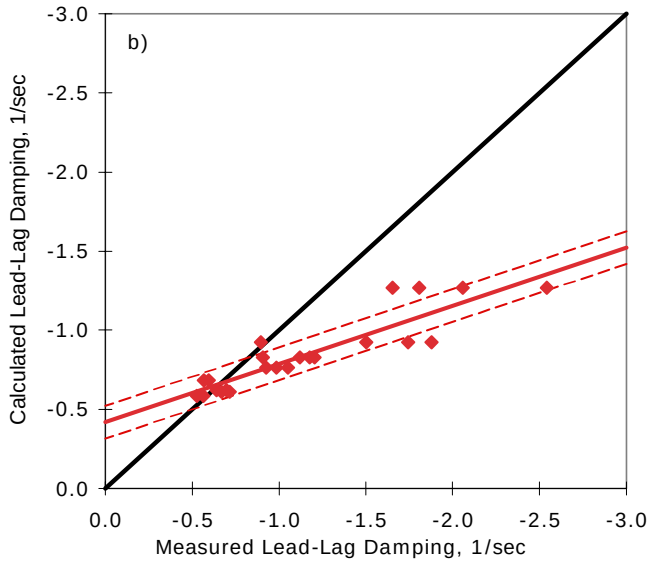

b) Linear regression: m = 0.368, S_e = ±3%

Figure 2.35. Predictive accuracy of CAMRAD/JA analysis for aeromechanical stability of a BO 105 rotor in hover [Peterson and Johnson, 1991].

Data limitations

Methods of measuring damping are most accurate at low damping levels but inaccurate at high damping levels, possibly causing difficulty in making an accurate assessment. Moreover, most measurement methods presume the damping is linear, and the results can be influenced when non-linearities are present. For modern soft inplane rotors, most dampers show numerous nonlinearities, and they affect the overall damping measurement.

Summary

The stability predictions show considerable variation, although at a stability boundary (or low damping levels) the measurements are generally quite accurate and the correlations are often improved. In general the results are poor to good and the samples shown here are probably representative of results obtained in recent decades.

FLUID MECHANICS FOR ROTORCRAFT APPLICATIONS

Innovative solutions to unsolved problems in aeromechanics and the application of technologies developed in the fixed-wing aerodynamics community are being investigated, both computationally and experimentally. These topics include dynamic stall, ice accretion, and the application of active flow control to rotor aerodynamics and fuselage drag reduction. The focus of these topics is the elucidation of the basic physics involved in these areas, with the assumption that this understanding will lead to accurate analytical models compatible with comprehensive analysis.

Dynamic Stall

Currently, multiple semiempirical models of the dynamic-stall process are used in comprehensive analyses. These methods attempt to model the effects of vortex shedding on the rotor blade induced by stall. This vortex shedding creates overshoots in lift, drag, and pitching moment. Moreover, these models must also properly account for a reduction of pitch damping that can occur at some pitch angles and oscillating frequencies. These models are based in part on wind tunnel tests of airfoils undergoing appropriate motions.

Dynamic-stall predictive capability

Dynamic stall refers to changes in lift, drag, and pitching moment that occur as one or more vortices are shed from the upper surface of a rotor blade as the blade is pitching up and the angle of attack exceeds the static stall angle. Dynamic stall is frequently modeled as a two-dimensional (2-D) process, based on dynamic-stall data obtained in wind tunnels. Bousman [2000] has shown that the extrema of lift, drag, and pitching moment in 2-D wind tunnel tests and in aircraft flight maneuvers are remarkably consistent, suggesting that comparing calculated and measured extrema is a valid test of dynamic-stall predictive capability. Bousman [2000] compared various semiempirical models for dynamic stall with the lift and moment extrema that were measured in a wind tunnel for three airfoils. Figures 2.36 and 2.37 show the linear regression for lift and moment, respectively. The prediction of the lift extrema is fairly good, the slope agreeing within –5% and scatter being roughly ±7%. But the prediction of the moment is only fair, the slope off by –23%, and the scatter is about ±40%. The moment extrema is important for the prediction of limit-control-system loads in rotorcraft maneuvers, and the poor predictive capability shown here suggests that the methods using these models will not be able to predict the control loads in maneuvers.

Ice Accretion

Two types of problems are usually considered in icing: ice accretion and icing effects. Ice accretion involves the prediction of ice shapes, in which geometries change over time. Simulation of ice growth requires frequent grid modifications and so is more suited to automated procedures. An icing-effects study, on the other hand, seeks to determine the flow field and performance degradation given an ice shape, and so is more suited to interactive tools.

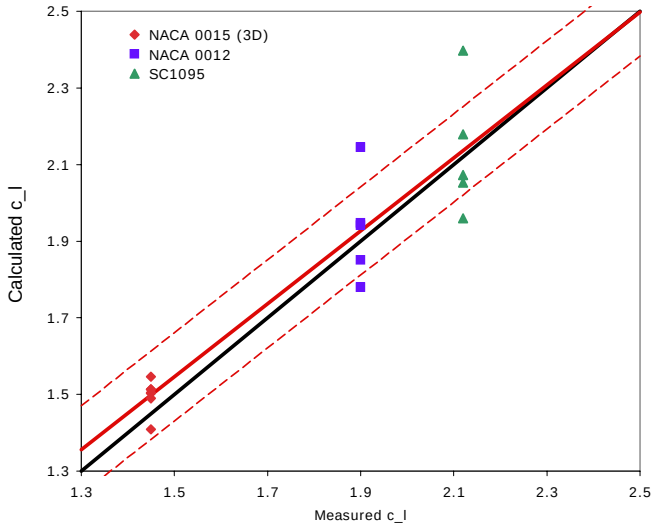

Figure 2.36. Predictive accuracy of various methods for prediction of dynamic-stall cl extrema; m = 0.953, S_e = ±5% [Bousman, 2000].

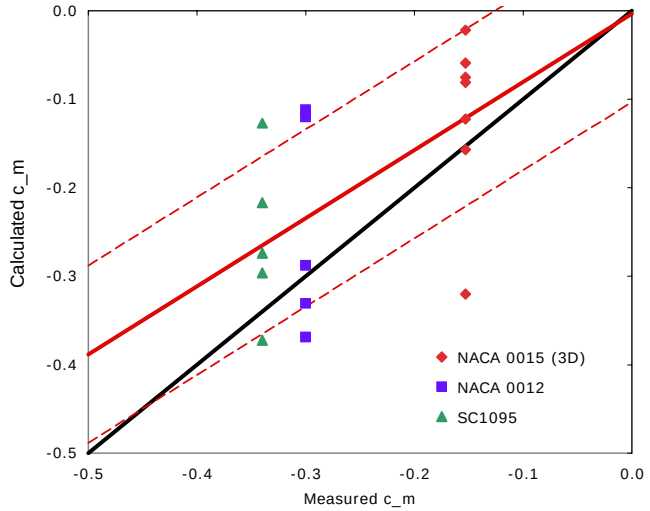

Figure 2.37. Predictive accuracy of various methods for prediction of dynamic-stall cm extrema; m = 0.770, S_e = ±20% [Bousman, 2000].

Ice-accretion predictions are typically two-dimensional in nature and based on the classical Messinger model. The analysis consists of four critical steps: flow-field calculation, water droplet impingement calculation, heat-transfer prediction, and ice accumulation normal to the surface.

LEWICE is the primary code for 2-D ice-accretion prediction, and it is the core of the 3-D ice accretion tools as well. The analysis uses a potential panel code to determine the flow field about a clean surface, and then calculates water-droplet trajectories from some upstream location until they impact on the surface or until the body is bypassed. Collection efficiency is then determined from the water-droplet impact location pattern between the impingement limits. A quasisteady analysis of the

control-volume mass and energy balance is next performed, using a time-stepping routine. Density correlations are used to convert ice-growth mass into volume. LEWICE also features multiple drop-size distributions, multiple airfoil elements, thermal models for antiicing/deicing systems, and an interface with structured grid codes, allowing the use of viscous Navier–Stokes flow solutions.

The LEWICE code is able to simulate rotor-blade accretions, but at a much lower level of fidelity than for fixed-wing aircraft. In part this is due to the assumptions made about the underlying physics. The software allows inputs for rotational speed to calculate an increase in the aerodynamic heating term in the energy balance. The rotational force is used to determine ice shedding and to find the resultant force of the shed ice particle, allowing it to be tracked. But the rotating-body information is not used by the potential flow solver in LEWICE, nor is it used in the droplet-trajectory calculations.

The second part of an icing calculation, icing effects or aerodynamic performance degradation, involves the calculation of the aerodynamic coefficients of the iced geometry. The section lift, drag, and moment characteristics with ice must be accurately known in order to predict the performance degradation from an icing encounter. Lifting-line theory is one commonly used method, but momentum-source methods coupled with blade-element theory are also widely used, as are panel methods. Often, proprietary methods or Navier–Stokes solvers are used to calculate aerodynamics. The SmaggIce interactive toolkit is a suite of codes used for ice-shape characterization and to prepare 2-D cross-sections of iced airfoils for a CFD icing-effects study. It allows for ice-geometry evaluation and preparation, grid generation (2-D, structured, and multiblock) and provides an interface with flow solvers to determine the aerodynamic flow characteristics.

Predictive capability

Ice accretion has been validated for a wide range of conditions and different geometries for fixed-wing applications and is used in reducing the cost of development and certification [Wright, 1999 and 2005]. But this acceptance does not exist for rotary-wing applications. Using a 2-D code to predict the ice accretion at a specified radial location on a rotor is not entirely straightforward. Current ice-accretion codes are quasi-steady-state, and make a 2-D assumption. Thus, an averaging technique is typically required for rotorcraft. The large aspect ratio of rotor blades still gives the 2-D assumption good results for certain applications, but not all. Most of the correlations used come from fixed-wing databases, and their application to rotary-wing problems has been only marginally successful.

The empirical methods for performance degradation and ice shedding generally show good agreement with experimental data taken on model rotors. Figure 2.38a, from Britton [1992], shows the torque rise on a model rotor in the Glenn Icing Research Tunnel (IRT). Initially, there is a fairly rapid increase in the torque rise, but the rise levels out after ice starts to shed from the outer portions of the blades. Correlation methods [Flemming and Lednicer, 1985] are able to accurately predict this torque rise; m = 0.995, S_e = ±3%. But because of the nature of empirical methods it is unclear whether these methods can be accurately and consistently applied to full-scale configurations. An analytical approach by Britton [1992], combining the Boeing B65 performance code, a modified version of the LEWICE ice-accretion code, an empirical routine to predict natural shedding, and an

interactive-boundary-layer (IBL) routine to determine the lift and drag characteristics, is shown in figure 2.38b. This method is not limited to model-scale data, but the predictive accuracy in this case is poor-to-fair as the method underpredicts the torque rise.

Ice shedding is typically predicted based on models of the failure stress of the ice bond. A typical model calculates the mass and centrifugal force at a given location. If this force exceeds a threshold value, then the model predicts shedding at that location. Actual determination of the failure stress of accreted ice is a surprisingly difficult task. Experimental results have been very dependent on surface roughness and temperature as well as velocity and drop size. These experiments show a good deal of data scatter, however, but empirical or semiempirical models are still widely used.

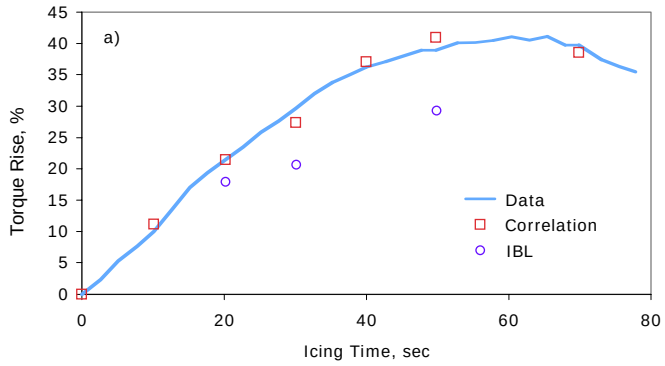

a) Torque rise as a function of exposure time to icing

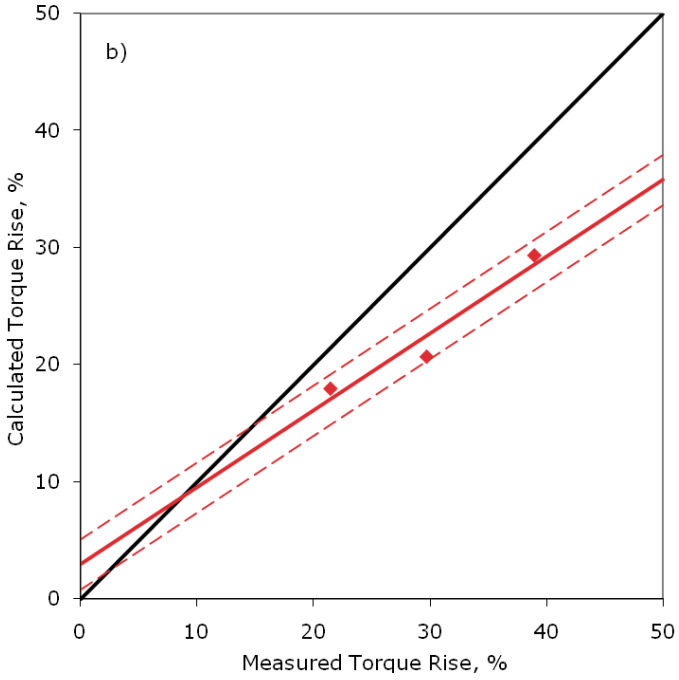

b) Linear regression: m = 0.656, S_e = ±4%

Figure 2.38. Predictive accuracy of Interactive Boundary Layer (IBL) method [Britton, 1992].

Application of Active Flow Control to Rotorcraft Components

Active flow control (AFC) is typically defined as positively altering a flow field by the introduction of periodic, as opposed to a steady, excitation. In addition, active flow control is typically thought of as something that can be turned on and off at will and adds momentum or energy to the flow being controlled. Active flow control can be applied to a rotary-wing aircraft to elevate the effect of dynamic stall, to tailor the lift distribution on the retreating side of the rotor, and to control separation at the aft end of the fuselage and appendages. A device that has had success as an active flow-control actuator for these types of situations on fixed-wing aircraft is the synthetic jet. The synthetic-jet concept is described simply as a closed cavity with an orifice and one active wall. The action of the active wall is to change the volume of the cavity. When the volume of the cavity is increased, external fluid is drawn into the cavity. When the cavity volume is decreased, fluid is expelled through the orifice and out into the external flow. This exhaust is highly directional and dominated by a vortex-ring structure. The repeated actuation of the synthetic jet generates a train of vortex rings that resemble, in the mean, a turbulent jet. The synthetic jet is attractive for application to rotary-wing aircraft, since it does not require any external plumbing; it requires only an electrical connection, and therefore can be completely mounted inside the blade or under the skin of a fuselage.

Fuselage drag reduction by active flow control

It has been often noted that the cruise drag of a fixed-wing aircraft is one order of magnitude lower than that of a helicopter of the same gross weight (Arad et al. [2006]; Fillipone and Michelson [2001]; Martin et al. [2003]; and Martin et al. [2005]). A clean rotary-wing configuration is considered to have a good drag coefficient if that drag coefficient is about unity. This drag coefficient is, in part, due to the interaction of the flow induced by the rotor and the fuselage. But it is also due to the fact that functionality to fulfill the mission usually takes precedence over aerodynamics for rotary-wing aircraft. The aerodynamic characteristics of a rotary-wing fuselage have more in common with bluff-body aerodynamics than the tube and wing aerodynamics of the fixed-wing world. Large separated regions and streamwise vortices dominate the aerodynamics of the fuselage of a rotary-wing aircraft.

This discussion leads to two observations. One is that there is an opportunity to minimize the drag on a rotary-wing aircraft fuselage by an application of AFC to minimize the size of the separated region. Secondly, to be able to predict the airloads on a fuselage, the computational approach must be able to predict a large separated flow and its interaction with the flow field induced by an AFC actuator, which is a challenge computationally.

Martin et al. [2005] showed that the application of AFC on a model of the Boeing MDX was able to reduce the drag by 10%. Additionally, the application of AFC has the potential of reducing the cruise download on the ramp area by as much as 40%. Ben-Hamou et al. [2004] demonstrated drag reductions of 3–11%, depending on the model incidence. This effort used a model that closely resembled the aft bode of the C-130 and CH-53.

The planned test for fuselage drag reduction builds upon these earlier works. The new experimental effort will feature a generic fuselage model based on an open geometry, which is well-known in the CFD community, the ROBIN. The ROBIN fuselage is a generic fuselage shape where the cross-sections are analytically defined. The new variation of the ROBIN will preserve the analytically defined cross-sections but move them along the length of the fuselage to create a ramp-like area of the other two geometries.

The experiment is to be designed from the beginning in cooperation with CFD researchers. This process will allow key areas for measurements to be identified. To facilitate validation efforts, high-fidelity measurements of the flow field with and without control will be made. Velocity measurements will be made using particle image velocimetry (PIV), both conventional and high-speed, and hot-wire anemometry. Drag measurements will be made with multiple balances.

Dynamic-stall control by application of active flow control

Numerous innovative approaches have been proposed for alleviating negative effects of dynamic stall, such as high pitching moments and drag. Within comprehensive analyses, little work has been done to incorporate analytic models to represent these approaches, and developments here will lag experiment. But various CFD models are being used to support experimentation.

The use of AFC to prevent dynamic stall will be evaluated experimentally using a two-dimensional model mounted on a dynamic-plunge pitch mechanism. Computational investigations on the use of AFC, specifically synthetic jets, indicate that it is possible to completely eliminate dynamic stall [Duraisamy et al., 2002], keeping the flow completely attached during the pitching motion ($15.0° + 4.2° \sin(wt)$). This result is a promising one that needs to be verified experimentally.

The same type of measurements used in the fuselage drag-reduction experiments would also be used here. Specifically, velocity measurements will be made using PIV, both conventional and high-speed, and hot-wire anemometry. These data will be useful for validation purposes and also for understanding the flow physics involved in dynamic stall and its control. It is anticipated that in order to simulate the effect of AFC on dynamic stall computationally, a time-accurate Navier–Stokes solver will need to be used. High-quality, detailed experimental data will be required to validate such computations. Once the simulations are validated, progress can be made on understanding the underlying flow physics in such a way as to allow development of a computationally simpler analytic model that is compatible with rotary-wing comprehensive analysis.

PLANS FOR IMPROVEMENT

There is a great need for improvement in many areas of aeromechanics, particularly if any of the new analytical methods being improved and developed are to be used by industry to support the design of new and improved rotorcraft. These needs include better analysis and better data. Many plans proposed for NASA rotorcraft research are discussed here, to suggest how they may fulfill these needs. But in other areas there are gaps and these will also be mentioned.

Rotor Aerodynamics and Interactions

Full-scale airloads and performance testing

As currently planned, the UH-60A wind tunnel test, with blade-mounted pressure transducers and a rotor balance, will provide an opportunity to measure performance data with significantly increased accuracy over that obtained in flight tests. The blade pressures can be measured, and integrated thrust and moments calculated and compared with balance results. Moreover, the integrated torque can be determined as well (using a viscous correction) and compared to shaft and balance torque measurements. Airspeed sweep data from the minimum power speed to maximum flight speed is of prime importance, preferably at multiple thrust values. Testing at maximum speed will provide an important opportunity to gather comprehensive data for airloads, structural loads, blade deformations, and balance steady and dynamic loads. Testing at high thrust, preferably with some blade dynamic stall, will also provide a comprehensive data set.

Rotor/fuselage separation effects tests

The testing of a small-scale slowed rotor compound model under the Isolated Rotor Test System (IRTS) in the Langley 14- by 22-Foot Subsonic Wind Tunnel provides an opportunity to evaluate the effects of rotor/fuselage separation distance on the body and rotor characteristics. Balance data will be measured for both the body and the rotor. Approximately 300 body-surface mean pressures will be measured along with 7 dynamic pressures on the model tail. Rotor/body separation distances of 4 in. and 8 in. are planned. Wake-velocity measurements will be made in front of the tail for a 12- by 20-in. data cross-flow plane. The measurements will be made using both a wide-field-of-view PIV system (under development) and a proven laser velocimetry (LV) system. Measurements are planned for one free-stream velocity, two rotor/body separation distances, and two rotor speeds.

Slowed-rotor performance

The testing of a small-scale rotor using the Langley IRTS will provide the opportunity to evaluate the rotor performance at rotor speeds substantially lower than 100% rpm (hover tip speed about 720 ft/sec). Reductions in rotor speed are planned to approach 50%. The rotor will be operated in the presence of a model with a large wing mounted high on the fuselage.

Active Control for Loads, Vibration, and Noise Alleviation

Active control using fixed system actuation, that is higher harmonic control (HHC) of the swashplate, has demonstrated reductions in vibration and external noise. But these benefits come with increased power, and sometimes loads. In the last 20 years, experimentation and calculations have suggested that on-blade systems with IBC may be more effective than HHC systems, particularly with the ability to control 2/rev. IBC systems using active pitch links have been tested twice before in the National Full-Scale Aerodynamics Complex (NFAC), once on a BO 105 rotor and once on a UH-60A rotor. Now, a new test of the UH-60A/IBC is scheduled in the 40- by 80-Foot Wind Tunnel, and two additional rotors with alternate designs will be tested by the NASA rotorcraft project:

the Boeing SMART rotor and the Active Elevon Rotor. This confluence of rotors to be evaluated over the next 5 to 10 years will provide a great deal of new and valuable information, in terms of both capability and understanding.

Active controls (pitch links)

A UH-60A rotor with active pitch links (UH-60A/IBC) will undergo a second test, this time in the 40- by 80-Foot Wind Tunnel. This test entry will provide high-speed and high-thrust flight conditions so that the IBC system can be evaluated for increased performance and reduced loading, vibration, and noise. Although the purpose of the test is to demonstrate improved performance and reduced loads, vibration, and noise, the resulting database will provide detailed measurements that can be used to resolve prediction accuracy problems with analytical models. These measurements will include both rotating-system oscillatory loads and fixed-system loads with a dynamically calibrated balance.

Test of the Boeing SMART Rotor

The SMART rotor, with a blade-mounted flap, will be tested in the 40- by 80-Foot Wind Tunnel to demonstrate the effects of an on-blade flap to control performance, vibration, and noise. The SMART rotor is an integrated design using a current technology rotor and an added blade-mounted flap that represents a first-generation design to demonstrate the use of on-blade active controls. Beyond the demonstration of improved performance and reduced noise and vibration, the data obtained will be used to understand deficiencies in current analytical methods.

Active Elevon Rotor

The Active Elevon Rotor (AER) is a design with two conformal elevons imbedded in each blade. The AER is just under 13 feet in diameter and will be tested to determine the effectiveness of the two-elevon design. Just as with the SMART rotor test, the extensive data obtained in testing will be used to demonstrate the capabilities of the rotor for increased performance and reduced loads, vibration, and noise, but also provide detailed data that can be used for improvements in analytical methods, which currently are inadequate for predictions of active-control rotor loads and performance.

Active controls (on-blade flow control)

Through a joint project with NASA, Boeing, and the U.S. Army, a small-scale rotor wind tunnel test will investigate the use of active flow control for retreating blade-stall alleviation. Using newly design flow-control actuators embedded in the blade spar, a flow-control slot is driven by an array of synthetic jet actuators. These actuators require zero net mass flow and therefore no plumbing from engine-bypass air. The purpose of the devices is to inject momentum into the turbulent boundary layer using an oscillatory jet created by the flow-control actuators. This added momentum energizes the flow and has been demonstrated to delay trailing-edge stall in oscillating 2-D airfoil testing. The objective of the test is to map out the rotor stall boundary in terms of blade loading and advance ratio with the slots sealed, and then repeat the measurements with the active flow control engaged. Part of the investigation involves changing the amount of coverage over the rotor disk where the active flow control is applied. The rotor itself is a simple untwisted two-bladed teetering configuration with a chord of 7.5 in. and a diameter of 7 ft. The test conditions will be at subscale tip speeds owing to the state of the art in actuator design and the desire to study trailing-edge stall instead of

shock-induced leading-edge stall. The test stand, hub hardware, and rotor balance have been carefully designed to withstand the severe control loads associated with operating the rotor beyond the stall boundary. This test will be the first attempt at using modern active flow-control technology in a rotating frame of reference.

Active flow controls for fuselage drag

Previous experiments have shown that fuselage drag can be significantly reduced with active flow control, such as zero-mass synthetic jet actuators [Ben-Hamou et al., 2004; and Martin et al., 2005]. A new experiment based on the ROBIN geometry will be used to demonstrate advances in drag reduction. The new variation of the ROBIN will preserve the analytically defined cross-sections, but move them along the length of the fuselage to create a ramp-like area (which on real aircraft tends to create separated flow regions).

The experiment will be designed from the beginning in cooperation with CFD researchers. This cooperation will allow key areas for measurements to be identified. To facilitate validation efforts, high-fidelity measurements of the flow field with and without control will be made. Velocity measurements will be made using PIV, both conventional and high-speed, and hot-wire anemometry. Drag measurements will be made using multiple balances. The resulting data will be used to demonstrate the effectiveness of the active control schemes and for validation of CFD methods.

Oscillatory Loads

Improvements in oscillatory and vibratory load predictions depend upon obtaining more accurate measurements, and in this regard the dynamic calibration of the fixed-system balance on the LRTA is key. Nonetheless, many issues remain in a dynamic calibration, and resolving these remains a challenge.

Test of UH–60A rotor for performance, loads, and vibration

The planned test of the UH–60A with pressure blades discussed previously includes the dynamic calibration of the LRTA balance and the measurement of vibratory loads in the fixed system. The comprehensive nature of measurements in both the fixed and rotating systems will provide a unique dataset that can be used to look at the transmission of oscillatory and vibratory loads. In the rotating system, on-blade measurements of bending moments and accelerations will provide information that can be used to identify the blade-state vector in a least-squares sense. Additional information will be obtained from optical deformation methods from off the blade. These blade loads then become the loads passed down to the rotor balance, and all parts of this rotor dynamics mélange must fit together.

Fluid Mechanics for Rotorcraft Applications

Dynamic stall and active flow control

The use of AFC to prevent dynamic stall will be evaluated experimentally using a two-dimensional model mounted on a dynamic-plunge pitch mechanism. Computational investigations on the use of AFC, specifically synthetic jets, indicate that it is possible to completely eliminate dynamic stall

[Duraisamy and Baeder, 2002], keeping the flow completely attached during the pitching motion. This result is a promising one that needs to be verified experimentally.

The synthetic-jet concept used here is simply a closed cavity with an orifice and one active wall that changes the volume of the cavity. When the volume of the cavity is increased, ambient fluid is drawn into the cavity. When the cavity volume is decreased, fluid is expelled through the orifice and out into the environment. This exhaust is highly directional and dominated by a vortex-ring structure. The repeated actuation of the synthetic jet generates a train of vortex rings that resemble, in the mean, a turbulent jet. The synthetic jet is attractive here since it does not require any external plumbing; only an electrical connection is required, and it can be completely mounted inside the blade.

The same type of measurements used in the fuselage drag-reduction experiments mentioned previously would be used here. Specifically, velocity measurements will be made using PIV, both conventional and high-speed, and hot-wire anemometry. These data will be useful for validation purposes and also for understanding the flow physics involved in dynamic stall and its control.

Ice accretion

The objective of the rotor icing task is to improve rotorcraft simulation capabilities by advancing the coupling methodology between fluid mechanics and icing physics models. The product will be a robust, validated coupling of rotor-performance codes with ice-accretion prediction codes.

Rough, highly irregular ice can induce complex, unsteady separation. There is a need for further microphysical research into quantifying roughness effects, in part to determine to what extent roughness elements can be modeled, how well they need to be characterized geometrically, and so on. Three-dimensional instability mechanisms can favor certain flow structures. Both 2-D and 3-D CFD may not be able to predict all of the flow features, either because of an inability to resolve instability mechanisms or because of limitations in turbulence modeling. A roughness model offers the potential advantage of reducing computational requirements.

The roughness parameter that affects transition and the magnitude of the heat transfer in the LEWICE icing calculations is necessary to accurately model the heat transfer and the resulting ice shape. For 2-D LEWICE, the roughness parameter uses a correlation based on a voluminous set of data. There is currently no such correlation for LEWICE3D, because of the limited set of 3-D ice-shape data.

This discussion leads to a number of experimental challenges. There is a need for subscale data to validate both ice accretion/shedding and performance models. Investigation of fundamental long-term icing physics issues such as roughness effects, three-phase flow fields, multiple scales, etc., is required to advance the most basic models of microphysical phenomena, in order to get away from current empirical correlations that may not apply to all rotorcraft scenarios. Most adhesion and shedding data in the literature, for example, are not applicable because of test-article geometry, test methodology, or the range of test conditions/materials.

Current experimental methods have challenges to overcome as well. Benchmarks have identified issues regarding the effects of wind tunnel turbulence levels on experimental results. Scaling of electrothermal systems remains a significant challenge, even for fixed-wing models. Novel methods for flow visualization are needed, or else improved methods for using existing instruments.

Current plans rely on augmentation funding for validation data. The current plan also does not include antiicing/deicing technologies, shedding and adhesion experiments, coupling with any performance codes other than FUN3D and OVERFLOW, or engine icing. The current plans also rely heavily on collaboration with other NASA programs, with industry partners, with other government agencies for validation data.

CROSS-CUTTING TECHNOLOGY REQUIREMENTS

Computational Fluid Dynamics (CFD)

Most calculations for performance, blade airloads, and structural loads need to be done in conjunction with the coupled CFD/CSD models to quantitatively compare the accuracy of these methods and classic comprehensive analyses. Such comparisons will provide a better knowledge of where the CFD/CSD analyses are critical and where they may not be necessary. In cases where there are strong aerodynamic nonlinearities or separated flow, it may not be possible to make suitable calculations with classical methods based on lifting-line theory. For example, it is unlikely that accurate performance or rotor loads can be obtained in high-speed flight where the blade aerodynamics are dominated by unsteady, nonlinear flow over the blade. Similarly, flight in maneuvers where there is extensive dynamic stall on the blade will require solutions using Navier–Stokes methods. But other problems, such as those dealing with multibody dynamics or higher harmonic loads, may never require the CFD/CSD analysis.

The highly nonlinear nature of dynamic stall, how this stall is influenced by active control, and the nonlinear ice accretion on airfoils are all fluid-mechanics problems for which classical methods are unsatisfactory. Eventual progress will require computations using CFD methods.

Acoustics

Emphasis on vortex-wake loading can benefit both aeromechanics and acoustics. Primary test cases should be selected for low-speed vibratory loading (level flight, about $\mu = 0.10$) and descent BVI (descending flight, $\mu > 0.10$) where there is a transition from states of high vibration and low noise to states of low vibration and high noise. Tests directed at these transitions will identify the phenomenological changes that affect the relationships of vibration and noise.

Noise reduction is a major objective of all of the active control schemes that will be tested. Just as testing will focus on control inputs that show improvement in performance or vibration, there will be a comparable effort for improvements in noise reduction.

Experimental Capabilities

New techniques for vortex-wake measurements will be important for validating methods of prediction of transition vibration. New measurements of blade deformations will provide a new means for looking at the blade-state vector and all of its aspects (displacements, angles, moments, and shears). These measurements will also contribute to understanding the oscillatory loads problems.

For vibration and noise reduction, it is anticipated that the vortex location and how it is affected by control inputs is a critical factor in any improvement. Thus accurate measurements using PIV techniques will be an essential component of these tests. The measurements of blade deflections will also be important in these cases.

REFERENCES

Anonymous: NASA/Army Rotorcraft Technology: Volume I–Aerodynamics, and Dynamics and Aeroelasticity. NASA CP 2495, Feb. 1988.

Arad, E.; Martin, P.; Wilson, J.; and Tung, C.: Control of Massive Separation over Thick-Airfoil Wing: A Computational and Experimental Study. AIAA Paper no. 2006-322, 44th AIAA Aerospace Sciences Meeting and Exhibit, Reno, Nev., Jan. 9–12, 2006.

Ben-Hamou, E.; Arad, E.; and Seifert, A.: Generic Transport Aft-Body Drag Reduction Using Active Flow Control. AIAA Paper no. 2004-2509, 2nd AIAA Flow Control Conference, Portland, Ore., June 28–1, 2004.

Berry, J. and Bettschart, N.: Rotor-Fuselage Interaction: Analysis and Validation with Experiment. AHS 53rd Annual Forum, Virginia Beach, Va., Apr. 29–May 1, 1997, pp. 343–367.

Bhagwat, M. J.; Ormiston, R. A.; Saberi, H. A.; and Xin, H.: Application of CFD/CSD Coupling for Analysis of Rotorcraft Airloads and Blade Loads in Maneuvering Flight. AHS 63rd Annual Forum, Virginia Beach, Va., 2007, pp. 2048–2077.

Bousman, W. G.: Airfoil Dynamic Stall and Rotorcraft Maneuverability. NASA/TM-2000-209601, July 2000.

Bousman, W. G.: Power Measurement Errors on a Utility Aircraft. AHS Aerodynamics, Acoustics, and Test and Evaluation Technical Specialists Meeting, San Francisco, Calif., Jan. 23–25, 2002.

Bousman, W. G. and Kufeld, R. M.: UH-60A Airloads Catalog. NASA/TM-2005-212827 and AFDD/TR-05-003, Aug. 2005.

Boyd, D. D., Jr.; Barnwell, R. W.; and Gorton, S. A: A Computational Model for Rotor-Fuselage Interactional Aerodynamics. AIAA Paper no. 2000-256, AIAA 38th Aerospace Sciences Meeting, Reno, Nev., Jan. 10–13, 2000.

Britton, R. K.: Development of an Analytical Method to Predict Helicopter Main Rotor Performance in Icing Conditions. AIAA Paper no. 1992-0418, AIAA 30th Aerospace Sciences Meeting, Reno, Nev., Jan. 6–9, 1992.

Caradonna, F. X.; Hendley, E.; Silva, M.; Huang, S.; Komerath, N.; Reddy, U.; Mahalingam, R.; Funk, R.; Wong, O.; Ames, R.; Darden, L.; Villareal, L.; and Gregory, J.: An Experimental Study of Rotors in Axial Flight. AHS Technical Specialists' Meeting for Rotorcraft Acoustics and Aerodynamics, Williamsburg, Va., 1997.

Corso, L. M.; Popelka, D. A.; and Nixon, M. W.: Design, Analysis, and Test of a Composite Tailored Tiltrotor Wing. AHS 53rd Annual Forum, vol. 1, Virginia Beach, Va., Apr. 29–May 1, 1997, pp. 209–219.

Duraisamy, K. and Baeder, J.: Active Flow Control Concepts for Rotor Airfoils Using Synthetic Jets. AIAA Paper no. 2002-2835, 1st Flow Control Conference, St. Louis, Mo., June 24–26, 2002.

Esculier, J. and Bousman, W. G.: Calculated and Measured Blade Structural Response on a Full-Scale Rotor. J. Amer. Hel. Soc., vol. 33, no. 1, Jan. 1988, pp. 3–16.

Felker, F. F.; Light, J. S.; Quackenbush, T. R.; and Bliss, D. B.: Comparison of Predicted and Measured Rotor Performance in Hover Using a New Free Wake Analysis. 44th Annual Forum of the AHS, Washington, D.C., June 16–18, 1988.

Filippone, A. and Michelsen, J. A.: Aerodynamic Drag Prediction of Helicopter Fuselage. J. Aircraft, vol. 38, no. 2, Apr. 2001, pp. 326–333.

Flemming, R. J. and Lednicer, D. A.: High Speed Ice Accretion on Rotorcraft Airfoils. NASA CR-3910, Aug. 1985.

Floros, M. and Johnson, W.: Performance Analysis of the Slowed-Rotor Compound Helicopter Configuration. AHS 4th Decennial Specialists' Conference on Aeromechanics, San Francisco, Calif., Jan. 21–23, 2004.

Gabel, R.; Sheffler, M.; Tarzanin, F.; and Hodder, D.: Wind Tunnel Modeling of Rotor Vibratory Loads. J. Amer. Hel. Soc., vol. 28, no. 2, Apr. 1983, pp. 47–54.

Hansford, R. E.: Considerations in the Development of the Coupled Rotor Fuselage Model. J. Amer. Hel. Soc., vol. 39, no. 4, Oct. 1994, pp. 70–81.

Hansford, R. E. and Vorwald, J.: Dynamics Workshop on Rotor Vibratory Loads Prediction. J. Amer. Hel. Soc., vol. 43, no. 1, Jan. 1998, pp. 76–87.

Harris, F. D.: AHIP: The OH-58D from Conception to Production. AHS 42nd Annual Forum, Washington, D.C., full-length version, June 2–4, 1986.

Harris, F. D.; Kocurek, J. D.; McLarty, T. T.; and Trept, T. J., Jr.: Helicopter Performance Methodology at Bell Helicopter Textron. AHS 35th Annual National Forum, Washington, D.C., May 21–23, 1979.

Ho, J. C.; Yeo, H.; and Ormiston, R. A.: Investigation of Rotor Blade Structural Dynamics and Modeling Based on Measured Airloads. AHS 63rd Annual Forum, Virginia Beach, Va., vol. 3, 2007, pp. 1720–1742.

Jacklin, S. A.; Haber, A.; de Simone, G.; Norman, T. R.; Kitaplioglu, C.; and Shinoda, P.: Full-Scale Wind Tunnel Test of an Individual Blade Control System for a UH-60 Helicopter. AHS 58th Annual Forum, Montreal, Canada, June 11–13, 2002.

Jacklin, S. A.; Swanson, S.; Blaas, A.; Richter, P.; Teves, D.; Niesl, G.; Kube, R.; Gmelin, B.; and Key, D. L.: Investigation of a Helicopter Individual Blade Control (IBC) System in Two Full-Scale Wind Tunnel Tests: Volume 1. NASA/TP-2003-212276, 2003.

Johnson, W.: Helicopter Theory. Princeton, N.J.: Princeton University Press, 1980.

Johnson, W.: Recent Developments in Rotary-Wing Aerodynamic Theory. AAIA J., vol. 24, Aug. 1986, pp. 1219–1244.

Johnson, W.: Technology Drivers in the Development of CAMRAD II. AHS Aeromechanics Specialists Conference, San Francisco, Calif., Jan. 1994.

Kocurek, J. D.; Berkowitz, L. F.; and Harris, F. D.: Hover Performance Methodology at Bell Helicopter Textron. AHS 36th Annual Forum, Washington, D.C., May 13–15, 1980.

Kottapalli, S.: Neural Network Research on Validating Experimental Tilt-Rotor Performance, J. Amer. Hel. Soc., vol. 45, no. 3, July 2000, pp. 199–206.

Kottapalli, S.: Calculation of Hub Loads at Low Airspeeds with Active Control. AHS 63rd Annual Forum, Virginia Beach, Va., May 1–3, 2007.

Kufeld, R. M.; Balough, D. L.; Cross, J. L.; Studebaker, K. F.; Jennison, C. D.; and Bousman, W. G.: Flight Testing of the UH–60A Airloads Aircraft. AHS 50th Annual Forum, vol. 1, Washington, D.C., May 11–13, 1994.

Kufeld, R. M. and Bousman, W. G.: High Load Conditions Measured on a UH-60A in Maneuvering Flight. AHS 51st Annual Forum, vol. 1, Fort Worth, Tex., May 9–11, 1995.

Leishman, J. G.: Principles of Helicopter Aerodynamics. Cambridge, U.K.; New York, N.Y.: Cambridge University Press, 2000.

Martin, P. B.; Tung, C.; Chandrasekhara, M. S.; and Arad, E.: Active Separation Control: Measurements and Computations for a NACA 0036 Airfoil. AIAA Paper no. 2003-3516, 21st AIAA Applied Aerodynamics Conference, Orlando, Fla., June 23–26, 2003.

Martin, P. B. and Tung, C.: Active Flow Control Measurements and CFD on a Transport Helicopter Fuselage. 61st Annual Forum of the AHS, Grapevine, Tex., June 1–3, 2005.

Mineck, R. E. and Gorton, S. A.: Steady and Periodic Pressure Measurements on a Generic Helicopter Fuselage Model in the Presence of a Rotor. NASA TM-2000-210286, 2000.

Ormiston, R. A. and Fulton, M. V.: Aeroelastic and Dynamic Rotor Response with On-Blade Elevon Control. 24th European Rotorcraft Forum, Marseilles, France, Sept. 15–17, 1998.

Peterson, R. L. and Johnson, W.: Aeroelastic Loads and Stability Investigation of a Full-Scale Hingeless Rotor. DGLR, AAAF, AIAA, RAeS International Forum on Aeroelasticity and Structural Dynamics, Aachen, Germany, June 3–6, 1991.

Quackenbush, T. R.; Wachspress, D. A.; Boschitsch, A. H.; and Curbishley, T. B.: A Comprehensive Hierarchical Aeromechanics Rotorcraft Model (CHARM) for General Rotor/Surface Interaction. CDI Report No. 99-03, 1999.

Saberi, H.; Khoshlahjeh, M.; Ormiston, R. A.; and Rutkowski, M. J.: Overview of RCAS and Application to Advanced Rotorcraft Problems. AHS 4th Decennial Specialist's Conference on Aeromechanics, San Francisco, Calif., Jan. 21–23, 2004.

Shinoda, P. and Johnson, W.: Performance Results from at Test of an S-76 Rotor in the NASA Ames 80- by 120-Foot Wind Tunnel. AIAA Paper no. 1993-3414, AIAA 11th Applied Aerodynamics Conference, Monterey, Calif., Aug. 9–11, 1993.

Torok, M. S.: Aeroelastic Analysis of Active Rotor Control Concepts for Vibration Reduction. AHS 52nd Annual Forum, Washington, D.C., June 4–6, 1996.

Wachspress, D. A.; Quackenbush, T. R.; and Boschitsch, A. H.: Rotorcraft Interactional Aerodynamics Calculations with Fast Vortex/Fast Panel Methods. AHS 56th Annual Forum, Virginia Beach, Va., May 2–4, 2000.

Wachspress, D. A.; Quackenbush, T. R.; and Boschitsch, A. H.: First-Principles Free-Vortex Wake Analysis for Helicopters and Tiltrotors. AHS 59th Annual Forum, Phoenix, Ariz., vol. 59, part 2, 2003, pp. 1763–1786.

Wang, J. M. and van Aken, J. M.: Correlation of Vibratory Hub Loads for a Sikorsky Full-Scale Bearingless Main Rotor. AHS 50th Annual Forum, Washington, D.C., May 11–13, 1994.

Wilbur, M. L.; Yeager, W. T., Jr.; Wilkie, W. K.; Cesnik, C. E. S.; and Shin, S.: Hover Testing of the NASA/Army/MIT Active Twist Rotor Prototype Blade. AHS 56th Annual Forum, Virginia Beach, Va., May 2–4, 2000.

Wright, W.: A Summary of Validation Results for LEWICE 2.0. AIAA Paper no. 1999-0249, AIAA 37th Aerospace Sciences Meeting and Exhibit, Reno, Nev., Jan. 11–14, 1999.

Wright, W.: Validation Results for LEWICE 3.0. AIAA Paper no. 2005-1243, AIAA 43rd Aerospace Sciences Meeting and Exhibit, Reno, Nev., Jan. 10–13, 2005.

Yeo, H. and Johnson, W.: Comparison of Rotor Structural Loads Calculated Using Comprehensive Analysis. 31st European Rotorcraft Forum, Florence, Italy, Sept. 2005.

Yeo, H. and Johnson, W.: Assessment of Comprehensive Analysis Calculation of Airloads on Helicopter Rotors. J. Aircraft, vol. 42, no. 5, Sept.–Oct. 2005, pp. 1218–1228.

Yeo, H.; Bousman, W. G.; and Johnson, W.: Performance Analysis of a Utility Helicopter with Standard and Advanced Rotors. J. Amer. Hel. Soc., vol. 49, no. 3, 2004, pp. 250–270.

CHAPTER 3

ACOUSTICS

Michael E. Watts (Ed.)[1]

Introduction, Noise Mechanisms: Fereidoun Farassat[1] and Thomas F. Brooks[1]
Noise prediction – Comprehensive Analysis: Casey L. Burley[1] and Douglas M. Nark[1]
Noise Prediction – CFD: D. Douglas Boyd, Jr. [1] and Douglas M. Nark[1]
Interior Noise: Randolph H. Cabell[1]
Gear and Drive-Train Noise: James J. Zakrajsek,[2] Fred B. Oswald,[2] and David Fleming[3]
Noise Propagation: Stephanie L. Heath[1] and Gerry L. McAninch[1]
Optimized Flight Paths: Michael A. Marcolini[1] and Sharon L. Padula[1]

ACRONYMS

ANOPP	Aircraft Noise Prediction Program
ARDS	Analysis of RotorDynamics Systems
BVI	blade vortex interaction
BWI	blade wake interaction
CAA	computational aeroacoustics
CAMRAD	Comprehensive Analytical Model of Rotorcraft Aerodynamics and Dynamics
CARMA	Comprehensive Analytical Model for Rotorcraft Acoustics
CFD	computational fluid dynamics
CSD	computational structural dynamics
DANST	Dynamic Analysis of Spur Gear Transmission
DARPA	Defense Advanced Research Projects Agency
DNS	direct numerical simulation
DyRoBes	Dynamics of Rotor Bearing Systems
EFEA	energy finite-element analysis
FAA	Federal Aviation Administration
F1A	Formulation 1A
FPR	Full Potential Rotor
FSC	Fast Scattering Code
FUN3D	Fully Unstructured Navier–Stokes 3D

[1] NASA Langley Research Center.
[2] NASA Glenn Research Center.
[3] Retired, NASA Glenn Research Center.

FW–H	Ffowcs Williams–Hawkings
GFPE	Green's Function Parabolic Equation Method
HART	higher harmonic control aeroacoustic test
HHC	higher harmonic control
HHC-MN	HHC minimum noise
HHC-MV	HHC minimum vibration
HIS	high speed impulsive noise
LIDAR	light detection and ranging
Navier–Stokes	N–S
OVERFLOW	OVERset grid FLOW solver
PE	parabolic equation
PVTM	Particle Vorticity Transport Method
RANS	Reynolds averaged Navier–Stokes
RNM	Rotorcraft Noise Model
RTP	Ray Tracing Propagation
SHCT	Short Haul Civil Tiltrotor
SEA	statistical energy analysis
SPL	sound pressure level
TRAC	Tillt Rotor Aeroacoustic Code

INTRODUCTION

Rotorcraft noise—external and internal—is a persistent and complex problem that continues to impede the acceptance of these aircraft within the community. NASA has been conducting research to understand and reduce rotorcraft noise since the 1950s, with increased funding and interest since the 1970s. The dominant external noise source of a rotorcraft is the rotor system. Thus, much of the research in rotorcraft noise reduction has focused on understanding and predicting source noise generated in the rotor system. The rotor system also affects cabin or interior noise, but the main offending sources of interior noise are found in the power train. Reducing the high-frequency content of power-train noise is critical for passenger comfort and health.

As the physics of noise-generation mechanisms of the rotor became known, efforts were made to develop physics-based computer codes for noise prediction. Advances in digital computers have influenced noise research and prediction in many ways. In addition to providing increased computational capability to the researchers, all aspects of experimental work such as data collection, data storage, and data analysis have been improved by modern digital computers. Advanced mathematics has also played a key role in modeling some of the noise-generation mechanisms of rotors because a purely computational approach can be highly inefficient or even impossible because of the lack of computing power. Nevertheless, significant advances since the 1970s have been made, though problems requiring experimental and theoretical research still remain. Several review articles on helicopter rotor acoustics have been written in the last few decades, including George [1997],

Brooks and Schlinker [1983], Schmitz [1991], Lowson [1992], Brentner and Farassat [1994 and 2003]. Of these, the articles by Schmitz [1991] and Brentner and Farassat [2003] are comprehensive.

This chapter covers three key areas of NASA rotorcraft acoustic research: External Noise Sources, Interior Noise Sources, and Noise Propagation Modeling and Optimized Flight Paths. The section on External Noise Sources provides a background on the different noise mechanisms of discrete and broadband noise. This discussion is followed by a description of predictive capabilities that include a system of interfaced non-computational fluid dynamics (CFD) and CFD codes and a higher-fidelity approach that is primarily CFD-based. Examples of noise predictions are provided for both predictive approaches. The section on Interior Noise Sources includes two main topics; the first discusses different types of cabin treatment for reducing interior nose and the attendant challenges in developing analytical models for these treatments. The second topic addresses gear-noise modeling and technologies to reduce the noise generated in the drive system. Propagation of source noise through the atmosphere is discussed in the third major section of this chapter. Effects of atmospheric conditions on noise propagation are discussed as well as different modeling approaches. Also included in the section on noise propagation is a topic on minimizing external rotorcraft noise at the macroscopic level by using low-noise flight operations. Optimized approach procedures for rotorcraft can be effective in reducing radiated noise generated by the rotor. The chapter concludes with a discussion on some interdependencies between acoustics research and other technical disciplines or areas.

EXTERNAL NOISE SOURCES

Noise Mechanisms

Helicopter rotor blades have complicated trajectories in space, and they operate in a flow field that is unsteady and highly complex, involving vortex shedding, separated flow, and turbulence (see fig. 3.1). The rotor-noise spectrum contains both discrete and broadband components. The discrete part of the spectrum is generally confined to lower frequencies, while the broadband part starts at midfrequencies and extends to high frequencies. Blade-vortex-interaction (BVI) noise and the high-speed blade-noise spectrum can reach the midfrequency range and, therefore, can overlap with the broadband noise spectrum. The discrete rotor noise is generated by the following mechanisms: thickness of the rotor blades (the thickness noise); steady and periodic blade loads (discrete loading noise); BVI noise; and periodic nonlinear sources (quadrupole noise). Broadband noise is generated by several different mechanisms [Brooks and Burley, 2004]: blade-wake interaction (BWI) noise; blade self-noise; unsteady BVI; and blade-atmospheric turbulence (ingestion) interaction. Burley and Brooks [2004] provides more detailed explanations of self-noise mechanisms such as turbulent boundary layer–trailing edge noise, laminar boundary later–vortex shedding noise, blunt trailing-edge noise, and blade-tip noise. In principle, each broadband noise mechanism may contribute to a different range of frequency. Some of acoustic energy at the lower end of the broadband spectrum of rotor noise is caused by the jitter of the BVI signature. Brooks showed that this broadening of the discrete frequency spectrum of BVI is caused by the random jitter of the BVI acoustic-pressure signature by phenomena such as blade-to-blade differences of vortex interaction [Brooks, 1988]. The general acoustic directivity of the rotor sources described previously are shown in figure 3.2 (from [Brentner and Farassat, 2003]).

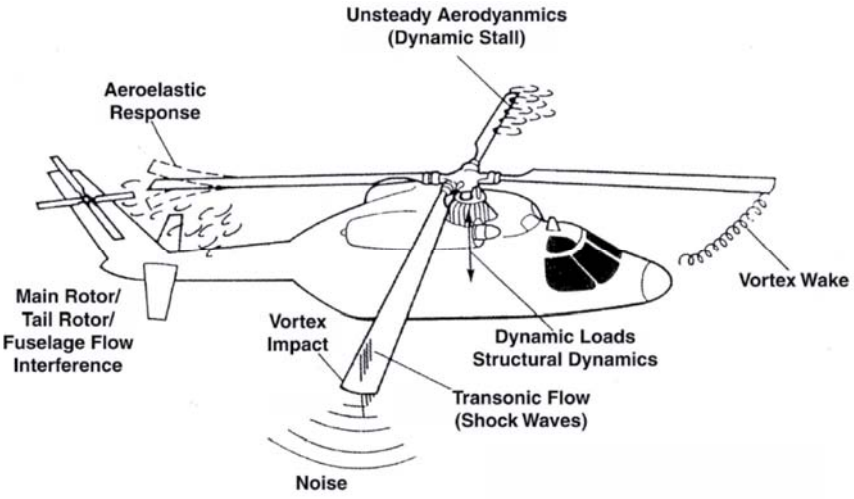

Figure 3.1. A schematic of the complicated aeromechanical environment in which a helicopter rotor operates (from [Brentner and Farassat, 2003]).

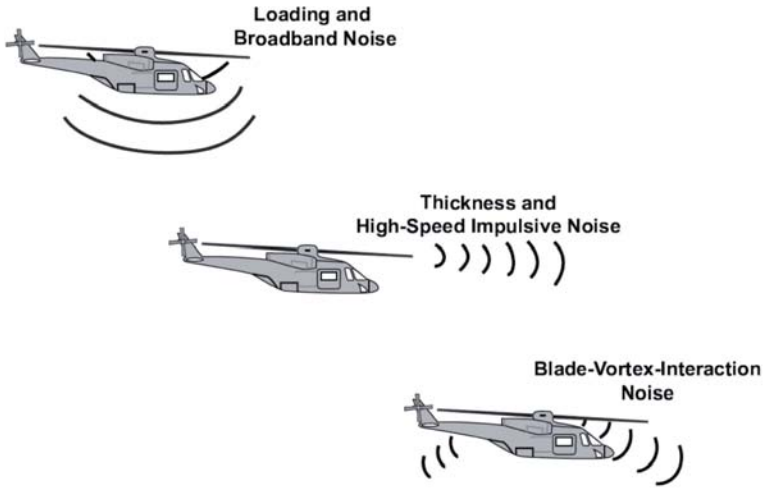

Figure 3.2. Typical direction of primary radiation for various rotor noise sources (from [Brentner and Farassat, 2003]).

BWI noise is a midfrequency broadband noise source that is due to the blade interaction with turbulent (nondeterministic) portions of the wakes of preceding blades. The interaction of the blades with the turbulence depends to a first order on the rotor tip-path-plane angle and speed for a given weight and number of blades. [Brooks, et al., 1988] measured a four-bladed BO 105 model rotor acoustic spectra, where the relative importance of different noise sources was determined for numerous flight speeds and descent angles. This testing was accomplished by scaling and frequency shifting the model with respect to a stationary observer of a full-scale flyover geometry. Figure 3.3 is a result from that study for an observer scaled to approximately 163 m below the rotor and 65 deg down from the flightpath of an equivalent full-scale rotor. On a dBA scale, which is used for determining certification metrics, a BWI noise region of dominance is seen to be significant for a large range of flight conditions. For some conditions near level flight and shallow-descent conditions, BWI noise may be as significant—if not more—as BVI and loading noise.

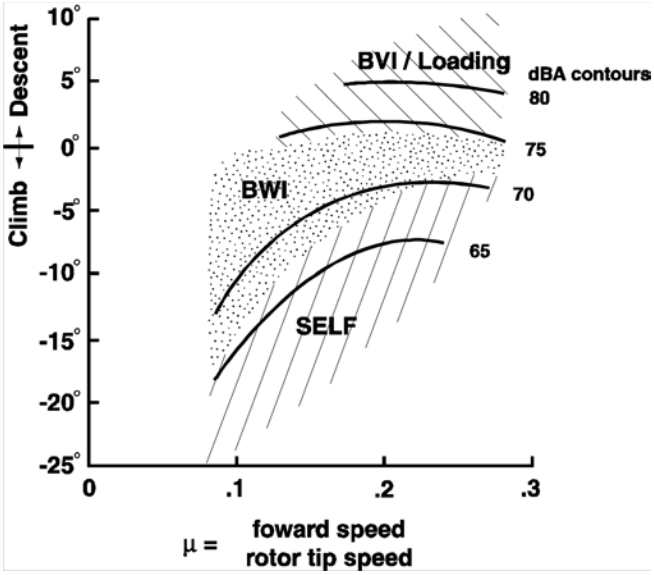

Figure 3.3. Regions where main-rotor noise sources (BVI/loading, BWI, and self) dominate for different operating conditions.

Ffowcs Williams–Hawkings (FW–H) Equation

Helicopter rotor noise prediction, particularly the prediction of the BVI noise and the broadband noise, is a very difficult problem of aeroacoustics. Currently, the acoustic analogy of Lighthill [1952] provides the most successful approach for rotor-noise analysis. The governing equation is the Ffowcs Williams–Hawkings (FW–H) equation [Ffowcs Williams and Hawkings, 1969], which is a rearrangement of the Navier–Stokes (N–S) equations. This rearrangement casts the N–S equations as a nonhomogeneous wave equation with source terms categorized as thickness noise, loading noise, and quadrupole noise. Formulation 1A (F1A) by Farassat [2007] is a solution to the FW–H equation for discrete frequency noise involving only the surface terms, i.e., thickness and loading. With the exception of the quadrupole noise that is modeled by volume sources, all the noise-generation mechanisms are modeled by surface sources. The thickness noise depends only on blade geometry and kinematics. The other mechanisms generated by surface sources are associated with blade deterministic (periodic) or random surface-pressure fluctuations.

The FW–H equation is used in two significant but different ways in rotor noise prediction: 1) as a means of classifying the rotor-noise sources and supplying a framework for qualitative analysis of the noise-generation mechanisms; 2) as the partial differential equation of noise generation and the basis for the analytical derivation of prediction formulas.

Current Status of Predictive Capability

In general, discrete frequency noise prediction is performed in the time domain, signifying the fact that the surface sources involved are relatively simple and can be obtained by using CFD. Broad-band noise prediction is generally performed in the frequency domain and involves turbulence

simulation. Quadrupole noise prediction involves extensive unsteady flow-field computation over a large region of space around the rotor. The following discussion first addresses analyses based on combining comprehensive rotorcraft analyses and/or early CFD codes with acoustic codes. Predictions for discrete and broadband noise predictions are presented. Acoustic predictions using higher-fidelity CFD codes coupled with computational-structural-dynamics (CSD) analyses are then discussed and discrete noise predictions are shown.

Noise predictions based on comprehensive rotorcraft analyses

Formulation 1A of Farassat programmed in various versions of WOPWOP in the time domain [Brentner, 1986; and Farassat, 2007] has proven to be useful in prediction of thickness and discrete loading noise. Aeroacoustic rotor codes were developed at NASA in support of Higher Harmonic Control (HHC)/ BVI noise-reduction studies [Brooks et al., 2000]. These codes evolved and became key elements of a system noise-prediction capability called Tilt Rotor Aeroacoustic Codes (TRAC). TRAC comprises sets of interfaced CFD and non-CFD codes, as illustrated in figure 3.4.

CAMRAD.Mod1 provides the performance/trim/wake information as input to the choice of alternate high-resolution blade-loads postprocessors One alternative was the use of a Full Potential Rotor code, FPRBVI [Prichard et al., 1994]. The other was the HIRES code, which used the multicore roll-up wake modeling approach developed by Brooks et al. [2002]. The high-resolution blade loading from either method was then employed in the acoustic code WOPWOP [Brentner, 1986], to predict the acoustic pressure.

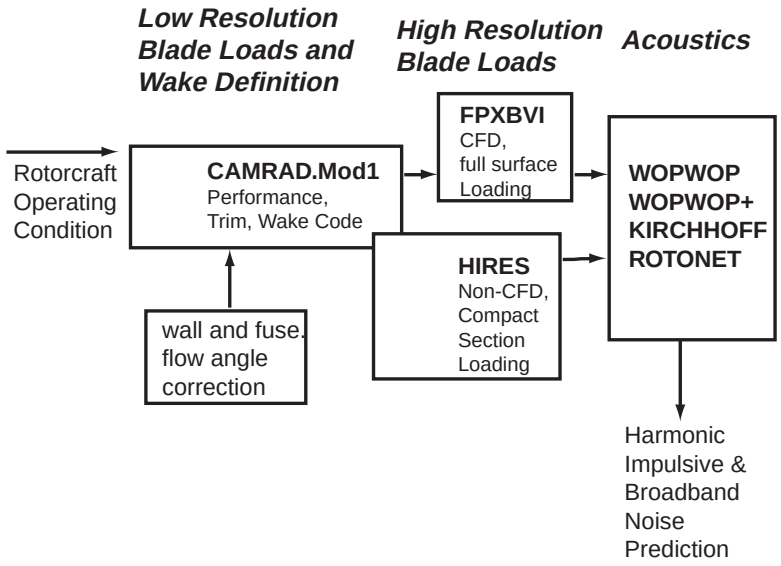

Figure 3.4. Key elements of the Titlrotor Aeroacoustics Codes (TRAC).

The use of FPRBVI provides chordwise distributions of the blade loading, whereas HIRES renders a chordwise compact loading. The choice of using one method of load determination over another would depend on the application. The FPRBVI approach may be preferred where flow over the blade is transonic or where substantial cross-flow (three-dimensional (3-D) effects) occurs because of blade curvature. The HIRES approach should be adequate for predicting noise for subsonic to low-transonic conditions where 2-D sectional loading, and thus a lifting-line analysis, is generally valid. An advantage of the lifting-line approach is that it can more readily account for full ranges of aerodynamic behavior such as unsteady separation and stall than can current CFD approaches. Also HIRES is much faster computationally than FPRBVI, and more appropriate for design and optimization applications.

Key features of the CAMRAD.Mod1 and HIRES methods, as well as partial validation of the codes using experimental results from several rotor model noise tests, especially from the HART Program, were presented by Brooks, et al. [2000]. Measured and predicted midfrequency noise contour plots are presented in figure 3.5. The measured noise-level contours are plotted over a plane defined from a linear array of microphones that is traversed upstream and downstream under the rotor. The rotor-tip path is shown as circles and the flow is from the top to bottom of the figure. The levels were obtained by integrating the noise spectra from the 6th through the 40th blade-passage harmonic. The spectra in these frequencies are dominated by BVI noise contributions in these descent cases. All cases show two distinct BVI noise-directivity lobes, one each on the advancing and retreating sides. The comparison for the baseline 5.3-deg tip-path plane descent angle (BL (5.3 deg)), in figure 3.5a, shows that the maximum levels and directivity of the lobes are generally well-predicted. Parts (b) and (c), for the HHC cases with the same nominal flight condition, show noticeable changes in the noise. For HHC-minimum noise (HHC-MN), the predictions appear to capture the basic directivity and amplitude changes. For HHC-minimum vibration (HHC-MV), the directivity but not the amplitudes are roughly captured. In part (d), the more vertical orientation of the shaft angle for BL (3.8 deg), compared to BL (5.3 deg), produces a forward shifting of the advancing side lobe with a slight drop in level. These features are predicted. In part (e), for the more aft shaft tilt of BL (6.8 deg), the advancing side-lobe shift to the side is predicted.

Measured and predicted acoustic-pressure time histories are shown in figure 3.6 for the corresponding conditions of figure 3.5. The measured time histories were obtained by averaging data over 30 revolutions. No frequency filtering was done—so the low-frequency harmonic noise is included. The microphone locations were on the advancing-side BVI lobes and are shown on the contour maps of figure 3.5. Figure 3.6a shows that for BL (5.3 deg), the basic impulsive BVI and harmonic noise characteristics are well-predicted. With the use of HHC, the character of the noise produced changes drastically. For the HHC-MN case, the large increase in harmonic noise and decreases in BVI noise, compared to the non-HHC BL (5.3 deg) case, are predicted. For the HHC-MV case, the more moderate increase in harmonic noise, compared to HHC-MN, and the appearance of additional BVI impulses are also seen in the prediction. However, here, the number of BVI occurrences is not captured. For the non-HHC cases, the basic amplitudes and features of the harmonic and BVI noise were captured, as well as shifts in the BVI impulses.

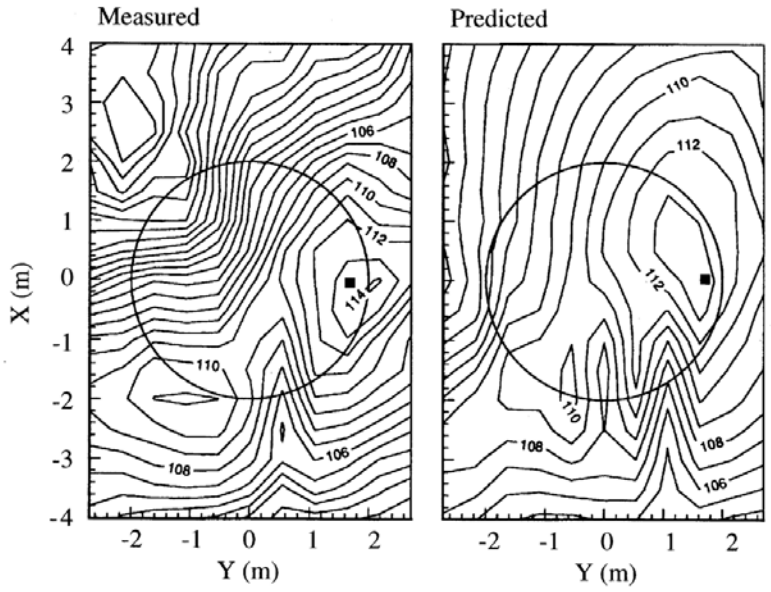

a) BL (5.3 deg)

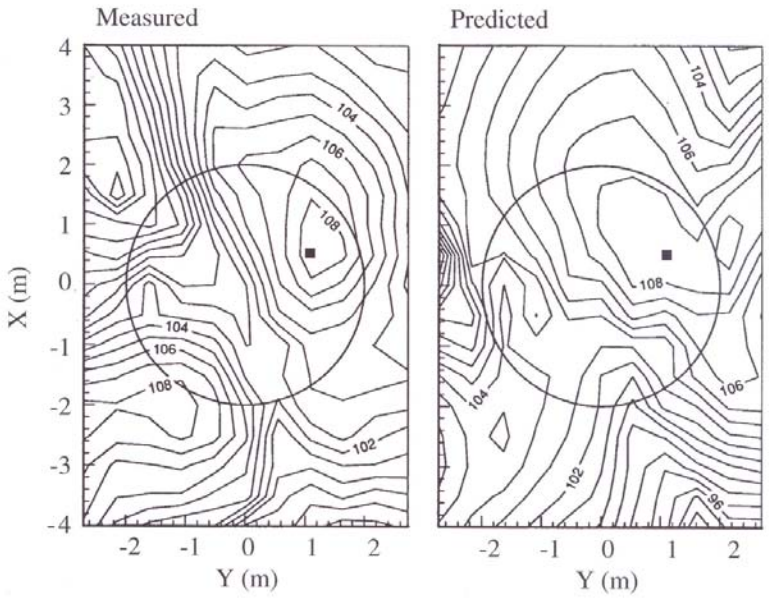

b) HHC-MN

Figure 3.5. Measured and predicted midfrequency noise contours for HART test conditions (from Brooks et al. [2000]).

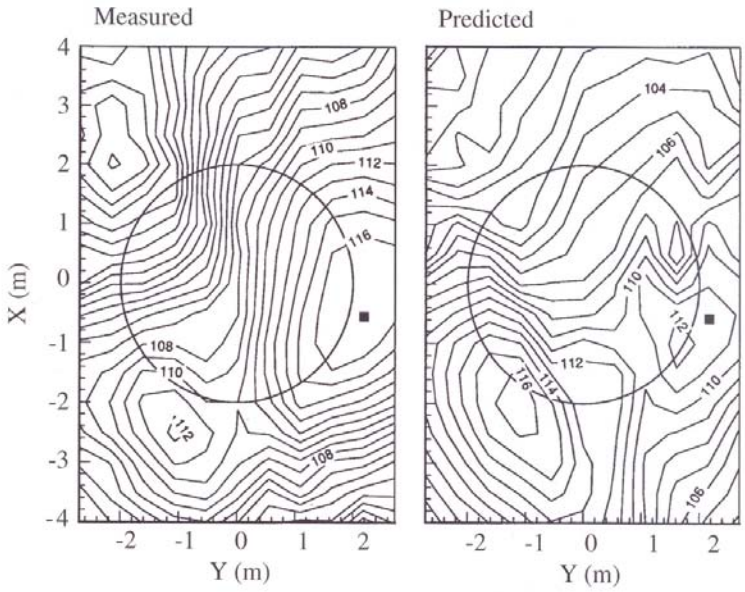

c) HHC-MV

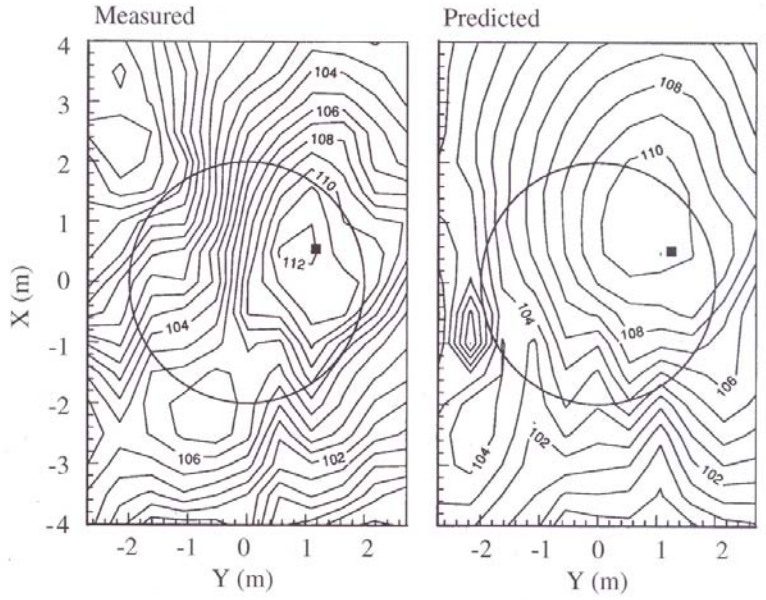

d) BL (3.8 deg)

Figure 3.5. Continued.

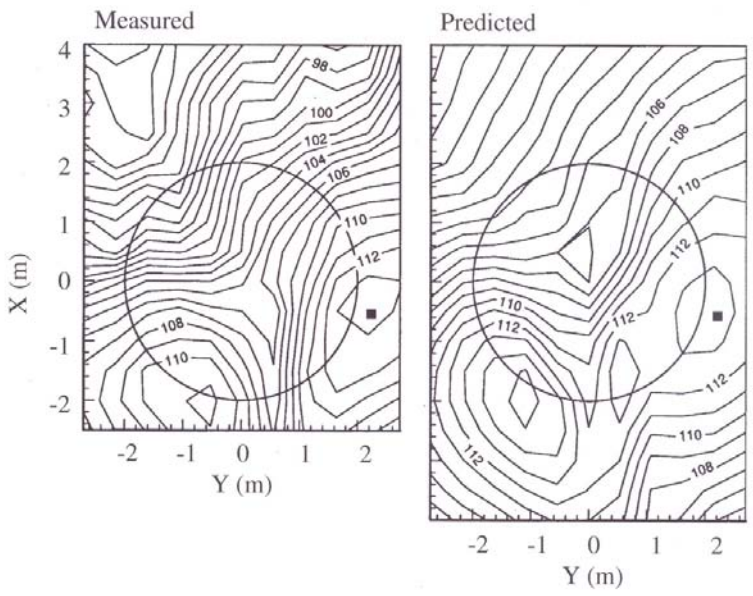

e) BL (6.8 deg)

Figure 3.5. Concluded.

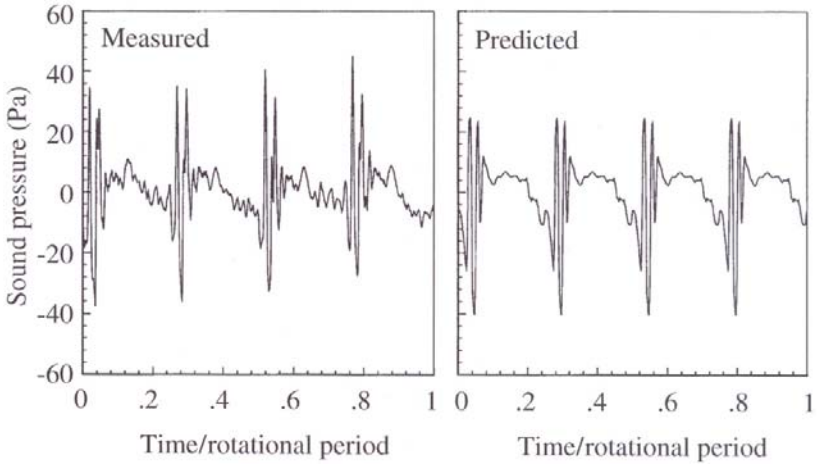

a) BL (5.3 deg)

Figure 3.6 Measured and predicted acoustic time histories for HART test conditions. Microphone position corresponds to locations noted in figures 3.5a–e, respectively (from Brooks et al. [2000]).

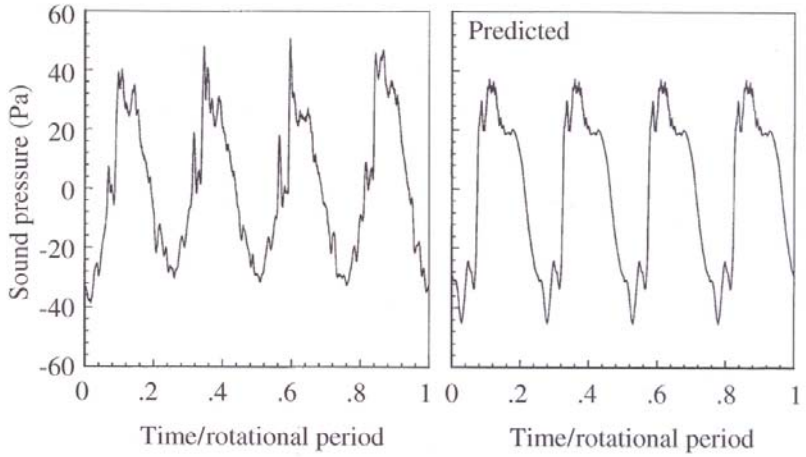

b) HHC-MN

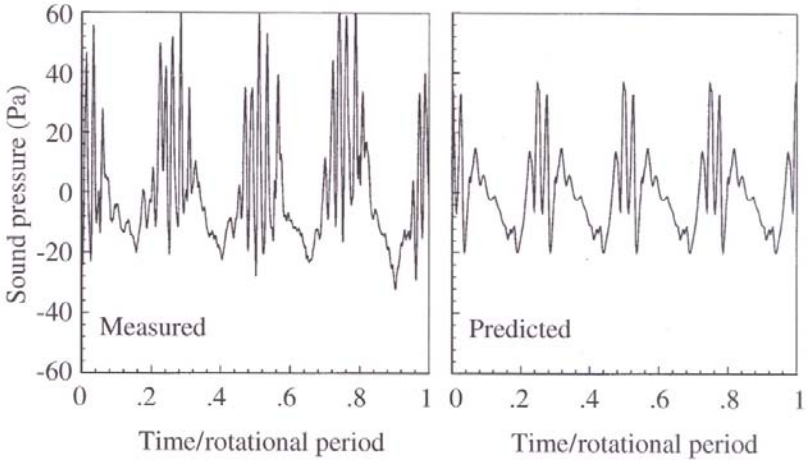

c) HHC-MV

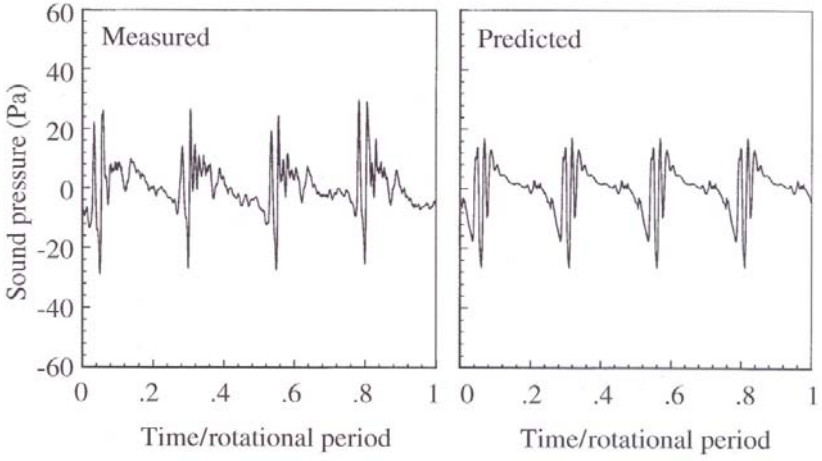

d) BL (3.8 deg)

Figure 3.6. Continued.

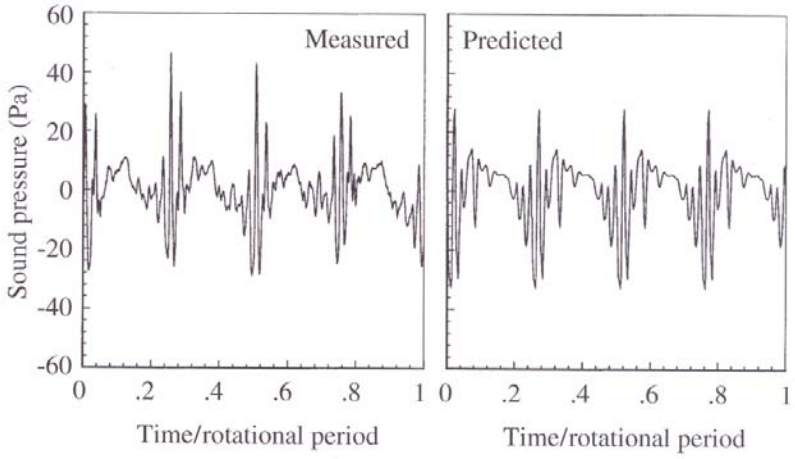

e) BL (6.8 deg)

Figure 3.6. Concluded.

Overall, the agreement with data from the HART program, using the BO-105 rotor model, was quite good. Generally, the success of the noise-prediction method was found to depend substantially on the multicore roll-up modeling of the rotor wake and resolution (temporal and spatial) definition of the blade loading. This wake modeling was developed from classical wake roll-up concepts for fixed wings and applied to the rotor problem. The method reduced the need for tweaking vortex parameters since the vortex character (size, strength, and distribution) was determined by the predicted local aerodynamics. However, improvements in the free-wake analysis, as well as the addition of multiple free-wake vortex trailers in CAMRAD.Mod1, further enhance the capability and dependability of the code.

CAMRAD.Mod1/HIRES appears to be sufficiently capable to be useful as a design tool. As an example, the calculations shown reveal the role that secondary vortices play in BVI noise production. A commonly held concept—that just relieving the tip loading would weaken the tip vortex and thus reduce or eliminate BVI noise—does not hold. The BVI-producing vortex may simply be released from a more inboard position. The vortex strength depends on the lift distribution, which is dependent on the rotor-blade design. The roll-up model implicitly accounts for the effect of blade design by using lift distribution in defining the wake structure and strength [Brooks et al., 2000].

To further illustrate the generality of the tools, a study to compare predictions using TRAC with data from the JVX Tiltrotor Test [Marcolini et al., 1995] was carried out by Burley et al. [2000]. The JVX Tiltrotor Test was a joint NASA/U.S. Army/Bell Helicopter Textron test of a 15%-scale model JVX proprotor conducted to obtain detailed maps of isolated tiltrotor noise directivity at numerous well-controlled operating conditions. These data were meant to provide insight into the various acoustic phenomena and to provide validation data for tiltrotor-prediction development.

For the tiltrotor, the blade loading, which directly determines the wake, can be quite different from that of a typical helicopter. For a helicopter (nominal twist of 8 deg and a blade aspect ratio on the order of 20) the peak loading is nominally in the tip region. For a tiltrotor (nominal twist of 35 to 45 deg and a blade aspect ratio on the order of eight), predicted results show the peak loading well inboard of the tip region. In this work, calculations for the tiltrotor reveal peak loading occurred anywhere from r/R = 0.30 to r/R = 0.75. Commonly, helicopter analyses intrinsically assume the maximum loading is near the tip and thus emit a single vortex at the tip. The resulting wake description (geometry and strengths) could be in error for a tiltrotor and thus make accurate noise prediction, particularly BVI noise, quite difficult.

Predictions for a wide range of forward-flight operating conditions were again made using the TRAC system: CAMRAD.Mod1-HIRES-WOPWOP (or WOPMOD) codes. To illustrate general results, figures 3.7a and 3.7b show a comparison of the maximum predicted and measured BVISPL levels for a sweep of tip-path-plane angles at C_T nominally 0.009 and 0.011, respectively. This is not a pure sweep of α'_{TPP}, since C_T varied by as much as 10% to 12% and was not held identically constant over the conditions. However, the specific measured thrust for a given condition was used in the corresponding prediction. In figure 3.7a for C_T = 0.009, the advancing side levels tend to agree, while on the retreating side, the shape of the trend curve is nearly identical, although there is a consistent 3- to 4-dB overprediction for all angles. For C_T = 0.011, the predicted and measured curves are similar, but the agreement is not good as C_T = 0.009, particularly on the retreating side. This exact reason for this phenomenon is not known. However, it is noted that, for these high disk loadings, establishing trim and wake convergence required more computational iterations, particularly for the blade motion, than were required for the low disk loading (C_T = 0.009) cases. Without measured results for blade motion and blade loading, the validation of the specific CAMRAD.Mod1 analysis could not be obtained. However, the trends indicate that there are significant differences between measured and prediction, even over the limited range of data that were available. To have a truly predictive capability, comparisons for a larger range of conditions are needed.

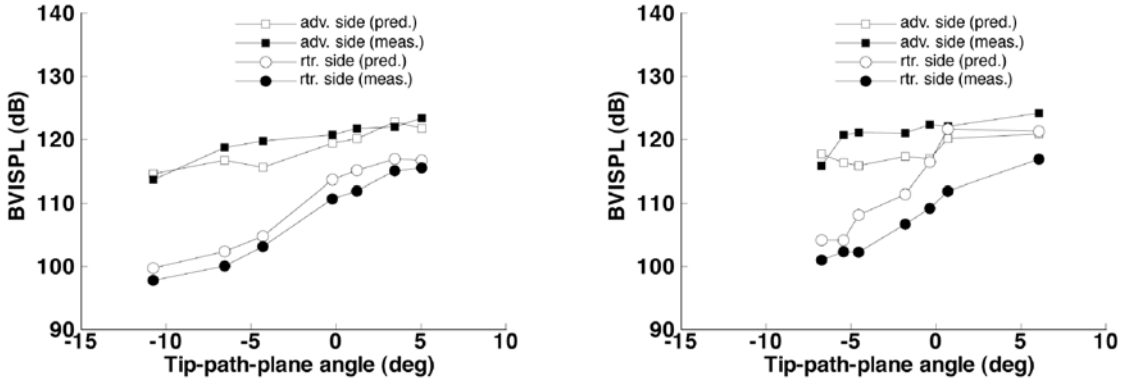

a) C_T = 0.009 b) C_T = 0.011

Figure 3.7. Measured and predicted maximum BVISPL vs. α'_{TPP} for two different rotor thrusts.

Aeroacoustic predictions for a wide range of forward-flight operating conditions were presented and compared to measured acoustic data from a model proprotor. The TRAC prediction system was shown to include the essential elements necessary to provide analysis for design and evaluation of low-noise proprotors, as well as support development of low-noise flight profiles.

More recently, the CAMRAD-II (C-II) analysis code, with its extended free-wake model, has been coupled to either WOPMOD or the newer PSU-WOPWOP. This C-II/PSU-WOPWOP coupled system has laid the foundation for the Comprehensive Analytical Model for Rotorcraft Acoustics (CARMA) [Boyd et al., 2005]. The CARMA code system builds upon the TRAC architecture and is a collection of standalone computer codes, linked by interface codes. The external-noise-prediction process starts with a physical description of the vehicle. The vehicle description consists of (1) CAMRAD-II input decks (including any airframe aerodynamics tables), which physically describe the vehicle, (2) airfoil tables, which provide sectional airfoil lift, drag, and moment information, and (3) airfoil section geometry, which provides the airfoil sectional shape required for the acoustic calculations. Note that although an extended and improved free-wake model of CAMRAD-II is used here, an equivalent to the roll-up modeling of CAMRAD.Mod1 is not. At this stage of development, the method uses only a nominal tip-vortex core size for the acoustic predictions. Still, this method is a transition to a more advanced CAMRAD version with an improved basic free wake, which is notable.

CAMRAD-II provides a comprehensive analysis of the vehicle. This analysis starts with physical description of the vehicle (including airframe aerodynamic information) and airfoil section data. These data are then used to determine the vehicle "trim" state for a given a flight condition. Once the vehicle trim state is known, CAMRAD-II is then executed as a "post-trim" procedure in order to compute the high-resolution rotor airloads and blade motion for use in the acoustic analysis. The high-resolution aerodynamic information is generated at the same radial stations on the rotor blade as used in the trim analysis, but the resolution azimuthally in the post-trim analysis is typically on the order of 1.5 degrees. This high resolution is required to adequately capture the impulsive character of a BVI event.

For the current assessment, the high-resolution airloads and blade motion predicted by C-II are input to WOPMOD, along with blade-section geometry, to compute the acoustic pressure time histories for the HART II rotor. The comparison between measured and prediction for the HART baseline rotor condition are shown in figure 3.8. The predictions are made in two ways; one uses the full-span wake model in C-II, and the other specifies just the single-tip-vortex model. The comparisons to the measured results are similar and are not as good as those previously made using the roll-up wake model of CAMRAD.Mod1. In figures 3.9a–f, predictions using the full-span model for a range of shaft angles are shown. The overall directivity and level trends appear to be captured with varying degrees of agreement for the different shaft angles, suggesting that the prediction of the rotor trim, blade motion, blade airloads, and rotor wake are not as accurate as required to predict accurate acoustics. Figure 3.10 shows a comparison of the predicted and measured maximum noise level on the advancing side. For advance ratio = 0.15, the trends are within 2–3 dB, except for the shaft angle of 2.3 degrees (mild descent) and 11.5 degrees (steep descent). The predicted level at the maximum BVI condition near 5.3 degrees compares very well with the measured level. It must be noted that this prediction was made using an unrealistic core size of 0.8 chord in order to match the

performance well and to obtain realistic acoustic levels. This core size is not accurate and is not representative of the actual physics. Although the trends can be assessed to some degree with this simple wake model, the levels are not accurate.

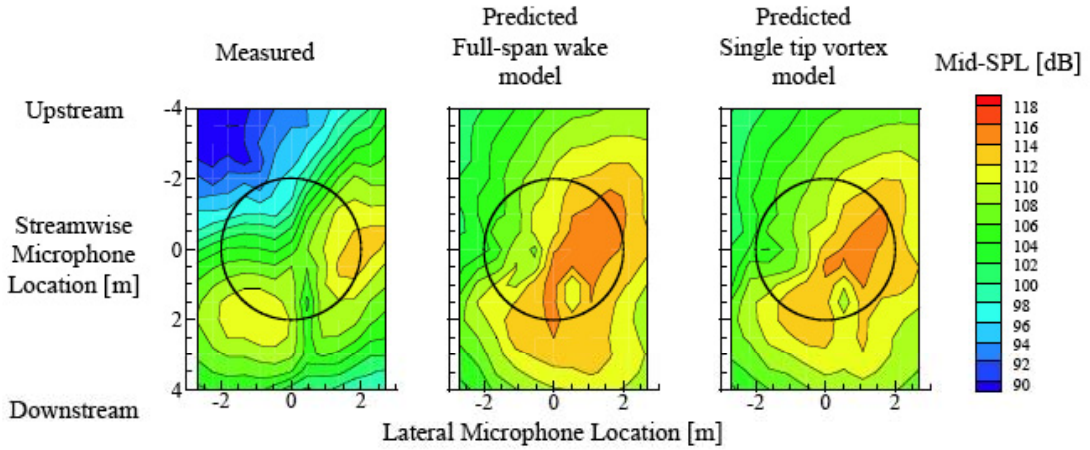

Figure 3.8. Measured and predicted noise-directivity maps of mid-SPL from the HART-II model rotor in the DNW for the baseline case (advance ratio = 0.15; shaft angle = 5.3 deg).

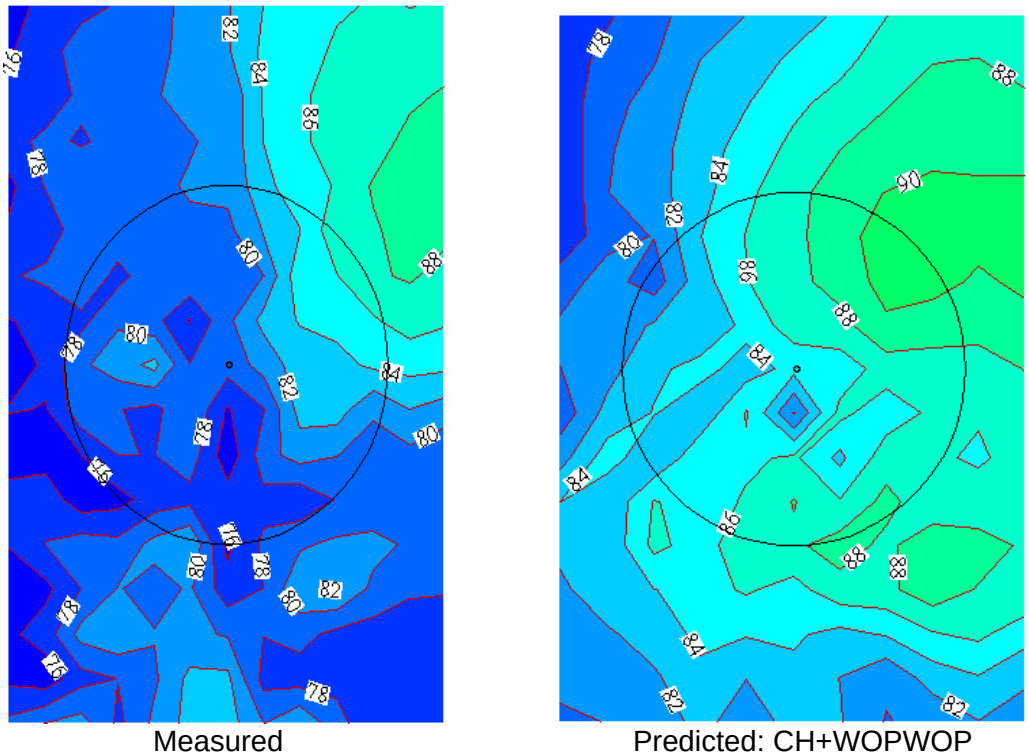

Measured Predicted: CH+WOPWOP

a) shaft angle = –6.9 deg

Figure 3.9 HART II contours of BVISPL for a range of shaft angles from descent to climb conditions at an advance ratio = 0.15.

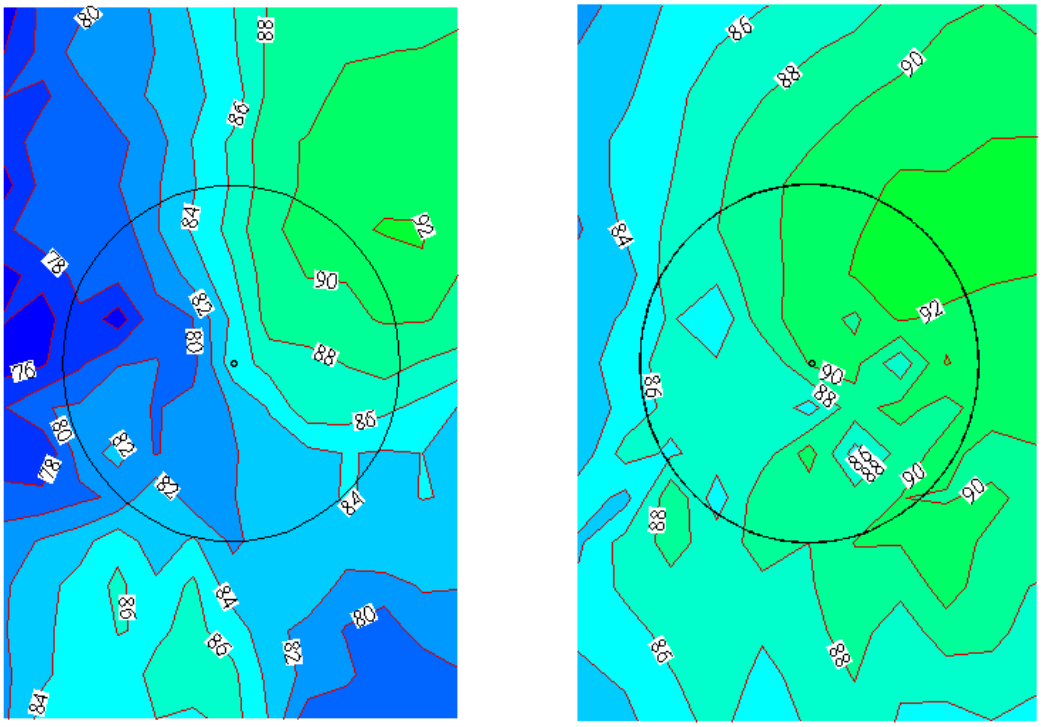

Measured Predicted: CH+WOPWOP

b) shaft angle = –3.7 deg

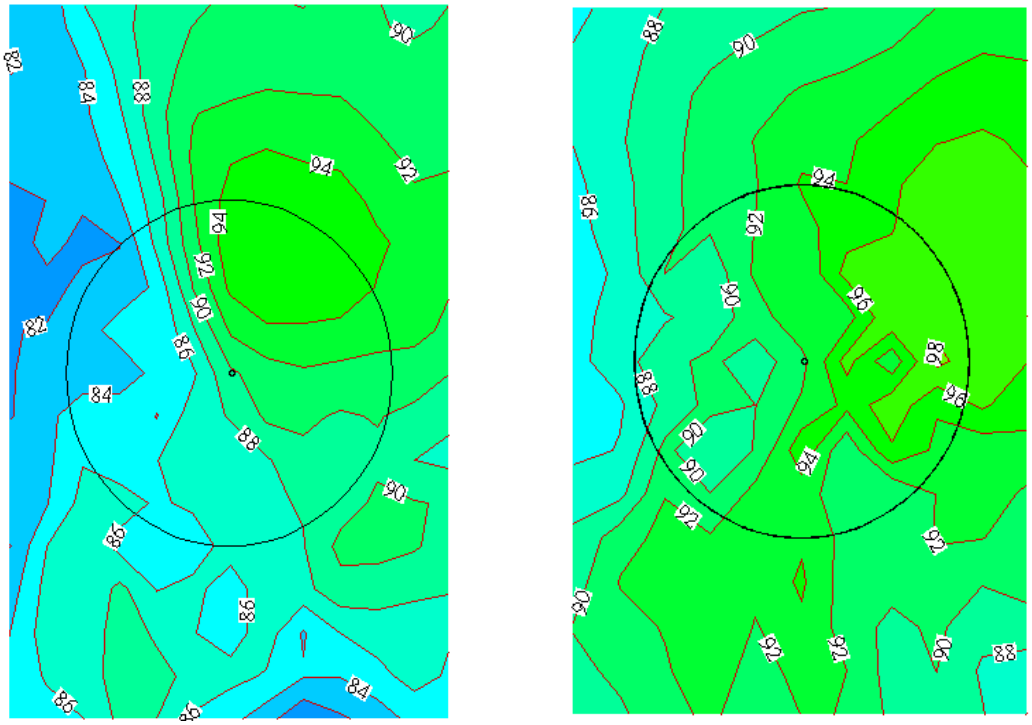

Measured Predicted: CH+WOPWOP

c) shaft angle = –0.6 deg

Figure 3.9 Continued.

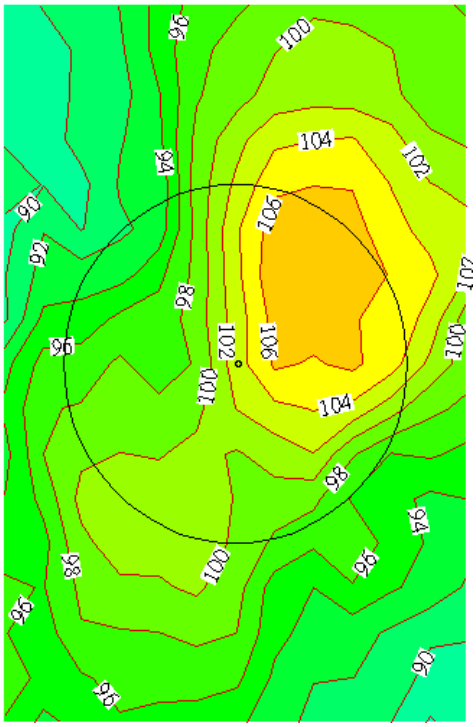

Measured

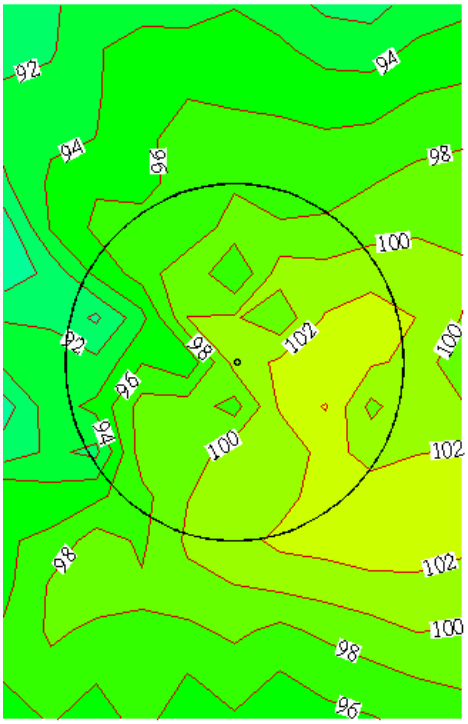

Predicted: CH+WOPWOP

d) shaft angle = 2.4 deg

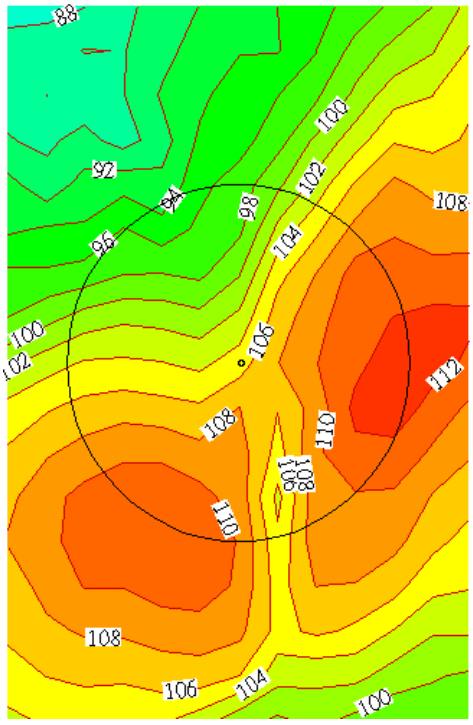

Measured

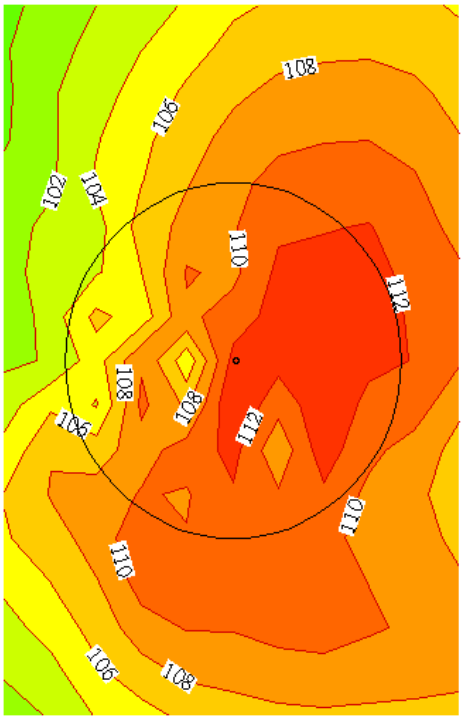

Predicted: CH+WOPWOP

e) shaft angle = 5.3 deg

Figure 3.9 Continued.

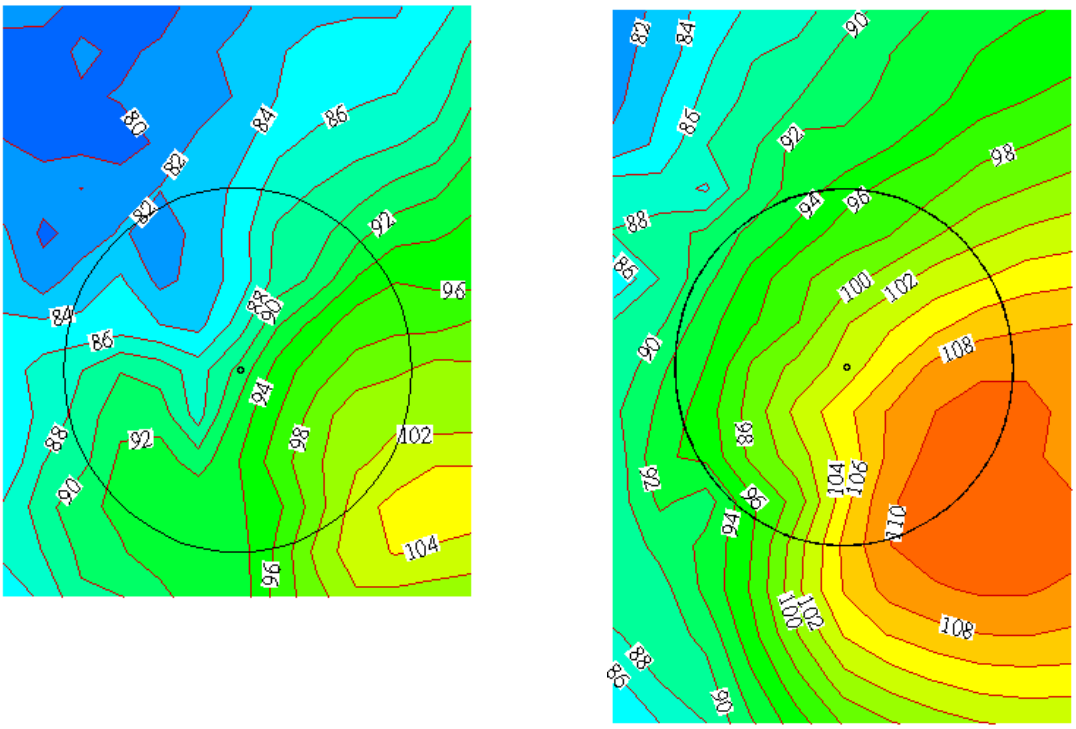

Measured Predicted: CH+WOPWOP

f) shaft angle 11.5 deg

Figure 3.9 Concluded.

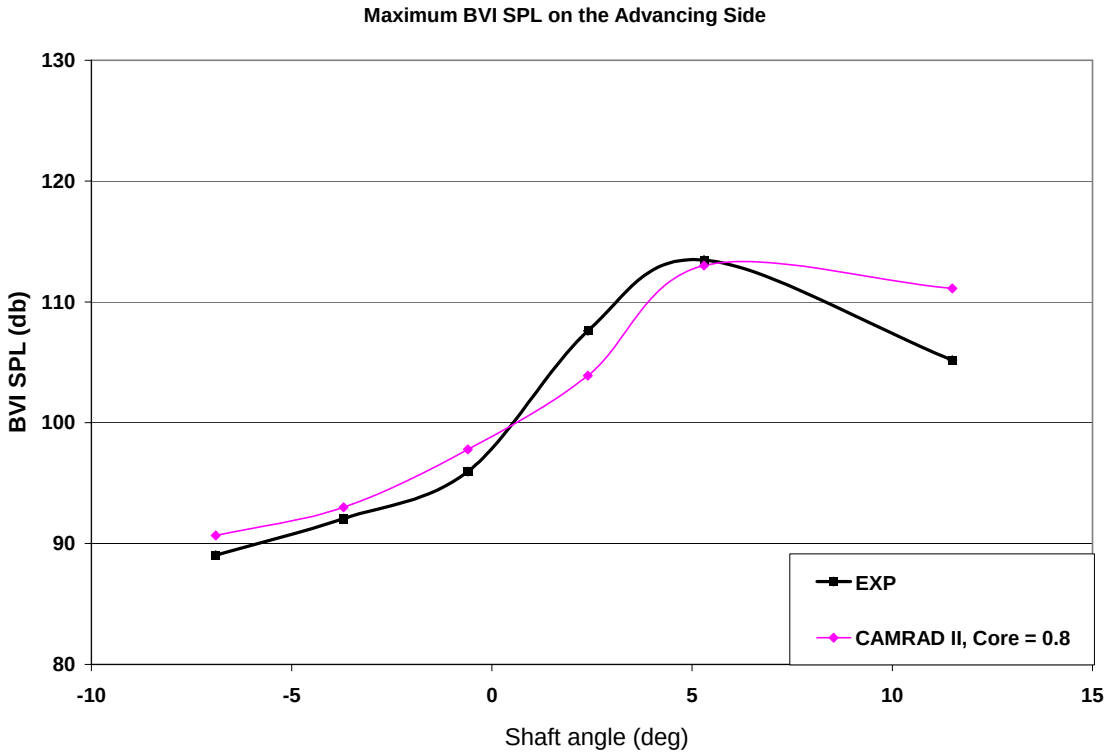

Figure 3.10 Predicted and measured maximum advancing-side BVISPL (presented in figs. 3.9a–f) of the HART rotor for a range of shaft angles for a constant advance ratio = 0.15.

Figure 3.11 presents an example of an excellent predicted acoustic pressure signature and spectrum and comparison with measured data (from figure 3 in Visintainer et al. [1993]). The microphone location for this comparison was nominally 25 deg below the rotor plane on the advancing side, ψ = 150 deg, 1.5 rotor radii from the rotor hub. This is a descent condition, μ = 0.152 and C_T/σ = 0.07.

Quadrupole noise

Several formulations by Farassat and Brentner programmed in the time domain have been shown to be very useful in prediction of discrete frequency quadrupole noise [Farassat and Brentner, 1998]. Note that the high-speed blade-slap noise of a helicopter is composed of the thickness noise as well as volume quadrupole noise. Farassat and Brentner showed that the sources on a rotating shock over an advancing blade are included in the quadrupole source term of the FW–H equation and rotating shocks are powerful sources of sound. Numerical experiments by these authors have shown that the peak of the signature of the high-speed blade slap can be calculated well by contributions from the thickness noise, the shock noise, as well as the volume quadrupoles near the leading edge of the blade near the blade tips. However, the width of the main pulse of the acoustic signature is under-predicted by a factor of 2. To calculate this width correctly, the quadrupoles in a large volume around the blade beyond the sonic surface must be included in the noise prediction. The main problem is that the fluid dynamic computations are time-consuming, particularly if all the blade kinematics are included. However, it appears that for high-speed blade-slap noise prediction, the details of the blade motion can be neglected.

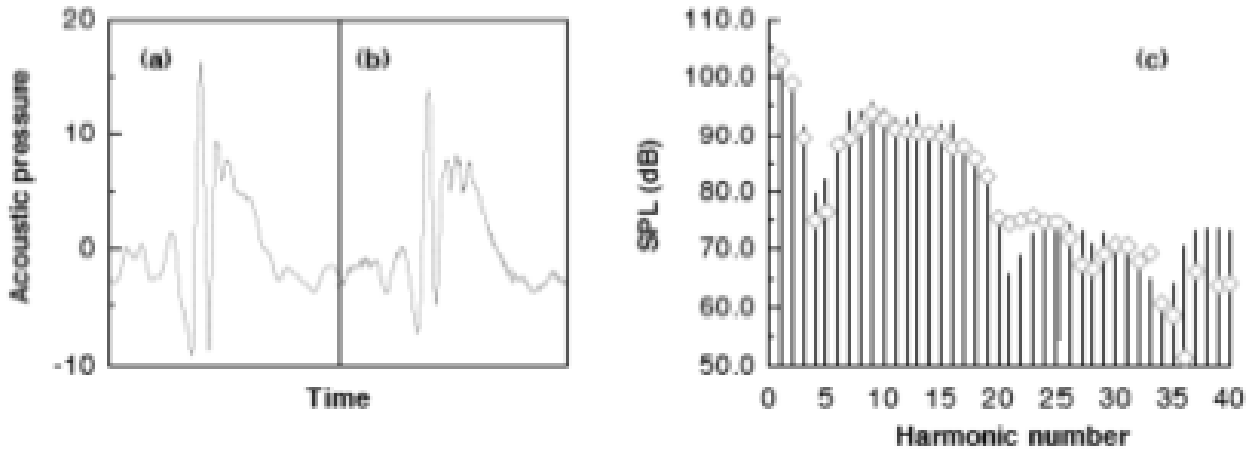

a) Measured time history;
b) predicted time history;
c) spectral comparison, –, measured; ◊, predicted.

Fig 3.11. Comparison of measured and predicted noise for a four-bladed Sikorsky model rotor.

Broadband noise

Calculation of the broadband noise of rotors is the most difficult part of helicopter noise prediction. As discussed previously, many mechanisms of broadband noise generation are difficult to model theoretically. Many of these mechanisms involve turbulent flow of various scales whose effect on surface-pressure fluctuations is poorly understood. At present there is not enough detailed surface-pressure fluctuation data to compute rotor broadband noise. The CFD problem that involves turbulence simulation is beyond the capability of the current computers. In this situation, frequency domain semiempirical formulations have been proposed by Brooks for the various mechanisms of broadband noise generation with empirically determined parameters derived from the measured HART data. These formulations have been verified for some reliable experimental data [Burley and Brooks, 2004]. Figure 3.12 shows measured spectra from the HART rotor taken at two locations under the advancing side for a range of shaft angles. The spectra in figure 3.12a are considerably different in character, particularly at the higher frequencies associated with BWI and blade self-noise, than those shown in figure 3.12b. A comparison of measured and predicted spectra obtained for a shaft angle of –5.3 degrees is shown in figure 3.13 for the measurement locations. Combined with the predictions of harmonic and BVI noise and broadband BWI noise, these were the first predictions of complete noise spectra compared to measurement. At present no other method is available for broadband noise prediction for realistic rotor designs and operating conditions. There are methods in basic research stage using extensive turbulence simulation that have not reached the degree of maturity of the semiempirical method of Brooks.

Noise predictions based on CFD analyses

The Navier–Stokes (N–S) equations, along with equations for conservation of mass and energy, and an equation of state govern the fluid flow fields and acoustics of interest. Solution of these equations constitutes a “first-principles” approach to determining a flow field. This set of equations can be cast in numerous different forms. These various forms can be exact (e.g., direct numerical simulation (DNS)), or approximate (e.g., Reynolds-averaged Navier–Stokes (RANS)). DNS-type methods attempt to solve the full N–S equations directly by resolving all temporal and spatial scales of interest, such as turbulent scales, acoustic waves, etc. Resolving these scales down to the smallest turbulent scales requires computational resources that are simply not available currently (nor will they be available in the foreesable future).

Approximations to the full N–S equations have been successfully used for many years for practical problems. One of the most prevalent approximations currently being used is the RANS equations. These equations are derived by splitting variables into two parts: a mean-flow part and a fluctuating part, leading to a set of equations for the mean flow (which can be “slowly” varying, or unsteady) and fluctuating part. The fluctuating part is usually associated with the turbulence of the flow and can be modeled using any of a vast array of turbulence closure methods.

Historically, CFD methods have focused on the hydrodynamic components of the flow field, such as the hydrodynamic pressure. Computation of these hydrodynamic quantities has typically been accomplished using relatively low-order methods (e.g., second order, third order, etc.). To compute acoustic quantities with these codes would require numerical methods that solve the equations with very high precision and accuracy. This requirement comes from the fact that the acoustic pressure is approximately 6 orders of magnitude smaller than the hydrodynamic pressure.

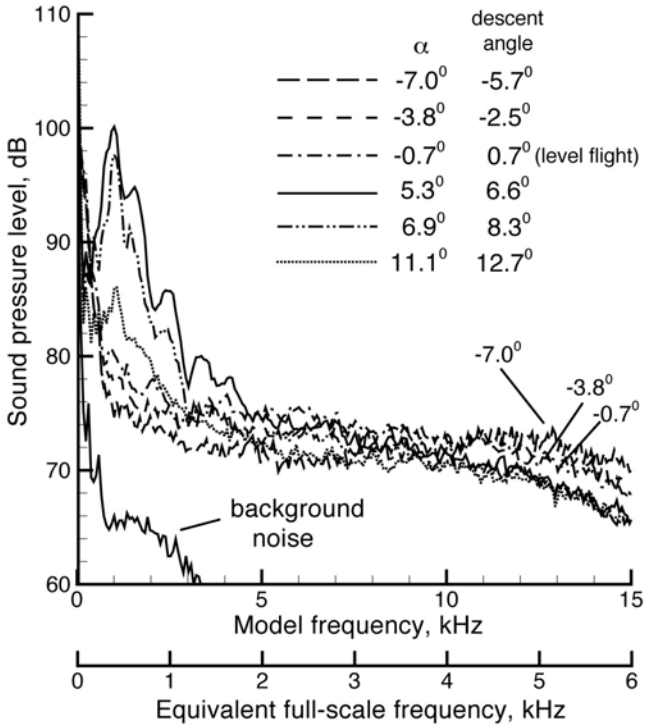

a) Measured by microphone located under and forward of rotor center on the advancing side

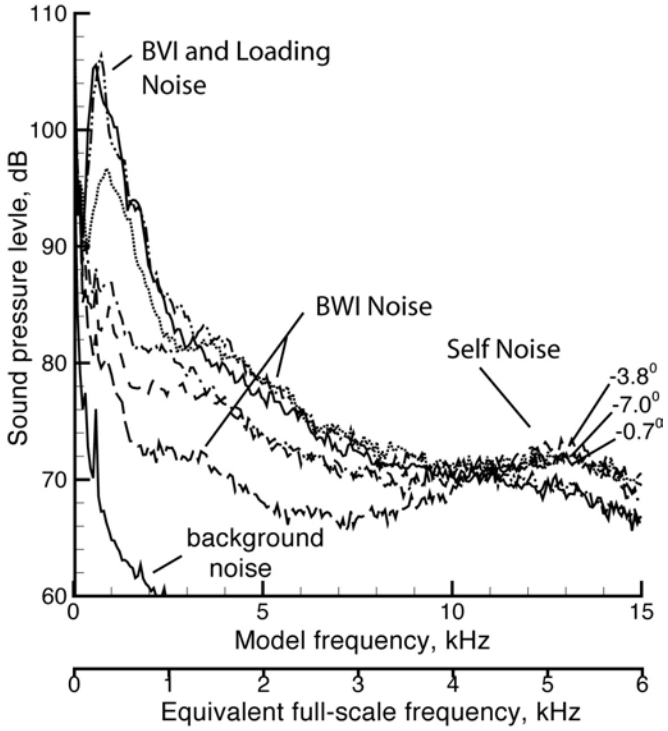

b) Measured by microphone located under and aft of rotor center on the advancing side

Figure 3.12. Measured noise spectra for a range of shaft angles showing the dominant noise sources for different frequency ranges.

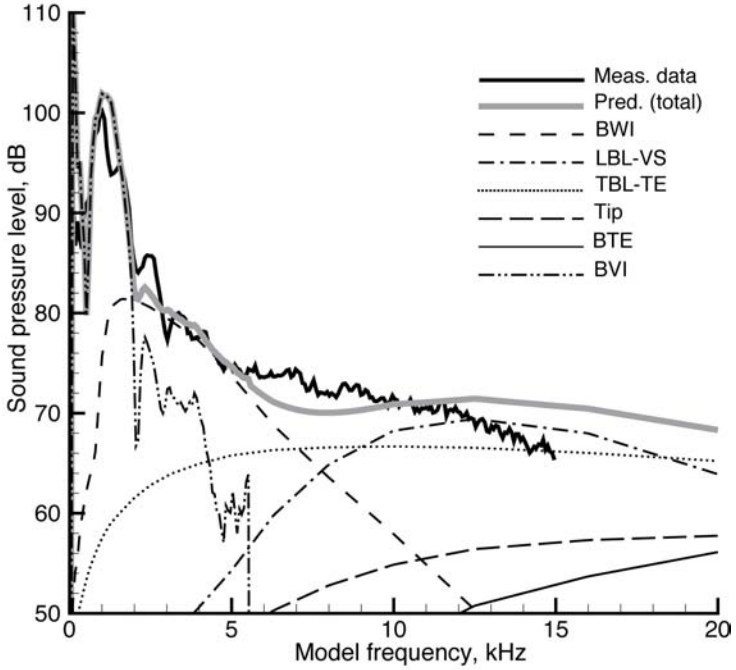

a) Measured spectrum compared to predicted total and component spectra for a location under and forward of rotor center on the advancing side

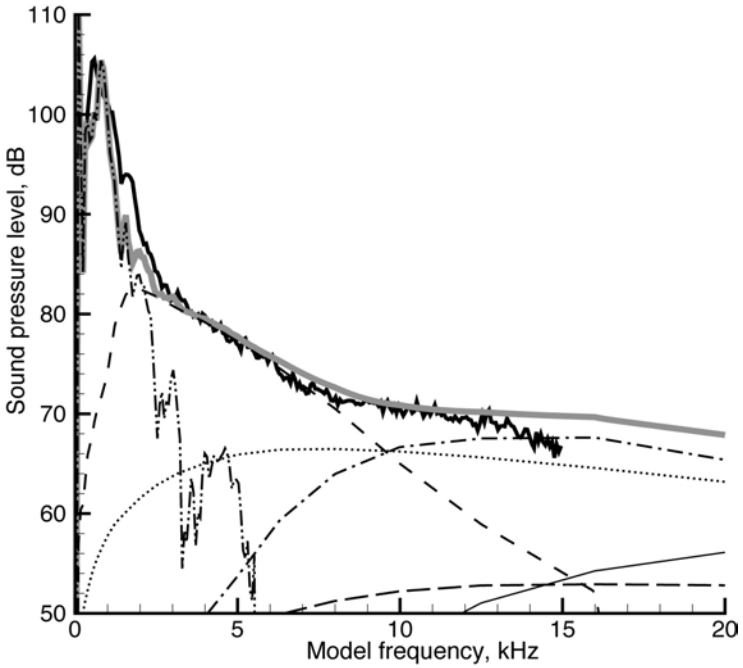

b) Measured spectrum compared to predicted total and component spectra for a location under and aft of rotor center on the advancing side

Figure 3.13. Measured and predicted noise spectra for shaft angle = –5.3 deg (descent condition).

The problem with the inability of CFD to compute acoustic parameters was recognized long ago. Efforts to develop this capability led to the field of computational aeroacoustics (CAA). The goal of CAA was to develop numerical methods capable of directly computing the acoustics in a flow field. Numerous methods were developed to aid in the numerical solution to equations such as the wave equation, the Euler equations, etc. For example, Tam developed a method called the Dispersion Relation Preserving (DRP) method. This method examines a given numerical stencil in wave-number space, and then optimizes the stencil coefficients to minimize the difference between the numerical solution and the exact solution. He then used these methods in the Euler equations to compute sound fields for various configurations. There are many other examples of this type of work in the literature. A decade or so ago, CAA was a distinct field of research and, in many areas, is still an active research topic. In recent years, the line between CAA and CFD has become blurred because many of the methods that were developed in the field of CAA have been imported into traditional CFD codes. This importation has resulted in more accurate CFD codes. Though these more accurate CFD codes are still not considered CAA methods, they do provide more accurate source terms for the acoustic equations such as the FH–W equation.

As described earlier in this chapter, Formulation 1A (F1A) [Farassat, 2007] is a solution to the FW–H equation for discrete frequency noise involving only the surface terms (thickness and loading). F1A requires accurate input of the body geometry, body kinematics, and surface-pressure data to compute discrete frequency thickness and loading noise. Recently, computation of cases with mild high-speed impulsive (HSI) noise has become feasible. This computation has been made possible by formulating the F1A as a penetrable surface solution instead of a nonpenetrable solution. However, this penetrable surface solution requires more data than the nonpenetrable F1A. All additional data required by the penetrable solution can be obtained from the conservative variables.

Recent efforts by groups such as the U.S. Army, Defense Advanced Research Projects Agency (DARPA), universities, etc. have advanced the state of rotorcraft such that it is possible to couple a CFD method with a CSD method for elastically deforming rotors. Though these methods are currently very computationally intensive, this CFD/CSD coupling provides a consistent solution for the aerodynamics and blade dynamics to a level of detail that has never existed before. Development of these coupling methods is still an area of intense research, further details of which are also discussed Chapter 4 of this document. NASA does not currently possess a full, independent capability to compute a complete CFD/CSD coupled solution with extraction of appropriate source data and subsequent discrete frequency noise calculation. Acquisition of an in-house capability is under way and will provide NASA the capability to assess noise from nonconventional rotorcraft configurations.

The current CFD/acoustic component of the research within NASA rotorcraft involves developing strategies to extract appropriate acoustic source information from the CFD/CSD coupled solution. Current NASA CFD efforts focus on two implementations of RANS. One implementation, OVERFLOW, [Potsdam et al., 2004; Lim and Strawn, 2007; and Dimanlig et al., 2007], solves the RANS version of the finite difference form using node-centered, structured, overset grids. OVERFLOW also can handle multiple moving bodies (e.g., rotating blades, store separation, etc.) The other implementation, FUN3D [Anderson and Bonhaus, 1994; Anderson et al., 1996; and Nielson, 1998], solves the RANS equations as well. However, FUN3D solves the integral form of the RANS equations using vertex-centered, unstructured grids. The source data from these CFD

codes coupled with various CSD approaches will then be transferred to discrete frequency noise computations. Computation of broadband noise components from CFD analyses is still not currently feasible. Extraction of this source information for discrete frequency noise prediction is not as straightforward. Currently two approaches are being pursued in the research community: co-processing and post-processing. Each has its own advantages and disadvantages.

Co-processing involves extraction of data on a small subset of user-defined grids. These grids can be solid surfaces, such as the rotor blade (used to extract the geometry and the surface pressure), or a penetrable surface ("off-body" surface) used to extract flow-field quantities away from solid surfaces. An advantage of co-processing is that it can drastically reduce the quantity of data that must be saved during a simulation. A disadvantage of this method is that, if later a different set of surfaces is desired after a computation is complete, the computation must be rerun.

Post-processing involves extraction of source information from the full set of output data from the CFD/CSD method after the solution is complete. A disadvantage of this method is that, because it is not known a priori which, where, or how often the data will need to be extracted, the entire flow field and solution must be saved at many time steps. This process can require storage of extremely large quantities of data. However, the advantage of the post-processing method is that the CFD/CSD computation does not need to be executed again if the user decides that a different set of data surfaces is needed.

Of these two methods, co-processing appears more developed than the post-processing model. Currently, however, NASA is sponsoring a Small Business Innovative Research (SBIR) program designed to address the problems associated with post-processing.

Rotorcraft Acoustic Characterization and Mitigation. The first step in the development of an internal NASA capability to predict discrete frequency noise, using CFD to compute the source-noise data, is to assemble the necessary computational tools and methods. Recently, NASA has obtained a suite of tools, including CAMRAD-II [Johnson, 2002], OVERFLOW2, PSU-WOPWOP [Hennes and Brentner, 2005], and several data-conversion codes to allow these tools to communicate (through file input/output (I/O)). New, more general, "conversion codes" have been developed. This section presents results from the most recent computations using this initial version of the assembled suite of tools.

The predictions in this section are for the HART-II rotor system in the DNW [Yu et al., 2002]. The complete coupling method uses the comprehensive rotorcraft analysis code CAMRAD-II to obtain the blade motion of a reference rigid blade set and the elastic motion relative to this rigid motion. This elastic motion is applied to the reference blade set during the subsequent execution of the CFD code OVERFLOW2. The airloads from the previous CAMRAD-II execution and the airloads from the CFD execution are then compared. The difference between these values is subsequently fed back into CAMRAD-II, where a new set of elastic blade motions is obtained. This iteration cycle continues until the solution has converged. Convergence for these cases is determined by examining (qualitatively at this point) the rotor-control settings and the airloads as a function of iteration. The full iteration method is now available and has been demonstrated. Currently, though, examination of

the CFD computations, and the resulting noise predictions with a known (measured) set of blade motions, is being examined. The measured flap, lag, and torsional blade motions have been recently made available. Ideally, using these measured blade motions in the CFD code should result in very reasonable airloads predictions. This process should, in turn, produce good noise predictions. If by performing these analyses the airloads or noise is not predicted well, the state of the art can be advanced by determining the cause of the differences.

The results presented here are from a fine-grid computation wherein the minimum background (off-body) Cartesian-grid resolution is 0.10c. Dual time stepping is used with physical time steps corresponding to 0.125 degrees. Fifteen Newton subiterations are used at each physical time step.

The three cases examined here are the Baseline (BL), Minimum Noise (MN), and Minimum Vibration (MV) cases. They are all at the same nominal flight condition where the advance ratio $\mu = 0.15$, a shaft tilt is 5.3 aft, and the rotor rotates at 1041 rpm. The predictions shown in this example include the full wind tunnel sting. Predictions of this nature are considered the state of the art and have not been shown previously for this rotor system.

Figure 3.14 shows the normal force coefficient multiplied by Mach number ($C_N M^2$) for the Baseline (BL), Minimum Noise (MN), and Minimum Vibration (MV) cases as a function of rotor azimuth. In all three cases, the gross features of the $C_N M^2$ quantity at r/R = 0.87 are shown in the predictions, though in general the mean value is underpredicted. This underprediction has been seen previously by other researchers, but the cause is still unknown. The measurements and predictions both contain distinct local BVI events for all three cases. Lim and Strawn [2007] estimated that to match vortex core sizes an off-body Cartesian spacing on the order of 0.0125c could be required. If a uniform Cartesian background mesh philosophy is maintained, the computational resources required are far beyond computer capabilities for the foreseeable future.

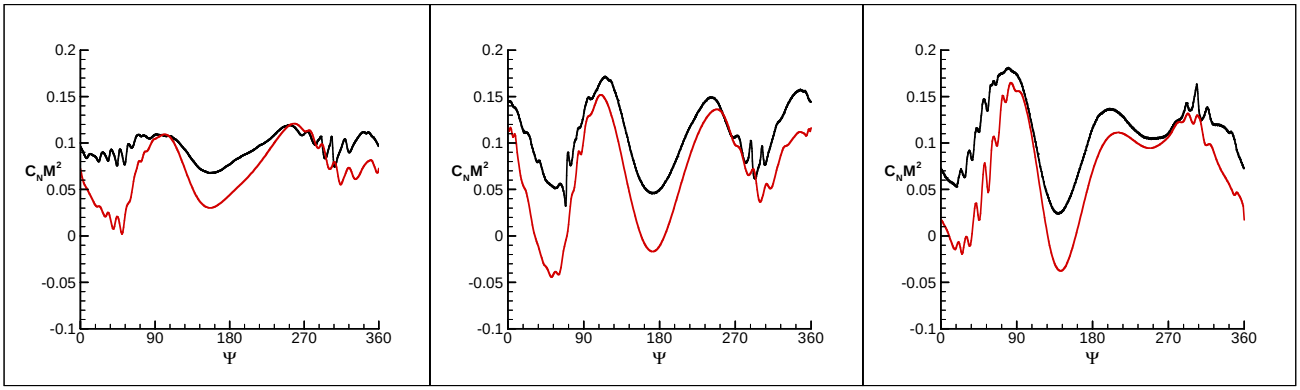

Figure 3.14. Measured (black line) and Predicted (red line) $C_N M^2$ for the HART.

Using co-processed data from these calculations, acoustic predictions can be made and are presented here. In this case, the acoustic source data are the elastically deforming blade surface and the pressure on the blade surface. The blade-surface data here were extracted every 1 degree of azimuth and used in the time-domain acoustic discrete-frequency noise-prediction code PSU-WOPWOP. The present predictions do not include any other effects, such as scattering. The noise predictions in figure 3.15 were performed for microphone locations that are on a plane below the rotor disc (corresponding to the microphone locations in the HART-II test). The midfrequency component (6th–40th blade-passage harmonic) of the predicted noise is plotted for all three cases along with their corresponding measured values. Even though the low-frequency components of the $C_N M^2$ do not compare as well as expected, the midfrequency components appear to compare well (based on the noise prediction). Further investigation is needed to examine the lower-frequency differences. The midfrequency (BVI) range SPL prediction using the measured blade motion show that the CFD code does reasonably well with airloads predictions that are used in the noise prediction when measured blade motion is used. For the BL and MV cases, the difference in the maximum noise levels (measured vs. predicted) is less than 0.5 dB. For the MN case, the difference between the measured and predicted maximum noise level is less than 2 dB. The directivity patterns, especially on the advancing side, are well-predicted. The retreating-side noise peaks, however, are not as well-predicted, though evidence of their presence is shown in the predicted contours.

In terms of level and directivity, these predictions can be considered very good. They indicate that that it *should* be possible to predict BVI noise levels within several dB, if all of the components provide accurate data to each other. The time required to process the data using the CFD/CSD method with the current computer resources is longer than initially expected. Though more and more computer resources are becoming available all the time, the burden placed on these resources seems to be increasing at an even larger rate. The high computational demands will significantly increase when additional capabilities, such as scattering, are included in the computations. These levels of computation appear to have been underestimated, while the availability of computer resources appears to have been overestimated.

Plans for improving predictive capabilities

Several tasks within NASA, in conjunction with other research areas, are directed toward improving rotorcraft acoustic predictive capabilities. At a fundamental level, research into the efficient extraction and transfer of source-data information is being conducted to improve the acoustic predictions provided by the aforementioned FW–H method. In conjunction with this effort, assessment of the CFD requirements for acceptable noise prediction is also ongoing. To this end, impenetrable and penetrable data surfaces are employed to study benchmark acoustic problems and identify optimal spatial and temporal resolution, permeable surface orientation, etc. Additionally, research being conducted to improve performance parameter prediction will also lead to improved acoustic prediction capabilities. In particular, investigation of the Particle Vorticity Transport Method (PVTM) [Anusonti-Inthra, 2006] is directed at using the vorticity transport equation to improve the blade-vortex definition obtained for CFD. Additionally, efforts to incorporate CFD/CSD coupling into FUN3D and the base version of OVERFLOW2 will provide improved performance prediction. Ultimately, the improved blade surface-pressure and vortex calculations will provide more accurate acoustic calculation input and ultimately improved acoustic prediction capabilities.

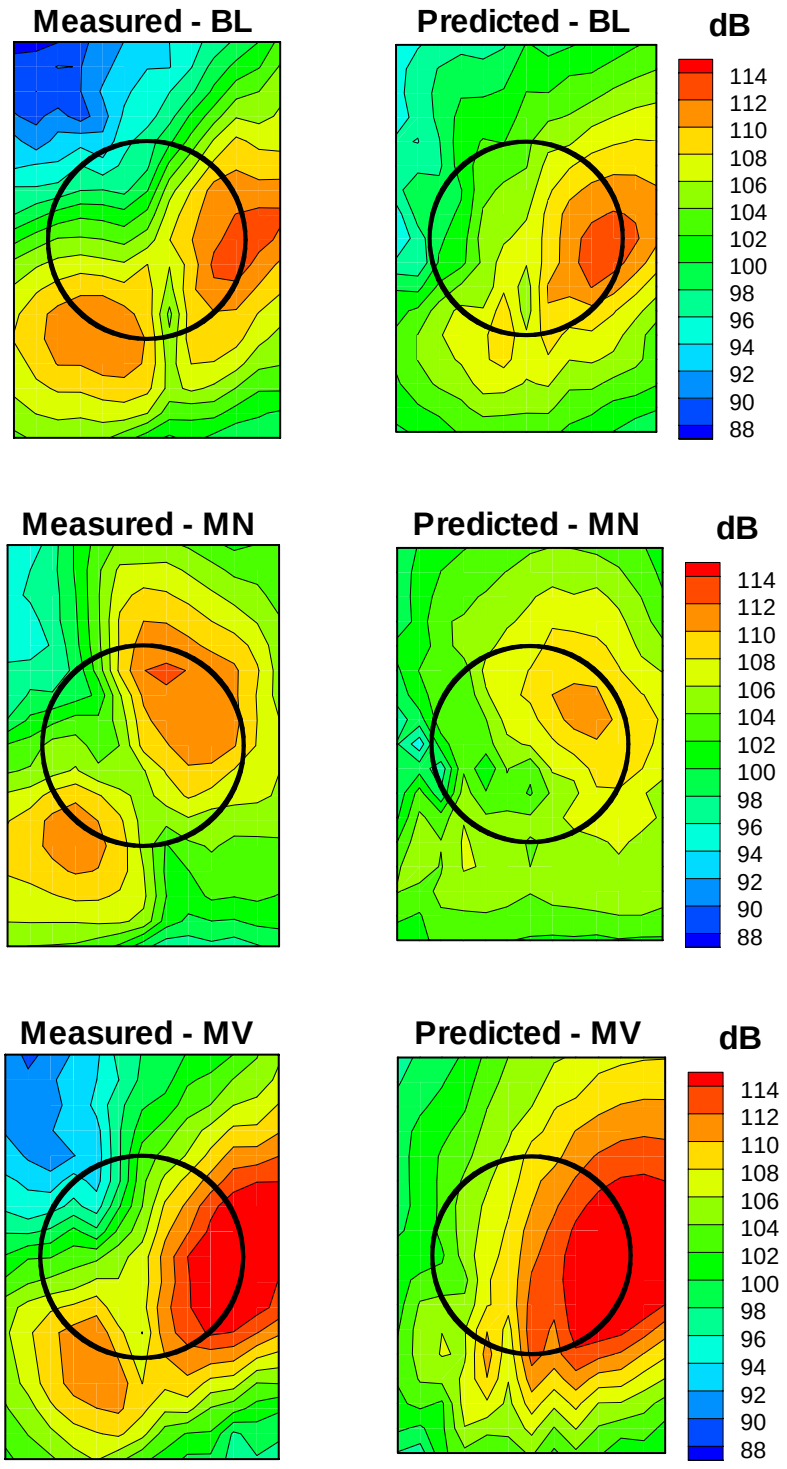

Figure 3.15. HART-II midfrequency measured versus predicted BVI SPL for Baseline (BL), Minimum Noise (MN), and Minimum Vibration (MV) cases. Predictions use measured blade motion.

The nature of the CFD/CSD coupled method requires that the accuracy of the CFD computation directly depends on the solution of the CSD, and visa versa. Unfortunately, therefore, if either the CFD or the CSD result is not accurate (because of modeling issues, assumptions made, etc.), then the entire solution is incorrect. It is desirable to examine each piece individually. So, to begin improvement of the computation of each piece, measured blade motion from the HART2 test has been imported into OVERFLOW2. Using the measured motion and the preliminary results discussed previously, CFD calculations are being examined to help understand the differences in the measured and predicted airloads. Once the CFD airloads predictions compare well with the measured airloads, these airloads can then be imported back into the CSD code (i.e., CAMRAD-II). This importation should result in a good CSD blade-motion prediction when compared with the measured blade motion. Again, if agreement is not good, then the CSD assumptions and modeling can be examined. This analysis should improve the overall modeling of the coupled CFD/CSD method.

In the area of quadrupole noise, the computation of the steepening of the acoustic-pressure signal for high-speed blade slap requires the integration of the quadrupoles source over a large volume beyond the sonic circle. Since the calculation of the peak acoustic pressure is relatively easy, the steepening effect can probably be corrected by a semiempirical method. Such a method should be explored in the future. A large amount of unsteady CFD data both on and off the blades must be computed and stored. The computation, storage, and retrieval of such a large amount of data can strain the most powerful existing computers, hence the need for efficent data-management strategies and architectures.

The current broadband noise models by Brooks depend substantially on an analytical model by Ffowcs Williams and Hall of a source passing the edge of an infinitely thin airfoil [Ffowcs Williams and Hall, 1970]. Such a model can perhaps be modified and improved by some basic experimental research focusing on airframe noise prediction. The results are relevant to rotor broadband noise prediction without requiring execution of a more complex rotor experiment.

Validation data requirements

As prediction techniques are enhanced and extended, the existence of quality validation data becomes increasingly important. Therefore, data from numerous tests are being used to validate various predictions. For example, the HART I and HART II databases are being used to validate CFD/CSD improvements in performance predictions, as well as subsequent improvements in acoustic predictions. For this comparison, measured blade motions will be required, along with an assessment of the blade-motion measurement uncertainty. Initial assessment of the PVTM methodology has been carried out using information from fixed-wing data with the hope of ultimately validating wake geometry and vortex definition with 20% predictive accuracy relative to measured HART II wake data. In addition, benchmark acoustic solutions are also available to begin the parameter assessment for accurate and efficient acoustic predictions. The insight gained from this research, coupled with the aforementioned improvements in performance prediction, will be brought together to validate acoustic predictions within 3 dB of measured peak noise levels. Quality experimental data including blade airloads, blade deflections, wake geometry, vortex size/strength, and acoustic flight-test data are desirable for different classes of rotors. Without these data, it is extremely difficult to measure success and/or identify gaps in prediction capabilities.

INTERIOR NOISE SOURCES

Introduction

Interior noise has always been a concern of the helicopter industry, although its importance relative to other design requirements varies considerably from vehicle to vehicle. The primary offending sources for helicopter interior noise are found in the power train, which tends to be located immediately adjacent to the passenger cabin. These sources include gear-mesh noise from the transmission, hydraulic-pump noise, and shaft vibrations. Sources of secondary importance include low-frequency rotor harmonics and broadband noise due to exterior flow excitation of the fuselage at high forward flight speeds. The high-frequency (kilohertz) nature of the power-train noise, coupled with the sensitivity of the human ear at these frequencies, make this noise source the most critical for passenger health and comfort.

Because of the proximity of the power train to the passenger cabin, reducing power-train noise is a challenge. The following traditional quieting methods require space and add weight to the vehicle:

- vibration isolation of power-train components from the airframe
- structural-damping treatment for locations where resonant response is a problem
- barrier treatments between radiating surfaces and passengers, such as heavily damped trim panels and dense treatments such as lead vinyl
- bulk absorbers, such as fiberglass, placed between the fuselage and trim panels to minimize acoustic resonances of the air gap between the trim panel and sidewall, and to attenuate high-frequency sound
- absorbent liners inside the passenger cabin to minimize the effect of reflected sound and cabin resonances

Early studies of combinations of these treatments demonstrated reductions in the A-weighted interior noise level of 30 dB relative to an untreated cabin [Howlett et al., 1977]. However, the resulting levels were still above the levels found in passenger aircraft, and were judged to be excessive. Advancements have been made in modeling methods and active and passive vibration control since these early studies of helicopter noise were performed. Despite these advancements, fully trimmed helicopter interiors are still several dB noisier than passenger jets. The tonal nature of helicopter interior noise also makes the interior noise environment even more annoying to passengers than a difference of several dBA would suggest.

Nontraditional approaches to cabin quieting include vibration isolators at the transmission mount points, active noise control, and optimized fuselage design for minimum noise radiation into the passenger compartment. Vibration isolators can introduce certification and shaft-alignment problems, and redesigning the primary structure to reduce interior noise is well beyond the comfort zone of most rotorcraft manufacturers. Active control has been extensively studied by the rotorcraft industry since that approach seems ideally suited to address the tonal nature of helicopter interior noise [Sutton et al., 1997; Millott et al., 1998; Maier and Tewes, 2005; Mathur et al., 2002; and LeHen et al., 2005]. The approach involves the introduction of energy to reduce vibrations transmitted from the gearbox to the airframe, disruption of the energy flow path through the structure, or

reducing the radiation efficiency of a trim panel. Despite the interest from the industry, relatively few active noise-control systems are offered on production helicopters. This situation may reflect the difficulty of fielding a robust, maintainable active noise-control system, especially at the high frequencies relevant to helicopter interior noise. Some important aspects of a successful active noise-control system include: obtaining a clean reference signal with minimal phase jitter; achieving a global reduction of cabin sound levels with a reasonable number of control actuators; implementing a high-performance control system with minimal complexity; and ensuring the robustness and maintainability of actuators and sensors.

In addition to these quieting methods, an important approach to the problem is source-noise reduction through low-noise power-train components [Coy et al., 1987; and Oswald et al., 1994]. Evaluating any one of these new approaches or optimizing a traditional approach requires an accurate interior noise-modeling tool. With such a tool, the acoustician and aircraft designer can strive to maximize performance with minimum added weight, and make an informed cost/benefit analysis on each quieting technology. For this reason, this section on Interior Noise Source is divided into two main sections: 1) Interior noise-prediction methods, including a novel actuator for active noise control, and 2) gear and drive-train noise.

Interior Noise-Prediction Methods

Interior noise-prediction tools are categorized depending on the frequency range being modeled, with a broad division between low- and high-frequency tools. The distinction between low and high frequency depends on the modal overlap of the system being studied, where low frequency corresponds to low modal overlap (an individual mode dominates the response in a given frequency band), and high frequency corresponds to high modal overlap (many modes contribute to the response in a given frequency band). A modal overlap threshold of 3 is usually used to distinguish between low- and high-frequency regions for acoustical spaces [Rabbiolo et al., 2004], and generally occurs around a few hundred hertz for the acoustic response of a helicopter cabin [Jayachandran and Bonilha, 2003]. The modal overlap-threshold frequency will vary for different components of the vehicle, occurring at higher frequencies for rigid airframe stiffeners and lower frequencies for less-stiff fuselage-sidewall panels. The term midfrequency range is sometimes used to denote the frequency range where the response of certain components exceeds the overlap threshold of 3, while the response of other components does not exceed the threshold.

At low frequencies, deterministic modeling methods such as finite elements, boundary elements, and modal expansion techniques are useful for predicting motion of the rotorcraft structure and the associated interior sound field [Atalla and Bernhard, 1994; Dowell, 1980; Rabbiolo et al., 2004; and Jayachandran and Bonilha, 2003]. The successful application of these methods depends on accurate characterization of material properties, boundary conditions, and external forces. These problems are difficult but not insurmountable ones that depend on the vehicle being studied.

Deterministic methods suffer from two significant drawbacks in the high-frequency range: the required mesh density exceeds current computational capabilities, and variations in material properties, joint properties, and dimensions collectively create a level of uncertainty that cannot be captured by deterministic methods. The dynamic response of the vehicle at high frequencies

becomes a random variable that can be described only using statistical methods. In other words, the apparent precision of prediction of response offered by large computational models of complex engineering structures is illusory at frequencies where more than a few modes contribute significantly to the response [Fahy, 1994].

As an illustration of this point, the cabin acoustic response due to an external force input was measured on 98 nominally identical automobiles coming off the same assembly line. Measured variations in the acoustic response from vehicle to vehicle were as high as 20 dB above a few hundred hertz [Kompella and Bernhard, 1996]. Thus, refining a deterministic model based on a single vehicle could produce prediction errors as large as 20 dB when applied to a second vehicle. This variability is most pronounced at high frequencies, which are particularly important for rotorcraft because of gear-mesh tones and the sensitivity of the human ear at those frequencies.

In recognition of the statistical nature of the acoustic response of a cabin and the vibration response of a structure, energy flow methods that predict frequency and space-averaged responses are favored at high frequencies. The most common such method is statistical energy analysis, or SEA [Lyon, 1995]. SEA was developed in the early 1960s for modeling spacecraft response to launch noise [Lyon and Maidanik, 1962; and Maidanik, 1962], and addressed the need for simplified, computationally feasible models of the high-frequency response of structures. To apply SEA, the system being analyzed is partitioned into subsystems that represent similar energy storage modes [Lyon and DeJong, 1995]. One such subsystem for a helicopter might be the flexural modes in a large section of the fuselage sidewall, or the acoustic modes in the passenger cabin. In contrast to the usual six degrees of freedom in a finite element analysis, SEA considers only a single degree of freedom for each subsystem: the time-averaged, total vibrational, or acoustic energy. After dividing the vehicle into subsystems, energy-dissipation factors for each subsystem, energy coupling factors between subsystems, and input powers from external sources are specified. A set of equations describing the equilibrium energy balance of the entire system can then be written and solved for unknown equilibrium subsystem energies. Because the vehicle is usually partitioned into relatively large subsystems, this solution step involves few equations and requires a trivial computational effort.

However, partitioning a large vehicle into SEA subsystems is not a trivial task, and little formal guidance exists for this task [Fahy and Walker, 2004]. The analyst must leave out unnecessary detail that complicates the model and may violate SEA assumptions, while including enough detail for the results to be relevant. Subsystems must satisfy certain assumptions for the analysis to be meaningful [Lyon and DeJong, 1995; and Langley, 1989]:

- Modes of a subsystem are nearly equally excited by sources, have similar damping, and have similar coupling to modes of connected subsystems.
- Force inputs to different subsystems are spatially and temporally uncorrelated.
- For a given frequency band of analysis, the power flow and energy variables are averaged across the band, and the spectra of excitation forces is assumed constant over that band.
- Many resonant modes are contained in a frequency band.
- Coupling between subsystems is conservative and light.

Each SEA subsystem is assumed to receive, dissipate, and transmit energy, hence, a critical part of SEA is the specification of loss factors that quantify these energy relationships. Commercially available software packages provide some help with these loss and coupling factors by providing libraries of standard structural components and coupling loss factors for common structural and acoustic joints and interfaces. However, unique joints or structural interfaces may require measurements or additional analysis, with numerous parameter updates before the analyst is confident in the model.

The subsystem approach of SEA leads to a low-order vehicle model that is easily solved to determine equilibrium subsystem energies resulting from input energies specified by the user. However, the cost of this simplicity is the loss of information on spatial variation of energy within a subsystem. The coarseness of the average energy results produced by an SEA model relative to a traditional finite-element analysis can be disconcerting to those unfamiliar with SEA. Nonetheless, the approach can be useful for providing guidance on potential vibration or acoustic problem areas during the early design phase where specific geometrical details may be vague. The approach can also be used to provide insight into energy flow in an existing structure using experimentally measured response data, and thereby provide guidance on methods to reduce unwanted energy flow using computational models instead of expensive experimental testing.

Recent research in SEA methods has involved the middle frequency range, where some structural components respond with low-frequency behavior (few modes contributing to the response) while other components respond with high-frequency behavior. A hybrid finite-element (FE/SEA) approach has been proposed, where finite elements are used to model the low-frequency components, and determine power inputs to the high-frequency components that are modeled using SEA [Langley and Bremner, 1999]. Other research involves adapting SEA methods to periodic structures such as a conventional aircraft fuselage [Jayanchandran and Bonilha, 2003; Cotoni et al., 2007; and Langley et al., 1997].

Actuators for interior noise control

Active noise and vibration control has been the subject of much attention during the past decade in the helicopter industry. This approach is particularly suited to the tonal-noise environment found in a helicopter. Much of this research focused on either reducing vibrational inputs from the transmission to the rotorcraft frame for cabin quieting [Sutton et al., 1997; LeHen et al., 2005; and Millott et al., 1998], or reducing noise radiated into the cabin from vibrating trim panels [Maier and Tewes, 2005; and Mathur et al., 2002] (these trim panels are generally excited by power-train vibrations). Laboratory results of this research have been promising, but there appear to be relatively few success stories of these systems installed on production helicopters. One exception is the Sikorsky S-76 helicopter, which has an active vibration-control system to reduce transmission noise [Millott et al., 1998]. Anecdotal evidence suggests that many active noise- and vibration-control projects have been discontinued after initial studies showed less-than-expected performance. It should be noted that active noise-control systems have been successfully applied to turboprop passenger aircraft, such as the Bombardier Dash 8 Q400.

Past investigations of active control for helicopters, and Sikorsky's current system, are generally based on a feed-forward noise-control approach [Elliott et al., 1987]. With this approach, a reference signal that is highly coherent with the offending noise field is measured somewhere in the vehicle.

An example of a suitable reference signal depends on the type of noise field: for noise from rotating shafts, a good reference is a once-per-revolution sensor on the shaft. For gear-mesh noise in a transmission, a suitable reference signal is a once-per-revolution sensor on the gear shaft or an accelerometer on the transmission housing. This reference signal is adaptively scaled, in amplitude and phase, by the control algorithm and the resulting signal is amplified and sent to actuators, which might be loudspeakers in the cabin, inertial force shakers at the gearbox mount points, or piezoelectric patches on trim panels. Error sensors, such as microphones in the cabin or accelerometers on the structure, are used by the adaptive-control algorithm to optimize the amplitude and phase adjustments made to the actuator input signals.

This type of feed-forward–based control system, and its variants, has been extensively studied [Elliott, 2000], but successfully applying the technology in the real world is not simple. Wires for sensors and actuators must be routed in the vehicle; actuators and sensors must be robust to environmental variations and allow for easy maintenance and replacement; and the entire system must perform better than an equivalent weight of passive treatment. The performance of an active system generally scales with the number of actuators and sensors, but more actuators and sensors means more computational resources, wiring, and power required. In addition to these hardware considerations, the high-frequency nature of helicopter interior noise creates additional complications. The helicopter cabin can have several hundred acoustic modes at high frequencies, hence loudspeaker-based noise cancellation systems tend to create very small quiet zones at the expense of increased global sound levels in the cabin. System response in the higher frequency range can be very sensitive to small structural variations, including the effects of temperature. Since a model of the frequency response is generally required for feed-forward noise-control systems, this model must be capable of online updating as conditions change, or the control system should be carefully designed to avoid being overly sensitive to these environmental changes.

Because of these issues with feed-forward noise control, an alternative approach based on collocated actuator and sensor pairs to dissipate energy in local structural vibrations has been studied [Elliott et al., 2002; MacMartin, 1996; and Gardonio et al., 2002]. An example of a collocated actuator and sensor pair is a force actuator and a sensor that measures the velocity of the structure at the point of the force input. With such an arrangement, a very simple feedback control loop can be implemented that, under certain conditions, is guaranteed to dissipate vibrational energy in the structure. This dissipative behavior is robust to environmental and structural variations. This control approach is often referred to as a decentralized approach, in contrast to the centralized approach of feed-forward control. The term centralized refers to the fact that in feed-forward control, all actuators and sensors are wired to a single computer, which then considers all of the sensor responses in order to determine the globally optimum actuator inputs. The decentralized approach is characterized by many actuator and sensor pairs that are not globally connected. Each decentralized actuator/sensor pair reduces only the local vibration response of the structure. The decentralized approach requires fewer wires and has simple computational requirements, but because it acts like additional structural damping, the approach generally does not reduce global or forced vibrations as well as a centralized approach. In practice, performance and robustness of the local-control approach can be limited by practical issues such as actuator and sensor dynamics, filter responses, and sampling delays if the controller is implemented digitally.

An experimental investigation of a practical implementation of the local-feedback approach for the reduction of radiated sound from a panel is described by Elliott et al. [2002]. The authors measured reductions in radiated sound power of 9 dB from a single panel using a 4 x 4 array of actuator/sensor pairs. The results indicated the need to carefully adjust the feedback gains in each control loop, especially if the ultimate goal is the reduction of sound radiation from the structure, because minimization of the kinetic energy at multiple points on the panel does not necessarily correspond to a minimization of radiated sound power.

Examples of current predictive capabilities for interior noise

The current state-of-the-art prediction capability for high-frequency rotorcraft interior noise is provided by SEA. As discussed earlier, SEA was developed nearly 50 years ago in order to provide a computationally feasible approach to modeling the high-frequency vibration response of structures. The foundation of the approach has not changed in those 50 years: the net power flow between two coupled systems is proportional to the difference in stored energy in the systems multiplied by a power-transfer coefficient, or coupling factor [Fahy and Walker, 2004]. In addition, the fundamental assumptions of SEA have not changed, hence advancements in computational capabilities since the birth of SEA have not necessarily enabled more complex SEA models. What has changed is that the community of practicing SEA engineers has accumulated techniques and standard practices for computing or measuring dissipation and coupling factors between subsystems, and has developed hybrid SEA methods to analyze systems that do not satisfy all SEA assumptions. One particular example is recent work to couple modally dense systems and systems with nonmodally dense systems [Langley and Bremner, 1999; Jayachandran and Bonilha, 2003; and Cotoni et al., 2007].

As a result, the successful application of SEA today depends on the same factors that determined a successful application 50 years ago: partitioning the system into subsystems that satisfy SEA assumptions, and specifying accurate energy-dissipation and energy-coupling factors within and between subsystems. Neither of these tasks is trivial, and there is a noted lack of formal guidance on how to best accomplish the partitioning task [Fahy and Walker, 2004]. The skill and experience of the practitioner is important, and SEA models of real structures are often updated and validated using experimental measurements on the structure. As with any numerical model of a production vehicle, SEA helicopter models are proprietary, as are the interior-noise and structural-response data used to develop and validate those models. This situation complicates the task of assessing prediction accuracy of these models. Nonetheless, some reports in the open literature provide insight into the accuracy of the method for the interior noise problem. The widespread use of SEA by the automotive, launch vehicle, commercial airliner, and helicopter industries provides some indirect validation of the value of the approach.

The most detailed description of SEA model development and validation for helicopter interior noise and vibration is found in a series of NASA contractor reports written over 20 years ago [Yoerkie et al., 1983, 1986a and 1986b]. The reports describe an SEA model of a Sikorsky S-76 helicopter that was used to evaluate and optimize a cabin-noise-control treatment. In spite of its age, the method described in the report largely corresponds to the state of the art today for interior noise prediction. The reports provide valuable insight into the subsystem partitioning task and determination of coupling-loss factors, both of which are critical for prediction accuracy.

The S-76 SEA model was developed using a procedure typical for modeling an existing vehicle where the modeler can update and validate the model using laboratory measurements on the vehicle. First, an SEA model was created by partitioning the airframe and acoustic spaces into 95 subsections by considering structural discontinuities (intersections between the skin and the frame, and intersections between frame sections). These subsections were further divided into 130 subsystems based on the likely types of energy propagation within the subsections. Junctions were specified between the subsystems, with the net result that the cabin acoustic space interacted with 110 subsystems in the model. Once the basic model was created, laboratory tests were conducted to determine accurate coupling-loss factors between subsystems and to validate modeling assumptions at frame junctions (i.e., energy coupling at complex joints). The entire analysis, as reported, concentrated on the vibratory and acoustic response at four octave-band-center frequencies: 500, 1000, 2000, and 4000 Hz. These frequency bands contain several gear-mesh tones in the S-76, and also constitute the range where the ear is most sensitive. Laboratory-measured frequency-response magnitudes and SEA predictions showed good agreement (within 10 dB) at the four octave-band-center frequencies.

Once the basic SEA model was updated and validated, further ground testing was done to collect frequency responses between force inputs at gearbox-attachment locations (which were assumed to be a significant source of power input to the structure) and panel-vibration responses. In-flight measurements were then made of the same panel-vibration responses as on the ground, and used to determine the actual in-flight power input at the gearbox mounts, since safety and complexity precluded the direct measurement of this in-flight input power.

The resulting computed in-flight gearbox input powers were used as inputs in the full SEA model to predict in-flight cabin interior acoustic levels. The predicted interior sound pressures and measured levels at the four octave-band-center frequencies, 500, 1000, 2000, and 4000 Hz, are shown in figure 3.16. SEA predictions of the average cabin sound pressure level are indicated by the + symbols. In order to compare this spatial average with measured data, several point pressure measurements in the cabin were averaged. The resulting measured spatial averaged is indicated by the square symbols in the plot. SEA slightly underpredicted the average measured sound pressure at the 500- and 1000-Hz bands, and slightly overpredicted the measurement at the 2000- and 4000-Hz bands. The maximum and minimum sound pressures at the measurement locations at each frequency are indicated by the diamond and triangular symbols, thus illustrating some of the spatial variation in sound levels within the cabin. The data show spatial variations about the average sound level of approximately 5 dB. At the far right of the plot, the SIL-4 level is shown, which is the speech-interference level averaged across the four octave-band-center frequencies. This metric provides some indication of how much the interior noise affects speech intelligibility. The symbols on the right indicate excellent agreement between predicted and measured average SIL-4 levels. These results illustrate the averaging inherent to SEA; levels are averaged over both space and frequency. Whether the spatial variation is important depends on the structure and frequency range. As the modal density of the structure or acoustic space increases in the frequency range of interest, the spatial variation of the response (either vibrational or sound pressure) should lessen. Nonetheless, the spread between the maximum and minimum measured sound pressures in figure 3.16 illustrates the variation that can be expected in a helicopter cabin.

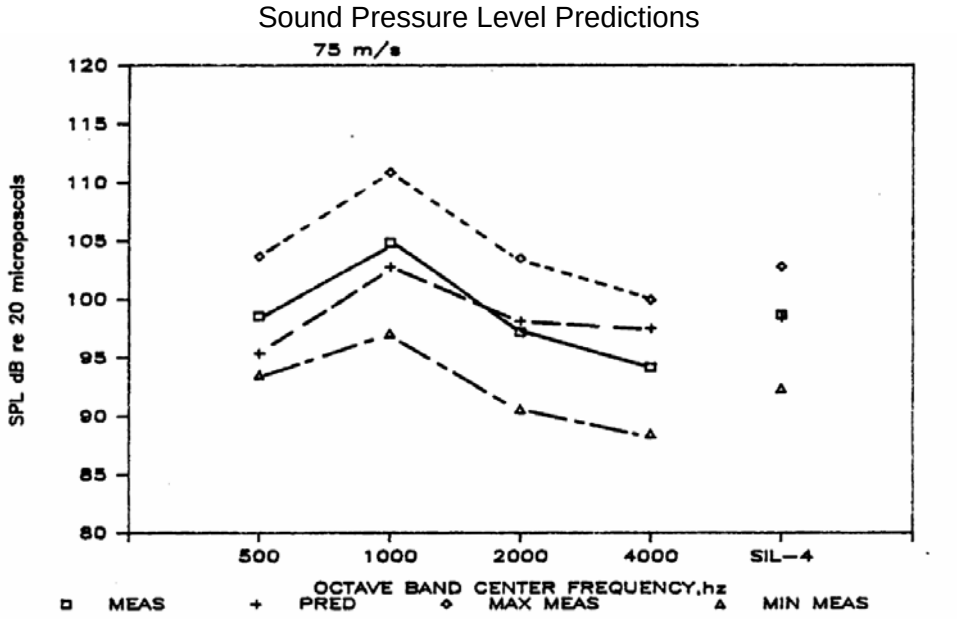

Figure 3.16. S-76 interior noise prediction using SEA [Yoerkie et al., 1986].

The authors of the S-76 report concluded that SEA provided a good description of energy flow in the structure using a relatively simple computational model. The model allowed them to understand energy flow within the structure and study treatment options for reducing interior sound levels.

A more contemporary SEA analysis for rotorcraft similar to the S-76 analysis is described by Cenedese et al. [2007]. The authors used SEA to model cabin noise in an AugustaWestland A109 helicopter. They relied on a combination of analytical and experimental modeling to tweak the SEA model to improve the correlation between modeled and measured values. As with the S-76 study, a primary goal of the model was to accurately describe energy flow paths from the gearbox mount points to sound pressure levels in the cabin. Once validated, the SEA model was then used to study noise-reduction solutions. Results of the model validation are shown in figure 3.17, which shows sound pressure levels at 1/3 octave-band-center frequencies from 400 to 3150 Hz. Average, measured sound levels are indicated by the dashed red line, while SEA predictions (for two modeling assumptions) are indicated by the solid blue lines. The predictions and measurements were made for a bare cabin configuration with no acoustic treatment. The dashed lines in the plot indicate 5-dB increments in sound pressure level. The data in the figure show the model agreed with measurements to within ±3 dB, except at 500 Hz.

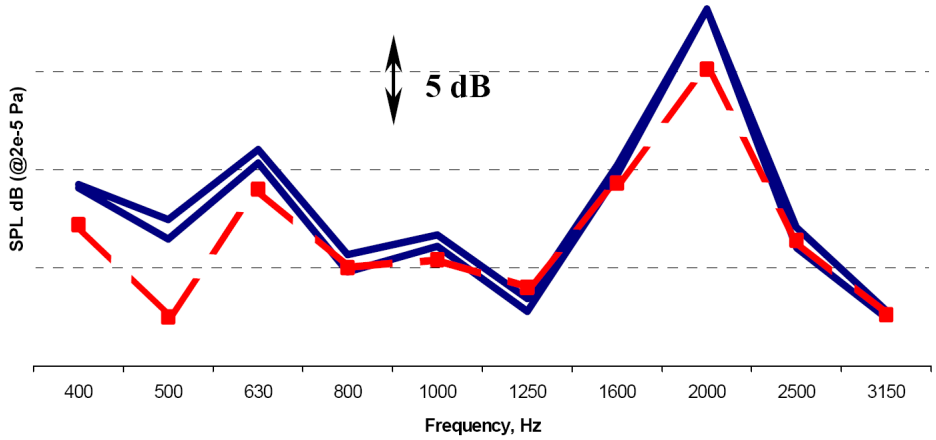

Figure 3.17. AgustaWestland A109 interior noise prediction using SEA (from Cenedese et al. [2007].

While relatively few other examples can be found in the literature of SEA applied to the entire rotorcraft, references can be found describing SEA predictions of component responses or systems of components found in aircraft and rotorcraft [Cotoni et al., 2007; Lin, 1999; and Langley et al., 1997]. Two of particular relevance to rotorcraft describe SEA for modeling a sidewall section of a Sikorsky S-92 [Bonilha et al., 2000], and a hybrid modal/SEA approach for modeling low-frequency noise in an S-92 cabin mockup [Jayachandran and Bonilha, 2003]. In the sidewall section study, SEA was used to predict transmission loss and space-averaged sidewall-vibration responses to acoustic and structural excitation of a sidewall section that included two windows, a trim panel, and sound insulation between the airframe and trim. One goal of the study was to use as little experimentally derived coupling information as possible, in order to illustrate the potential use of SEA on a structure that exists only on paper. To this end, only damping-loss factors were measured, while all other coupling-loss factors were computed analytically. The transmission loss of the sidewall assembly was predicted within ±3 dB from 50 to 8000 Hz, although there were some modeling discrepancies below 250 Hz when the vibration responses of individual components of the sidewall assembly were examined.

The cabin mockup study [Jayachandran and Bonilha, 2003] illustrates a hybrid SEA/modal analysis, where SEA was used to model the response of the structure while a modal model was used for the cabin acoustics. This approach was used because the structural response was modally rich at frequencies where the cabin acoustic response was not modally rich. As a result of the low modal density of the cabin response, a pure-SEA model of the entire system was hypothesized to be inaccurate at low frequencies. In this hybrid SEA/modal approach, the sidewall-vibration amplitudes predicted by SEA were used as inputs to the interior acoustic-modal-response model. One advantage of this approach was that it enabled the authors to predict spatial variation of the cabin acoustic field, although the predictions were limited to below 500 Hz. The agreement between measurements and predictions was generally within ±3 dB above 40 Hz.

Plans for improving predictive capabilities

Although the results described in the previous section showed generally good agreement between SEA interior noise predictions and measurements, there are at least three areas where current predictive capabilities can be improved:

- predicting the spatial variation of energy within a structure or acoustic space
- predicting high-frequency acoustic and vibration responses directly from a finite-element model
- predicting energy flow within sandwich composites, and between metallic and composite sections of the airframe

Information on spatial variation of energy within a structure can provide detailed insight into energy flow in a structure, and therefore be useful for evaluating localized damping treatments and optimizing the location of a damping treatment (passive or active). The second area for improvement is driven by the desire to integrate interior acoustic requirements into the vehicle design process. A high-frequency interior noise-prediction method that can use models generated for other disciplines, such as low-frequency vehicle dynamics, could allow greater integration of interior acoustic considerations into the vehicle design stage. The third area relates to future rotorcraft structures that may contain exotic composite laminates or sandwich components, and combinations of composite and metallic components.

An alternative high-frequency prediction method that addresses the shortcomings of SEA was developed recently and is called energy finite-element analysis, or EFEA [Bouthier and Bernhard, 1995b]. EFEA assumes the vibrational energy flow vector in a structure is proportional to the gradient of the energy density in that structure [Bouthier and Berhnard, 1995b; and Langley, 1995]. By averaging the energy density over time and local space, a relatively simple differential equation that relates energy density and intensity can be derived that resembles Fourier's law for heat conduction [Smith, 1997]. This differential equation can be solved using traditional finite-element methods, so the subsystem partitioning required for SEA is not needed for EFEA, and predictions can be done using existing finite-element models and solvers. In addition, EFEA predicts energy levels at the detail of the finite-element model, so the spatial variation of energy in a structure or acoustic space can be studied at a greater level of detail than is provided by SEA. It should be noted that even though EFEA can use a finite-element model, the user or software must still specify energy-dissipation factors and coupling-loss factors between elements, so this step has not been eliminated.

EFEA is not a technology without risks, however. The method is relatively young, with principal development having been done in the early 1990s [Wohlever and Bernhard, 1992; and Bouthier and Bernhard, 1995a and 1995b], and it has yet to gain wide acceptance. The underlying conductivity model for EFEA has been criticized as being insufficient to accurately describe the spatial distribution of energy density in a two-dimensional structure, particularly for a point-excited plate [Langley, 1995]. A solution to that particular criticism is to use a hybrid EFEA approach that divides the structural response into a reverberant field and a direct field, with different modeling approaches for the corresponding energy distributions in these fields [Smith, 1997]. For lightly damped structures, EFEA and SEA are likely to offer the same prediction results, since the vibration or acoustic response is predominantly reverberant and uniform in this case. The principal strength of EFEA is primarily for spatially varying response fields, as occur when a structure is heavily damped, or when localized damping is applied to a structure [Smith, 1997].

Plans for improving high-frequency prediction of vibration and acoustic response are focused on validating EFEA and documenting the relative strengths and weaknesses of EFEA and SEA for excitations and structures relevant to rotorcraft interior acoustics. Plans also include extending the capabilities of EFEA to model vibrational propagation in sandwich composites, and combination composite-metallic structures. The first step in validating EFEA is to compare EFEA predictions of the vibration response of a stiffened metallic structure due to a point-force input on the structure. The same comparison will be done on a stiffened composite structure. Accurately predicting the vibration response of built-up structures, such as those used in helicopters, is needed in order to predict the sound radiated from such a structure. The prediction will be considered accurate if it is within ±3 dB of measured results when averaged across 1/3 octave bands. Prediction discrepancies that exceed ±3 dB will be investigated and documented. The ability of EFEA to correctly model spatial variation in the response will also be documented.

It is important that EFEA also model the coupling between a stiffened structure and an enclosed acoustic space. Hence, validation plans include using EFEA to predict interior sound pressure levels in a stiffened composite cylinder excited by one or more point-force inputs. Fiberglass or foam-absorber material may be added to the interior of the cylinder to reduce the effect of acoustic resonances of the interior space.

If EFEA appears to be a viable and valuable alternative to SEA for interior noise prediction, the methods will be compared using data collected on a more realistic rotorcraft structure. A common approach for collecting such data in a laboratory setting is to instrument the interior cabin of a helicopter with microphones and attach an inertial-force actuator to the gearbox mount points. The interior acoustic response due to force inputs can then be measured and compared with predicted values.

Plans for improving the performance of a collocated active control system are focused on periodic arrangements of piezoelectric shunt circuits. Periodic structures are known to have a frequency-filtering property, whereby energy in certain frequency bands is reduced while energy in other bands passes through unattenuated [Richards and Pines, 2003]. The work in this area will look at optimal arrangements of negative-capacitance piezoelectric shunt circuits to create a periodic structure with tunable attenuation bands [Cunefare, 2006]. The resulting periodic structure can be used to disrupt energy flow from vibrating power-train components to the passenger cabin.

Gear and Drive-Train Noise

Cabin noise is a major concern to manufacturers and users of helicopters. Modern helicopter transmissions may operate with input speeds of 20,000 rpm. In addition, helicopter designers strive to keep weight to a minimum. High speed and low weight, with resulting high power density, make transmission noise a major problem. Much of the noise originates in the gear meshes. The noise travels by various paths into the helicopter crew and passenger compartments, where it contributes to fatigue and hearing loss.

One of the significant noise paths is from the gear mesh, through the transmission shafts and bearings, into the transmission case. From there it may travel through the transmission mounts into the

airframe structure, or be radiated through the air. There are two major research areas involved when addressing rotorcraft transmission-generated cabin noise. The first research area is the actual modeling of the gear-mesh vibrations through the shafts and bearings to the transmission housing and structural supports. The second area is the development of technologies to reduce the gear-mesh–generated vibration transmission to the structure.

Numerous papers have been published on the development of techniques to model the vibration transmission through bearings and housings. An extensive review of gear-housing dynamics and acoustics literature was published by Lim and Singh [1989]. In this review, they note that gearbox vibration and noise are due to transmission error, which is a measure of the accuracy with which the driven gear follows the driver gear. Transmission error is due to imperfection in gear manufacture, and also to elastic deformation of the gear teeth as they move through mesh. Transmission designers strive to minimize the error, but it can never be eliminated. The vibration frequency of transmission error is the gear-mesh frequency and multiples thereof, and also sidebands of these frequencies; that is, the mesh frequencies plus or minus the gearbox-shaft frequencies. Lim and Singh followed their literature survey with a five-part study of vibration transmission through rolling element bearings [Lim and Singh, 1990a, 1990b, 1991, 1992, and 1994]. In these papers, they note that bearing translational properties alone do not adequately explain how vibration is transferred from the rotating shaft to the transmission case. They propose use of a 6 × 6 matrix of bearing stiffness (including cross-coupling coefficients), which includes radial, angular, and axial motion. They calculate stiffness matrices for one example each of ball and roller bearings. Liew [2002] and Liew and Lim [2005] calculated the time-varying bearing stiffness as the balls orbit in their track. The authors termed the new analysis a “slight improvement” over earlier work. Joshi [2004] refined the elastic contact analysis to include deformation of the raceway as well as the ball. He also calculated the time-varying bearing stiffness due to ball orbiting. Royston and Basdogan [1998] analyzed spherical rolling-element bearings, also including the cross-coupling terms. In this case, the bearing has no angular stiffness. Bearing damping was not considered in any of these analyses, but it is usually assumed to be very low [Royston and Basdogan, 1998; and Zeillinger and Köttritsch, 1996]. Fleming [2002] conducted a study in which the effects of bearing translational stiffness and damping on transmission error were investigated. In this case, static transmission error was given; proper choice of bearing properties reduced dynamic transmission error up to 10 dB. Transmission-case flexibility was not accounted for.

The second major area of research in gear-mesh–generated cabin noise is the development of technologies to reduce the generation or transmission of this vibration. One approach taken is to reduce the vibration at the source by modifying tooth geometry. A computer model (DANST) was developed to predict the static transmission error, dynamic load, and tooth-bending stress of spur gears as they are influenced by operating speed, torque, stiffness, damping, inertia, and tooth profile [Oswald et al., 1996]. An extensive computer simulation was conducted using DANST to investigate the effectiveness of profile modification for reducing dynamic loads in gear [Padmasolala et al., 2000]. Both linear and parabolic tooth-tip relief were used in the analysis. Results show that linear-tip relief is more effective in reducing dynamic loads on gears with small spacing errors but parabolic-tip relief becomes more effective as the amplitude of spacing error increases. In addition, it was found that parabolic-tip modification is more effective for the severe case where the error is spread over a longer span of teeth.

Similarly, an integrated computerized approach was developed to design the tooth geometry of spiral bevel gears to reduce mesh and misalignment induced vibration [Litvin et al., 2002]. Studies have shown that spiral bevel gears are the main source of transmission-generated noise in a helicopter cabin [Lewicki and Coy, 1987; and Mitchell et al., 1986]. The approach used is to develop a spiral bevel tooth geometry that results in a parabolic transmission-error function that reduces the vibration caused by misalignment of the gears. Spiral bevel gears for an OH-58D helicopter transmission were fabricated using this design methodology and tested in a 500-Hp transmission test facility at NASA Glenn Research Center. The results of the tests show that a 7-dB noise reduction was achieved with the new design methodology as compared to the baseline gear designs [Lewicki and Woods, 2003]. A major drawback of using tooth-profile modification to reduce gear-mesh vibration is the sensitivity of this method to changing system operating loads and speeds.

Another approach to reduce the gearbox-induced vibration and noise in a helicopter cabin is to isolate the vibration from the structure. If gear-mesh–induced vibration can be prevented from traveling through the transmission bearings, significant quieting of the helicopter may occur. One way proposed to prevent the travel is to replace the normally used rolling-element bearings, which have very little damping, with fluid-film bearings. The much higher damping in fluid-film bearings is expected to significantly reduce vibration transmission and noise.

Fluid-film bearings have not traditionally been a consideration for rotorcraft transmissions because of inherent shaft-imbalance issues and low survivability under oil-starvation conditions. However, a new bearing with a wave geometry [Dimofte et al., 2006] has been developed that is an order of magnitude more stable than traditional fluid-film bearings. In addition, current coatings technologies have been experimentally proven to allow continued operation of the bearing under severe oil-off conditions. The current NASA gear-noise-reduction research focuses not only on developing accurate vibration-transmission modeling tools, but also on validating these tools with this new approach to vibration isolation using fluid-film bearings.

Examples of current predictive capability for gear noise

As mentioned previously, methods developed to model gear-vibration transmission through a shaft/bearing/housing system have not used accurate damping parameters in the model. To effectively model and evaluate all possible solutions to reducing and isolating helicopter gear-box–induced vibration models need to be developed that can simulate the complex damping conditions of all possible shaft/ bearing systems. A simplified model was recently developed to include stiffness and damping to evaluate the effects of gear-mesh vibration transmission through two bearing systems [Fleming, 2007]. The model developed in this study is shown in figure 3.18.

The model stems from the gear-noise rig at NASA Glenn Research Center. This rig has two counter-rotating shafts, each with a 28-tooth gear. Noise is generated by the gear mesh due to transmission error; it manifests itself as a periodic force between engaging gear teeth. This force may be resolved into a radial force on the shafts plus shaft torque; it is the radial force that is felt by the bearings and is analyzed here.

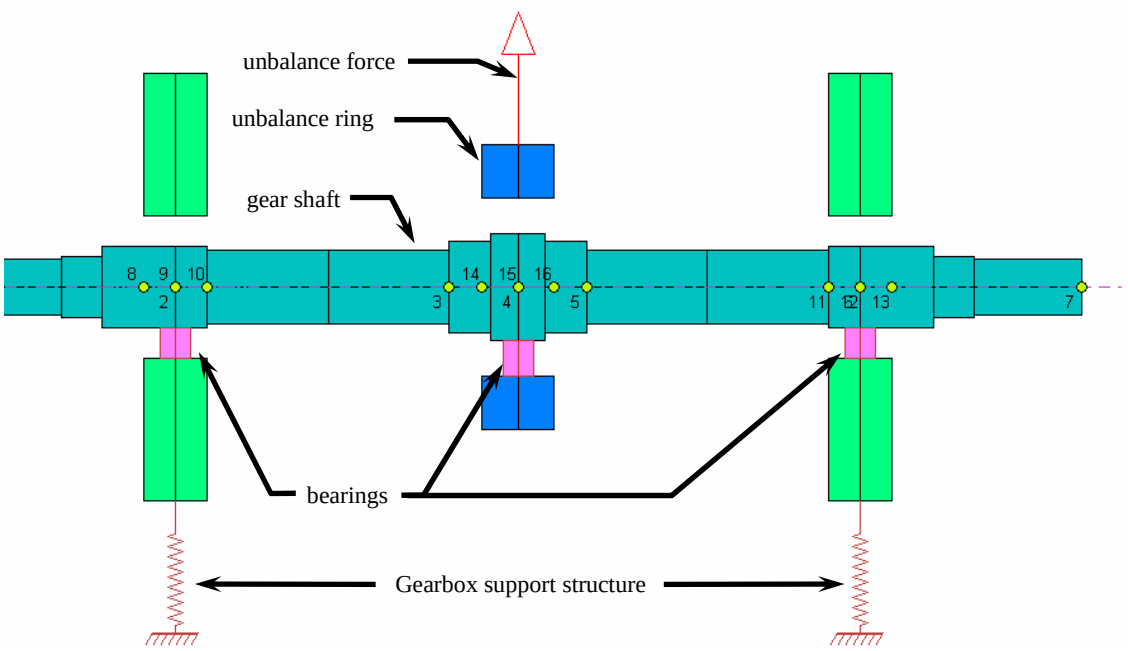

Figure 3.18. Analytical model of a shaft/bearing/housing system.

In the model, only one of the shafts is considered. Rather than a periodic radial force, an unbalanced ring (shown in blue in figure 3.18) at the shaft midspan applies a rotating load to the shaft; the unbalance force is represented in figure 3.18 by the red arrow. The ring is assumed to be very light, so that it does not affect the model dynamics except through the unbalance force. It is connected to the shaft by very stiff bearings (1.75 GN/m). Having the ring separate from the shaft allows the use of nonsynchronous excitation frequencies; for the present work, mesh frequency (28 times shaft speed) and twice mesh frequency (56 times shaft speed) were used. Use of a rotating unbalance load is obviously different than the periodic unidirectional force assumed in an actual transmission; however, the technique should be useful in evaluating the effect on vibration of different bearings.

The shaft was modeled after the one in the noise rig; however, it was made symmetric from end to end for simplicity in interpreting results. Two bearings with a span of 245 mm support the shaft. The small numerals along the shaft centerline in figure 3.18 are the station numbers of the rotordynamic model. The portions of the transmission case near the bearings are modeled by nonrotating shafts (shown as green rings in fig. 3.18). They are connected to the remainder of the case (assumed to be rigid and unmoving) by the bearings shown as the red sawtooth lines, and to the shaft by bearings shown in pink. The shaft and case-simulating rings are taken to be steel. At this point a finite-element model of the actual transmission case has not been employed; the hollow shafts representing the case were merely sized to “look” right.

Two well-known rotordynamics codes, DyRoBeS [2006] and ARDS [Fleming, 1996], were used to carry out the analysis. DyRoBeS is a Windows development of ARDS and is the more user-friendly code. However, availability of the ARDS source code allowed output to be tailored to the present application.

The first bearing type simulated was that of a ball bearing. The stiffness of the ball bearing was calculated previously by Lim and Singh [1990a] for a bearing similar to the ones traditionally used in the gear noise rig. The bearing is a 25-mm bore, light-series bearing. This size is close to one that could be used in the noise rig, so the direct radial-stiffness coefficient and direct angular-stiffness coefficient calculated by Lim and Singh [1990a] were used in the analysis. Cross-coupled coefficients were not used, nor were axial coefficients since it was assumed that the bearings do not carry any thrust load.

The other bearing type that was simulated was the wave bearing [Dimofte et al., 2006]. This bearing is similar to a full circular journal bearing, but there is a variation in clearance around the circumference that greatly reduces bearing instability tendencies. In common with other fluid-film bearings, and in contrast to rolling-element bearings, the wave bearing has substantial damping. Wave bearings were specifically designed for the noise rig; they have a 32-mm diameter and are 20 mm long.

There is some ambiguity in choosing stiffness coefficients for the wave bearing, since fluid-film bearing stiffness varies with both load and speed. The load that the bearing will experience in the noise rig is not precisely known, and the rig will operate over a range of speeds. Values of stiffness were chosen for a moderately loaded bearing corresponding to an eccentricity ratio of 0.34 and a speed of 4000 rpm. Angular stiffness coefficients for the wave bearing were not supplied; they were approximated by assuming that the bearing film pressure profile is parabolic in the axial direction. Thus,

$$K_\theta = K_x L^2 / 24$$

where L is the bearing length; angular damping was calculated similarly. Bearing properties are shown in table 3.1. The case stiffnesses were arbitrarily chosen to be the same as those of the ball bearing. Ball-bearing damping was estimated from Lewis and Malanoski [1965] and Zeillinger and Köttritsch [1996]; the radial damping is much less than that of the wave bearing, but the angular damping is comparable.

For the analysis, excitation was applied to the shaft by means of 7.2-g cm imbalance on the balance ring. Since a linear system has been assumed, the amount of imbalance is immaterial to understanding the results; the results scale linearly. Figures 3.19 and 3.20 show the “case” radial amplitude (microns) and angular amplitude (milliradians slope), respectively, for excitation at 28 times shaft speed (corresponding to the mesh frequency of the 28-tooth gears in the NASA Glenn Research Center noise rig). The angular vibration occurs because of shaft bending and the angular bearing stiffness and damping. This vibration mode is a significant means of noise transmission into the atmosphere surrounding the transmission. Both figures exhibit resonance peaks for both bearing types within the speed range plotted. The lower stiffness and higher damping of the wave bearing do not seem to confer an overall advantage regarding noise.

TABLE 3.1. BEARING AND CASE PROPERTIES

	Radial stiffness Kx, MN/m	**Angular stiffness Kθ, N m/rad**	**Radial damping Bx, kN s/m**	**Angular damping Bθ, N m s/rad**
Ball bearing	175	15	3.5	2.3
Wave bearing	46.6	0.78	144	2.4
Case	175	15	3.5	2.3

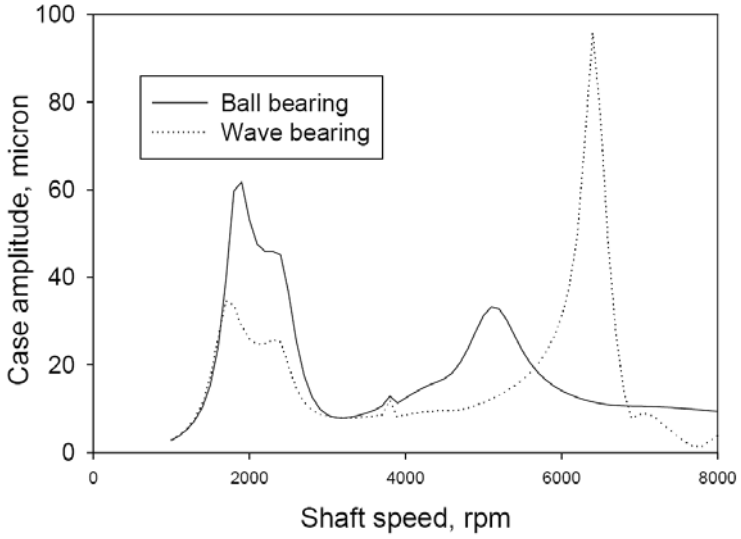

Figure 3.19. Radial vibration amplitude of transmission case for 28× excitation.

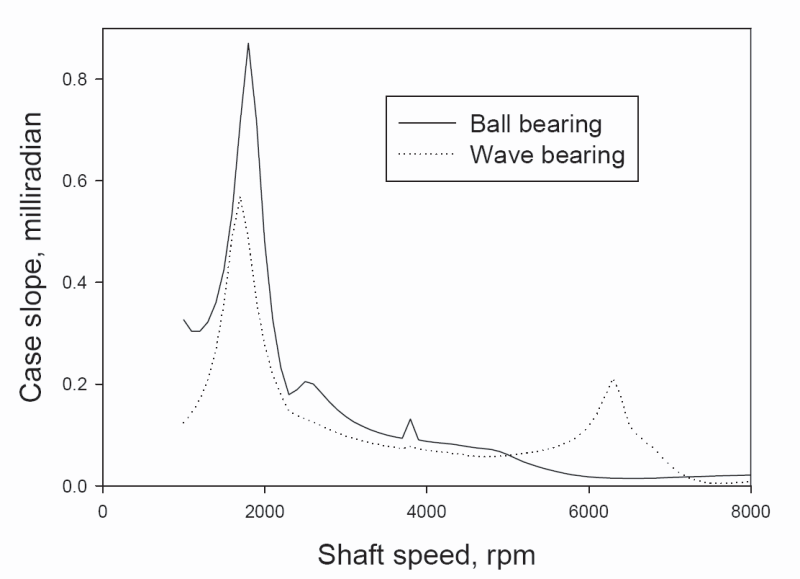

Figure 3.20. Angular vibration of transmission case for 28× excitation.

Contrary to the results shown in the figures, experimental data for rotors supported on wave bearings indicate that high-frequency vibration is effectively damped [Dimofte, 2007]. Apparently wave-bearing damping drops at high frequency in a manner that is not accounted for in the data used herein.

Plans for improving predictive capability of gear noise

Plans for improving predictive capabilities of gear-mesh–induced vibration transmission through a shaft/bearing/housing system include developing a more comprehensive vibration-transmission model that includes cross coupling effects of the shaft and bearing, and accurate damping models of the complex damping associated with fluid-film bearings.

Validation Data Requirements

Required validation data for the interior noise modeling consists of component-level vibroacoustic responses for the composite-model development and vehicle-level responses for the EFEA/SEA evaluation and trade studies. The component-level data will be used to validate energy density relations for sandwich composites and provide data on energy coupling between metallic and composite components, and composite-to-composite components (such as composite stiffeners on a composite plate). The vehicle-level data will be used for validating EFEA for vehicle-level predictions, and for comparing EFEA with SEA. These data should consist of vibration responses of important radiating components such as skin panels, in addition to the vibration response of stiffeners that conduct energy around the fuselage, and the acoustic response in the passenger cabin. These responses should be collected for point-force inputs at the gearbox-mount points. This type of excitation is felt to be the most important for interior noise, although additional studies could examine other sources such as force inputs from other power-train components, or broadband input such as turbulent boundary layer excitation.

To prepare for the vehicle-level dataset and develop confidence in basic model development and modeling assumptions, vibroacoustic data will be collected on progressively more complicated structures and enclosed spaces excited by one or more force inputs. The most basic structure will be a stiffened metallic panel excited by a point force. A typical dataset should contain measurements of the out-of-plane velocity response of the structure to a point-force input at different locations on the structure. Localized damping should be applied to the structure to create spatial variation in the response. The boundary of the structure can be either simply supported or clamped, as long as it presents a significant barrier to energy flow. Both stiffened metallic and composite structures should be tested. If the velocity-response data is collected over a sufficiently dense grid, the sound radiation from the structure can be modeled using a boundary-element method or other appropriate method. The resulting prediction of radiated sound can be compared with EFEA and SEA predictions. A candidate starting structure is a stiffened aluminum panel owned by the Structural Acoustics Branch at NASA Langley Research Center. This panel was built to resemble the stiffened sidewall of an aircraft fuselage, and contains ring frames and stringers with representative spacing and cross section. Once confidence has been gained on the metallic structure, a similar stiffened composite panel should be tested. No specific composite structure has been identified, although collaboration with a rotorcraft manufacturer would be suitable for the design and manufacture of a test article.

Beyond the stiffened panels, the next level of validation data should come from stiffened structures enclosing an acoustic space. Two such structures are owned by NASA: the first is a stiffened aluminum cylinder that is 12 feet long and 4 feet in diameter, and the second is a similarly sized filament-wound, carbon fiber cylinder with composite stiffeners. Vibration data have already been collected on the aluminum cylinder as part of a previous finite-element model-validation study, so interior

acoustic responses have to be measured to complete the dataset. Similar data will be collected on the composite cylinder and used for the composites modeling task and the vehicle-level response modeling.

The final validation dataset will need to be measured on an actual helicopter fuselage. Ground testing with inertial force shakers exciting the structure should be sufficient; in-flight data are not needed. The fuselage should be instrumented with accelerometers to measure vibrations of important structural components (those involved in the radiation of sound into the passenger cabin, or those significantly involved in energy transmission from the input source to the cabin). The cabin should be instrumented with a sufficient number of microphones to compute a spatial average sound level and to quantify spatial variation in the sound level.

In addition to the modeling effort, validation data are needed to document the performance of the periodic arrays of piezoelectric shunt circuits. These data can be collected on a simple structure such as a panel or beam, as long as the structure can be used to demonstrate the bandpass filtering properties of the shunt circuit array.

Validation of the gear-noise model will be performed using data from tests to be conducted in the gear-noise test facility at NASA using several bearing arrangements. Data required will include shaft movement, vibration in all axes at the bearing locations, experimentally obtained damping properties of the bearings under various operating conditions, sound-pressure-level noise measurements at specific locations around housing, and overall sound power integrated over a hemispherical sphere of the housing.

Cross-Cutting Technology Needs

The accurate prediction of interior noise levels will depend on accurate characterization of the materials and structures used in the fuselage and accurate specification of noise and vibration inputs to the fuselage. With respect to materials and structures, noise-prediction accuracy depends on accurate modeling of vibrational-energy density in airframe components, whether they are metallic, next-generation composite, or a hybrid of composite and metallic materials. As new material systems and structures appear in the fuselage, additional model development and validation data will be needed to ensure interior noise predictions remain meaningful. With respect to noise and vibration inputs to the fuselage, frequency ranges, levels, and types of energy will need to be specified for the interior noise model. For example, a future quiet-transmission design may produce less airborne sound radiating from the gearbox, but may produce the same vibration levels at the mount points as the old gearbox. The planned validation work on an actual helicopter fuselage should provide information on prediction sensitivity to source input levels. This information will be useful for determining the fidelity of input levels needed from power-train designers in order to evaluate the interior noise benefits from a proposed design change.

The success of periodic arrays of piezoelectric shunt circuits may depend on materials issues such as packaging, electronics miniaturization, and the structure of the helicopter. Packaging may be important for ensuring robustness of the actuator to the normal operating environment, as well as installation and maintenance. The structure of the helicopter is important since the array of shunts may be

more effective if the structure is periodic where the shunts are mounted. This setup might necessitate a change in the geometry of a stiffener near the gearbox, for example. These cross-cutting requirements should become more apparent as the period shunt technology matures.

NOISE PROPAGATION MODELING AND OPTIMIZED FLIGHT PATHS

Introduction

A key goal for NASA is the mitigation of community aircraft noise generated by rotorcraft. Progress toward this goal is enabled not only by understanding and reducing noise at specific sources (i.e., the rotor and power-train system) described in previous sections of this chapter, but also by improving propagation tools and optimized low-noise flight profiles that are incorporated into overall aircraft system noise-prediction tools. Atmospheric propagation modeling describes the effects of the atmosphere on the acoustic disturbance as it travels through the atmosphere from the source to the observer. Optimized low-noise flight procedures are critical for rotorcraft approaches but are constrained by the limits of passenger comfort and Federal Aviation Administration (FAA) helicopter rules.

The following sections discuss current NASA research in propagation modeling and optimized approaches for rotorcraft. Plans for improving predictive capability in these areas are also included.

Noise Propagation Modeling

Propagation modeling may be divided into two areas: near-field modeling and far-field modeling. NASA is addressing both areas. The goal of near-field modeling is the accurate description of the acoustic field of new aircraft designs that incorporate shielding to create quieter aircraft. The goal of far-field modeling is the accurate description of the effects of the atmosphere and terrain on the acoustic disturbance generated by rotorcraft, and using this knowledge to limit the effects of rotorcraft noise on the community.

Historically, NASA's acoustic programs have included only far-field effects and have used line-of-sight propagation techniques to propagate noise from a source to an observer. NASA's main system noise-prediction tools are Rotorcraft Noise Model (RNM) [Page, 2002] and the Aircraft Noise Prediction Program (ANOPP) [Zorumski, 1982]. RNM and ANOPP account for numerous propagation phenomena, including spherical spreading, characteristic impedance corrections, frequency corrections, atmospheric attenuation, and ground effects (which includes the reflected sound fields, interference of the reflected fields with the direct sound field, and complex impedance effects due to varying ground materials). These propagation effects have been studied and improved over many years.

Because RNM and ANOPP assume that the acoustic disturbance travels along a straight line connecting the source and the receiver, they cannot account for the effects of wind shear and temperature gradients. These effects have been dramatically observed during recent flight tests. The red

curve in figure 3.21 shows the temperature profile measured early in the morning. This profile has a positive temperature gradient (or inversion), and the blue curve shows a late morning profile with a negative temperature gradient (a standard lapse rate). These two temperature profiles produce very different sound fields. The early-morning profile bends the acoustic rays toward the ground and traps the acoustic energy in a thin acoustic duct near the ground. However, the late-morning profile bends the acoustic rays away from the ground, and the acoustic energy is transported away from the ground. The different distributions of acoustic energy are reflected in the plots of SPL vs. distance shown in figure 3.22. Note that the SPL decreases more slowly with distance for the inverted profile than for the standard lapse rate case. Both ANOPP and RNM would predict that the SPL falls off at 6 dB per doubling of distance as seen for the predicted constant temperature profile in figure 3.22.

Current tools available or in development at NASA

NASA's main acoustic codes are: (1) ANOPP (Aircraft Noise Prediction Program), which has been the standard for fixed-wing aircraft noise assessments since the early 1980s and which is maintained and continually improved as new technologies and codes become available, and (2) RNM (Rotorcraft Noise Module), which was originally a subset of ANOPP used to predict rotor noise. During the last decade RNM has been linked with advanced rotor-prediction codes (such as CAMRAD II [Johnson, 1997]), and is currently the standard code used to assess detailed rotorcraft noise.

Historically, sound propagation has been modeled by ray-tracing methods, parabolic-equation methods, finite-difference time-domain methods, fast-field methods, boundary-element methods, and more. Ray-tracing methods, the Crank Nicholson Parabolic Equation Method (CNPE), the Green's Function Parabolic Equation Method (GFPE), and a fast-field method are most frequently used to solve the propagation problem [Salomons, 2001]. Each method is obtained using its own assumptions and approximations, and each method has its own range of applicability in solving atmospheric acoustic-propagation problems.

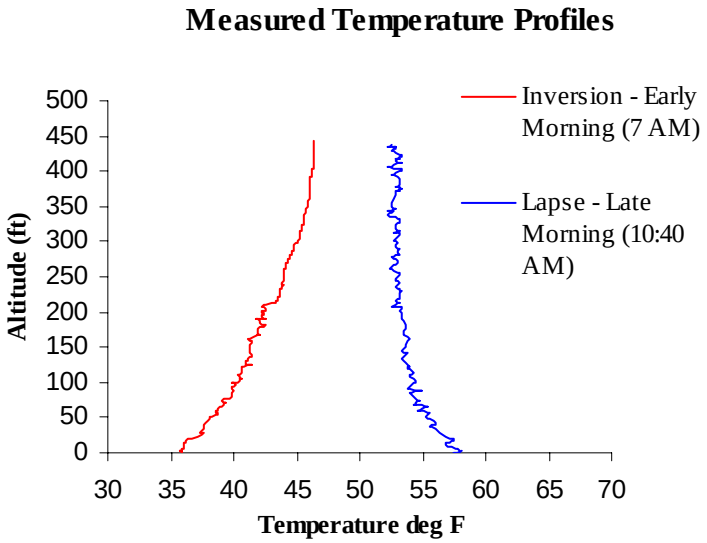

Figure 3.21. Morning temperature variations during 2005 Eglin Test.

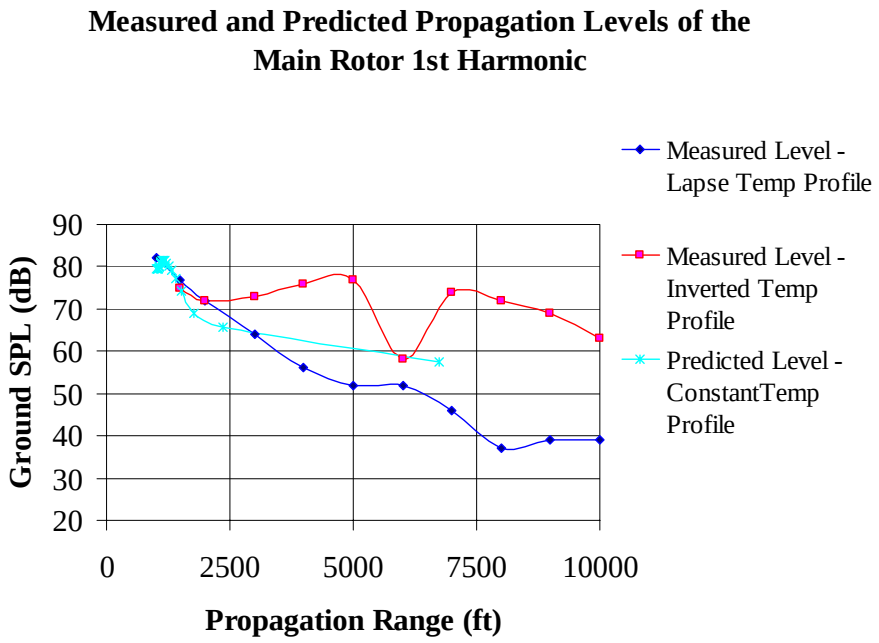

Figure 3.22. Large variances in acoustic levels are observed at propagation ranges of 5000 and 7500 feet from a rotorcraft source. These differences between the early- and late-morning sound levels are greater than 25 dB at certain ranges. The rotorcraft was flown at level conditions with a speed of 110 knots, and at an altitude of 150 ft.

NASA is currently developing two atmospheric propagation tools: a ray-tracing method (RTP) [Heath, 2007], and the GFPE through a contract with the University of Mississippi [Gilbert and Xiao, 1993]. NASA is enhancing the two methods to account for wind shear and temperature gradients, and intends to fully integrate the RTP, the GFPE, and a hybrid method combining the GFPE and ray methods with the system noise-prediction tools (RNM and ANOPP).

Examples of current predictive and testing capabilities

A ray-tracing code was developed to account for the wind and temperature gradients. While developing the ray-tracing method to account for wind and temperature gradient effects, an increased understanding of complex propagation paths and explicit characterization of ground contour patterns was obtained [McAninch and Heath, 2006].

The shadow boundary regions (or zones of silence) on the ground are characterized by an asymptotic limiting angle. This angle, which is set by wind and temperature conditions, is illustrated by examining the 1921 explosion of a chemical plant in Oppau, Germany [Mitra, 1952]. By interviewing observers on the ground, the Oppau study mapped out a complicated acoustic pattern (fig. 3.23) defining alternating audible and silent zones. Over the years, the radial patterns of the Oppau acoustic footprint have been attributed to turning (refracting) and trapping (ducting) of sound waves from a layer of air in the upper atmosphere. Instead of characterizing the radial pattern of silent zones, as was done in previous works, [Pierce, 1981; Cook, 1962; and Jones et al., 2004], NASA has identified an angle, ζ, that envelopes the audible region, as shown in figure 3.23.

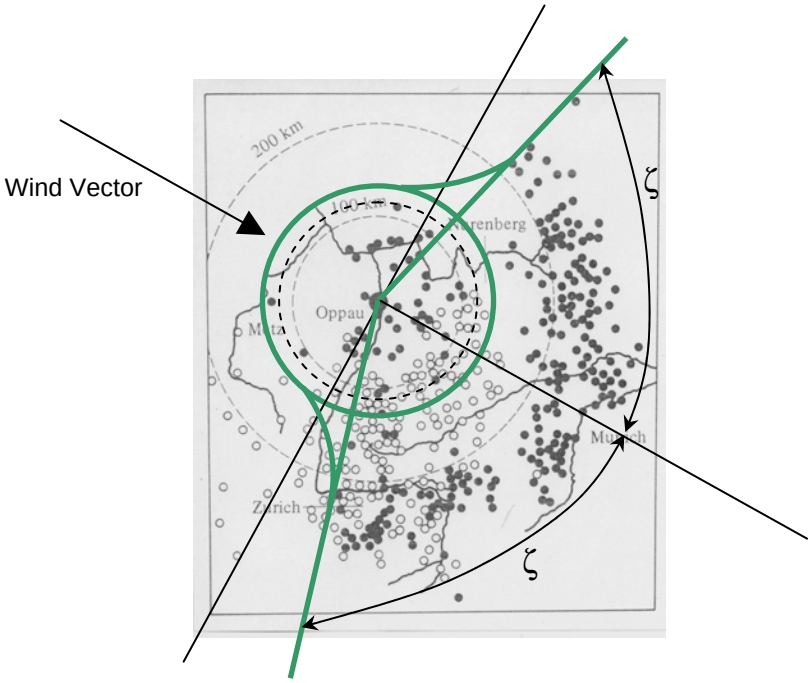

● – Explosion heard, ○ – Explosion not heard.

Figure 3.23. Results of audibility survey for a large ground-based explosion at Oppau, Germany in 1921.

This characteristic angle, ζ, is particularly useful in that it quickly defines the angular confines of the shadow boundary on the ground before any effort is put forth to trace the acoustic rays [Heath, 2006].

In addition to the characteristic angle, NASA has quantified general ground-contour characteristics apparent when including both wind and temperature atmospheric effects.

Current system noise-prediction tools assume a homogeneous atmosphere, and do not accurately capture the physics imposed by the combined wind and temperature gradients. Temperature variations within the atmosphere are described using a lapse rate, β, which is defined as the negative rate of change of temperature with altitude (–dT/dz). Standard-temperature profiles (which are described with a positive lapse rate) cause acoustic rays to refract upward, creating a shadow zone. On the other hand, inverted temperature profiles (described with a negative lapse rate) refract the ray toward the ground. For the constant temperature case, the rays are straight lines connecting the source and observer.

The acoustic field is cylindrically symmetric about a source in a stationary or uniformly moving medium, even with a temperature gradient. However, wind shear complicates the picture even when no temperature gradient is present. In this case, the rays on the upwind side of the source are refracted upward, the same as for a standard lapse rate atmosphere, while the rays on the downwind side of the source are bent downward, generating an acoustic duct, as if the temperature gradient

were positive. If both wind shear and temperature gradients exist, as, for example, in the real atmosphere, the ray picture becomes even more complicated. The combined interactions create interesting acoustic contours (including the shadow zones) that can be described using two angles (the critical emission angle and the critical shadow boundary angle, ζ) [Heath, 2006]. Figure 3.24 graphically shows the resulting ground contour for two combined wind and temperature cases. The figure was generated using the newly developed ray-tracing propagation code (RTP v1.0) [Heath, 2007].

In addition to contour characteristics, a method to identify the various propagation regions corresponding to phenomena such as ducting or evanescent propagation has been developed. Propagation characteristics within each region are determined using the Ellipse of Turning Points (ETPs) [McAninch and Heath, 2006].

Plans for improving predictive and testing capabilities

The propagation research plan concentrates on predicting wind and temperature effects, terrain effects, and multipath ray effects. Since RNM and ANOPP do not have the ability to account for these effects, two new tools are under development, the ray-tracing code (RTP) [Heath, 2007] and the GFPE code [Gilbert and Xiao, 1993].

The propagation effects of wind and temperature result in shadow zones, caustic regions, ducted regions, and numerous other multipath propagation effects. Currently, version 1.0 of RTP predicts the shadow-zone effects for single-path downward propagating rays. However, there are more phenomena (such as the dip in the Eglin rotorcraft propagation data as seen in figure 3.22 between ranges of 5000 and 6000 feet) that are believed to be the result of destructive interference between multiple rays. In order to account for these interferences, NASA is enhancing the Ray Tracing Propagation code to handle the multipath effects.

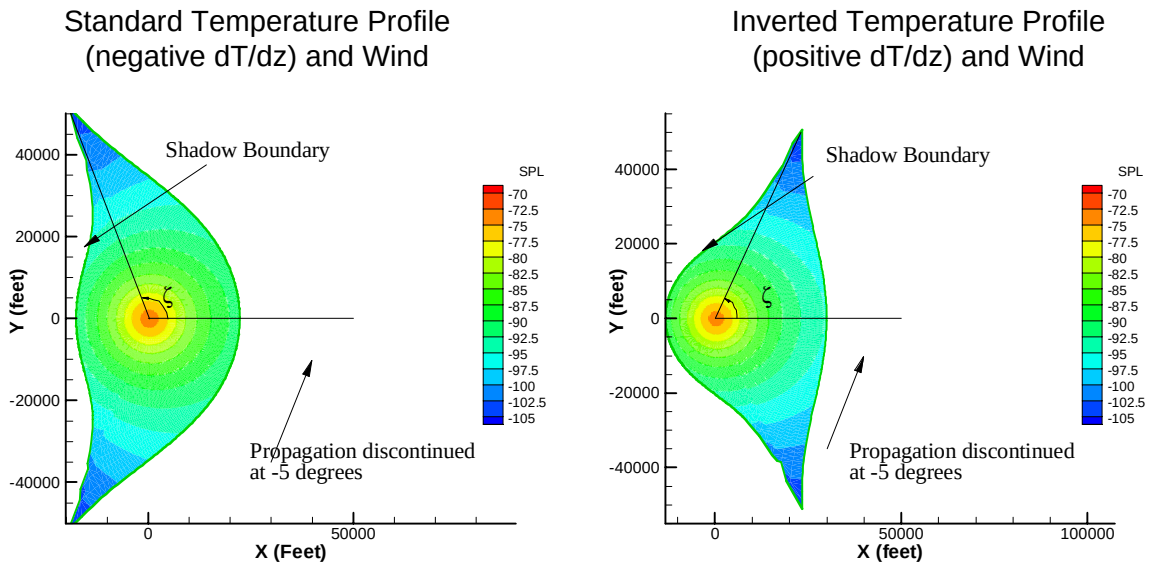

Figure 3.24. Combined wind and temperature acoustic contour levels. Figure shows acoustic contour characterization for wind and temperature gradients for a wind blowing from left to right in the frames.

Multipath rays are a direct result of reflections, and upward and downward refraction effects. The propagation phenomena include constructive and destructive interference, ray ducting and caustic zones, and some types of diffraction. The latest advances from the ETPs will be used to create an efficient multipath code.

Terrain also significantly affects propagation. Terrain may be defined as the physical ground attributes, such as mountains, hills, and valleys, or it could consist of tall buildings and skyscrapers. The uneven surfaces may cause focusing, shielding, or diffractive effects. Terrain effects may be incorporated in both the GFPE and the ray-tracing methods; however, as the codes are presently, it is available only in the GFPE method. Research will be completed to add terrain capabilities to the ray-tracing propagation code and the resulting hybrid methods. The current terrain methods are simplistic (i.e., the assumed impacting ray paths are assumed to be curved circular arcs with no flow adjustment due to terrain). Even so, the current terrain model will be used as a first approximation to terrain effects.

In order to add these phenomena, certain advances are required for the RTP and the GFPE. All ray-tracing methods are based on the principles of the geometric acoustic theory. The geometric acoustic theory [Lewis and Keller, 1964; and Blokhintsev, 1946] provides a very flexible method for the study of sound propagation in the Earth's atmosphere. The challenge is to adequately account for the physical effects desired without having to solve multiple simultaneous equations. To this end, the RTP ray-tracing code with simplifying assumptions was created. The two simplifications necessary to achieve this code creation are representation of the atmosphere as a stratified medium and representation of the atmosphere with linearly varying properties within stratified layers. RTP will be expanded to include solutions in the shadow and caustic regions, and research complex rays to explain and characterize the acoustic-ray solutions within various regions. Research in other propagation fields (such as underwater acoustics, electromagnetic, and seismology [Ceverny, 2001]) can provide valuable insight, even though they do not account for wind.

The GFPE is a two-dimensional (2-D) method based on the axis symmetric assumption [Salomons, 2001]. The GFPE provides a simplified governing equation with solutions that are easily obtained, and can account for irregular terrain and numerous atmospheric conditions (including turbulence). But the GFPE also has disadvantages. The main disadvantage of the GFPE method is that it neglects changes in the sound field due to the effects of large elevation angles with respect to the wave-front direction. Therefore, it is valid only for narrow propagation angles. The GFPE also uses an "effective" sound speed to account for flow conditions. This method further restricts the conditions at which the GFPE is valid. Advances to the GFPE and other parabolic-equation (PE) techniques, such as those suggested by Kriegsmann, and Larsen [1978], may be necessary to obtain accurate solutions.

Together the advancements in the ray-tracing and parabolic codes will enable NASA to predict low-frequency noise propagation within 5 dB of measured peak noise levels in a nonuniform atmosphere.

As seen previously both the ray-tracing and GFPE methods have advantages and disadvantages. A hybrid model will be created to automatically switch between the two methods. The valid frequency range of each method leads us to formulate a hybrid solution capturing the best of the ray methods and the GFPE methods. The ray-tracing methods are formulated based on a high-frequency assump-

tion, and therefore are best when used for higher frequencies, whereas the GFPE methods (as formulated) are better for lower frequencies. The limits of both codes are under investigation, but hybrid logic will be initially chosen based on frequency. The logic will also look at the different propagation regions (such as the shadow and ducted regions where the narrow-angle assumption of the PE methods are valid) and the parameters controlling the solution accuracies. Eventually the development of an advanced hybrid method to predict some of the more complicated phenomena by combining advanced ray and PE methods will allow the prediction of peak levels of the scattered noise fields within 3 dB of that measured.

Near-field propagation is also important in reducing community noise. Scattering of source noise from the aircraft or other interfaces near the source can be used as a shielding effect for various aircraft configurations. Recent research has been productive in this area, resulting in the first and second versions of the Fast Scattering Code (FSC) [Tinetti et al., 2006]. NASA plans to continue to advance FSC methods and capabilities, as well as to investigate lower-fidelity energy boundary methods. The following work is planned:

- Research regarding the parameter resolution within FSC is ongoing to define good parameter ranges.
- Application of FSC to applicable scattering problems will continue. This research involves linear algebra techniques using fast multipole and other methods to allow the computer to handle the full-scale geometry for midrange frequency problems.
- Optimization capabilities to assess absorbent walls are currently being added to the Fast Scattering Code. These capabilities will allow NASA to investigate various liners to aid in shielding noise sources from observers.
- The energy boundary-element formulations used in scattering problems [Wang and Wu, 2004] will be investigated. This method has advantages and disadvantages and is based on assumptions that limit the applied acoustics scattering problems.

In terms of the entire scope of the propagation problem, the near-field scattering techniques will be used to alter the source noise prior to far-field atmospheric-propagation calculations.

In summary, plans for analysis, tool development, and validation over the next 5 years will address cases for wind, temperature, terrain, and multipath effects. There is a need to gain better physical understanding of the solutions in order to yield more realistic propagation predictions. Better prediction tools will greatly impact the airport community planning tools, and will allow us to better mitigate noise exposure to the community. By developing and incorporating the research tools listed previously, the existing system noise-prediction tools will be infused with the propagation methods required to predict the 25-dB change in sound levels seen during the 2005 Eglin Acoustic Flight Test.

Optimized Flight Paths

Efforts to develop techniques whereby helicopters and other rotorcraft can “fly neighborly” have been attempted for many years with varying degrees of success [Yoshikami, 1985]. Early efforts to modify operating procedures to produce less objectionable community noise were developed using

an ad hoc approach because data were limited and rotor-noise directivity was less well-understood. In fact, most available data were based on listening and/or measurement by acousticians riding in the cockpit of the test vehicle. The guidance given to pilots was rule-based. For example, the white region in figure 3.25 indicates combinations of descent rate and speed that should be avoided in order to reduce approach noise [HAI, 1993].

By the early 1990s, efforts to develop low-noise operating procedures began to incorporate a more systematic approach. Under NASA's Short Haul (Civil Tiltrotor) program, tiltrotor noise reduction was being simultaneously attacked at the source (i.e., low-noise proprotor designs) and via operations [Marcolini et al., 1996]. The development of low-noise procedures itself used a three-pronged approach centered on the XV-15 tiltrotor aircraft. First, a detailed mapping of the noise generated by the XV-15 in a wide range of level flight and (primarily) descent conditions were acquired in a joint NASA/U.S. Army/Bell Helicopter test program [Conner et al., 1997], using measurement techniques originally incorporated on the Airloads UH-60 test program [Wilson et al., 1995]. This technique involved flying the vehicle at a constant operating condition over a linear array of microphones placed perpendicular to the flight path. The multisource, time-dependent data were then "depropagated" to produce an equivalent point source that models the noise-directivity characteristics for that particular operating condition. The technique to transform flyover data into noise hemispheres is graphically represented in figure 3.26.

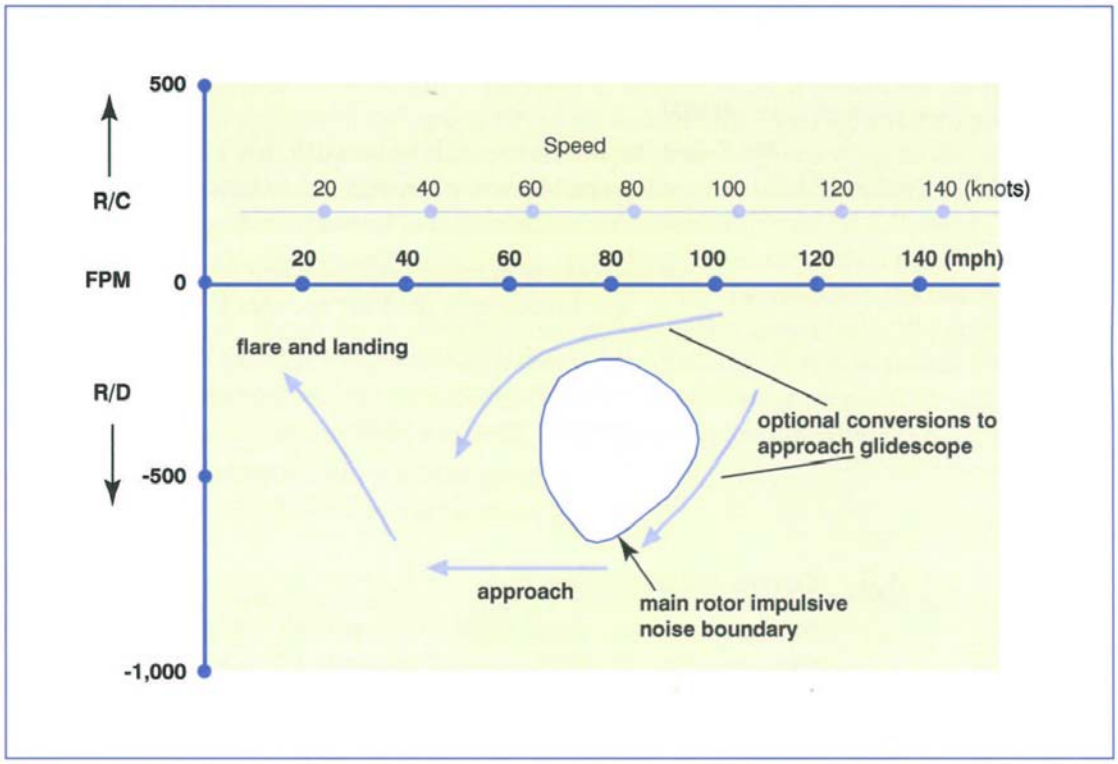

Figure 3.25. HAI Fly Neighborly noise abatement technique for light helicopters.

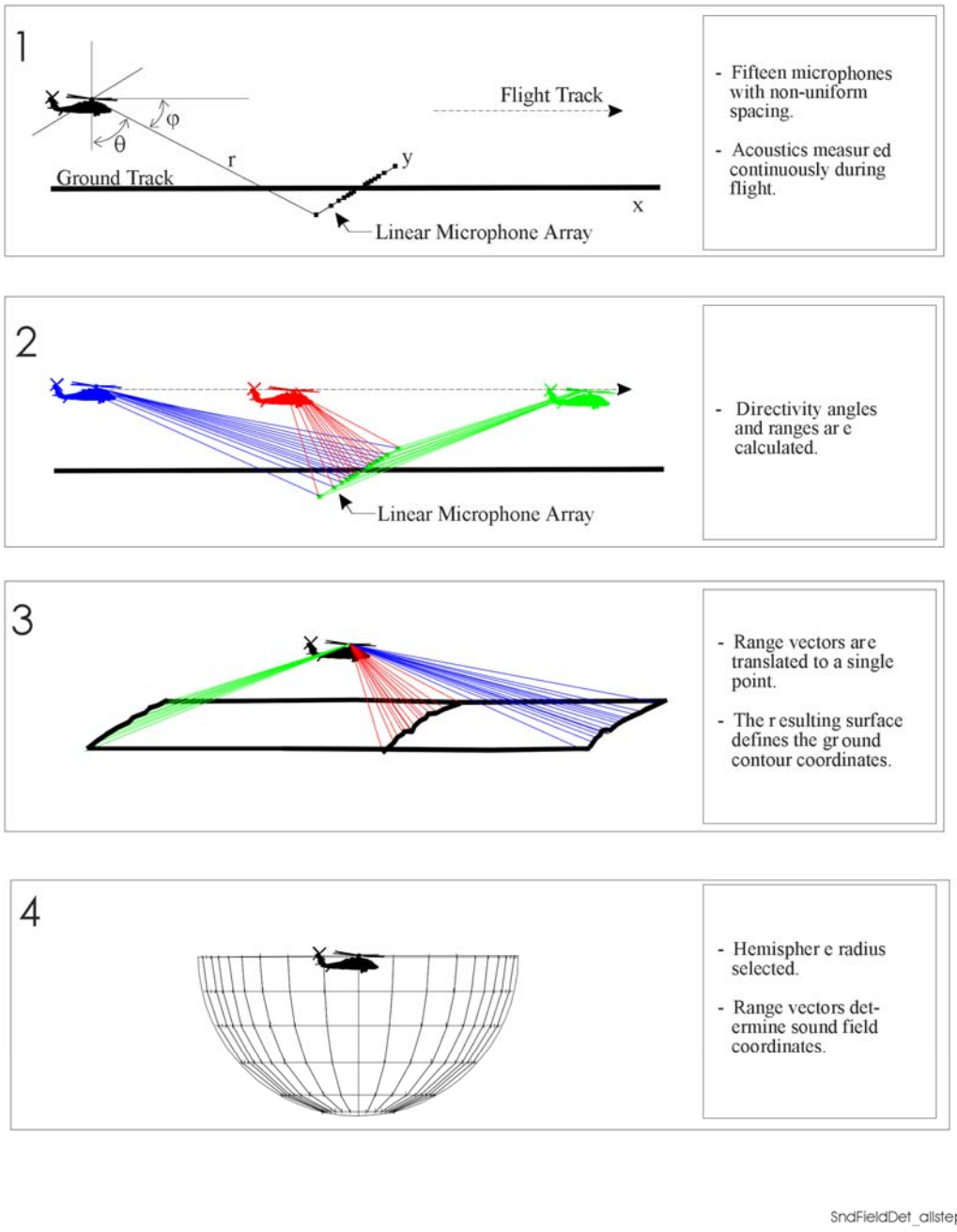

Figure 3.26. Single-source effective surface contour calculation.

The second element of this three-pronged approach was the development of the Rotorcraft Noise Model (RNM) [Lucas and Marcolini, 1997]. RNM is a tool to convert flight-track and noise-hemisphere input into community noise footprints. RNM was originally developed to take noise hemispheres from the XV-15 testing and allow the user to construct and compare candidate low-noise approach procedures.

Given a large number of measured hemispheres, constraints developed jointly by acousticians and handling qualities experts and a validated RNM modeling capability, the final step was to design approach procedures that were quiet, safe, and easy to fly. This process began by coupling RNM with iSIGHT [Padula et al., 1999], a commercially available optimization software package. The candidate procedures were then tested in the Vertical Motion Simulator at NASA Ames Research Center, and then in the XV-15 simulator at Bell. Both of these efforts were designed to produce procedures that were quiet and had acceptable handling qualities, within the limitations of the XV-15 controls system. A graphical depiction of this approach is shown in figure 3.27.

Results from the final XV-15 flight test in this series [Conner et al., 2002] demonstrated up to 10-dB reductions in sound-exposure level along the flightpath when compared with a typical 6-degree approach in helicopter mode.

Since the successful completion of the SH(CT) program, numerous improvements and refinements have been made to this basic process. In the collection of the acoustic data used to construct the noise hemispheres, a pure linear array has been replaced by a U-shaped array, with microphones on both sides of the flightpath suspended on cranes, as shown in figure 3.28 [Conner et al., 2006]. This array provides much-improved data at the shallow sideline angles, as well as more complete capturing of the directivity angles nearest to the rotor tip-path plane. Numerous refinements have been made to RNM as well, with both improved propagation modeling and a better means of interpolating between noise hemispheres being major improvements. Additionally, multidisciplinary integration and optimization software has developed new capabilities for optimizing and validating flight procedures [Padula and Gillian, 2006].

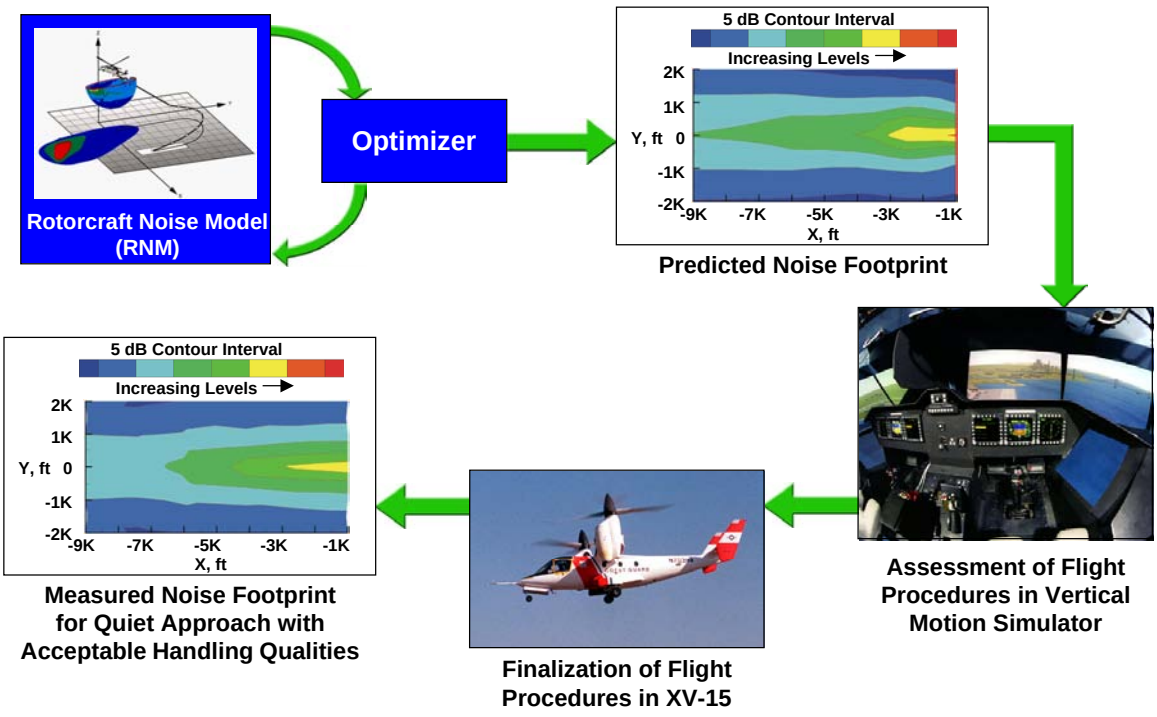

Figure 3.27. Development of XV-15 low-noise approach procedures.

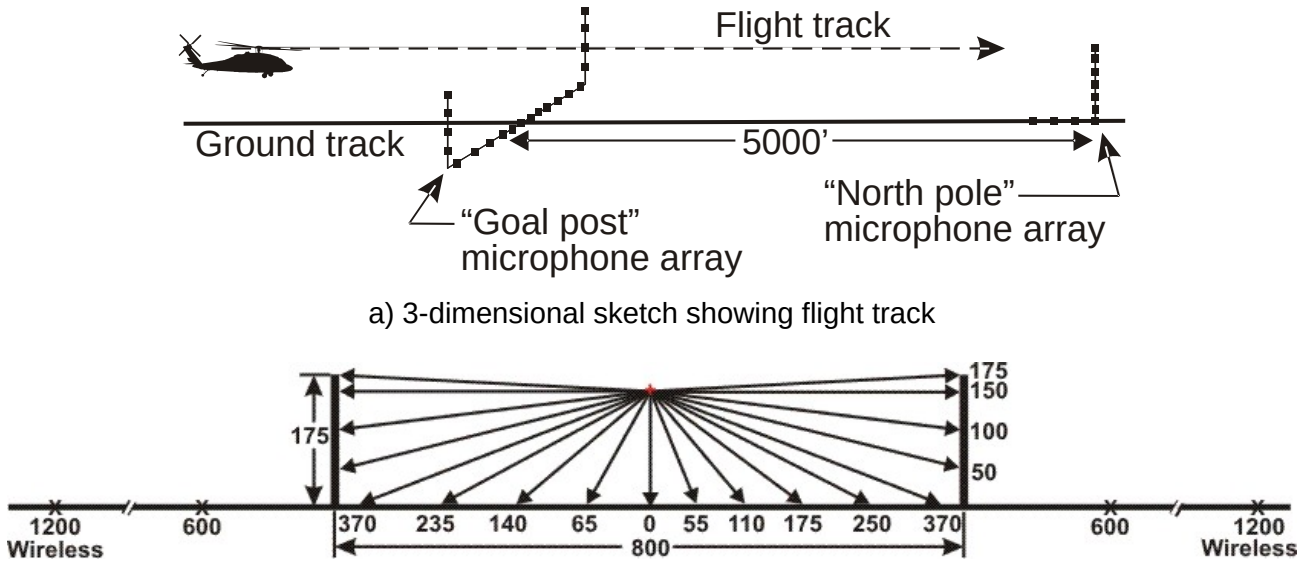

a) 3-dimensional sketch showing flight track

b) Goal post array details

Figure 3.28. Improved flyover data collection array.

Limitations of the process used in the XV-15 testing and acoustic predictions are now being addressed. Most notably among them is the incorporation of limited unsteady effects (decelerations, turns, etc.) in the approaches [Schmitz et al., 2007]. Challenges facing the inclusion of maneuvering flight into low noise profiles include properly quantifying the relevant parameters for optimization and then developing a method of testing to acquire data for those parameters. Finally, it must be recognized that the "Holy Grail" of low-noise flight-procedure design will not be achieved until it is no longer necessary to use measured noise hemispheres. Efforts to improve first-principles rotorcraft noise-prediction capability have been under way for many years, and dramatic improvements in capability and understanding have been achieved (for details on these efforts, see the Noise Prediction section of this chapter). Still, we have not yet reached the state where we can design low-noise procedures based solely on predicted hemispheres. These plans will enable the development and validation of low-noise flight procedures within 5 dB of maximum contour-area level.

Validation Data Requirements

Propagation validation has been a topic of discussion for several years. It is very important to know both the source noise and the atmospheric conditions. Therefore, propagation validation is a very difficult task. Validation data cannot be obtained in a controlled environment, and weather conditions vary with both location and time.

Detailed 3-D measurements of wind and temperature require more advanced instrumentation. Instrumentation such as LIDAR and SONAR would be extremely useful in obtaining real 3-D/4-D weather data to accompany acoustic data, but these systems are very expensive and difficult to obtain. There are currently no plans to use these systems with planned flight tests. NASA does, however, have wireless microphones for upcoming tests that will enable longer-range propagation data.

Other possible sources of validation data may come from within different disciplines. Some such liaisons could be NLR, airport data, coupling efforts with Colorado State [Jones et al., 2004] and other ongoing European entities such NORTRIAL and Attenbourough, who presented explosion data at the Inter-Noise 2006 conference [Madshus et al., 2006].

A systematic approach to information exchange between researchers engaged in the development of advanced propagation technologies is needed in order to yield the highest-accuracy assessments of the public-good benefits. Incorporation of up-to-date experimental and analytical propagation information into system noise-prediction tools will allow us to weigh the benefits and deficits of individual propagation technologies.

NASA is using PSU-WOPWOP [Brentner, 1986] predictions for the Eurocopter BO-105 configuration at various blade-passing frequencies to validate the near-field scattering technologies.

Cross-Cutting Technology Needs

NASA can take advantage of the same theories, and in some cases the same propagation codes, throughout all aircraft disciplines (subsonic rotary-wing, subsonic fixed-wing, and supersonic aircraft). Research into rotorcraft noise propagation aligns closely with research plans for fixed-wing aircraft, and the advances made apply to both fixed-wing and rotary-wing aircraft. The curved-ray stratified-media codes with supersonic propagation methods are also synonymous with rotary- and fixed-wing propagation (with slight modifications). The only difference would be the integration of new propagation codes into existing system noise-prediction tools (RNM for rotary wing and ANOPP for fixed wing) and, of course, source-noise influences such as frequency content. Supersonic propagation has an added complexity due to shock waves that is not seen in either rotary- or fixed-wing subsonic aircraft, but in general most of what is learned for one class of vehicles is applicable to the others. Propagation technology is also used by the U.S. Army/Department of Defense (DOD)/DARPA for aircraft detection. DARPA is currently investigating 4-D (x, y, z, and t) weather capabilities for propagation as part of the Helicopter Quieting Program. Eventually, as weather data become available, the 4-D weather capability will prove advantageous to NASA rotorcraft as well. It is anticipated that the propagation techniques currently under development will be applicable to all rotorcraft configurations and will be valid for various atmospheric and terrain conditions. A set of atmospheric cases defining key propagation parameters constitutes the benchmark for verification and validation for the wind and temperature cases. And, as research progresses, a benchmark for the terrain and other cases will also be established. These benchmark cases will establish the “known” quantity required to periodically evaluate the assumptions against the physics and will be shared by all vehicle types.

The ability for a pilot to manually follow a prescribed approach or to set an autopilot for a constant operating condition promises repeatable data collection and an expanded operating envelope [Schmitz et al., 2007]. This recent advancement will be key for future low-noise approaches. Although the coupling between rotorcraft noise and handling qualities is still being handled manually or by incorporating basic guidelines and constraints in the optimization procedure, the stage is set to combine these research areas. Such improvements are beyond the horizon of our current efforts, but they remain a long-term vision.

REFERENCES

Anderson, W. K. and Bonhaus, D. L.: An Implicit Upwind Algorithm for Computing Turbulent Flows on Unstructured Meshes. Computers and Fluids, vol. 23, no. 1, Jan. 1994, pp. 1–21.

Anderson, W. K.; Rausch, R. D.; and Bonhaus, D. L.: Implicit/Multigrid Algorithm for Incompressible Turbulent Flows on Unstructured Grids. J. Computational Physics, vol. 128, no. 2, Oct. 1996, pp. 391–408.

Anusonti-Inthra, P.: Development of Rotorcraft Wake Capturing Methodology Using Fully Coupled CFD and Particle Vortex Transport Method. Proc. of the AHS Annual Forum, Phoenix, Ariz., vol. 1, 2006, pp. 333–342

Atalla, N. and Bernhard, R.: Review of Numerical Solutions for Low-Frequency Structural-Acoustic Problems. Applied Acoustics, vol. 43, no. 3, 1994, pp. 271–294.

Blokhintsev, D. I.: Acoustics of a Nonhomogeneous Moving Medium. NACA TM-1399, 1946.

Bonilha, M. W.; Han, F.; and Wadey, B.: Application of Predictive and Experimental SEA to a S-92 Helicopter Sidewall Section. 6th AIAA/CEAS Aeroacoustics Conference, AIAA Paper no. 2000-2054, Lahaina, Hawaii, 2000.

Bouthier, O. M. and Bernhard, R. J.: Simple Models of Energy Flow in Vibrating Membranes. J. Sound and Vibration, vol. 182, no. 1, Apr. 1995a, pp. 129–147.

Bouthier, O. M. and Bernhard, R. J.: Simple Models of the Energetics of Transversely Vibrating Plates. J. Sound and Vibration, vol. 182, no. 1, Apr. 1995b, pp.149–166.

Boyd, D. D., Jr.; Burley, C. L.; and Conner, D. A.: Acoustic Predictions of Manned and Unmanned Rotorcraft Using the Comprehensive Analytical Rotorcraft Model for Acoustics (CARMA) Code System. AHS International Specialists' Meeting on Unmanned Rotorcraft, Phoenix, Ariz., 13–20 Jan., 2005.

Brentner, K. S.: Prediction of Helicopter Rotor Discrete Frequency Noise: A Computer Program Incorporating Realistic Blade Motions and Advanced Acoustic Formulation. NASA/TM-87721, Oct. 1986.

Brentner, K. S. and Farassat, F.: Helicopter Noise Prediction: The Current Status and Future Direction. J. Sound and Vibration, vol. 170, no. 1, Feb. 1994, pp. 79–96.

Brentner, K. S. and Farassat, F.: Modeling Aerodynamically Generated Sound of Helicopter Rotors. Progress in Aerospace Sciences, vol. 39, no. 2, Apr. 2003, pp. 83–120.

Brooks, T. F. and Schlinker, R. H.: Progress in Rotor Broadband Noise Research. Vertica, vol. 7, no. 4, 1983, pp. 287–307.

Brooks, T. F.: Effect of Signal Jitter on the Spectrum of Rotor Impulsive Noise. Vertica, vol. 12, no. 3, 1988, pp. 257–265.

Brooks, T. F.; Jolly, J. R., Jr.; and Marcolini, M. A.: Helicopter Main Rotor Noise: Determination of Source Contribution using Scaled Model Data. NASA TP 2825, Aug. 1988.

Brooks, T. F.; Boyd, D. D., Jr.; Burley, C. L.; and Jolly, J. R., Jr.: Aeroacoustic Codes for Rotor Harmonics and BVI Noise–CAMRAD.Mod1/HIRES. J. Amer. Hel. Soc., vol. 45, no. 2, Apr. 2000.

Brooks, T. F. and Burley, C. L.: Blade Wake Interaction Noise for a Main Rotor. J. Amer. Hel. Soc., vol. 49, no. 1, 2004, pp. 11–27.

Burley, C. L.; Brooks, T. F.; Marcolini, M. A.; Brand, A. G.; and Conner, D. A.: Tiltorotor Aeroacoustic Code (TRAC) Predictions and Comparisons with Measurements. J. Amer. Hel. Soc., vol. 45, no. 2, 2000, pp. 80–89.

Burley, C. L. and Brooks, T. F.: Rotor Broadband Noise Prediction with Comparison to Model Data. J. Amer. Hel. Soc., vol. 49, no. 1, 2004, pp. 28–42.

Cenedese, F.; Perazzolo, A.; Costa, A.; and Forghieri, A. et al.: Helicopter's Vibroacoustic Solutions Using Hybrid SEA Validated Model. 13th AIAA/CEAS Aeroacoustics Conference, AIAA Paper no. 2007-3577, Rome, Italy, May 21–23, 2007.

Ceverny, V.: Seismic Ray Theory. 1st ed., Cambridge University Press, Cambridge, U. K., 2001.

Conner, D. A.; Marcolini, M. A.; Edwards, B. D.; and Brieger, J. T.: XV-15 Tiltrotor Low Noise Terminal Area Operations. AHS 53rd Annual Forum, Virginia Beach, Va., Apr. 29–May 1, 1997.

Conner, D. A.; Edwards, B. D.; Decker, W. A.; Marcolini, M. A.; and Klein, P. D.: NASA/Army/Bell XV-15 Tiltrotor Low Noise Terminal Area Operations Flight Research Program. J. Amer. Hel. Soc., vol. 47, no. 4, Oct. 2002, pp. 219–232.

Conner, D. A.; Burley, C. L.; and Smith, C. D.: Flight Acoustic Testing and Data Acquisition for the Rotor Noise Model (RNM). AHS 62nd Annual Forum, Phoenix, Ariz., May 9–11, 2006.

Cook, R. K.: Strange Sounds in the Atmosphere. I. Sound, vol. 1, no. 13, 1962, pp. 12–16.

Cotoni, V.; Gardner, B.; Shorter, P.; Carneal, J.; and Fuller, C.: Recent Enhancements to SEA for Predicting the High-Frequency Structure-Borne Noise Response of Aerospace Structures. AHS 63rd Annual Forum, Virginia Beach, Va., 2007, pp. 16–27.

Coy, J. J.; Handschuh, R. F.; Lewicki, D. G.; Huff, R. G.; Krejsa, E. A.; and Karchmer, A. M.: Identification and Proposed Control of Helicopter Transmission Noise at the Source. USAVVCOM-TR-87-C-2 and NASA/TM-89312, NASA, 1987.

Cunefare, K. A.: Negative Capacitance Shunts for Vibration Suppression: Wave-Based Tuning and Reactive Input Power. Proc. of Active 2006: 6th International Symposium on Active Noise and Vibration Control, Adelaide, Australia, 2006.

Dimanlig, A. C. B.; Meadowcroft, E. T.; Strawn, R.; and Potsdam, M.: Computational Modeling of the CH-47 Helicopter in Hover. AHS 63rd Annual Forum, Virginia Beach, Va., 2007.

Dimofte, F.; Ene, N.; Keith, T. G., Jr.; and Handschuh, R. F.: Investigation of the Stability of a Rotor Supported by Oil Journal Wave Bearing. Proc. of the IFToMM Seventh International Conference on Rotor Dynamics, H. Springer and H Ecker, eds., Technical University of Vienna, Vienna, Austria, Sept. 25–28, 2006.

Dimofte, Florin: University of Toledo, personal communication, 2007.

Dowell, E. H.: Master Plan for Prediction of Vehicle Interior Noise. AIAA J., vol. 18, no. 4, 1980, pp. 353–366.

DyRoBeS, version 11.3 (2006), Eigen Technologies Inc., http://www.DyRoBeS.com/ accessed Nov. 29, 2008.

Elliott, S. J.; Stothers, I. M.; and Nelson, P. A.: A Multiple Error LMS Algorithm and its Application to the Active Control of Sound and Vibration. IEEE Transactions on Acoustics, Speech, and Signal Processing (ASSP), vol. 35, no. 10, Oct. 1987, pp. 1423–1434.

Elliott, S.: Signal Processing for Active Control. Academic Press, Oct. 2000.

Elliott, S. J.; Gardonio, P.; Sors, T. C.; and Brennan, M. J.: Active Vibroacoustic Control with Multiple Local Feedback Loops. J. Acoustical Society of America, vol. 111, no. 2, Feb. 2002, pp. 908–915.

Fahy, F. J.: Statistical Energy Analysis: A Critical Overview. Philosophical Transactions of the Royal Society of London, Series A, vol. 346, no. 1681, Mar. 1994, pp. 431–447.

Fahy, F.; and Walker, J.: Advanced Applications in Acoustics, Noise, and Vibration. Spon Press, 2004.

Farassat, F. and Brentner, K. S.: Supersonic Quadrupole Noise Theory for High-Speed Helicopter Rotors. J. Sound and Vibration, vol. 218, no. 3, Dec. 1998, pp. 481–500.

Farassat, F.: Derivation of Formulations 1 and 1A of Farassat, NASA/TM-2007-214853, Mar. 2007.

Ffowcs Williams, J. E. and Hawkings, D. L.: Sound Generation by Turbulence and Surfaces in Arbitrary Motion. Philosophical Transactions of the Royal Society of London, A264, 1969, pp. 321–342.

Ffowcs Williams, J. E. and Hall, L. H.: Aerodynamic Sound Generation by Turbulent Flow in the Vicinity of a Scattering Half-Plane. J. Fluid Mechanics, vol. 40, no. 04, 1970, pp. 657–670.

Fleming, D. P.: Rotordynamics on the PC: Transient Analysis with ARDS. Rotating Machinery, Proc. of the Sixth International Symposium on Transport Phenomena and Dynamics of Rotating Machinery, vol. I, Maui, Hawaii, 1996, pp. 367–375.

Fleming, D. P.: Effect of Bearing Dynamic Stiffness on Gear Vibration. Proc. of Ninth International Symposium on Transport Phenomena and Dynamics of Rotating Machinery (ISROMAC-9), Yoshinobu Tsujimoto, ed. Pacific Center of Thermal-Fluids Engineering, Kihei, Maui, Hawaii, 2002.

Fleming, D. P.: Vibration Transmission through Bearings with Application to Gearboxes. ISCORMA-4, Calgary, Alberta, Canada, Aug. 27–31, 2007.

Gardonio, P.; Bianchi, E.; and Elliott, S.: Smart Panel with Multiple Decentralised Units for the Control of Sound Transmission. Part II: Design of the Decentralised Control Units. Proc. of Active 2002, Southampton, U.K., 2002, pp. 487–498.

George, A. R.: Helicopter Noise - State of the Art. AIAA Paper no. 1977-1337, 4th Aeroacoustics Conf., Atlanta, Ga. Oct 3–5, 1977.

Gilbert, K. E., and Xiao D.: A Fast Green's Function Method for One-Way Sound Propagation in the Atmosphere. J. Acoust. Soc. Am., vol. 94, no. 4, Oct., 1993, pp. 2343–2352.

HAI: HAI Fly Neighborly Guide, Cox, C. and Leverton, J. eds., Helicopter Association International, Alexandria, Va., 1993.

Heath, S. L., and McAninch, G. L.: Propagation Effects of Wind and Temperature on Acoustic Ground Contour Levels. AIAA Paper no. 2006-411, 44th AIAA Aerospace Sciences Meeting and Exhibit, Reno, Nev., Jan. 9–12, 2006.

Heath, S. L.: RTP - Ray Tracing Propagation Code User's Manual. NASA Technical Memorandum, NASA Langley Research Center, Hampton, Va., 2007.

Hennes, C. C., and Brentner, K. S.: The Effect of Blade Deformation on Rotorcraft Acoustics. 31st European Rotorcraft Forum, Florence, Italy, Sept. 13–15, 2005.

Howlett, J. T.; Clevenson, S. A.; Rupf, J. A.; and Snyder, W. J.: Interior Noise Reduction in a Large Civil Helicopter. NASA TN-D-8477, 1997.

Jayachandran, V., and Bonilha, M.: A Hybrid SEA/Modal Technique for Modeling Structural-Acoustic Interior Noise in Rotorcraft. J. Acoustical Society of America, vol. 113, no. 3, 2003, pp. 1448–1454.

Johnson, W. R.: CAMRAD II, Comprehensive Analytical Model of Rotorcraft Aerodynamics and Dynamics. Johnson Aeronautics, Palo Alto, Calif., 1997. (Also NASA-TM-81182; AVRADCOM-TR-80-A-5-PF-1, 1980.)

Johnson, W. R.: Influence of Wake Models on Calculated Tiltrotor Aerodynamics. AHS Aerodynamics, Acoustics, Testing, and Evaluation Technical Specialists' Meeting, San Francisco, Calif., Jan. 2002.

Jones, R. M.; Gu, E. S.; and Bedard, A. J., Jr.: Infrasonic Atmospheric Propagation Studies Using A 3-D Ray Trace Model. Amer. Meteorol. Soc. 22nd Conference on Severe Local Storms, Hyannis, Maine, Oct. 2004.

Joshi, P. R.: An Elastic Contact Theory for Modeling Vibration Transmissibility through Rolling Contact Bearings. MS Thesis, University of Cincinnati, Cincinnati, Ohio, 2004.

Kompella, M. and Bernhard, R.: Variation of Structural-Acoustic Characteristics of Automotive Vehicles. Noise Control Engineering J., vol. 44, no. 2, Mar.–Apr. 1996, pp. 93–99.

Kreigsmann, G. A., and Larson, E. W.: On the Parabolic Approximation to the Reduced Wave Equation. SIAM J. Appl. Math., vol. 34, no. 1, Jan. 1978, pp. 200–204.

Langley, R. S.: A General Derivation of the Statistical Energy Analysis Equations for Coupled Dynamic Systems. J. Sound and Vibration, vol. 135, no. 3, Dec. 1989, pp. 499–508.

Langley, R. S.: On the Vibrational Conductivity Approach to High Frequency Dynamics for Two-Dimensional Structural Components. J. Sound and Vibration, vol. 182, no. 4, May 1995, pp. 637–657.

Langley, R. S.; Smith, J.; and Fahy, F.: Statistical Energy Analysis of Periodically Stiffened Damped Plate Structures. J. Sound and Vibration, vol. 208, no. 3, Dec. 1997, pp. 407–426.

Langley, R. S. and Bremner, P.: A Hybrid Method for the Vibration Analysis of Complex Structural-Acoustic Systems. J. Acoustical Society of America, vol. 105, no. 3, Mar. 1999, pp. 1657–1671.

LeHen, F.; Smith, E. C.; Lesieutre, G. A.; and Szefi, J. T.: Actively-Enhanced Periodically-Layered Mount for Helicopter Gearbox Isolation. AIAA Paper no. 2005-2250, 46th AIAA/ASME/ASCE/AHS/ASC Structures, Structural Dynamics, and Materials Conference, Apr. 2005.

Lewicki, D. G., and Coy, J. J.: Vibration Characteristics of OH-58A Helicopter Main Rotor Transmission. NASA TP-2705, AVSCOM TR-86-C-42, Apr. 1987.

Lewicki, D. G., and Woods, R. L.: Evaluation of Low-Noise, Improved-Bearing-Contact Spiral Bevel Gears. NASA/TM-2003-212353, ARL-TR-2970, June 2003.

Lewis, R. M., and Keller, J. B.: Asymptotic Methods for Partial Differential Equations: The Reduced Wave Equation and Maxwell's Equations. New York University Research Report EM-194, Jan. 1964.

Lewis, P., and Malanoski, S. B.: Rotor-Bearing Dynamics Design Technology. Part IV: Ball Bearing Design Data. AFAPL-TR-65-45, Part IV, May 1965 (Restricted Distribution).

Liew, H.: Analysis of Time-Varying Rolling Element Bearing Characteristics. MS Thesis, University of Alabama, 2002.

Liew, H., and Lim, T. C.: Analysis of Time-Varying Rolling Element Bearing Characteristics. J. Sound and Vibration, vol. 283, 2005, pp. 1163–1179.

Lighthill, M. J.: On Sound Generated Aerodynamically, I: General Theory. Proc. of the Royal Society, vol. 211, no. 1107, Mar. 1952, pp. 564–587.

Lim, T. C., and Singh, R.: A Review of Gear Housing Dynamics and Acoustics Literature: Topical Interim Report. NASA CR 185148, 1989.

Lim, T. C., and Singh, R.: Vibration Transmission through Rolling Element Bearings. Part I: Bearing Stiffness Formulation. J. Sound and Vibration, vol. 139, no. 2, June 1990a, pp. 179-199.

Lim, T. C., and Singh, R.: Vibration Transmission through Rolling Element Bearings. Part II: System Studies. J. Sound and Vibration, vol. 139, no. 2, 1990b, pp. 201–225.

Lim, T. C., and Singh, R.: Vibration Transmission through Rolling Element Bearings. Part III: Geared Rotor System Studies. J. Sound and Vibration, vol. 151, no. 1, Nov. 1991, pp. 31–54.

Lim, T. C., and Singh, R.: Vibration Transmission through Rolling Element Bearings. Part IV: Statistical Energy Analysis. J. Sound and Vibration, vol. 153, no. 1, 1992, pp. 37–50.

Lim, T. C., and Singh, R.: Vibration Transmission through Rolling Element Bearings. Part V: Effect of Distributed Contact Load on Roller Bearing Stiffness Matrix. J. Sound and Vibration, vol. 169, no. 4, Jan. 1994, pp. 547–553.

Lim, J. W., and Strawn, R. C.: Prediction of HART II Rotor BVI Loading and Wake System Using CFD/CSD Loose Coupling. AIAA Paper no. 2007-1281, American Institute of Aeronautics and Astronautics Aerospace Sciences Meeting and Exhibit, Reno, Nev., Jan. 2007.

Lin, J. A.: Airplane Interior Noise Modeling Using Statistical Energy Analysis Approach. AIAA Paper no. 99-1903, 5th AIAA/CEAS Aeroacoustics Conference, Bellevue, Wash., 1999.

Litvin, F. L.; Fuentes, A.; Mullins, B. R.; and Woods, R.: Design and Stress Analysis of Low-Noise Adjusted Bearing Contact Spiral Gears. NASA CR-2002-211344, ARL-CR-486, Jan. 2002.

Lowson, M. V.: Progress Towards Quieter Civil Helicopters. Aeronautical J., vol. 96, no. 956, June–July 1992, pp. 209–223.

Lucas, M. J., and Marcolini, M. A.: Rotorcraft Noise Model. AHS Technical Specialists' Meeting for Rotorcraft Acoustics and Aerodynamics, Williamsburg, Va., 1997.

Lyon, R., and Maidanik, G.: Power Flow between Linearly Coupled Oscillators. J. Acoustical Society of America, vol. 34, no. 5, May 1962, pp. 623–639.

Lyon, R. H., and DeJong, R. G.: Theory and Application of Statistical Energy Analysis. Butterworth-Heinemann, 2nd Ed., 1995.

MacMartin, D. G.: Collocated Structural Control for Reduction of Aircraft Cabin Noise. J. Sound and Vibration, vol. 190, no. 1, Feb. 1996, pp. 105–119.

Madshus, C.; Lovholt, F.; Kaynia, A. et al.: Air-Ground Interaction in Long Range Propagation of Low Frequency Sound and Vibration – Field Tests and Model Verification. Applied Acoustics, vol. 66, no. 5, 2006, pp. 553–578.

Maidanik, G.: Response of Ribbed Panels to Reverberant Acoustic Fields. J. Acoustical Society of America, vol. 34, no. 6, June 1962, pp. 809–826.

Maier, R., and Tewes, S.: Active Trim-Panel Suspension for Interior Noise Control. AIAA Paper no. 2005-3036, 11th AIAA/CEAS Aeroacoustics Conference, Monterey, Calif., 2005.

Marcolini, M. A.; Conner, D. A.; Brieger, J. T.; Becker, L. E.; and Smith, C. D.: Noise Characteristics of a Model Tiltrotor. Proc. of the AHS 51st Annual Forum, Fort Worth, Tex., vol. 2, May 1995, pp. 1217–1226.

Marcolini, M. A.; Burley, C. L.; Conner, D. A.; and Acree, C. W., Jr.: Overview of Noise Reduction Technology in the NASA Short Haul (Civil Tiltrotor) Program. SAE Technical Paper 962273, SAE International Powered Lift Conference, Jupiter, Fla., Nov. 1996.

Mathur, G.; O'Connell, J.; JanakiRam, R.; and Fuller, C.: Analytical and Experimental Evaluation of Active Structural Acoustic Control of Helicopter Cabin Noise. AIAA Paper no. 2002-1035, 40th AIAA Aerospace Sciences Meeting and Exhibit, Reno, Nev., Jan. 2002.

McAninch, G. L., and Heath, S. L.: On the Determination of Shadow Boundaries and Relevant Eigenrays for Sound Propagation in Stratified Moving Media. AIAA Paper no. 2006-0412, 44th AIAA Aerospace Sciences Meeting and Exhibit, Reno, Nev., Jan. 2006.

Millott, T. A.; Welsh, W. A.; Yoerkie, C. A., Jr.; MacMartin, D. G.; and Davis, M. W.: Flight Test of Active Gear-Mesh Noise Control on the S-76 Aircraft. Proc. of the AHS 54th Annual Forum, Washington, D.C., May 1998, pp. 241–249.

Mitchell, A. M.; Oswald, F. B.; and Coe, H. H.: Testing of UH-60A Helicopter Transmission in NASA-Lewis 2240-kW (3000-hp) Facility. NASA TP-2626, Aug. 1986.

Mitra, S. K.: The Upper Atmosphere. The Asiatic Society, 2nd. Ed., 1952, pp. XXIV, 713.

Nielson, E. J.: Aerodynamic Design Sensitivities on an Unstructured Mesh Using the Navier–Stokes Equations and a Discrete Adjoint Formulation. Ph.D. thesis, Virginia Polytechnic Institute and State University, Blacksburg, Va., 1998.

Oswald, F. B.; Townsend, D. P.; Valco, M. J.; Spencer, R. H.; Drago, R. J.; and Lenski, J. W., Jr.: Influence of Gear Design Parameters on Gearbox Radiated Noise. NASA/TM-106511, Mar. 1994.

Oswald, F. B.; Lin, H. H.; and Delgado, I. R.: Dynamic Analysis of Spur Gear Transmissions (DANST) PC Version 3.0 User Manual. NASA/TM-107291, ARL-TR-1189, Aug. 1996.

Padmasolala, G.; Lin, H. H.; and Oswald, F. B.: Influence of Tooth Spacing Error on Gears With and Without Profile Modifications. NASA/TM-2000-210061, PTG-14436, Oct. 2000.

Padula, S. L.; Korte, J. J.; Dunn, H. J.; and Salas, A. O.: Multidisciplinary Optimization Branch Experience Using iSIGHT Software. NASA/TM-1999-209714, Nov. 1999.

Padula, S. L., and Gillian, R. E.: Multidisciplinary Environments: A History of Engineering Framework Development. AIAA Paper no. 2006-7083, 11th AIAA/ISSMO Multidisciplinary Analysis and Optimization Symposium, Portsmouth, Va., Sept. 2006.

Page, J. A.: Rotorcraft Noise Model (RNM 3.0) Technical Reference and User Manual. Wyle Report 02-05, Mar. 2002.

Pierce, A. D.: Acoustics: An Introduction to Its Physical Principles and Applications. 1st ed., McGraw-Hill, New York, N. Y., 1981.

Potsdam, M.; Yeo, H.; and Johnson, W.: Rotor Airloads Prediction Using Loose Aerodynamic/ Structural Coupling. AHS 60th Annual Forum, Baltimore, Md., 2004.

Prichard, D. S.; Boyd, D. D.; and Burley, C. L.: NASA/Langley's CFD-Based BVI Rotor Noise Prediction System: (ROTONET/BVI) An Introduction and Users' Guide. NASA/TM-109147, Nov. 1994.

Rabbiolo, G.; Bernhard, R.; and Milner, F.: Definition of a High-Frequency Threshold for Plates and Acoustical Spaces. J. Sound and Vibration, vol. 277, no. 4-5, 2004, pp. 647–667.

Richards, D., and Pines, D. J.: Passive Reduction of Gear Mesh Vibration Using a Periodic Drive Shaft. J. Sound and Vibration, vol. 264, no. 2, 2003, pp. 317–342.

Royston, T. J., and Basdogan, I.: Vibration Transmission through Self-Aligning (Spherical) Rolling Element Bearings: Theory and Experiment. J. Sound and Vibration, vol. 215, no. 5, Sept. 1998, pp. 997–1014.

Salomons, Erik M.: Computational Atmospheric Acoustics. 1st ed., Kluwer Academic Publishers, Boston, Mass., 2001.

Schmitz, F. H.: Chapter 2: Rotor Noise. Aeroacoustics of Flight Vehicles: Theory and Practice. Volume 1: Noise Sources, NASA RP-1258, vol. 1, Aug. 1991, pp. 65–149.

Schmitz, F. H.; Greenwood, E.; Sickenberger, R. D.; Gopalan, G.; Sim, B.; Conner, D.; Moralez, E.; and Decker, W. A.: Measurement and Characterization of Helicopter Noise in Steady-State and Maneuvering Flight. AHS 63rd Annual Forum, Virginia Beach, Va., May 1–3, 2007.

Smith, M. J.: A Hybrid Energy Method for Predicting High Frequency Vibrational Response of Point-Loaded Plates. J. Sound and Vibration, vol. 202, no. 3, May 1997, pp. 375–394.

Sutton, T. J.; Elliott, S. J.; Brennan, M. J.; Heron, K. H.; and Jessop, D. A. C.: Active Isolation of Multiple Structural Waves on a Helicopter Gearbox Support Strut. J. Sound and Vibration, vol. 205, no. 1, 1997, pp. 81–101.

Tinetti, A. F.; Dunn, M. H.; and Pope, D. S.: Fast Scattering Code (FSC) User's Manual, Version 2.0. NASA/CR-2006-214510, 2006.

Visintainer, J. A.; Marcolini, M. A.; Burley, C. L.; and Liu, S. R.: Acoustic Predictions Using Measured Pressures from a Model Rotor in the DNW. J. Amer. Hel. Soc., vol. 38, no. 3, July 1993, pp. 35–44.

Wang, A.; Vlahopoulosa, N.; and Wu, K.: Development of an Energy Boundary Element Formulation for Computing High-Frequency Sound Radiation from Incoherent Intensity Boundary Conditions. J. Sound and Vibration, vol. 278, no. 1-2, Nov. 2004, pp. 413–436.

Wilson, M. R.; Mueller, A. W.; and Rutledge, C. K.: A New Technique for Estimating Ground Footprint Acoustics for Rotorcraft Using Measured Sound Fields. AHS Vertical Lift Aircraft Design Conference, San Francisco, Calif., Jan. 1995, pp. 5.3-1–5.3-9.

Wohlever, J. C., and Bernhard, R. J.: Mechanical Energy Flow Models of Rods and Beams. J. Sound and Vibration, vol. 153, no. 1, Feb. 1992, pp. 1–19.

Yoerkie, C. A.; Moore, J. A.; and Manning, J. E.: Development of Rotorcraft Interior Noise Control Concepts: Phase I: Definition Study. NASA CR-166101, May 1983.

Yoerkie, C. A.; Gintoli, P. J.; and Moore, J. A.: Development of Rotorcraft Interior Noise Control Concepts: Phase II: Full Scale Testing. NASA CR-172594, Rev. 1, Feb. 1986a.

Yoerkie, C. A.; Gintoli, P. J.; Ingraham, S. T.; and Moore, J. A.: Development of Rotorcraft Interior Noise Control Concepts: Phase III: Development of Noise Control Concepts. NASA CR-178172, July 1986b.

Yoshikami, S. A.: Flight Operations Noise Tests of Eight Helicopters. FAA/EE-85-7, Aug. 1985.

Yu, Y. H.; Gmelin, B. L.; Heller, H. H.; Philipe, J. J.; Mercker, E; and Preisser, J. S.: HHC Aeroacoustic Rotor Test at the DNW—The Joint German/French/US HART Project. 20th European Rotorcraft Forum, Amsterdam, The Netherlands, Sept. 1994.

Yu, Y. H.; van der Wall, B. G.; Pausder, H.; Burley, C.; Brooks, T.; Beaumier, P.; Delrieux, Y.; Mercker, E.; and Pengel, K.: The HART-II Test: Rotor Wakes and Aeroacoustics with Higher-Harmonic Pitch Control (HHC) Inputs – The Joint German/French/Dutch/US Project. AHS 58th Annual Forum, Montreal, Canada, June 2002.

Zeillinger, R., and Köttritsch, H.: Damping in a Rolling Bearing Arrangement. Evolution, issue 1/96, 1996.

Zorumski, W. E.: Aircraft Noise Prediction Program Theoretical Manual, Parts 1 and 2. NASA/TM-83199, Pt. 1 and 2, Feb. 1982.

CHAPTER 4

COMPUTATIONAL FLUID DYNAMICS (EXTERNAL FLOW)

Terry L. Holst,[1] Elizabeth M. Lee-Rausch,[2] Robert T. Biedron,[2] Guru P. Guruswamy,[1] and Richard E. Kreeger[3]

NOMENCLATURE

c	rotor-blade chord
C_m	pitching moment coefficient
C_n	normal force coefficient
C_Q	coefficient of torque
C_T	coefficient of thrust
D_{V360}	vortex core diameter (= distance between vortex cross-flow velocity component peaks at ψ = 360 deg)
FM	figure of merit (= $C_T^{3/2}/C_Q\sqrt{2}$)
M	Mach number
M_{tip}	rotor-tip Mach number
M_∞	free-stream Mach number
r	radial coordinate along the rotor blade
R	rotor-blade maximum radius
x, y, z	nonrotating Cartesian coordinate system fixed to the rotor center of rotation with x extending straight back, y positive along the ψ = 90-deg direction, and z positive upward
μ	advance ratio (= M_∞/M_{tip})
ψ	azimuth angle measured in the counterclockwise direction when looking down on the rotor

[1] NASA Ames Research Center.
[2] NASA Langley Research Center.
[3] NASA Glenn Research Center.

ACRONYMS

BDF	backward difference formulae
BVI	blade–vortex interaction
CAD	computer-aided design
CFD	computational fluid dynamics
CSD	computational structural dynamics
DARPA	Defense Advanced Research Projects Agency
DES	detached-eddy simulation
DOD	Department of Defense
FEM	finite-element method
HIC	Helicopter Icing Consortium
LES	large-eddy simulation
NFAC	National Full-Scale Aerodynamics Complex
NFV	nonsteady-flow visualization
RANS	Reynolds-averaged Navier–Stokes
SOA	state of the art
UAV	uncrewed air vehicle

INTRODUCTION

The simulation of rotorcraft flow fields is a challenging multidiscipline problem that lags in development over its counterpart in the fixed-wing world by more than a decade. Successful aerodynamic simulation of a rotor/fuselage system requires the modeling of unsteady three-dimensional (3-D) flows that include transonic shocks, dynamic stall with boundary layer separation, vortical wakes, blade/wake and wake/wake interactions, rigid-body motion, blade deformations, and the loss of performance caused by ice accretion. The accurate simulation of these physical elements is required for the accurate prediction of aeromechanics and acoustics performance for rotorcraft. This problem has been addressed in the engineering design environment using simplified codes, called comprehensive codes, in which all facets of the rotorcraft problem—aerodynamics, structural dynamics, trim, etc.—are combined using simplified analyses. For example, aerodynamics is modeled using lifting-line theory and/or airfoil table lookups, and structural dynamics is modeled using nonlinear beam theory. A survey of comprehensive codes, including an historical development, is presented in Kunz [2005]. A few specific examples of comprehensive codes include 2GCHAS [Rutkowski et al., 1995], CAMRAD II [Johnson, 1986] and UMARC [Bir and Chopra, 1994].

Though the various comprehensive codes have provided significant benefits for understanding rotorcraft aeromechanics, more detailed analysis and design approaches based on first-principle methods are needed to help quantify the complex nonlinear interactions that exist between the various rotorcraft aeromechanics disciplines. These first-principle methods are the main emphasis of this chapter. In particular, the rotorcraft aeromechanic analyses described and surveyed in this chapter focus on computational-fluid-dynamics (CFD) approaches that solve the Reynolds-averaged Navier–Stokes (RANS) equations coupled with nonlinear computational-structural-dynamics (CSD) approaches. The only non-first-principle modeling performed in this context is that associated with turbulence. The survey results presented in this chapter are from the published literature or are new results produced within NASA. A review of rotorcraft CFD in general can be found in Strawn et al. [2006].

Flow-solver research with the main focus on rotorcraft aeromechanic applications is the subject of this chapter. Structured and unstructured CFD approaches are considered, with these presentations generally split into separate sections. Using these two approaches for aeromechanics CFD, with suitable comparisons along the way, is deemed appropriate, as each approach brings different attributes to aeromechanic simulations. The unstructured-grid CFD approach provides the mechanism for rapid grid generation for complex geometries and for the application of solution-adaptive grids. The structured CFD approach allows efficient execution efficiency, which is especially beneficial for database generation involving a large number of solutions or for path-finding solutions on exceptionally large grids. The ultimate approach for solving aeromechanics CFD problems could quite likely be a hybrid approach, combining these two methodologies. CSD models including both loose- and tight-coupling techniques are discussed. Ice-accretion prediction techniques and the resulting losses in aeromechanic performance are also highlighted. Lastly, a variety of computer science issues—including frameworks for implementing/combining the various CFD, CSD, and other modules; job setup automation; graphical result analysis, and parallelization—are also discussed.

State-of-the-art (SOA) metrics are presented for key areas pacing the development of aeromechanics simulations. These metrics are generally limited to simulation aspects, such as sectional normal force or pitching moment coefficient, for which enough data are available to establish a statistically valid baseline. Nevertheless, some metrics are proposed, those associated with unstructured flow-solver analysis, for example, without the establishment of a baseline with the hope that enough computational experimental comparisons can be performed in the near future to establish a baseline.

CURRENT TOOLS AVAILABLE OR IN DEVELOPMENT AT NASA

The primary CFD tools being used and/or developed within NASA for unsteady aerodynamic analysis are presented and discussed in this section. These tools include the FUN3D flow solver, which uses an unstructured-grid approach, the OVERFLOW2 flow solver, which uses an overset zonal-grid approach in which each grid zone is structured, and numerous icing tools for the prediction of ice accretion and the resulting loss in aerodynamic performance it causes.

FUN3D

FUN3D uses a node-based finite-volume scheme to solve both the steady and unsteady Euler and Navier–Stokes equations on mixed-element grids, including tetrahedra, pyramids, prisms, and hexahedra [Anderson and Bonhaus, 1994]. The flow-solver suite also has a two-dimensional (2-D) option for triangular and quadrilateral grids. The suite can handle either the compressible or incompressible RANS equations, using the artificial-compressibility method of Chorin for the incompressible equations. The inviscid fluxes are computed in an upwind fashion at control-volume faces using an approximate Riemann solver such as that of Roe. For second-order spatial accuracy the dual-cell interface values are obtained by extrapolation of the neighboring nodal quantities based on gradients computed using an unweighted least-squares technique. The full Navier–Stokes terms are evaluated with a Galerkin-type formulation. Domain decomposition and the message-passage-interface (MPI) standard are used to achieve a portable and scalable multiprocessor implementation of all code capabilities.

For steady flows, the solution at each time step is updated with a backwards Euler time-differencing scheme and the use of local time stepping. At each time step, the linear system of equations is relaxed in a red-black fashion with either a point- or line-implicit procedure [Nielsen et al., 2004]. For time-dependent simulations, a range of time-integration schemes is available, including first- through third-order backward difference formulae (BDF), and a fourth-order Explicit, Singly Diagonally Implicit Runge-Kutta (ESDIRK4) scheme [Carpenter et al., 2003]. A pseudotime term is typically added to enhance stability for large time steps, with subiterations used to converge each time step in pseudo time [Biedron et al., 2005]. Either a fixed number of subiterations are performed per time step, or preferably, a “temporal error controller” [Vatsa and Carpenter, 2005] is used. The temporal-error controller terminates the subiteration process when the residual drops below an estimate of the temporal error by a prescribed amount, typically one order of magnitude, so that excessive subiterations are not needlessly performed.

For turbulent flows, the eddy viscosity can be modeled using the Spalart–Allmaras one-equation model or two-equation models, including Menter's shear stress transport (SST), k-ω, and k-ε. An option for detached-eddy simulation (DES) is provided with the Spalart–Allmaras model.

Moving-body simulations may be accommodated using rigid [Biedron et al., 2005], overset, or deforming meshes. Body motion can be specified in a general form, although for rotorcraft applications a simplified input option is available wherein blade motion is specified as a combination of collective pitch, cyclic pitch, lead-lag, and flap, with hinge offsets. Overset grids are used for simulations involving large relative motion between bodies, such as those occurring in rotorcraft applications [O’Brien, 2006]; the overset meshes may themselves be rigid or deforming. Figure 4.1 illustrates a typical overset unstructured mesh for the HART II wind tunnel model. The single background mesh (blue) contains the fuselage and most of the volume nodes; the densely clustered region near the blade is created using volume sourcing in the VGRID mesh-generation software [Pirzadeh, 1996]. Each blade mesh (red) extends only a short distance from the blade surface, typically 1–2 chords. The fuselage/background grid and a blade grid are generated independently, and then the SUGGAR domain connectivity software [Noack, 2005] is used to assemble the composite mesh (fuselage/background plus multiple blades) and establish connectivity data between the component meshes.

For rotorcraft applications in which detailed rotor loads are not required, a source-based actuator-disk model with constant, linear, user-specified, and blade-element loading options is available [O'Brien, 2006]. Actuator-disk simulations do not require overset grids.

OVERFLOW2

The OVERFLOW2 computer program uses an overset or chimera zonal-grid approach to solve the RANS equations for the flow about general geometries, including geometries with relative motion. Thus, it is ideally suited to the solution of rotorcraft flow fields. OVERFLOW2 was developed by combining the original OVERFLOW flow solver [Benek et al., 1985; and Buning et al., 1988] with the six-degree-of-freedom moving-body capability within the OVERFLOW-D flow solver [Meakin, 2001a and 2001b; and Chan et al., 2001]. A description of this development process is presented in Nichols et al. [2006].

The original OVERFLOW code incorporated the diagonal form of the implicit approximate-factorization algorithm from Pulliam and Chaussee [1981] and a second-order-accurate in-space central-difference approximation for the inviscid fluxes. Mixed second- and fourth-order smoothing was added to the explicit and implicit sides of the equations to provide numerical stability.

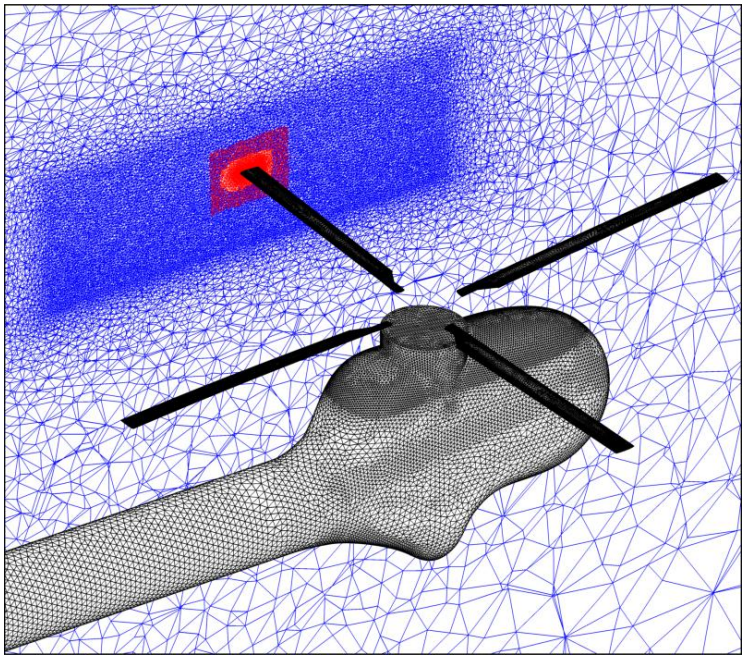

Figure 4.1. Unstructured-overset grid for the HART II model. Surface meshes are shown in black. A slice through the volume along a blade shows the background mesh (blue) and the blade mesh (red).

The OVERFLOW2 flow solver, while retaining the algorithmic features described previously, has been enhanced over the years with many additional options, which are described in Nichols et al. [2006]. A few of these include a Lower Upper-Symmetric Gauss Seidel (LU-SGS) implicit-solution algorithm with a Roe upwind inviscid-flux scheme [Kandula and Buning, 1994], a multigrid solution-acceleration procedure, low-Mach-number preconditioning, a central-difference matrix-dissipation inviscid-flux scheme [Jespersen et al., 1997], parallelization capabilities using both OPENMP and MPI [Jespersen, 1998], an AUSM inviscid-flux scheme [Liou and Buning, 2000], and a dual time-stepping implicit-solution algorithm [Pandya et al., 2003]. In addition, numerous turbulence models, including three hybrid RANS/large-eddy simulation (LES) models, have been added to OVERFLOW2 [Nichols et al., 2006].

The general concept behind the OVERFLOW2 chimera or overset zonal-grid approach is to divide the flow domain into a series of simple regions, with each region being covered by a separate structured grid. Such a scenario is displayed in figures 4.2 and 4.3. Figure 4.2 shows selected surfaces from a chimera grid generated about a Comanche helicopter fuselage, while figure 4.3 shows a half-span slice through a chimera grid for the V-22 tiltrotor. Boundary conditions for all grid zones that terminate in an overlap region are supplied by interpolating the solution from the interior of a grid zone with which they overlap. This chimera-interpolation feature is a steadfast characteristic of all overset zonal-grid approaches. For rotorcraft applications in which one set of grids, those fixed to the rotor, move relative to those fixed to the fuselage, the interpolation coefficients must be recomputed each time step.

Because each grid zone in the OVERFLOW2 code is structured, a high level of execution efficiency can be obtained from the OVERFLOW2 solver. This advantage is offset by the increased difficulty in generating overset grids, particularly for complex geometry applications. Fitting a structured-volume grid to an arbitrary surface, especially when the surface contains slope and/or feature discontinuities, can be a time-consuming, not to mention error-prone, process. Chan [2002] wrote a specialized software package, called OVERGRID, to deal with this problem. OVERGRID greatly simplifies the surface and volume grid-generation process for overset grids, but the process still involves a significant amount of human intervention.

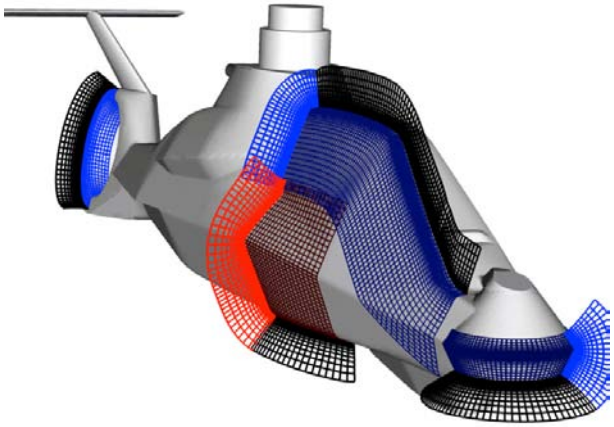

Figure 4.2. Selected surfaces from a volume grid about a Comanche helicopter fuselage showing how a complex geometric shape is discretized using the overset-grid approach. Taken from Chan et al. [2002].

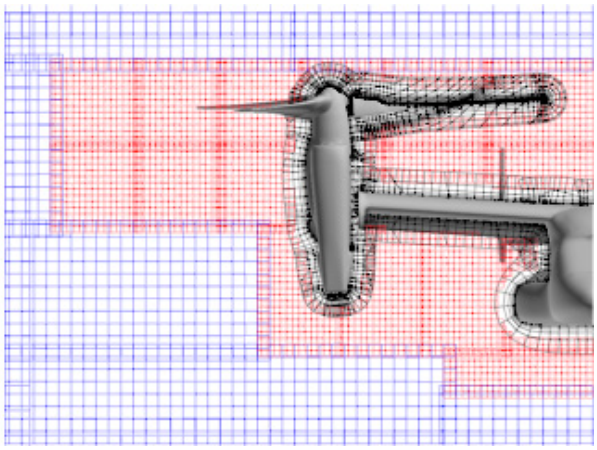

Figure 4.3. Slice through a V-22 tiltrotor half-span volume grid (every third point) showing a typical chimera-grid arrangement. Black grids are near-body grids (body-fitted). Red grids are finest-level off-body grids (Cartesian). Blue grids are next-finest-level off-body grids (Cartesian). Taken from Potsdam and Strawn [2002].

Icing Tools

The last time NASA did significant research in the area of rotorcraft icing was under the auspices of the Helicopter Icing Consortium [Britton and Bond, 1991]. At the time, no civilian helicopter had been certified for flight into known icing conditions. Civil rotorcraft operations are now entering the regularly scheduled revenue service market and need performance capabilities for all-weather operations. Current and future military systems will be required to operate continuously in moderate-icing conditions.

The rate of ice accumulation on an aircraft depends on the icing potential, which is a function of the characteristics of the airframe and the environmental conditions. Wing geometry, angle of attack, and velocity all have a strong influence on ice accretion. Environmental parameters of interest include cloud liquid-water content and droplet spectra, ambient temperature, relative humidity, degree of droplet supercooling, and even the distribution of liquid water along the flightpath.

Rotorcraft are more susceptible to icing than fixed-wing aircraft. They typically cannot fly fast enough (greater than Mach 0.6) to prevent icing by kinetic energy heating much beyond the blade tips, and usually cannot gain enough altitude to fly above the weather. Helicopter operations require remaining in an area for long periods of time, and the potential for severe vibration or damage due to ice shedding is more of a concern for helicopters relative to fixed-wing aircraft. The small chord length of rotor blades compared to the width of aircraft wings makes them less tolerant of icing. Mechanical and pneumatic de-icing systems are generally not practical for rotors, so conventional rotor deicing systems use electrothermal technologies, which can have power-consumption and reliability issues.

Analysis of helicopter icing is more complex than for fixed-wing aircraft or even engine icing because there are numerous issues specific to rotorcraft. These include the effects of centrifugal and adhesive forces; wake/vortex interactions within the rotor disk; the tracking of particle trajectories through complex flow fields; highly three-dimensional blade geometries; the presence of both rotating and nonrotating parts; large spanwise variations in flow properties; and multiple, complex scaling issues.

Design tools are required to assure safe operations in icing conditions. Icing can be considered early in the design process at relatively low additional cost only if well-integrated analytical tools are available. Analytical tools can be especially useful when design changes or retrofits to an existing ice protection system or rotor are made. Besides their use in the design process, analytical methods are also needed for certification. Addressing the entire icing envelope in flight is not practical or possible. Codes are useful to determine the most critical conditions for tunnel, flight, and natural ice testing. Analytical tools can thus be used to focus development and certification testing, thereby reducing the cost and/or risk. The accurate prediction of ice accretion requires a multidiscipline approach, incorporating elements of aerodynamics, heat transfer, structures and materials, and dynamics and controls.

Current Icing tools available or in development

The current SOA of subsonic rotary-wing icing is quasisteady and quasi-3-D. There is a loose coupling between the aerodynamics and the ice accretion—not a true, multiphase solution. This approach, developed as the result of a significant research effort, is acceptable for most fixed-wing applications, such as general aviation, business jets, or commercial transports. But there are still shortcomings for some vehicle types, such as axisymmetric and slender bodies, engines and turbomachinery, aircraft with swept wings, and, notably, rotorcraft. These cases all exhibit flow-field or ice features that are not well-predicted by the current SOA.

The icing analysis procedure for prediction of performance degradation must address both aerodynamic performance and ice accretion. Several tools, for example, LEWICE3D and FENSAP-ICE [Baruzzi et al., 2003; and Hartman et al., 2006], have begun to address this complexity by combining a suite of high-fidelity tools into an integrated icing environment. These tools typically consist of an aerodynamic flow calculation, droplet trajectory and impingement calculations for collection efficiency, and a heat transfer calculation for ice growth. For robustness, these codes often include tools for geometry preparation, grid generation, and various postprocessing utilities. There are typically other physical models, too, such as anti-icing/de-icing system performance, splashing, runback, and shedding. The importance of the physical models cannot be overstated, because the accuracy of the predictive tools can spell the difference between the critical ice shape and an unreliable prediction.

LEWICE3D is a suite of codes, developed by NASA and used widely by industry, to determine the amount and location of ice accretion on an aircraft. It is used to calculate water loading on aircraft surfaces so that the size and location of ice protection systems can be determined, to optimize the placement of icing sensors, and to determine ice shapes used in failed ice protection system tests. LEWICE3D is also used to determine corrections for cloud-measurement instruments, such as droplet size probes or liquid-water content probes on NASA research aircraft.

LEWICE3D uses a Monte-Carlo-based collection efficiency calculation using droplet-impact counts. Trajectories are calculated using an Adams-type predictor-corrector method developed by Norment [1985] with modifications by Bidwell and Potapczuk [1993]. Tangent trajectories and collection efficiencies for simple 2-D or 3-D regions can also be calculated using a modified version of the 2-D LEWICE method. Streamlines are calculated using a fourth-order Runge–Kutta integration scheme, which is highlighted in figure 4.4. In this figure A0 is the area per particle in the free stream, and Am is the area of the surface element.

The ice-growth methodology in LEWICE3D uses a single-time-step strip approach (see fig. 4.5) and requires a steady or time-averaged flow solution supplied by the user. The strip approach is based on the classical Messinger energy-balance procedure with an integral boundary layer technique used to generate heat transfer coefficients and is a modified version of the method used in the LEWICE2D code applied along streamlines [Wright, 2002]. LEWICE3D supports multiblock structured grids, adaptive Cartesian grids, and unstructured grids, as well as panel-based binary-tree grids.

LEWICE3D includes extensions that allow generation of a full 3-D ice accretion for surfaces and generation of a new iced surface, calculation of off-body concentration factors, and determination of shadow zones. The program has been parallelized using Open Multi-Processing (OpenMP) and MPI to complete jobs faster on parallel machines. The parallel version has been ported to SGI and Linux machines.

EXAMPLES OF CURRENT PREDICTIVE CAPABILITIES

SOA performance levels are established in this section for CFD simulations that solve the RANS equations for the flow about rotorcraft configurations. Most of the results presented are for isolated rotor geometries, because first-principle results for the more-difficult rotor/fuselage problem have not been published in sufficient numbers to form a statistically valid SOA. This discussion typically involves solvers that use wake capturing with coupled CSD routines (or the direct specification of rotor deflections).[4] All flight conditions are considered. The metrics used to establish SOA performance levels include both computational accuracy and expense. For the area of computational accuracy, numerous parameters are used in the SOA assessment, including both integrated and sectional or localized quantities, for example, normal force and pitching moment coefficients for various blade sectional positions. This section is subdivided into several subsections for which hover performance, performance in forward flight, and maneuver are discussed. Lastly, a section is presented in which the important problem of predicting ice accretion on rotor blades and the resulting loss in aerodynamic performance is considered.

[4] The tiltrotor results do not have structural deflections included in the calculation procedure as the blades are low aspect ratio and relatively stiff. The structural deflections are assumed to be negligible.

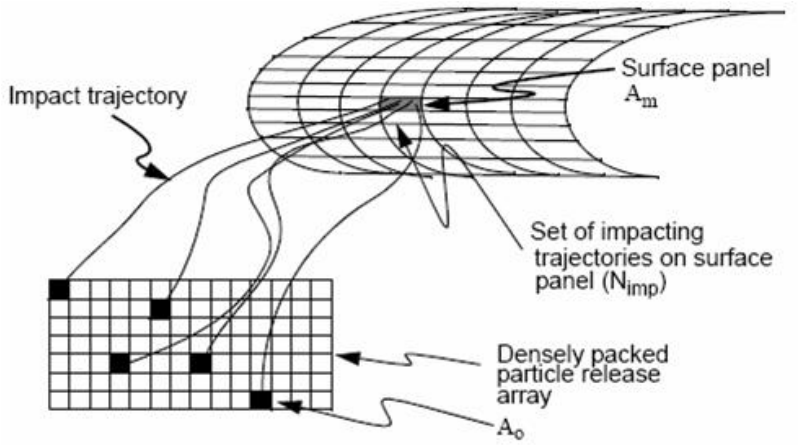

Figure 4.4. Monte-Carlo-based collection-efficiency calculation using droplet-impact counts.

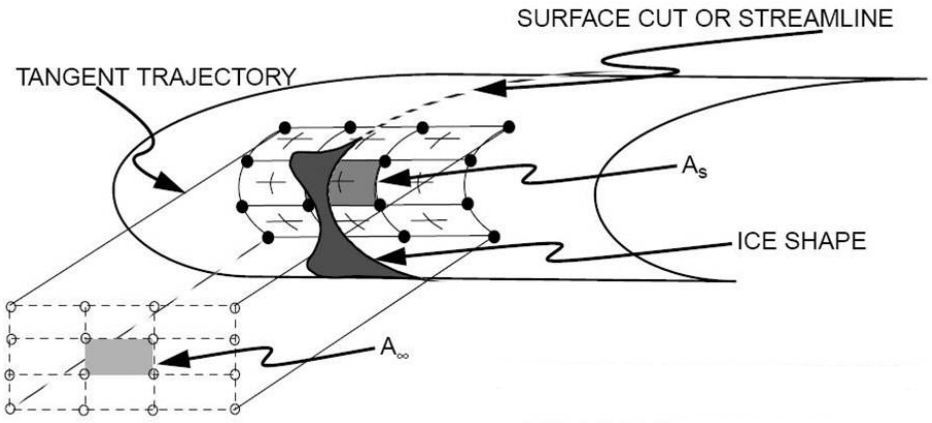

Figure 4.5. Tangent trajectories used to predict ice shapes at a typical leading-edge surface.

Hover Computations

The first CFD rotorcraft computations considered herein are those associated with isolated-rotor hover flight conditions. Flow-field simulations for the hover of an isolated rotor can be simplified by fixing the computational grid to the spinning rotor, requiring the addition of special rotational terms to the governing equations. The problem so configured has a steady state, which can be approached using standard steady-state convergence-acceleration algorithms that are routinely available within the RANS CFD community. In addition, this approach eliminates the need for having two sets of grids with relative motion—one set fixed to the spinning rotor blades, the other set fixed to the free stream.

A sample of results from the literature showing measured versus computed values for figure of merit (FM), coefficient of torque (C_Q), and coefficient of thrust (C_T) are presented in figures 4.6 through 4.8. These results have been compiled from six separate studies that involved computational/ experimental comparisons for five different hovering rotors: the TRAM tiltrotor [Potsdam and

Strawn, 2002] and Pulliam, 2007;[5] the Eurocopter 7A Rotor [Pomin and Wagner, 2002]; the UH-60A [Strawn and Djomehri, 2002; Ahmad and Strawn, 1999; and Wake and Baeder, 1994]; the Caradonna-Tung NACA 0012 rotor [Ahmad and Strawn, 1999]; and a modified UH-60 with a tapered tip [Wake and Baeder, 1994]. These results are from a large number of structured-grid solutions involving many different grid sizes and orientations.

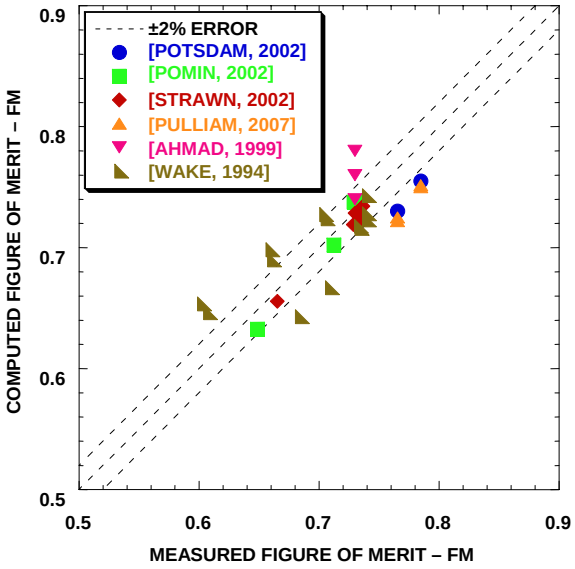

Figure 4.6. Measured versus computed FM for numerous isolated rotor simulations appearing in the literature, all using Navier–Stokes solvers with captured wakes.

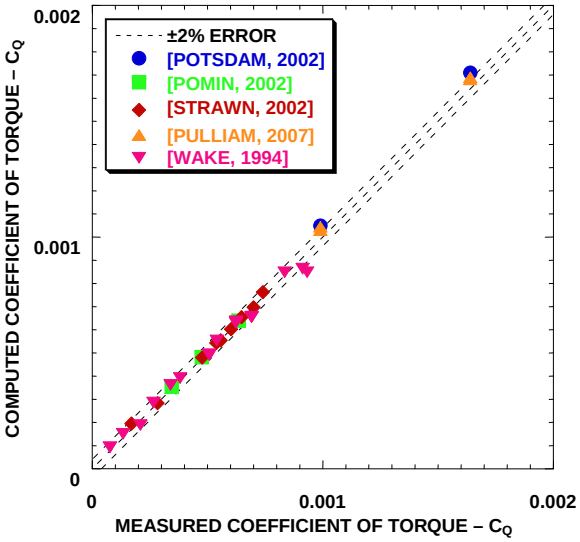

Figure 4.7. Measured versus computed coefficient of torque (C_Q) for numerous isolated rotor simulations appearing in the literature, all using Navier–Stokes solvers with captured wakes.

[5] Private communication. NASA Ames Research Center, Moffett Field, Calif.

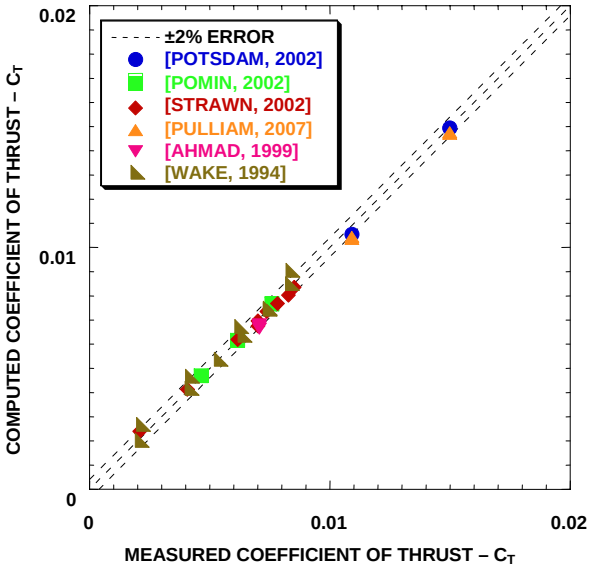

Figure 4.8. Measured versus computed coefficient of thrust (C_T) for numerous isolated rotor simulations appearing in the literature, all using Navier–Stokes solvers with captured wakes.

The results presented in figure 4.6 show measured versus computed FM values. The centered diagonal line indicates 0% error, while the dashed lines above and below indicate ±2% error. The base for computing error percentages for this figure was chosen to be FM = 1.0. The computed value of FM error, averaged over all data points in figure 4.6, is 0.0241. Thus, the average percent error, using the FM = 1.0 base, is 2.41%. This process establishes the SOA for FM for hovering rotorcraft calculations involving the structured-grid RANS formulation.

The results presented in figure 4.7 show measured versus computed C_Q values for the same rotors used in figure 4.6 (five of the six authors). The centered diagonal line indicates 0% error, while the dashed lines above and below indicate ±2% error. The base for computing error percentages for this figure was chosen to be C_Q = 0.002, which is also the horizontal or vertical axis length. The computed value of C_Q error, averaged over all data points in figure 4.7, is 0.0000233. Thus, the average percent error, using the C_Q = 0.002 base, is 1.16%. This process establishes the SOA for C_Q for hovering rotorcraft calculations involving the structured-grid RANS formulation.

The results presented in figure 4.8 show C_T results for the same rotors used in figures 4.6 and 4.7 (all six authors). The centered diagonal line indicates 0% error, while the dashed lines above and below indicate ±2% error. The base for computing error percentages for this figure was chosen to be C_T = 0.02—the horizontal or vertical axis length. The computed value of C_T error, averaged over all data points displayed within figure 4.8, is 0.000216. Thus, the average percent error, using the C_T = 0.02 base, is 1.08%. This process establishes the SOA for C_T for hovering rotorcraft calculations involving the structured-grid RANS formulation.

CFD/CSD Coupling Approaches

Computational aeromechanics, that is, the coupling of CFD and CSD solvers to obtain accurate simulations about rotorcraft, is one of the most challenging problems in the field of aeronautical science. The aerodynamics and structural dynamics associated with rotorcraft rotor systems are inherently nonlinear and intimately interrelated. To obtain an accurate prediction of rotor performance, it is imperative that both these disciplines be combined within a single simulation in a reasonable and thoughtful manner.

Many different aerodynamic and structural dynamic formulations are available to solve the rotorcraft aeromechanics problem, as exemplified by figure 4.9. SOA simulations for fixed-wing applications with complex nonlinear physics have generally gravitated to Navier–Stokes formulations with a suitable RANS turbulence model for the aerodynamics discipline and to a suitable 3-D finite-element method (FEM) approach for the structural dynamics discipline.

SOA rotary-wing applications with nonlinear physics are generally paced by RANS solvers, with the structural-dynamics discipline typically receiving less-sophisticated treatment. Taking advantage of the long, slender nature of most rotor blades, structural-dynamics solvers for rotary-wing applications have gravitated to nonlinear one-dimensional beam theory, as exemplified by the structural dynamics routines that most rotorcraft comprehensive codes use. The other main advantage of using beam theory is the ability to express linear aerodynamic quantities as a function of structural parameters. However, the need for more accurate 3-D FEM structures has also been presented [Das et al., 2007].

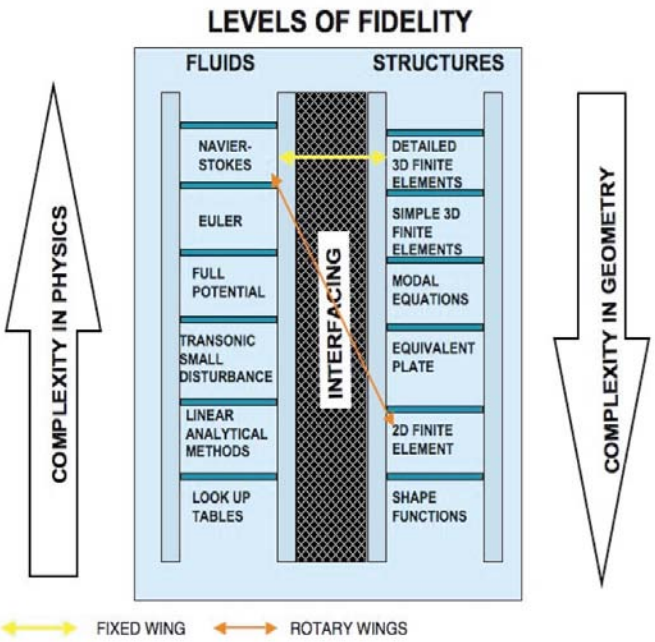

Figure 4.9. Levels of fidelity available for aeroelastic applications. A typical high-fidelity fixed-wing formulation uses a RANS/3-D–FEM approach (yellow line), while a rotary-wing formulation uses a RANS/beam-theory approach (orange line).

For rotorcraft applications the coupling procedure by which the two disciplines are combined typically follows one of two different approaches—loose coupling or tight coupling.[6] For the loose-coupling approach, first suggested by Tung et al. [1984], the structural deflections from the CSD solver and loads from the CFD solver are exchanged only a small number of times per revolution, for example, once per blade passage. This approach works well for straight and level flight in which a periodic steady state has been reached and is more computationally efficient than tight coupling. The loose-coupling approach is also the current standard for CFD/CSD coupling methods within the rotorcraft simulation field [Kunz, 2005]. In conjunction with the loose-coupling approach, an externally prescribed trim algorithm is often included, allowing adjustment of various control parameters, for example, the pitch collective angle, so that trimmed flight is achieved simultaneously as the CFD/CSD solution converges. The basic loose-coupling approach has many variations within the literature, but most of them use the general theme described here.

A typical convergence history for a loosely coupled CFD/CSD approach, taken from Nygaard et al. [2006] is presented in figure 4.10 in the form of normal force versus azimuth curves plotted during successive iterations. The RANS flow solver used in this study was OVERFLOW2, and the structural-dynamics solver was Rotorcraft Comprehensive Analysis System (RCAS). In this implementation each iteration corresponds to one revolution of the rotor system. The first revolution

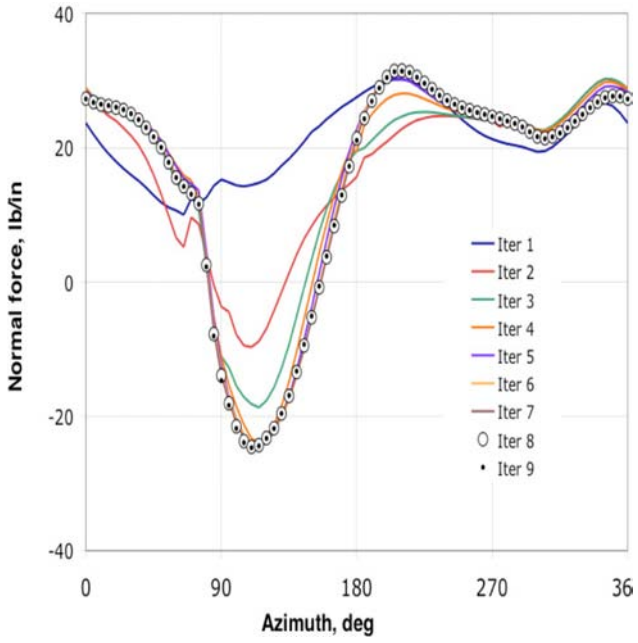

Figure 4.10. Convergence of normal force for a typical loose-coupling algorithm (OVERFLOW2/RCAS), UH-60 rotor, 158 knots forward-flight condition, $\mu = 0.368$, $C_T/\sigma = 0.0843$, $r/R = 0.965$; taken from Nygaard et al. [2006].

[6] The loose- and tight-coupling terminology used for rotary-wing applications is also used for fixed-wing applications, but with different implementations. For fixed-wing applications loose coupling typically requires a single explicit fluid/structure exchange during each time step. Tight coupling requires an implicit fluid/structure exchange during each time step, which is typically implemented using a sub-iteration process. For additional discussion on fixed-wing CFD/CSD coupling approaches, see Bathe and Wilson [1976] or Guruswamy and Yang [1981].

corresponds to the OVERFLOW2 airloads from the initial blade deflections obtained from an isolated RCAS computation, while each subsequent iteration corresponds to OVERFLOW2 outputs with updated blade motion and trim information, obtained from the RCAS comprehensive code. As can be seen from the figure, the loose-coupling algorithm for this computation converges after approximately 8 iterations.

The tight-coupling approach is simple in concept, but not as well developed as the loose-coupling approach, partly because it is more computationally expensive than loose coupling. In the tight-coupling approach airloads from the aerodynamics solver are supplied to the structural-dynamics solver as input. Geometric deflections from the structural-dynamics solver are supplied as input to the aerodynamics solver. This interchange is typically performed once during each time step. If this interchange is performed iteratively in advancing from one time step to the next, i.e., via a sub-iteration process, the coupling methodology is typically improved in robustness and accuracy. Such an implementation is often called a "strong-coupling" approach. Care must be taken in the transfer of loads and deflections so as to maintain the proper conservation of energy. The use of tight- or strong-coupling is most important in maneuver computations that do not reach a periodic steady state. As such, this coupling approach is neither well-developed nor well-validated because of the lack of suitable maneuver-flight validation data. More discussion on rotorcraft maneuver computations will be provided in a subsequent section.

Issues that need additional research attention in the CFD/CSD area are associated with improving accuracy of the coupling process. Since the CFD/CSD coupling process is largely ad hoc, current methodologies may not be adequate to maintain time accuracy in nonlinear flow regimes [Kunz, 2005]. The current inability to predict phase angles for flapping motion may be a strong indication of inadequacies associated with current CFD/CSD coupling approaches [Bhagwat et al., 2007].

Forward-Flight Computations

SOA performance levels are established in this section for CFD simulations that solve the RANS equations for the flow about rotorcraft configurations in steady forward flight. This discussion is restricted to solvers that use wake capturing with coupled CSD routines (or the direct specification of rotor deflections). The metrics used to establish these SOA performance levels include both accuracy and computational efficiency/expense. For the area of performance accuracy two parameters are used, normal force and pitching moment coefficient.

Results based on structured CFD solvers

Computed results for normal force coefficient taken from four different studies [Sitaraman and Baeder, 2006; Potsdam et al., 2006; Duque et al., 2006; and Bhagwat et al., 2007] are compared with experiment in figure 4.11 for the UH-60A high-speed forward-flight test (C8534), at $\mu = 0.368$ and $M_{tip} = 0.6415$. All of these results are taken from structured-grid RANS solvers. Sectional results scaled by Mach number squared are presented for two different radial stations, r/R = 0.865 and 0.965. These data (including the experimental data) were obtained by digitizing graphical results from the literature across the entire azimuth range at 15-deg intervals.

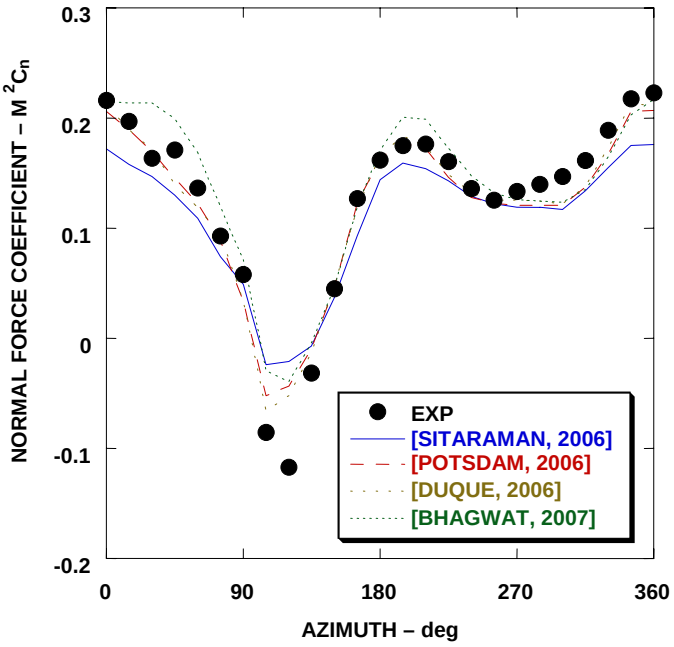

a) r/R = 0.865

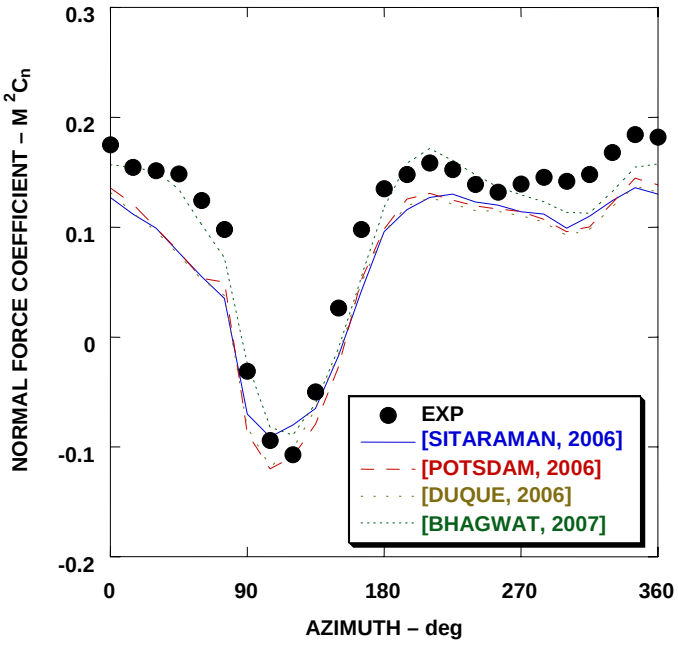

b) r/R = 0.965

Figure 4.11. Computed normal force coefficients from four structured-grid RANS codes compared with experiment for the UH-60A rotor, high-speed forward-flight case, C8534, μ = 0.368, M_{tip} = 0.6415.

Computed results for pitching moment coefficient (with the mean removed) taken from three different structured-grid studies [Sitaraman and Baeder, 2006; Potsdam et al., 2006; and Bhagwat et al., 2007] are compared with experiment in figure 4.12 for the UH-60A high-speed forward-flight test (C8534), at $\mu = 0.368$ and $M_{tip} = 0.6415$. Sectional results scaled by Mach number squared are presented for two different radial stations, r/R = 0.865 and 0.965. As with figure 4.11, the data in figure 4.12 (including the experimental data) were obtained by digitizing graphical results from the literature across the entire azimuth range at 15-deg intervals. Note the generally good agreement between all results presented.

To obtain a more concise statement of error with regard to comparisons between RANS computations and experiment, it is of interest to plot computed air-load results versus experimental data as was done in figures 4.6 through 4.8. A sample of results in this format obtained from the literature showing measured versus computed normal force and pitching moment coefficients (sectional values) scaled by M^2 are presented in figures 4.13 and 4.14. As with figures 4.11 and 4.12, these data were obtained by digitizing graphical results from the literature across the entire azimuth range at 15-deg intervals.

The results presented in figure 4.13 show Mach-number-scaled normal force coefficient values from 14 solutions involving seven studies [Sitaraman and Baeder, 2006; Potsdam et al., 2006; Lim and Strawn, 2007; Pomin and Wagner, 2004; Duque et al., 2006; Dietz et al., 2006; and Bhagwat et al., 2007]. Data obtained from a total of 33 radial stations ranging from r/R = 0.55 to 0.965 for three different rotor geometries (UH-60A, HART II, and Eurocopter 7A) and eight different flight conditions are displayed. The center diagonal line indicates 0% error, while the two diagonal lines above and below indicate ±10% error. The base for computing error percentages for this figure was chosen as the axis length—that is, $M^2C_n = 0.6$. The computed value of M^2C_n, averaged over all data points within figure 4.13, is 0.11705, and the average measured value of M^2C_n is 0.13201. The average M^2C_n error (summed over all data points in fig. 4.13 using absolute values) is 0.02477. Thus, the average percent error for the data presented in figure 4.13, using the $M^2C_n = 0.6$ base, is 4.1%. This process establishes the SOA for sectional normal force coefficient for rotorcraft calculations involving the structured-grid RANS formulation with a captured wake and coupled CSD solver.

The results presented in figure 4.14 show Mach-number-scaled pitching moment coefficient values (mean removed) from nine solutions involving four studies [Sitaraman and Baeder, 2006; Pomin and Wagner, 2004; Potsdam et al., 2006; and Bhagwat et al., 2007]. Data obtained from a total of 26 radial stations ranging from r/R = 0.55 to 0.965 for two different rotor geometries (UH-60A and Eurocopter 7A) and eight different flight conditions are displayed. The center diagonal line indicates 0% error, while the two diagonal lines above and below indicate ±10% error. The base for computing error percentages for this figure was chosen as the axis length—that is, $M^2C_m = 0.05$. The computed value of M^2C_m averaged over all data points within figure 4.14, is 0.0000070, and the average measured value of M^2C_m is –0.0001427. The average M^2C_m error (summed over all data points in fig. 4.14 using absolute values) is 0.002338. Thus, the average percent error for the data presented in figure 4.14, using the $M^2C_m = 0.05$ base, is 4.7%. This process establishes the SOA for sectional pitching moment coefficient (mean removed) for rotorcraft calculations involving the structured-grid RANS formulation with a captured wake and a coupled CSD solver.

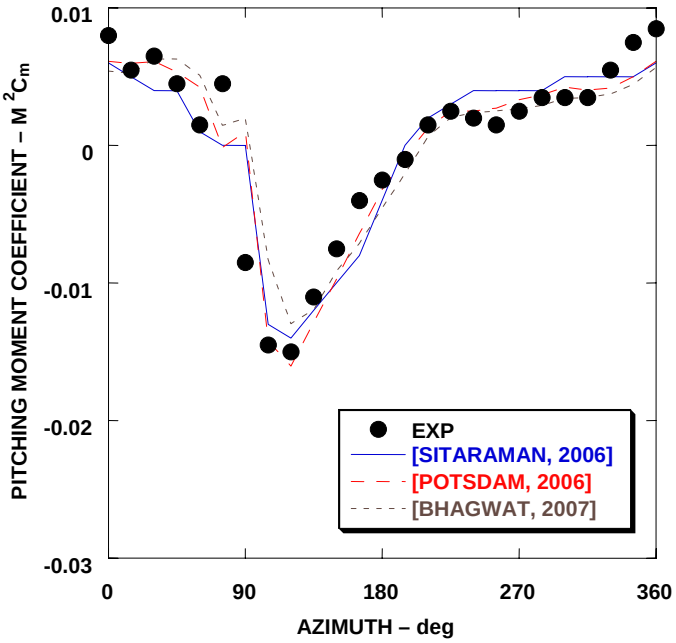

a) r/R=0.865

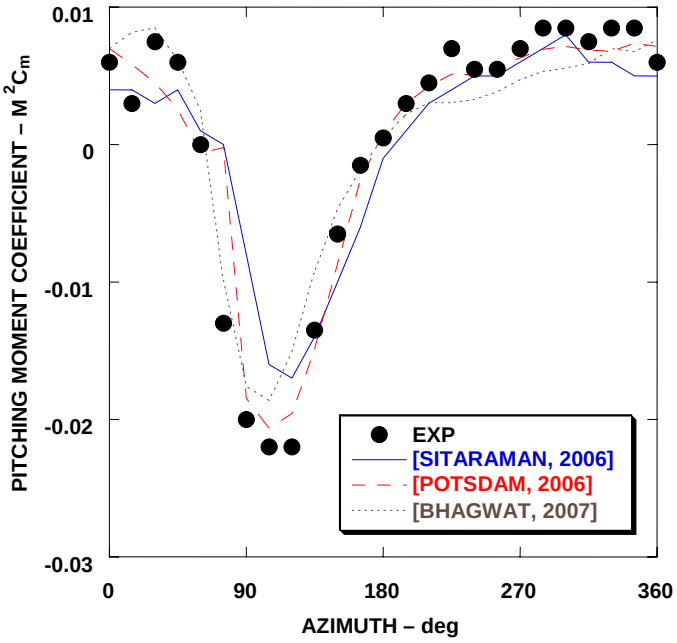

b) r/R = 0.965

Figure 4.12. Computed pitching moment coefficients from three structured-grid RANS codes compared with experiment for the UH-60A rotor, high-speed forward-flight case, C8534, μ = 0.368, M_{tip} = 0.6415.

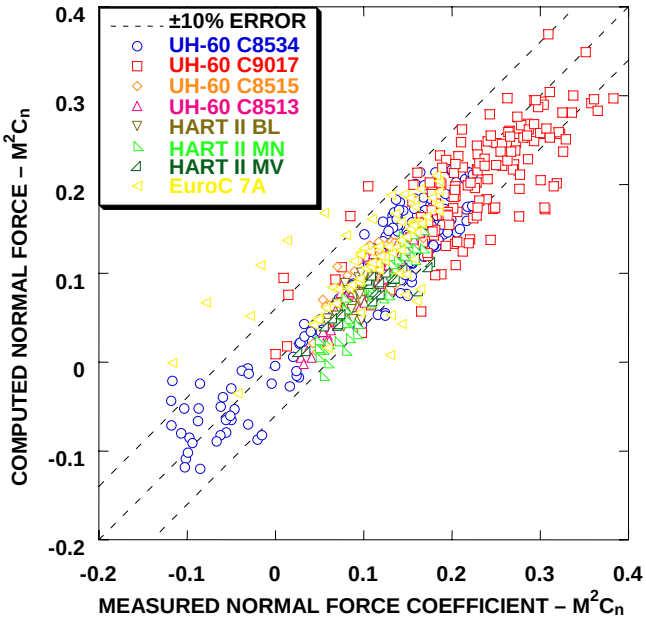

Figure 4.13. Measured versus computed normal force for numerous rotorcraft simulations appearing in the literature involving structured-grid Navier–Stokes solvers with captured wakes.

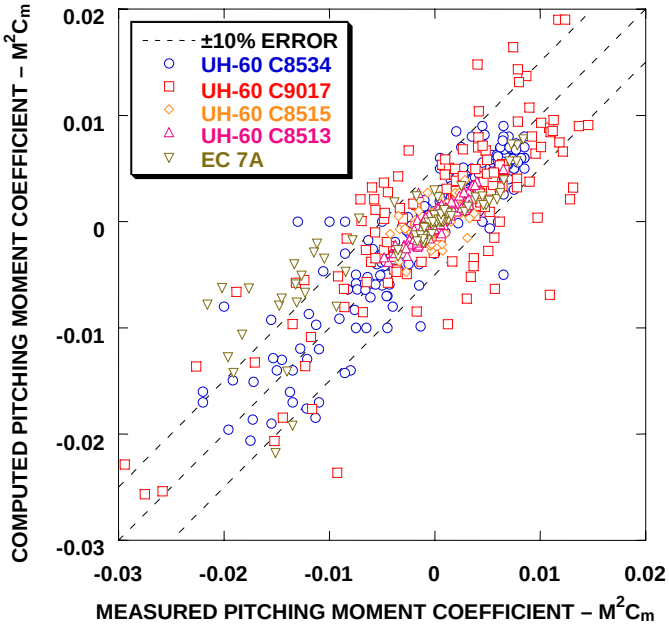

Figure 4.14. Measured versus computed pitching moment (with mean removed) for several rotorcraft simulations appearing in the literature involving structured-grid Navier–Stokes solvers with captured wakes.

An additional area of interest for rotorcraft forward flight—because it affects not only aeromechanic performance but also the acoustics signature—is being able to simulate the rotor wake. Accurate simulation of the rotor-wake geometry includes the prediction of wake-vorticity distribution and position as a function of wake age. This simulation is particularly difficult because rotorcraft wakes contain steep gradients that experience large, rapid spatial excursions that are difficult to anticipate. Thus, achieving adequate grid resolution for accurate wake computation is a formidable problem. In addition, producing accurate and sufficiently detailed experimental data for the purpose of validating computed wake geometries is an equally daunting task.

Largely because of these difficulties, few studies have been performed in which computed rotor-wake vorticity distributions and position have been compared with experimental results. One exception in which wake position for the HART II baseline case was compared with experimental data (taken from Lim and Strawn [2007]) is shown in figures 4.15 and 4.16. Figure 4.15 shows a diagram of the particle-image-velocimetry (PIV) measurement stations used in the experiment. Comparisons between experiment and OVERFLOW2 computations using two different grids are presented in figure 4.16 for the experimental positions 17–23 from the advancing side of the rotor (y = +1.4 m) and positions 43–47 from the retreating side (y = –1.4 m). The snb/sob and fnb/fob designations correspond to standard-near-body grid (6.8 million points) and standard-off-body grid (12.6 million points), and fine-near-body grid (12.1 million points) and fine-off-body grid (100.8 million points), respectively. The wake location predicted by the standard-grid result (snb/sob) differs from its experimental counterpart by as much as one blade chord (0.121 m) while the fine-grid result (fnb/fob) shows an improved prediction. These comparisons are all made during the first two rotor revolutions.

Because of the lack of experimental/computational comparisons, establishing suitable metrics (with associated SOA numerical target values) for measuring improvement in the area of rotorcraft wake simulation is difficult. The single metric presented at the end of this presentation—vortex core

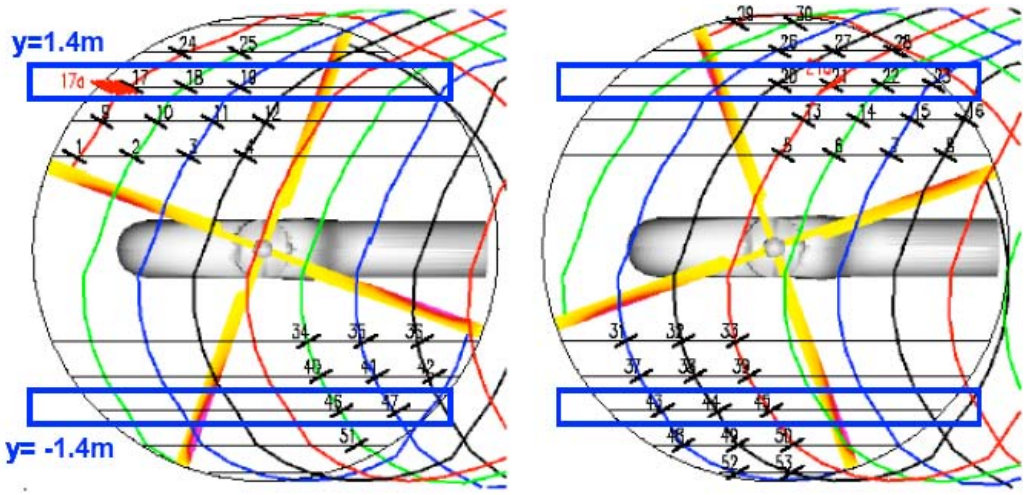

a) Ψ = 70° b) Ψ = 20°

Figure 4.15. Particle image velocimetry (PIV) measurement-plane positions for the HART II baseline case, taken from Lim and Strawn [2007].

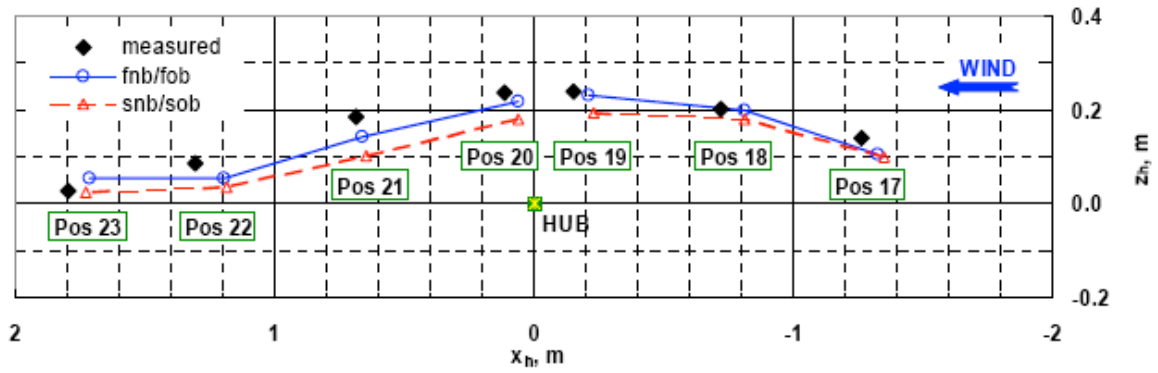

a) Advancing side, y = 1.4 m

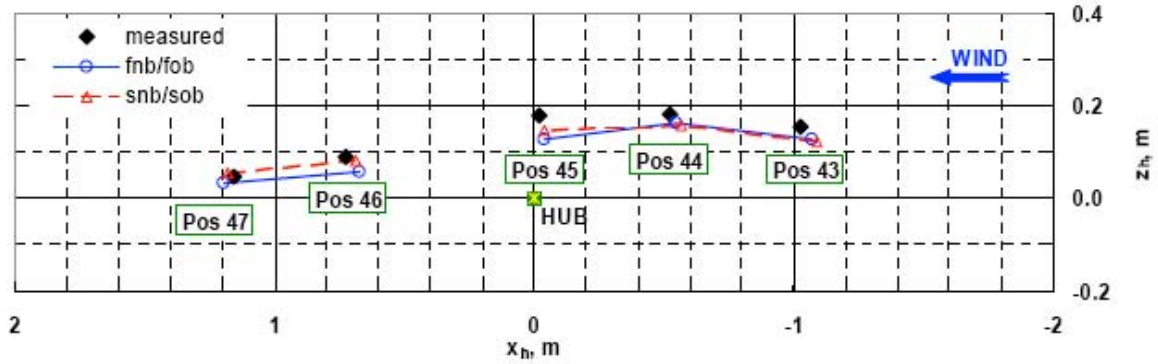

b) Retreating side, y = –1.4 m

Figure 4.16. Computed rotor-blade wake positions compared with measurement for two longitudinal cutting planes on the advancing and retreating sides (y = ±1.4 m) for the HART II baseline case, taken from Lim and Strawn [2007].

diameter at ψ = 360 deg—is a first cut in this regard and is being presented without a SOA measurement baseline. This metric will be especially important for measuring improvement associated with advanced computational methods, as their inherent numerical dissipation, which tends to smear vortical flow detail, needs to be carefully evaluated. As time progresses, additional metrics will most likely be needed for this important area.

Results based on unstructured CFD solvers

The FUN3D solver provides two levels for rotor simulation, an actuator disk and rotating overset blades. The actuator-disk simulation is suitable for steady-state calculations in which detailed simulation of the individual rotor blades is of secondary importance, such as investigating the interaction of the rotor wake on various components of the airframe. The overset blade simulation is needed for time-varying calculations in which the local flow field in the vicinity of the rotor is important, such as investigation of rotor performance. Since the capability for rotorcraft simulations in the unstructured-grid RANS area is relatively recent (and indeed, actively ongoing through developments with the FUN3D solver), there are far fewer examples to illustrate the SOA for this formulation.

Several rotorcraft case studies using the actuator disk to represent the rotor and an unstructured Navier–Stokes analysis to model the body have been presented in O'Brien and Smith [2005]. The configurations included the generic ROBIN and Georgia Tech research test articles and a Dauphin production helicopter model [O'Brien, 2006].

Computations have also been performed on two small-scale uncrewed air vehicle (UAV) rotorcraft configurations described in Jones et al. [2006]: one with a triangular-shaped cross-section (Tri model), the other with a hexagonal-shaped cross-section (Hex model). These configurations have been tested with and without the main rotor over a notional operating envelope. Pressure distributions from FUN3D are compared with experiment at several longitudinal stations on the body for the Hex model with rotor in figure 4.17. Results are typical for a Navier–Stokes solver. In general, agreement of the computed and measured pressure distributions is very good. However, FUN3D underpredicts both the download and the drag.

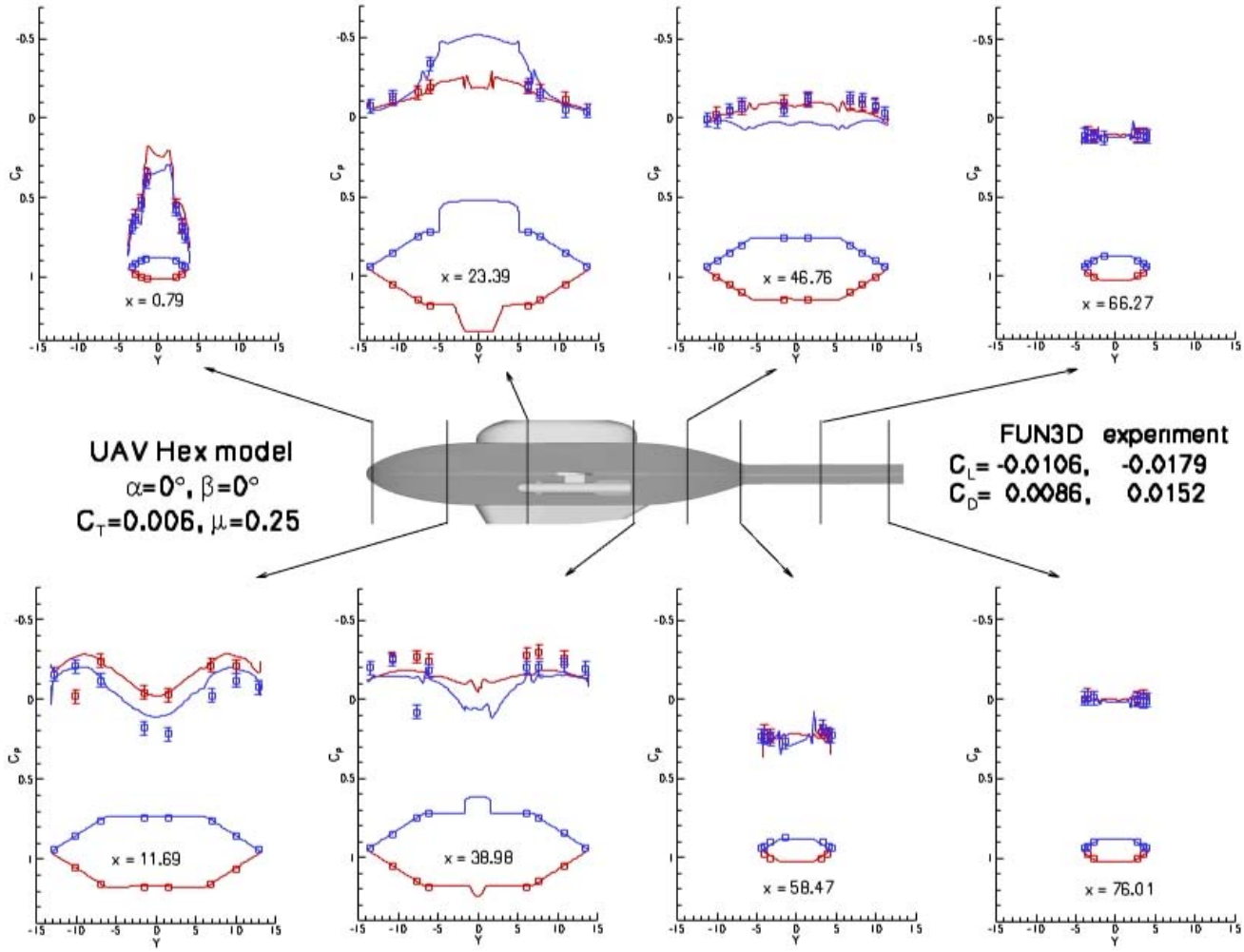

Figure 4.17. Computational pressures from FUN3D using an actuator-disk model compared with experiment for the UAV Hex model [Jones et al., 2006], taken from Mineck and Jones [to be published].

Computed downloads from FUN3D compared with experiment for the Tri-model geometry in forward flight are presented in figure 4.18. FUN3D predictions follow the experimental variation of the fuselage lift with advance ratio but the computed magnitude does not match the measurements. Prediction of the rotor-induced download on helicopter fuselages has always been a difficult challenge. No experimental pressures are available for this case, making explanations for the discrepancy between calculated and measured lift coefficient ($C_{L)}$ speculative.

Figures 4.17 and 4.18 show the rotor-induced download on the fuselage was underpredicted for the UAV and Tri-model configurations, respectively. For both configurations, a simple linear radial variation of the rotor loading was assumed. A more representative rotor loading based on the local blade lift should improve the fidelity of the rotor simulation and possibly improve the prediction of the download on the fuselage.

The FUN3D solver has been coupled to the CSD code CAMRAD II [Biedron, 2007]. Airload data and structural response data are exchanged between the codes once per revolution. The HART II Baseline, Minimum Noise, and Minimum Vibration cases have been analyzed using the coupled scheme [Biedron and Lee-Rausch, 2008]. In all three cases the simulation includes both the rotor and the fuselage/sting of the HART II wind tunnel model; wind tunnel walls are not included. Measured-force data in the HART II experiment were limited to normal force at a single span station r/R = 0.87; no moment data were taken. However, extensive measurements of blade motion were taken, allowing for an assessment of the computed structural response. A comparison of the

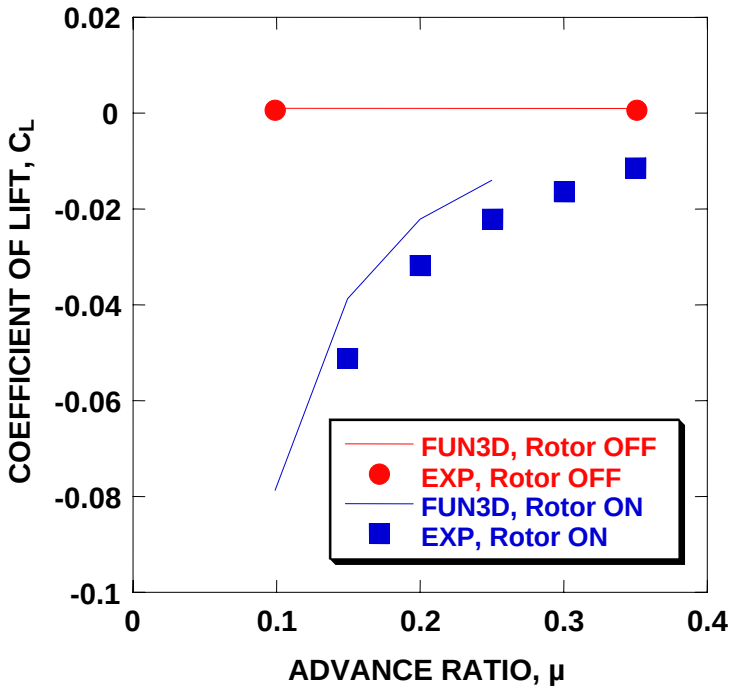

Figure 4.18. Comparison of computed and experimental downloads for the UAV Tri model in forward flight, FUN3D with rotor actuator disk turned on and off, $\alpha = 0°$, $\beta = 0°$, $C_T = 0.006$, taken from Mineck and Jones [to be published].

experimentally measured and computed data for sectional normal force coefficient (scaled by Mach number squared) at r/R = 0.87 is shown in figure 4.19 for the Baseline case. Also shown in the plot is the convergence of the computed results with coupling cycle. As for the structured-grid approach, the loose-coupling method converges within several trim cycles. Although the coupling has captured the basic three-per-revolution load variation, the blade–vortex interaction (BVI) is not well-captured by the relatively coarse 6.9-million-node grid. Figure 4.20 shows the corresponding comparison and convergence history for the tip (r/R = 1.0) elastic torsion. Elastic torsion is the blade pitch with the collective, cyclic, and built-in blade twist removed, and thus indicates the aeroelastic deformation in pitch.

Analogous to the structured-grid results shown in figure 4.13, figure 4.21 illustrates the quantitative comparison between the computed results and the experimental data. The experimental and computational data have been interpolated to 15-deg increments. The same base for computing error is used in both figures to allow direct comparison.

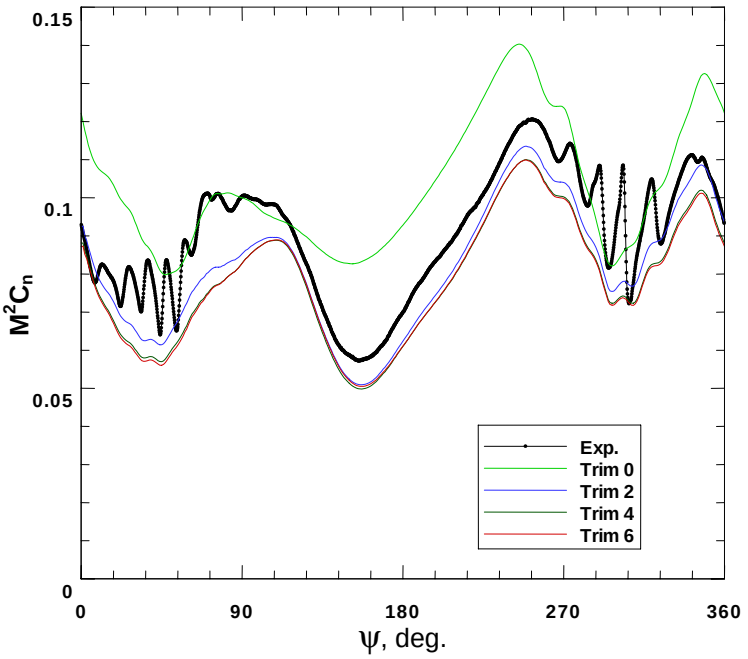

Figure 4.19 Convergence of normal force for loose coupling using unstructured grids (FUN3D/ CAMRAD II), HART II wind tunnel model, Baseline case, r/R = 0.87. Experimental data shown for comparison.

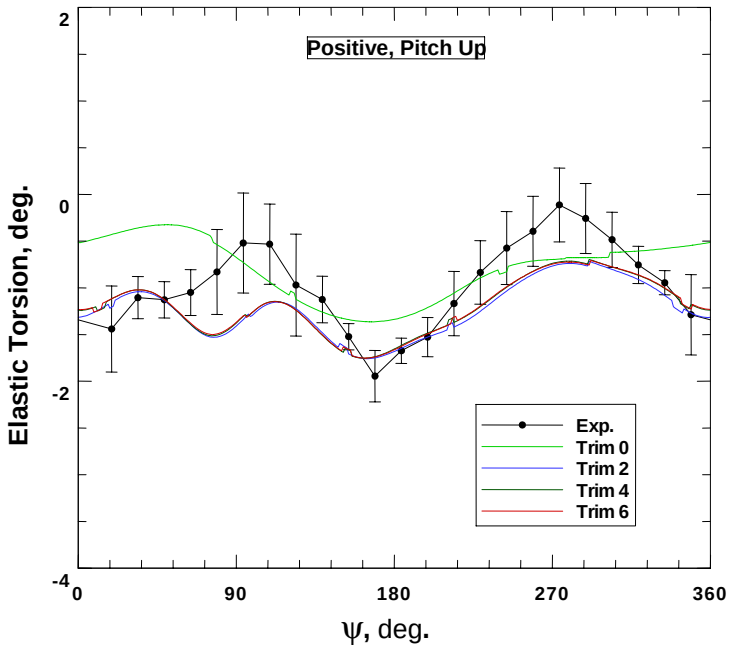

Figure 4.20. Convergence of elastic torsion for loose coupling using unstructured grids (FUN3D/ CAMRAD II), HART II wind tunnel model, Baseline case, r/R = 1.0. Experimental data shown for comparison; error bars represent blade-to-blade scatter.

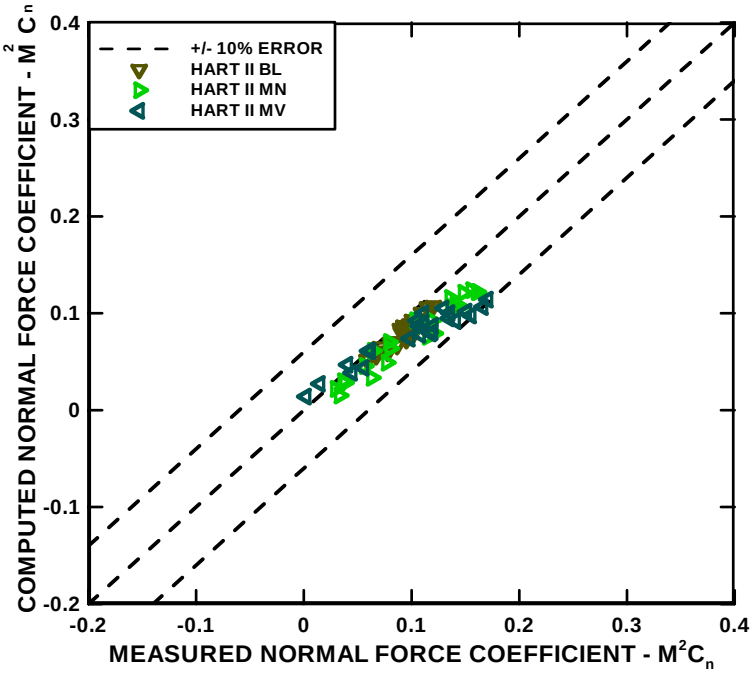

Figure 4.21. Measured versus computed normal force for the HART II wind tunnel model using the FUN3D solver with captured wakes. Same error base as for figure 4.13.

Maneuver Computations

This section describes aeromechanic computations associated with rotorcraft maneuver conditions. This type of computation is more difficult than those associated with straight and level flight because a new time scale is introduced via the maneuver and because the loose-coupling approach, which is so successful for straight and level flight, generally is not applicable for maneuver conditions.

The first example simulation for this section is the vertical gust and/or plunge maneuver computation taken from Bhagwat et al. [2007] for a UH-60A rotorcraft. This computation used the OVERFLOW2 flow solver to simulate the aerodynamics and the RCAS comprehensive analysis code to simulate the structural dynamics. The two solvers were combined using a tightly coupled algorithm in which airloads and structural deformations were exchanged at the end of each time step. The maneuver was implemented, after a trimmed forward flight was achieved, in two different ways. First, the aircraft was moved downward at a constant 20-ft/sec rate for one-quarter revolution and then moved upward at the same rate over the next quarter revolution. Second, the aircraft was forced to encounter a vertical gust of the same magnitude. If the rotor is completely rigid, these two excitations are equivalent. The resulting two responses should be identical.

These two calculations were performed using a rigid-body assumption. The resulting two responses in the form of Mach-number-scaled normal-force perturbations at r/R = 0.77 are presented in the upper portion of figure 4.22. Both results are identical, consisting of an initial increase in normal force as the gust/vehicle motion is started. For this rigid-body case, the oscillations damp out quickly.

For the flexible-rotor case, however, the two excitations are not equivalent, as can be seen from the lower portion of figure 4.22. The effect of the gust is seen immediately at the 77% spanwise location, as manifested by an immediate increase in normal force. When the excitation is imparted by a change in vehicle motion, which is imparted to the rotor through the hub, the affect at the 77% span station is delayed, as required by proper blade dynamics. In addition, it is seen that the oscillations in the time response for the flexible case persist for a considerably longer time than for the rigid case.

Another result demonstrating a SOA maneuver computation that used a strongly coupled CFD/CSD formulation is presented in figure 4.23 (taken from Nygaard et al. [2006]). This computation used the OVERFLOW2 RANS solver in conjunction with the RCAS CSD solver. A trimmed four-bladed UH-60 rotor solution, developed with loose coupling, was restarted with a strongly coupled algorithm and run for one-quarter revolution (approximately) and then excited with a pitch doublet of moderate strength. The pitch doublet consisted of a 2-deg negative pitch input for approximately one-quarter revolution followed by a 4-deg positive pitch input for approximately one-quarter revolution. At the end of the pitch excitation the rotor was returned to the original pitch state. The pitch angle was changed at a one-degree-of-pitch to one-degree-of-azimuth rate.

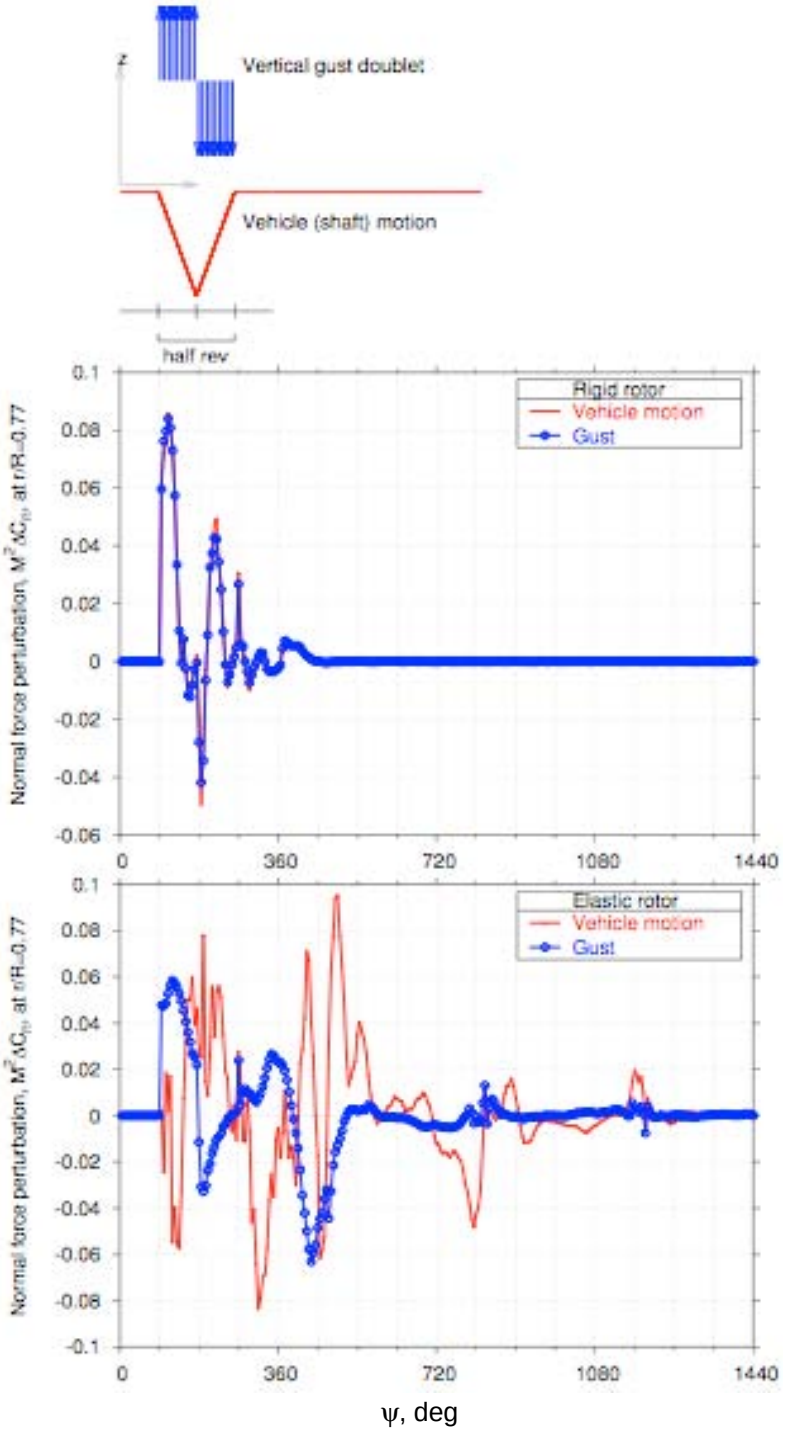

Figure 4.22. Normal-force perturbation resulting from two different but related maneuvers, vehicle plunge (red curves) and a vertical gust (blue curves), for two formulations, a) Rigid rotor, b) Elastic rotor. Taken from Bhagwat et al. [2007].

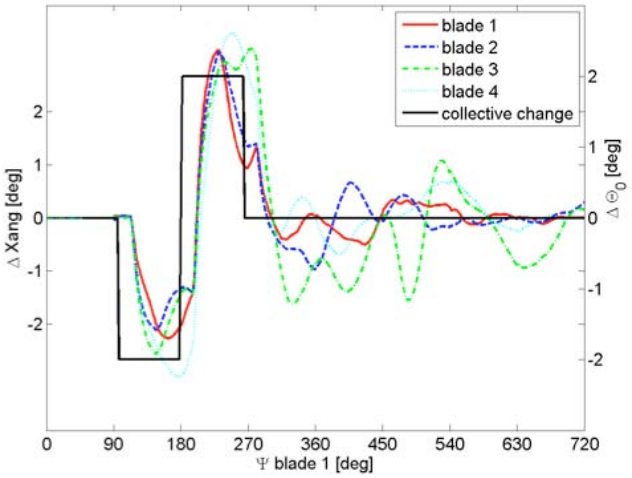

a) Perturbation pitch angle response, r/R = 0.965

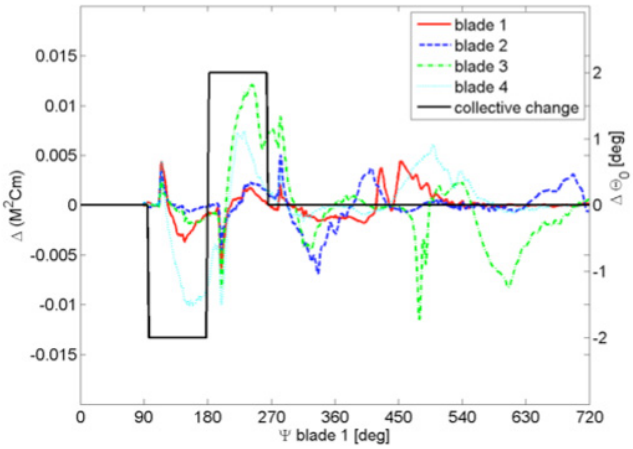

b) Perturbation pitch moment response to collective pitch doublet, r/R = 0.965

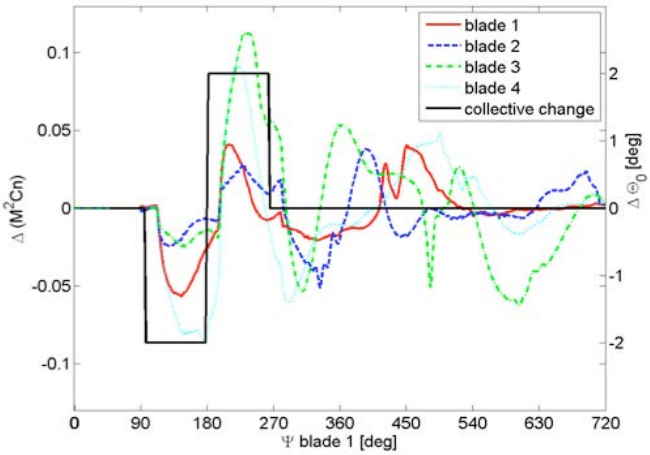

c) Perturbation normal force response to collective pitch doublet, r/R= 0.965

Figure 4.23. Response from a collective pitch doublet for a UH-60 rotor operating at 158 knots in steady-state forward flight, taken from Nygaard et al. [2006].

The perturbation pitch motion for all four blades at a radial station of 0.965 is displayed in figure 4.23a in conjunction with the pitch-angle excitation. The perturbation motion is obtained by subtracting the steady-state periodic pitch motion from the total blade pitch motion. Note that blade 3 shows clear evidence of self-excited oscillations, or torsional instability, for nearly one full rotor revolution.

The pitching moment and normal-force perturbations for all four blades at a radial station of 0.965 are presented in figures 4.23b and 4.23c, respectively, also in conjunction with the pitch-angle excitation. The perturbation airloads are far from proportionate to the pitch-angle perturbation, as numerous frequencies are excited, which persist far beyond the original excitation. This result demonstrates the dramatically nonlinear nature of the rotor dynamics problem. See Nygaard et al. [2006] for a detailed discussion of the physics associated with this simulation, especially in how the CFD and CSD disciplines interact.

Maneuver computations, such as those described in Bhagwat et al. [2007], Nygaard et al. [2006], and Bhagwat and Ormiston [2008] are just now within reach using first-principle methods because the simulation methodology and required computer power are now available. These anticipated first-principles maneuver computations assume that the additional frequencies introduced by these maneuver scenarios are not dissimilar to the frequencies already present in forward-flight simulations. Maneuver computations, such as a tiltrotor transition from vertical to forward flight in which the newly introduced time scales are significantly larger than traditional blade rotational time scales, are still beyond the scope of first-principle analysis. It is important to note that, although certain maneuver computations are now possible, they still have been neither fully explored nor validated with experimental data.

Ice-Accretion Predictions

Previous research has indicated that proper modeling of the iced surface and a grid-sensitivity study are essential for the accurate prediction of aerodynamic properties. For rime ice, which typically occurs at lower temperatures where supercooled liquid water freezes on impact, steady RANS solutions can adequately predict the aerodynamics up to near stall, both with and without wall functions, using a variety of turbulence models.

Glaze ice accretes at temperatures close to freezing in encounters with higher liquid-water content than rime ice. For glaze ice near stall it has been found that both steady and unsteady RANS solutions are unsatisfactory, regardless of the code or turbulence model used, even with a high-quality 2-D structured grid. Time-averaged DES provides some improvement in lift and drag predictions near stall for glaze ice shapes compared to steady RANS results, but in-depth comparisons [Mogili et al., 2005; and Pan and Loth, 2004] indicate that some details of the flow field are still not being captured.

Despite these challenges the current SOA is such that, given an ice shape, aerodynamic prediction is close to being a tractable problem. Significant effort still remains, however, to improve code throughput and address the means of obtaining a valid ice shape. Figures 4.24a through 4.24d show

typical results of a RANS study on a 2-D airfoil [Chi et al., 2004]. These predictions of accretion are for a 2-D rotor airfoil. Generally the computed results (figures 4.24a and 4.24b) compare well with experiment everywhere except near CL_{max}.

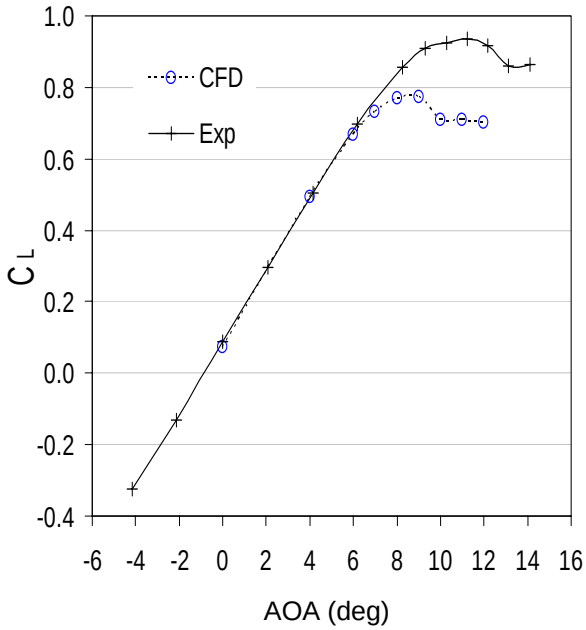

a) Lift coefficient vs. angle of attack, computational vs. experimental

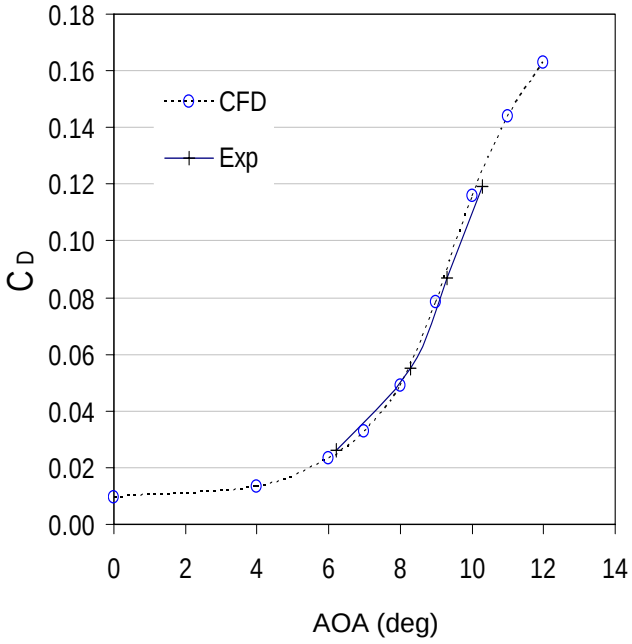

b) Drag coefficient vs. angle of attack, computational vs. experimental

Figure 4.24. Ice-accretion results from a RANS flow solver for a nonrotating airfoil geometry, taken from Chi et al. [2004].

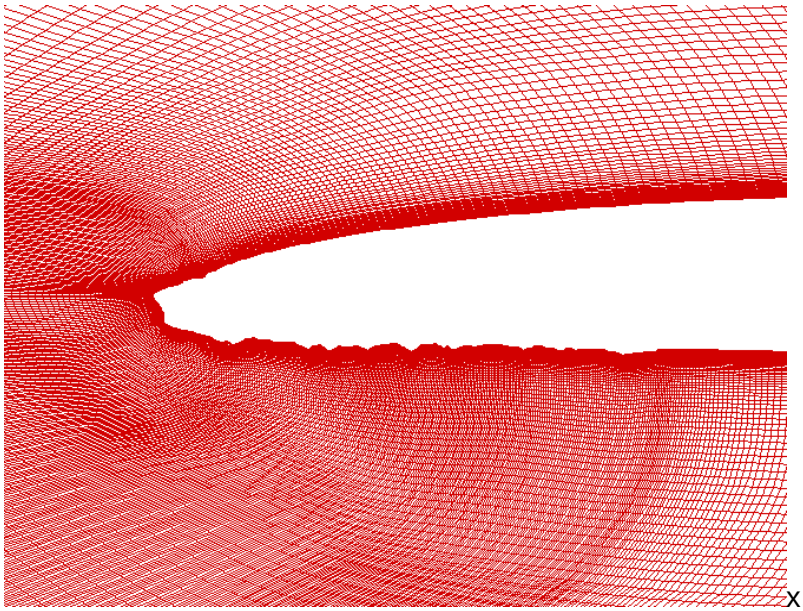

x.

c) Structured grid used for RANS CFD study

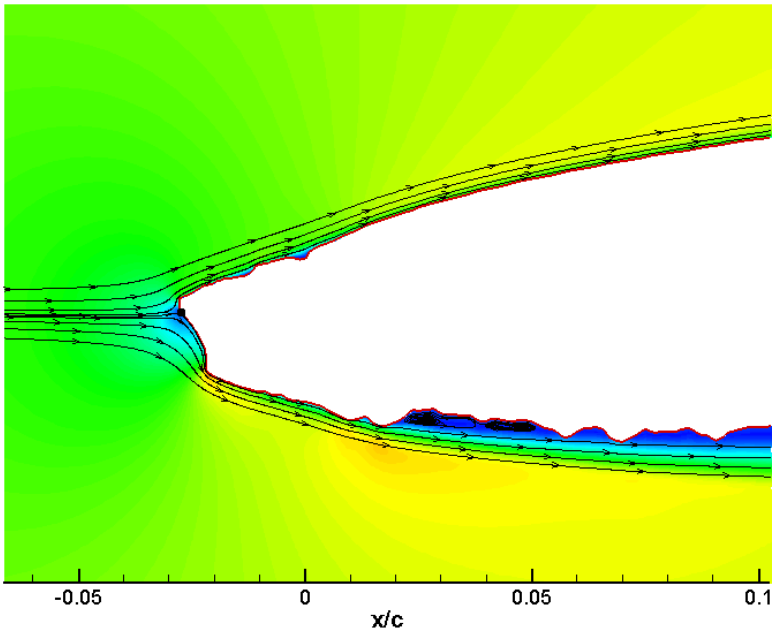

d) Ice accretion on the forward portion of an airfoil with selected streamlines from the RANS computed solution

Figure 4.24. Concluded.

Computational Cost/Efficiency

Computational cost is a difficult metric to evaluate because of the large number of dependent factors. A few pertinent cost factors are presented in table 4.1 for results presented in the literature. Many entries in table 4.1 are blank because of the lack of a published response in the associated category. The last item, wall-clock time, is presented in two ways, on a per-revolution basis and on a per-solution basis. There are not many responses in this area, especially on a per-solution basis. Even if this table were fully completed, an important additional question associated with computational efficiency is the level of accuracy that is produced. To be correct the computational efficiency of two approaches/solutions should be compared only at fixed accuracy. Thus, computational cost of a RANS solution for a rotorcraft flow field cannot be established without additional detailed information. Improvements in this area, which typically call for a multiplicative factor improvement/ reduction in wall-clock time, can still be measured using a different approach, as discussed later in this section.

Metrics Used for Monitoring Rotorcraft Aeromechanic Simulation Improvements

Specific SOA performance metrics that are deemed important for monitoring the field of rotorcraft aeromechanics simulations are presented in table 4.2. Each of the metrics, whenever possible, is presented with a SOA value that has been defined and numerically established in a preceding section, which is indicated on the “Basis” line in table 4.2. A plan for how to achieve improvements in these metrics is presented in the next section.

As can be seen from table 4.2, aeromechanic simulation metrics are being proposed for three main areas: structured CFD/CSD code enhancements, unstructured CFD/CSD code enhancements, and ice-accretion modeling improvements. There are generally two types of metrics for measuring progress, those associated with simulation accuracy and those associated with simulation cost. The accuracy metrics include rotorcraft performance, specifically, FM; airloads, which are represented by Mach-number-scaled sectional normal force and pitching moment coefficients; and vortex core diameter—D_{V360}.

The vortex core diameter, D_{V360}, is defined as the distance between the vortex cross-flow velocity component peaks at a wakeage of 360 deg. The goal is to continually reduce numerical smearing associated with rotorcraft vortical flow solutions, as measured by this parameter in comparison with experiment. For ice-accretion modeling the chief accuracy metric is associated with the prediction of the ice mass.

TABLE 4.1. COMPUTATIONAL COST STATISTICS ASSOCIATED WITH ROTORCRAFT COMPUTATIONS FROM THE LITERATURE. ALL COMPUTATIONS ARE FOR RANS SOLVERS WITH CAPTURED WAKES AND GRIDS THAT ARE FITTED TO THE ROTOR-BLADE SURFACE, I.E., NO ACTUATOR DISK SIMULATIONS ARE INCLUDED. BLANK TABLE ENTRIES HAVE NO REPORTED DATA.

Reference date	Geometry	Codes CFD/CSD	Coupling type/ frequency	Computer/chip speed	No. of procedures	Grid size	Grid spacing in wake	Wall-clock time	
								/revolution	/solution
			deg	GHz		x10^6	Tip chords	hr	hr
Potsdam et al. [2006]	UH-60A	OVERFLOWD CAMRADII	loose 90	IBM 690 1.4	80	26.1		18.8	
Potsdam et al. [2006]	UH-60A	OVERFLOWD CAMRADII	loose 90	IBM 690 1.4	16	3.3		8.0	20–28 12–20[b]
Lim and Strawn [2007]	HART II	OVERFLOW2 CAMRADII	loose 360			2.9 19.4 113	0.2 0.1 0.05		
Pomin and Wagner [2004]	ONERA/ Euro 7A	INROT DYNROT	strong 0.5	NEC SX5	8 16	15.6 42.6		80 171	
Sitaraman and Baeder [2006]	UH60A & HART II	TURNS UMARC	loose 360	Intel Xenon 3.2	1	5.2		75	
Pulliam [2007][7]	V-22 Tiltrotor	OVERFLOW2 rigid	n/a	SGI Altix 1.5	32 64	14 14	0.1 0.1	hover hover	10.5 5.7
Nygaard et al. [2006]	UH-60	OVERFLOW2 RCAS	loose & strong	IBM P4 1.7	16	4.4		1.4	
Ahmad and Strawn [1999]	Caradonna-Tung NACA0012	OVERFLOW rigid	n/a	Cray C90	1 1 1	0.41 2.5 16.2	0.2 0.1 0.05	hover hover hover	11.5 64.8 118.1
O'Brien [2006]	Robin	FUN3D prescribed motion	n/a	IBM P3 0.4	72	2.7		57[c] (39)	228[c] (156)

a Hover computations converge to steady state, and thus do not have a /rev wall-clock time.

b These times are with restart capability.

c Top number is CPU time for domain connectivity + CFD computation. The number in parentheses is for CFD computation only.

[7] Private communication. NASA Ames Research Center, Moffett Field, Calif.

TABLE 4.2. METRICS FOR MONITORING ROTORCRAFT AEROMECHANIC SIMULATION IMPROVEMENT

	Accuracy Metrics				Simulation Cost Metrics	
Structured CFD/CSD code enhancements						
Simulation metric	FM	M^2C_n	M^2C_m	D_{V360}	CC	ST
SOA	2.4%	4.4%	4.7%	IDA	variable	IDA
Basis for determining SOA	fig. 4.6	fig. 4.13	fig. 4.14	--	table 4.1	--
Unstructured CFD/CSD code enhancements						
Simulation metric	FM	M^2C_n	M^2C_m	D_{V360}	CC	ST
SOA	IDA	IDA	IDA	IDA	IDA	IDA
Advanced ice-accretion model						
Simulation metric	ice mass				CC	ST
SOA	IDA				IDA	IDA

CC—Computational cost (measured in hours of wall-clock time)
ST—Solution turnaround (measured in hours of wall-clock time)
IDA—Insufficient data available

Establishing SOA values for the ice-mass metric, the vortex-core metric, or any of the accuracy metrics for the unstructured CFD code category is not statistically possible at this time because of insufficient data. Furthermore, these metrics are a first cut in what will be required to adequately track improvements for aeromechanics simulations. As time progresses, additional metrics will most likely be needed for this important area.

Simulation cost includes two separate metrics, computational cost (execution wall-clock time) and solution turnaround time. Because the computational-cost metric is a function of so many dissimilar quantities—for example, grid resolution, time-step size, hardware speed, number of processors, system software efficiencies, convergence efficiency, parallel efficiency, etc.—establishing a quantitative basis for this metric a priori is difficult. See, for example, the variations in computational statistics that are displayed in table 4.1.

The intent of the computational-cost metric is to provide a quantitative measure by which improvement in computational cost at fixed accuracy can be monitored. Improvement can be determined by performing two separate computations for the same problem at fixed accuracy. The first will use 2007 code technology and the second current code technology. The computational cost improvement will be determined by comparing the two computational costs (execution wall-clock times) that are obtained.

The solution turnaround-time metric is composed of three factors: grid-generation time, solution-setup time, and the previously defined computational cost. Result analysis could be added as a fourth factor, but for the sake of simplicity is not included. Grid-generation time includes surface-grid-

generation time and volume-grid-generation time. In measuring grid-generation time it is assumed that a geometry file in the proper format exists prior to the start of the grid-generation process. If a file does not exist, or if a geometry file exists that has to be "repaired" in any way, then this geometry-file-creation step, because it comprises so much uncertainty, should not be included in the grid-generation time. Solution-setup time is the time required to prepare all input files, including control-parameter-input files, geometry-motion files, and grid-connectivity files, but the time excludes the actual grid file preparation, which is included under grid-generation time.

The intent of the solution turnaround-time metric is to provide a quantitative measure by which improvements in total solution turnaround time can be monitored. This metric will be computed by comparing two computations for the same problem at fixed accuracy. The first will use FY07 technology and the second current technology. The turnaround-time improvement will be determined by comparing the two turnaround times that are obtained. For consistency sake, the problem used for this purpose should be varied so that problem familiarity will not unduly cause improvements in the evaluation of this metric.

RECOMMENDATIONS FOR IMPROVING PREDICTIVE CAPABILITIES

Activities in the area of aeromechanic simulations for achieving the improvements in the metrics listed in table 4.2 are outlined in this section.

Unstructured CFD flow solver improvements

This section describes recommendations for the continued development and enhancement of unstructured-grid RANS codes for solving rotorcraft aeromechanic problems. To provide a proper focus, this discussion centers on the unstructured-grid FUN3D flow solver. A key assumption is that most features currently associated with the FUN3D code (as stated previously) will be retained. The general objective of this work is to develop an integrated, unstructured-grid rotorcraft simulation tool that overcomes the shortcomings associated with existing simulation tools. The specific goal is to efficiently perform unsteady Navier–Stokes flow-field simulations about rotorcraft flight vehicles with deforming overset grids to model flexible rotating blades. This set of recommendations will advance the SOA in the areas of accuracy and computational/throughput efficiency for unstructured-grid rotorcraft analysis.

A major stumbling block to the throughput of numerical simulation is rooted in the poor definition of the subject geometry. More often than not, the definition fails to provide a watertight representation of the geometry model required by 3-D mesh generation, and labor-intensive procedures are needed to impose this requirement. In addition, topological artifacts resulting from the creation of the model may impose unnecessary constraints on the meshing process. Therefore, additional effort must be expended to reduce the complexity of the model topology before meshing can commence. In order to improve the quality of geometry models, the adoption of solid modeling practices from the onset of computer aided design (CAD) will effectively eliminate the need to repair models prior to analysis. A robust procedure to quilt together geometric entities, thereby reducing the topological complexity of the model, will allow the development of an engineering topology. This engineering

topology can be tailored to meet the needs of a given discipline without loss of accuracy or model validity. The quilting process must include a global parameterization that is based on the underlying constituent entities.

The computational efficiency of the core FUN3D solver needs to be improved by implementing an agglomeration multigrid method for the solution of turbulent viscous flows and for the solution of the deforming mesh equations. Also the efficient higher-order time-integration schemes developed for the flow equations must be extended to the time integration of the deforming grid. In addition, a robust hybrid scheme to use the incompressible, preconditioned, or compressible equations on different parts of the domain should be implemented. Mesh adaptation aimed at improving solution accuracy is a key to resolving the rotorcraft wake system. Improvement of the current SOA for mesh adaptation to enhance robustness and applicability for rotorcraft applications should be developed. Solution criteria from both detected features and adjoint error estimates should be used to drive the adaptation process.

Recently the FUN3D solver was modified to include the basic components for coupling to the CAMRAD II CSD code, including the combination of overset and deforming grids. Although the initial coupling is tailored to a specific CSD code, it is anticipated that the Fluid Structure Interface used in Nygaard et al. [2006] could also be implemented as a means of coupling with other comprehensive codes. The initial loose-coupling implementation requires extensive user intervention, first running the CSD code, and then using an intermediate code to process the CSD output and generate the required motion data file for the flow solver. After the flow solver is run for at least one complete revolution, a second set of intermediate codes is required to generate the delta airloads file needed by the CSD code. This complete process must be done for every trim cycle, so there is plenty of opportunity for user error. The complex coupling process needs to be automated to reduce the chance of error, and to make rotorcraft simulations more routine. In addition to the basic flow-solver improvements described in the preceding paragraph, other enhancements are required for efficient rotorcraft simulations. Specific areas needing improvement include the computational cost of establishing overset connectivity and the computational cost of deforming the mesh; both must be done at each time step. In addition, the restriction of the loose-coupling frequency to once per revolution should be removed to allow coupling once per $1/N_{blade}$ revolutions.

Once the coupled, elastic simulation capability has been fully developed, attention should focus on improving the wake-capturing capability. The accurate prediction of airloads requires both accurate blade motion (addressed previously) and accurate representation of the rotor-wake system. Focus on this aspect would be best initiated after the basic coupling capability described previously is in place and a reasonable amount of experience has been obtained.

Several technology areas might be used by the unstructured-grid approach for improved wake capturing, including coupling to a wake model (either continuum or lumped-particle), higher-order schemes, and mesh adaptation. Several coupled CFD-wake-model approaches have been published that show promising improvements over uncoupled CFD results. Although gains from wake-coupling methods are notable, this approach is somewhat ad hoc. Higher-order and adaptive methods are more attractive, as they are closer to the overall first-principles philosophy of this discussion. Ongoing work on mesh adaptation within FUN3D could be leveraged for rotorcraft applications [Lee-Rausch et al., 2005; Bibb et al., 2006; and Biedron and Thomas, 2009].

Validation cases

Validation of rotorcraft-simulation capabilities achieved by FUN3D is in progress for a rigid blade, and thus, coupling to a comprehensive code is not necessary. The Tilt Rotor Aeroacoustic Model (TRAM) rotor (isolated rotor, similar to V-22) has been identified as this rigid-blade case. This configuration has been studied with OVERFLOW [Potsdam and Strawn et al., 2002], and experimental data is also available [Swanson et al., 1999]. Once the baseline coupling with CAMRAD II is in place, numerous validation cases will be computed. The HART-II baseline case is being used during the development of the coupling, and will serve as the validation case for a trimmed, elastic blade. The HART-II case has been computed by using various flow solvers and comprehensive codes, and detailed experimental data are available as well [van der Wall et al., 2002; and Yu et al., 2002]. The HART-II data include extensive measurements of vortex-core position that can be used to assess improvements of the wake resolution in FUN3D as they are implemented. A third set of validation cases will be for the UH-60, where extensive airloads data are available.

Structured CFD Flow-Solver Improvements

Recommendations for the continued development and enhancement of structured-grid RANS codes for solving rotorcraft aeromechanic problems are described in this section. To provide a focus for these plans, the discussion centers on the structured-grid OVERFLOW2 flow solver. A key element of this discussion is the assumed retention of most features that are currently associated with the OVERFLOW2 code. The flow solver uses a chimera, zonal-grid method to solve the unsteady RANS equations. The zonal-grid system consists of a set of curvilinear, near-body grids that retain the full Navier–Stokes terms and a set of Cartesian off-body grids that are used to solve the Euler equations. Initially, emphasis focuses on the development of an advanced off-body solver. For computational tests in which a full simulation is required, the current OVERFLOW2 near-body solver is used with minimal modifications in conjunction with the evolving off-body solver. Details are presented in five subtasks as follows:

Subtask 1: Advanced CFD methods

A new family of compact (and noncompact), higher-order, spatial-differencing schemes (up to eighth order) is being developed, implemented, and tested for an off-body Cartesian-grid solver that is used in OVERFLOW2. These schemes are currently limited to seven-point stencils and triple-fringe chimera logic. A new higher-order artificial dissipation scheme is being developed in concert with the spatial scheme. A new suite of higher-order time-stepping schemes (up to fourth order), including fully implicit multistage and compact schemes, is being developed to improve time accuracy and stability. These improvements are required for rotorcraft flows to help in improving performance and airloads accuracy, as well as capturing the vortex wake system, including wake-wake and blade-wake interactions for acoustics applications.

Subtask 2: Solution-adaptive methods for accurate rotorcraft-wake simulation

A new dynamic solution-adaptive-grid approach for the off-body grids used within the OVERFLOW2 flow solver is being developed to allow accurate simulation of the rotorcraft-wake system. The main focus in this subtask is to produce a solution-adaptation capability that uses the existing chimera zonal-grid framework. A detection algorithm is used within the Cartesian zonal-grid set to determine where flow-field gradients exist, that is, where the vortical wake is located. Once this location is determined, a new Cartesian zonal-grid system is generated with a series of new, finer grid zones where the gradients exist and coarser grid zones where flow gradients are lacking. This process will be periodically applied to the rotorcraft solution process, once per revolution at first, and then as the procedure is refined, at increasingly smaller time intervals. This approach, coupled with a higher-order method described in subtask 1, will reduce the required grid size for fixed accuracy or increase the accuracy for larger grids. This approach will improve performance and airloads accuracy, as well as the accuracy associated with acoustics computations, thus impacting all of the accuracy metrics. This solution-adaptive-grid approach is being demonstrated in stages, first for an isolated rigid rotor in hover—ostensibly the V-22 tiltrotor—and then for an isolated flexible rotor in forward flight.

Subtask 3: Computer science enhancements

The objective of this subtask is to reduce execution time and turnaround time for Navier–Stokes simulations and improve data mining. A multipronged approach, including domain decomposition, MPI, and loop-level parallelization, is being used to make the applications software more efficient with scalability to at least 1000 processors. This process will improve the computational-cost metric. Grid-generation automation, including the development of automated scripts for generating rotor-surface grids, will improve the solution turnaround-time metric. Nonsteady-flow visualization is required to understand the physics of complex flow fields, particularly for rotorcraft simulations because of the large amounts of data involved. Graphical routines are being developed and added to compute visualization data as the solution evolves, thus reducing solution file size by orders of magnitude over the traditional postprocessing approach. The visualization of vortex wakes through the use of total pressure iso-surfaces and/or helicity contours will be used in this effort.

Subtask 4: Validation/application for next-generation rotorcraft

The objective of this subtask is to exercise software tools for aeromechanics applications, including prediction and validation of airloads, performance, blade loads, etc. There are two elements in this subtask: (1) Computations with wind tunnel wall effects and (2) computations for next-generation helicopter/tiltrotor designs. Element 1 is an experimental support activity that is of great interest to the National Full-Scale Aerodynamics Complex (NFAC) facility. The OVERFLOW2 flow solver (including appropriate enhancements) will be employed to analyze aerodynamic interference effects produced by wind tunnel walls and model supports. Interference caused by the fuselage on the rotor system will also be evaluated. One example of this interference is the simulation of a full-scale UH-60 rotor in the NFAC with the Large Rotor Test Apparatus included. Another example is the simulation of wall effects on full-scale rotors in the 40 x 80-Foot Wind Tunnel. Element 2 is an ongoing validation effort in which newly added software enhancements are continuously validated using a standard set of test cases as well as new tests that are used to evaluate new rotorcraft concepts including concepts in active flow control. Specific existing experimental databases used for validation include V-22 tiltrotor, UH-60, HART II, and slowed-rotor tests completed in 2007 in the NASA Langley 14- by 22-Foot Wind Tunnel. Future tests should include new and improved 3-D

measurements for both the global rotor-wake flow field and new detailed measurements that focus on the tip-vortex structure. Additional details on this are presented in the succeeding section, "Validation Data Requirements."

Subtask 5: OVERFLOW2 enhancements

The objective of this subtask is to incorporate improvements into the NASA-supported version of OVERFLOW2 for application to rotorcraft problems, including advanced turbulence models; high-order accuracy numerical methods; support for deforming grids; coupling to rotorcraft comprehensive code(s); and grid-adaptation techniques. These improvements are either already available from an outside source or are under development in one of the subtasks listed previously. Outside sources include various U.S. Army-funded activities, the various Defense Advanced Research Projects Agency (DARPA) Helicopter Quieting Program teams, and other Department of Defense (DOD)-funded activities at other government labs within academia or industry. Code improvements will be tested against suitable model and/or rotorcraft problems to identify specific improvements in accuracy and efficiency for simulating performance and acoustics applications.

CFD/CSD Coupling Improvements

The general objective of this task is to develop more accurate and efficient coupling strategies/ algorithms for combining two or more disciplines in the same simulation for rotorcraft applications. This task will be subdivided into two subtasks: (1) Aerodynamics/Rotor Dynamics Coupling for Structured CFD and (2) Aerodynamic/Rotor Dynamics Coupling for Unstructured CFD.

Subtask 1: Aerodynamics/rotor dynamics coupling for structured CFD solvers

The objective of this subtask is to develop a tightly coupled interaction between an unsteady RANS flow solver using structured grids and a suitable rotor-dynamics code and to perform simulations using the coupled methodology for a range of rotorcraft configurations. The rotor-dynamics code will use an existing finite-element-based solver that is coupled time accurately to the OVERFLOW2 flow solver (i.e., tight coupling). This work will be accomplished using the following steps:

1) Add modal structures to OVERFLOW2 using tightly coupled Arbitrary Lagrangian–Eulerian procedure.
2) Acquire modal structural data for a single-blade configuration from selected second-generation rotor-dynamics code and/or ground vibration test.
3) Compute tightly coupled computations and validate with available experimental data and/or with results from other codes (DARPA/U.S. Army).
4) Develop script to run multiple cases on supercluster.
5) Add FEM structures or third-generation rotor-dynamics code to improved version of OVERFLOW2 using higher-order coupling method available through either DOD or open literature.
6) Validate coupled responses for the same test case.

Use of a “strong-coupling” approach, i.e., the implicit coupling between fluids and structures on a per-time-step basis, may be studied as an alternative to tight coupling as it may provide an enhancement to the computational-cost metric and/or to the simulation-accuracy metrics. Strong coupling would be implemented for the rotorcraft CFD/CSD problem by using a “dual time-stepping” approach, which already exists within the OVERFLOW2 flow solver. The coupling between CFD and CSD would be iterated to achieve a separate convergence during each time step. This iteration requires the added expense of multiple coupling operations during each time step, but may allow for the use of larger time steps, thus leading to an overall cost savings and/or increased simulation accuracy (especially temporal accuracy).

Subtask 2: Aerodynamics/rotor dynamics coupling for unstructured CFD solvers

The first approach examined in this subtask is to loosely couple the unstructured-grid Navier–Stokes code FUN3D to the rotorcraft comprehensive code CAMRAD II. The interface between the two codes is currently being developed, tested, and documented. A rotor-airloads-integration capability will be developed in FUN3D for the transfer of airloads to CAMRAD II via file transfer. Similarly, the rotor-blade rotation and deformation as defined by the CAMRAD II analysis output will be transferred back to FUN3D via file transfer. Subsequently, the same coupling will be examined using a tightly coupled approach.

Ice-Accretion-Prediction Improvements

The objective of this subtask is to implement recent advances within an existing framework of tools to reduce wall-clock-time requirements, improve accuracy for multiphase ice-accretion modeling, and improve the coupling algorithms between the fluid-mechanics and icing models. New techniques in grid generation and CFD will be developed to advance the SOA in ice-accretion and performance-prediction tools. The final product will be a robust, validated coupling of rotor-performance codes with ice–accretion-prediction codes. Such a tool must be able to simulate fully 3-D geometries with highly irregular ice, and be capable of handling complex rotating and nonrotating geometries in order to determine degraded performance. This code (or suite of codes) should also be upgradeable and modular in order to leverage breakthroughs in other branches of CFD to improve physical models, accuracy, robustness, speed, and hardware requirements. Finally, the effort will be validated using the ice-mass metric with results being compared to experimental data.

VALIDATION DATA REQUIREMENTS

This section describes requirements for validating CFD and CFD/CSD aeromechanic computations for isolated rotor and rotor/fuselage configurations. For this purpose, validation is defined to mean the process by which the level of error existent within a numerical simulation relative to physical reality is quantified. Several different types of errors exist within a numerical simulation—physical model error, numerical error, lack-of-convergence error, etc. In the present discussion there is no attempt to discern simulation error type—only its magnitude is considered.

A numerical simulation can be validated in several ways, including comparisons with exact analytic solutions, grid-refinement analysis, comparisons with other numerical results in which the error is known, and comparison with experimental data. For rotorcraft aeromechanic simulations the primary method for effecting validation is via the latter approach—comparison with experimental data. Thus, the central task of this section is the development of data requirements for the numerical-simulation-validation process.

In this regard it is an easy task to state that highly accurate experimental data are required across the entire flow field of interest for a suitably large range of time. This statement is, of course, not very useful, as it does not account for what experimental measurements can be obtained or the cost of obtaining them. Thus, a more in-depth listing of required measurements is presented in Chapter 5.

An experimental database for rotary-wing-icing validation is also required. Microphysical experiments should be used to develop new capabilities, while static- and powered-force rotor-blade models are required for thorough ice-shape validation. Research-quality aerodynamic data using simulated ice shapes are needed to validate aerodynamic performance degradation. Industry partnerships are needed both to help set requirements for the codes and to enhance experimental validation. More detail on validation data requirements for icing is given in Chapter 2.

AREAS BENEFITING FROM A CROSS-CUTTING TECHNOLOGY APPROACH

This section discusses the concept of cross-cutting technology development and coordination within the various rotorcraft disciplines—aeromechanics, acoustics, propulsion, flight dynamics and control, structures and materials, and experimental capabilities—as well as among the various vehicle classes—rotorcraft, fixed-wing vehicles, supersonic vehicles, and hypersonic vehicles. The main reason to consider a cross-cutting developmental approach is that many developmental efforts are multidiscipline in nature, and thus a coordinated cross-cutting approach is more efficient. In addition, many vehicle classes have problems that can be solved using common technology, i.e., technology developed under one vehicle class might solve a similar problem in a different vehicle class. A final reason for using a cross-cutting technology approach is associated with the pooling of expertise. The experts working under one discipline or vehicle class may provide a fresh or innovative approach into solving related problems within a different discipline or vehicle class. Thus, coordinated cross-cutting activities can improve developmental efficiency in several different ways. The purpose of this section is to list the pertinent areas where such an approach would be beneficial for rotorcraft aeromechanic simulations.

Potential Areas Benefiting from a Cross-Cutting Approach

The key technology areas within the field of aeromechanic simulations that could benefit from a cross-cutting approach include the following: problem setup automation, simulation-code-execution efficiency, accuracy and reliability, result analysis automation, physical-modeling improvements, validation enhancement, ice-accretion technology needs, and optimization. Each of these is now discussed.

Problem setup automation

This technology area includes geometry definition, typically performed with CAD software; surface-grid generation; volume-grid generation; and input-control file preparation. Because all vehicle classes require each of these elements, a cross-cutting approach for developing technology enhancements in this area would be beneficial. The rotorcraft vehicle class has certain problem setup attributes that are not generally found in other vehicle classes, limiting the degree to which a single development effort could successfully be used for rotorcraft applications. One example of this limitation is the input file that describes geometry motion, i.e., the motion of the rotor relative to the fuselage.

Simulation-code execution efficiency, accuracy, and reliability enhancements

This technology area includes enhancements for single discipline solvers and multidiscipline coupling methods. In particular, more accurate spatial and temporal algorithms with less numerical dissipation, better convergence robustness, and better efficiency are desired. Related improvements in execution efficiency, which includes more efficient single-processor coding and more efficient parallel scalability, are also included in this topic. Because all vehicle classes generally require these elements, a cross-cutting approach for developing improvements in this technology area would be beneficial. Because rotorcraft aeromechanic simulations are strongly forced by highly flexible, moving-geometry components with special requirements on CFD/CSD coupling, many developments in the area of rotorcraft are unique to that vehicle class. Thus, a cross-cutting approach in this technology area should be limited to basic developments.

Result analysis automation

This technology area includes flow-field/solution visualization and result-processing automation, which is the conversion of raw data into knowledge that is easily usable by end users (data mining). The result-analysis-automation process should be applicable not just to a single simulation but to entire databases comprising integrated computational and experimental results. In addition, the process should infuse the actual database-generation-automation process. As such, result-analysis automation is a multidiscipline and multivehicle class undertaking that would benefit from a cross-cutting approach. Within the rotorcraft vehicle class a result-automation process would be particularly useful for an experimental capabilities/aeromechanics/acoustics cross-cutting effort aimed at an automated identification/quantification of the vortical-wake system generated by a rotorcraft.

Physical-modeling improvements

This technology area includes efforts to improve the physical models associated with the aeromechanic simulations area. The primary models needing improvement in this regard are associated with turbulence and transition. Such is the case for nearly every problem in aerodynamics for sufficiently high Reynolds numbers, and thus, this area is a multidiscipline and multivehicle class area that could benefit from a cross-cutting approach. For aeromechanic simulations the chief areas needing improved turbulence and transition models are associated with blade dynamic stall, blade-shock boundary layer interactions, and bluff-body flow separation at the hub or on the fuselage. An

additional area in which model improvements are needed is within ice-accretion prediction. The formation of ice on an aerodynamic surface strongly interacts with turbulence and transition, as well as the heat transfer. Developing physical model improvements would best be achieved across the disciplines of aeromechanics, propulsion, and experimental capabilities.

Validation enhancements

This technology area is associated with the improvement of the aeromechanic simulation validation process, i.e., the more accurate categorization and reduction of aeromechanic-simulation error. As all vehicle classes have simulation errors, and the requirement to categorize and reduce those errors, validation enhancement would benefit from a cross-cutting approach. However, within a specific vehicle class the interaction between aerodynamic or aeroelastic simulations and experimental capabilities is much more important than inter-vehicle-class interactions and should be the primary emphasis of any validation-enhancement cross-cutting activity. Within the rotorcraft vehicle class, for example, having a strong interaction between aeromechanic/acoustic simulations and experimental capabilities is of paramount importance and should be undertaken using a cross-cutting approach.

The area associated with innovative rotorcraft concepts might also benefit from a cross-cutting approach. For example, the computational challenges associated with modeling synthetic-jet-type active flow-control actuators embedded within a rotor blade are significant. The best approach for doing this modeling is a combined simulation/experimental approach.

Ice-accretion technology needs

Ice accretion includes a variety of technology topics, many of those mentioned previously, with one additional feature—the formation of ice on aerodynamic surfaces. Thus, a cross-cutting approach is essential for the development of computational tools that predict ice accretion and the resulting loss in aerodynamic performance. There are simply too many technical development issues to be addressed solely within an icing-tool development program. These areas include turbulence modeling, especially in the presence of roughness caused by ice; grid generation in the presence of ice; heat transfer models over complex 3-D roughness; and the general computational framework required to implement large CFD and CFD/CSD codes. The crosscutting characteristic for iced aerodynamic predictions spans many disciplines within the rotorcraft vehicle class, including aeromechanics, propulsion, and experimental methods.

Optimization

An analysis capability, once developed, should be used to produce optimal vehicle or vehicle-component performance. For the present discussion involving first-principle methods applied to rotorcraft vehicle analysis, optimization is not a significant near-term objective, simply because of the extreme computational cost. Ultimately, however, the ability to optimize performance of a rotorcraft will become achievable. In this context, having a rotorcraft presence within an optimization cross-cutting development effort should be considered, as it will pave the way to the time when rotorcraft optimization is an achievable goal.

REFERENCES

Ahmad, J. and Strawn, R.: Hovering Rotor and Wake Calculations with an Overset-Grid Navier–Stokes Solver. AHS 55th Annual Forum, Montréal, Canada, May 25–27, 1999.

Anderson, W. and Bonhaus, D. L.: An Implicit Upwind Algorithm for Computing Turbulent Flows on Unstructured Grids. Computers and Fluids, vol. 23, no. 1, 1994, pp. 1–21.

Baruzzi, G.; Tran, P.; Habashi, W.: Akel, I.; Balage, S.; and Narramore, J.: FENSAP-ICE: Progress Towards a Rotorcraft Full 3-D Icing Simulation System. AIAA Paper no. 2003-0024, 41st AIAA Aerospace Sciences Meeting and Exhibit, Reno, Nev., Jan. 6–9, 2003.

Bathe, K. and Wilson, E.: Numerical Methods in Finite Element Analysis. Prentice Hall, New York, N.Y., 1976.

Benek, J.; Buning P.; and Steger, J.: A 3-D CHIMERA Grid Embedding Technique. AIAA Paper no. 1985-1523-CP, 7th AIAA Computational Fluid Dynamics Conference, Cincinnati, Ohio, July 15–17, 1985. Technical Papers (A85-40926 19-34). New York, N.Y., 1985, p. 322–331.

Bhagwat, M., and Ormiston, R. A.: Examination of Rotor Aerodynamics in Steady and Maneuvering Flight Using CFD and Conventional Methods. AHS Aeromechanics Specialist's Conference, San Francisco, Calif., Jan. 23–25, 2008.

Bhagwat, M.; Ormiston, R.; Saberi, H.; and Xin, H.: Application of CFD/CSD Coupling for Analysis of Rotorcraft Airloads and Blade Loads in Maneuvering Flight. AHS 63rd Annual Forum, Virginia Beach, Va., 2007.

Bibb, K.; Gnoffo, P.; Park, M.; and Jones, W.: Parallel, Gradient-Based Anisotropic Mesh Adaptation for Re-entry Vehicle Configurations. AIAA Paper no. 2006-3579, 9th AIAA/ASME Joint Thermophysics and Heat Transfer Conference, San Francisco, Calif., June 5–8, 2006.

Bidwell, C. and Potapczuk, M.: User's Manual for the NASA Lewis Three-Dimensional Ice Accretion Code (LEWICE 3D). NASA TM-105974, 1993.

Biedron, R. T. and Lee-Rausch, E. M.: Rotor Airloads Predictions Using Unstructured Meshes and Loose CFD/CSD Coupling. AIAA Paper no. 2008-7341, 26th AIAA Applied Aerodynamics Conference, Honolulu, Hawaii, Aug. 18–21, 2008.

Biedron, R. T. and Thomas, J. L.: Recent Enhancements to the FUN3D Flow Solver for Moving-Mesh Applications. AIAA Paper no. 2009-1360, 47th AIAA Aerospace Sciences Meeting, Orlando, Fla., Jan. 5–8, 2009.

Biedron, R.; Vatsa, V.; and Atkins, H.: Simulation of Unsteady Flows Using an Unstructured Navier–Stokes Solver on Moving and Stationary Grids. AIAA Paper no. 2005-5093, 23rd AIAA Applied Aerodynamics Conference, Toronto, Ontario, June 6–9, 2005.

Biedron, R.: Unstructured CFD Developments In The Subsonic Rotary Wing Project. NASA Fundamental Aeronautics 2007 Annual Meeting, New Orleans, La., 2007.

Bir, G. and Chopra, I.: Status of University of Maryland Advanced Rotorcraft Code (UMARC). AHS Aeromechanics Specialist Conference, San Francisco, Calif., 1994.

Britton, R. K., and Bond, T. H.: A Review of Ice Accretion Data from a Model Rotor Icing Test and Comparison with Theory. AIAA Paper no. 1991-0661, 29th AIAA Aerospace Sciences Meeting, Reno, Nev., Jan. 7–10, 1991.

Buning, P.; Chiu I.; Obayashi, S.; Rizk, Y.; and Steger, J.: Numerical Simulation of the Integrated Space Shuttle Vehicle in Ascent. AIAA Paper no. 1988-4359, AIAA Atmospheric Flight Mechanics Conference, Minneapolis, Minn., Aug 15–17, 1988.

Carpenter, M.; Viken, S.; and Nielsen, E.: The Efficiency of High Order Temporal Schemes. AIAA Paper no. 2003-0086, 41st AIAA Aerospace Sciences Meeting and Exhibit, Reno, Nev., Jan. 6–9, 2003.

Chan, W.: The OVERGRID Interface for Computational Simulations on Overset Grids (for Flow Solver). AIAA Paper no. 2002-3188, 32nd AIAA Fluid Dynamics Conference and Exhibit, St. Louis, Mo., June 24–26, 2002.

Chan, W.; Gomez III, R.; Rogers, S.; and Buning, P.: Best Practices in Overset Grid Generation. AIAA Paper no. 2002-3191, 32nd AIAA Fluid Dynamics Conference and Exhibit, St. Louis, Mo., June 24–26, 2002.

Chan, W.; Meakin, R.; and Postdam, M.: CHSSI Software for Geometrically Complex Unsteady Aerodynamic Applications. AIAA Paper no. 2001-0593, 39th AIAA Aerospace Sciences Meeting and Exhibit, Reno, Nev., Jan. 8–11, 2001.

Chi, X.; Zhu, B.; Shih, T.; Addy, H.; and Choo, Y.: CFD Analysis of the Aerodynamics of a Business-Jet Airfoil with Leading-Edge Ice Accretion. AIAA Paper no. 2004-0560, 42nd AIAA Aerospace Sciences Meeting and Exhibit, Reno, Nev., Jan. 5–8, 2004.

Das, M.; Madenci, E.; and Straub, F.: Aeroelastic Analysis of Rotor Blades Using Three Dimensional Flexible Multibody Dynamic Analysis. AIAA 2007-2295, 48th AIAA/ASME/ASCE/AHS/ASC Structures, Structural Dynamics, and Materials Conference, Honolulu, Hawaii, Apr. 23–26, 2007.

Dietz, M.; Krämer, E.; and Wagner, S.: Tip Vortex Conservation on a Main Rotor in Slow Descent Flight Using Vortex-Adapted Chimera Grids. AIAA Paper no. 2006-3478, 24th AIAA Applied Aerodynamics Conference, San Francisco, Calif., June 5–8, 2006.

Duque, E.; Sankar, L.; Menon, S.; Bauchau, O.; Ruffin, S.; Smith, M.; Ahuja, K.; Brentner, K.; Long, L.; Morris, P.; and Gandhi, F.: Revolutionary Physics-Based Design Tools for Quiet Helicopters. AIAA Paper no. 2006-1068, 44th AIAA Aerospace Sciences Meeting and Exhibit, Reno, Nev., Jan. 9–12, 2006.

Guruswamy, P. and Yang, T.: Aeroelastic Time Response Analysis of Thin Airfoils by Transonic Code LTRAN2. Computers and Fluids, vol. 9, no. 4, Dec. 1981, pp. 409–425.

Hartman, P.; Narducci, R.; Peterson, A.; Dadone, L.; Mingione, G.; Zanazzi, G.; and Brandi, V.: Prediction of Ice Accumulation and Airfoil Performance Degradation: A Boeing-CIRA Research Collaboration. AHS 62nd Annual Forum, Phoenix, Ariz., May 9–11, 2006.

Jespersen, D.; Pulliam, T.; and Buning, P.: Recent Enhancements to OVERFLOW (Navier–Stokes Code). AIAA Paper no. 1997-0644, 35th AIAA Aerospace Sciences Meeting and Exhibit, Reno, Nev., Jan. 6–9, 1997.

Jespersen, D.: Parallelism and OVERFLOW. NAS Technical Report NAS-98-013, NASA Ames Research Center, Moffett Field, Calif., 1998.

Johnson, W.: Recent Developments in Rotary Wing Aerodynamic Theory. AIAA J., vol. 24, no. 8, Aug. 1986, pp. 1219–1244.

Jones, H.; Wong, O.; Watkins, A.; Noonan, K.; Reis, D.; Malovrh, B.; and Ingram, J.: Initial Assessment of Surface Pressure Characteristics of Two Rotary Wing UAV Designs. AHS 62nd Annual Forum, Phoenix, Ariz., May 9–11, 2006.

Kandula, M.; and Buning, P.: Implementation of LU-SGS Algorithm and Roe Upwinding Scheme in OVERFLOW Thin-Layer Navier–Stokes Code. AIAA Paper no. 1994-2357, 25th AIAA Fluid Dynamics Conference, Colorado Springs, Colo., June 20–23, 1994.

Kunz, D.: Comprehensive Rotorcraft Analysis: Past, Present and Future. AIAA Paper no. 2005-2244, 46th AIAA/ASME/ASCE/AHS/ASC Structures, Structural Dynamics and Materials Conference , Austin, Tex., Apr. 18–21, 2005.

Lee-Rausch, E.; Park, M.; Jones, W.; Hammond, D.; and Nielsen, E.: Application of Parallel Adjoint-Based Error Estimation and Anisotropic Grid Adaptation for Three-Dimensional Aerospace Configurations. AIAA Paper no. 2005-4842, 23rd AIAA Applied Aerodynamics Conference, Toronto, Ontario, Canada, June 6–9, 2005.

Lim, J. and Strawn, R.: Prediction of HART II Rotor BVI Loading and Wake System Using CFD/CSD Loose Coupling. AIAA Paper no. 2007-1281, 45th AIAA Aerospace Sciences Meeting and Exhibit, Reno, Nev., Jan. 8–11, 2007.

Liou, M. and Buning, P.: Contribution of the Recent AUSM Schemes to the OVERFLOW Code: Implementation and Validation. AIAA Paper no. 2000-4404, 18th AIAA Applied Aerodynamics Conference, Denver, Colo., Aug. 14–17, 2000. Collection of Technical Papers, vol. 2 (A00-39837 10–02), 2000.

Meakin, R.: Object X-Rays for Cutting Holes in Composite Overset Structured Grids. AIAA Paper no. 2001-2537, 15th AIAA Computational Fluid Dynamics Conference, Anaheim, Calif., June 11–14, 2001a.

Meakin, R.: Automatic Off-Body Grid Generation for Domains of Arbitrary Size. AIAA Paper no. 2001-2536, 15th AIAA Computational Fluid Dynamics Conference, Anaheim, Calif., June 11–14, 2001b.

Mineck, R. E. and Jones, H. E.: CFD Predictions of Body Force and Pressure Data for Two Rotary Wing UAV Designs. To be published as NASA TM.

Mogili, P., Thompson, D.; Choo, Y.; and Addy, H.: RANS and DES Computations for a Wing with Ice Accretion. AIAA Paper no. 2005-1372, 43rd AIAA Aerospace Sciences Meeting and Exhibit, Reno, Nev., Jan. 10–13, 2005.

Nichols, R.; Tramel, R.; and Buning, P.: Solver and Turbulence model Upgrades to OVERFLOW2 for Unsteady and High-Speed Applications. AIAA Paper no. 2006-2824, 24th AIAA Applied Aerodynamics Conference, San Francisco, Calif., June 5–8, 2006.

Nielsen, E.; Lu, J.; Park, M.; and Darmofal, D.: An Implicit, Exact Dual Adjoint Solution Method for Turbulent Flows on Unstructured Grids. Computers and Fluids, vol. 33, no. 9, Nov. 2004, pp. 1131–1155.

Noack, R.: SUGGAR: a General Capability for Moving Body Overset Grid Assembly. AIAA Paper no. 2005-5117, 17th AIAA Computational Fluid Dynamics Conference, Toronto, Ontario, Canada, June 6–9, 2005.

Norment, H.: Calculation of Water Drop Trajectories To and About Arbitrary Three-Dimensional Lifting and Non-Lifting Bodies in Potential Airflow. NASA CR-3935, Oct. 1985.

Nygaard, A.; Saberi, H.; Ormiston, R.; Strawn, R.; and Potsdam, M.: CFD and CSD Coupling Algorithms and Fluid Structure Interface for Rotorcraft Aeromechanics in Steady and Transient Flight Conditions. AHS 62nd Annual Forum, Phoenix, Ariz., May 9–11, 2006.

O'Brien, D., Jr.: Analysis of Computational Modeling Techniques for Complete Rotorcraft Configurations. PhD Thesis, Aerospace Engineering, Georgia Institute of Technology, Spring, 2006.

O'Brien, D. and Smith, M.: Analysis of Rotor-Fuselage Interactions Using Various Rotor Models. AIAA Paper no. 2005-0468, 43rd AIAA Aerospace Sciences Meeting and Exhibit, Reno, Nev., Jan. 10–13, 2005.

Pan, J. and Loth, E.: Detached Eddy Simulations for Airfoil with Ice Shapes. AIAA Paper no. 2004-0564, 42nd AIAA Aerospace Sciences Meeting and Exhibit, Reno, Nev., Jan. 5–8, 2004.

Pandya, S.; Venkateswaran, S.; and Pulliam, T.: Implementation of Preconditioned Dual-Time Procedures in OVERFLOW. AIAA Paper no. 2003-0072, 41st AIAA Aerospace Sciences Meeting and Exhibit, Reno, Nev., Jan. 6–9, 2003.

Pirzadeh, S.: Three-Dimensional Unstructured Viscous Grids by the Advancing-Layers Method. AIAA J., vol. 34, no. 1, Jan. 1996, pp. 44–49.

Pomin, H. and Wagner, S.: Navier–Stokes Analysis of Helicopter Rotor Aerodynamics in Hover and Forward Flight. AIAA J. of Aircraft, vol. 39, no. 5, Sept.–Oct. 2002, pp. 813–821.

Pomin, H. and Wagner, S.: Aeroelastic Analysis of Helicopter Rotor Blades on Deformable Chimera Grids. AIAA J. of Aircraft, vol. 41, no. 3, May 2004, pp. 577–584.

Potsdam, M. and Strawn, R.: CFD Simulations of Tiltrotor Configurations in Hover. Proc. of the AHS 58th Forum, Montreal, Canada, vol. 58, part 1, 2002, pp. 681–696.

Potsdam, M., Yeo, H.; and Johnson, W.: Rotor Airloads Prediction Using Loose Aerodynamic/ Structural Coupling. AIAA J. of Aircraft, vol. 43, no. 3, May–June 2006, pp. 732–742.

Pulliam, T. and Chaussee, D.: A Diagonal Form of an Implicit Approximate Factorization Algorithm. J. Computational Physics, vol. 39, no. 2, Feb. 1981, pp. 347–363.

Rutkowski, M.; Ruzicka, C.; Ormiston, R.; Saberi, H.; and Jung, Y.: Comprehensive Aeromechanics Analysis of Complex Rotorcraft Using 2GCHAS. J. Amer. Hel. Soc., vol. 40, no. 4, 1995, pp. 3–17.

Sitaraman, J. and Baeder, J.: Evaluation of the Wake Prediction Methodologies Used in CFD Based Rotor Airload Computations. AIAA Paper no. 2006-3472, 24th AIAA Applied Aerodynamics Conference, San Francisco, Calif., June 5–8, 2006.

Strawn, R. and Djomehri. M.: Computational Modeling of Hovering Rotor and Wake Aerodynamics. AIAA J. of Aircraft, vol. 39, no. 5, Sept. 2002, pp. 786–793.

Strawn, R., Caradonna, F. X.; and Duque, E. P. N.: 30 Years of Rotorcraft Computational Fluid Dynamics Research and Development. J. Amer. Hel. Soc., vol. 51, no. 1, Jan. 2006, pp. 5–21.

Swanson, S., McCluer, M.; Yamauchi, G.; and Swanson, A.: Airloads Measurements from a ¼-Scale Tiltrotor Wind Tunnel Test. Proc. of the 25th European Rotorcraft Forum, Rome, Italy, vol. 2, Sept. 14–16, 1999.

Tung, C.; Caradonna, F.; Boxwell, D.; and Johnson, W.: The Prediction of Transonic Flows on Advancing Rotors. AHS 40th Annual Forum, Arlington, Va., May 16–18, 1984.

van der Wall, B., et al.: The HART II Test in the LLF of the DNW–A Major Step towards Rotor Wake Understanding. 28th European Rotorcraft Forum, Bristol, England, Sept. 17–20, 2002.

Vatsa, V. and Carpenter, M.: Higher Order Temporal Schemes with Error Controllers for Unsteady Navier–Stokes Equations. AIAA Paper no. 2005-5245, 17th AIAA Computational Fluid Dynamics Conference, Toronto, Ontario, Canada, June 6–9, 2005.

Wake, B. and Baeder, J.: Evaluation of a Navier–Stokes Analysis Method for Hover Performance Prediction. AHS Aeromechanics Specialists Conference, San Francisco, Calif., Jan. 19–21, 1994.

Wright, W. User's Manual for the NASA Glenn Ice Accretion Code LEWICE. NASA CR-2002-211793, Aug. 2002.

Yu, Y., et al.: The HART-II Test: Rotor Wakes and Aeroacoustics with Higher-Harmonic Pitch Control (HHC) Inputs–The Joint German/French/Dutch/US Project. AHS 58th Annual Forum, Montreal, Canada, 2002.

CHAPTER 5

EXPERIMENTAL CAPABILITIES

Luther N. Jenkins,[1] Danny A. Barrows,[1] Benny K. Cheung,[2] Benton H. Lau,[2] Robert S. Okojie,[3]
Alan J. Wadcock,[2] Anthony Neal Watkins,[1] and Chung-Sheng Yao[1]

ACRONYMS

2MRTS	2-Meter Rotor Test Stand
ATR	Active twist rotor
BVI	blade-vortex interaction
CCD	charged-coupled device
CFD	Computational fluid dynamics
CSD	Computational structural dynamics
DARPA	Defense Advanced Research Projects Agency
DGV	Doppler global velocimetry
DNW	Duits-Nederlandse Windtunnels
FOV	field of view
GPS	global positioning system
FS TRAM	Full-span Tilt Rotor Aeroacoustic Model
HART	Higher Harmonic Control Aeroacoustic Rotor Test
IBC	Individual Blade Control
LDV	laser Doppler velocimetry
LRTA	Large Rotor Test Apparatus
LSDR	Large Scale Dynamic Rig
LV	laser velocimetry
MDART	McDonnel Douglas Advanced Rotor Technology
NFAC	National Full-Scale Aerodynamics Complex
PDV	planar Doppler velocimetry
PFM	Powered Force Model
PIV	particle image velocimetry
PMI	projection Moire interferometry

[1] NASA Langley Research Center.
[2] NASA Ames Research Center.
[3] NASA Glenn Research Center.

PSP	pressure-sensitive paint
RTA	Rotor Test Apparatus
SBMR	Sikorsky Bearingless Main Rotor
SiC	Silicon Carbide
SMART	Smart Material Actuated Rotor Technology
TDT	Transonic Dynamics Tunnel
VMD	videogrammetric-model-deformation

INTRODUCTION

The term “experimental capability” refers to a measurement technique or measurement techniques that can be applied in a wind tunnel or other test facility to obtain suitable data for satisfying a research objective. These objectives may include providing understanding and insight, conducting performance assessments, validating predictive design tools, characterizing new designs and concepts—or in the case of NASA rotorcraft research—establishing databases for the development of design and analysis methods based on “first principles.” Because the research objectives and data requirements are ever-increasing, experimental capabilities must be continually enhanced and developed to meet these growing needs.

Prior to 1970, experimental capabilities for rotorcraft testing consisted mainly of measurement of aerodynamic parameters for performance characterization, visualization of rotor wakes, and limited flow-field measurements using intrusive techniques. These techniques provided sufficient data to develop and validate analytical tools for rotorcraft design, but as design tools began to rely more heavily on computational models, experimental databases with the appropriate types of information became a pacing item for their development and validation. This situation inspired the application and development of a host of new experimental methods. Many of these methods use laser, optical, and imaging techniques to measure flow parameters nonintrusively. Although a considerable amount of time is often required for setup, these optical techniques proved to be highly effective in providing both qualitative and quantitative information about the complex flows produced by rotorcraft.

This chapter assesses optical and other advanced measurement techniques that are considered state-of-the-art techniques for rotorcraft testing. It also outlines plans for the enhancement and development of experimental capabilities to satisfy the critical data requirements of NASA rotorcraft research. The discussion focuses on the following four technical areas based on measurement type: surface-pressure measurements, flow-field measurements, blade-deformation measurements, and aerodynamic-performance measurements. Within these areas, factors such as scope, accuracy, and efficiency are also addressed. The scope of the capability refers to its applicability (i.e., the type of information provided and its uses). Efficiency is a measure of the amount of data that can be acquired during a given operation time of the test facility/apparatus. Accuracy is a measure of data quality and degree to which the true value or state of the parameter being measured is captured. Often, incremental improvements in these areas can result in significant advances to the state of the art.

EXAMPLES OF CURRENT EXPERIMENTAL CAPABILITIES FOR ROTORCRAFT TESTING

This section surveys some experimental techniques and capabilities that are currently considered to be advanced or state-of-the-art techniques for rotary-wing testing. Although the origins and basis for many of these techniques can be traced back to fixed-wing testing, their implementation in the rotorcraft test environment requires unique approaches and methods to accommodate the inherent dynamics of the model and surrounding flow field.

Surface-Pressure Measurements

For rotorcraft, steady and unsteady surface-pressure measurements provide critical information about the integrated and local effects of the air flow on the fuselage as well as the rotor blades. For example, surface pressures can be integrated over a given area to provide total as well as sectional loads. They can also be used to identify features that can impact performance, such as flow acceleration and separation. Unsteady surface pressures are essential to understand unsteady airloads, buffeting resulting from the interaction between the rotor wake and other parts of the vehicle, and impulsive airloads associated with blade–vortex interaction (BVI).

Traditionally, surface pressure has been measured via transducers connected to orifices drilled in the surface of the fuselage or rotor blade. With this approach, a sufficient number of orifices must be installed in a given area to adequately resolve pressure variations. While the fuselage can accommodate a large number of orifices, typically rotor blades cannot. The thickness of a blade can only accommodate a certain number of orifices and conduits for cables and tubing before structural integrity is compromised. One measurement technique that addresses some of these issues is pressure-sensitive paint (PSP).

PSP technology involves the application of paints or coatings containing a luminescent material to a model or vehicle surface. This material is excited using blue or ultraviolet (UV) light and the luminescence measured. The luminescent material is chosen such that its excited-state lifetime (i.e., the amount of time that a molecule resides in an excited state) is long enough so that when it interacts with molecular oxygen, the material is quenched to the ground state. Thus, PSP is an oxygen-sensitive coating as opposed to pressure-sensitive. However, if oxygen is present in the testing media (as in the case of wind tunnels operating in an air environment), then with Henry's Law, the pressure can be inferred from measuring the relative luminosity of the molecule. Figure 5.1 shows typical functional relationships between pressure and fluorescence intensity for different temperatures.

PSP is a ratiometric technique where an image acquired at a certain pressure is referenced to an image acquired at known conditions. The two standard methods of acquiring these images are the intensity-based method and the lifetime method. In the intensity-based method, the reference image is acquired when the tunnel is at isobaric and isothermal conditions, generally at wind-off or at very slow operation. This reference image is then used to compute pressures in images acquired during run conditions. Certain limitations are inherent in this technique. First, reference images must be

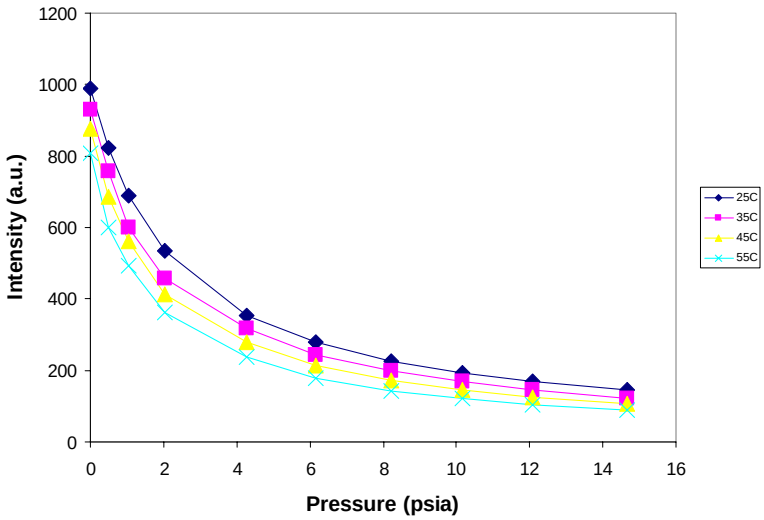

Figure 5.1. Typical PSP calibration trends showing fluorescence intensity versus pressure.

taken at each model position. Second, slight model movement between the reference and run images can cause registration errors. Third, large temperature differences on the model due to significant time differences between run images and reference images can introduce additional measurement errors.

In the lifetime method, the paint is excited using very short pulses of light (10–30 μs) and a short exposure reference image is collected during the pulse or shortly after the light is pulsed. The run image is then collected after the excitation pulse is finished and the molecules have begun to relax back to the ground state. The analysis is similar to the intensity-based method in that the "run" image is ratioed with the "reference" image, but all data are collected at condition, thus minimizing registration and temperature-difference errors.

The accuracy of PSP is generally 1–2% of the absolute pressure, but it depends on the pressure regime in question. At low pressures (typically less than 4 psia), the sensitivity of PSP is greater than at higher pressure regimes, providing improved accuracy. Uncertainty in standard pressure instrumentation (e.g., pressure orifices) can be as low as 0.05% psid. Table 5.1 summarizes additional pros and cons of PSP compared to discrete transducers.

Some of the first applications of PSP to measure the surface pressure on rotating objects were tests involving propeller models [Hubner et al., 1996] and rotating machinery [Burns and Sullivan, 1995]. This testing paved the way for application of PSP on a three-blade rotor. PSP was used to measure the pressure distribution over the entire length of the rotor blade, thus establishing the feasibility of the technique [Bosnyakov et al., 1997]. At NASA, PSP has been used to acquire surface pressures on an isolated rotor in hover [Wong et al., 2005; and Watkins et al., 2007] and several rotor-fuselage combinations in forward flight [Jones et al., 2006; and Watkins et al., 2007]. Figure 5.2 shows the

TABLE 5.1. PROS AND CONS OF USING PSP VERSUS ORIFICES TO MEASURE PRESSURE

Pros	• PSP provides a global pressure map as opposed to localized pressures. • Good dynamic range (vacuum to atmospheric and above). • PSP can significantly decrease model fabrication time/costs (uses only a fraction of the taps typically required). • PSP can provide information in places that are hard to instrument (wing/body junctures, leading edges, etc.). • PSP can be applied to most materials (metals, ceramics, some plastics, etc.).
Cons	• Temperature is the largest source of error (but can be mitigated using a few pressure taps to "anchor" data). • Data analysis requires much longer time than pressure taps. • Care must be used when handling the model (minimize skin contact due to oils and greases in skin, minimize light exposure, etc.). • Data must be collected without tunnel lights (resulting in potentially inadequate observation of the model during operation). • PSP requires the upper and lower surfaces of the blade to be painted and imaged to measure airloads.

experimental setup used for the isolated rotor in hover tested in the Rotor Test Cell at NASA Langley Research Center. Since this test was a proof-of-concept test, PSP was applied only to the outer 15% of each blade. Figure 5.3 shows pressure contours acquired at several different thrust conditions.

The results are only qualitative since the blades were not instrumented, but they show the ability of PSP to capture pressure changes associated with the different thrust conditions. Figure 5.4 shows PSP results for a rotor-fuselage combination and highlights an additional benefit of PSP. Besides providing a global view of the surface-pressure distribution, data can also be extracted to obtain line plots for more detailed analysis and comparisons. The large spikes in the line plot correspond to a joint between exterior panels on the model.

In addition to steady pressures, PSP can also be used to acquire unsteady pressures. Paint formulations are now available that have frequency responses on the order of several kilohertz. During a recent experiment on the U.S. Army's Slowed Rotor Model, a fast-response paint formulation was applied to the fuselage and compared with unsteady pressure transducers. Although the results are not published yet, preliminary results show good agreement. The next step is to apply these fast-response paints on the rotor blades. These efforts are discussed later in this chapter.

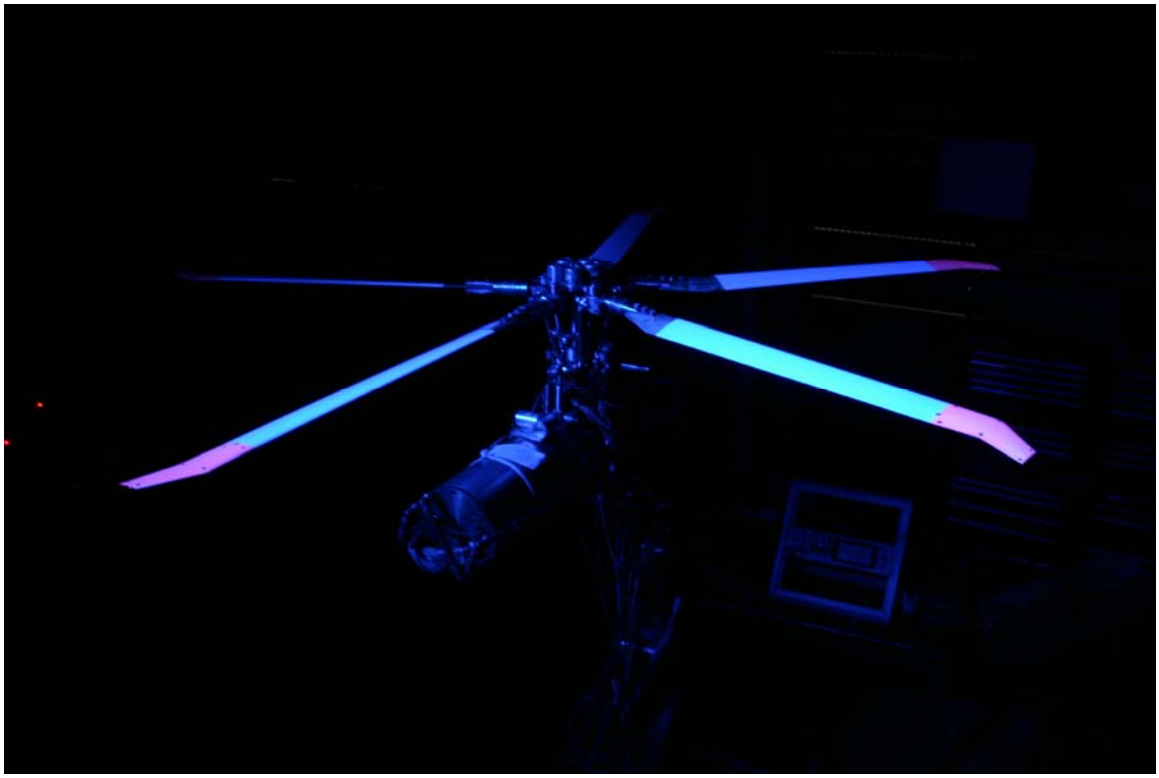

Figure 5.2. PSP application to rotor blades for blade-pressure measurements in hover.

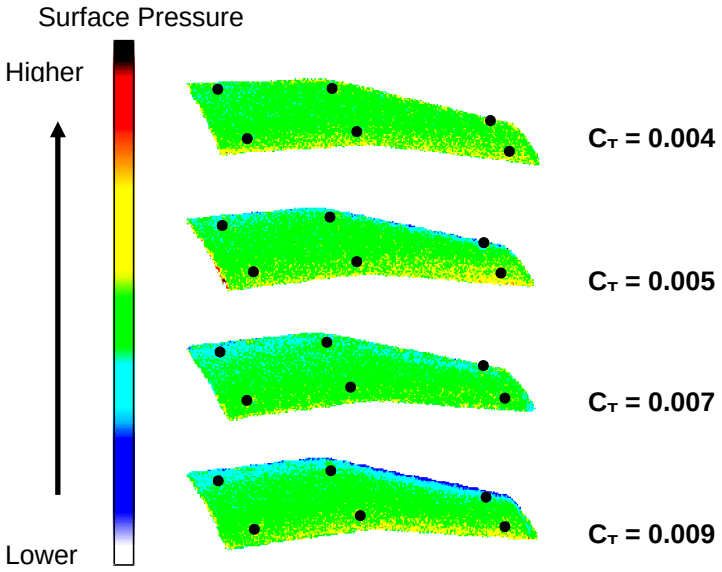

Figure 5.3. Pressure contours acquired at different thrust conditions using PSP.

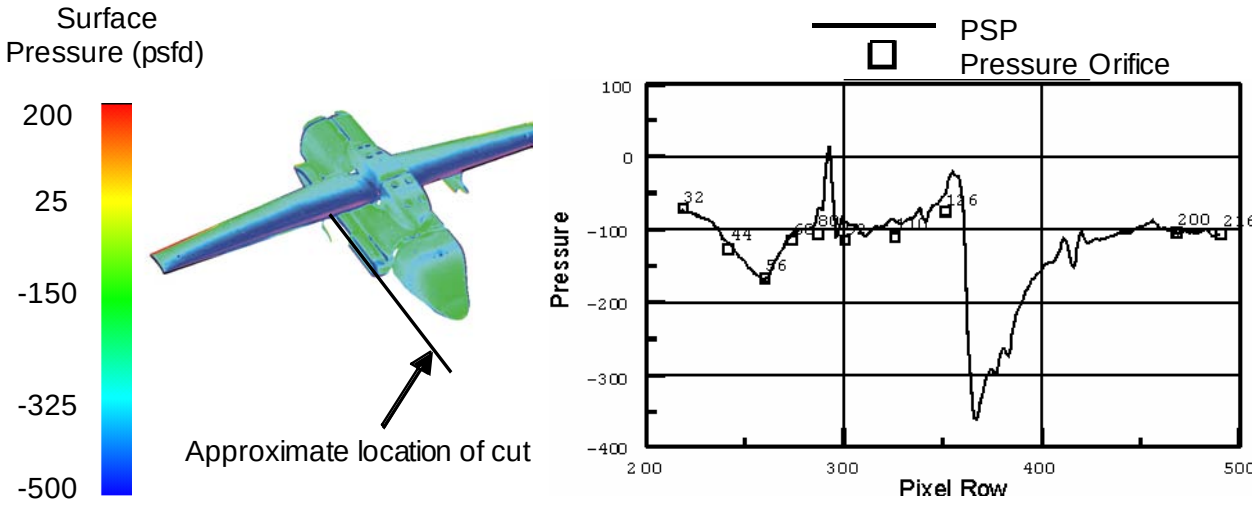

Figure 5.4. Pressure contours acquired on the Slowed Rotor Model using PSP and extracted data compared to pressure orifices.

Flow-Field Measurements

Flow-field measurements enable the documentation of flow conditions such as pressure, velocity, and temperature around individual rotors or rotor-fuselage combinations. Besides detailed quantitative information, flow-field measurements can be used to examine the structure and characteristics of important flow features associated with the rotor and its wake. These features include tip vortices, vortex sheets, flow induced by the main and tail rotors, and the interaction of the rotor wake with both the fuselage and the tail rotor. Insight into these complex flow interactions is necessary to fully understand the rotor aerodynamics and the influence of off-body flow on the overall performance characteristics of the vehicle. Such insight is also essential for performing more stringent assessments of predictive tools and methods.

For many years, pressure probes and hot wires were the primary techniques for measuring rotorcraft flow fields [Tangler et al., 1973]. Although these methods were reliable, they were intrusive and time-consuming, and they created a potential collision hazard with the moving rotor. To address the flow and structural interference issues and exploit the advances in optical methods, researchers began to apply nonintrusive techniques such as laser velocimetry (LV), Doppler global velocimetry (DGV), and particle image velocimetry (PIV) in rotorcraft tests. Table 5.2 compares some basic characteristics of these techniques to traditional techniques for quantitative flow-field measurements.

Even though the advanced techniques offer improved capability with regard to scope, efficiency, and accuracy, they also require optical access, seeding systems, and in-situ calibration. These additional requirements can impact the test facility, test objectives, and data requirements, so due consideration must be given to them when developing test plans. The next few sections discuss LV, DGV, and PIV and their application to rotorcraft testing.

TABLE 5.2. CHARACTERISTICS OF SYSTEMS USED TO MEASURE ROTOR WAKES

	LV	DGV	PIV	Hot Wire	Multihole Pressure Probe
Intrusive				X	X
Pointwise measurement	X			X	X
Planar measurement		X	X		
Multiple velocity components (u,v,w)	X	X	X	X	X
Average velocity data	X	X	X	X	X
Fluctuating velocity data	X	X	X	X	
Seeding required	X	X	X		
Calibration required		X	X	X	X
Optical access required	X	X	X		
Temperature dependence		X		X	

Laser velocimetry

Laser velocimetry (LV) is a laser-based flow diagnostic technique that measures the frequency of laser light scattered off a particle passing through a fringe pattern created at the intersection of two coincident laser beams having the same wavelength. Velocity is computed by multiplying the measured frequency, which is actually a count of the number of fringes traversed by the particle within a given period of time, and the distance traveled by the particle. This distance is determined using Bragg's Law, the wavelength of the laser light, the angle between the intersecting laser beams, and the number of fringes. Figure 5.5 shows an LV system used at the NASA Langley Research Center 14- by 22-Foot Subsonic Wind Tunnel. In addition to being nonintrusive, LV can measure unsteady and periodic flow fields, making it well-suited for rotorcraft testing. However, as shown in table 5.2, it does require optical access to the measurement area, and seed material or particulates must be introduced into the air stream to scatter light. These requirements can prohibit its use in certain facilities and in flows where the particles may fail to properly follow the flow.

Despite these requirements, LV has provided detailed insight into the complexity of the rotor wake, blade-tip vortices, and their interaction with other components. In the early 1970s, Sullivan and Ezekiel [1974] developed a two-component laser Doppler velocimeter (LDV) specifically to make measurements within the core of a blade-tip vortex and obtain detailed information regarding its structure. The system was able to measure the flow above the rotor blade, but measurements of the tip vortex were not as successful because of the inability of the frequency counters to handle the large and rapid changes in the flow field. This effort was followed by many others where two-component [Landgrebe and Johnson, 1974; and Biggers et al., 1975 and 1977] and three-component [Gorton et. al., 2002] systems were used to establish quantitative databases for developing rotor-wake theories. Figure 5.6 shows an example of induced air-flow ratios measured using LV on a torsionally stiff rotor (2MRTS) and an aeroelastically-scaled rotor (PFM) at similar operating conditions. As mentioned previously, the only way to obtain these types of data and level of detail prior to the application of LV was through the use of intrusive probes.

Figure 5.5. LV system in the NASA Langley 14- by 22-Foot Subsonic Wind Tunnel.

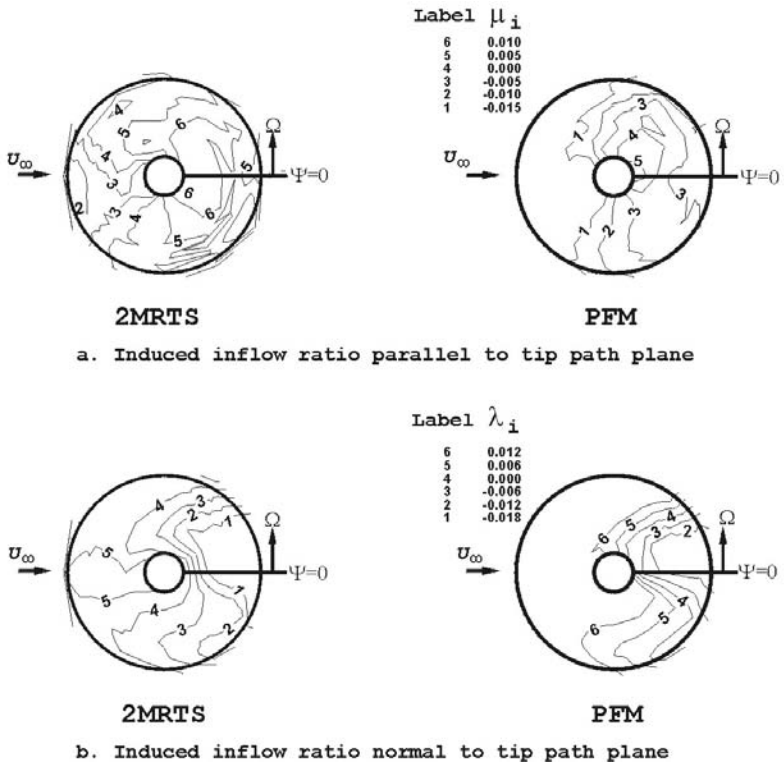

Figure 5.6. Time-averaged induced inflow velocity ratios obtained using LV and computed using PFM [Gorton and Hoad, 2002].

Despite the ability of LV to provide information for these types of comparisons, its use in large wind tunnels and test facilities has not been widespread because of its poor efficiency. In most cases, the technique requires several minutes to acquire enough samples for statistical significance. Because this sampling is done one point at a time, run times can be quite long, making specific flow conditions difficult to maintain. To improve efficiency while maintaining scope and accuracy, planar velocity-measurement techniques such as DGV and PIV were pursued.

Doppler global velocimetry

Doppler global velocimetry (or planar Doppler velocimetry (PDV)) is a planar technique that measures three components of velocity at numerous points over a large area simultaneously. The flow field of interest is seeded and illuminated by laser light. By measuring the Doppler-shifted light scattered by the illuminated seed particles, the fluid velocity is determined. Samimy and Wernet [2000], and McKenzie and Reinath [2005] provide reviews of the technique. PDV can be a useful technique for capturing flow structures such as blade-tip vortices and characterizing inflow into the main or tail rotors. An additional benefit is the adjustable spatial resolution. Because each pixel of the camera sensor is essentially a measurement point, different lenses can be used to increase or decrease the number of pixels over a given area. PDV is better suited for high-speed flows where the Doppler shift is large; consequently, applications to rotorcraft flows have been limited.

The initial application of DGV in a rotorcraft test was performed in the Langley 14- by 22-Foot Subsonic Wind Tunnel using a continuous-wave laser and charged-coupled-device (CCD) cameras [Gorton et al., 1996]. Using the setup in figure 5.7, velocity information was obtained by integrating the measurements over the camera exposure time. The results showed that the technique was promising but more development was needed to improve its accuracy and reliability. In a follow-on application, the continuous-wave laser was replaced with a pulsed laser to obtain instantaneous velocity measurements [Meyers et al., 1998a]. The system was successful in capturing the rotor-wake skew angle; however, the full capability was not realized because of vibration and temperature, which affected critical system components such as the laser and iodine cells. Additional work has been

Figure 5.7. Doppler global velocimetry in use at the Langley 14- by 22-Foot Subsonic Wind Tunnel.

done to “harden” the system [Meyers et al., 1998b] and make it more durable for large wind tunnel environments. Application of PDV to a full-scale rotor wake is reported in McKenzie and Reinath [2005]. Figures 5.8a and 5.8b show the installation of the three-dimensional (3-D) PDV system in the 80- by 120-Foot Subsonic Wind Tunnel at NASA Ames Research Center for measuring the wake of a full-scale UH-60 rotor. Measured velocity contours of the wake behind a blade are shown in figure 5.9.

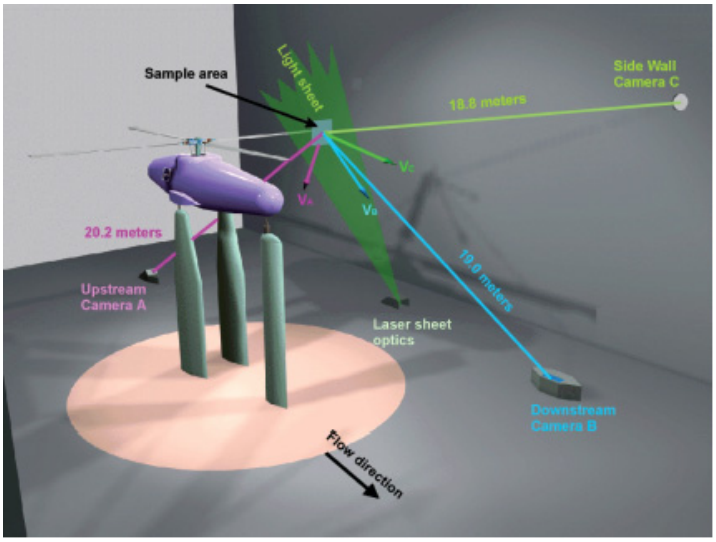

a) Schematic PDV installation

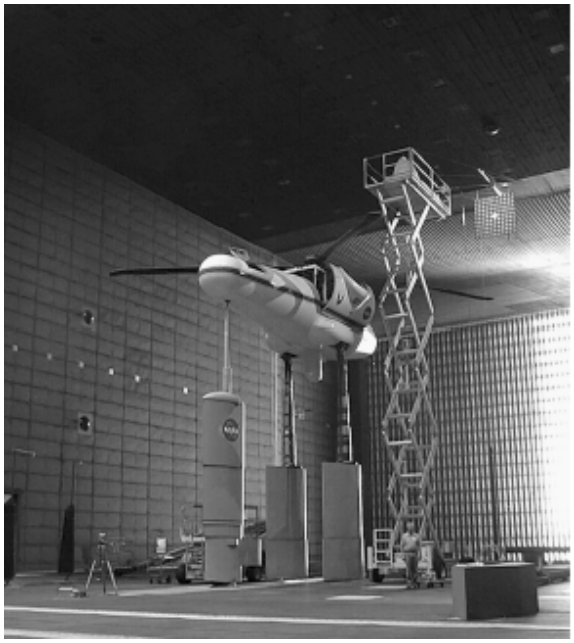

b) Mapping target elevated into position

Figure 5.8. PDV installation in the 80- by 120-Foot Subsonic Wind Tunnel at NASA Ames Research Center; reproduced from McKenzie and Reinath [2005].

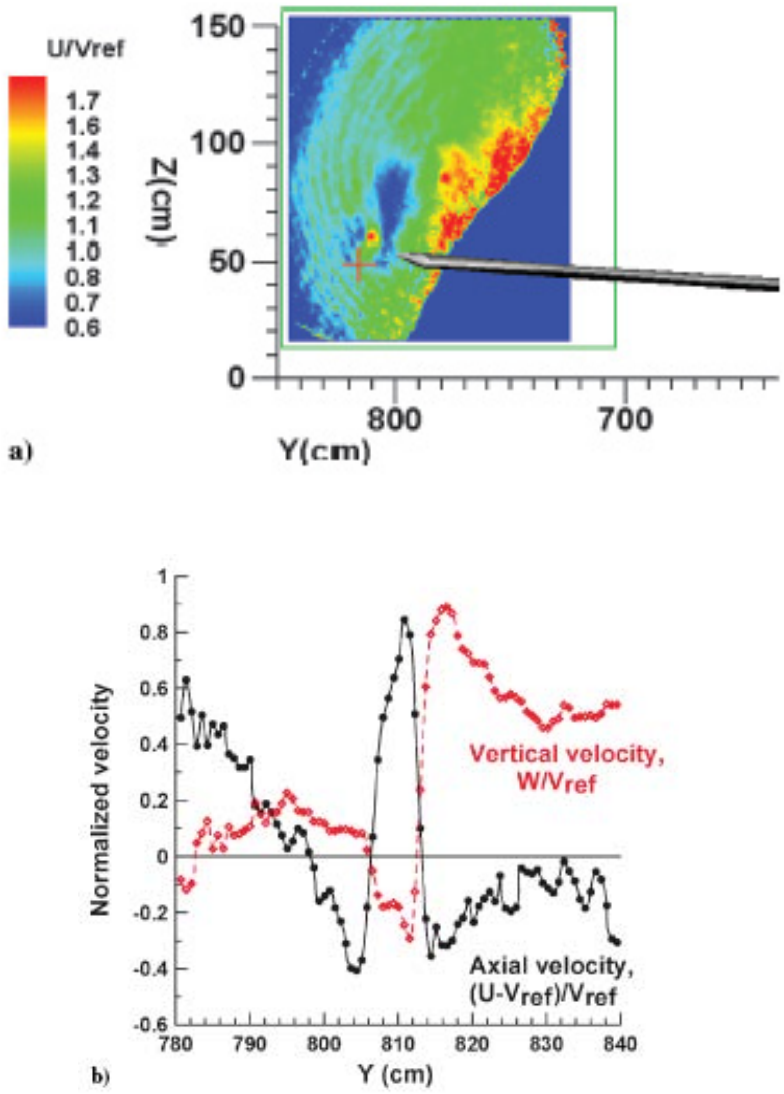

Figure 5.9. Blade-wake velocity fields: normalized axial a) velocity field contours (U/Vref) for blade trailing-edge azimuth of 15 deg upstream of light sheet, primary tip vortex core center in upper right quadrant of cross at Y,Z = (810.9, 60.0); b) [(U−Vref)/Vref] and vertical [W/Vref] velocity profiles through the primary tip-vortex core at constant Z = 60.0 cm, plotted along a line parallel to the Y axis; reproduced from McKenzie and Reinath [2005].

Particle image velocimetry

Despite the limited success of DGV, the potential increase in efficiency afforded by planar measurement techniques paved the way for the use of PIV in rotorcraft testing. Similar to instantaneous DGV systems, PIV uses a pulsed laser-light sheet to expose particles introduced into the air stream. The laser is synchronized with a digital camera such that the particles are exposed and their position recorded during successive pulses of the light sheet. The images are then interrogated to determine the displacement of a group of particles between the two laser pulses. The displacement and the time between laser pulses are then used to calculate velocity. PIV can be configured for two-dimensional (2-D) measurements (two velocity components) or 3-D measurements (three velocity components).

The latter is sometimes referred to as a stereoscopic PIV (SPIV) system and is more complicated than the 2-D systems in terms of setup and operation. Early systems were film-based, and several days were required to develop and process the images. In the early development of 2-D PIV, a film-based PIV system was shown to approach the accuracy level of a conventional LV system. With the advance of the digital-imaging system, digital PIV can conveniently acquire more PIV samples for turbulence statistics estimation and permits data reduction in a fraction of the time when compared to film-based systems. These improvements in efficiency as well as the potential to provide instantaneous measurements of vortex strength, structure, size, and location (independent of vortex wander) established PIV as a viable measurement technique for rotor-wake assessment.

NASA has amassed considerable PIV experience in a wide range of testing facilities and velocity ranges using commercial as well as indigenous PIV hardware and software. As with most experimental techniques, this experience was acquired mainly through research activities involving fixed-wing vehicles and then applied in tests involving rotorcraft. Initially, the size of the digital-camera sensors and resolution requirements limited the size of the measurement area, also known as the field of view (FOV), to approximately 1 foot by 1 foot. This limitation made PIV appropriate for measuring blade-tip vortices on small, isolated rotors [McAlister et. al., 2001; and McAlister and Heineck, 2002], but inappropriate for capturing the evolution of the wake when rotor diameters exceed 1 meter. Increases in camera-sensor size and a commensurate increase in the number of pixels made it possible to enlarge the FOV and capture a large portion of the rotor wake without sacrificing resolution. As a result, the costly and very time-consuming task of repositioning the cameras to cover a measurement area was eliminated and the development of *large-field PIV* systems began in earnest.

Large-field PIV has been used in both the U.S. Army Hover Chamber [Heineck et. al., 2000] and the 7- by 10-Foot Subsonic Wind Tunnel at NASA Ames Research Center, where flow fields have been routinely measured using FOVs as large as 3 x 6 feet [Wadcock et. al., 2002; Wadcock et. al., 2004; and Silva et. al., 2004]. Figures 5.10 through 5.14 illustrate some representative results from this research. The investigations and figures focus on three different categories of flow-field measurements. Category 1, shown in figure 5.10, consists of detailed 3-D measurements of the velocity and vorticity of the near- and midfield trailed vortices from the rotor-blade tips at various wake ages for the rotor operating in hover conditions. This test enables improved comprehensive modeling by establishing semiempirical trends of vortex core size and strength. Category 2, shown in figure 5.11, consists of global measurements of an isolated vortical structure and its evolution. Category 3 consists of global (though likely small-scale) measurements of the rotor-wake interactions around and between complete vehicles and other bodies/structures such as naval ships or vertiport sites. The experimental setup is shown in figure 5.12, and PIV results are shown on figure 5.13. Computational results for this configuration are included in figure 5.14 to show how comparisons with large-field PIV results can be used for both qualitative and quantitative validation.

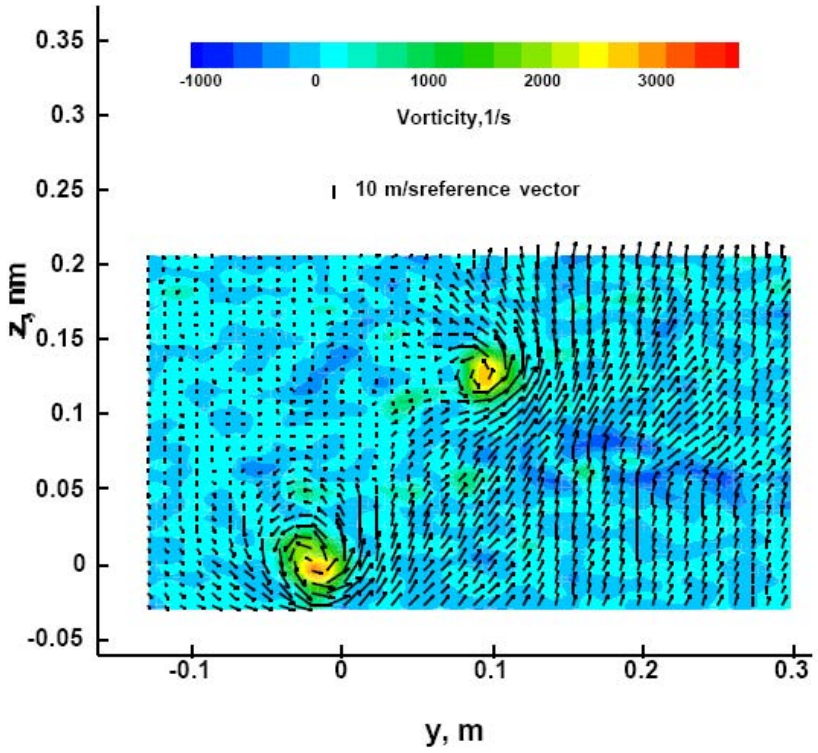

Figure 5.10. Trailed tip vortex tangential velocity and vorticity distributions (early- to midstage wakes ages from isolated rotor hover test [Heineck et al., 2000].

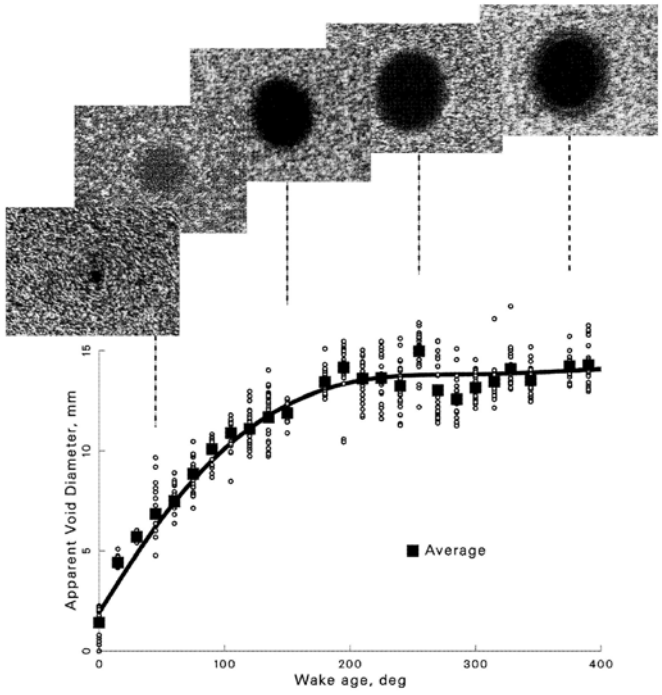

Figure 5.11. Raw PIV images showing rotor-wake structure and evolution [McAlister and Heineck, 2002].

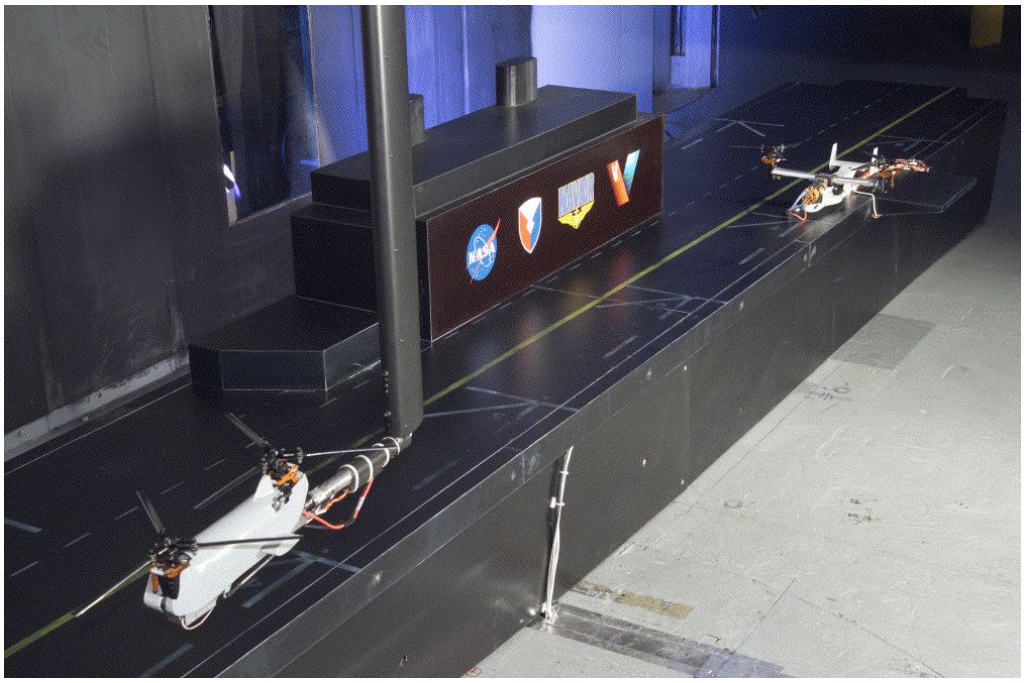

Figure 5.12. Scaled ship and aircraft wind tunnel models in U.S. Army 7- by 10-Foot Wind Tunnel.

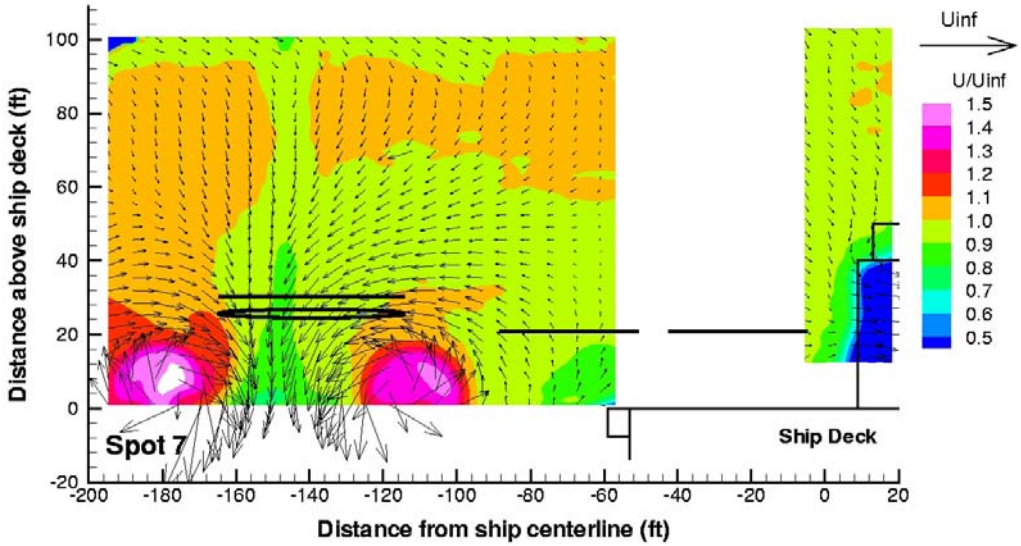

Figure 5.13. PIV measurements acquired at landing spot 7. CH-46 longitudinal location is landing spot 6, lateral offset = 4(b/2), wheels above deck = 10 ft (full-scale). [Wadcock et al., 2004].

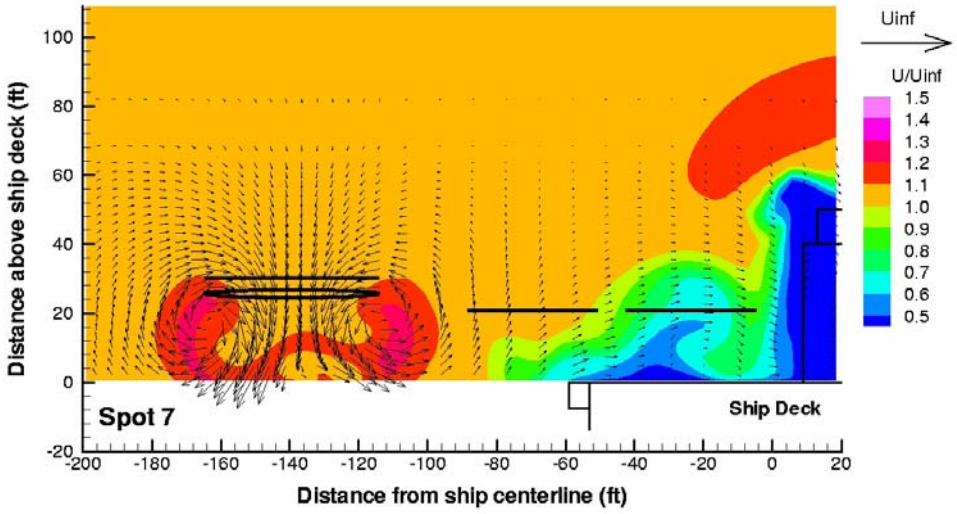

Figure 5.14. CFD calculation at landing spot 7. CH-46 longitudinal location is landing spot 6, lateral offset = 4(b/2), wheels above deck = 10 ft (full-scale). [Rajagopalan et al., 2005].

In addition to these applications, an attempt was made in 2001 to apply the large-field PIV technique in the National Full-Scale Aerodynamics Complex (NFAC) 40- by 80-Foot Wind Tunnel during testing of the Full-Span Tilt-Rotor Aeroacoustic Model (FS TRAM). Although the test ended prematurely because of model hardware issues, sufficient information was acquired to show the feasibility of using large-field PIV in the NFAC despite the challenges of seeding the facility and the long distances over which the cameras and lasers were required to operate.

Today, large-field PIV systems are commonly used in rotorcraft research. In addition to the various systems developed by NASA, European researchers have also used the technique to measure blade-tip vortices during the HART II Test in Germany's DNW Wind Tunnel [Raffel et al., 2004]. The success of these applications has established large-field PIV as the state-of-the-art technique for rotorcraft flow-field measurements and spawned numerous efforts to improve its scope, efficiency, and accuracy. Specific efforts planned by NASA are discussed later in this chapter.

Blade-Deformation Measurements

Blade-deformation measurements are used to resolve blade shape, attitude, and deflection. When combined with blade airload and rotor-wake measurements, a comprehensive dataset is formed that directly relates the physical properties of the flow to rotor performance. Such information is critical in the development of design tools and methods based on "first principles" and can potentially be used to help validate CFD-computational structural dynamics (CSD) coupled solvers. It is also a crucial measurement for testing rotor designs that use active twist, flow control, or other adaptive technologies to enhance performance and minimize noise.

Traditionally, blade-deformation measurements have been made using strain gauges, accelerometers, and other measurement devices imbedded in the rotor blade. Because of limitations in blade size and channels on the slip ring, the number of possible sensors is usually insufficient to fully resolve the blade geometry. As an alternative, optical methods can now be used to provide a fairly accurate description of the blade geometry over its entire length, with the additional benefit of reduced fabrication costs and sensor count. Two optical techniques that have been used for rotorcraft testing are projection moire interferometry (PMI) and photogrammetry.

Projection moire interferometry

PMI is a laser-based technique that provides spatially continuous structural-deformation measurements. The technique involves using a CCD camera to image equally spaced, parallel lines projected on the blade surface. An image is acquired with the blade "unloaded" to obtain a reference image and then images are acquired while the blade is spinning or in the "loaded" condition to record changes in the projected line pattern due to blade deformation. The "unloaded" and "loaded" images can then be ratioed to produce a moiré fringe pattern that equates to deformation contours.

PMI was first used to measure blade deformation during a rotorcraft test in the 14- by 22-Foot Subsonic Wind Tunnel [Fleming and Gorton, 1998] at NASA Langley Research Center. During this proof-of-concept test, the projector-camera system was mounted in the floor to image the underside of the blades on the advancing side of the rotor. Figure 5.15 shows dewarped PMI data and corresponding blade-deflection contours measured at 5 azimuths. The accuracy for these measurements was estimated to be 3%, with a minimum resolution of 0.08 mm. Following this initial test, an extensive development effort was conducted to improve the accuracy by identifying and mitigating significant error sources and reducing the cost per point when applying PMI in large wind tunnels [Fleming et. al., 1999]. One potential error source identified and examined during this effort was the refractive index of different tunnel test media. Differences in refractive index affect the pitch of projected grid lines imaged by the PMI camera. For R134a gas, the error was determined to be negligible. This result was extremely significant because it paved the way for PMI to be used during the U.S. Army's Active Twist Rotor (ATR) test in the Transonic Dynamics Tunnel (TDT), which uses R143a gas [Fleming, et. al., 2002]. Figure 5.16 shows deformation contours and individual data points extracted along the blade span to provide blade-bending and -twist information. Despite the scatter, bending and twist distributions like those provided in figures 5.16b and 5.16c are required to improve the fidelity of computational models and to perform detailed assessments of rotor performance.

PMI has been used in numerous wind tunnels and appears applicable on rotor test stands; however, because the technique relies on light intensity, it may not be as well suited for facilities like the NFAC, where large distances between the blades and the projector can reduce the visibility of the projected line pattern. An alternate technique that may be better suited for large facilities such as the NFAC is photogrammetry.

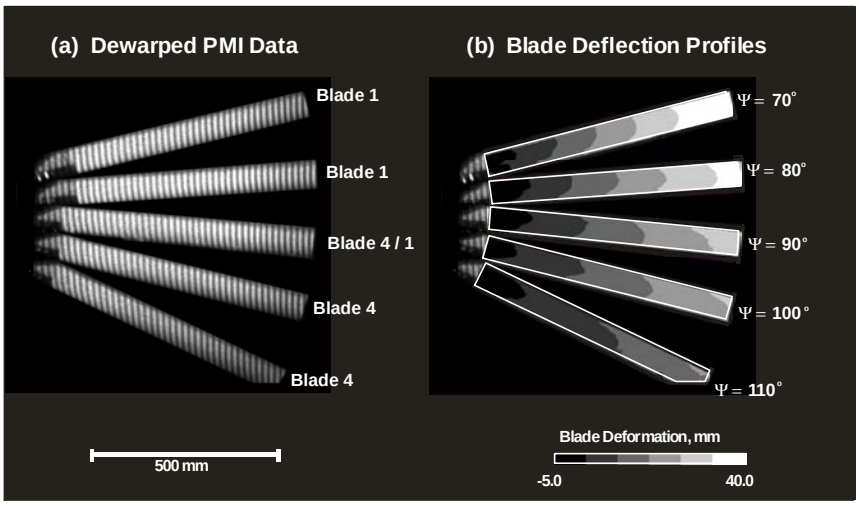

Figure 5.15. Azimuth-dependent PMI measured blade-deformation profiles, rotor shaft angle = –3 deg [Fleming and Gorton, 1998].

Photogrammetry

Photogrammetry, known within NASA as the videogrammetric-model-deformation (VMD) measurement technique, has been used extensively to measure aeroelastic deformation for fixed-wing models and in aerospace-related activities at NASA [Burner, 1997; Burner and Liu, 2001; and Barrows, 2007]. Current VMD measurement systems use digitized images from CCD cameras to determine the spatial coordinates of retro-reflective targets attached to the model surface. Since the light returned from retro targets can be much larger than from white diffuse targets, use of high-output light strobes to reduce target motion during image acquisition can enable use of photogrammetry at large facilities where PMI would be very difficult to implement. For test articles where the target displacement is constrained in one of the coordinate directions, the single-camera-view technique is typically used. For models like rotor blades that typically morph, move out of plane, or do not have a constrained coordinate in the field of motion, multiple cameras are used to resolve the coordinates of each target.

Rotorcraft research programs in both Russia and Europe have used photogrammetry for rotorcraft testing. The Russian system, referred to as the Blade Deformation Measuring System (BDMS), used CCD cameras imbedded in the hub to measure blade movement and deformation on the rotor system of a Ka-25 helicopter [Bosnyakov et al., 1997]. This arrangement was unique in that the images were acquired in the rotating frame. In Europe, a stationary stereo-pattern-recognition (SPR) measurement technique was used during the Higher Harmonic Control Aeroacoustic Rotor Test (HART II) in the German-Dutch wind tunnel (DNW). In this application, tip-flap, lead-lag, and torsion information were obtained by using overlapping stereo-camera images to reconstruct 3-D blade spatial locations [Schneider, 2005]. Successes in both Russia and Europe have established photogrammetry as a viable technique for blade-deformation measurements in both rotating and fixed frames. As a result, NASA has identified photogrammetry as a critical experimental capability for its rotorcraft research and is implementing photogrammetry systems in its primary research facilities.

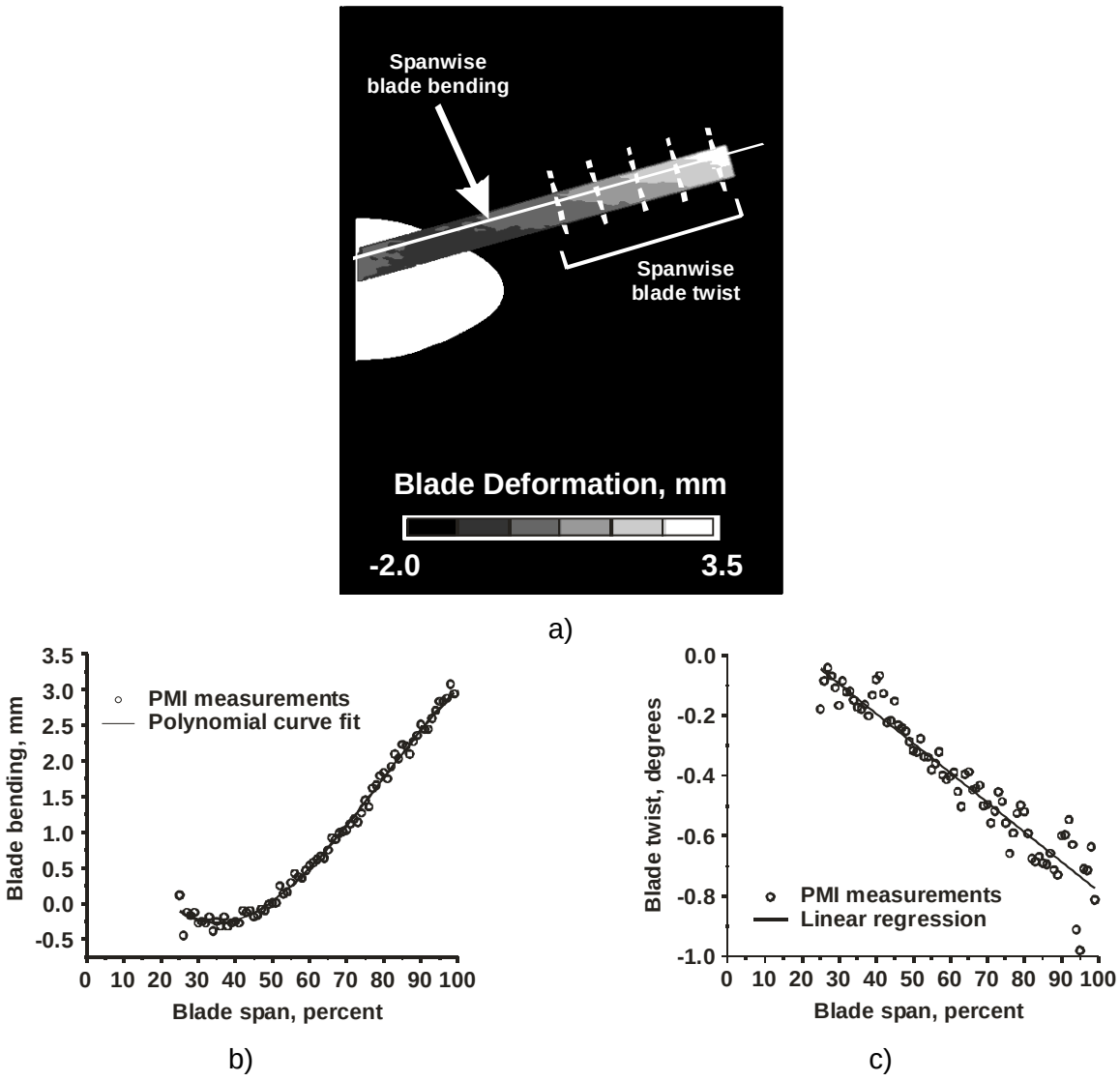

Figure 5.16. Blade-deformation measurements on Active Twist Rotor blades using PMI: (a) blade-deformation contours, (b) blade-bending distances as a function of span, and (c) blade-twist measurements as function of span [Fleming, 2002].

Aerodynamic Performance Measurements

Rotor and/or model six-component balances are commonly used to measure forces and moments acting on the test model in wind tunnel testing. Prior to testing, the balance is often calibrated statically, either separately in the calibration lab or in situ with the test model in the wind tunnel. Static calibration is suitable for mean measurement of loads acting on the model. However, when the loads acting on the test model are dynamic, a static calibration does not provide a measure of the true loads. The measured loads are always modulated by the dynamics of the rotor balance and the model due to the rotating hardware comprising the rotor and control systems. For rotorcraft, the major components of the dynamic loads come from the 1/rev and the *N*/rev harmonics of the rotor-rotating speed.

NASA has been developing methods and procedures for performing dynamic calibrations to measure unsteady hub loads for several years. A calibration study of the rotor test apparatus (RTA) was performed in the NFAC 40- by 80-Foot Wind Tunnel in 1993. Because the balance of the RTA was asymmetric, the balance responded differently when a vertical dynamic load was applied forward of the rotor shaft center than when applied aft of the rotor shaft center. The multiple load path of the RTA design also complicated the calibration and the analysis. The study raised many issues in the dynamic calibration, such as the effect of the hub mass, the effect of the shaft angle on the balance response, and the effect of multiple load paths. The calibration data were applied in the Sikorsky Bearingless Main Rotor (SBMR) tests on the RTA.

The dynamic calibration, however, was limited to an applied load of 250 lbf for both in-plane and out-of-plane shaking. Ideally, the load should have been more than twice that amount for the in-plane shaking. Nevertheless, the data showed that at the 5/rev harmonics, the dynamic correction could reduce the side-force magnitude at the rotor hub by up to two-thirds, increase the axial-force magnitude up to one-half, and reduce up to one-half the magnitudes of the rolling and pitching moments. These results show the importance of dynamic calibrations, especially when the data are being used to validate computational models that are not coupled with CSD solvers.

PLANS FOR IMPROVING TEST CAPABILITIES

This section discusses technical plans for improving and developing experimental capabilities within NASA rotorcraft. Areas of emphasis have been selected based on critical data required by other disciplines to verify and validate design tools and methods. Within this discussion, only measurement techniques applicable to isolated rotors and rotor/fuselage simulations in hover and/or constant-speed forward flight are addressed. Measurement techniques for maneuver applications have not been considered to date.

The approach for developing advanced experimental capabilities can be divided into three stages. The first stage is *fundamental research*, in which techniques are developed and evaluated for suitability and feasibility. Fundamental research may also include research on existing measurement techniques to develop a better understanding of the underlying principles on which it is based and to enhance or extend the capability. The second stage is *system development and implementation*, where promising techniques emerging from the fundamental research stage are advanced and used to design measurement/instrumentation systems that can be implemented and evaluated in appropriate testing environments. The third stage is *system integration*, which involves the application of several measurement systems to acquire a variety of flow parameters simultaneously for improved operational efficiency.

Pressure Measurements

The primary focus in this area is to use PSP to gain better insight into rotor-fuselage aerodynamic interactions (with the emphasis on the pressure distribution of the nonrotating body) and to gain insight into rotor-blade airloads, with the initial emphasis on hover results. The latter objective entails extending coverage of surface-pressure measurements using PSP to include larger regions of the rotor disk (azimuth and blade span) and the blade lower surface. NASA has extensive experience in the development and use of PSP for measuring both steady and unsteady pressure, but making measurements over such large areas and on both the upper and lower surfaces is challenging, especially with the potential changes in blade shape and position. To develop this capability, NASA plans to leverage advances in paint formulations, lighting techniques, and camera technology and extend existing methods for applying PSP to develop new systems and implementation strategies for NASA's primary rotorcraft test facilities. These systems and implementation strategies will attempt to mitigate error sources and streamline the acquisition process so as to meet the following target metrics for unsteady and steady pressure measurements:

- Unsteady pressures: Pressure sensitivity, accuracy, dynamic range, and time response within 30% compared to conventional surface pressure transducers.

- Steady pressures: Verify pressure-measurement accuracy based on PSP technology within 2% of reference pressure transducers.

To improve accuracy and overall robustness, several improvements are planned. A new system will be designed and developed to acquire data from multiple views using the lifetime method. This system will enable blade pressures to be acquired simultaneously at multiple blade positions. The robustness and applicability of PSP systems to rotorcraft testing is highly dependent on their ability to adapt to various tunnel environments. Sometimes other tunnel light sources cast shadows on the surfaces, and distances between model and illuminating light sources can be considerable. Therefore, improved lighting will be incorporated by using newer, brighter sources as well as by developing focusing strategies. The ability of the PSP to respond to the rapidly changing pressure environment on the rotor blades is a critical requirement. Depending on initial results, new paint chemistries will be explored to enhance time response.

Development and enhancements to the PSP system will be evaluated through tests in wind tunnels and rotor test stands. The tests are designed to progress systematically from measuring pressures on a fuselage to measuring blade pressures on a rotor in hover and then to measuring blade pressures on a rotor in forward flight. The first test will be the Slowed Rotor Test in the Langley 14- by 22-Foot Subsonic Wind Tunnel where surface pressures will be measured on the fuselage to supplement data acquired in 2006. Next, a test will be conducted in the Hover Test Cell at Langley Research Center on an instrumented blade in hover. The results of this test will permit extensive comparisons between PSP and surface orifices, thus establishing the benchmark for the system and helping to identify other necessary modifications and enhancements. From here, system performance will be further evaluated in a small-scale test scheduled for 2009 in the Langley 14- by 22-Foot Subsonic Wind Tunnel to measure blade pressures on a rotor in forward flight.

Flow-Field Measurements

With regard to flow-field measurements, NASA intends to improve rotor-wake diagnostics by developing large-field PIV systems for the NFAC and the Langley 14- by 22-Foot Subsonic Wind Tunnel that are capable of measuring flow velocities with an uncertainty of 1.5 m/s over extended areas within the rotor disk. In the NFAC, the current goal is to document an area 14 feet wide by 4 feet high with sufficient spatial resolution to define the structure of the trailed tip vortex of a full-scale UH-60 rotor blade. In the Langley 14- by 22-Foot Subsonic Wind Tunnel, the current goal is to document an area 8 feet wide by 3 feet high to resolve the wake behind a fuselage-rotor combination. Measuring three velocity components in such a complex flow over such large areas poses a unique challenge to NASA experimental groups. In addition, establishing these systems as a full-fledged capability in these facilities requires that they be versatile, accurate, and efficient. A significant portion of the development process will seek to evaluate the performance of these large-field PIV systems and address specific issues related to accuracy and operational efficiency.

One consideration in the use of large-field PIV is the ability to determine particle displacements. In some cases, a single pixel on the camera sensor may correspond to several millimeters in the measurement plane, so the displacement may be undetectable even though most PIV algorithms can resolve displacements as small as 0.1 pixels. To guarantee proper detection of particle displacement, NASA plans to develop and evaluate high-performance PIV image recording systems, including state-of-the-art imaging optics and sensors, to obtain the proper FOV and pixel resolution. These parameters determine the system accuracy and spatial resolution of the velocity-field measurement. The goal is for the large-field systems to have the same resolution as lab-scale PIV systems, where the particle diameter covers 2 to 3 pixels and displacements are on the order of 6 to 8 pixels. Since most commercial PIV packages base their proprietary calibration and correlation algorithms on this criterion, achieving these conditions should result in optimal accuracy and system performance.

A second consideration in applying large-field PIV in facilities like the Langley 14- by 22-Foot Subsonic Wind Tunnel and the NFAC is seeding the flow. Seeding material, seed density, and particle size greatly affect the quality of PIV signal and the ability to resolve flow structures in the rotor wake. Particles of diameter 1 micron or smaller are adequate for most flows (in the sense that they will follow a fluid streamline). Current seeders in use at NASA Ames and Langley Research Centers generate a fairly mono-disperse seed with diameters ranging from 0.2 to 0.5 microns, but increasing the particle size would increase particle visibility and permit the FOV to increase without having to increase laser power. One drawback to using larger particles is the difficulty to get them into a rotor-tip vortex and remain there. Heavy particles are naturally centrifuged out of the vortex, sometimes leaving a particle void. A particle void can be advantageous in identifying the location of a vortex, but the absence of particles inside the vortex core makes measuring the flow velocity in this area almost impossible. As part of the development effort, the spectra characteristics of different types of seed (e.g., smoke, mineral oil, and polystyrene latex spheres) will be evaluated in a laboratory environment.

After the cameras and other hardware have been integrated into systems, the challenge becomes implementing them in the various facilities and addressing operational issues. One difficulty in using optical–flow-field measurement techniques in the NFAC—or any facility for that matter—is limited optical access. In the case of the NFAC, the test section is totally enclosed by a steel shell, so using a traversable PIV system would be extremely complicated. Currently, PIV cameras are mounted in existing camera ports in the NFAC and the laser sheet must be directed into the required location with some difficulty, essentially limiting PIV measurements to a single plane for each installation. The Langley 14- by 22-Foot Subsonic Wind Tunnel offers more options for camera placement, but moving the system can be time- and labor-intensive. Calibration of a PIV system is also labor-intensive. Options for addressing these issues and optimizing system performance will be considered and explored as part of the development effort. Some proposed options include establishment of effective and efficient PIV transport systems, remote monitoring and adjustment of seeding systems and laser/optics, vibration monitoring, simplified calibration, reliable independent measurements to validate the PIV data, and using multiple camera/lens systems for variable spatial resolution and optimal PIV parameter operation.

Primary applications of large-field PIV systems to acquire critical data are scheduled to occur in 2009 as part of the UH-60 Airloads Test in the NFAC 40- by 80-Foot Wind Tunnel and as part of the Pressure Instrumented Blade test in the Langley 14- by 22-Foot Subsonic Wind Tunnel. Prior to these tests, the systems were evaluated during the 2008 NFAC UH-60 Individual Blade Control test and the 2007 Langley 14- by 22-Foot Subsonic Wind Tunnel slowed-rotor compound helicopter test as risk reduction.

Structural Measurements

The focus in this area is to extend the application of the VMD system and methodology developed by NASA for fixed-wing vehicles to rotating blades. Efforts will focus on developing a fully outfitted optical measurement system to acquire deformation information over the entire UH-60 rotor disk in the NFAC with 0.5-mm accuracy.

To accomplish this goal, a 2-camera photogrammetric measurement system was developed to precisely capture still-frame blade motions and provide calculations of object space coordinates of discrete points on rotor blades from coordinates obtained in pairs of images. With 2 cameras, one rotor quadrant (or 90 deg of rotor azimuth) of the UH-60 rotor can be imaged. Multicamera views will increase the global coverage in the FOV, thus adding a stronger solution to the triangulation computations. The synchronized high-resolution, multicamera system leverages some of the advancements in commercially available photogrammetric measurement systems developed primarily for the movie industry and for medical applications. The present 2-camera system used for wind tunnel applications at Langley Research Center uses (640 x 480) CCD analog cameras with typical displacement accuracies of 0.03 to 0.05 inches and angular accuracies of 0.05 to 0.10 degrees during tests in transonic wind tunnels. To accommodate applications to rotor blade measurements, the system was upgraded to 2K- by 2K-pixel digital cameras for improved resolution.

In 2008, a DARPA/NASA/Army/Boeing test of the SMART rotor was conducted in the NFAC 40- by 80-Foot Wind Tunnel. To explore the feasibility of using the photogrammetric technique for full-scale blade deformation measurements, the 2-camera VMD system was installed in the wind tunnel. Using retro-reflective targets placed on the underside of one of the SMART blades, the VMD technique was proved feasible for imaging one-quadrant of the rotor disk. Based on this successful demonstration, the VMD system will be expanded to 4 cameras to image 2 quadrants of the rotor disk during the UH-60 IBC test. Camera-calibration techniques will be refined and measurement uncertainties will be assessed after each stage of development. Checkouts during hover tests in the Hover Test Cell at Langley Research Center are also anticipated. The VMD system will then be expanded to 8 cameras/4 quadrants for the UH-60 Airloads test where the system will provide critical blade-deformation data. The system will be used in subsequent tests where multiple measurement techniques will be used simultaneously.

Aerodynamic Performance Measurements

To increase accuracy in aerodynamic force measurements on large-scale rotors in wind tunnel tests, an experimental technique will be developed to calibrate the rotor balance dynamically and to measure the true dynamic loads acting on the rotor hub within 10% accuracy. Unlike static calibrations where the applied static loads are typically in the expected range of the actual test, the applied dynamic loads in dynamic calibrations are limited to a small range because of the structural dynamic limit on mechanical components. Another complication in the development of the technique is the specialized equipment and hardware required to perform the calibration. Figure 5.17 shows a calibration fixture around the Large Rotor Tests Apparatus (LRTA) at NASA Ames Research Center, which permits testing and evaluation on the hub alone in a laboratory-type environment. Once the LRTA is installed in the NFAC, an extensive shaker apparatus like that shown in figure 5.18 will be required. The major emphasis of this effort is to establish an appropriate procedure for performing the calibration and determining the accuracy. The plan is to develop the technique in the laboratory and evaluate it during the UH-60 Airloads test in the NFAC.

Additional Areas of Research

In addition to the areas already discussed, NASA plans to use both in-house and NASA-funded research to advance techniques for propulsion-system measurements, shear-stress measurements on rotor blades, nonintrusive rotorcraft-state measurements in flight, and wireless data transmission.

Propulsion-systems measurements

Two areas related to propulsion-systems measurements are actively being investigated: drive-train vibration and bearing-failure monitoring systems, and high-temperature and high-pressure sensors. The goal is to develop sensors/systems that can operate reliably in a 500-deg C operational environment without water-cooling requirements and measure pressure and/or vibration with a resolution of ±3 psi or ±1 kG, respectively. These sensors/systems will be used in evaluating engine and drive-train performance parameters such as pressure, temperature, and vibration so as to enhance vehicle health monitoring and provide critical data for validating design tools and methodologies.

Figure 5.17. Dynamic calibration setup for Large-Scale Rotor Test Apparatus (LRTA).

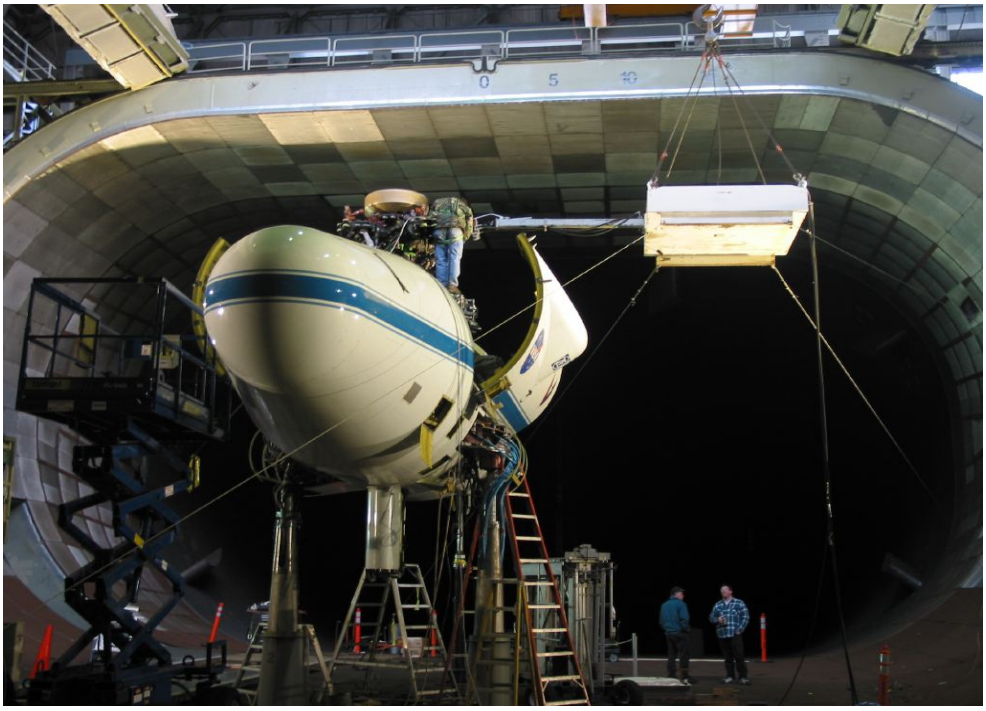

Figure 5.18. Dynamic calibration setup for LRTA in the NFAC.

Drive-Train Vibration and Bearing-Failure Monitoring Systems. The experimental capability under development is to implement in-situ monitoring of the drive-train environment within a rotorcraft to more accurately determine precursors to component mechanical failure. Conventional monitoring of drive trains is performed by ex-situ measurement of vibration characteristics to extrapolate failure. The problem associated with the conventional approach is that signal accuracy could be compromised because of signal attenuation.

High Temperature and Pressure Sensors. Conventional engine transducers are generally water-cooled, adding to cost and bulkiness. The proposed approach is to develop low-cost, reliable pressure sensors that have a smaller footprint in the test apparatus and can survive the high-temperature environments of the rotorcraft engines and drive trains. Silicon Carbide (SiC) transducers under development do not require cooling since the material is inherently thermomechanically stable at higher temperatures, relative to the conventional transducers.

The current research strategy is to leverage and further resolve the newly discovered effect/influence of the separation of the sensor bond-pad from the gold die-attach material at the bond interface, thus effectively disconnecting the sensor from the external circuit. Solving this reliability problem will allow sensor operation beyond 400 deg C. Another goal in this area is to develop thermally stable SiC piezoresistive pressure transducers that can operate reproducibly over time at 500 deg C without significant parametric degradation. This work will extend pressure and vibration measurements beyond temperatures previously possible and will provide three immediate significant technological benefits: wider frequency bandwidth (overcomes acoustic attenuation associated with pitot tube), stable output, and reduced packaging complexity (no cooling tubes). Key to the validation of this sensor technology is the extraction of sensor long-term operating parameters in the “field”; these sensor-performance data will then be used as benchmarks for further future sensor-development efforts.

Shear-stress measurements

Shear stress on the rotor-blade surface is a measurement that would greatly benefit validation of high-fidelity CFD tools. To date, these measurements have been made only in hover. Wadcock and Yamauchi [1998] and Wadcock et al. [1999] describe shear-stress measurements on a full-scale XV-15 tiltrotor blade in hover. Using the oil-film interferometric technique, shear stress on an XV-15 blade surface was measured and the chordwise distribution of skin-friction coefficient was determined for multiple radial stations. Natural transition, leading-edge laminar separation followed by turbulent reattachment, and reverse flow regions were also identified. Figure 5.19 shows a fringe pattern at 50% radial station with the transition location identified. The transition location for a range of collective pitch is presented in figure 5.20. The oil-film interferometric technique is applicable only to steady flows such as hover- or axial-flow conditions. Enabling shear-stress measurements in unsteady flows is a challenge for future experimental research.

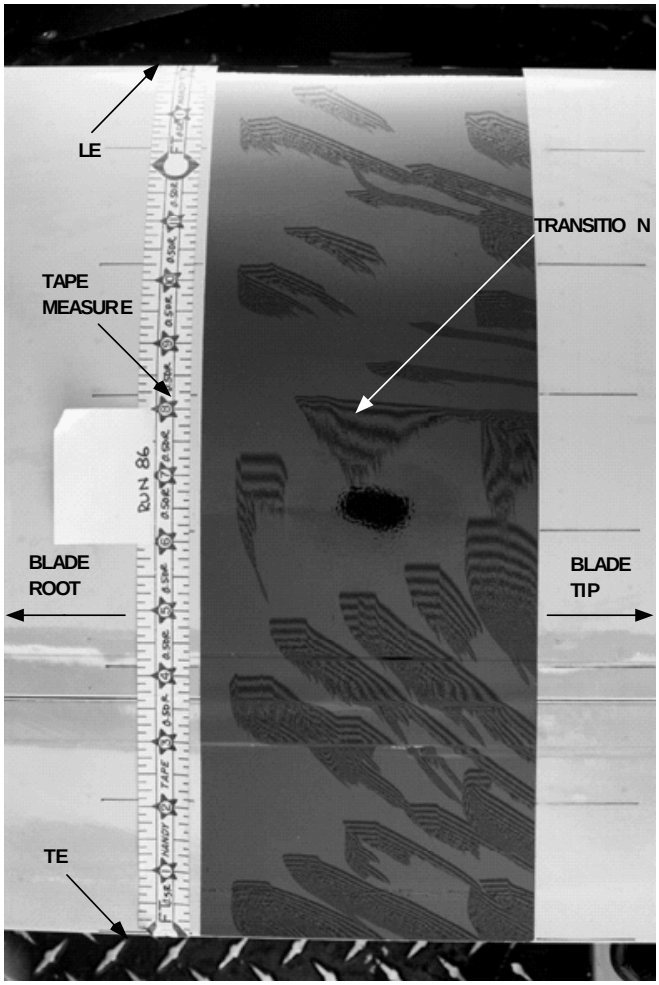

Figure 5.19. Fringe pattern at r/R = 0.50, collective pitch = 2.9 deg, rotor thrust coefficient = 0.0033, blade-tip Mach number = 0.56. Reproduced from Wadcock and Yamauchi [1998].

Vehicle-state measurements

Research in this area will focus on the development of a portable, nonintrusive flight-control measurement system that can be installed on a variety of rotorcraft platforms for flight testing without having to recertify the aircraft. The first system will provide global positioning system (GPS), navigation, attitude, and heading reference as well as measurements of cyclic, collective, and yaw. These measurement signals will be interfaced to a laptop to provide a navigation display on a 6-inch LCD for use by the pilot. Additional details about the development and implementation of this system is discussed in Chapter 6. The second system will measure the blade-tip-path plane of the rotor to help perform comprehensive assessments of rotor performance and noise. After evaluating candidate techniques, a system will be assembled and demonstrated in flight with a goal of measuring blade position within 0.25 inch. This work will be performed under the auspices of a NASA Research Announcement.

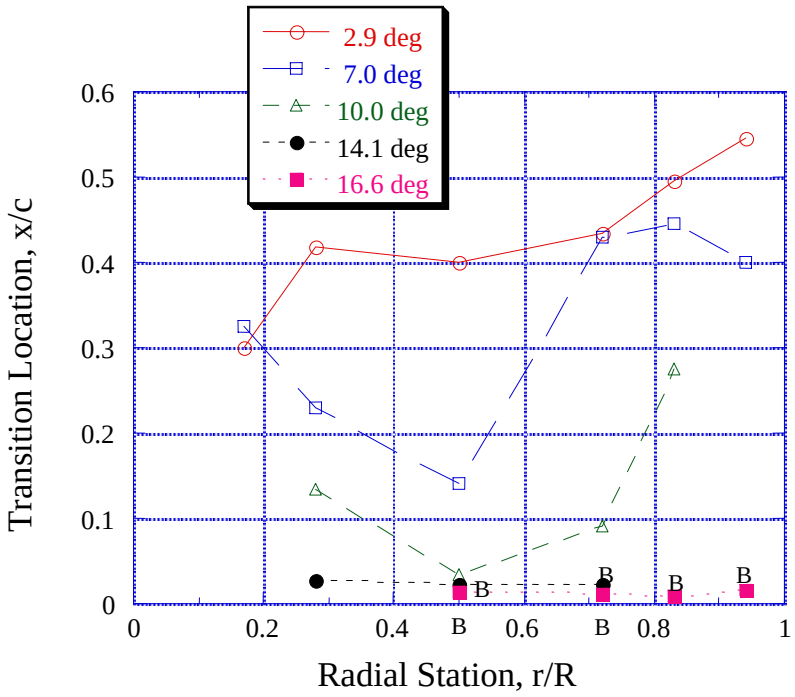

Figure 5.20. Transition location as a function of collective pitch, blade-tip Mach number = 0.56. "B" indicates presence of a leading-edge bubble. Reproduced from Wadcock and Yamauchi [1998].

Wireless data transfer

As new wireless data-transfer protocols are developed and throughput speeds increase, the use of wireless data transfer is becoming widespread in test facilities throughout the world. Telemetry and optical systems are routinely used to transfer data in component tests and tests involving fixed-wing vehicles. However, the use of wireless data transfer in rotorcraft testing is not as prevalent because of the difficulties associated with transferring data from a rotating frame to a fixed frame at high data rates. This data transfer usually requires multiple receivers to capture signals transmitted at different rotor positions and sophisticated algorithms to produce a continuous data record.

Work in this area will look at leveraging existing and emerging wireless data-transfer methods to develop hub-mounted systems capable of transferring data at rates as high as 3.25 Mbps for both wind tunnel and flight testing. Key challenges include miniaturization of system components to reduce weight and their ability to operate reliably when exposed to large vibrations and high temperatures. The potential impact of such systems is quite significant in that they would alleviate channel count limitations associated with slip rings. Increasing the potential number of sensors on the rotor blades will improve spatial resolution, permit in-situ calibrations for off-surface measurement techniques, and provide additional information to satisfy safety-of-flight requirements.

CROSS-CUTTING TECHNOLOGIES

As mentioned in previous chapters, experimental capabilities provide critical technologies for advancing the state of the art in the other rotorcraft disciplines, especially as new computational tools and frameworks are established. Therefore, advances among the various disciplines are not mutually exclusive and depend on effective communication, collaboration, and integration to ensure that the requirements and critical data needs of the each discipline are carefully considered and addressed. Table 5.3 shows some of the critical data required by some of the rotorcraft disciplines. Data identified as critical by more than one discipline indicate areas where the development or enhancement of an experimental capability could have significant impact. These areas are also potential areas where a multidisciplinary approach can lead to better understanding and an enhanced verification and validation process.

TABLE 5.3. CRITICAL DATA NEEDS IDENTIFIED BY DISCIPLINES WITHIN NASA ROTORCRAFT

Critical Data	Aeromechanics	Acoustics	Flight Dynamics	Propulsion
Aircraft state		X	X	
Blade surface pressures	X	X		
Boundary layer transition location	X	X		
Surface shear stress	X			
Tip-vortex characteristics	X	X		
Blade torsion	X	X	X	
Blade deflection	X	X	X	
Rotor wake	X	X		
Flow interactions	X	X	X	
Pressure and temperature				X

REFERENCES

Barrows, D.: Videogrammetric Model Deformation Measurement Technique for Wind Tunnel Applications. AIAA Paper no. 2007-1163, 45th AIAA Aerospace Sciences Meeting and Exhibit, Reno, Nev., Jan. 8–11, 2007.

Biggers, James C. and Orloff, Kenneth L.: Laser Velocimeter Measurements of the Helicopter Rotor-Induced Flow Field. J. Amer. Hel. Soc., vol. 20, no. 1, Jan. 1975, pp. 2–10.

Biggers, J. C.; Lee, A.; Orloff, K. L.; and Lemmer, O. J.: Laser Velocimeter Measurements of Two-Bladed Helicopter Rotor Flow Fields. NASA/TM–X-73238, May 1977.

Bosnyakov, S.; Bykov, A.; Coulech, V. et al.: Blade Deformation and PSP Measurements on the Large Scale Rotor by Videometric System. ICIASF 1997 – 17th International Congress on Instrumentation in Aerospace Simulation Facilities, Pacific Grove, Calif., Sept. 29–Oct. 2, 1997. Record (A98-18712 03-35), Piscataway, N.J., Institute of Electrical and Electronics Engineers, Inc., 1997, pp. 95–104.

Burner, A. W.: Model Deformation Measurements at NASA Langley Research Center. Technical Report, UMI Order No.: NASA-97-81agard-awb, NASA Langley Technical Report Server, 1997.

Burner, A. W.: Model Deformation Measurements at NASA Langley Research Center. AGARD Conference Proceedings CP-601: Advanced Aerodynamic Measurement Technology. 81st Meeting and Symposium of the Fluid Dynamics Panel, Seattle, Wash., Sept. 22–25, 1997, pp. 34-1 to 34-9.

Burner, A. W. and Liu, T.: Videogrammetric Model Deformation Measurement Technique. AIAA J. of Aircraft, vol. 38, no. 4, July–Aug., 2001, pp. 745–754.

Burns, S. P., and Sullivan, J. P.: The Use of Pressure Sensitive Paints on Rotating Machinery. 16th ICIASF Record, International Congress on Digital Object Identifier 10.1109, July 18–21, 1995, pp. 32.1–32.14.

Fleming, G. A., and Gorton, S. A.: Measurement of Rotorcraft Blade Deformation Using Projection Moir Interferometry. Proceedings SPIE Third International Conference on Vibration Measurements by Laser Techniques, Ancona, Italy, vol. 3411, June 16–19, 1998, pp. 514–527.

Fleming, G. A.; Soto, Hector L.; South, Bruce W.; and Bartram, Scott M.: Advances in Projection Moiré Interferometry Development for Large Wind Tunnel Applications. AIAA Paper no. 1999-01-5598, SAE/AIAA World Aviation Congress, San Francisco, Calif., Oct. 19–21, 1999.

Fleming, G. A.; Soto, H. L.; and South, B. W.: Projection Moire Interferometry for Rotorcraft Applications: Deformation Measurements of Active Twist Rotor Blades. AHS 58th Annual Forum, Montreal, Canada, vol. 1, June 11–13, 2002.

Gorton, S. A.; Berry J. D.; Hodges, W. T.; and Reis, D. G.: Rotor Wake Study Near the Horizontal Tail of a T-Tail Configuration. AIAA J. Aircraft, vol. 39, no. 4, July–Aug., 2002, pp. 645–653.

Gorton, S. A.; Meyers, J. F.; and Berry, J. D.: Velocity Measurements Near the Empennage of a Small-Scale Helicopter Model. AHS 52nd Annual Forum, vol. 1, Wash., D.C., June 4–6, 1996, pp. 517–531.

Gorton, S. A. and Hoad, D. R.: Assessment of Rotor Blade Angle of Attack from Experimental Inflow Data. J. of Aircraft, vol. 39, no. 5, Sept.–Oct. 2002, pp. 772–730.

Heineck, J. T.; Yamauchi, G. K.; Wadcock, A. J.; Lourenco, L.; and Abrego, A. I.: 2000. Application of Three-Component PIV to a Hovering Rotor Wake. AHS 56th Annual Forum, Virginia Beach, Va., May 2–4, 2000.

Hubner, J. P.; Abbitt, J. D.; and Carroll, B. F.: Pressure Measurements on Rotating Machinery Using Lifetime Imaging of Pressure Sensitive Paint. AIAA Paper no. 96-2934, 32nd ASME, SAE, and ASEE Joint Propulsion Conference, Lake Buena Vista, Fla., July 1–3, 1996.

Jones, H. E.; Wong O. D.; Watkins, A. N.; Noonan, K. W.; Reis, D. G.; Malovrh, B. D.; and Ingram, J. L.: Initial Assessment of Surface Pressure Characteristics of Two Rotary Wing UAV Designs. AHS 62nd Annual Forum, Phoenix, Ariz., May 9–11, 2006.

Landgrebe, A. J. and Johnson, B. V.: Measurement of Model Helicopter Rotor Flow Velocities with a Laser Doppler Velocimeter. J. Amer. Hel. Soc., vol. 19, July 1974, pp. 39–43.

McAlister, K. W.; Tung, C.; and Heineck, J. T.: Devices that Alter the Tip Vortex of a Rotor. NASA/TM–2001-209625, Feb. 2001.

McAlister, K. W. and Heineck, J. T.: Measurements of the Early Development of Trailing Vorticity from a Rotor. NASA/TP–2002-211848, July 2002.

McKenzie, R. L. and Reinath, M. S.: Three-Dimensional Planar Doppler Velocity Measurements in a Full-Scale Rotor Wake. AIAA J., vol. 43, no. 3, 2005, pp. 489–499.

Meyers, J. F.; Lee, J. W.; Fletcher, M. T.; and South, B. W.: Hardening Doppler Global Velocimetry Systems for Large Wind Tunnel Applications. AIAA Paper no. 98-2606, 20th AIAA Advanced Measurement and Ground Testing Technology Conference, Albuquerque, N.M., June 15–18, 1998a.

Meyers, J. F.; Fleming, G. A.; Gorton, S. A.; and Berry, J. D.: Instantaneous Doppler Global Velocimetry Measurements of a Rotor Wake: Lessons Learned. 9th International Symposium on Applications of Laser Technologies to Fluid Mechanics, Lisbon, Portugal, July 13–16, 1998b.

Raffel, M.; Richard, H.; Ehrenfried, K.; Van der Wall, B.; Burley, C.; Beaumier, P.; McAlister, K.; and Pengel, K.: Recording and Evaluation Methods of PIV Investigations on a Helicopter Rotor Model. Experiments in Fluids, Springer-Verlag, vol. 36, no. 1, 2004, pp. 146–156.

Rajagopalan, G.; Niazi, S.; Wadcock, A. J.; Yamauchi, G.; and Silva, M. J.: Experimental and Computational Study of the Interaction Between a Tandem-Rotor Helicopter and a Ship. AHS 61st Annual Forum, Grapevine, Tex., June 1–3, 2005.

Samimy, M. and Wernet, M. P.: Review of Planar Multiple-Component Velocimetry in High-Speed Flows. AIAA J., vol. 38, no. 4, 2000, pp. 553–574.

Schneider, O.: Analysis of SPR Measurements from HART II. J. Aerospace Science and Technology, vol. 9, no. 5, Rotorcraft Research, July 2005, pp. 409–420.

Silva, M. J.; Yamauchi, G. K.; Wadcock, A. J.; and Long, K. R.: Wind Tunnel Investigation of the Aerodynamic Interactions Between Helicopters and Tiltrotors in a Shipboard Environment. AHS 4th Decennial Specialist's Conference on Aeromechanics, San Francisco, Calif., Jan. 21–23, 2004.

Sullivan, J. P. and Ezekiel, S.: Two-Component Laser Doppler Velocimeter for Periodic Flow Fields. J. of Physics E: Scientific Instruments, vol. 7, no. 4, Apr. 1974, pp. 272–274.

Tangler, J. L.; Wohlfeld, R. M.; and Miley, S. J.: An Experimental Investigation of Vortex Stability, Tip Shapes, Compressibility, and Noise for Hovering Model Rotors: Final Report. NASA-CR-2305, Sept. 1973.

Wadcock, A. J. and Yamauchi, G. K.: Skin Friction Measurements on a Full-Scale Tilt Rotor in Hover. AHS 54th Annual Forum, Washington, D.C., 1998.

Wadcock, A. J.; Yamauchi, G. K.; and Driver, D. M.: Skin Friction Measurements on a Hovering Full-Scale Tilt Rotor. J. Amer. Hel. Soc., vol. 44, no. 4, 1999, pp. 312–319.

Wadcock, A. J.; Yamauchi, G. K.; and Heineck, J. T.: Three-Component Velocity Measurements in the Wake of a Rotor in Hover. Highlights of Aero-Space Technology Enterprise, Research and Technology Report 1999, Dec. 2000.

Wadcock, A. J.; Yamauchi, G. K.; Heineck, J. T.; Silva, M. J.; and Long, K. R.: PIV Measurements of the Wake of a Tandem-Rotor Helicopter in Proximity to a Ship. AHS 4th Decennial Specialist's Conference on Aeromechanics, San Francisco, Calif., Jan. 21–23, 2004.

Watkins, A. N.; Leighty, B. D.; Lipford, W. E.; Wong, O. D.; Oglesby, D. M.; and Ingram, J. L.: Development of a Pressure Sensitive Paint System for Measuring Global Surface Pressures on Rotorcraft Blades. ICIASF 2007, 22nd International Congress on Instrumentation in Aerospace Simulation Facilities, Pacific Grove, Calif., June 10–14, 2007.

Wong, O. D.; Watkins, A. N.; and Ingram, J. L.: Pressure Sensitive Paint Measurements on 15% Scale Rotor Blades in Hover. AIAA Paper no. 2005-5008, 35th AIAA Fluid Dynamics Conf., Toronto, Ontario, June 6–9, 2005.

CHAPTER 6

FLIGHT DYNAMICS AND CONTROL

William A. Decker,[1] Chad R. Frost,[1] Barbara T. Sweet,[1] and Colin R. Theodore[1]

ACRONYMS

Apex	Autonomous system software tool
CAMRADII	Comprehensive Analytical Model of Rotorcraft Aerodynamics and Dynamics
CIFER	Comprehensive Identification from Frequency Responses
CONDUIT	Control Designer's Unified Interface
CTR	Civil Tiltrotor
DOF	Degree of Freedom
DVE	Degraded Visual Environment
FBW	Fly by Wire
FDC	Flight Dynamics and Control
FOV	Field of View
GTRS	Generic Tilt Rotor Simulation
GVE	Good Visual Environment
HQR	Handling Qualities Rating
HHC	Higher Harmonic Control
HSI	Human System Integration
IBC	Individual Blade Control
ICAB	Interchangeable Cab
ISA	Instantaneous Self-Assessment
IVHM	Intelligent Vehicle Health Monitoring
LRTA	Large Rotorcraft Test Apparatus
MDATD	Multi-Disciplinary Analysis and Technology Development
MIMO	Multiple Input Multiple Output
NASA-TLX	NASA Task Load Index
NFAC	National Full-scale Aerodynamics Complex

[1] NASA Ames Research Center.

OBC	Onboard Blade Control
OTW	Out of the Window
PAX	Passengers
PIO	Pilot Induced Oscillation
PPGD	Portable Programmable Guidance Display
RASCAL	Rotorcraft Aircrew Systems Concepts Airborne Laboratory
RCAS	Rotorcraft Comprehensive Analysis System
RFCS	Research Flight Control System
RTA	Rotor Test Apparatus
SIRCA	Super-Integrated Rotorcraft Control Architecture
SISO	Single Input Single Output
SSC	Sequential Shifting Control
UCE	Useable Cue Environment
UMARC	University of Maryland Advanced Rotorcraft Code
VCR	Visual Cue Rating
VMS	Vertical Motion Simulator

INTRODUCTION

Flight dynamics and control (FDC) for rotorcraft pose unique challenges due to the inherent instabilities of the flight vehicle, the aerodynamic and mechanical complexity of the system, and the operational environment, which is often obstacle-rich with poor visibility at low altitude. As new technologies are integrated into existing rotorcraft configurations and designs for future advanced rotorcraft are contemplated, it is essential that control of flight and the capabilities of the pilot be integrated in the design process from the beginning. The area of flight dynamics and control is highly integrated with other technical disciplines, especially the aeromechanics, acoustics, and propulsion disciplines. As described in Chapter 2, rotors incorporating active control technology such as individual blade control (IBC) and on-blade control (OBC) are promising methods for improving rotor performance and reducing vibration and noise. Measuring the effect of high-frequency (that is, greater than 1/rev) inputs to the rotor control system during a wind tunnel test does not simulate the effect on the primary control system with a pilot in the loop, however. Active rotor control must be considered in the context of the complete vehicle, including the pilot, not just for an isolated rotor. In Chapter 3, optimized low-noise approaches are discussed. The effectiveness of these approaches depends on the pilot's ability to accurately and consistently execute the approach. A key focus of the propulsion research within NASA is developing a variable or multispeed drive system to enable slowed rotor operation of future large, high-speed rotorcraft. Varying the rotor speed up to 50%, depending on the flight state and rotor capabilities, is sought for enhanced performance, yet has serious unexplored implications for dynamics and handling qualities that directly affect operational utility.

In anticipation of the advanced technologies and configurations being investigated by NASA and others in the rotorcraft community, FDC research within NASA focuses on an overarching goal of developing a Super-Integrated Rotorcraft Control Architecture (SIRCA). SIRCA is an envisioned integrated, broadband rotorcraft-control-system architecture incorporating a flight-control system, engine control, airframe/drive-train/rotor-load control, active-rotor control, vehicle-health management, and precision guidance for low-noise operation. Supporting tasks focus on developing new approaches to control design for broadband control, and integrating acoustic, aeromechanic, and propulsion predictive models with handling-qualities analysis and design tools. Fundamental research will also be conducted to develop real-time predictive acoustic models that account for dynamic flight conditions and control inputs. Precision guidance, navigation, and control capabilities will be developed to enable data collection and evaluation for rotorcraft flight experiments, including studies of vehicle-acoustic characteristics, vehicle-dynamics modeling, noise reduction, and terminal-area operations.

The following sections of this chapter begin with a description of current analysis tools and testing facilities for rotorcraft flight dynamics and control research. These tools and facilities were developed and used in collaboration over many years with the U.S. Army Aeroflightdynamics Directorate. NASA FDC research is described next, beginning with the SIRCA. The major components of SIRCA that are emphasized within NASA are then discussed: Advanced Aeromechanics Concepts; Multispeed Rotor Control; Flight Dynamics of Large Rotorcraft; Human System Integration; and Guidance and Navigation Displays. Relevant modeling and analysis tools are described within each of these topics. Examples of current application of tools in support of SIRCA are provided, and plans for improving methodologies and tools are discussed.

CURRENT CAPABILITIES IN ROTORCRAFT FLIGHT DYNAMICS AND CONTROL

Flight dynamics and control design typically progresses through three major stages: desktop and workstation analysis and design; simulated response testing, often leading to piloted simulation studies; and flight trials.

With human control desired and incomplete or simplified dynamic models employed, the design process is often iterative. The thrust of flight dynamics and control development over the past couple of decades has been aimed at achieving more satisfactory and complete design solutions earlier in the process, where the costs and risks of design validation are lower.

The following sections describe the tools and facilities NASA uses for FDC research. Examples are provided for each of the three stages of design and validation.

Control-System Design Tools

The efficient design and optimization of control systems for rotorcraft involve numerous key components and tools. The first of these components are flight-dynamics models that accurately represent the time- and frequency-domain response characteristics of the vehicle through the flight envelope. The second are control-system design specifications that include control-system and

handling-qualities design requirements and specifications. Examples of these design requirements and specifications for civilian rotorcraft are the Federal Aviation Administration (FAA) Airworthiness Standards contained in Part 27 for Normal Category Rotorcraft and in Part 29 for Transport Category Rotorcraft. For military rotorcraft, ADS-33E [Anonymous, 1975] lists handling-qualities requirements and MIL-F-9490D [Anonymous, 1999] lists general control-system characteristics. The third component comprises the toolsets that are used to efficiently evaluate and optimize the control system to the set of desired design specifications and requirements with the rotorcraft-dynamics models.

In order for flight-dynamics models to be used for flight-control design purposes, they must be accurate over a wide frequency range around the fundamental frequency of the closed-loop control system, or crossover frequency. A general rule is that the models should be accurate down to at least one-fifth of the control crossover frequency, and accurate to frequencies up to at least 5 times the crossover frequency. Control systems for conventional helicopters typically have a fundamental closed-loop control frequency (crossover frequency) in the range of 2–3 rad/sec, which requires models that are accurate from about 0.4 to 15 rad/sec. For the design of higher-bandwidth flight control systems, the models must be accurate to even higher frequencies. In such cases, the dynamics of the rotor system should be explicitly included in the dynamics models to obtain the required levels of accuracy. For larger rotorcraft, the effects of fuselage bending and torsion modes may be important for flight-control design, and should also be included in the dynamics models.

There are two basic approaches to generating helicopter-dynamics models for flight-control design and analysis applications. The first uses system-identification techniques to extract models of the flight dynamics from test data collected on the actual vehicle in flight. System identification typically produces the most accurate flight-dynamics models. The current industry-standard system-identification package is CIFER (Comprehensive Identification from Frequency Responses). The CIFER package [Tischler and Remple, 2006] was developed by the U.S. Army Aeroflightdynamics Directorate at Ames Research Center. CIFER provides an integrated set of tools for the frequency-domain analysis of flight-test data to identify frequency responses, transfer function models, and state-space models. CIFER has been used extensively in government and industry for model identification of rotorcraft, including the BO-105 at the Deutsche Forschungsanstalt für Luft- und Raumfahrt (DLR) [Tischler and Cauffman, 1992], the Sikorsky S-92 [Tischler et al., 2001], and the Apache AH-64D [Harding and Moody, 2005]. CIFER has also seen widespread application for model identification of unmanned aerial vehicles (UAVs) [Theodore et al. 2004], and to support wind tunnel tests [Tischler, 1999]. SIDPAC [Klein and Morelli, 2006], developed at NASA Langley Research Center, is another system-identification tool that is used.

The second approach to generating flight-dynamics models is to use rotorcraft analysis tools such as CAMRADII [Johnson, 1994], RCAS [Saberi et al., 2004], or GenHel [Ballin and Dalang-Secretan, 1991; and Howlett, 1989]. This approach is often the only one that can be used if the vehicle does not currently exist or is to be significantly modified. Some comprehensive codes, such as CAMRADII, can generate linear state-space models directly that can be used in flight-control law design and analysis. Other codes, such as GenHel, cannot extract linear models directly. For these codes, time-domain simulation data must be generated and system identification of the simulation data used to extract the linear models.

Numerous control-system design tools are available commercially that can also be used for rotorcraft flight-control design. For example, control-system design toolboxes are available as part of the MATLAB and LabVIEW software packages produced by MathWorks, Inc., and National Instruments, respectively. These control design toolboxes are used for a wide variety of applications [Gomez and Goethert, 2006; Gu et al., 2005; and Tewari, 2002]. These software packages, however, were not specifically developed for fixed-wing and rotorcraft applications and do not integrate the various rotorcraft control-system and handling-qualities specifications directly into the control-system design and optimization task.

The software tool that is becoming the industry standard for helicopter and fixed-wing flight control system development in the United States is CONDUIT (Control Designer's Unified Interface). CONDUIT [Tischler et al., 1997] was developed by the U.S. Army Aeroflightdynamics Directorate at Ames Research Center. The CONDUIT software package is a state-of-the-art tool for the design, evaluation, and optimization of aircraft flight-control systems. CONDUIT combines the fields of control-system design and handling-qualities analyses into a single package by allowing the user to define a set of design specifications (such as ADS-33E, MIL-F-9490D, etc.) with which the control system will be automatically evaluated and optimized. CONDUIT has been used for control-system analysis on many rotorcraft programs in the United States, including the modernization of the control laws for the Apache AH-64D [Harding et al., 2007] and UH-60 Black Hawk [Tischler et al., 2005] helicopters.

The CIFER and CONDUIT control-system design tools are described in detail here since they will be used to support NASA FDC research activities. For example, the tools will be used to support the UH-60A IBC wind tunnel test to be performed in the National Full-Scale Aerodynamics Complex (NFAC) 40- by 80-Foot Wind Tunnel that was previously described in Chapter 2. The control design tools will be used in the development of an automatic rotor-trim controller to study the stability and performance of the closed-loop IBC vibration/noise reduction systems and to assess the level of interactions between the closed-loop IBC systems and the dynamic response of the rotor system to swashplate control inputs [Cheng et al., 2006]. CIFER and CONDUIT were also used during a test of the Boeing SMART rotor in the NFAC in 2008 to extract the rotor-dynamics modes, including the regressive lag mode characteristics.

In addition to wind tunnel tests, CIFER and CONDUIT will be used to support data analysis for planned Vertical Motion Simulator (VMS) experiments.

Flight-Simulation Test Facilities

The second phase of flight dynamics and control analysis and design involves validation testing of the design using nonlinear simulation models. Often these models are developed to operate in real time with a human pilot. Simulation models range from simple models such as "ARMCOP" [Talbot et al., 1982] to more complex models employing substantial empirical or experimental data as part of their calculations. Two such models, dating from the 1980s, have provided the backbone for NASA and U.S. Army research simulation. Representing single main rotor helicopters has been the Sikorsky-developed GENHEL model of the UH-60 helicopter [Howlett, 1981]. Representing tilt-rotor aircraft has been the Bell-NASA-STI-developed Generic Tilt Rotor Simulation [Hanson and

Ferguson, 1991; Ferguson, 1991] developed to support XV-15, V-22, and NASA CTR-4/95 (civil tiltrotor) development and studies. The latter (CTR-4/95) represented a NASA conceptual airplane used for civil transport requirements and operations studies. These models often rely on extensive wind tunnel testing or computational-fluid-dynamics (CFD) simulations to capture physical effects. The nonlinear simulation models can be used for control-system or dynamic-response validation using standardized control inputs or as the aircraft and control-system model element of a piloted simulation.

Pilot-controlled flight simulation tests are used to verify flight-control and cockpit-guidance designs and overall flight-dynamics response. The objective for cockpit design is achieving desired performance of a task with satisfactory handling qualities. A combination of objective measures, such as flightpath tracking performance and pilot-workload assessment, usually using the Cooper-Harper Handling Qualities Evaluation Scale (fig. 6.1) [Cooper and Harper, 1969], are used to establish whether the design goal has been met. Research efforts aimed at defining quantitative models of pilot performance and workload assessment are under development; they are discussed later in the Human Systems Integration section of this chapter. Human pilot assessment, however, remains the standard for final validation and acceptance.

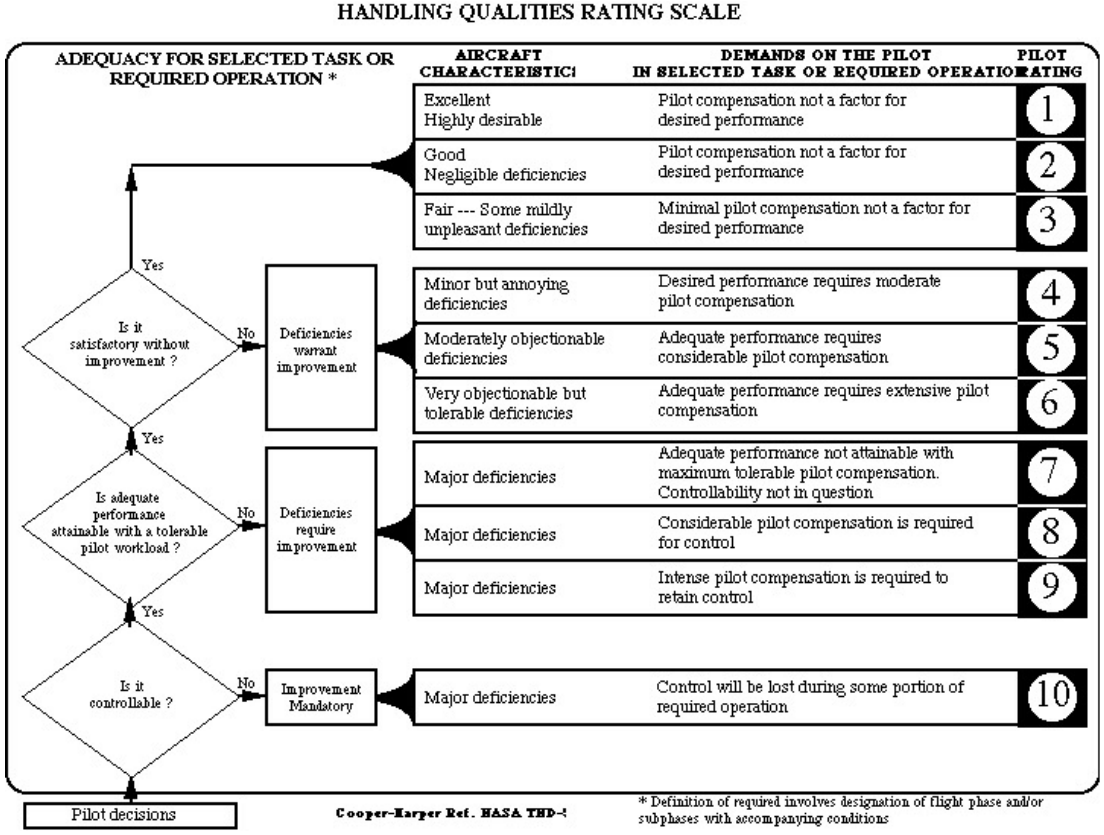

Figure 6.1. Cooper-Harper Handling Qualities Rating Scale [Cooper and Harper, 1969].

Human-piloted simulation can take many forms, ranging from desktop simulation using simple "joystick" control sticks to flight simulators with large motion-cuing capability. Desktop simulators, such as that shown in figure 6.2, are useful for developing complex simulation environments for subsequent assessment using a large motion-cueing platform, assessments of instrument guidance, or flight-procedure development. As the need for pilot sensing and interaction with the resulting aircraft motions becomes more important to the control task, more complete cockpit cueing environments are necessary in simulation.

One of the most critical control tasks that rotorcraft must perform is precision hover. This task requires high-fidelity multisensory cueing. Most precision hover is performed with reference to outside visual cues. Wide field of view (FOV), up to that of a full aircraft cockpit with lots of scene detail and texture, becomes necessary for conventional hover. The alternative, for degraded visual conditions (an issue for civil transport rotorcraft as well as military aircraft), requires instrument aids, typically as a head-up or helmet-mounted display. Motion cueing is important for the hover task, as a pilot senses much of the aircraft acceleration via proprioceptive cues ("seat-of-the-pants"). While "onset cueing"—high frequency, limited motion—has been used successfully for higher-speed control tasks, hover benefits greatly from very-low-frequency acceleration cueing, which requires large motion travel to sustain for meaningful periods. Sound can be a useful auxiliary cue, complementing other cues rendered at reduced fidelity. Finally, the control inceptors (control sticks,

Figure 6.2. Desk-top development simulation work station.

pedals, or switches) need appropriate force and damping characteristics, as these are useful to the control designer to tame poor control-response characteristics. Ironically, the hover-flight regime often finds pilots preferring minimal control-stick forces, a characteristic that can require more complex simulation hardware. All of these cues are provided by the Ames VMS [Aponso et al., 2008].

The VMS combines a high-fidelity simulation capability with an adaptable simulation environment that allows the simulator to be customized to a wide variety of human-in-the-loop research applications. The distinctive feature of the VMS is its large amplitude, high-fidelity motion capability. The high level of simulation fidelity is achieved by combining this motion fidelity with excellent visual- and cockpit-interface fidelities. An interchangeable cab arrangement allows different crew vehicle interfaces and vehicle types to be evaluated, allowing fast turnaround times between simulation projects. The VMS motion system is a six-degree-of-freedom combined electromechanical/ electrohydraulic servo system, shown in figure 6.3. It is located in and partially supported by a specially constructed 120-ft tower. The motion platform consists of a 40-ft-long beam that travels ±30 ft vertically. On top of the beam is a carriage that traverses the 40-ft length of the beam. A sled sits atop the carriage, providing the ±4 ft of travel in a third translational degree of freedom. A conically shaped structure is mounted on the sled and rotates about the vertical axis, providing yaw motion. A two-axis gimbal allows pitch and roll motion. The interchangeable cab (ICAB) is attached to the top gimbal ring. The motion capability of the VMS is summarized in table 6.1.

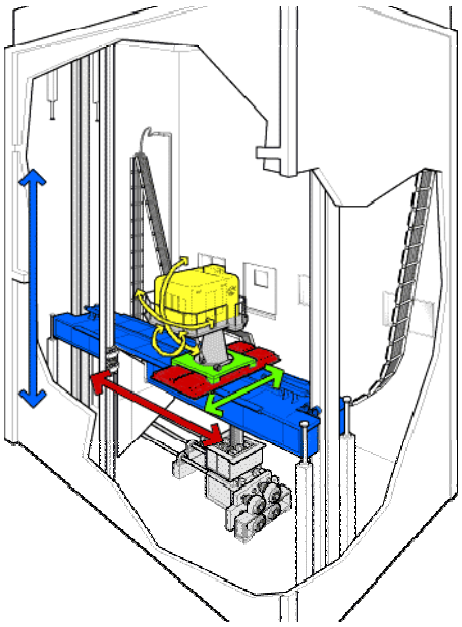

Figure 6.3 Cutaway diagram of the VMS facility.

TABLE 6.1. VMS MOTION CAPABILITY

VMS NOMINAL OPERATIONAL MOTION LIMITS			
Axis	**Displacement (ft)**	**Velocity (ft/sec)**	**Acceleration (ft/sec^2)**
Vertical	±30	16	24
Lateral	±20	8	16
Longitudinal	±4	4	10
Yaw	±24 (deg)	46 (deg/sec)	115 (deg/sec^2)
Roll	±18	40	115
Pitch	±18	40	115

The ICAB capability in the VMS allows the cockpit to be tailored to the research application. The VMS has five portable ICABs with different out-the-window (OTW) visual FOVs. For each simulation study, the cab is equipped based on the study requirements and tested fixed-base with the complete simulation environment except for motion. Equipping the cab (fig. 6.4) includes installation of flight controls, flight instruments and displays, and seats (fig. 6.5). Following equipage and checkout, the ICAB is transported and installed on the motion system. The ICAB capability allows the VMS facility to conduct fixed-base and moving-base simulation studies simultaneously.

Tiltrotor handling qualities, controls, and terminal-area operations studies using the VMS have also been conducted in parallel with helicopter investigations. The original XV-15 selection and development were conducted on the predecessor facility, the Flight Simulator for Advanced Aircraft (FSAA), with later developments conducted on the VMS as it began operations in 1979. The XV-15 work led to definition of requirements for a medium-lift transport tiltrotor aircraft through the Joint Vertical Aircraft (JVX) program that led to the V-22 Osprey. Tiltrotor studies using the VMS considered civil operations and requirements through a series of 10 experiments conducted throughout the 1990s and ending in 2001. Key topics included: steep approaches; instrument-approach guidance; engine-out operations, noise-abatement operations (done in concert with XV-15 flight research); and simultaneous, noninterfering operations that are independent of the main runways of a major airport. The large vertical and longitudinal motion capability of the VMS led to development of a discrete nacelle position-control system and acceptance of its use during final approach by airworthiness authorities. The VMS is ideally suited for evaluating future large civilian rotorcraft, and NASA has begun investigating unique issues associated with these types of aircraft.

Flight Research Aircraft

The final phase of flight-control and cockpit-interface design involves flight validation. For research and design criteria development this validation usually involves flight trials intended to provide a benchmark for comparison to ground-based flight-simulation results. For production designs, flight tests provide the ultimate validation of the design and verification of satisfying the design requirements. The expense and potential risk of flight trials is necessary because the theoretical knowledge

and mathematical modeling of the total flight environment is incomplete. The modeling includes knowledge of all aircraft dynamics, aerodynamics, and the cueing environment used by the imperfectly understood human pilot. Aiken et al. [1991] and Borchers et al. [1998] describe some of the key rotorcraft flight-test activities and accomplishments at NASA.

Figure 6.4. VMS at NASA Ames Research Center.

Figure 6.5. VMS ICAB interior view.

While research work can and does use existing production aircraft where appropriate, the very nature of flight dynamics and controls research requires investigation of a range of dynamic responses not available in production aircraft. Variable stability research helicopters have been developed to provide “flying simulators” wherein an experimental flight control system attempts to provide the desired dynamic responses in spite of the natural response of the base aircraft.

The key flight platform available to NASA embodying the state of the art in flight-control architectures for rotorcraft research is the U.S, Army/NASA Rotorcraft Aircrew Systems Concepts Airborne Laboratory (RASCAL) [Aiken et al., 1991]. The RASCAL (fig. 6.6) is a modified JUH-60A Black Hawk helicopter operated by the Army and used by NASA at the Ames Research Center. The RASCAL facility has been in operation, in various research and development phases, since 1989. The fourth phase of development, currently in progress, focuses on a full-authority fly-by-wire (FBW) flight control system, known as the Research Flight Control System (RFCS), which has been integrated into the helicopter. The aircraft provides an easily reconfigurable, fully programmable capability to investigate a wide range of flight-control, cockpit-display, and crew-systems concepts, including integration of mission equipment.

Figure 6.6. RASCAL helicopter.

The RASCAL is supported by a broad array of in-house-developed tools and commercial software tools for control synthesis, simulation, and dynamic analysis. Although control-system design methods and vehicle-modeling tools have also advanced markedly over the last five decades, in-flight simulation remains the superior method for assuring reality and minimizing risk prior to design decisions. RASCAL is especially suited to serve as a system-integration platform or systems-requirements tool for new rotorcraft technologies. Though based on a medium-sized military platform, RASCAL can enable evaluation of large civil rotorcraft and will play a primary role in demonstrating and validating key aspects of SIRCA.

Wind Tunnel Testing

Wind tunnel tests of small- and full-scale actively controlled rotors provide opportunities for close collaboration between FDC and aeromechanics researchers. As described in Chapter 2, past and expected tests of active rotors in the NASA 40- by 80-Foot Wind Tunnel, the Transonic Dynamics Tunnel, and the U.S. Army 7- by 10-Foot Wind Tunnel provide data to evaluate the effect of higher harmonic inputs to the rotor on the primary control system. Figure 6.7 shows some installation photos for rotor wind tunnel tests in the NFAC 40- by 80-Foot and 80- by 120-Foot Wind Tunnels.

a) XV-15 rotor with higher-harmonic control installed on the Rotor Test Apparatus in the 80- by 120-Ft Wind Tunnel

Figure 6.7. Active rotor tests in the NFAC.

b) UH-60 rotor with individual blade control installed on the Large Rotor Test Apparatus in the 40- by 80-Ft Wind Tunnel

c) Boeing SMART rotor with active flaps installed in the 40- by 80-Ft Wind Tunnel

Figure 6.7. Concluded.

SUPER-INTEGRATED ROTORCRAFT CONTROL ARCHITECTURE (SIRCA)

Control and management of rotary-winged flight vehicles is an inherently multidisciplinary activity, including domains such as flight control, human factors, structures, acoustics, aeromechanics, and propulsion. Predictive capabilities and models developed in one discipline must be commanded by, communicated to, and shared with the control and management functions developed under other disciplines. Existing architectures for aircraft control and management generally exhibit some combination of being proprietary, not well-suited to a research environment, not readily extensible, focused on only one or a few disciplines, and cumbersome for integrating new research nodes.

A key goal of NASA FDC research is to address the absence of an open, highly integrated, research-oriented system architecture for management and control of rotary-winged aircraft. NASA is developing a Super-Integrated Rotorcraft Control Architecture (SIRCA) in response to increasingly complex rotorcraft systems envisioned for the future. SIRCA is an integrated, broadband rotorcraft-control architecture linking the systems for flight control, engine control, airframe/drive-train/rotor-load control, active rotor control of vibration and noise, vehicle health management, and guidance and cueing. SIRCA development aims to enable new types of holistic control design approaches that use acoustic, aeromechanic, and propulsion predictive models to achieve specified performance metrics. Figure 6.8 shows a conceptual layout of SIRCA.

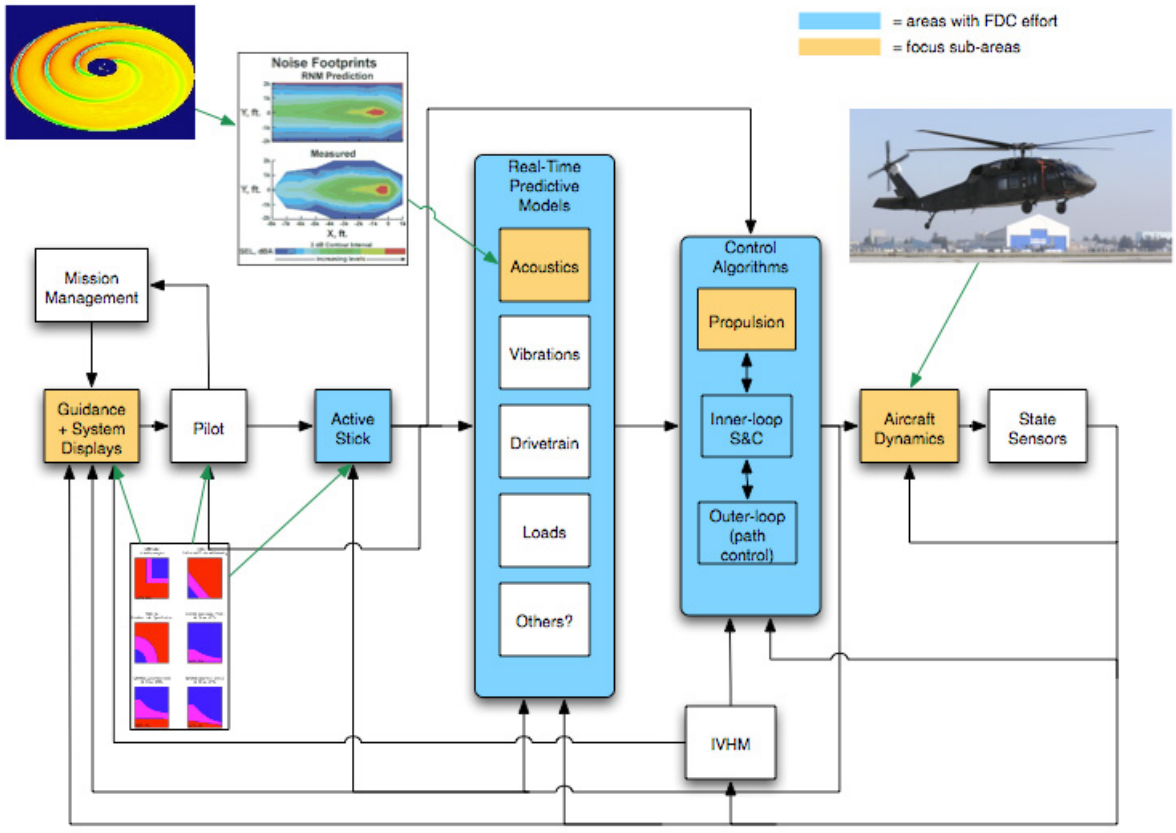

Figure 6.8. Conceptual schematic of the SIRCA for rotorcraft.

The primary objective in developing SIRCA is to accommodate research, development, test, and evaluation activities of advanced rotorcraft systems that enable integrated management and control of the flight vehicle. Top-level goals of this effort are to:

- Facilitate the easy integration of stakeholders' technologies into research aircraft and simulations.
- Enable connectivity between disparate system elements operating on a wide range of timescales (e.g., milliseconds for inner-loop control, and minutes for route planning).
- Provide capabilities in an open and extensible format to allow the widest and most flexible possible use.

Initial work in defining SIRCA required identifying stakeholders and their concerns, and developing a draft architecture. FDC will leverage NASA's significant experience in developing integrated architectures for spaceflight, planetary rover, and unmanned-aerial-system (UAS) missions. A brief review of relevant architectures to be leveraged or considered in developing SIRCA is provided next.

An example of the current state-of-the-art research-oriented control architecture is that developed for the U.S. Army/NASA RASCAL JUH-60 in-flight simulator. RASCAL employs a fail-safe hardware/software system, as shown in figures 6.9 and 6.10, with flight-critical elements segregated from the research elements, such that failures on the research side of the architecture are identified

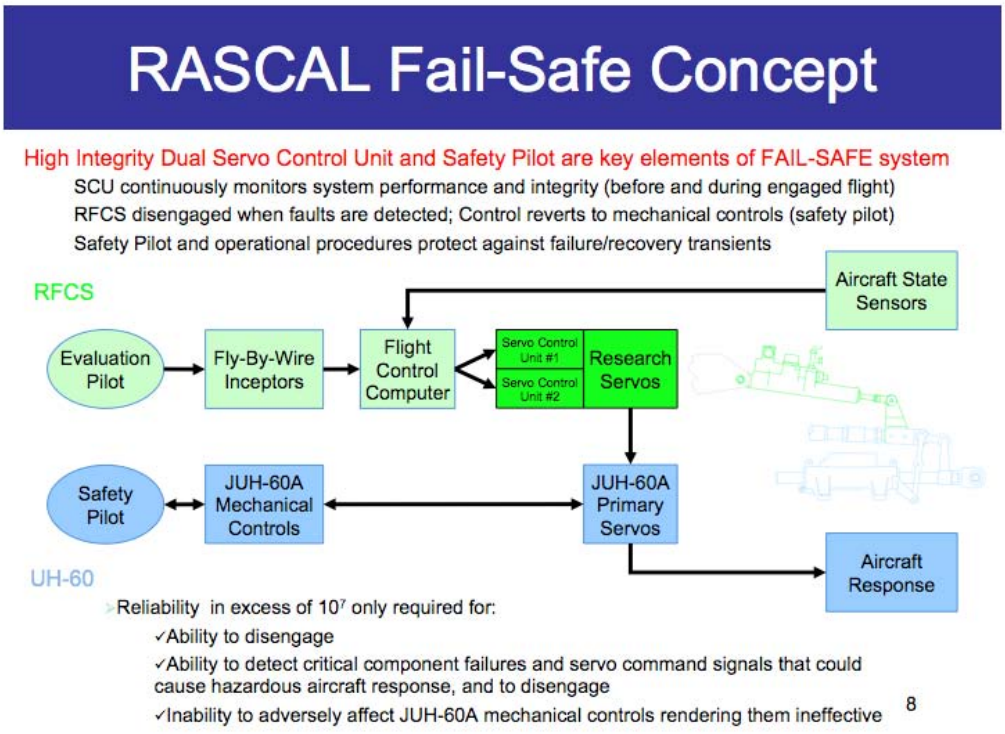

Figure 6.9. U.S. Army/NASA RASCAL fail-safe concept.

and safe operation is restored promptly. The general principles of this architecture (if not the specific details of implementation) are common among other variable-stability aircraft in operation today, both fixed- and rotary-wing: the CALSPAN VISTA F-16, NASA F-15 ACTIVE and F-18, the NRC's Bell 205 and 412, JAXA's MuPAL-alpha and -epsilon, and the DLR FHS EC-135. RASCAL was designed as a flight-control and handling-qualities research platform, and thus the architecture has limitations on how easily new and different research components can be integrated. In part, this limitation is illustrated by the MIL-STD-1553 data-bus-message format shown in figure 6.11; interfacing a research element into a system using this communications system is complicated by the need to propagate changes to the message structure across the nodes involved. Some of the platforms that have been developed since RASCAL have implemented newer communications protocols and busses to alleviate this problem.

An additional architectural approach is exemplified by autonomous rotorcraft developed by NASA and the U.S. Army, by Georgia Tech, and by the University of California, Berkeley. In these vehicles, and others, an emphasis was placed on research system integration and the use of open standards [Whalley et al., 2005]. However, as they are not human-occupied aircraft, the approach taken to system robustness, reliability, and response to failures is not as rigorous as in the case of RASCAL and other occupied variable-stability research aircraft.

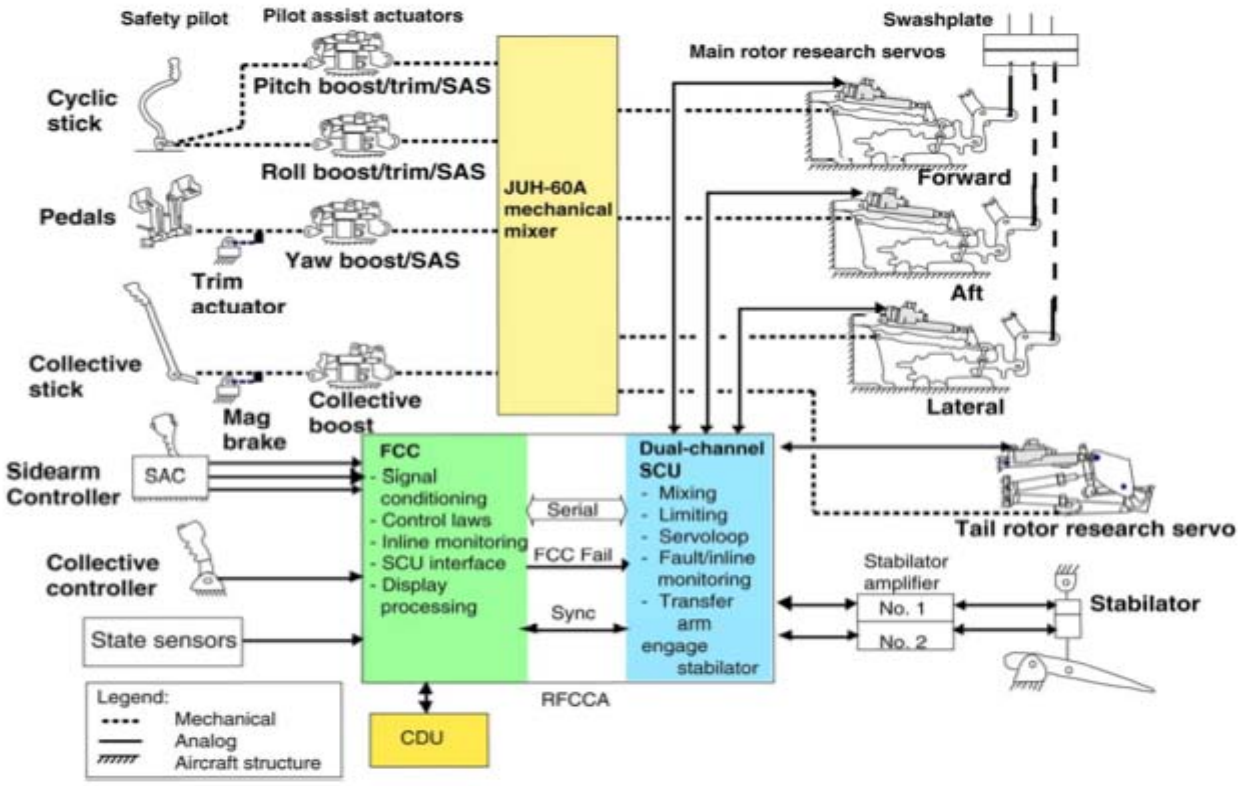

Figure 6.10. Key components of RASCAL system architecture.

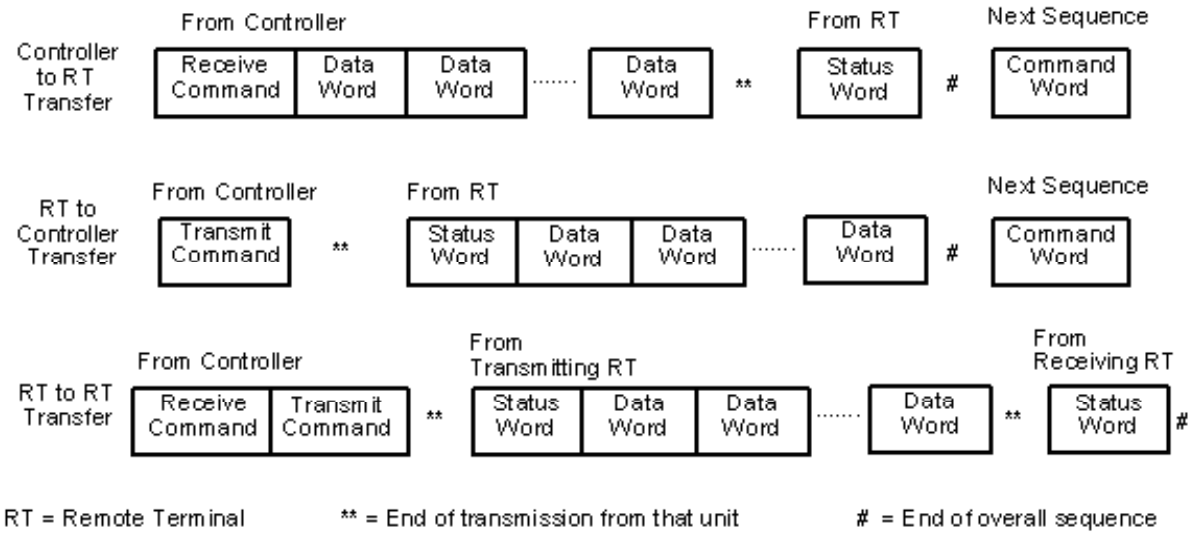

Figure 6.11. MIL-STD-1553 data-message formats [Garlington, 2000].

A third example is afforded by the Lockheed Martin Common Cockpit™ avionics suite, as used in the MH-60R and MH-60S. Based on an "open architecture," the Common Cockpit™ integrates numerous standard elements into a comprehensive networked system [Lockheed Martin, 2008].

With over 60 cockpits fielded (out of a contracted 172 systems), the cockpits have achieved over 40,000 flight hours during worldwide operations [Hatcher, 2004]. This architecture, and other comparable highly integrated systems developed by other commercial companies, places the emphasis on reliability; while standards-based, the details of the system are proprietary, and integrating new pieces into the system requires close cooperation with the manufacturer as well as thorough testing and qualification. While not specific to the MH-60 implementation, figure 6.12 illustrates a typical production military aircraft avionics architecture based on MIL-STD-1533. As noted, this architecture emphasizes reliability over ease of experimentation.

SIRCA is expected to draw upon the RASCAL control architecture to develop a baseline, but will also rely on the work developed under the Autonomous Rotorcraft Project [Whalley et al., 2005]. For example, a central element identified as part of the draft SIRCA architecture, which is absent from existing inhabited research rotorcraft architectures, is the "control agent." An example of a control agent is Apex [Freed et al., 2005], which has been used in the Autonomous Rotorcraft Project and the Intelligent Mission Management project, among others. The Apex architecture is shown in figure 6.13. The possible roles for a control agent are too numerous to list, but can be generalized as taking on some of the workload of a human pilot in integrating numerous, diverse sources of information, making decisions about them, and taking appropriate action. In the case of

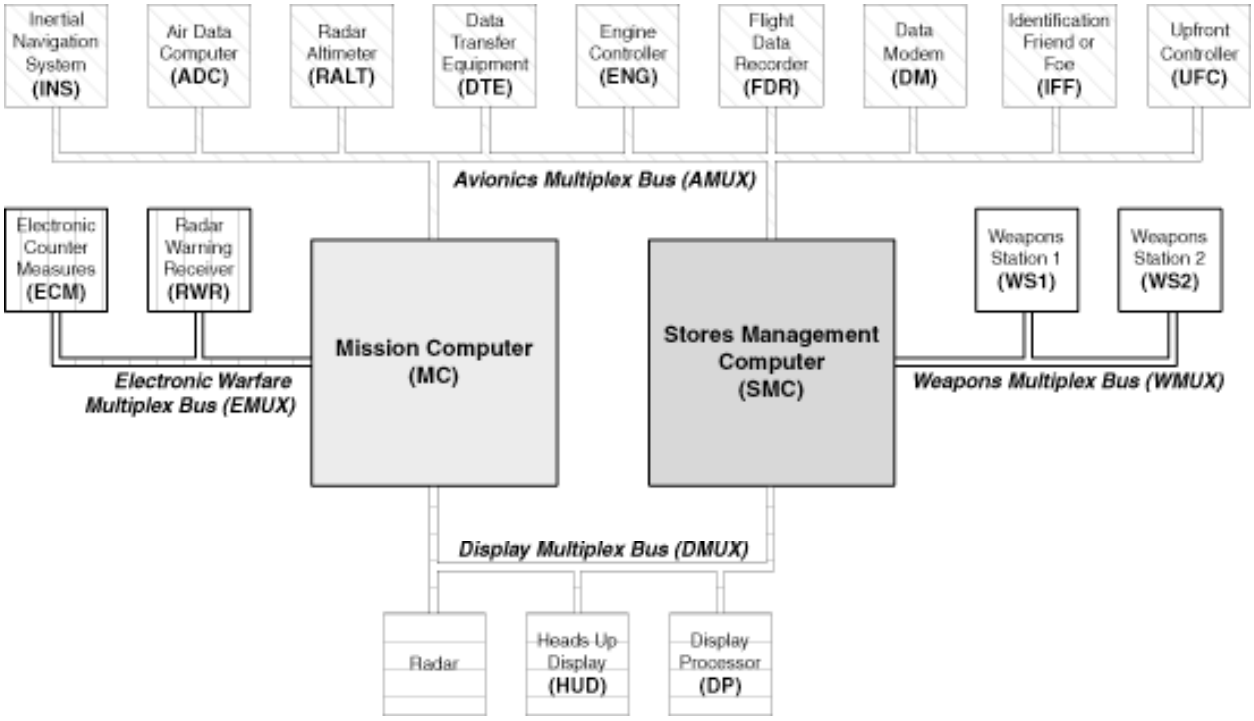

Figure 6.12. MIL-STD-1553 multiple-bus avionics architecture [Garlington, 2000].

an autonomous system, these roles would include directing most or all of the functions of the system; for a vehicle with a pilot in the loop, a control agent might work behind the scenes, examining events and information and routing them effectively, and directing the execution of higher-level resources (such as predictive models). Such a role is represented by the "goal executive" block shown in figure 6.14.

The trade-off between pilot input versus automated task is a crucial aspect of the proposed SIRCA architecture. Higher bandwidth and increased number of control systems dictates more automation while preserving essential pilot contributions.

Continued development work on SIRCA by NASA FDC research is planned, working towards a demonstrated capability to efficiently integrate nodes from multiple disciplines. Planned development includes specification of interfaces; selection of an execution engine and language [Verma et al., 2006], and development of the planning and execution vocabulary required to integrate systems in the architecture; and selection of a common interface middleware that can be used throughout the architecture.

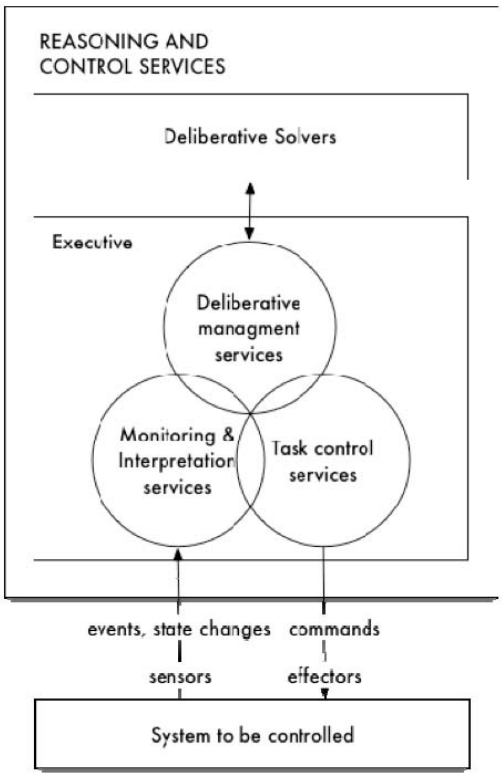

Figure 6.13. The Apex integration architecture, an example of a control agent architecture [Freed et al., 2005].

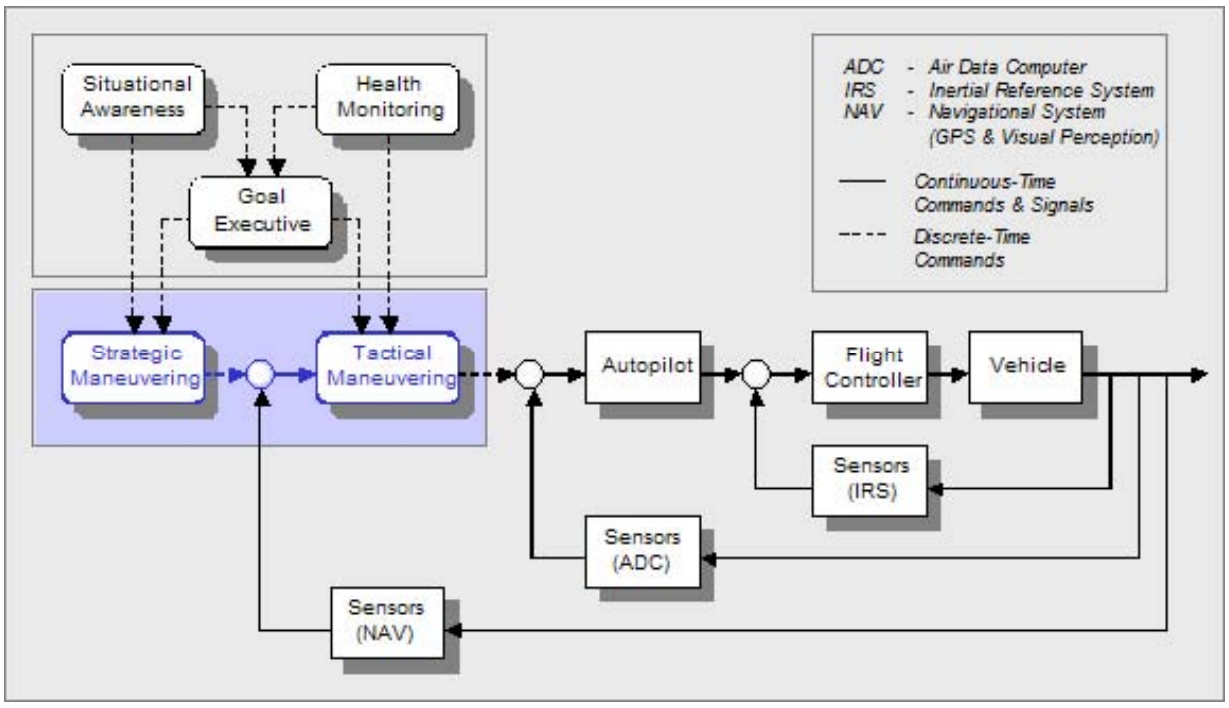

Figure 6.14. Intelligent vehicle control architecture [Patterson-Hine et al., 2008].

As shown in the conceptual architecture (fig. 6.8), SIRCA must respond to distinct but complementary technology advances in other disciplines. In addition to developing the SIRCA architecture, specific discipline-oriented topics currently supported by NASA FDC research to enable SIRCA include:

- Advanced aeromechanics concepts
- Control of variable or multispeed propulsion systems
- Flight dynamics of large rotorcraft
- Human-system integration
- Guidance and navigation displays

The following sections describe the FDC ongoing work, predictive capability, and planned research in each of these topics.

Advanced Aeromechanics Concepts

Recently interest in the development and testing of various advanced aeromechanical devices and concepts for use on current and future rotorcraft has increased. The objectives of using these devices and concepts include the reduction of the helicopter noise signature for both military and civil applications; the reduction in the vibration environment to improve passenger and pilot comfort, improve the fatigue life on mechanical components, and reduce vibration for the avionics and other electronic systems; and the improvement in helicopter performance by reducing the rotor torque and power required, and increasing the thrust, range, endurance, and/or speed. As described earlier, the envisioned SIRCA addresses the emerging need for an onboard executive or management framework that will interact with and coordinate the actions of the various control systems. These control systems include the primary flight control system as well as any active control systems associated with the advanced aeromechanics concepts. Without SIRCA, each of the control systems would operate independently and would not coordinate their activities with the other systems. The key to successfully developing and implementing SIRCA is to have predictive capabilities that accurately model all of the important dynamics and systems. In addition, these predictive tools must generate models in a form appropriate for flight-control-system design, and for flight-dynamics simulations and handing-qualities analyses.

Some of the advanced aeromechanical devices and concepts being developed include higher harmonic control (HHC), IBC, on-blade control (OBC), variable-speed rotors, etc. These advanced aeromechanics concepts (also discussed in Chapters 2, 3, and 7) have the potential to significantly affect the dynamics of the helicopter in the frequency ranges that are important for flight control from DC to about 2 Hz, and thus can affect the flight-control-system design and performance—particularly where the concepts themselves contain active control systems that can maximize their performance over varying flight regimes and there is potential for interaction between the various onboard control systems.

With such devices moving from initial concepts and simulation to full-scale experimentation and eventually on to production, it is important that the effects of these advanced aeromechanics concepts on the flight dynamics, control system, and handling qualities be clearly understood. In addition to understanding their effects, accurate predictive capabilities and mathematical models are required so that flight-control-system design can account for advanced aeromechanical concepts. These models should therefore be compatible with current flight controls and handling-qualities analysis techniques and tools, including real-time simulation capabilities to evaluate handing qualities with the pilot in the loop. Many flight control design and handling-qualities evaluation tools require models in a linear state-space form, and compatibility with these tools should be accounted for when developing predictive capabilities.

Key areas where advanced aeromechanics concepts could potentially impact the helicopter flight dynamics, flight control design, and handling qualities are discussed next.

The advanced aeromechanics concepts or mechanisms may change the dynamic response characteristics of the helicopter from a baseline case where the concept/mechanism is not present. The effects caused by these mechanisms could be seen as additional higher-order dynamics, changes to the higher-order dynamics from alteration of the rotor modes, and changes to the lower-frequency rigid-body response characteristics. The design of the flight control system must therefore account for these changes in the dynamic characteristics, and this process requires accurate predictive capabilities and models that are compatible with flight control design tools. In addition, the flight control system must be robust enough to provide the required level of handing qualities with and without the advanced aeromechanics concepts being active. The FDC group is currently working in this area as part of a UH-60 rotor IBC wind tunnel test. One of the test objectives is to evaluate the effects of IBC advanced control on the dynamic response of the UH-60 rotor by measuring the rotor dynamic response with and without the IBC system active. This work could be used as a prototype exercise for SIRCA, where the trim controller and IBC systems would be operating together and the SIRCA architecture provides an overall “control agent” for the independent control systems.

The advanced aeromechanics concepts may also produce time-varying dynamics of the rotor system and helicopter response. These variations in dynamics would likely occur on a much smaller time scale (particularly in maneuvering flight) compared to variations in dynamics resulting from changes in airspeed, altitude, weight, etc. Again the flight control system must be robust enough to account for these changes or uncertainties in the vehicle dynamic response. The FDC group is currently studying the effects of time-varying dynamics on piloted handling qualities as part of NASA-funded research with industry. This work includes a VMS simulation of time-varying higher-order dynamics to determine at what point the pilot is able to detect the change in dynamics and what impact these changing dynamics have on piloted handling qualities.

Another key area involves control-system interactions between actively controlled advanced aeromechanics concepts and the primary flight control system. If these interactions are present, they could negatively impact the stability and performance of one or both of the active control systems. To ensure that no negative effects are possible, the various control systems would have to be designed, or at least evaluated, in parallel rather than independently. This process requires the availability of accurate models of both the vehicle dynamics and the advanced aeromechanics devices

that can be used together in the control-system development. Through NASA-funded research, development of predictive modeling capabilities that include the rigid-body, rotor, and inflow dynamics as well as the outputs of the vibration and noise effects for a variety of advanced aeromechanics concepts (such as IBC/HHC/OBC) is under way. The resulting models will be in state-space form and could be used with current control-system-design and handling-qualities evaluation tools. Another study is being performed as part of the UH-60 rotor IBC wind tunnel test that will address the stability and performance of an IBC system in steady testing as well as during maneuvers. Results from this wind tunnel experiment will provide insight into any potential interactions with a primary flight control system and the piloted-handling qualities.

In addition to the effects of advanced aeromechanics concepts on rotorcraft flight dynamics and control, the basic aeromechanics modes (such as those resulting from blade flexibility, hingeless and bearingless rotors, rotor wakes and inflow, etc.) of the rotor are becoming more important to rotorcraft flight dynamics and flight control design. Traditionally, the frequency separation between primary flight control systems (lower band of frequencies from DC to about 2 Hz) and the aeromechanics modes of the rotor has been large enough that the primary flight control system could be largely designed using only simple rotor models. In some cases, the lower-frequency rotor modes such as the regressive lag mode and the coupled inflow-coning mode, which do affect the flight control design in some cases, were included using lower-order models to produce the correct dynamics effects in the frequency range of the primary flight control system. These basic aeromechanics effects (blade flexibility and inflow dynamics, etc.) are becoming more important because the frequency separation between primary flight control and the basic helicopter aeromechanics modes is decreasing. One reason for this phenomenon is that modern flight control systems are becoming more highly augmented with higher bandwidths to improve maneuverability and performance, a situation that drives up the frequencies of interest to the primary flight control system. On the other hand, the progression towards larger rotorcraft with larger rotors and the integration of slowed rotor concepts act to reduce the frequencies of the rotor modes, increasing their effects in the primary flight control range.

Current and planned analytical capability

Significant progress has been made—and continues to be made—towards improving the fidelity of aeromechanics comprehensive codes such as CAMRAD II, RCAS, etc. to predict the effects of these advanced aeromechanics concepts. However, these predictive analyses are developed primarily for the purpose of aeromechanics predictions and the models are often not available in a form required for flight dynamics and control analyses. On the other hand, flight-dynamics codes (such as GENHEL and Forecast) can be used directly for real-time simulation and flight control analysis and design, but do not model helicopter aeromechanics with sufficient fidelity to investigate the effects of advanced aeromechanics concepts on helicopter flight control and handling qualities.

FDC efforts are addressing the limitations in the current state of the art in modeling techniques to develop predictive capabilities that are appropriate for rotorcraft flight dynamics and control purposes and that accurately model the advanced aeromechanics concepts. NASA-funded research in this area includes two key activities. The first activity focuses on developing a free-wake model formulation in a first-order state-space form that will be directly compatible with flight control

design and handling-qualities analysis tools, and can be used in real-time simulations. This model formulation will improve the fidelity of flight-mechanics models that are used in flight-control-system development and handling-qualities assessments.

A second effort expands the work of Cheng et al. [2006] in developing modeling techniques for integrating higher-harmonic vibration predictions in a linear state-space model form that can be used for flight dynamics and control analysis. In addition, this activity aims to accurately predict the vibration environment in maneuvering flight for numerous different advanced aeromechanics concepts. These predictive capabilities will allow advanced aeromechanics concepts for vibration reduction and primary flight control to be developed and evaluated simultaneously rather than independently. This modeling can also be used to study the potential interactions between the primary flight control systems and advanced active aeromechanics concepts for vibration reduction since the underlying dynamics model includes both flight dynamics and vibration predictions. Such modeling capability is particularly important for maneuvering flight, where rapid changes occur in the vibration environment.

The impact of the advanced aeromechanic concepts on handling qualities is also being addressed by FDC. For example, the effects of added higher-order dynamics on handling qualities and the effect that these time-varying dynamics have on rotorcraft piloting is being assessed through NASA-funded research. Results from this investigation will provide valuable data on the impact of advanced aeromechanics concepts that produce time-varying dynamics on the piloting task and handling qualities, and on flight control design. A planned NASA wind tunnel test of the UH-60 rotor with IBC will investigate the effects of active individual blade control for noise and vibration reduction on the lower-frequency dynamic response of the rotor system and determine any potential for interaction between the actively controlled IBC system and primary flight control. Cheng et al. [2006] studied the potential interactions between an IBC vibration-reduction controller and the helicopter dynamic response using analytical models. Their results showed that the IBC system did not significantly affect the vehicle dynamic response and concluded that the IBC system would also not affect the primary flight control system. This study also showed that maneuvering flight can significantly reduce the effectiveness of the IBC system to reduce vibrations in certain flight regimes, and concludes that changes to the IBC system bandwidths (crossover frequencies) may be required for these systems to continually reduce vibrations during transient maneuvers. The SMART rotor wind tunnel test will also provide data on rotor dynamic response with on-blade flap-control surfaces that can be used for tool development and validation.

Variable Rotor Speed

Recent system analysis work has shown the potential benefit of substantial reductions in rotor tip speed in cruise (versus hover tip speeds) for tiltrotor aircraft and other rotary-wing platforms (see fig. 6.15, from Johnson et al. [2007]). However, implementing systems that efficiently enable such large variations in vehicle rotor tip speeds in flight will require substantial progress in multiple disciplines, including advances in flight dynamics and control.

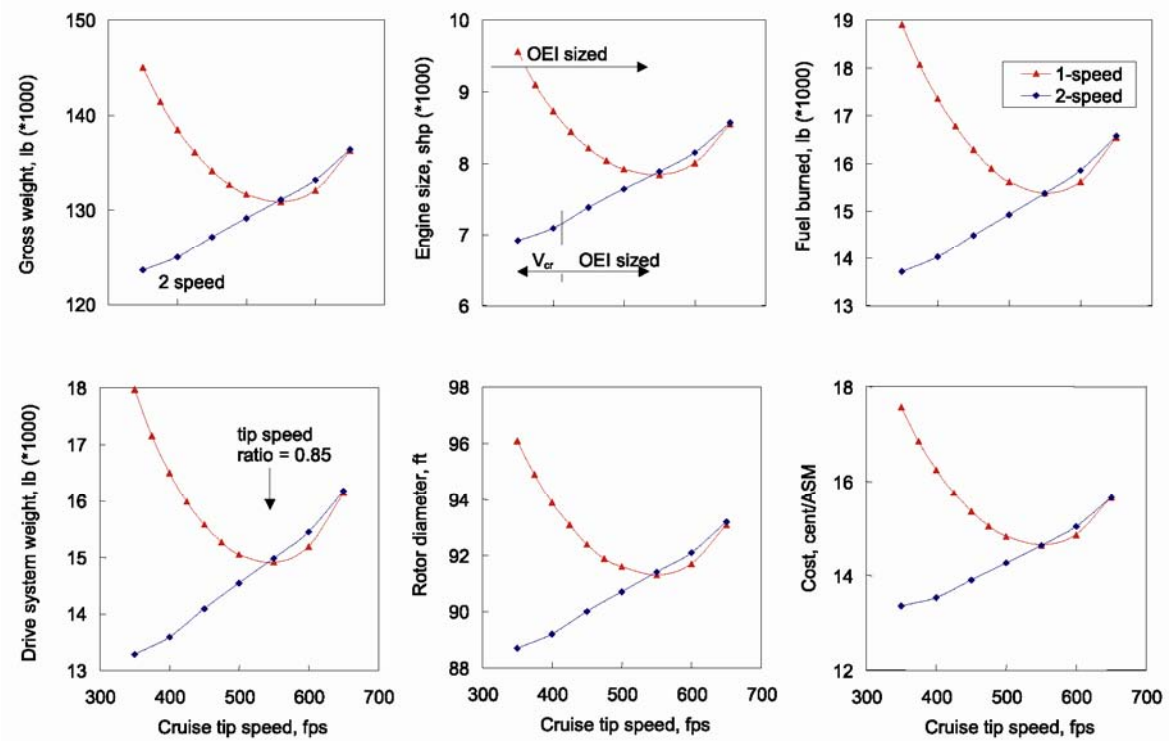

Figure 6.15. Representative heavy-lift tiltrotor weight reduction resulting from reduced cruise tip speeds and multispeed transmissions (from Johnson et al. [2007]).

FDC research aims to provide a variable-rotor-speed methodology that can vary continuously between 100% and 50%, as opposed to current practice in which the rotor is controlled to a constant speed. Currently, rotorcraft flight control systems are designed with a constant-rotor-speed assumption, even though variations of a few percent in rotor speed occur transiently because of load changes, for example. However, rotor-speed variations during maneuvers such as the bob-up have been shown in simulation to provide benefits in agility such as reduced time to climb (by exchanging rotor speed for increased available collective) [Iwata and Rock, 1993], and there is evidence that experienced pilots purposely allow rotor-speed droop to improve performance [Iwata, 1996]. Thus the idea of variable rotor speed for rotorcraft is attractive in certain situations because of its ability to improve responsiveness. However, because of high pilot workload and the complexity of performing aggressive maneuvers in a near-optimal manner, automation of the optimal control law has been investigated [Iwata and Rock, 1996]. In contrast, by allowing large (30% of nominal) rotor-speed variations, dramatic improvements have been demonstrated through simulation in agility and maneuverability during a 180-degree, maximum-performance decelerating turn [Schaefer, 1991].

Another consequence of the current fixed-rotor-speed approach is that turboshaft engines are designed to operate at a fixed power turbine speed, and performance significantly degrades for off-design operation. In fact, engine-speed variation is restricted to a maximum of about 15% because of fuel-efficiency and stall-margin considerations. Thus, in order to achieve useful variable-rotor-speed control over a significant range, either engine operability range needs to be expanded [D'Angelo, 1995] or some of the speed variability must be accounted for though the transmission. A study of several competing approaches incorporating a combination of engine and transmission modifications

concluded that the baseline turboshaft engine coupled with a variable-speed transmission is the best configuration. It would be able to produce nearly constant output power with good fuel-consumption characteristics over a 100% to 50% output speed range with little technology risk [Bettner et al., 1992]. Thus the issue becomes one of determining a way to vary the gear ratio in a transmission connected to a standard turboshaft engine.

Continuously variable transmissions have been developed that allow speed variation over a wide range while providing continuous power. However, they are usually based on a traction drive or friction drive, where the power is transferred though nonpositive engagement frictional contacts. These drives are relatively large and heavy, and their efficiency and reliability are poor compared to those of gearboxes. Two-speed transmissions have been proposed for tiltrotor concepts, which often employ two-speed operation, one for vertical mode and one for forward flight; however, transmissions designed for two discrete speeds do not provide continuously variable rotor speed. Additionally, while two-speed transmissions that use gears to transmit torque and power are very efficient, shifting from one speed to another could cause a momentary loss of output power, and the large power changes can damage the transmission or drive train.

FDC is investigating a sequential shifting control (SSC) with baseline turboshaft engines [Litt et al., 2007]. The SSC requires the addition of two multispeed gearboxes to a standard drive train. Two engines work together to vary the rotor speed over a range much larger than either could achieve individually. The engines are coordinated to vary their power turbine speeds sequentially, synchronized with the gear shifting, to produce smooth, continuous rotor-speed variations over a wide operating range. The target test platform used here is the T700 propulsion/rotor system in an Apache or Blackhawk helicopter.

The approach for SSC is illustrated in figure 6.16. There are two engines, each with a multispeed gearbox inserted between the nose box and freewheeling clutch. Any approach to large rotor-speed variations must meet the following requirements: power turbine speed variation must be limited to about 15%, and continuous torque must be applied to the rotor. The SSC meets the first requirement by dividing the rotor-speed range up into speed bands, each corresponding to about 15% of power turbine speed times the gear ratio. A small amount of overlap with the neighboring speed bands at each end allows one engine to “hand off” the rotor to the other engine during the synchronized gear-shifting process. If 50% speed variation is specified, six overlapping speed bands are required to implement the algorithm. The second requirement is met by always having one engine engaged while the other is shifting (unless the rotor is overspeeding, when neither is engaged). This way the rotor speed can vary over a wide range while the engines each remain within their smaller speed band. Since the highest rotor-speed band includes the nominal rotor speed, the engines do not have to work as hard in the other speed ranges. This conceptual approach addresses the issue of available power and the ability of a single engine to drive the rotor while the other is shifting—if the procedure can be accomplished in the highest gear, it can be accomplished in lower gears where less torque is required. In fact, it is anticipated that there would be shifting constraints into high gear that are related to power and life, but procedures such as the maximum power check that are performed with only one engine operating at full power indicate that the SSC approach is feasible.

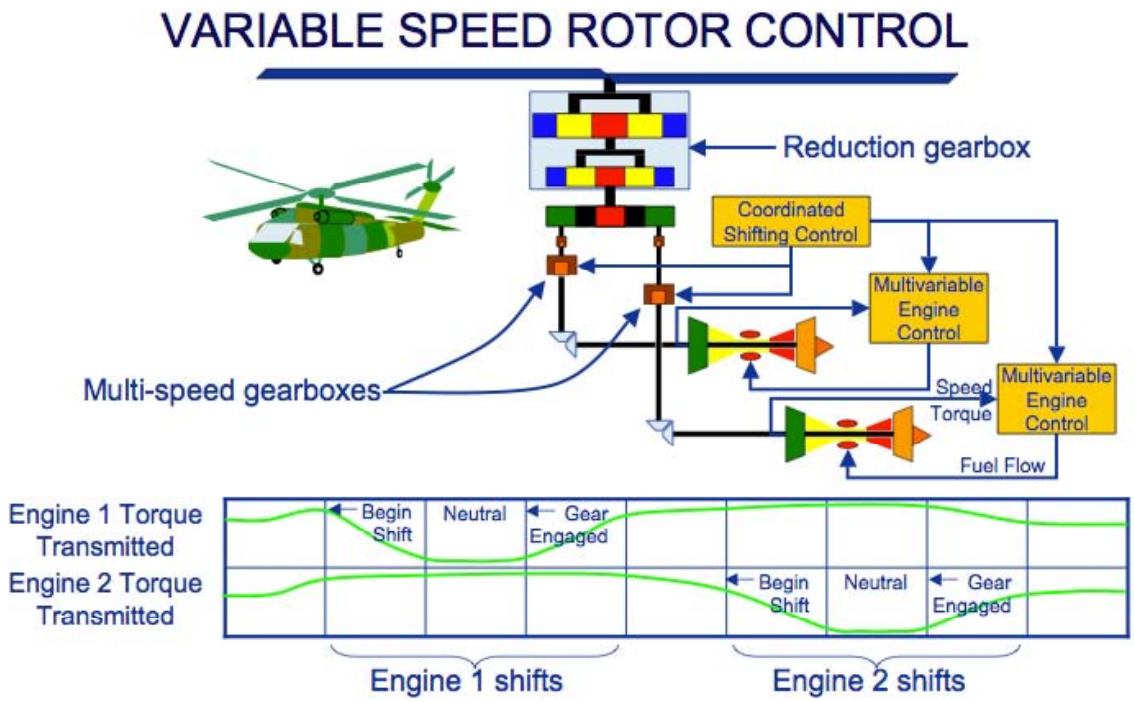

Figure 6.16. Overall concept of the sequential gear-shifting strategy for multispeed rotor control (Litt et al., 2007].

As shown in figure 6.17, the SSC requires a high level of coordination between the propulsion system and the gearboxes. Conceptually, a command (presumably from a pilot) to vary rotor speed from one speed band to another would result in generation of a trajectory (potentially by an automated system). This trajectory would involve the synchronized operation of the two engines and gearboxes to adjust the rotor speed while maintaining rotor torque. Thus the rotor trajectory would be decomposed into an individual speed profile for the power turbine of each engine that accounts for the constraints associated with the shifting procedure. The actual procedure involves a sequence of events to make the transition, taking advantage of the existing freewheeling clutches to disengage the power turbines from the main gearbox to facilitate the shifting process. The overall concept has been demonstrated in simulation in several hand-tuned examples [Litt et al., 2007]. Work is ongoing to develop control algorithms to facilitate the switching process that provide feasible trajectories resulting in smooth transitions between speed regimes.

Currently, simplified models from the literature are being used for testing purposes. Linear T700 turboshaft engine models and dynamometer-like load models have been implemented. The transmission is modeled as a set of gear ratios, providing a simple testbed for evaluating algorithms and developing control laws. More complex nonlinear models are available for evaluation testing of control laws.

Along with the inclusion of nonlinear engine models, better multispeed transmission models are being developed, as well as rotor models. The interaction between the engine/transmission/rotor system and the airframe will be captured to evaluate the approach from a high-level system perspective.

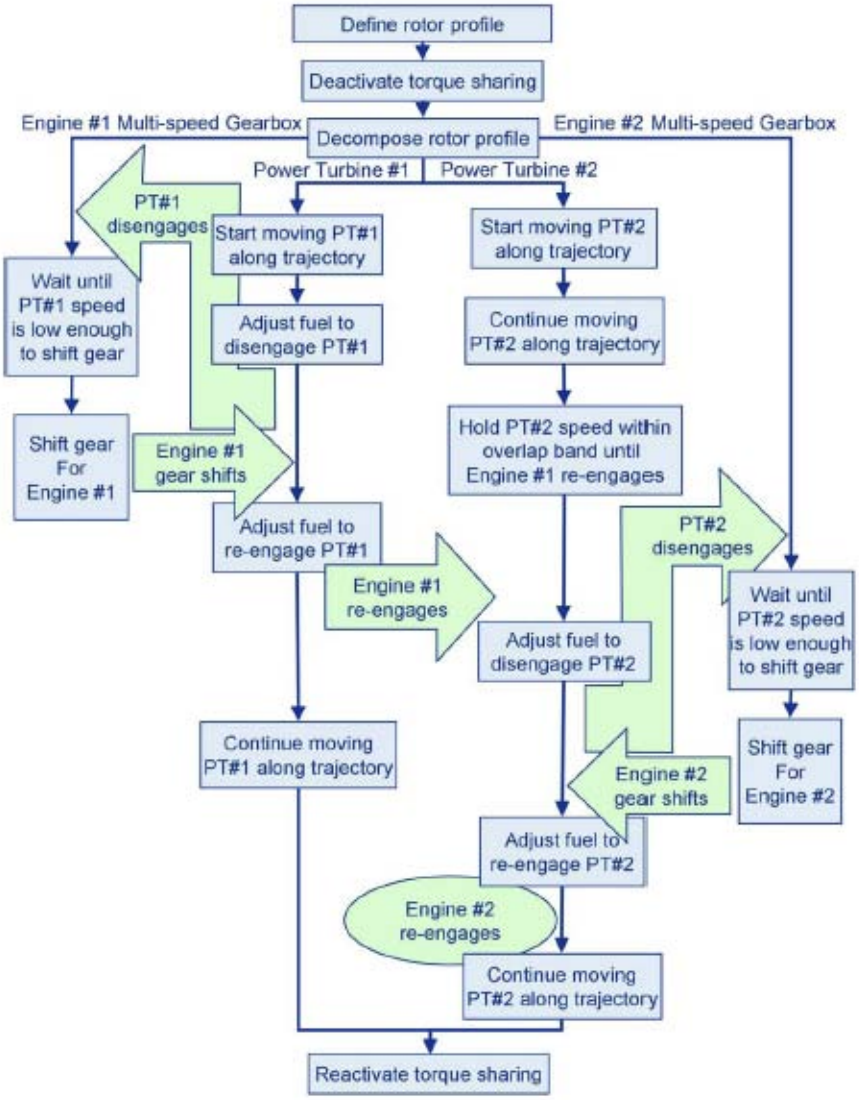

Figure 6.17. Logic flow diagram for SSC approach (Litt et al., 2007].

Flight Dynamics of Large Rotorcraft

The design of increasingly large rotorcraft results in the flexibility of the fuselage and wing structures becoming a more important component of the overall flight-control-system design because the frequencies of the fuselage and wing structural modes decrease as the overall size of the rotorcraft increases, and the lower-frequency structural modes have a greater impact on the vehicle dynamic response. In addition to large size, the strength of the structural components are often being constrained by weight, size, and cost considerations, and the increased use of composite structures for weight reduction results in more flexible structures that drive down the structural mode frequencies, thereby increasing their impact on the vehicle dynamic response. This increased likelihood for structural mode coupling with vehicle flight dynamics is exacerbated by the structural modes typically having low damping where their effects can be seen at frequencies significantly below the natural frequencies of the modes themselves.

While the structural mode frequencies are decreasing, the requirements for increased performance and maneuverability push the flight control frequencies higher, resulting in a greater impact of structural flexibility. The confluence of flight control frequencies and structural mode frequencies with larger rotorcraft make it increasingly important to account for the fuselage and wing structural flexibility in the efficient design of flight control systems. Another impact of structural flexibility is in aeroservoelastic stability where the pilot biodynamic feedback and flight-control-system feedback can couple with the rotorcraft structure, resulting in pilot- or control-system–assisted excitation of the structural modes. Aeroservoelastic stability is an important consideration that should be accounted for in the control system design.

The key to properly accounting for structural flexibility effects in the control-system design task is to have predictive capabilities that accurately model the vehicle dynamics, including the effects of structural flexibility. This predictive capability must also include pilot biodynamic and control models to accurately assess aeroservoelastic stability characteristics. Finally, the rotorcraft models must include sensor models that account for the structural flexibility effects on the dynamic response characteristics at the sensor locations, which are used for pilot and control-system feedback. Having these accurate predictive capabilities available in the control-system design phase will ultimately decrease the amount of flight-test time required to assess the impact of structural flexibility on the control system and to tune the control system to get the desired performance.

The following section discusses challenges of modeling and predicting flight dynamic response of large rotorcraft.

Predictive capability

From a historical perspective, much of the work in the modeling of flexible rotorcraft structures has been made to improve the prediction of vibration and loads within the fuselage such as at the pilot seat, avionics bay, passenger compartment, engine, and drive-train positions. Structural flexibility is an important consideration since the loads for the rotor system can be amplified or attenuated depending on where the vibrations or loads are resolved within the fuselage structure. For example, the design of fixed-frame, vibration-reduction devices is highly dependent on accurate predictions of fuselage loads and vibration. An example of this application is the work of Cribbs et al. [2000], who used a coupled rotor/fuselage aeroelastic response model to study vibration reduction based on Active Control of Structural Response (ACSR). Fuselage structural flexibility was modeled using finite element methods where thousands of degrees of freedom are commonly used to model the fuselage structure. This study showed that the vibration accelerations at various fuselage locations depend on the locations where they are measured, with vibration levels higher in the rear cabin than at the pilot seat. This predictive modeling capability was then used to develop an ACSR system that was able to reduce vibration levels at all advance ratios and illustrated the importance of accurate fuselage structural modeling. Another example is the work of Yeo and Chopra [2001], who incorporated fuselage flexibility to perform a comprehensive vibration analysis of a coupled rotor/fuselage system for the AH-1G. This study used UMARC with an elastic-line airframe structural model of the main fuselage, tailboom, wing, and main rotor shaft with a total of 39 beam elements. Comparisons with NASTRAN predictions and test data for the airframe natural frequencies showed a good predictive accuracy with this structural modeling technique. The study also showed a general improvement in fixed-frame vibratory-load prediction at the pilot seat with an elastic fuselage model when compared with experimental operation load survey test data. A study by Bauchau et al. [2004] used a

finite element analysis to compute the flexible modes of the fuselage; the model represents the elastic fuselage using a modal approximation to reduce the number of degrees of freedom in the fuselage. This model was then used to study the vibration environment in forward flight and during maneuvers.

These examples illustrate methods for integrating fuselage flexibility effects into comprehensive rotorcraft models for the purpose of improving the prediction of rotor loads and vibrations and showing that predicting the structural modes of the fuselage, wings, etc. is possible. These studies, however, have not attempted to model the overall effects of structural flexibility on the dynamic response of the rotorcraft. With the proposed design of larger rotorcraft, additional studies and modeling capabilities are needed to specifically model the effects of structural flexibility on the flight dynamics and aeroservoelastic characteristics of rotorcraft.

Aeroservoelastic stability characteristics of rotorcraft are becoming significant considerations in the design of flight control systems because of the proximity of fuselage and wing structural modes with the piloted and automatic control frequency ranges. Aeroservoelastic stability will likely become a more significant consideration for larger rotorcraft that have structural modes at lower frequencies, but is also a significant issue for many nontraditional rotorcraft configurations (such as tiltrotors) that have some unique structural flexibility modes that can couple with the flight control system and the pilot biodynamic feedback.

One prime example is in the development of the V-22 [Landis et al., 1996], wherein in-flight pilot-assisted oscillations were encountered in initial flight tests due to the tendency of the pilot/control system to couple with the aircraft structural response when flying in airplane mode. One of the destabilizing effects observed in flight testing was a coupling between the longitudinal acceleration and the symmetric wing chordwise bending mode at a natural frequency of about 4.2 Hz. For this coupling in airplane mode, the thrust-control lever command increased the thrust and excited the chordwise bending mode of the wings. The excitation of this mode resulted in fore-aft motion at the cockpit producing a biodynamic feedback through the pilot, which was observed to decrease the damping of the symmetric wing chordwise bending mode with increasing airspeed. To eliminate this destabilizing effect, a digital notch filter was included in the pilot thrust-control-lever command that effectively removed the coupling and resulted in symmetric wing chordwise bending-mode damping that did not decrease with airspeed and was therefore not affected by the pilot biodynamic feedback. Other such aeroservoelastic stability issues in rotorcraft have used notch filters in the control systems that effectively break the feedback loops at the critical structural-flexibility frequencies. The use of notch filters also has the added advantage of not introducing unacceptable phase lag in the flight control frequency ranges up to about 2 Hz.

It is worth noting that in the initial development of the V-22 flight control system the aeroservoelastic analyses did not include models of the pilot biodynamic feedback, and therefore did not predict the resulting pilot-assisted oscillations. Subsequent to initial flight tests, aeroservoelastic analyses were run using generalized pilot/control models that were derived from measured data taken from ground-shake tests to design system enhancements, and these models were correlated to measured stability data collected in flight.

This example illustrates a need for additional work in developing models that include the interactions between the vehicle flight dynamics response, structural flexibility modes, the flight control system, and pilot biodynamic feedback in order to assess the aeroservoelastic stability and to identify potential pilot or control-system–assisted oscillations. Such modeling capabilities would also be able to examine aeroservoelastic stability at all parts of the flight envelope and with different pilot biodynamic models. Finally, the rotorcraft models must include sensor models that accurately calculate the dynamic-response characteristics as the sensor locations of the flexible structure that can influence the aeroservoelastic stability characteristics, particularly in coupling with the control system. Having accurate predictive capability would ultimately decrease the amount of flight testing by being able to assess and account for flexible structure effects in the design phase rather than solely in flight.

As rotorcraft become larger the potential for structural flexibility to impact the overall flight dynamics response of the vehicle increases. Structural flexibility could ultimately negatively affect the stability margins and performance of the vehicle and control system. These effects of structural flexibility on dynamic response are different from the aeroservoelastic effects described in the previous section that are often mitigated with the use of notch filters. The effects of structural flexibility on the dynamic response are seen over a wider frequency range and are something that the fixed-wing community has had to account for in flight-control-system design for many years because the long and slender fuselage and wing structures that characterize larger fixed-wing aircraft typically have lightly damped low-frequency structural modes. In the rotorcraft community, the fuselage and wing structures have typically been compact and rigid enough that there has been no impact of structural flexibility on the dynamic response in the flight control frequency range up to about 2 Hz. However, as rotorcraft become larger, with decreasing structural frequencies because of size, this situation will no longer hold true and the flexibility of the rotorcraft structure will affect the rotorcraft dynamic response that will have to be accounted for in the flight-control-system design.

A fixed-wing example for a large transport aircraft is shown in figure 6.18 (from Theodore et al. [2008]). This figure shows the effect of wing bending on the body roll-rate response for aileron inputs in a low-speed cruise condition. The solid line shows the frequency response obtained from flight-test data and the dashed line shows the response from a rigid-body simulation model that did not include wing-bending structural degrees of freedom. Two wing-bending structural modes are visible by the two peaks in the magnitude curve and the large phase rolloff at the higher end of the spectrum. The increase in magnitude and decrease in phase associated with the wing-bending modes for this case would negatively affect the stability margins and performance of the system. In fact, if the rigid-body simulation model were used to design the flight control system for this aircraft, the stability margins measured in flight would be lower than those predicted in the design. This study also used a state-space model structure that includes coupled rigid-body and structural dynamics; the study simultaneously identified the rigid-body and structural dynamics from flight data. This state-space model could then be used for flight control design to properly account for the structural flexibility effects. The model structure used here is adapted from the work of Waszak et al. [1992] and Meirovitch and Tuczu [2003], who also incorporated structural flexibility into flight-dynamics models for fixed-wing applications.

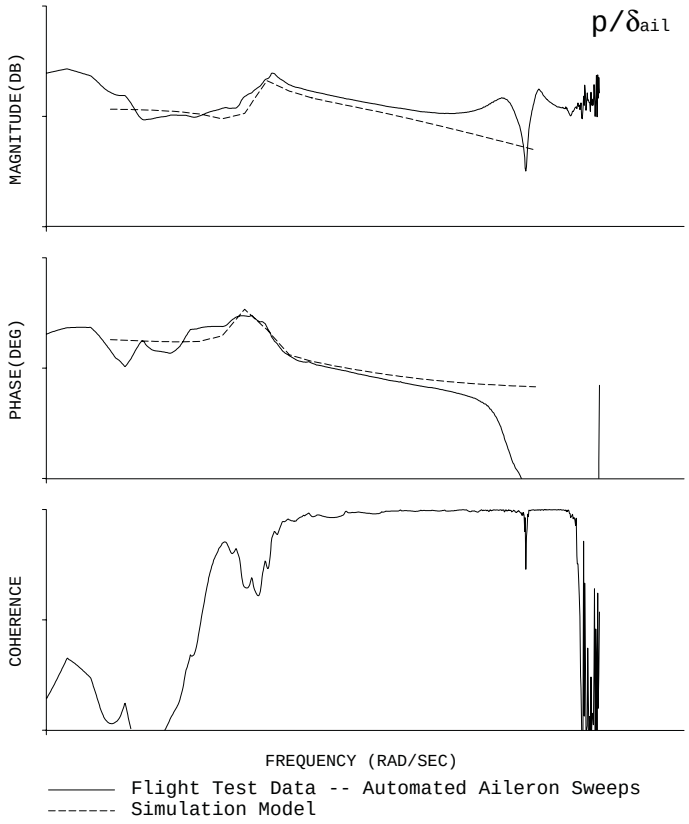

Figure 6.18 [Theodore et al., 2008]: Roll rate due to aileron frequency response for a large transport aircraft comparing flight data response and a rigid-body simulation model. Effects of two wing-bending modes are seen as twin peaks in magnitude curve at the higher-frequency end.

The approach taken by Theodore et al. [2008] was to use system identification to determine a coupled state-space model for a large fixed-wing transport aircraft, but the same approach could be used to identify similar models for rotorcraft. The ultimate goal for rotorcraft work would be to have a design and modeling capability that can accurately predict the effects of structural flexibility on the flight-dynamics response of the rotorcraft and produce this model in a format that is conducive to flight-control and handling-qualities design.

A performance-metric goal within NASA is to have the ability to accurately model the effects of structural flexibility of the helicopter dynamic response to within 10% of that observed in flight over the flight control frequency range up to about 2 Hz. Current flight-dynamics modeling techniques do not include the effects of fuselage structural flexibility and therefore do not account for this effect during flight control design. Control systems have been tuned in flight using an iterative process to meet the required levels of performance and handling-qualities specifications. Models that accurately represent the helicopter dynamics (including structural flexibility) would produce an improved initial control-system design and would require less flight-test time for control-system tuning.

Human-System Integration

The rotorcraft operational environment (as compared with other vehicle classes) offers a unique set of challenges to the pilot and crew. While fixed-wing aircraft typically have relatively high levels of natural stability, rotorcraft typically have less-stable vehicle dynamics, requiring specialized vehicle-specific skills and producing higher workloads. In addition to the challenge of piloting, the rotorcraft crew typically operates in environments that are more hazardous and less controlled than fixed-wing aircraft. A partial list of typical rotorcraft operations includes medivac, logging, surveying, inspection, air taxi/transportation, surveillance, and law enforcement. Many of these operations require operation into or out of minimally or unprepared landing sites, while others require extended operations in close proximity to structures and other obstacles. These types of operations additionally require the crew to rely extensively on out-the-window visual information; sometimes, close integration with other information sources is also required (such as sensor information, Global Positioning System (GPS) location, etc.).

The technologies being developed under SIRCA have the potential to pose unique challenges to the human pilot. Advanced blade-control concepts will likely introduce additional, higher-order dynamics to the vehicle. Variable-rotor-speed–control concepts will produce temporally varying vehicle dynamics, potentially much more rapid variations than are typically encountered because of changes due to operational environment or nominal vehicle states (e.g., airspeed, altitude, flightpath). Lastly, advances in control technologies such as fly-by-wire control systems enable greater flexibility in designing the response characteristics, thereby enabling potential new control modes.

The potential exists for negative interactions between the SIRCA technologies and the human pilot. Time-varying and higher-order dynamics could confound the task of fault or failure detection by the human pilot. Additionally, time-varying and higher-order dynamics as well as mode-control changes have the potential of increasing susceptibility to pilot-induced oscillations. Lastly, criteria and benchmarks currently used to assess flying quality and safety may need to be reexamined to determine appropriate standards for piloted control of rotorcraft incorporating these advanced design concepts.

The following discussion describes current predictive capabilities and modeling techniques for handling qualities, useable cue environment, workload, aircraft-pilot coupling, mode control, failure recovery, and pilot modeling.

Handling qualities

Although modern aircraft design automates much of the traditional piloting role, the ability to fly with a human controlling the aircraft remains as a primary means of operation for less-augmented aircraft, a means of dealing with unexpected or constantly changing missions (such as for military aircraft), or reversion to human control upon failure of parts of the automated system. As such, design for human control remains an important metric for the aircraft-control designer. Evaluation of piloted handling qualities remains a critical metric for satisfactory aircraft-control design. As defined by the seminal work by Cooper and Harper [1969] on the topic, Handling Qualities is defined as "those qualities or characteristics of an aircraft that govern the ease and precision with which a pilot is able to perform the tasks required in support of an aircraft role."

Pilot assessment and assignment of a Cooper-Harper Handling Qualities Rating (HQR) has served the aeronautics enterprise with an effective metric for the four decades since its development in the 1960s. Use of this evaluation system requires definition of an evaluation task and performance (precision) metrics that a pilot uses to arrive at a numerical rating. The rating is arrived at by working through the dichotomous decision tree involving both task performance and pilot workload, as illustrated in figure 6.1. Careful description of the task and required performance with evaluation pilots has generally produced consistent evaluation results, augmented by pilot standardization through the auspices of various flight-test schools.

Core concepts of the HQR are the definitions of desired or acceptable task performance and a discussion of satisfactory or adequate workload. With these parameters defined, a pilot can work through the decision blocks on the left side of figure 6.1. These decisions produce three bands of handling-qualities assessments plus the totally unacceptable uncontrollable result. The three bands are further discriminated by sets of adjectives describing both task performance and pilot assessment of workload, from which a pilot arrives at a single rating. The three bands are often referred to in association with handling-qualities "levels" which roughly translate into:

- Level 1: Satisfactory without improvement
- Level 2: Adequate performance, but improvement required
- Level 3: Unacceptable performance and/or workload

Note that although one might refer to numerical handling-qualities levels or the numerical HQR, the decision process that produced the rating is dichotomous. An average HQR may be used when looking at results from a group of pilots, but the individual assessments still need to be examined, particularly where there are significant outliers.

The goal of a controls designer is to achieve at least level-1 handling qualities. A design with level-2 handling qualities may be accepted for some adverse tasks (such as extreme winds and turbulence) or for recovery from a major system failure (such as an engine failure). Since the goal of a controls designer is to achieve "level-1" handling qualities, progress in controls and cockpit interface rarely can be measured by average HQR. Instead, one must seek metrics that define improvements in terms of task performance (e.g., closer tracking of a desired approach path), more complex operations, or worse task conditions (winds, turbulence, visibility). Rarely are existing successful designs (level-1 HQR) evaluated against more stringent performance criteria or task conditions, unless they are serving as a baseline for a product improvement.

For rotary-wing aircraft, a significant effort was made to summarize flight characteristics that lead to level 1, 2, or 3 handling-qualities assessments. This effort has resulted in the U.S. Army (with participation from other services and NASA) Aeronautical Design Standard-33 [Anonymous, 2000]. That effort has produced a quantifiable set of metrics that could be used by design and analysis tools such as CONDUIT [Tischler et al., 1997] that seek an optimized design solution. While such design tools produce a design predicted to have the specified handling-qualities assessment, it still remains for a human pilot to make the final assessment and acceptability determination.

Useable cue environment

The Useable Cue Environment (UCE) is an empirical method used to identify the loss of visual cues when using vision aids in a Degraded Visual Environment (DVE), and to determine the level of stabilization augmentation (response type) necessary to offset the loss of visual cues. Based on the hypothesis that stability and control issues associated with a loss of visual cues could be offset with increased vehicle stabilization, the method was developed and refined through a series of flight-test [Hoh, 1984 and 1986; and Hoh et al., 1987] and simulator [Ferguson et al., 1984] experiments. The rationale and supporting data are well summarized in Hoh et al.[1989].

The ADS-33E-PRF Specification [Anonymous, 2000] calls for assessment of the UCE for several hover and low-speed tasks, specifically hover, landing, pirouette, acceleration and deceleration (or depart/abort), sidestep (or lateral reposition), and vertical maneuver. It is a requirement that the test aircraft exhibit level-1 handling qualities (nominally rate response-type) for these tasks when performed in a Good Visual Environment (GVE). UCE is a function of the visual aid, not a function of the helicopter; assessment of UCE can be done in any helicopter possessing level-1 Rate Response-Type handling qualities. In the degraded visual environment with vision aids, UCE is determined by first rating the Visual Cue Rating (VCR) for both translation and attitude (see fig. 6.19a). Following each task, the pilot is asked to rate all attitude and translational cues; the numerically worst (highest) cues for attitude and translational cueing are then entered into the UCE template (see fig. 6.19b), and a UCE level is determined. ADS-33E-PRF [Anonymous, 2000] specifies response types that are necessary for each UCE, and are chosen such that the task can be performed, under DVE, to level-1 handling-quality ratings. In general, levels of stabilization required are as follows:

UCE = 1: rate response
UCE = 2: attitude-command-attitude-hold + height-hold (ACAH + HH)
UCE = 3: translational-rate-command + position hold + height hold (TRCPH + HH)

The UCE method was developed to specifically address the loss of visual cues required for hover, and its use for this purpose was extensively validated before inclusion in the ADS-33E specification. The method was not developed to assess overall FOV requirements, ability to see and avoid large objects, or determine the suitability of simulator visual systems. Also, the UCE method is not a measure of perceived quality of the visual environment; it is determined from pilot-in-the-loop assessment following the execution of the tasks.

Pilot workload, awareness, error, and trust

Design features can influence a variety of human factors that determine the success of any human-automation control system. Among the most important of these are:

- Workload: an umbrella term used to describe the demands placed on the pilot while performing pilot duties. These demands can take the form of mental or physical work, time pressure, frustrations, feeling involvement or engagement, and others.
- Awareness: the pilot's cognizance of relevant aspects of the task and environment such as aircraft position, altitude, operating modes of the automation, and the future intentions of both pilot and automation.

- Error: deviations from the planned or nominal course of events that can range from simple slips and omissions to larger errors in planning or understanding.
- Trust: the pilots' confidence in the human-automation system for accomplishing the mission.

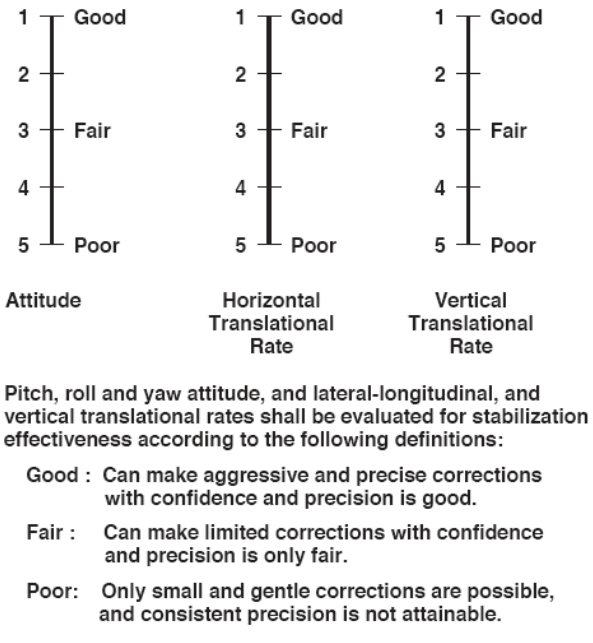

a) VCR scale (from ADS-33E-PRF)

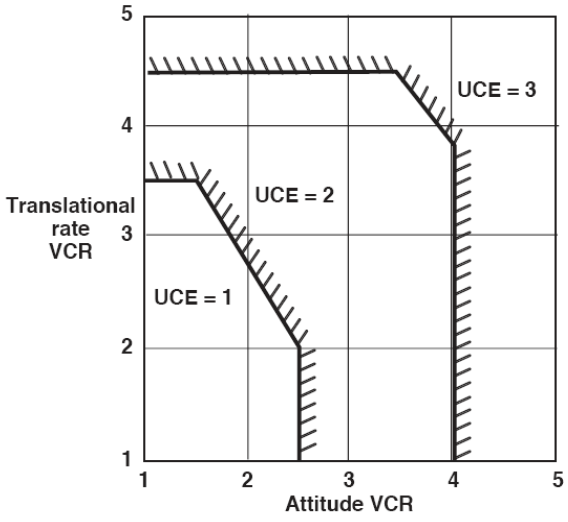

b) UCE template (from ADS-33E-PRF)

Figure 6.19. Usable Cue Environment (UCE) method.

It is important to recognize that these four factors are tied together, and that a change in one typically results in a change to one or more of the others. For example, high levels of pilot workload can lead to an increase in the number of errors, and thereby a decrease in pilots' trust in—and usage of—the automation. Low levels of pilot workload can often lead to decreased awareness and an increase in error [Casner, 2005 and 2006; and Endsley, 1995].

As a pilot-automation system is being designed, it is possible to maintain a good awareness of how specific design features are affecting these variables. The following describes practical techniques for measuring these four human-factors variables.

Workload

Techniques for measuring pilot workload can be grouped into two basic categories. Physiological workload measures monitor one or more physiological states of the human operator to arrive at an estimate of workload. For example, heart rate has been demonstrated to be a good indicator of physical workload [Wierwille, 1979], while heart-rate variability is known to be a reasonable indicator of mental workload [Aasman et al., 1987]. There are numerous problems with using physiological measures in a practical design setting. First, they can be cumbersome and costly to use. Second, some aspects of workload have no clear physiological means to measure (e.g., frustration).

Subjective workload measures allow pilots to provide estimates of their workload as they themselves perceive it. Numerous techniques are available. The instantaneous self-assessment (ISA) technique [Tattersall and Foord, 1996] allows pilots to provide numerical ratings of their perceived workload along a 20-point scale. While clearly the simplest technique to use, ISA can lead to wide variability among perceived workload between pilots performing the same task. This variability happens when different pilots think about workload in different ways. For example, one pilot may consider workload to mean "physical workload". This pilot might give low workload ratings for any task that does not involve physical labor. Meanwhile, a different pilot might believe that "time pressure" is the essence of workload and assign a high workload rating to any time-crunched situation. To get around these problems of different interpretations of the notion of workload, the NASA Task Load Index (NASA-TLX) technique was developed [Hart and Staveland, 1988]. The NASA-TLX technique asks pilots to provide six different workload measures, each one designed to assess a different aspect of workload that the pilot might have in mind when the notion of workload is mentioned. NASA-TLX measures include mental and physical workload, feelings of time pressure and frustration, an overall estimation of effort being put forth, and a self-assessment of the pilots' own performance of the task.

Awareness

Several techniques exist for the measurement of pilot awareness. Before attempting to measure pilot awareness, it is important to detail the information of which the pilot must remain aware. This information might naturally include geographical position and altitude [Casner, 2005 and 2006], proximity to terrain and other hazards, current operating modes of the automation [Casner, 2004; and Sarter and Woods, 1995], and the future intentions of both the pilot and the automation.

Testing done in flight simulators often uses a stop-and-freeze technique [Endsley, 1987 and 1995]. Using this method, the simulator is frozen at random points while the pilot can be questioned about present position, the surrounding environment, the state or modes of the automation, future intentions, etc.

A more realistic technique is a performance measurement technique that asks pilots to continue to perform a task when one or more functions of the automation become inoperative [Casner, 2005]. Success at this task implies that the pilot has remained aware of all of the relevant details of a task that had been delegated to the automation.

A subjective self-assessment technique for measuring awareness asks pilots to rate their own awareness as they perform a task [Taylor, 1989].

Error

Error is the simplest of all factors to measure. The designer must simply identify which performance parameters are most important and record any pilot deviations from what is considered a normal performance. These deviations might include navigation and control accuracy, poor decisions, or procedural missteps. Several useful taxonomies of human error can be used to help designers understand the types of errors that are useful to measure and track [Norman, 1981; and Reason, 1990]. Interestingly, error rate has also been proposed as a means of measuring pilot workload [Hart and Bortolussi, 1984].

Trust

One technique for measuring pilot trust in automation is to use a simple survey that asks pilots to rate their trust or confidence using particular features of the automation. Asking pilots to supply these ratings before and after they use the system is informative since pilot trust will change as the pilot gains experience using a system. Comparing pilot trust and confidence with the actual performance of the pilot-automation system also provides useful information. Discrepancies between pilot trust and the actual performance of the pilot-automation system are often found.

Tuning workload, awareness, error, and trust for best performance. It is every designer's intention to create a human-machine system that keeps human operators at a level of workload that maintains their interests and skills, ensures awareness of all things relevant to the mission, results in zero errors, and perfectly matches the reliability of the system. However, it is unclear that such a system could ever be designed. Difficult situations require pilots to work hard—sometimes unusually hard—while routine situations inevitably lead to periods of inactivity and occasional boredom.

Human attention and memory are naturally limited, and it is never possible to remain aware of everything that is or could be mission-relevant. Errors are a natural part of human performance at any level of skill and experience, while complicated technology systems continue to harbor surprises among the thousands of pages of computer code that define their behavior. For these reasons, perhaps the best design approach is design for overall performance. The techniques mentioned previously can be used to continually track pilot workload, awareness, error, and trust as a design progresses, and to help understand changes in performance that are observed. When problems with workload, awareness, error, and trust are identified, the designer is then left with the problem of

attempting to make changes to these factors, through changes in the system design. Relationships between design and operating procedures and these four human factors are known.

Workload can be increased and decreased by selectively making available different features of an automated system. When workload is too high, tasks can be automated. When workload is too low, automation features can be withheld and the pilot can be required to manually perform these tasks. Workload and awareness are often tightly intertwined. In the case that the pilot is using many automated features at once, and a misunderstanding or unexpected event arises between pilot and automation, workload levels can instantly spike as the pilot is thrown into a state of confusion.

Awareness is perhaps the most difficult factor to manage with design. The simple strategy of displaying information to pilots, and asking them to passively monitor the information, does not seem to guarantee awareness [Mumaw et al., 2000]. Rather, awareness of any task springs from having a direct involvement with that task [Casner, 2005 and 2006]. Again, note how attempting to raise awareness by keeping the pilot directly engaged will also likely result in increased pilot workload.

Errors can result from any number of design features, including inappropriate levels of workload and awareness. Once other factors have been tuned to satisfactory levels, it is wise to design a process that anticipates pilot error and provides a means by which errors can be detected and corrected [Reason, 1990; and Wiener, 1993].

Trust is a measure that is ideally aligned with the actual reliability of the human-automation system. A first design step that can help align pilot trust and system reliability is to provide good feedback to the pilot [Norman, 1990]. This feedback can be provided in the form of information displays to be used during flight, or through training in which pilots are made aware of the reliability and vulnerability of the pilot-automation system.

Aircraft-pilot coupling

Aircraft-pilot coupling can encompass a range of pilot/vehicle interactions from pilot-induced oscillations to biodynamic interference. A pilot-induced oscillation (PIO) can be described as an "unwanted, inadvertent, and atypical closed-loop coupling between a pilot and two or more of the independent response variables of an aircraft" [Smith, 1977]. The PIO phenomenon has received considerable attention in the literature over the past 45 years, e.g., Anonymous [1997 and 2000]; Ashkenas et al. [1964]; Hess [1984 and 1997a]; McRuer [1994]; and Smith and Berry [1975]. PIOs are generally organized into three categories: 1) Linear Pilot-Vehicle Oscillations, 2) Quasi-Linear Pilot-Vehicle System Oscillations with Rate Position Limiting, and 3) Non-Linear Pilot-Vehicle Oscillations with Transitions. Aircraft characteristics in Category 1 oscillations are essentially linear and pilot behavior is typically quasi-linear or quasi-stationary. The two aircraft-associated factors that contribute most to Category 1 are excessive phase (or time) lag and inappropriate effective aircraft gain, either too high (too sensitive) or too low (too sluggish). Category 2 events are typically produced position-limiting (i.e., control surface stops) or rate-limiting (i.e., actuator) elements in the control system. Category 3 PIOs typically occur because of a change in the pilot's behavior dynamics or nonlinear transitions within the control system, such as can occur with a mode change in a flight control system.

Most of the PIO research reported has focused on fixed-wing vehicles. Concern with rotorcraft PIO tendencies, however, has not been ignored, e.g., Hamel [1966] and Ockier [1996]. In Anonymous [2000], the following characteristics that make rotorcraft prone to PIO are cited:

- limited stability
- significant delays in control effectors because of the time required for rotor response (typically 70 msec) and power actuation (20 to 30 msec)
- coupling of rigid-body modes with rotor and transmission modes
- significant inherent cross-coupling of control that is highly nonlinear
- potential coupling with external slung loads

Additionally, the application of rotorcraft fly-by-wire systems is noted for its potential to significantly increase PIOs.

Biodynamic interference has been known for some time to adversely affect rotorcraft performance. This effect occurs when accelerations and/or vibrations of the vehicle cause generation of nonvoluntary manual-control commands. One of the more serious examples occurred with Navy CH-53E rotorcraft operating with slung loads, as described briefly in McRuer [1994]. Here pilot biodynamic coupling with lower-frequency rotor degrees of freedom occurred, and the load accentuated the problem. Another documented incident occurred with the U.S. Army's Advanced Digital Optical Control System (ADOCS) rotorcraft, as reported in Glusman et al. [1986]. This incident was also briefly discussed in Gibson and Hess [1997].

Mode control

By their nature, rotorcraft operate over a range of airspeeds, from hover to 100+ knots. In absolute terms, this range is small when compared to that of high-performance, fixed-wing vehicles. Tiltrotor aircraft such as the BA 609 will exhibit greater airspeeds in "airplane" mode. The rotorcraft-response characteristics, however, vary significantly over this speed range, with unaugmented vehicles exhibiting oscillatory instabilities at hover and modal characteristics resembling those of fixed-wing aircraft at higher speeds [Norris, 2008]. Rotorcraft Stability and Command Augmentation System (SCAS) designs often demand tailoring response characteristics with airspeed. The manner in which mode transitions are integrated into the flight control laws can significantly affect flight safety and perceived handling qualities. Little research has been conducted on optimizing the dynamics of mode transition on pilot behavior, particularly in terms of the rapidity in these changes. In rotorcraft operations, mode transition also includes the dynamic effect of variable rotor speeds, as currently being demonstrated on the Boeing's A160T Hummingbird unmanned vehicle [Norris, 2008].

ADS-33E-PRF [Anonymous, 2000] specifies multiple modes and response types. In most helicopters, where multiple response modes are available, they are selectable by the pilot. The recent advent of fly-by-wire control architectures have allowed for the development of new concepts for mode control. Recently, the U.S. Army Aeroflightdynamics Directorate tested the UH-60M Upgrade Control Laws (MUCLAWS) using the RASCAL JUH-60A In-Flight Simulator [Fletcher et al.,

2008]. It featured an “automoding” system, which was designed to automatically select basic flight control modes and appropriate response type on the basis of a blended airspeed/groundspeed; control laws as a function of airspeed are shown in the “keyhole” diagram in figure 6.20.

In-flight assessment of the handling qualities with both the MUCLAWS and EH-60L baseline control laws was performed in both GVE and DVE conditions. The MUCLAWS yielded significant improvements in handling qualities over the baseline. In GVE conditions, average handling quality with MUCLAWS was 2.76, compared with 4.25 in the baseline condition. Handling qualities were assessed for precision hover, right-hovering turn, left-hovering turn, right lateral reposition, left lateral reposition, depart/abort, and vertical maneuver. Even more noticeable improvement was attained in DVE; the MUCLAWS handling-quality average was 3.23, compared with 5.21 in the baseline condition.

While excellent handling qualities and platform stability were attained with the MUCLAWS, certain aspects of the automoding instantiation led to some objectionable qualities for certain task elements. As an example, during constant turns above 50-knot airspeed, the roll-attitude characteristics are attitude command and attitude hold. While centering the cyclic ensures a level-flight attitude, it is at the price of maintaining constant control forces during a constant bank. In the future, it is envisioned that “task-tailoring” modes can be developed in addition to the “automode,” which can be used to adapt the control system for specific aircraft configurations and tasks.

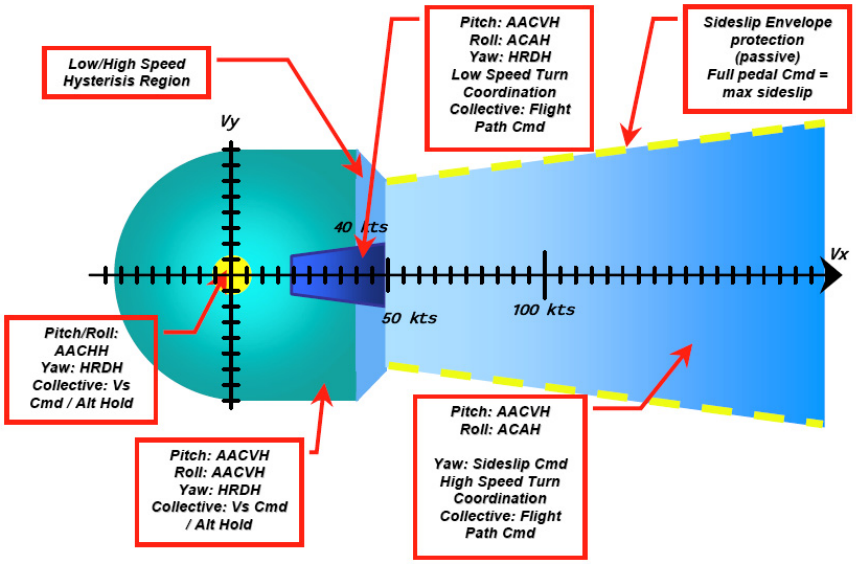

Figure 6.20. MUCLAWS control-mode selection diagram.

Failure recovery

The ability of the human pilot to recover and maintain control of a rotorcraft following system failures such as a SCAS failure is of obvious importance to safe operation. The system failures may also be accompanied by automatic reconfiguration of the flight control system to accommodate these failures, a goal currently being pursued for fixed-wing aircraft, e.g., Steinberg [2005].

Interest in modeling the adaptive characteristics of the human operator/pilot began over five decades ago, e.g., Curry and Govindaraj [1977]; Delp and Crossman [1972]; Elkind and Miller [1966]; Gilstead and Fu [1970]; Gould and Fu [1966]; Hess [1965]; Krendal and McRuer [1960]; Li [1966]; Niemela and Krendal [1974]; Phatak and Bekey [1968 and 1969]; Preyss and Meiry [1968]; Smith [1963]; Weir and Johnston [1968]; Weir and Phatak [1966]; and Young [1969]. Recent research in adaptive and reconfigurable flight control systems, however, has rekindled interest in the adaptive pilot, as questions naturally arise as to the ability of the human pilot to adapt to changing vehicle dynamics during and after the reconfiguration process. Again, when specific vehicle types were considered in these studies, e.g., Weir and Johnston [1968], they were fixed-wing vehicles. Some recent research in developing a model that could model pilot adaptation to sudden and significant change in vehicle dynamics was reported in Hess [2008]. The encouraging aspect of this modeling effort was that the pilot model used has also been employed in modeling the multiaxis control behavior of a rotorcraft pilot as described in Hess [2006]. Thus, there is some optimism that the model could be used for analyzing and predicting pilot behavior in multiaxis rotorcraft failure-recovery scenarios.

Pilot modeling

Manual control is the study of human behavior when controlling a system that requires continuous control inputs, such as piloting a helicopter. It has enabled the development of mathematical models describing the human operator's actions as part of a closed-loop control system. These models have been used extensively to describe, understand, and predict pilot behavior in many classes of vehicles, including rotorcraft. While a full review of this body of manual-control and human-operator modeling is outside the scope of this report, the work that is highly relevant to SIRCA application is identified in this section.

Models can be categorized in many ways. They can be characterized by the type of information the human operator is using as input to base control movements on. Another characterization is related to how many specific control "loops" the operator is "closing", which is a function of the number and types of control effectors, the dynamics of the vehicle being controlled, information sources, and the task. Yet another important defining characteristic is related to the control paradigm, specific assumptions regarding the underlying structure and philosophy of the model. The simplest manual-control model is demonstrated in figure 6.21. The human operator is represented by the block Y_p; the system being controlled is the block Y_c. The operator here has one control effector (δ), the controlled element Y_c has one state that defines it (m), and it is responding to the error (e) between the commanded state (i) and actual state (m).

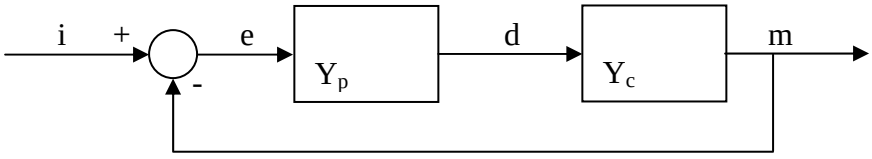

Figure 6.21. Diagram of single-input, single-output compensatory control paradigm.

Four basic categories of mathematical pilot models are addressed in this section: Isomorphic, Algorithmic, Behavior-Based, and Qualitative.

Isomorphic models refer to those models of pilot behavior in which some effort has been directed toward explicitly modeling the dynamics of the human-sensory and control-effector systems. Two prominent examples are the so-called crossover and the structural models of the human pilot [Hess, 2003]. Other examples of isomorphic models are biophysical models [van Paasen, 1994] and biodynamic models [Jex, 1971].

Algorithmic models refer to those representations of pilot control behavior that are created through the use of control-system synthesis techniques that have been successfully applied to the design of inanimate controllers. Some isomorphism may be retained in this modeling. A prominent example of an algorithmic model is the optimal control model of the human pilot [Hess, 2003; and Kleinman et al., 1970].

Behavior-based models rely upon novel and often detailed representations of human signal-processing behavior. Two prominent examples are fuzzy-logic models, e.g., Hess [1997a] and Zeyada and Hess [2003], and neural-net models, e.g., such as discussed in Jagacinski and Flach [2003].

In contrast to the preceding three pilot-model formulations, qualitative models of human pilot behavior have been proposed, e.g., Hess [1987]. While not capable of producing the fine-grained nature of human pilot-control activity, the models provide a useful framework within which to place and evaluate the more detailed models discussed previously.

Model Complexity

While most pilot models were originally developed with a single input and single output (termed SISO tasks), the job of piloting a helicopter is a significantly multiinput, multioutput (MIMO) task. The pilot has available multiple sources of helicopter state information; in addition to flight-display information, information can be obtained from perception of the external visual scene, and from direct perception of motion and orientation. The pilot typically has 4 to 5 control-effector degrees of freedom, typically the longitudinal cyclic, the lateral cyclic, collective, pedals, and, in some helicopters, continuous control of throttle.

The three major pilot modeling techniques, the crossover model, optimal-control model, and structural pilot model, have all been adapted to describe MIMO conditions. In order to apply the crossover model or structural model, some assumptions need to be made regarding the architecture to

limit the number of transfer functions associated with the loop closures. A common assumption that has been adopted and demonstrated extensively is that of sequential loop closures; control of helicopter states that exhibit different bandwidths are considered sequentially (starting with the highest bandwidth state) rather than consecutively. For example, helicopter position is ultimately controlled through the cyclic, but helicopter attitude is the highest bandwidth state, then velocity, then position. Application of either the crossover or structural model to this task would incorporate first a pilot-control element for pitch attitude, then velocity, then position.

The optimal-control model is well-suited to MIMO tasks and can be applied without additional structural assumptions. However, although algorithmically it is possible to close all of the loops consecutively, model complexity increases with each state and control effector. Methods have been considered to constrain model complexity while retaining the underlying optimal pilot-model paradigm ([Davidson and Schmidt, 1994]; [Garg and Schmidt, 1989]; Innocenti and Schmidt, 1984]; and [Ryu and Andrisani, 2000]).

A series of early tutorial examples of applying the crossover, structural, and optimal-control models to a simplified rotorcraft hovering task (both SISO and MIMO) can be found in Hess [1997a].

Model Information Source(s)

As noted earlier, the simplest modeling paradigm, single-input, single-output compensatory control, is shown in figure 6.21. Compensatory control refers to control loops in which the input to the operator is the error between the commanded or reference state. Pursuit refers to tasks in which the operator has both the reference state and actual state available; preview control consists of presentation of not only the current reference state and actual state, but also information regarding the future of the reference state (hence the name preview). Properly presented, preview and pursuit information can improve task performance while lessening workload because the pilot can make more anticipatory control movements.

Although most models have been developed with the assumption that the state information is being provided explicitly through a display, realistic pilot modeling for SIRCA applications needs to incorporate other information sources, specifically visual perception of the external scene and motion perception.

Visual scene perception has been considered and incorporated into the model structure for the crossover [Johnson et al., 1988; Johnson and Phatak, 1989 and 1990; Johnson et al., 1987; and Sweet, 1999], optimal [Baron et al., 1980; Grunwald and Merhav, 1974 and 1976; and Wewerinke, 1978 and 1980], and structural [Hess, 1997b] pilot models. Just as early pilot models were based on simplified information sources, the work accomplished to date incorporating visual scene perception has been largely based upon relatively simple simulated visual scenes—current models of all forms are some ways from analytical representations of natural scene perception.

A thorough review, extension, and application of the optimal-control pilot model, first introduced in Kleinman et al. [1970], can be found in the Ph.D. dissertation of Wewerinke [1989]. This work addresses modeling human perception, information processing, decision making, and control, with the resulting model applied to the control of aircraft and ships.

Models to Predict and Understand

The various rating techniques (handling qualities, workload, usable cue environment, PIO susceptibility, failure recovery) described previously are typically used empirically. During simulation or flight test, values of these ratings scales are determined as a function of control-system configuration or other independent variable. Given the expense and time involved with both flight testing and simulation, methods to predict these characteristics—or to better understand underlying causalities—are highly valuable, particularly with the SIRCA technologies. The significant variability of the underlying helicopter dynamics caused by the proposed technologies will be difficult to predict based only on current experience.

Delft University in the Netherlands has examined the utility of pilot models as applied to rotorcraft research. One such study is noteworthy as the pilot model results were compared directly with flight-test results [van der Vorst, 1998]. The rotorcraft in question was the Eurocopter BO-105. Two ADS-33 maneuvers were selected, acceleration/deceleration and sidestep [Heffley et al., 1981]. Of particular interest was the ability of the pilot model to capture off-axis pilot/vehicle control/response behavior (not shown). More recent applications of this modeling approach, with emphasis on predicting fixed-wing pilot/vehicle performance and handling qualities, can be found in Weber et al. [2005], a report produced by the Moscow Aviation Institute.

Research summarized in Zeyada and Hess [2003] demonstrated how the structural pilot model could be employed to produce estimates of flight-simulator fidelity for a six-degree-of-freedom model of a rotorcraft performing a vertical remask maneuver [Anonymous, 2000]. The pilot model used the three major cues employed in human vehicular control, i.e., proprioceptive, visual, and vestibular. The modeling approach also allows prediction of task-dependent handling qualities of the nominal flight article (without simulator limitations) in the maneuver being simulated.

One of the primary uses of pilot models stems from their ability to understand the nature and sensory demands of particular vehicles performing well-defined tasks. An early example of this ability can be found in Heffley et al. [1981]. Sponsored by the U.S. Army, the research reported focused upon rotorcraft flight-simulator training requirements and effectively summarized the state of the art in application of frequency-domain models of the human pilot. The pilot modeling work extends the pilot modeling approach described in McRuer and Krendel [1974], based upon the precision crossover model of the human pilot.

Work in prediction of handling qualities through application of pilot models has been extensive. The optimal-control model was used over 30 years ago to the assessment of rotorcraft handling qualities [Hess, 1977]. The precision pilot model (a more detailed version of the crossover model) was used to study rotorcraft handling qualities as described in Cameron et al. [2003], and the structural model was used to predict both handling qualities and pilot-control activity in comparison to a pilot-in-the-loop simulation on the NASA Ames Vertical Motion Simulator [Hess et al., 2002]. Work remains to be done to provide good absolute correlation between predicted and measured handling qualities, although these models have proven valuable in making relative predictions, i.e. predicting trends in handling-qualities ratings as a function of design or other independent variable.

NASA is currently working with the University of California, Davis, to develop pilot models for rotorcraft that account for time-varying dynamics and biodynamic interference. Time-varying dynamics that are being considered include dynamic changes resulting from control-mode transitions and variable rotor speeds, although the resulting models will have the potential to also address failure-recovery scenarios and determination of useable cue environments. Hess [2008] and Hess and Marchesi [2008] describe the current status of this modeling effort.

Guidance and Navigation Displays

As shown in the notional SIRCA architecture in figure 6.8, guidance and system displays will synthesize multiple inputs to the pilot. These inputs may include aircraft-state sensors, IVHM data, feedback from real-time models, and mission-management information. Guidance and navigation cues must be concisely displayed to enable the pilot to fly safely, accurately, and with repeatability. NASA FDC research has made significant progress toward this goal by developing a Portable Programmable Guidance Display (PPGD) that has been successfully demonstrated during helicopter noise testing [Decker et al., 2007]. The programmable guidance system uses a pursuit guidance philosophy developed for panel-mounted displays from a head-up display design to provide pilot guidance for researcher-specified flightpaths and flight conditions The underlying system has been applied to a wide range of aircraft, including conventional airplane transports, vertical/short takeoff and landing (V/STOL) attack aircraft, and civil tiltrotor operations and control requirements studies [Decker, 2001; and Hardy, 2002]. From the tiltrotor application, the guidance system was adapted for use on the NASA-U.S. Army JUH-60A Rotorcraft Aircrew Systems Concepts Airborne Laboratory (RASCAL) research aircraft in support of civil terminal airspace studies [Moralez et al., 2004]. The current-generation guidance system was designed as an interim step toward portability for use in less-augmented and -instrumented aircraft. Figures 6.22a and 6.22b show the PPGD display format and key elements.

As reported in Decker et al. [2007], the PPGD was used during an acoustic flight test of a Bell 206 helicopter. Flightpath-position (height and lateral error) and velocity-tracking results were collected and analyzed for steady-condition testing, decelerations, and accelerations on glide slope. Figures 6.23 through 6.25 show composite test results for 53 steady-speed descent data runs.

Figure 6.23 shows a standard deviation of 8.4 feet for the height tracking error, which is exceptional repeatability for flight testing. The lateral-position error, shown in figure 6.24, has a standard deviation of 18.5 feet, primarily because of reduced lateral-guidance sensitivity compared to the vertical-guidance sensitivity. The airspeed tracking, shown in figure 6.25, resulted in a standard deviation of 0.6 knots. Overall, the trajectories and speed profiles flown with the aid of the PPGD are considered much more repeatable than previous acoustic flight tests. The PPGD is a new tool for flight testing that requires precise position and speed guidance.

a) Display format

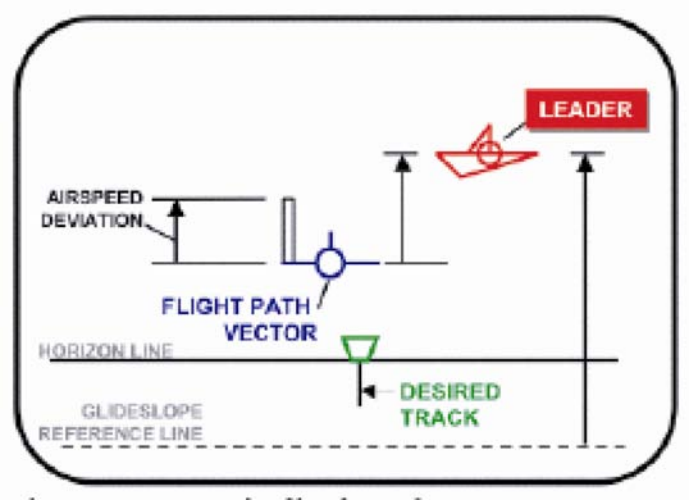

b) Primary display elements

Figure 6.22. Programmable Pursuit Guidance Display [Decker, 2007].

Planned enhancements to the PPGD include incorporation of nonintrusive collective and cyclic stick positions measurements, a portable air data boom, and rotor tip-path-plane measurement system. These enhancements are described in Chapter 5. The goal is to maintain the portability of the entire instrumentation package so that the system can be installed with minimal effort on most rotorcraft.

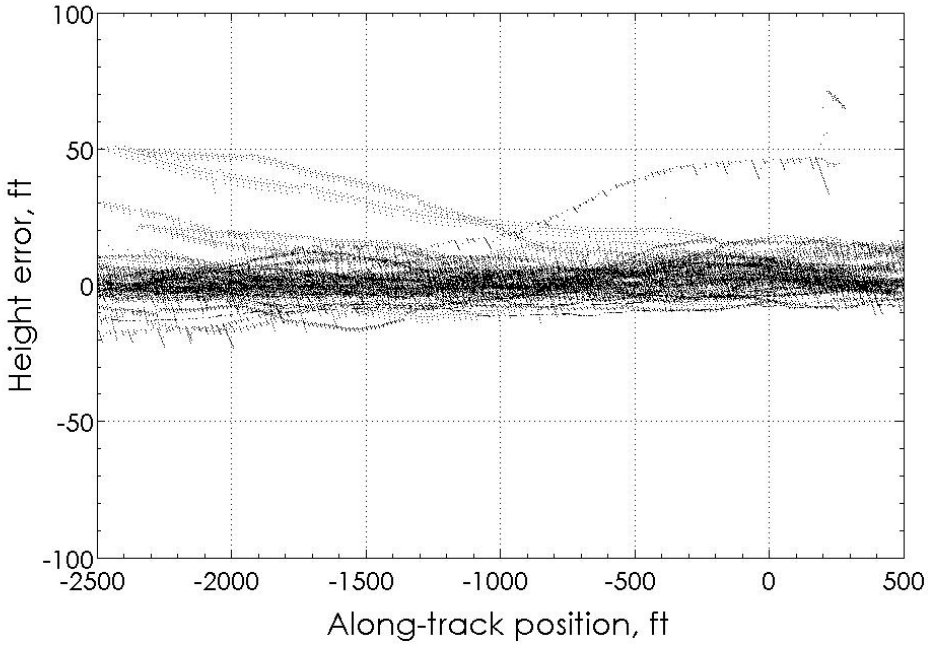

Figure 6.23. Height tracking error [Decker et al., 2007].

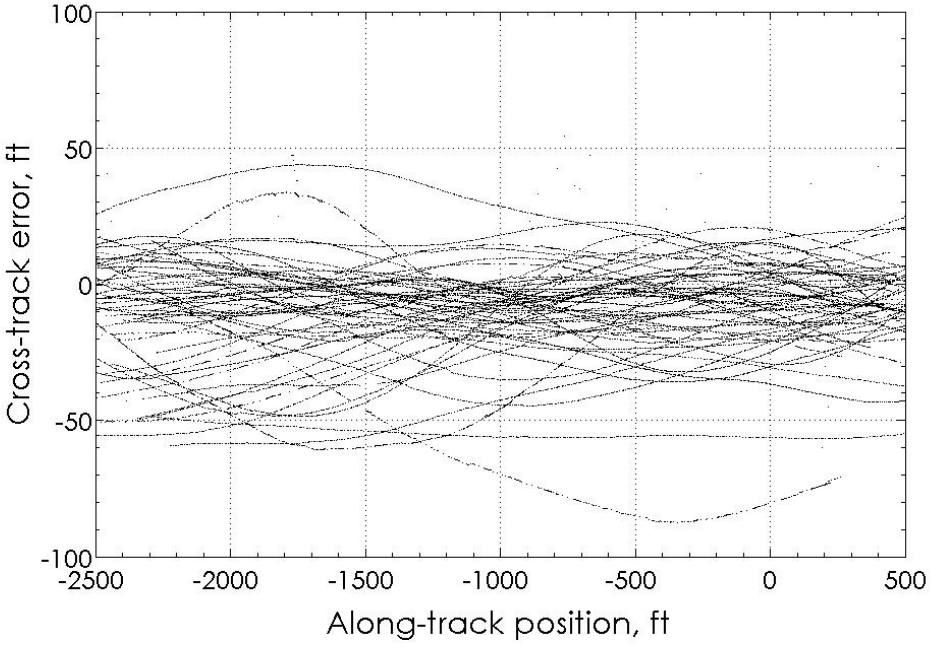

Figure 6.24. Lateral tracking position error [Decker et al., 2007].

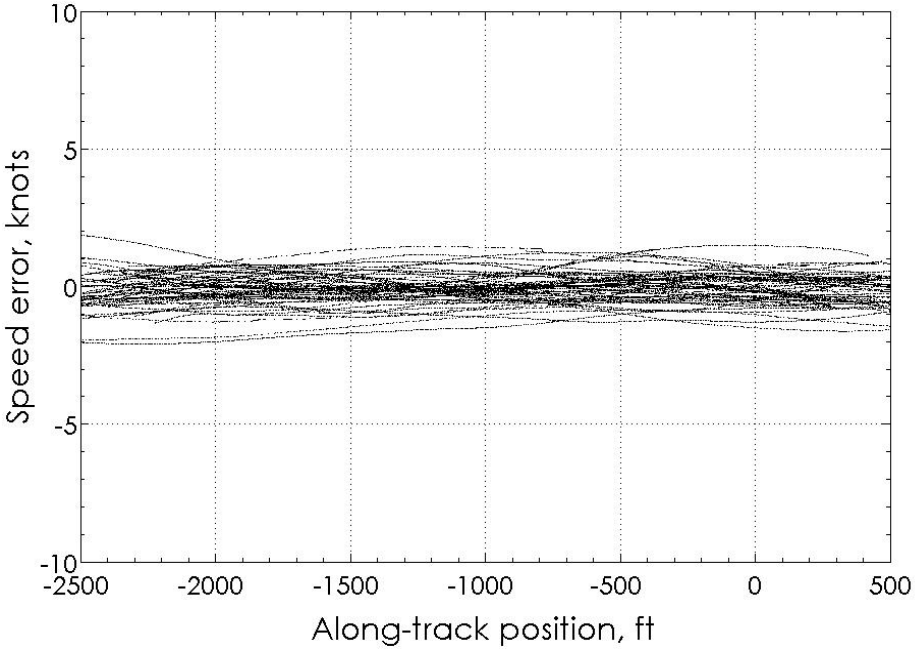

Figure 6.25. Airspeed tracking [Decker et al., 2007].

SUMMARY

The NASA flight dynamics and control discipline over many decades—principally through partnership with the U.S. Army, Industry, and Academia—has developed and gained access to an extensive array of rotorcraft design and analysis tools, as well as world-class flight test and simulation capabilities. However, many new challenges are presenting themselves for the rotorcraft FDC discipline. New heavy lift rotorcraft concepts are being proposed for development. New active rotor and flow control systems and devices are being developed and tested in the laboratory, in large-scale wind tunnels, and in flight. New variable-geometry and variable-speed vehicle configurations are being studied for their performance potential. New strategies for flight-trajectory planning are being developed to provide for low-noise flight profiles and simultaneous non-interfering flight in the airspace. New human-system integration architectures, seeking to define an optimum balance between man and machine for aircraft control, are also being explored. All of these emerging vehicle design and operational trends will demand the FDC discipline, and its associated tools, techniques, and technologies, evolve to meet these challenges.

A key theme of this overall NASA rotorcraft research state of the art assessment has been the identification of metrics to judge future technical progress. The FDC discipline is no different: definition and tracking of metrics will be essential to assess progress within the discipline. For the FDC handling qualities efforts, beyond the conventionally accepted HQR metrics such as the Cooper-Harper ratings, new HQR metrics—and their associated acceptable threshold limits—will likely need to be defined and evaluated for an emerging class of large/advanced rotorcraft. For control law design and analysis development efforts, key metrics need to be defined to assess: 1) net reductions in time associated with new design and analysis tools and, correspondingly, 2) the predictive accuracy of these tools. Finally, new safety, efficiency (including appropriateness), and performance metrics need to be defined for highly automated rotorcraft systems, as represented in part by the SIRCA concept. In particular, the potentially highly coupled nature of variable-speed rotor operations for rotorcraft will require performance metrics that can balance the array of aeromechanics issues that will inevitably be manifested with such systems.

Several challenging near-term FDC research activities are currently planned. For FDC handling qualities research, a series of VMS simulations are being conducted for existent and notional large transport rotorcraft to assess the unique HQR aspects of these vehicles. In particular, the work will provide new insights into flight control design and pilot handling quality issues for the new generation of large-passenger (90-120 PAX) civil tiltrotor aircraft being studied by NASA. This work will help inform other NASA rotorcraft research disciplines – particularly the Multi-Disciplinary Analysis and Technology Development (MDATD) discipline's efforts (refer to Chapter 9) to refine NASA CTR reference designs. Near term plans for the human-system integration effort focus on refined HQR metrics applicable to large/advanced rotorcraft configurations. Finally, the SIRCA conceptual architecture is currently being jointly developed by a team of both rotorcraft and automation experts. Recent work has focused on the design and evaluation of a proof-of-concept trim-controller computer system to maintain satisfactory rotor trim while simultaneously effecting active rotor control via individual blade control (IBC) and onboard blade control (OBC) devices. This proof-of-concept

trim-controller is being evaluated as a part of large-scale rotor wind tunnel tests being conducted by the NASA Aeromechanics discipline (Chapter 2). Another noteworthy effort with respect to the realization of the SIRCA concept is the incorporation of a variable-speed propulsion system model (Chapter 9) into a FDC vehicle simulation model.

In many regards, the final proof-of-concept for new technologies continues to require flight test and evaluation. “Concept to flight” remains a key feature of NASA rotorcraft research.

REFERENCES

Aasman, J.; Mulder, G.; and Mulder, L. J. M.: Operator Effort and the Measurement of Heart-rate Variability. Human Factors, vol. 29, no. 2, 1987, pp. 161–170.

Aiken, E. W.; Hindson, W. S.; Lebacqz, J. V.; Denery, D. G.; and Eshow, M. E.: Rotorcraft In-Flight Simulation Research at NASA Ames Research Center: A Review of the 1980's and Plans for the 1990's. NASA-TM 103873, Aug. 1991.

Andrisani, D., II, and Gau, C-F: A Nonlinear Pilot Model for Hover, AIAA J. Guidance and Control, vol. 8, no. 3, May–June, 1985.

Anonymous: Military Specification, Flight Control Systems—General Specifications for Design, Installation, and Test of Piloted Aircraft (MIL-F-9490D), 1975.

Anonymous: Aviation Safety and Pilot Control—Understanding and Preventing Unfavorable Pilot-Vehicle Interactions. National Academic Press, Washington, D. C., 1997.

Anonymous: Handling Qualities Requirements for Military Rotorcraft (Aeronautical Design Standard-33E-PRF), U.S. Army Aviation Systems Command, St. Louis, Mo., Mar. 2000.

Aponso, B. L.; Tran, D. T.; and Schroeder, J. A.: Rotorcraft Research at the NASA Vertical Motion Simulator. AHS 64th Annual Forum, Montreal, Canada, Apr. 29, 2008.

Ashkenas, I.; Jex, H.; and McRuer, D. T.: Pilot-Induced Oscillations: Their Cause and Analysis. Northrop-Norair Report NCR-64-143, June 20, 1964.

Ballin, M. G. and Dalang-Secretan, M. A.: Validation of the Dynamic Response of a Blade Element UH-60 Simulation Model in Hovering Flight. J. Amer. Hel. Soc., vol. 36, no. 4, Oct. 1991.

Baron, S.; Lancraft, R.; and Zacharias, G. L.: Pilot/Vehicle Model Analysis of Visual and Motion Cue Requirements in Flight Simulation. NASA CR-3312, Oct. 1980.

Bauchau, O.; Rodriquez, J.; and Chen, S.-Y.: Coupled Rotor-Fuselage Analysis with Finite Motions Using Component Model Synthesis. J. Amer. Hel. Soc., vol. 49, no. 2, Apr. 2004.

Bettner, J. L.; Hawkins, J. M.; and Blandford, C. S.: High Speed Rotorcraft Propulsion Concepts to Control Power/Speed Characteristics. AIAA Paper no. 1992-3367. 28th SAE, ASME, and ASEE, Joint Propulsion Conference and Exhibit, Nashville, Tenn., July 6–8, 1992.

Borchers, P. F.; Franklin, J. A.; and Fletcher, J. W.: Flight Research at Ames: Fifty-Seven Years of Development and Validation of Aeronautical Technology. NASA/SP-1998-3300, 1998.

Cameron, N.; Thomson, D. G.; and Murray-Smith, D. J.: Pilot Modeling and Inverse Simulation for Initial Handling Qualities Assessment. The Aeronautical J., vol. 107, no. 1074, 2003, pp. 511–520.

Casner, S. M.: Flying IFR with GPS: How Much Practice is Needed? International J. Applied Aviation Studies, vol. 4, no. 2, 2004.

Casner, S. M.: The Effect of GPS and Moving Map Displays on Navigational Awareness while Flying under VFR. International J. Applied Aviation Studies, vol. 5, no. 1, 2005.

Casner, S. M.: Mitigating the Loss of Navigational Awareness while Flying with GPS and Moving Map Displays under VFR. International J. Applied Aviation Studies, vol. 6, no. 1, 2006.

Cheng, R. P.; Tischler, M. B.; and Celi, R.: A High-Order, Linear Time-Invariant Model for Application to Higher Harmonic Control and Flight Control System Interaction. NASA/TP-2006-213460, AFDD/TR-04-005, Aug. 2006.

Cooper, G. E., and Harper, R. P., Jr.: The Use of Pilot Rating in the Evaluation of Aircraft Handling Qualities. NASA TN-D-5153, Apr. 1969.

Cribbs, R. C.; Friedmann, P. P.; and Chiu, T.: Coupled Helicopter Rotor/Flexible Fuselage Aeroelastic Model for Control of Structural Response. AIAA J., vol. 38, no. 10, Oct. 2000, pp. 1777–1788.

Curry, R. E., and Govindaraj, T.: The Human as a Detector of Changes in Variance and Bandwidth. Proc. 13th Annual Conference on Manual Control, Jan. 1977, pp. 217–221.

D'Angelo, M.: Wide Speed Range Turboshaft Study. NASA CR-198380, Aug. 1995.

Davidson, J. B. and Schmidt, D. K.: Extended Cooperative Control Synthesis. NASA TM-4561, 1994.

Decker, W. A.: Handling Qualities Evaluation of XV-15 Noise Abatement Landing Approaches Using a Flight Simulator. AHS 57th Internl. Annual Forum, Washington, D. C., May 9–11, 2001.

Decker, W. A.; Tucker, G. E.; Moralez III, E.; Hardy, G. H.; and Lewis, E. K.: Use of a Portable Programmable Guidance Display in Support of Helicopter Noise Testing. AHS 63rd Annual Forum, Virginia Beach, Va., May 2007.

Delp, P., and Crossman, E. R.: Transfer Characteristics of Human Adaptive Response to Time-Varying Dynamics. Proc. 8th Annual Conference on Manual Control, Ann Arbor, Mich., May 17–19, 1972, pp. 245–271.

Elkind, J. I., and Miller, D. C.: Process of Adaptation by the Human Controller. Proc. 2nd Annual NASA-University Conference on Manual Control, Cambridge, Mass., Feb. 28–Mar. 2, 1966, pp. 47–63; also NASA SP-128, Model Control, Jan. 1966.

Endsley, M. R.: SAGAT: A Methodology for the Measurement of Situation Awareness (NOR DOC 87-83), Northrop Corporation, Hawthorne, Calif., 1987.

Endsley, M. R.: Measurement of Situation Awareness in Dynamic Systems. Human Factors, vol. 37, no. 1, 1995, pp. 65–84.

Ferguson, S. W.; Clement, W. F.; Cleveland, W. B.; and Key, D. L.: Assessment of Simulation Fidelity Using Measurements of Piloting Technique in Flight. AHS Paper A-84-40-08-4000, AHS 40th Annual Forum, Arlington, Va., May 16–18, 1984.

Ferguson, S. W.: A Mathematical Model for Real Time Flight Simulation of a Generic Tilt-Rotor Aircraft. NASA CR-166536, June 1991. (Limited Distribution)

Fletcher, J. W.; Lusardi, J.; Mansur, M.; Morales, E.; Robinson, D. et al.: UH-60M Upgrade Fly-By-Wire Flight Control Risk Reduction Using the RASCAL JUH-60A In-Flight Simulator. Proc. AHS 64th Annual Forum, Montreal, Canada, Apr. 29–May 1, 2008.

Freed, M.; Bonasso, P.; Dalal, K. M.; Fitzgerald, W.; Frost, C. R.; and Harris, R.: An Architecture for Intelligent Management of Aerial Observation Missions. AIAA Paper no. 2005-6938, Proc. AIAA Infotech@Aerospace Technical Conference, Arlington, Va., Sept. 26–28, 2005.

Garg, S. and Schmidt, D. K.: Cooperative Synthesis of Control and Display Augmentation. J. Guidance, Control, and Dynamics, vol. 12, no. 1, 1989, pp. 54–61.

Garlington, K.: The MIL-STD-1553 Local Area Network. Aug. 2003. http://home.flash.net/~kennieg/cse5344/paper/. Accessed Nov. 24, 2008.

Gibson, J. C., and Hess, R. A.: Stick and Feel System Design. AGARDograph 33, Mar. 1997.

Gilstead, D. W., and Fu, K. S.: A Two Dimensional, Pattern Recognizing, Adaptive Model of a Human Controller. Proc. 6th Annual Conference on Manual Control, Wright Patterson AFB, Ohio, Apr. 7–9, 1970, pp. 553–569.

Glusman, S. I.; Landis, K. H.; and Dabundo, C.: Handling Qualities Evaluation of the ADOCS Primary Flight Control System. Proc. AHS 42nd Annual Forum, Washington, D. C., June 2–4, 1986, pp. 727–737.

Gomez, A., and Goethert, E. Control System Design using LabVIEW FPGA for a Digital Picture Kiosk. Proc. 2006 American Control Conference, Minneapolis, Minn., June 14–16, 2006, pp. 1406–1409.

Gould, E. E., and Fu, K. S.: Adaptive Model of the Human Operator in a Time-Varying Control Task. Proc. 2nd Annual NASA-University Conference on Manual Control, Cambridge, Mass., Feb. 28–Mar. 2, 1966, pp. 85–97; also NASA-SP-128, Model Control, Jan. 1966.

Grunwald, A. J., and Merhav, S. J.: An Analytical Model for Visual Field Control—A Parametric Study (TAE-217). Israel Institute of Technology, 1974.

Grunwald, A. J., and Merhav, S. J.: Vehicular Control by Visual Field Cues—Analytical Model and Experimental Validation. IEEE Transactions on Systems, Man and Cybernetics, vol. 6, no. 12, Dec. 1976, pp. 835–845.

Gu, D.-W.; Petkov, P. H.; and Konstantinov, M. M.: Robust Control Design with MATLAB. Springer, Aug. 2005.

Hamel, P. G.: Rotorcraft-Pilot Coupling: A Critical Issue for Highly Augmented Helicopters? AGARD-CP-592, Advances in Rotorcraft Technology, Ottawa, Canada, May 27–30, 1966.

Hanson, G. D., and Ferguson, S. W.: Generic Tilt-Rotor Simulation (GTRSIM) User's and Programmer's Guide. Vol. 1: User's Guide. NASA CR-166535, June 1991.

Harding, J. W.; Mansur, M. H.; Tischler, M. B.; Moody, S. J.; and MaCann, R. C.: Optimization and Piloted Simulation Results of the AH-64D Modern Control Laws. Proc. AHS 63rd Annual Forum, Virginia Beach, Va., vol. 2, 2007, pp. 883–896.

Harding, J. W., and Moody, S.: Identification of AH-64D Dynamics to Support Flight Control Systems Evaluations. Proc. AHS 61st Annual Forum, vol. 1, June 1–3, 2005.

Hardy, G. H.: Pursuit Display Review and Extension to a Civil Tilt Rotor Flight Director. AIAA Paper no. 2002–4925, AIAA Guidance, Navigation, and Control Conference and Exhibit, Monterey, Calif., Aug. 5–8, 2002.

Hart, S. G., and Bortolussi, M. R.: Pilot Errors as a Source of Workload. J. Human Factors and Ergonomics Soc., vol. 26, no. 5, Oct. 1984, pp. 545–556.

Hart, S. G., and Staveland, L. E.: Development of NASA-TLX (Task Load Index): Results of Empirical and Theoretical Research. In P. A. Hancock and N. Meshkati (Eds.), Human Mental Workload, North Holland Press, Amsterdam, 1988, pp. 239–250.

Hatcher, R.: PMA-299 Multi-Mission Helicopter Team awards MH-60 Common Cockpit multi-year contract. NAVAIR Release, Jan. 6, 2004. http://www.globalsecurity.org/military/library/news/2004/01/mil-040106-navair01.htm. Accessed Nov. 24, 2008.

Heffley, R. K.; Clement, W. F.; Ringland, R. F.; Jewell, W. F.; Jex, H. R.; Meruer, D.; and Carter, V. E.: Determination of Motion and Visual System Requirements for Flight Training Simulators. Technical Report 546, U.S. Army Research Institute for the Behavioral and Social Sciences, Fort Rucker, Ala., Aug. 1981.

Hess, R. A.: The Human Operator as an Element in a Control System with Time Varying Dynamics. AFFDL-FDCC-TM-65-34, U.S. Air Force Flight Dynamics Lab, June 1965.

Hess, R. A.: Prediction of Pilot Opinion Ratings Using an Optimal Pilot Model (of Aircraft Handling Qualities in Multiaxis Tasks). Human Factors, vol. 19, no. 5, Oct. 1977, pp. 459–476.

Hess, R. A.: Analysis of Aircraft Attitude Control Systems Prone to Pilot-Induced Oscillations. J. Guidance, Control, and Dynamics, vol. 7, no. 1, 1984, pp. 106–112.

Hess, R. A.: A Qualitative Model of Human Interaction with Complex Dynamic Systems. IEEE Transactions on Systems, Man, and Cybernetics, vol. SMC-17, no. 1, Jan. 1987, pp. 33–51.

Hess, R. A.: A Unified Theory for Aircraft Handling Qualities and Adverse Aircraft-Pilot Coupling. J. Guidance, Control, and Dynamics, vol. 20, no. 6, 1997a, pp. 1141–1148.

Hess, R. A.: Feedback Control Models—Manual Control and Tracking. In G. Salvendy (Ed.), Handbook of Human Factor and Ergonomics, John Wiley & Sons, Inc., New York, 1997b, pp. 1249–1294.

Hess, R. A.: Pilot Control. In P. S. Tsang and M. A. Vidulich (Eds.), Principles and Practice of Aviation Psychology, Lawrence Erlbaum, Mahwah, N.J., 2003.

Hess, R. A.: Simplified Approach for Modeling Pilot Pursuit Control Behaviour in Multi-Loop Flight Control Tasks. Proc. Institution of Mechanical Engineering, J. Aerospace Engineering, vol. 220, no. G2, Apr. 2006, pp. 85–102.

Hess, R. A.: Modeling the Adaptive Human Pilot Accommodating Sudden Changes in Vehicle Dynamics. Unpublished Paper. Dept. of Mechanical and Aeronautical Engineering, 2008.

Hess, R. A. and Marchesi, F.: Pilot Modeling with Applications to the Analytical Assessment of Flight Simulator Fidelity. AIAA Paper no. 2008-6682, AIAA Modeling and Simulation Technologies Conference, Honolulu, HI, Aug. 18–21, 2008.

Hess, R. A.; Zeyada, Y.; and Heffley, R. K.: Modeling and Simulation for Helicopter Task Analysis. J. Amer. Hel. Soc., vol. 47, no. 2, Oct. 2002, pp. 243–252.

Hoh, R. H.: Investigation of Outside Visual Cues Required for Low Speed and Hover (TR-1213-1): Systems Technology, Inc., 1984.

Hoh, R. H.: Handling Qualities Criterion for Very Low Visibility Rotorcraft. AGARD-CP-423, Rotorcraft Design for Operations, Proc. AGARD Flight Mechanics Meeting, Amsterdam, Netherlands, Oct. 13–16, 1986.

Hoh, R. H.; Baillie, S. W.; and Morgan, J. M.: Flight Investigation of the Tradeoff between Augmentation and Displays for NOE Flight in Low Visibility. AHS National Specialists' Meeting on Flight Controls and Avionics, Cherry Hill, N.J., Oct. 13–15, 1987.

Hoh, R. H.; Mitchell, D. G.; Aponso, B. L.; Key, D. L.; and Blanken, C. L.: Background Information and User's Guide for Handling Qualities Requirements for Military Rotorcraft. USAAVSCOM TR 89-A-008 and NASA/CR-187878, 1989. (Limited Distribution)

Howlett, J.: UH-60A Black Hawk Engineering Simulation Program: Volumes I and II. NASA/CR-166-309 and NASA/CR-166310, Dec. 1981. (Limited Distribution)

Howlett, J.: UH-60A Black Hawk Engineering Simulation Program: Volume I - Mathematical Model. NASA CR-177542, USAAVSCOM TR-A-001, 1989.

Innocenti, M, and Schmidt, D. K.: Quadratic Optimal Cooperative Control Synthesis with Flight Control Application. J. Guidance, Control, and Dynamics, vol. 7, no. 2, 1984, pp. 206–214.

Iwata, T., and Rock, S. M.: Benefits of Variable Rotor Speed in Integrated Helicopter/Engine Control. AIAA Paper no. 93-3851, AIAA Guidance, Navigation, and Control Conference, Monterey, Calif., 1993.

Iwata, T.: Integrated Flight/Propulsion Control with Variable Rotor Speed Command for Rotorcraft. Final report for NASA Ames Research Center Grant NCA2-594, and Ph.D. dissertation, Stanford University, Palo Alto, Calif., 1996.

Iwata, T., and Rock, S. M.: Learning-Based Implementation of Minimum-Time Control with an Application to Rotorcraft. AIAA Paper no. 96-3774, AIAA Guidance, Navigation and Control Conference, San Diego, Calif., July 29–31, 1996.

Jagacinski, R. J., and Flach, J. M.: Control Theory for Humans: Quantitative Approaches to Modeling Performance. Erlbaum, Mahwah, N.J., 2003.

Jex, H. R.: Problems in Modeling Man-Machine Control Behavior in Biodynamic Environments. NASA SP-281, Proc. 7th Annual Conference on Manual Control, USC, Los Angeles, Calif., June 2–4, 1971.

Johnson, W.: Technology Drivers in the Development of CAMRAD II. AHS Aeromechanics Specialists Meeting, San Francisco, Calif., Jan. 19–21, 1994.

Johnson, W.; Yeo, H.; and Acree, C. W.: Performance of Advanced Heavy-Lift, High-Speed Rotorcraft Configurations. 1st AHS/KSASS International Forum on Rotorcraft Multidisciplinary Technology, Seoul, Korea, Oct. 15–17, 2007.

Johnson, W. W.; Bennett, C. T.; O'Donnell, K.; and Phatak, A. V.: Optical Variables Useful in the Active Control of Altitude. 23rd Annual Conference on Manual Control, Cambridge, Mass., June, 1988.

Johnson, W. W., and Phatak, A. V.: Optical Variables and Control Strategy Used in a Visual Hover Task. Proc. 1989 IEEE Internl. Conference on Systems, Man and Cybernetics, Boston, Mass., Nov. 14–17, 1989.

Johnson, W. W., and Phatak, A. V.: Modeling the Pilot in Visually Controlled Flight. IEEE Control Systems Magazine, vol. 10, no. 5, 1990, pp. 24–26.

Johnson, W. W.; Bennett, C. T.; Tsang, P. S.; and Phatak, A. V.: The Visual Control of Simulated Altitude. Proc. 4th Symposium on Aviation Psychology, Columbus, Ohio, 1987, pp. 216–222.

Klein, V., and Morelli, E. A.: Aircraft Systems Identification: Theory and Practice, AIAA Publications, 2006.

Kleinman, D. L.; Baron, S.; and Levison, W. H.: An Optimal Control Model of Human Response, Parts I and II. Automatica, vol. 6, no. 3, May 1970, pp. 357–383.

Krendal, E. S., and McRuer, D. T.: A Servomechanisms Approach to Skill Development. J. Franklin Institute, vol. 269, Jan. 1960, pp. 24–42.

Landis, K. H.; Davis, J. M.; Dabundo, C.; and Keller, J. F.: Advanced Flight Control Research and Development at Boeing Helicopters. In Advances in Aircraft Flight Control, Mark B. Tishler (Editor), Taylor and Francis, London, England, 1996, pp. 103–142.

Li, Y. T.: Man in an Adaptive and Multiloop Control System. NASA SP-128 and Proc. 2nd Annual NASA-University Conference on Manual Control, Feb. 28–Mar. 2, 1966, pp. 99–105.

Litt, J. S.; Edwards, J. M.; and DeCastro, J. A.: A Sequential Shifting Algorithm for Variable Rotor Speed Control. NASA/TM-2007-214842, ARL-TR-4086, June 2007.

Lockheed Martin: Common Cockpit™ Avionics Suite. http://www.lockheedmartin.com/products/CommonCockpit/index.html. Accessed Nov. 24, 2008.

McRuer, D. T.: Pilot-Induced Oscillations and Human Dynamic Behavior. NASA CR-4683, July, 1995.

McRuer, D. T., and Krendel, E. S.: Mathematical Models of Human Pilot Behavior. AGARD-AG-188, Jan. 1974.

Meirovitch, L., and Tuzcu, I.: Integrated Approach to the Dynamics and Control of Maneuvering Flexible Aircraft. NASA CR-2003-211748, July 2003.

Moralez, III, E.; Tucker, G. E.; Hindson, W. S.; Frost, C. R.; and Hardy, G. H.: In-Flight Assessment of a Pursuit Guidance Display Format for Manually Flown Precision Instrument Approaches. (Reprint) AHS 60th Annual Forum, Baltimore, Md., June 8–10, 2004.

Mumaw, R.; Sarter, N.; Wickens, C.; Kimball, S.; Nikolic, M.; and Marsh, R., et al.: Analysis of Pilots' Monitoring and Performance on Highly Automated Flight Decks. NASA CR NAS2-99074, 2000.

Niemela, R. J., and Krendal, E. S.: Detection of a Change in Plant Dynamics in a Man-Machine System. AF Inst. of Technol., Proc. 10th Annual Conference on Manual Control, Wright-Patterson AFB, Ohio, Apr. 9–11, 1974, pp. 97–111.

Norman, D. A.: Categorization of Action Slips. Psychological Review, vol. 88, no. 1, Jan. 1981, pp. 1–15.

Norman, D. A.: The Problem of Automation: Inappropriate Feedback and Interaction, not Over-Automation. Philosophical Transactions of the Royal Society of London, vol. 327, no. 1241, 1990, pp. 585–593.

Norris, G.: Rotary Restart. Aviation Week and Space Technology, vol. 168, no. 10, Mar. 2008, p. 49.

Ockier, C.: Pilot-induced Oscillations in Helicopters—Three Case Studies. Report No. IB111-96/12, DLR Institut fur Flugmechanik, Braunschweig, Germany, 1996.

Patterson-Hine, A.; Christian, D.; Iverson, D.; Kaneshige, J.; Poll, S.; Sanderfer, D.; Felix Shung, F.; and Spirkovska, L.: Research in Intelligent Vehicle Automation Group. http://ti.arc.nasa.gov/projects/ne/riva.html. Accessed Nov. 24, 2008.

Phatak, A. V., and Bekey, G. A.: Model of the Adaptive Behavior of the Human Operator in Response to Sudden Change in the Control Situation. NASA SP-192, Proc. 4th Annual NASA-University Conference on Manual Control, Jan. 1969, pp. 361–381.

Phatak, A. V., and Bekey, G. A.: Decision Processes in the Adaptive Behavior of Human Controllers. NASA SP-215, Proc. 5th Annual NASA-University Conference on Manual Control, Jan. 1970, pp. 429–451.

Preyss, A. E., and Meiry, J. L.: Stochastic Modeling of Human Learning Behavior. IEEE Transactions on Man-Machine Systems, vol. MMS-9, no. 2, June 1968, pp. 36–46.

Reason, J.: Human Error. Cambridge University Press, Cambridge, Mass., Oct. 26, 1990.

Ryu, S. and Andrisani, D.: Controller Design for Longitudinal Flying Qualities Improvement in Nonlinear Aircraft. AIAA Paper no. 2000-3988, AIAA Atmospheric Flight Mechanics Conference, Denver, Colo., 2000.

Saberi, H. M.; Khoshlahjeh, M.; Ormiston, R. A.; and Rutkowski, M. J.: Overview of RCAS and Application to Advanced Rotorcraft Problems. AHS Aeromechanics 4th Decennial Specialists Meeting, San Francisco, Calif., Jan. 21–23, 2004.

Sarter, N. B., and Woods, D. D.: How in the World Did We Ever Get into That Mode? Mode Error and Awareness in Supervisory Control. Human Factors, vol. 37, no. 1, Mar. 1995, pp. 5–19.

Schaefer, C. G., and Lutze, F. H., Jr.: Enhanced Energy Maneuverability for Attack Helicopters Using Continuous, Variable (C-V) Rotor Speed Control. AHS 47th Annual Forum, 1991.

Schmidt, D. K.: The Integrated Manual and Automatic Control of Complex Flight Systems. NASA/CR–2009-188664, Aug. 1991.

Smith, J., and Berry, D.: Analysis of Longitudinal Pilot-Induced Oscillation Tendencies of YF-12 Aircraft. NASA TN D-7900, Feb. 1975.

Smith, R. H.: On the Limits of Manual Control. IEEE Transactions on Human Factors in Electronics, vol. 4, no. 1, Sept. 1963, pp. 56–59.

Smith, R. H.: A Theory for Longitudinal Short-Period Pilot Induced Oscillations. AFFDL-TR-77-57, Air Force Flight Dynamics Laboratory, Wright-Patterson AFB, Ohio, June 1977.

Steinberg, M.: Historical Overview of Research in Reconfigurable Flight Control. Proc. Institution of Mechanical Engineers, Part G, J. Aerospace Engineering, vol. 219, no. G4, 2005, pp. 263–272.

Sweet, B. T.: The Identification and Modeling of Visual Cue Usage in Manual Control Task Experiments. NASA TM-1999-208798, Sept. 1999.

Talbot, P. D.; Tinling, B. E.; Decker, W. A.; and Chen, R. T. N.: A Mathematical Model of a Single Main Rotor Helicopter for Piloted Simulation. NASA TM-84281, Sept. 1982.

Tattersall, A. J., and Foord, P. S.: An Experimental Evaluation of Instantaneous Self-Assessment as a Measure of Workload. Ergonomics, vol. 39, no. 5, Jan. 1996, pp. 740–748.

Taylor, R. M.: Situational Awareness Rating Technique (SART): The Development of a Tool for Aircrew Systems Design. In AGARD-CP-478, Proc. AGARD Symposium, Copenhagen, Denmark, Oct. 2–6, 1989.

Tewari, A.: Modern Control Design with Matlab and Simulink. John Wiley & Sons, Inc., 2002.

Theodore, C.; Ivler, C.; Tischler, M.; Field, E.; Neville, R.; and Ross, H.: System Identification of Large Flexible Transport Aircraft. AIAA Paper no. 2008-6894, Atmospheric Flight Mechanics Conference, Honolulu, Hawaii, Aug. 18–21, 2008.

Theodore, C.; Tischler, M. B.; and Colbourne, J. D.: Rapid Frequency-Domain Modeling Methods for Unnamed Aerial Vehicle Flight Control Application. J. Aircraft, vol. 41, no. 4, 2004.

Tischler, M. B.: Identification of Bearingless Main Rotor Dynamic Characteristics from Frequency-Response Wind-Tunnel Test Data. J. American Helicopter Society, vol. 44, no. 1, Jan. 1999.

Tischler, M. B.; Blanken, C. L.; Cheung, K. K.; Swei, S. S.; Sahasrabudhe, V.; and Feynberg, A.: Modernized Control Laws for UH-60 BLACK HAWK Optimization and Flight-Test Results. J. Guidance, Control, and Dynamics, vol. 28, no. 5, 2005.

Tischler, M. B., and Cauffman, M. G.: Frequency-Response Method for Rotorcraft System Identification: Flight Applications to BO-105 Coupled Rotor/Fuselage Dynamics. J. American Helicopter Society, vol. 37, no. 3, Jan. 1992.

Tischler, M. B.; Colbourne, J. D.; Jenkins, J. L.; Cicolani, L. S.; Cheung, K. K.; and Wright, S. C., et al.: Integrated System Identification and Flight Control Optimization in S-92 Handling Qualities Development. AHS 5th Internl. Annual Forum, May 2001.

Tischler, M. B.; Colbourne, J. D.; Morel, M. R.; Biezad, D. J.; Levine, W. S.; and Moldoveanu, V.: CONDUIT: A New Multidisciplinary Integration Environment for Flight Control Development. NASA TM-112203, USAATCOM TR-97-A-009, June 1997.

Tischler, M. B., and Remple, R. K.: Aircraft and Rotorcraft System Identification: Engineering Methods with Flight Test Examples, AIAA Education Series, 2006.

van der Vorst, J.: A Pilot Model for Helicopter Manoeuvers. 24th European Rotorcraft Forum, Marseille, France, Sept. 15–17, 1998.

van Paasen, R.: Biophysics in Aircraft Control: A Model of the Neuromuscular System of the Pilot's Arm. Faculty of Aerospace Engineering, Delft University of Technology, The Netherlands, 1994.

Verma, V.; Jonsson, A.; Pasareanu, C.; and Iatauro, M.: Universal-Executive and PLEXIL: Engine and Language for Robust Spacecraft Control and Operations. AIAA Paper no. 2006-7449, AIAA Space Conference, San Jose, Calif., Sept. 19–21, 2006.

Waszak, M. R.; Buttrill, C. S.; and Schmidt, D. K.: Modeling and Model Simplification of Aeroelastic Vehicles: An Overview. NASA TM-107691, Sept. 1992.

Weber, G.; Efremov, A. V.; and Ogloblin, A. V.: Development of Criteria for Flying Qualities Prediction Using Structural Modeling of Human Pilot Behaviour in the Longitudinal Precise Tracking Task. European Conference for Aerospace Sciences, Moscow, Russia, July 4–7, 2005.

Weir, D. H., and Johnson, W. A.: Pilot's Response to Stability Augmentation System Failures and Implications for Design. NASA SP-192, Proc. 4th Annual NASA-University Conference on Manual Control, Ann Arbor, Mich., Mar 21–23, 1968, pp. 341–360.

Weir, D. H., and Phatak, A. V.: Model of Human-Operator Response to Step Transitions in Controlled Element Dynamics. NASA SP-128, Proc. 2nd Annual NASA-University Conference on Manual Control, Cambridge, Mass., Feb 28–Mar. 2, 1966, pp. 65–83.

Wewerinke, P. H.: The Visual Scene Perception Process Involved in Manual Approach Landing. Report no. NLR-TR-78130-U, National Aerospace Lab, Amsterdam, Netherlands, Oct. 1978.

Wewerinke, P. H.: Visual Scene Perception in Manual Control. J. Cybernetics and Information Science, vol. 3, no. 1-4, 1980, pp. 3–26.

Wewerinke, P. H.: Models of the Human Observer and Controller of a Dynamic System. Dissertation Abstracts Internatl., vol. 51, no. 01-C, Twente University of Technology, The Netherlands, 1989, pp. 157.

Whalley, M.; Freed, M.; Harris, R.; Schulein, G.; Takahashi, M.; and Howlett, J.: Design, Integration, and Flight Test Results for an Autonomous Surveillance Helicopter. Proc. AHS UAV Specialist Meeting, Jan. 19, 2005.

Wiener, E. L.: Intervention Strategies for the Management of Human Error. NASA-CR-4547, Aug. 1993.

Wierwille, W. W.: Physiological Measures of Aircrew Mental Workload. Human Factors, vol. 21, no. 5, Oct. 1979, pp. 575–593.

Wright, Greg P., and Lappos, Nick D.: Helicopter Maneuver Envelope Enhancement (HelMEE) Study: Topical Report. NASA/CR-177542, USAAVSCOM TR-89-A-001, 1989.

Yeo, H., and Chopra, I.: Coupled Rotor/Fuselage Vibration Analysis for Teetering Rotor and Test Data Comparison. J. Aircraft, vol. 38, no. 1, Jan.–Feb. 2001, pp. 111–121.

Young, L. R.: On Adaptive Manual Control. Ergonomics, vol. 12, no. 4, 1969, pp. 635–674.

Zeyada, Y., and Hess, R. A.: Computer-Aided Assessment of Flight Simulator Fidelity. J. Aircraft, vol. 40, no. 1, Jan.–Feb. 2003, pp. 173–180.

CHAPTER 7

PROPULSION

Christopher DellaCorte,[1] Isaac Lopez,[1] and Robert C. Bill[2]

ACRONYMS

CFD	computational fluid dynamics
DOF	degree of freedom
EHL	elastohydrodynamic lubrication
FE	finite-element
Glenn-HT	NASA Glenn Research Center Multi-Block Navier-Stokes Heat Transfer Code
HUMS	Health Usage Monitoring Systems
LES	large-eddy simulation
NPSS	National Propulsion System Simulator
PIV	particle image velocimetry
SBG	spiral bevel gear
SFC	specific fuel consumption

INTRODUCTION

The primary purpose of this report is to identify key areas that we do understand and key areas in which our basic understanding has significant gaps. The limits of validation of our analytical tools and the challenges involved in incorporating them into higher-level system models are also highlighted. This discussion will provide a basis for future research and development (R&D) investment decisions as well as a basis for measuring progress.

The propulsion system of a rotary-wing aircraft comprises the engines, drive system, and all of the ancillary supporting subsystems necessary to provide the power for lift and forward thrust. The range/payload flight characteristics of a rotary-wing aircraft are particularly dependent on the efficiency and power density of the propulsion system. This dependency is driven by propulsion system weight, engine fuel efficiency, and operational characteristics of the propulsion system (range of output speeds; stable operation limits).

[1] NASA Glenn Research Center.
[2] Retired, U.S. Army Research Laboratory.

As shown in table 7.1, in a typical state-of-the-art (SOA) helicopter the propulsion system (less fuel tankage) accounts for about 25% of the operational empty weight, clearly a major fraction of the airframe weight. The highest power densities (horsepower per pound of engine weight) available in today's turboshaft engines are in the 5–7 hp/lb range. Increasing power density beyond this SOA would be very beneficial to the powered lift world, but would entail very highly loaded turbomachinery stages with attendant control, stability, and high rotational speed issues. With regard to the latter issue, there may be an opportunity for breakthrough improvements in bearing performance and complete elimination of the engine lubrication system (accounting for about 10–15% of engine weight) through application of emerging oil-free bearing technology.

The power density of SOA drive systems (input horsepower per pound of drive-system weight) is about 3 hp/lb, and efforts to substantially increase this power density require increased loading of mechanical components and ways to achieve much higher speed-reduction ratios in fewer reduction stages. The transmission lubrication system (size, weight, effectiveness) may benefit from development of oil-free engine-bearing technology if lubricants optimized for transmission application can be used instead of using a common lubricant for both engine and drive system, as is current general practice.

Engine fuel efficiency, best expressed as specific fuel consumption (SFC, pounds of fuel consumed per horsepower hour), significantly affects the range/payload attributes of a rotorcraft; for each pound reduction in mission fuel, more than a pound increase in payload can be realized. Conversely, for a given range/payload mission profile, reduction in SFC can substantially reduce the necessary size and gross weight of the aircraft. SFC is directly related to the engine overall pressure ratio and component efficiencies, and as shown in figure 7.1, currently available engine SFCs are in the 0.45–0.55 lb/hphr range, depending on engine size. Also, the SFC of turboshaft engines increases substantially as the engine operating point (output power, speed) deviates from the optimum design point, resulting in a rather narrow range of efficient operation.

TABLE 7.1. ROTORCRAFT WEIGHT BREAKDOWN SUMMARY

Type	Drivetrain Weight*	Engine Weight*	Mas Gross Weight*	Empty Weight*
CH-47D	4000	1160	53888	25408
UH-60M	1400	950	23472	11501
AH-64D	1200	950	22950	11952
CH-53E	6500	2250	73348	33372
CH-46	950	700	24250	
UH-1	600	500	10476	5388
OH-58	300	135	5493	3293
AH-1	600	500	14733	10006

*All weights are in pounds. Engine weights from "The History of Gas Turbine Development in the United States" by Peter St. James (1960). ASME. Airframe weights are from Flight International, August 2002 and July 1996.

Conclusion: Exclusive of fuel tankage, propulsion system comprises about 24% of empty weight and 10-15% of maximum gross weight.

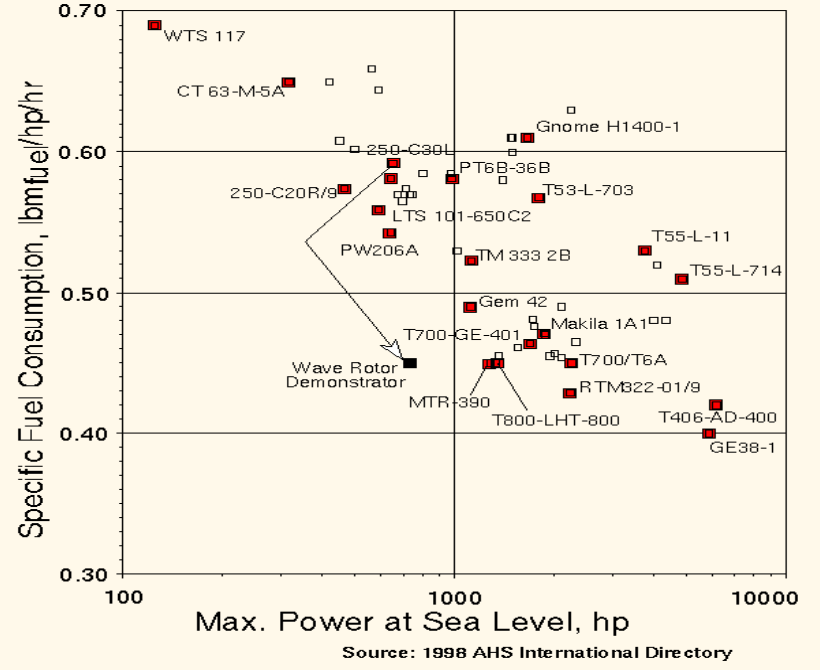

Figure 7.1. Turboshaft engine-specific fuel consumption as a function of rated power.

Over the past four decades, significant progress has been made in the propulsion arena, particularly in the areas of engine power density, and in the performance and reliability of both engines and drive systems. However, the basic concept defining turboshaft-powered rotorcraft propulsion systems has actually changed very little since the 1950s. Virtually all drive systems currently on U.S. helicopters (and on the V-22 as well) are based on planetary gear configurations and are single-reduction-ratio systems. The engines are set up in a constant power-turbine-output-speed mode, hence the rotor systems are nominally constant-speed systems. Although this current situation contributes to a relatively simple and robust control system, major benefits could be realized from the overall flight efficiency and performance and noise standpoints if we could safely and reliably vary the rotor speed on the order of 50% over the aircraft mission profile. Previous studies have considered propulsion-system approaches to varying the main rotor sspeed of helicopters and advanced tiltrotor concepts. Power-turbine technologies capable of efficient operation over wide speed ranges under high-output power conditions were analytically investigated in the early 1990s, and showed a potential for about 15–20% speed variation with an accompanying 5% or so SFC increase without resorting to variable-geometry hardware in the hot section. Several years later, variable-speed drive-system approaches were evaluated for application to an advanced heavy-lift tiltrotor concept aircraft with major transmission efficiency and weight issues identified for each approach when a 30% speed variation was to be achieved through the transmission (planetary drive basis in all cases) system alone [Kish, 2002]. Not considered in either of these studies was the possibility of parsing the overall speed change over both the engine and the drive system.

The following three sections of this report discuss in more depth the SOA of engines and drive systems, and the report concludes with a Summary section. Particular attention is given to the capabilities and limitations of currently used analytical tools, plans for improving those capabilities, and validation requirements necessary for support of improvements to the analytical tools.

ENGINES

The key to developing future high-efficiency, wide-operating-range engines depends on our ability to sustain stable engine operation at high overall pressure ratios. Current turboshaft engines operate at relatively modest pressure ratios of less than 20:1. In comparison, modern large turbofan engines operate at roughly twice that pressure ratio. The special challenges for rotary-wing turboshaft engine developers in reaching the desired cycle pressure ratios reside in the comparatively small size of even the largest turboshaft engines: core engine air-flow rates are measured in 10s of lb/sec, as opposed to 100s for large turbofans. That means airfoils are small and clearances are proportionally large, as are the scale sizes of many secondary flow phenomena that are important in sustaining efficiency and stability. Concepts such as advanced tip or casing treatments have been applied with some success to large engine stages for enhancement of compressor stability, but may or may not be so effective in smaller engine applications. Similarly, concepts such as aspirated stages wherein flow circulation control is effected over compressor airfoil surfaces via "blowing" schemes have been shown to benefit large stages; the same benefits may or may not be realizable for smaller stages. The history of active stall/stabilization has been recently summarized [Hathaway, 2006]; schemes are in the process of being evaluated and need substantial further work before they can be effectively applied to turboshaft engines. Finally, in the hot section, the potential benefits from applying variable-geometry nozzles or other flow-control concepts to the power turbine for an extended efficient operating-speed range need to be thoroughly analyzed.

In addition to high pressure ratio, high rotating speed is essential to keeping engine size and weight as low as possible. Current engines depend on oil-lubricated rolling-element bearings for reliable mechanical operation at high speeds, but the operating speed and lubrication temperature limit for conventional rolling-element bearings has been reached. Glenn Research Center was a leader in rolling-element bearing research and advanced the state of the art for high-speed, high-temperature, long-life bearings for use in gas-turbine engines. Research on rolling-element bearings was concluded in 1984. Zaretsky [1997] provides a good summary of this research. Oil-free fluid-film foil air bearings afford the opportunities to sidestep the rolling-element bearing speed limits (the faster an oil-free fluid-film foil air bearing goes, the better), and at the same time rid the engine of the bulky, weighty lubrication system altogether. Significant improvements in thrust/weight ratio and lowered maintenance can be realized by incorporating oil-free fluid-film foil air bearings into rotorcraft propulsion engines. To achieve this goal, improved fundamental understanding of compliant surface foil gas bearing technology is required to ready oil-free rotorcraft turbine engines. Research is needed to develop accurate hydrodynamic fluid-film modeling of a nonisothermal case with a fluid, pressure-dependant, moveable boundary. This problem is highly nonlinear and needs to be addressed in order to obtain the prediction accuracy needed. The unique opportunity exists for thrust load sharing between an oil-free engine and an optimized gearbox. Research will be performed to study the coupling of an oil-free engine core and power shaft with an optimized gearbox. This novel arrangement could allow higher-power-density engines and drive systems.

The key to realizing the potential advances in turbomachinery and in oil-free fluid-film foil air bearing technology rests primarily with the analytical tools at our disposal or under development. New and improved first-principle and computational models exist, and their potential has generally been demonstrated. These models must be validated and/or have their validation envelope substantially expanded, addressing rotorcraft-specific operating conditions and environments. Modifications to

and further development of these models must be validated and guided by experimental work at the NASA Glenn Research Center, and in some cases in academia and industry. Historically, this experimental work basis has provided the physical and phenomenological underpinnings that were enabling to the modeling and analytical work in the first place. The following subsections highlight some of the more important analytical tools available to support the engine technology concepts, and address validation limits.

Current Tools Available or in Development at NASA

NASA has developed numerous design and analysis tools for turbomachinery applications. One-dimensional (1-D) meanline design and analysis tools provide rapid capability for exploring design space based on overall pressure ratio, mass flow rate, etc., and geometric constraints, and for predicting off-design performance or generating maps for use in system studies. The two-dimensional (2-D) tools provide capability for establishing stage-work split and spanwise loading distributions, and then generating velocity triangles and preliminary blade shapes. Higher-order analysis tools include single-passage isolated blade row to multiple-passage multiblade row steady and unsteady simulation capability for axial and centrifugal compressors and turbines. The most recently developed codes that NASA has invested in are 3-D multistage-capable. These codes are distinctly complementary in their capabilities, ranging from 3-D multistage transient to single-stage steady capability, and a summary of their applications was provided by Adamczyk et al. [1998]. A recent review of NASA-developed turbomachinery codes was provided by Mazumder [2007]. A brief description of the major codes in NASA's turbomachinery computational-fluid-dynamics (CFD) arsenal follows.

TURBO, a NASA-sponsored code developed at Mississippi State University, is capable of time-accurate 3-D multistage analyses. TURBO predictions of overall compressor efficiency has been shown to agree within a couple of percent with validation experimental data, and internal flow measurements have generally validated the ability of the code to predict stage-level phenomena such as flow separation (a precursor to compressor stall). The code is limited mainly by its validation envelope, defined by stage loading, 3-D geometric details, and overall configuration. Also we need to better understand how to effectively yet efficiently grid the geometry being analyzed, and to rationally select appropriate turbulence models suitable for specific flow situations (e.g., passage flow, tip flow). Of particular interest is code applicability to turboshaft engines wherein nonaxial turbomachinery is generally employed; validation of TURBO for application to centrifugal compressor stages is an area needing additional work. Also, enhanced validation of the ability of the code to predict tip flows and injected flow phenomena is needed.

Another widely used and continuously evolving NASA-developed CFD code is APNASA [Adamczyk, 2000], derived from an earlier developmental code called "Average Passage." As the name implies, APNASA is not strictly a time-accurate code; individual blade and blade/vane interactions are time-averaged. As such, APNASA possesses a computational efficiency not featured in other multistage 3-D CFD codes, and provides accurate multistage 3-D flow and performance predictions. APNASA can also capture transient flow and performance phenomena on a stage spatial scale. Overall axial-compressor predictions for TURBO and APNASA are seen to be in very close agreement (within 1–2%) in figure 7.2, which shows a single axial passage row with the flow moving from the inlet through successive sequences of rotor/stator stages, five axial stages in all. The

absolute scale pertaining to figure 7.2 is unavailable because of proprietary concern by the engine manufacturer, but the plot does show static pressure contours. The main point of the comparison is the agreement between the time-accurate TURBO predictions and the time-averaged APNASA predictions. APNASA is especially useful in guiding design and configuration adjustments for full-compression-system (and turbine system) performance optimizations, and will be an especially valuable tool in defining multi-stage configurations and accurately predicting the performance of highly loaded compressors. APNASA is an important complementary tool to the time-accurate codes, and provides an excellent starting point for obtaining time-accurate solutions.

Like TURBO and most other turbomachinery CFD codes, APNASA was developed and validated with axial turbomachinery in mind (limited application experience to centrifugal stages), and its potential for dealing with tip flows and injected-flow phenomena needs to be assessed. Together, applied in tandem, APNASA and TURBO are essential parts of our arsenal of tools.

H3D [Hah et al., 2006] is a 3-D code capable of predicting transient, unsteady flow solutions. The code has been extensively applied to single-stage analyses, and was successfully used in centrifugal compressor-impeller analyses. H3D has been extensively validated against a wide range of compressor stages, turbine stages, propellers, and pumps. Glenn HT is a steady state 3-D heat transfer and aero code, especially capable of treating blade-tip and internal-cooling flows for single-stage turbine analyses. Validation cases supporting Glenn HT include research data on tip flows, internal-coolant passage flows, and turbine aerodynamics from rotating and cascade facilities.

The SWIFT code is a widely disseminated 3-D steady-state finite-difference code applicable to single-blade-row analyses and is capable of analyzing axial and radial (centrifugal) turbomachinery stages. Viscous terms are included in the circumferential and radial directions, but a thin-layer approximation is applied in the streamwise direction [Chima and Liou, 2003]. SWIFT has been validated against numerous compressor research rotors, turbine stages, centrifugal machinery, and fan stages.

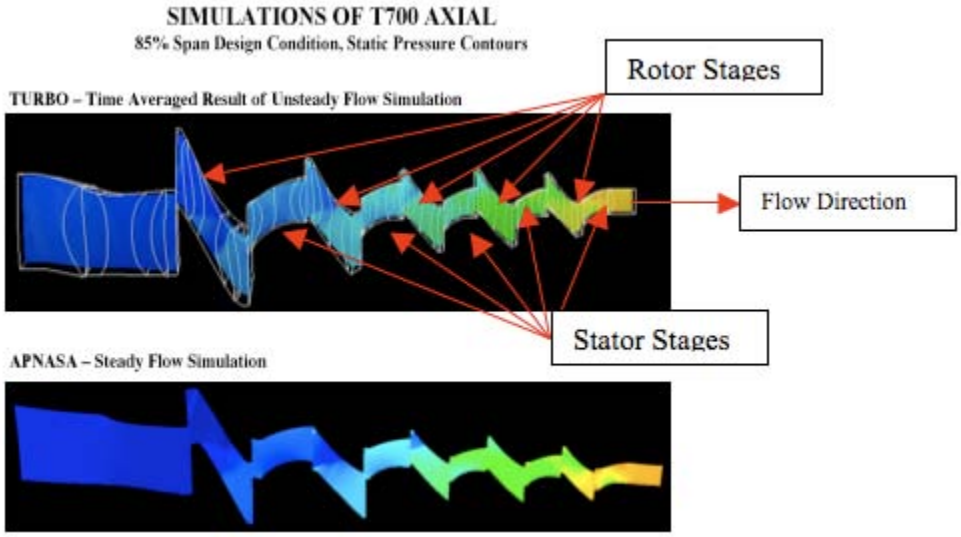

Figure 7.2. TURBO and APNASA predictions of T700 axial-compressor performance.

CSTALL is a recently developed 3-D unsteady, Euler equation-based code specifically designed to address compressor instability. CSTALL has multistage capability but does require independent Navier–Stokes analysis input for turning-loss calibration between blade rows [Chima, 2006]. Computationally, CSTALL is very efficient, and is still in the relatively early stages of validation.

At the other end of the spectrum is the NASA-developed National Propulsion System Simulator (NPSS). NPSS was developed as an overall framework for analysis of full propulsion systems, mainly with large turbomachinery in mind. Individual codes can be embedded in NPSS to give it a component-level zoom capability for CFD, structural, and dynamic insights. For purposes of engine-related research and development within NASA rotorcraft, however, the most applicable tools are component-level CFD codes like TURBO and APNASA that can provide insight and guidance for developing highly loaded wide-operating-range turbomachinery concepts.

Supporting the development and validation of these codes is a comprehensive array of experimental research facilities, including the Large Low Speed Compressor facility [Hathaway et al., 1993] shown in figure 7.3a, that uses substantial geometric upscaling to allow direct measurement of detailed secondary flow structures (tip and hub flows, vortices, wakes). Figure 7.3a shows the up-scale rotor of a four-stage axial compressor model; casing and stators have been removed. Full-size compressor and turbine single-stage and multistage facilities are available, equipped with laser velocimetry and comprehensive flow, pressure, and temperature measurement capabilities. An example is shown in figure 7.3b, which illustrates the small compressor facility used to make detailed flow measurements on small axial and centrifugal stages.

The central technology of oil-free turbomachinery is the compliant surface gas bearing (foil bearing). Both thrust and journal foil bearings are key enabling technologies for this development. Historically, the field of hydrodynamics and bearing development has relied heavily upon experimental investigations. To a somewhat lesser, but still nontrivial, extent analytic methods have been developed to enhance the understanding of bearing design and operation. Therefore, over the past decade the Oil-Free Turbomachinery team at Glenn Research Center has designed and developed seven high-speed (>10 krpm) rotating-machinery test rigs for research and technology development on foil bearings. These test rigs cover the entire test range of speed, pressure, and temperature that a bearing location in a gas turbine engine would experience. In most cases the test rigs exceed the current SOA in the gas turbine engine operating parameter that allows for potential future requirements to be met. Typical test data include bearing performance measures such as load capacity and friction coefficient, two parameters that are critical to the systems integration of foil bearings. Some experimental capability does currently exist for point-wise field measurements of pressure and temperature in the gas film. Analytic codes have been developed over the past five years for both thrust and journal bearings through cooperative agreements with The Pennsylvania State University and Case Western Reserve University. These predictive tools were the first attempts at physics-based tools as opposed to the empirically based tools that have dominated the field to date [Agrawal, 1997; and Heshmat and Hermel, 1993].

a) Large Low Speed Compressor facility

b) Small compressor facility

Figure 7.3. Examples of turbomachinery research facilities at Glenn Research Center.

Current Predictive Capabilities

NASA has provided several benchmark datasets for assessing the predictive capability of turbomachinery flow solvers, including overall performance measurements from choke to stall at various rotor speeds and selected probe surveys at different operating conditions. The earliest widely referenced test case for axial-flow compressors was NASA rotor 67 [Strazisar et al., 1990] for which the detailed velocity field was measured at several spanwise locations and for different operating conditions using laser anemometry and conventional survey instrumentation. The most recent NASA test case reported in the open literature became the basis of a blind test case for assessing the predictive capability of turbomachinery flow solvers. The results of the blind test case were first reported in [Wisler et al., 1994; and Denton, 1996] and later formed the basis of another CFD assessment in [Dunham, 1998]. For centrifugal compressors the detailed laser-anemometer measurements of the NASA low-speed centrifugal compressor [Hathaway et al., 1995] and a high-speed compressor stage [Skoch et al., 1997) have been widely used for validating turbomachinery flow solvers for centrifugal compressor applications. Detailed geometry, inlet-flow conditions, and conventional aerodynamic probe-survey measurements as well as detailed laser-anememometer measurements are provided in the previously mentioned benchmark datasets. In addition, NASA researchers have published papers, only a few examples of which are referenced herein, that provide CFD guidance for improved predictive capability [Hathaway and Wood, 1997; Adamczyk, 2000; and VanZante et al., 2000] or provide insight into or measure characteristics of the fundamental flow physics [Hathaway et al., 1986; and Suder et al., 1987]. The capability for predicting the flow physics associated with the onset of stall are currently being investigated and show some promise in acquiring insight into the flow physics of stall inception.

Predictive capabilities of the turbomachinery CFD codes can be indirectly validated through comparison of measured performance of well-characterized research stages with predicted performance. The performance parameters compared are typically stage pressure ratio, mass flow rates, and efficiency. For example, figure 7.4a shows a comparison between TURBO-predicted rotor 35 speedlines versus experimental measurements; in terms of predicted versus actual mass flow, the agreement is quite good, being within a few percent. Rotor 35, a NASA designation, is a widely accepted validation testbed, data from which has been used to help in validation of a wide range of CFD codes. In figure 7.4b predicted pressure and temperature spanwise profiles are compared with measured profiles; the TURBO predictions were in excellent agreement with the measurements, generally within 1%. The most notable discrepancies are in the blade-tip region, especially with regard to temperature profile, indicative of the need to develop rational ways to enable CFD codes to capture phenomena in this critical region without sacrificing efficiency and accuracy elsewhere. Within the bounds of their respective validation envelopes, all of the turbomachinery CFD codes are capable of this level of accuracy in terms of predicted global flow parameters; it is mainly a question of specified grid fineness and availability of supporting computational facilities. For instance, the speedline and pressure-profile results from SWIFT analyses [Chima, 2006] compared to rotor 35 data show similar close agreement, as illustrated in figure 7.5. These predictive capabilities directly support objectives toward compressor stall-control modeling for highly loaded, wide-operating-range turbomachinery.

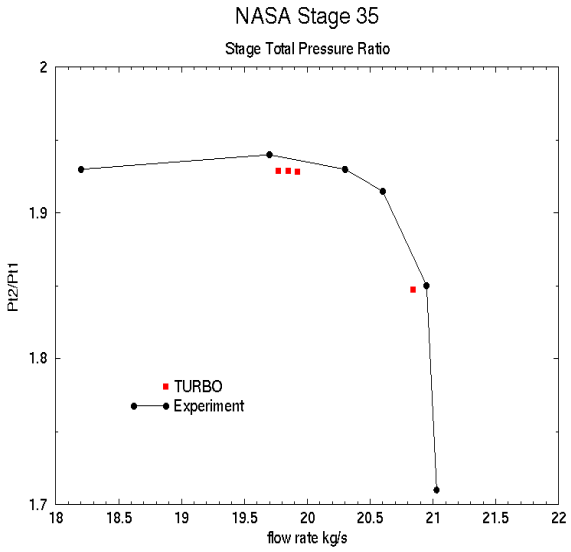

a) Predicted vs. measured speedline

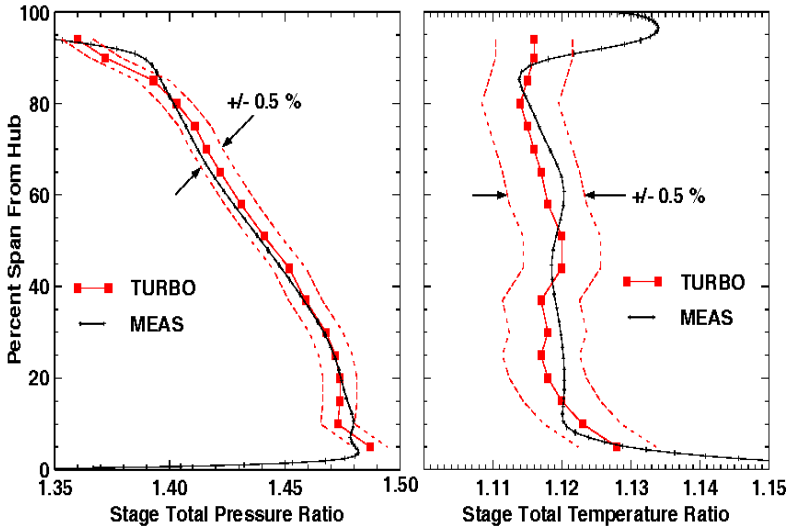

b) Pressure and temperature profiles

Figure 7.4. CFD-predicted speedline, and total pressure and total temperature comparisons with experimental data.

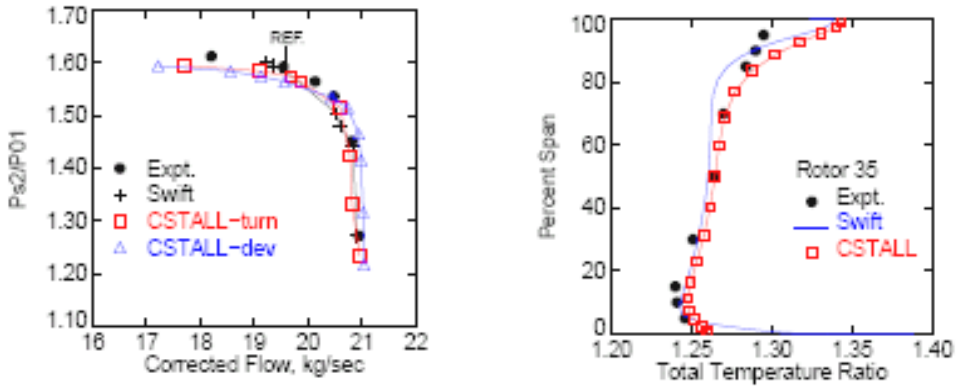

Figure 7.5. Comparison of SWIFT and CSTALL data with rotor 35 results.

From a flow phenomenon standpoint, documentation of predictive capability is more inferred. Using TURBO as an example again, the predicted scenario for onset of compressor stall is a progressive coalescing of small rapidly rotating (about 80% rotor speed) cells into ever larger and more slowly rotating cells (40–50% rotating speed) followed by the onset of full stall. These TURBO predictions, summarized in figure 7.6a, are in agreement with predicted measurements from numerical static pressure probes located around the compressor stage passage annulus at the same locations as in the actual supporting experiment. The predicted speed of the stall cells and the overall evolving stall scenario are consistent with what has been reported in the open literature [Day, 1993; and Cumptsy, 2004] wherein initial small high-speed instabilities (close to rotor speed) rotating around the annulus grow into large stall cells rotating around the annulus at about one-half rotor speed.

Dynamic pressure measurements are taken at very high frequency, approaching blade pass frequencies, and there is no doubt some distortion in the measurements. Likewise, the analytical results are somewhat a function of local gridding structure, but the predicted local pressure levels are considered to be within a few percent of the measured fluctuations. Of more importance than accuracy of predicted pressure levels is the ability to successfully predict the onset of rotating stall cells and their evolution toward full stall. Onset prediction accuracy was within about 1% (referenced against measured mass flow rate) of the experimentally observed onset of stall, and progression tracked almost in lock step with the experimental pressure measurements. The real value here is that we not only have the predictive accuracy represented by the speedline predictions (figs. 7.4 and 7.5), but we also have confidence that the predicted phenomenology is correct. The next step is to apply these analytical tools to multistage and full engine configurations, and of course validate the predictions at that level.

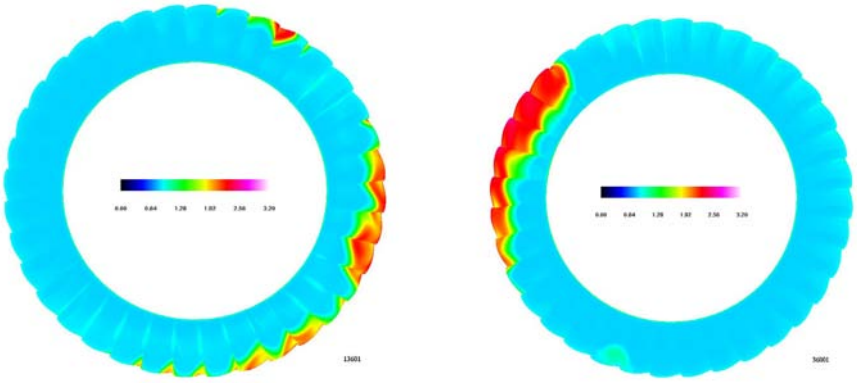

3.8 revolutions 10 revolutions

a) Predicted annular stall cell formation

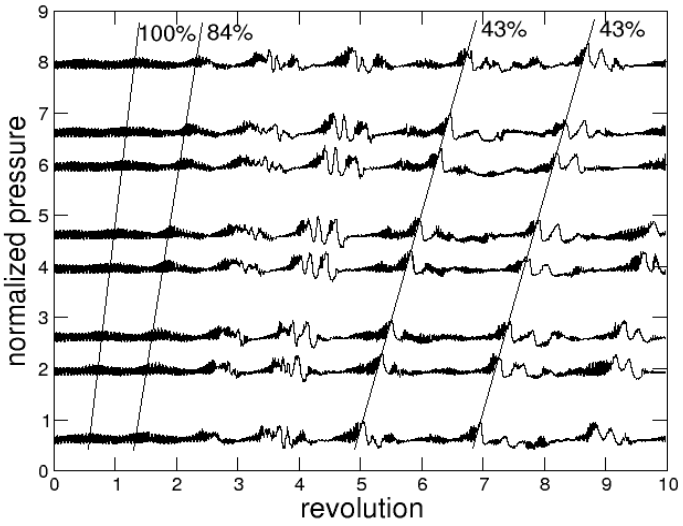

b) Predicted static pressures

Figure 7.6. Turbo CFD predictions of stall cell formation compared to dynamic pressure measurements.

Other correlations of experimental flow data (laser velocimetry, detailed probe measurements) with predictions from various codes show generally good agreement with respect to detailed flow phenomena around blade tips, blade/wake interactions, and hub-flow effects. Figure 7.7a shows a detailed predicted velocity flow-field map for a centrifugal compressor diffuser, in which the major features (flow-reversal regions) are consistent with laser particle-image-velocimetry (PIV) measurements shown in figure 7.7b for the same diffuser (image is rotated 90 degrees) under almost the same operating conditions.

As a final example, the detailed flow structure over compressor blade tips as predicted by H3D and compared with direct experimental observation are shown in figure 7.8 [Hah et al., 2006]. The colors represent static-pressure contours (scale not available for the experimental measurements). The important thing from this comparison is not the actual static-pressure levels, but rather the general consistency seen in the predicted and observed flow structures. The measurements show that the tip leakage vortex oscillates significantly near stall, even with a uniform flow-inlet condition. The H3D prediction, based on large-eddy simulation (LES), reproduces this vortex oscillation very well, and accurately calculates the measured dominant frequency component of this vortex oscillation as well as the angular relationship between the tip vortex and the airfoil leading edge. These tip-flow phenomena are especially significant with respect to stall inception, and the ability to accurately predict them in a full compressor or engine environment is essential to the development of wide-operating-range, highly loaded turbomachinery.

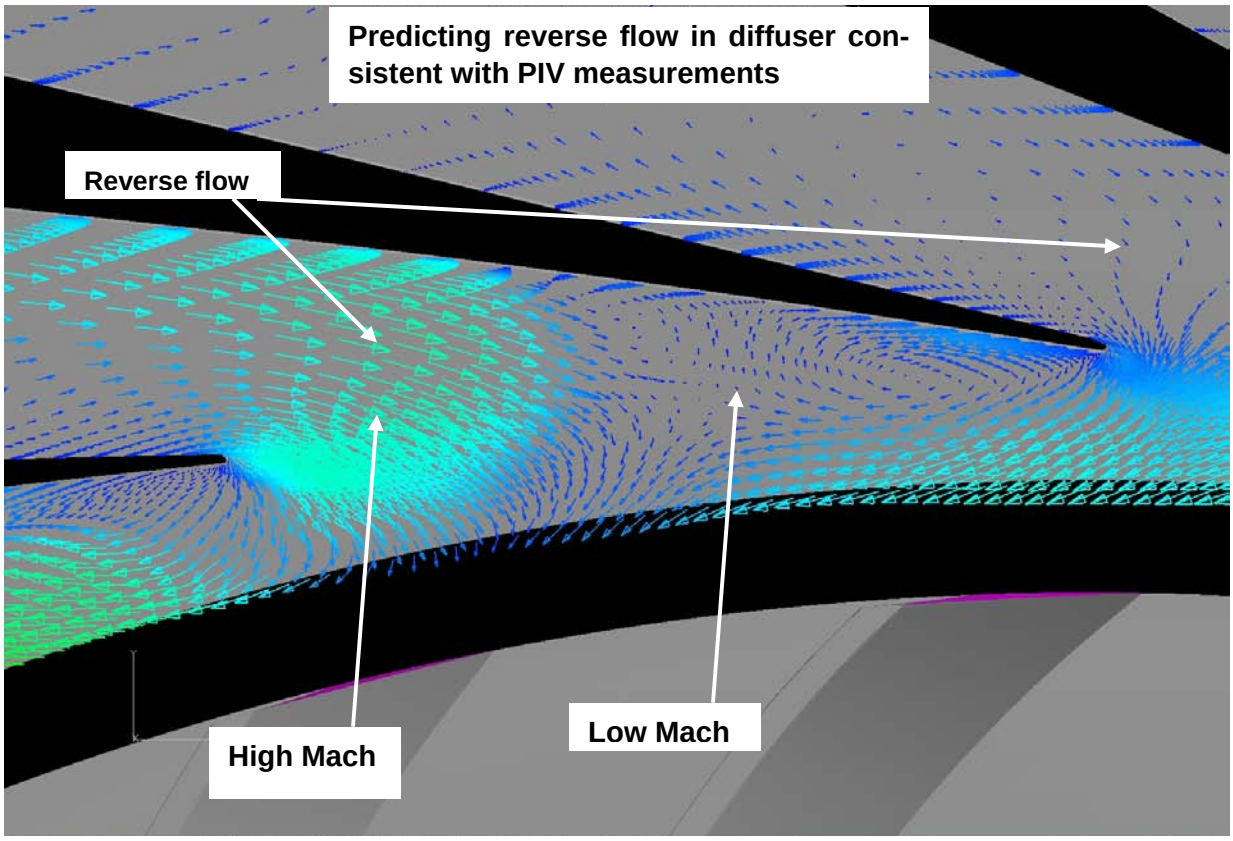

a) TURBO full-annulus simulation of CC3 centrifugal compressor diffuser. Instantaneous snapshot without stall-control technology

Figure 7.7. TURBO-predicted flow field versus PIV data in centrifugal compressor diffuser.

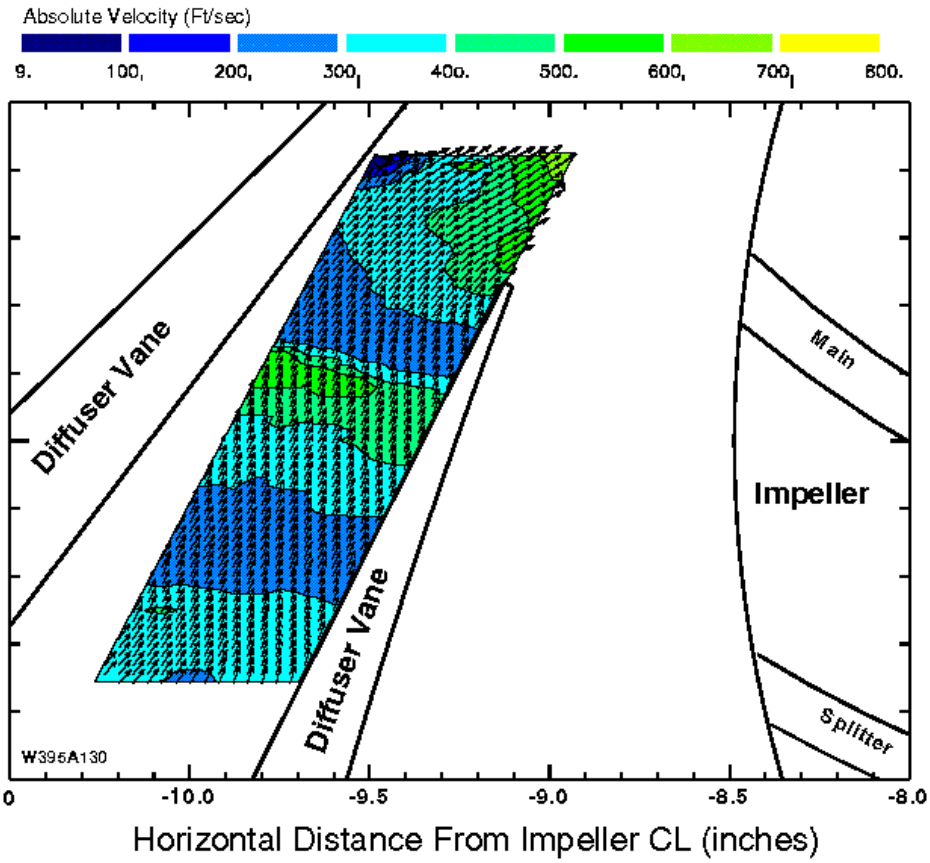

b) Instantaneous PIV measurement of velocity in CC3 centrifugal compressor diffuser

Figure 7.7. Concluded.

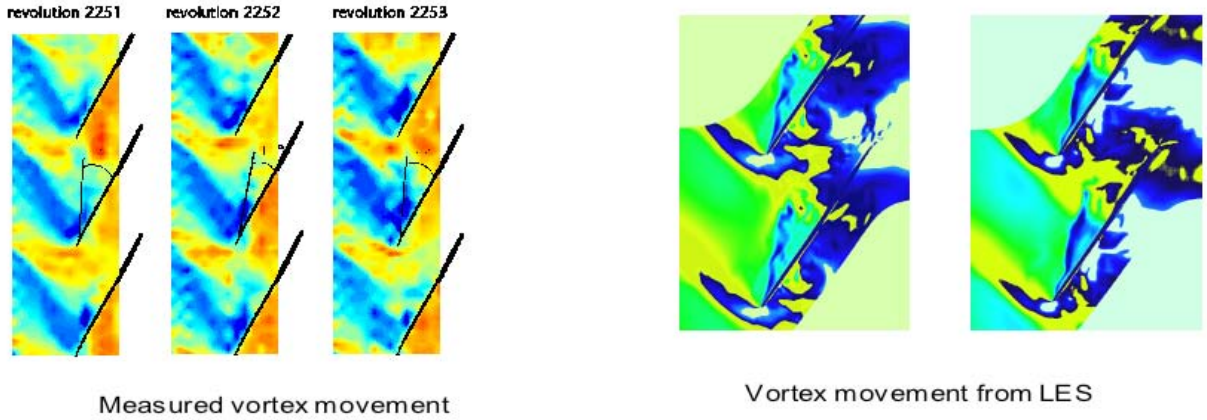

Figure 7.8. H3D predicted tip-leakage vortex structure compared to experiment.

Properly applied and adapted, the turbomachinery CFD tools in conjunction with the supporting experimental facilities constitute critically enabling assets for accurately predicting the onset of stall, and providing optimum strategies for stall prevention or active stabilization. In the following subsection, some approaches for adapting these tools to the specific requirements and component level concepts are discussed.

Current predictive capabilities addressing oil-free fluid-film foil air-bearing performance include the ability to predict thrust and journal performance parameters for foil-bearing operating in isothermal conditions [DellaCorte and Valco, 2000; and Howard et al., 2001]. Load-capacity predictions based on this methodology are summarized for three technology levels of journal bearings in figure 7.9a; the key is the semiempirical load-capacity coefficient, which is related to the stiffness characteristics of the foil support structure. The power-dissipation predictions are shown in figure 7.9b [DellaCorte et al., 2006] as a function of Modified Sommerfeld Number, S', which is related to the thickness of the air film; power dissipation is an essential to the thermal analysis of the bearing. Although the approach outlined is based on a curve fit through available data, the methodology is well-founded on basic tribological concepts that form the underpinnings of our physical understanding of bearings. Specifically, friction (power dissipation in this case) is seen as being bound to follow a Stribeck type of variation over a very broad range of value for S'. At low values of S', intermittent solid contact will occur, resulting in high frictional loads and energy dissipation. At high values, large masses of lubricant (air) are subjected to large momentum changes, thus resulting in large dissipation values at the high end. Ideally we strive to operate near the minimum-dissipation part of the curve, where just a sufficient amount of lubricant (air) is drawn into the contact region to effect 100% separation of the opposing surfaces. The theoretical insight behind this predictive methodology is represented by the idea of extending the Stribeck analogy to the oil-free fluid-film foil air-bearing concept.

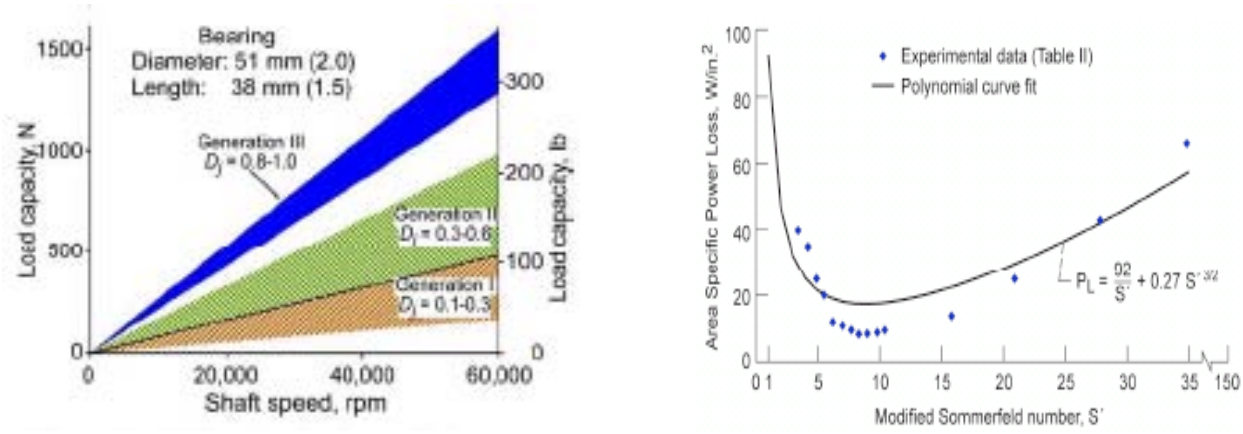

a) Load capacity versus shaft speed

b) Power dissipation vs. Modified Sommerfeld Number

Figure 7.9. Predicted foil journal-bearing load-capacity and power-dissipation performance.

The predictive accuracy of this approach is on the order of 10–15%, which is good enough for initiating a test-intensive bearing-development project, but more is needed to support an analytical approach to an oil-free fluid-film air-bearing-supported engine design. Dynamic stiffnesses and damping characteristics have to be addressed, as do bearing thermal effects.

Current proprietary codes are primarily research tools and not necessarily efficient bearing-design tools. They are specific to the developer's particular approach to bearing support structure, and are heavily laced with empirical factors of limited validation range. Analytical approaches to nonuniform, unsteady load distributions due to shaft dynamics and misalignments and temperature gradients need to be developed and validated. Testing capabilities are similar to predictive capabilities in that performance parameters such as load and torque are measured experimentally.

Plans for Improving Predictive Capability

NASA is continuing to invest in the support of two test facilities that are germane to rotorcraft development: Test cell CE18 for testing small (up to 20-in. diameter) centrifugal, axial, or axicentrifugal compressors up to 30:1 pressure ratio and 60,000 rpm; and, the Engine Components Research Laboratory that currently supports testing of a T700 engine for development of stall-control technology, and is capable of testing small engines (35 lbm/sec) up to 25000 SHP. Other turbomachinery test facilities at NASA Glenn Research Center that can support rotorcraft research are a low-speed compressor facility and high-speed single-stage and high-speed multistage compressor facilities. In addition, NASA has some small standalone test facilities that do not require additional support beyond that of a single research investigator; for example: isolated airfoils, small wind tunnels, and diffusers.

The predictive capabilities are continually being improved as dictated by research requirements. The main improvements required for achieving the NASA rotorcraft wide operability (in concert with the highly loaded) turbomachinery goals are driven by the expected reliance on flow control and the need to model flow-control concepts and incorporate the effects of such concepts in the design process. The following capabilities are also important for rotorcraft: meshing complex 3-D geometries (e.g., pipe diffusers, axicentrifugal compressors), including flows associated with flow control; accurately predicting laminar/turbulent transition; and improving predictive capability for separated and secondary flows, especially over a wide operating range. These simulating capabilities must be able to predict the effects of inlet-flow distortions and the onset of compressor stall. The available analytical tools can be applied at the subcomponent (e.g., compressor stage) level and yield results that are at least adequately in agreement with experimental data. There are two major areas of challenge, however: the gridding scheme can be optimally set up for high-quality high-resolution results only if the phenomenological and spatial details of the problem to be addressed are generally known a priori; and the tools need to be applied and validated at the full component (e.g., multistage compressor or turbine) level at least, and ultimately at the engine level. The full component-level application is being pursued, combining the APNASA and TURBO codes and applying them to the T700 compressor as a validation case. Overall, steady performance is well-represented, but the ability to successfully predict transient phenomena such as compressor stall and to support stall-prevention methodologies has yet to be developed and validated.

Supported by NASA, two independent predictive tools for oil-free fluid-film foil journal bearing will be developed over the next three years. These tools will require high-fidelity instrumentation and testing capabilities in order to provide the level of validation necessary of a predictive tool.

Validation Data Requirements

Detailed measurements with pressure, thermal, and swirl inlet distortions are needed to validate predictive models. Detailed measurements of boundary layer flows during laminar/turbulent transition and separated flow conditions to develop improved modeling and improved predictive capability are also required. Measurements in multistage and axicentrifugal compression systems with stall control technology are required to provide validation data for codes that predict the effects and sensitivity of stall-control technology on multistage matching, compressor performance, and stall margin. Design methodologies have to be developed for advanced SOA compression systems for rotorcraft, accounting for the effect of stall-control technology that the design depends on for wide operability.

For oil-free fluid-film foil air bearings, proper validation of the predictive tools will require a multi-fidelity process. From the macroscopic viewpoint the tools will be required to initiate calculation from gross parameters such as the geometry of the compliant layer, friction coefficient, and preload force. Thus the validation-data requirements will include meticulous documentation of the bearing conditions prior to testing. Additionally, the models will be required to “roll up” the calculations into performance parameters such as load capacity and reaction torque at various speeds, pressures, and temperatures. To accomplish this task a rigorous dataset must be established with carefully conducted experiments and open-source bearing designs in order for the data to be of high value. The requirement of additional, higher-fidelity data, not traditionally obtained in foil bearing tests, also exists. These types of data are invaluable for validating the physics of the underlying models. Data that would fit this description include point-wise or field-wise measurements of pressure, temperature, material stress, and film thickness.

Cross-Cutting Technology Needs

Interdependencies between engine disciplines and other subsonic rotary-wing disciplines reside heavily in the flight control domain, particularly if variable-speed rotors are considered. Gas-generator time-lag effects and power turbine inertial time lags will need to be addressed in the overall flight control algorithms. Also, stall is a fundamental limitation of compression systems. Stall bounds the operability envelope, limits efficiency, and requires that the compressor be designed with sufficient stall margin to allow for blade erosion, inlet distortions, and other effects that degrade the stall margin. The stall characteristics will need to be incorporated in the overall rotorcraft control architecture to assure safe, efficient operation over the intended flight envelope.

The Oil-Free Turbomachinery technology has seen application to air-cycle machines, and is in the late demonstration phase for application to ground-based turbocharger and distributed-power applications. In the aeropropulsion arena, besides being strongly applicable to rotary-wing turboshaft

engines, oil-free technology has strong potential for application to regional jet and supersonic business jet primary propulsion engines. The technology issues, barriers, and approaches are generally unique to oil-free technology. The Oil-Free Turbomachinery technology is largely transparent as far as interdependencies with other rotary-wing disciplines are concerned.

DRIVE SYSTEMS

Drive-system technology has progressed in a very evolutionary manner to its present state. Since drive-system reliability is so closely tied to rotorcraft flight safety, this conservative approach is understandable. A failure in any major drive component (gears, bearings) downstream from the isolating overrunning clutch, always located very near the engine-output shaft, can potentially, if not certainly, result in loss of aircraft and crew. Design practice is to follow widely accepted and validated procedures for calculating gear (American Gear Manufacturers Association) and bearing loading (American Bearing Manufacturers Association) so that a high confidence in required component life results. Manufacturers perform their own material testing for gears followed by rig testing and qualification systems tests. Load safety factors as high as 40% are typically applied, reflecting uncertainties associated with envelope-limiting dynamic and maneuver loads for which reliable, drive-system level predictive tools are lacking.

Windage is an important consideration from the standpoints of drive-system life, lubrication, and thermal management. The models currently used are very approximate and inadequate, especially when applied to epicyclic gear motion. At high speeds, windage can account for a major portion of the energy dissipation associated with current gearboxes [Krantz and Handschuh, 1990], hence driving the size and capacity of lubricant supply and cooling susbsystems. The fluid-dynamics environment inside a gearbox is extremely complex, being excited by epicyclic gear motion, displacement of fluid by meshing gear teeth, a potentially two-phase CFD environment (air and liquid lubricant), and many complex-shaped structures that can disturb/upset flow fields. Work in this area supports NASA goals aimed at improving drive lubrication models and concepts and gear windage models through development of better characterized and understood lubrication and heat transfer inside the gearbox.

All of the current dynamic analysis tools that are applicable at the propulsion-system level (rotor, drive system, engines) were developed with main rotor dynamics and control in mind. As such, they generally treat the drive system as a series of course, lumped masses connected by rigid or at best, 1-degree-of-freedom (DOF) elastic shafts. Engines are similarly treated from an overly simplified standpoint. What is needed is an analytical capability that can resolve dynamic loads through the drive system, down to subcomponent (e.g., gear mesh) levels.

Current rotorcraft systems operate with single-speed transmissions and achieve a limited rotor-speed variation based upon changes in engine speed, limiting the ability to fly at widely varying speeds with acceptable efficiency and noise signature. While multispeed transmissions dominate the automotive power trains, such concepts do not exist for rotorcraft, nor do system-level performance models, controls, and rotor designs. Variable-speed propulsion, without loss of efficiency and torque, is necessary to permit high-speed operation with reduced noise. Speed variations in excess of

50% will have a dramatic effect on reducing external noise while increasing rotorcraft performance. To achieve this large speed-variation capability, advanced variable/multispeed drive-system modeling tools and concepts (e.g., Stevens et al. [2008]) are underway. A combination of university-based and government-led investigations are ongoing in concert with industry to enable the design and development of such systems through the development of working drive-system concepts, and analytical architecture to capture the significant dynamic phenomena associated with variable-speed drive.

Most SOA rotorcraft gearboxes share their lubrication system with the engine, resulting in a compromised lubrication system for both engine and drives but low weight. Advances in engines may allow the deployment of oil-free turbines enabling a gearbox to be deployed with an optimized lubrication system. Laboratory tests by Townsend and Shimski [1994] have shown greater than eightfold improvement in gear-surface-fatigue life using transmission-optimized lubrication as compared to standard turbine oil.

On the system level, assessments focus on determining a conceptual approach to developing an optimized propulsion system for rotorcraft. Both advanced drive technology, enabled by the use of high-viscosity gear oil, and oil-free turbine engine technology, enabled by high-temperature foil air bearings, are being assessed. The advantages of each technology are assessed and compared to technical challenges, such as increased gearbox windage loss, introduced by this propulsion concept. Accurate assessments are predicated by the availability of existing data and testbeds for highly loaded drive-system components, such as gears, and oil-free engine technology. The goal of the effort is to determine the benefits and drawbacks such an optimized propulsion system provides as well as a deeper understanding of the challenges and roadmap to implement such a system.

Current Tools Available or in Development at NASA

Current analytical tools available at NASA Glenn Research Center are applied at the component level. These tools have been developed in-house, under grant, or via contract for application to gear geometry (spur, helical, spiral bevel, face gears), gear dynamics (spur and helical), gear life calculations, gear-tooth bending stress, gear-tooth contact stress, thermal behavior of spur gears, thermal behavior of spiral-bevel gears, gear fatigue life, gear crack propagation, and gear health-monitoring techniques (vibration techniques, fuzzy logic). They are based on many of the mainstream modeling codes such as PATRAN, ANSYS, MARC, etc. that are used for the finite element (FE), boundary element, or specialized gearing-related elements, and are typically used for stress analysis, thermal behavior, or gear crack propagation of meshing gear teeth addressing the various gear failure mechanisms. A qualitative representation of gear failure modes is shown in figure 7.10.

Other tools that are based on current industry practice such as the American Gear Manufacturers Association are also used for rapid modeling results and for comparison to contractor-generated data in some instances. Available to anyone, these codes provide a necessary function of being able to access many different designs in a short amount of time. Many of these codes have menu-driven data input and produce design data that provide conservative designs.

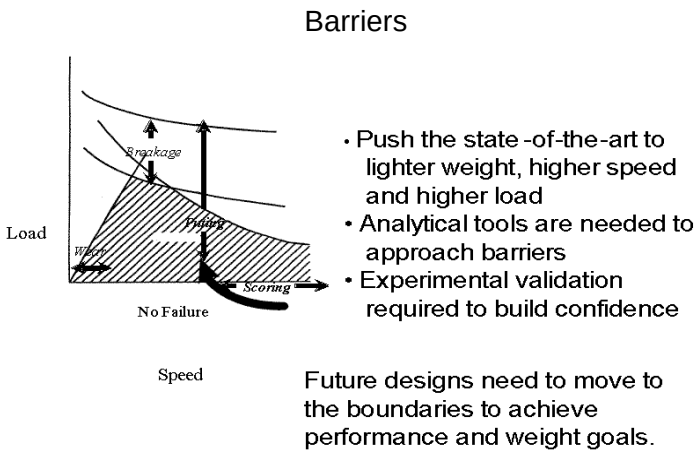

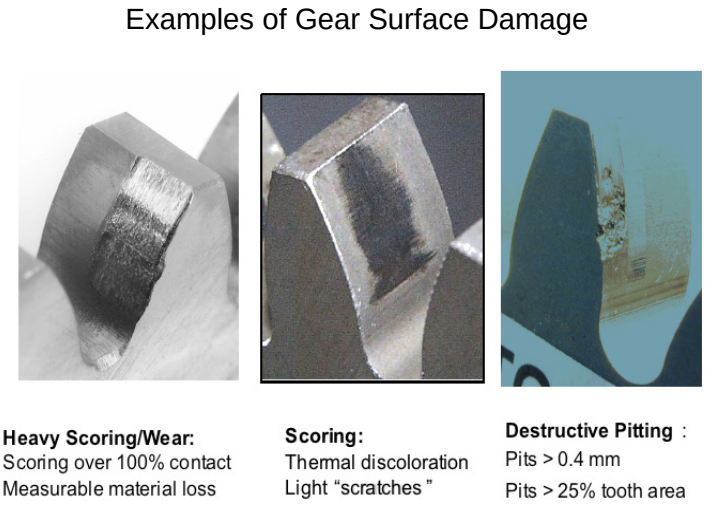

Figure 7.10. Conceptual gear failure mechanism map.

Another available capability is to analyze rolling-element and fluid-film bearings. These programs were developed under contract and grant for many of the common types of bearings used in existing rotorcraft. The programs for rolling-element bearings have been available for over 10 years and the codes for nominal fluid-film bearings, including cavitation, have been studied extensively.

In addition to the analytical tools mentioned previously, there is an extensive testing capability at Glenn Research Center. The component test capability includes single-tooth bending and contact fatigue of spur gears and face/spiral bevel gear dynamic bending and contact fatigue. These facilities (figure 7.11) are used to generate statistically significant gear fatigue data that can be used to compare materials, manufacturing techniques, lubricants, etc. A facility also exists for testing gear noise/vibration on the single-component level. This facility can be used to understand the effects of gear-design changes such as profile modification to reduce noise and vibration.

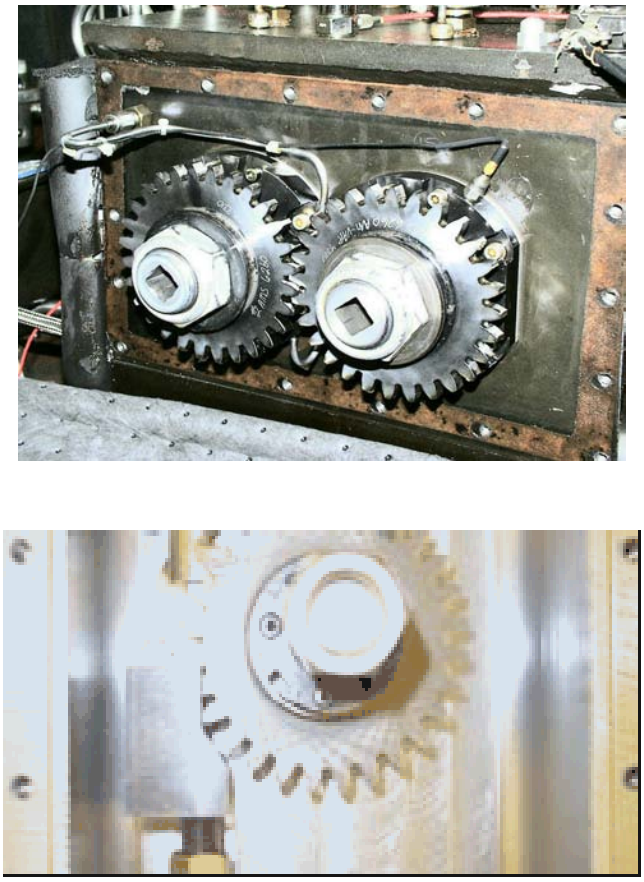

Figure 7.11. Gear-surface-fatigue and gear-bending-fatigue test facilities.

Facilities also exist to test subsystems and complete rotorcraft transmissions. These facilities permit testing of improved /modified components in a rotorcraft-relevant environment. These facilities have been used to measure gear-tooth bending strain dynamically, gear noise/vibration, gear thermal behavior, and several other aspects of interest to gear researchers; they are essential for validating improved drive-system analytical tools.

Current Predictive Capabilities

Like bearing life predictions, gear-design life predictions are probabilistic, and are based on a surface-pitting fatigue failure mode in well-characterized gear and bearing specialty steels [Townsend, 1983; and Zaretsky, 1990]. Based on steady, defined loads within the domain of pitting fatigue failure, probabilistic lives can be predicted to a very high confidence level [Townsend et al., 1978]. The limiting consideration in accuracy of gear-fatigue failure lives is our ability to accurately represent all of the meshing and dynamic-load components the gear-tooth surface and supporting structure actually experiences.

Finite-element models have been developed that can accurately predict gear meshing and structural loads for drive-system subelements like a planetary stage or a spiral bevel gear (SBG) under steady-input torque conditions. Comparisons of the FE predicted ring gear-tooth root and fillet stresses are

generally in excellent agreement with experimentally measured stresses from planetary-ring gears (within a few percent). For a detailed investigation of gear-tooth profile and gear stiffness-related meshing dynamics, of dominant importance in controlling transmission noise and vibration, computationally efficient analytical models are under development [Ambarisha and Parker, 2007]. These analytical models can quickly capture the effects of subtle gear-tooth profile modifications and changes in tooth stiffness without having to develop costly, time-consuming FE gridding approaches to resolve such fine geometric changes. These analytical models have demonstrated comparable predictive accuracy for complex dynamic phenomena associated with nonlinear mesh stiffnesses, as illustrated in figure 7.12 for a planetary stage. The baseline for comparison is a well-gridded and -validated (from a stress-prediction standpoint) FE model. The important point for comparison between the analytical predictions and the FE results is the nearness of the resonance peaks (within about 50 Hz in all cases), the consistency in prediction of the jump phenomenon (note ascending and descending rotational-speed paths in figure 7.12), and the consistency in predicting the onset of gear-tooth separation (with its consequent loss in control of tooth load sharing). Improvements are needed, of course, including more accurate representation of tooth stiffnesses, and structural representation of ring, carrier, housing, and bearing dynamic properties, including damping effects. Also, a more direct comparison with experimental results is highly desirable.

On the isolated component or single-stage level, static load measurements generally agree with dynamic meshing data, and analytical predictions are consistent with experimental results. Particularly notable is the ability to predict dynamic tooth loads and noise of SBGs, as described by Lewicki et al. [2007]. Theoretically developed SBG pinion-tooth modifications were predicted to

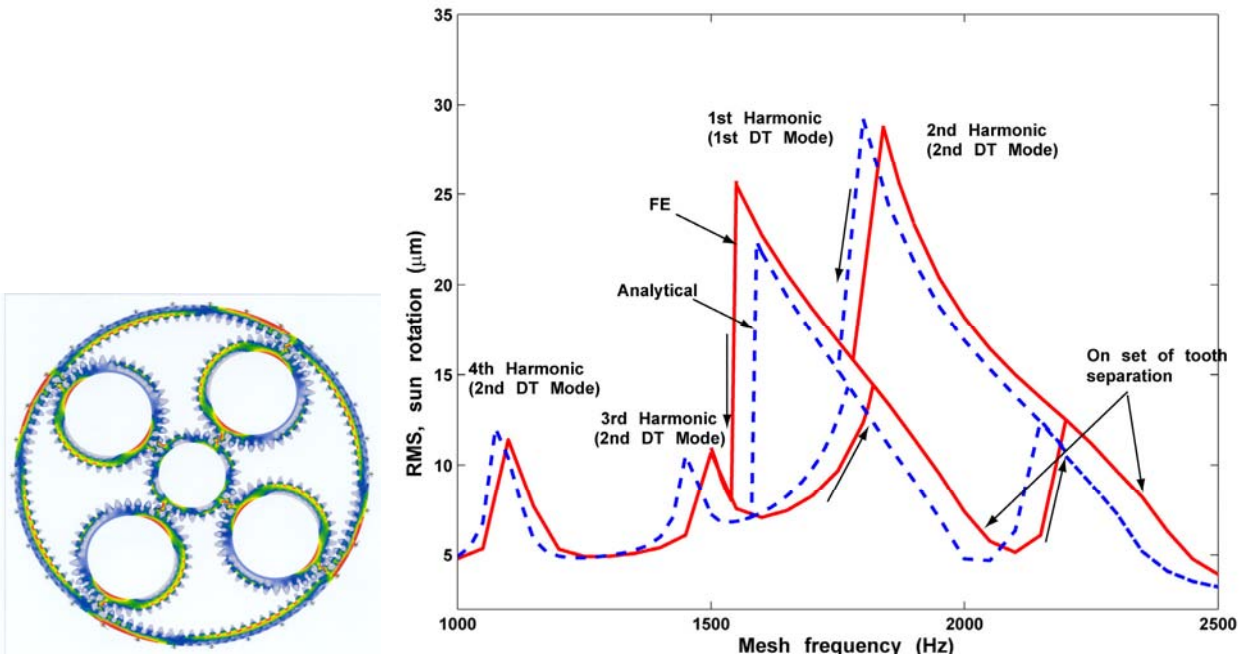

Figure 7.12. Comparison of analytically predicted gear-mesh dynamic phenomena with well-vetted FE predictions.

give simultaneous benefits of reduced mesh noise and increased load-carrying capacity. The theoretical predictions were borne out by experimental results conducted on highly instrumented modified tooth-profile gear sets, summarized in figure 7.13. The measured sound power results include two baseline gear sets plus two variations each of low-noise and low-stress gear-tooth modifications, and a final modified low-noise design. A 10- to 20-dB sound power reduction was predicted for the low-noise modifications, depending on transmitted torque level (and therefore gear-tooth load deflection), and that is fairly consistent with the experimental sound power measurements shown in figure 7.13a. The low-noise variations tested represented various compromises between near-perfect conjugate gear action and desired improvements in manufacturing details and load-carrying capacity. The stress measurements associated with baseline and selected high-strength and selected low-noise modifications are summarized in figure 7.13b; the measurements are actually pinion-tooth fillet stresses at five locations along the tooth under the maximum tooth-loading condition. The results are very close, within a few percentage points of predicted fillet stress levels for the various modifications. The important point is that the tooth modifications, made on the basis of theoretical gear-geometry modeling, provided substantial simultaneous improvements in both noise characteristics and load capacity.

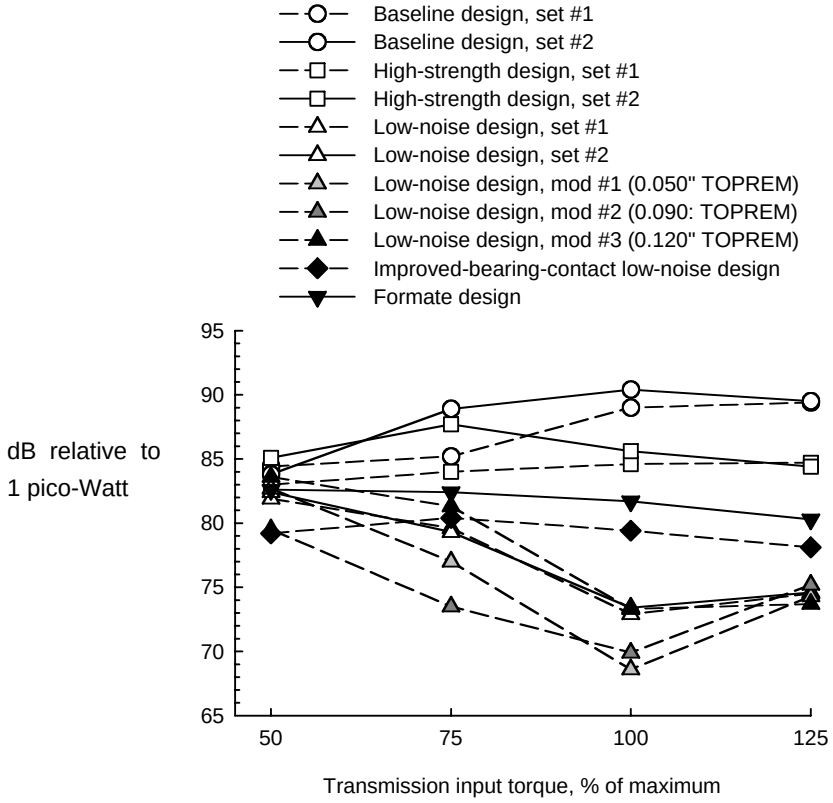

a) Sound power at spiral-bevel mesh frequencies

Figure 7.13. Effect of applying theoretically developed spiral-bevel gear-tooth modifications on gear-mesh noise and load capacity.

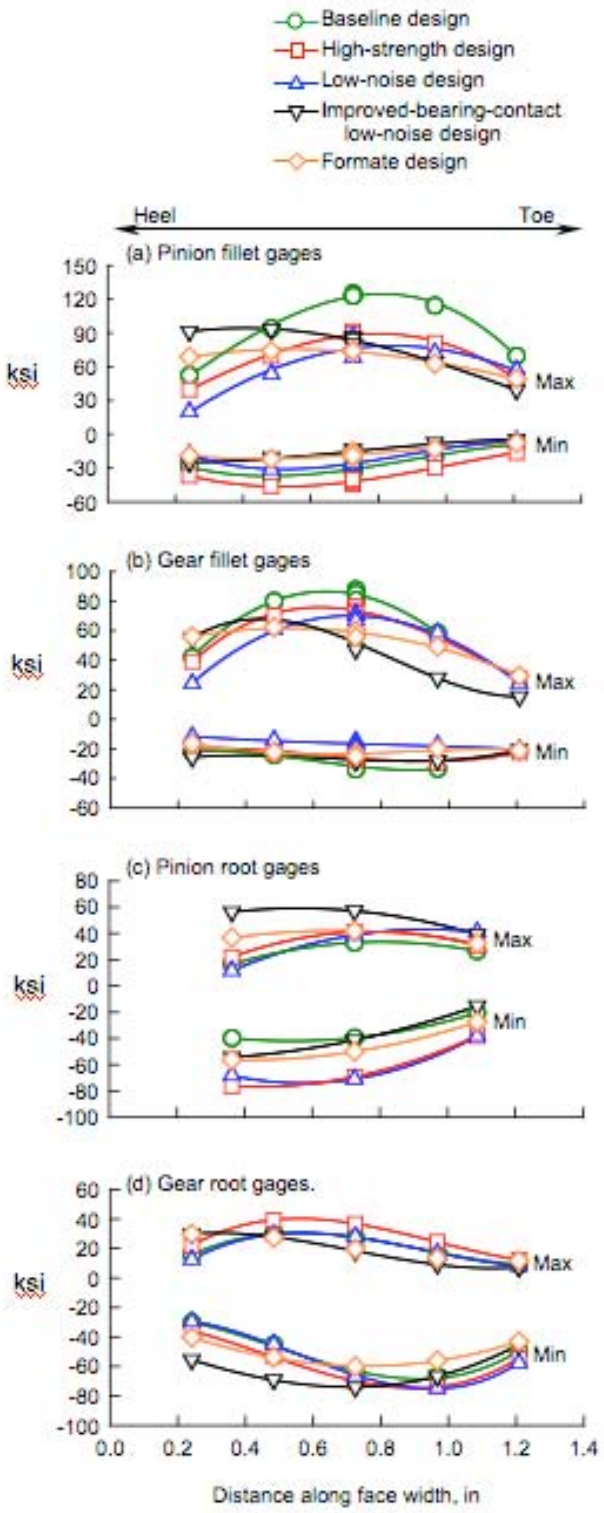

b) Maximum and minimum gear-tooth stress distribution along tooth-face width, static strain tests

Figure 7.13. Concluded.

Another example of component-level predictive capability is provided by Krantz et al. [1994]. An analytical model based on newly developed gear-mesh indexing theory was successfully applied to a split-torque transmission design, correcting a load-sharing developmental problem as illustrated in figure 7.14. The potential for power-density benefit associated with the split-torque transmission concept can be realized only if the power is shared nearly equally between the four paths shown in the example. In the prototype design with traditional synchronous meshing, mesh 3 was forced to carry about 10% more than its nominal 25% load share, while mesh 4 was about 10% underused. The concept of indexing shifts the timing of the gear meshes so that the net loading can be shared more uniformly, theoretically each mesh carrying 25% of the total loading. As can be seen in figure 7.14, experimental results showed only a slight deviation from the analytically predicted ideal load sharing, with mesh 3 being about 1% more highly loaded than ideal, and mesh 4 still about 1% underloaded. The slight discrepancy between the analytical prediction and the experimental result can be largely attributed to unaccounted-for deflections and misalignments in the drive train.

The previous three examples, represented by figures 7.12 through 7.14, are essential elements in addressing the ability to accurately predict power density, lubrication performance, and system life.

Advances have also been made in the analytical modeling of fatigue crack growth in gear-tooth roots by Lewicki [1995]. A 3-D linear elastic fracture mechanics code (FRANK 3-D) has been adapted to gear-tooth geometry and loads, and resulting analyses have successfully predicted crack-growth trajectories. The dependence of this crack-growth trajectory on certain gear-component structural parameters is a critical predictive feature from the standpoint of drive-system integrity and safety. The primary crack-trajectory issue of concern is whether the path originating at the tooth fillet extends through the tooth base, ultimately resulting in loss of a single tooth, or whether the path turns radially inward through the gear rim, ultimately resulting in catastrophic failure of the entire gear structure; the first situation is bad, but the second is inevitably catastrophic. FRANK 3-D based predictions compared with crack-growth experimental results are shown to be in excellent agreement in figure 7.15, particularly with regard to resolving those conditions (gear rim thickness, gear speed) that tend to promote the catastrophic through-rim crack trajectory. Accuracy in the ability to predict

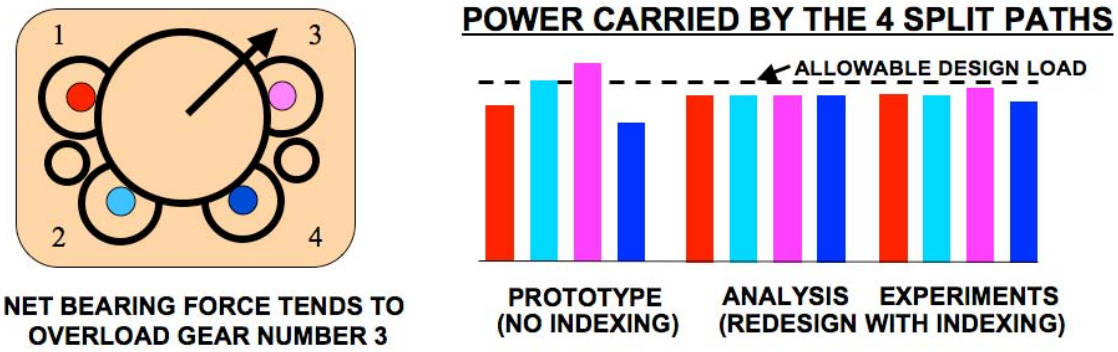

Figure 7.14. Improved torque split through mesh indexing.

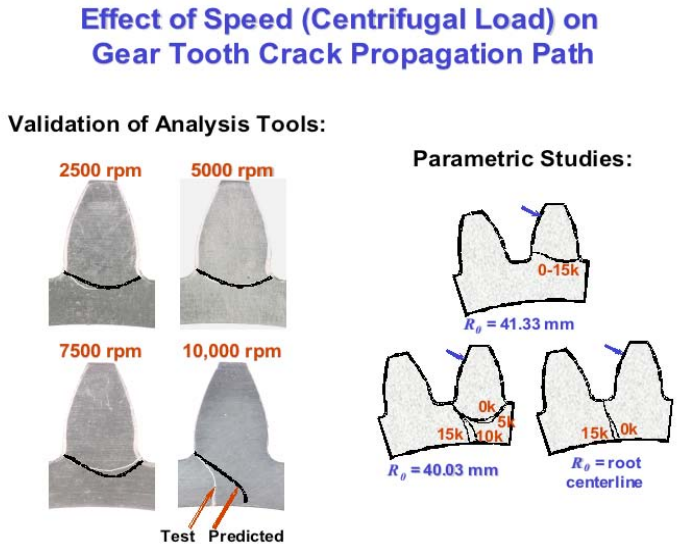

Figure 7.15. Comparison of analytically predicted and experimental gear root crack trajectories.

the threshold for transition from under-the-tooth to gear rim cracking depends, of course, on analytical meshing structure and the degree of structural fidelity represented in the FE model, but well-controlled experiments on laboratory gears have shown accuracy within a few percent in terms of gear rim thickness and gear rotational speed. The model and methodology have been accepted by American Gear Manufacturers Association as a basis for a new gear design standard.

All gears and bearings comprising the drive system operate in the elastohydrodynamic lubrication (EHL) regime. Traditional tools and models can accurately predict the lubricant film thickness separating the loaded surfaces (gear tooth, bearing surface) in relative motion under steady geometric and loading conditions where lubricant supply is not an issue. Highly loaded drive systems with variable-speed features and time-varying geometric distortions introduce conditions that the present EHL models are not equipped to handle.

The SOA in gear windage power-loss prediction is based on a simple empirical model derived from turbine disk aerodynamic drag data. The windage losses are embedded in an overall power-loss prediction, and development of the power-loss model has been heavily focused on gear and bearing tribological loss mechanisms. The windage part of the model has been calibrated (empirical constants defined) for simple spur gear/pinion meshes only. Analytical estimates of power losses for such simple meshes show windage contributions to be on the order of 10–15% of total losses at high pitch-line velocities [Anderson and Lowenthal, 1980]. Validation experiments conducted on planetary gear sets [Krantz and Handschuh, 1990] include loss contributions from carrier drag and complex epicyclic gear motion. In these situations, measured losses exceeded analytically predicted losses by as much as a factor of 2, as can be seen in figure 7.16. Though Krantz and Handschuh did not attribute the discrepancies to windage specifically, no doubt windage did play a significant role.

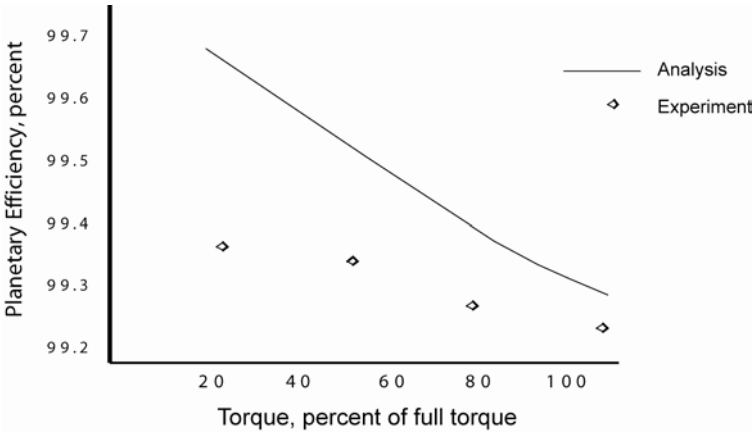

Figure 7.16. Comparison of analysis with experiment for planetary efficiency.

Plans for Improving Predictive Capability

Drive-system fundamental technology centers on gears, bearings, seals, and the transmission structures that support these mechanical components. Such technologies are mature and fairly well-understood based upon many decades of empirically based modeling corroborated and supplemented by analytical approaches. Despite advances in basic understanding, drive-system analytical tools are lacking in several key areas specific to and vital to advanced, high-power-density, highly reliable rotorcraft drive systems. For example, relationships between elastohydrodynamic film thickness, contact and bending fatigue, and gear surface finish are needed to develop accurate tools to design highly efficient drive systems with a high level of confidence. Another example of an advanced tool that is needed is an accurate gear-windage-prediction model. This prediction capability will be necessary as future transmissions will be run at higher operating temperatures with minimal lubrication. Power loss due to windage can be high, and the resulting heat load to the system requires additional cooling capacity that adds significant weight.

In addition, advanced diagnostics and prognostics technologies to detect and predict the health and usage of rotorcraft dynamic mechanical systems in the engine and drive system will be developed to address technology shortfalls in the current SOA. Although commercially available Health Usage Monitoring Systems (HUMS) are providing significant safety benefits when installed on rotorcraft, the fault detection success rate of today's helicopter health monitoring systems through vibration analysis is still in need of improvements. HUMS experience, documented by the Civil Aviation Authority, shows a success rate of 70 percent in detecting faults [McColl, 1997].

Over the past several decades, a number of diagnostic techniques have been developed to detect damage and abnormal conditions of the dynamic mechanical components in rotorcraft propulsion systems. A majority of the technologies developed are vibration based and focus on the gears, bearings and drive shafts of the main transmission system. Based on the physical phenomena of the rotating component interacting with its environment, specific fault patterns are produced in accelerometer vibration signatures for the component fault under investigation. Numerous condition indicators, the vibration characteristics extracted from these signatures, have been developed to characterize

component health: [Stewart, 1977], [Zakrajsek, 1989], [Zakrajsek et al. 1993], [Zakrajsek et al. 1994], [Howard, 1994], [Randall, 2001].

Multi-Sensor Data Fusion is another technique that has shown great promise for improving current HUMS performance. Similar to how we use our multiple senses to make decisions, data from multiple sensors of different measurement technologies are combined to make better decisions about the state of a system. Results from gear rig testing has shown integrating oil and vibration results in a health monitoring system with improved damage detection and decision-making capabilities as compared to using individual measurement technologies [Dempsey and Afjeh, 2004; Dempsey et al. 2006]. Some commercial HUMS use data fusion to integrate condition indicators into one health indicator that provides an overall assessment of the state of the component [Bechhoefer and Bernhard, A., 2004b; Bechhoefer, E., and Mayhew, E., 2006].

Usage monitoring, another important aspect of diagnostics and prognostics, consists of measuring torque, engine operating hours and flight hours to track usage of aircraft components. Flight regimes and environmental operating conditions can also be included. Limited work, correlating usage monitoring to diagnostics and prognostics, has been performed in this area: [Huff et al., 2000], [Bechhoefer and Bernhard, 2004a], [Vaughan and Tipps, 2008].

Further work is needed to achieve true condition-based maintenance and operational quality while increasing the safety of rotorcraft to that comparable to large fixed wing aircraft. To achieve these goals, the following technologies need to be developed [Zakrajsek et al., 2006]:

- Tools to increase fault detection coverage and decrease false alarm rates
- Technologies to accurately detect onset of failure and isolate damage, and assess severity of damage magnitude.
- Life prediction technologies to assess effects of the damage on the system and predict remaining useful life and maintenance actions required
- Integration of the health monitoring outputs with the maintenance processes and procedures
- Data management and automated techniques to obtain and process the diagnostic information with minimal specialist involvement
- System models, material failure models and correlation of failure under bench fatigue, seeded fault test and fielded data.
- Generic data collection and management scheme for analysis of operational data.

Developing these technologies will enable helicopter operators to obtain maintenance credits, increase the time between expensive overhauls, and facilitate using HUMS as a practical tool for on-condition maintenance.

Beyond the component level, there is a need for a system-level analytical tool capable of predicting dynamic loads arising from rotor lead/lag excitations, engine control oscillations, and nonlinear time-varying effects resulting from couplings, shaft dynamics, and mesh loads. Under a NASA-sponsored research program, a Simulink-based approach is being developed incorporating structural

dynamic models of the drive-system components and addressing unique excitations and nonlinearities that are encountered when rotor-speed variations of up to 50% are realized.

An assessment will be performed to determine tools and technologies currently available to predict fatigue, life, durability, etc., of drive systems and related components. Based on the assessment, specific tools and technologies will be developed in the areas of gear bending and surface-fatigue modeling, online gear-damage-magnitude assessment, gear windage power-loss prediction model, gear-life models, and surface-lubrication-technology development. These fundamental model and technology development efforts will be validated using experimental data from gear surface and bending-fatigue component test facilities (fig. 7.10). The improved drive lubrication model will be validated in the high-speed gear test facility at the Glenn Research Center. Tests in the high-speed gear facility will also be used to validate improved lubrication concepts capable of at least 2x life extension at loss of lubrication conditions.

Predictive (analytical) testing initiated in 2007 includes NASA-funded efforts in 3-D CFD modeling of a gearbox to investigate windage losses associated with high-speed operation and dynamic mechanical-system modeling of the propulsion system to include variable or multispeed drive systems and variable-speed gas turbine engines. These efforts will provide tools necessary to improve gear-system performance and minimize dynamic sensitivity of future rotorcraft propulsion systems.

Development of a unique gear windage test facility is under way with 2x current SOA for gear pitch-line velocity maximum used in typical aerospace applications. This facility will enable the systematic study of the effect of internal gearbox geometry, structure, and features on windage-related energy-loss mechanisms.

The Variable/Multi-Speed Drive System Simulator Test Facility is under development for testing concepts on a scaled version of a propulsion system with respect to speed, inertias, etc. to make a reasonable assessment of concepts for future rotorcraft operation.

A High Load Contact Fatigue Test Rig is under development to permit testing at higher contact stress levels necessary for enhanced materials, coatings, and manufacturing methods that will require high loading to develop fatigue data of future enhancements.

Validation Data Requirements

The data generated by the existing and planned test facilities at NASA will be necessary for validation of the enhanced analytical capabilities that have been initiated under NASA funding. These test facilities along with those existing at our university partners will provide the required validation test data that will enhance user confidence when applying existing and new analytical capabilities to current and future drive systems.

Cross-Cutting Technology Needs

As was the case for engine technologies, the inertial and dynamic effects associated with variable-speed drive systems will have to be incorporated into the overall flight control architecture. Also, overall drive-system layout and structural-support requirements will need to be addressed under airframe-structure disciplines.

Windage-loss modeling associated with the drive-system mechanical elements will use some of the CFD modeling tools developed for engine components and main rotor/airframe components, particularly for turbulence modeling and gridding schemes.

SUMMARY

NASA rotorcraft propulsion research is comprised of two major parts: engines and drive systems. The engine research focuses on ways of achieving high power density and wide operating range to meet the NASA rotorcraft performance requirements. Three key developmental thrusts are essential to the engine research: concepts to extend the stable operating range of highly loaded compressors; development of wide-speed-range power turbine concepts; and development of oil-free bearing technology to enable application of airfilm foil bearings to future turboshaft engines.

An array of CFD tools is in hand to support turbomachinery component and concept-level development. These tools do need some enhancement though: an expanded validation envelope addressing compressor operation near stability limit, with and without active stall control; and improved approaches to grid generation and turbulence modeling consistent with local flow phenomena associated with component details. In addition, for airfilm foil bearing development, analytical models need to be developed and validated, incorporating the latest foil bearing material and support structure concepts along with air film lubrication principles. These foil bearing models must be incorporated into engine-system structural dynamic models. NASA rotorcraft program elements are in place addressing these CFD and air film bearing requirements.

Drive-system component-level modeling is a well-developed area with reliable models describing gear and bearing performance (life, mesh loads, structural reaction loads) under prescribed, steady input load and speed conditions. What is needed is a high-fidelity system-modeling capability. At the system level, dynamic and transient loads and nonlinearities associated with coupled rotor blade lead/lag dynamics, inertias, and loading nonlinearities arising from meshing loads and mechanical couplings, and interconnecting shaft dynamics all have to be modeled together as an integral system. Especially challenging are variable-speed requirements from the standpoints of both drive-system conceptual complexity and added dynamic and nonlinearity issues. NASA rotorcraft propulsion plans address these issues at the conceptual modeling level.

REFERENCES

Adamczyk, J. J.; Hathaway, M. D.; Shabbir, A.; and Wellborn, S. R.: Numerical Simulation of Multi-Stage Turbomachinery Flows. RTO Applied Vehicle Technology Panel (AVT) Symposium, AGARD Propulsion and Energetics Panel (PEP), Toulouse, France, May 11–15, 1998.

Adamczyk, J. J.: Aerodynamic Analysis of Multistage Turbomachinery Flows in Support of Aerodynamic Design. IGTI Scholar Lecture, ASME Paper no. 99-GT-80, J. Turbomachinery, vol. 122, no. 2, Dec. 2000.

Agrawal, G. L.: Foil Air/Gas Bearing Technology – an Overview. ASME Paper no. 97-GT-347, 1997 International Gas Turbine and Aeroengine Congress, Orlando, Fla., June 2–5, 1997.

Ambarisha, V. K., and Parker, R. G.: Nonlinear Planetary Gear Dynamics Using Analytical and Finite Element Models. J. Sound and Vibration, 2007, vol. 302, no. 3, pp. 577–595.

Anderson, N. E., and Lowenthal, S. H.: Spur-Gear Systen Efficiency at Part and Full Load. NASA/TP-1622, Feb. 1980.

Bechhoefer, E., and Bernhard, A. P. F.: Setting HUMS Condition Indicator Thresholds by Modeling Aircraft and Torque Band Variance. Proc. 2004 IEEE Aerospace Conference, Big Sky, Mont., March 6–13, 2004a.

Bechhoefer, E., and Bernhard, A. P. F.: HUMS Optimal Weighting of Condition Indicators to Determine the Health of a Component. Proc. AHS 60th Annual Forum, Baltimore, Md., vol. 60, no. 1, May 7–10, 2004b.

Bechhoefer, E., and Mayhew, E.: Mechanical Diagnostics System Engineering in IMD–HUMS. Proc. 2006 IEEE Aerospace Conference, Big Sky, Mont., July 14, 2006.

Chima, R. V., and Liou, M. S.: Comparison of the AUSM+ and H-CUSP Schemes for Turbomachinery Applications. NASA/TM–2003-212457, June 2003.

Chima, R. V.: A Three-Dimensional Unsteady CFD Model of Compressor Stability. NASA/TM-2006-214117, Feb. 2006.

Day, I. J.: Stall Inception in Axial Flow Compressors. ASME J. Turbomachinery, vol. 115, no. 1, Jan. 1993, pp. 1–9.

DellaCorte, C., and Valco, M. J.: Load Capacity Estimation of Foil Air Journal Bearings for Oil-Free Turbomachinery Applications. STLE Tribol. Trans., vol. 43, no. 4, 2000, pp. 795–801.

DellaCorte, C.; Radil, K. C.; Bruckner, R. J.; and Howard, S. A.: A Preliminary Foil Gas Bearing Performance Map. NASA/TM–2006-214343, Oct. 2006.

Dempsey, P. J., and Afjeh, A. A.: Integrating Oil Debris and Vibration Gear Damage Detection Technologies Using Fuzzy Logic. J. Amer. Hel. Soc., vol. 49, no. 2, April 2004.

Dempsey, P. J.; Kreider, G.; and Fichter, T.: Tapered Roller Bearing Damage Detection Using Decision Fusion Analysis. NASA/TM–2006-214380, July 2006.

Denton, J.: Lessons from Rotor 37. Presented at the Third International Symposium on Experimental and Computational Aerothermodynamics of Internal Flows (ISAIF), Beijing, China, Sept. 1–6, 1996.

Dunham J.: CFD Validation for Propulsion System Components. AGARD AR-355, May 1998.

Hah, C.; Bergner, J.; and Schiffer, Heinz-Peter: Short Length Scale Rotating Stall Inception in a Transonic Axial Compressor—Criteria and Mechanism. Paper no. GT2006-90045. ASME Turbo Expo 2006, Barcelona, Spain, May 8–11, 2006.

Hathaway, M. D.; Gertz, J.; Epstein, A.; and Strazisar, A. J.: Rotor Wake Characteristics of a Transonic Axial Flow Fan. AIAA Journal, vol. 24, no. 11, Nov. 1986, pp. 1802–1810.

Hathaway, M. D.; Chriss, R. M.; Wood, J. R.; and Strazisar, A. J.: Experimental and Computational Investigation of the NASA Low-Speed Centrifugal Compressor Flow Field. ASME J. Turbomachinery, vol. 115, no. 3, July 1993, pp. 527–542.

Hathaway, M. D.; Chriss, R. M.; Strazisar, A. J.; and Wood, J. R.: Laser Anemometer Measurements of the Three-Dimensional Rotor Flow Field in the NASA Low-Speed Centrifugal Compressor. NASA/TP-3527, June 1995.

Hathaway, M. D., and Wood, J. R.: Application of a Multi-Block CFD Code to Investigate the Impact of Geometry Modeling on Centrifugal Compressor Flow Field Predictions. ASME J. Turbomachinery, vol. 119, Oct. 1997, pp. 820–830.

Hathaway, M. D.: Passive Endwall Treatments for Enhancing Stability. Lccture Series 2006-06, Advances in Axial Compressor Aerodynamics, von Karman Institute for Fluid Dynamics, ed: Denos, R. and Broukaert, J.-F., May 15–18, 2006. NASA/TM–2007-214409, ARL-TR-3878, July 2007.

Heshmat, H., and Hermel, P.: Compliant Foil Bearings Technology and Their Application to High Speed Turbomachinery. Thin Films in Tribology, Elsevier Science Publ. B. V., 1993, pp. 559–575.

Howard, I.: A Review of Rolling Element Bearing Vibration "Detection, Diagnosis and Prognosis." DSTO Aeronautical and Maritime Research Laboratory, DSTO–RR–0013, Oct. 1994.

Howard, S.; DellaCorte, C.; Valco, M.-J.; Prahl, J.-M.; and Heshmat, H.: Dynamic Stiffness and Damping Characteristics of a High-Temperature Air Foil Journal Bearing. STLE Tribol. Trans., vol. 44, no. 4, 2001, pp. 657–663.

Huff, E. M.; Tumer, I. Y.; Barszcz, E.; Lewicki, D. G.; Decker, H.; and Zakrajsek, J. J.: Experimental Analysis of Mast Lifting and Bending Forces on Vibration Patterns Before and After Pinion Reinstallation in an OH-58 Transmission Test Rig. AHS 56th Annual Forum, Virginia Beach, Va., May 2–4, 2000.

Kish, J.: Vertical Lift Drive System Concept Studies: Variable Speed/Two-Speed Transmissions. Final Report. NASA/CR–2002-211564, June 2002. [Limited Distribution]

Krantz, T. L., and Handschuh, R. F.: Efficiency Study Comparing Two Planetary Reduction Stages. NASA/TM-83740, AV5COM TM 90-C-005, 1990.

KrantZ, T. L.; Rashidi, M.; and Kish, G. J.: Split Torque Transmission Load Sharing. Proc. of The IMechE-PartG: J. Propulsion and Power, vol. 208, no. 2, 1994, pp. 137–148.

Lewicki, D. G.: Crack Propagation Studies to Determine Benign or Catastrophic Failure Modes for Aerospace Thin Rim Gears. Dissertation, Case Western Reserve University, May 1995 (also NASA/TM-107170, May 1996).

Lewicki, D. G.; Woods, R. L.; Litvin, F. L.; and Fuentes, A.: Evaluation of Low-Noise Formate Spiral-Bevel Gear Set. Proceedings of the ASME 2007 IDET/CIE, 2007, and NASA/TM–2007-215032 and ARL-TR-4135, Dec. 2007.

Mazumder, Q. H.: Preliminary Assessment of Turbomachinery Codes. Final Report. NASA/CR–2007-214687, Mar. 2007.

McColl, J.: Overview of Transmissions HUM Performance in UK North Sea Helicopter Operations. Rotorcraft Transmission Systems Health Monitoring Seminar S553, UK Civil Aviation Authority, Institution of Mechanical Engineers, London, England, Nov. 18, 1997.

Skoch, G. J., et al.: Laser Anemometer Measurements of the Flow Field in a 4:1 Pressure Ratio Centrifugal Impeller. ASME Paper no. 97-GT-342, ASME International Gas Turbine and Aeroengine Congress, Orlando, Fla., June 2–5, 1997.

Stevens, M. A.; Handschuh, R. F.; and Lewicki, D. G.: Concepts for Variable/Multi-Speed Rotorcraft Drive System. NASA/TM-2008-215276, ARL-TR-4564, Sept. 2008.

Stewart, R. M.: Some Useful Data Analysis Techniques for Gearbox Diagnostics. Machine Health Monitoring Group, Institute of Sound and Vibration Research, University of Southhampton, Report MHM/R/10/77, July 1977.

Strazisar, A. J.; Wood, J. R.; Hathaway, M. D.; and Suder, K. L.: Single Stage Transonic Fan Rotor. Test Cases for Computation of Internal Flows in Aero Engine Components, AGARD Advisory Report 275, 1990.

Suder, K. L.; Strazisar. A. J.; Adamczyk, J. J.; Hathaway, M. D.; and Okiishi, T. O.: Measurements of the Unsteady Flow Field Within the Stator Row of a Transonic Axial-Flow Fan, Part I: Measurement and Analysis Techniques. ASME Paper no. 87-GT-226, ASME Gas Turbine Conference, Anaheim, Calif., May 31–June 4, 1987.

Townsend, D. P.; Coy, J. J.; and Zaretsky, E.V.: Experimental and Analytical Load-Life Relation for AISI 9310 Steel Spur Gears. J. Mechanical Design, vol. 100, no.1, 1978, pp. 54–60.

Townsend, D. P.: Status of Understanding for Gear Materials. Tribology In The 80's, vol. 2, 1983, pp. 795–609; also NASA-CP-2300, vol. 2, Aug. 1984.

Townsend, D. P., and Shimski, J.: Evaluation of EHL Film Thickness and Extreme Pressure Additives on Gear Surface Fatigue Life. NASA/TM-106663, July 1994.

VanZante, D. E.; Strazisar, A. J.; Wood, J. R.; Hathaway, M. D.; and Okiishi, T. H.: Recommendations for Achieving Accurate Numerical Simulation of Tip Clearance Flows in Transonic Compressor Rotors. ASME J. Turbomachinery, ASME 99-GT-390, vol. 122, Oct. 2000, pp. 733–742.

Vaughan, R. E., and Tipps, D. O.: A Condition Based Maintenance Approach to Fleet Management. AHS CBM Specialists' Meeting, Huntsville, Ala., Feb. 12−13, 2008.

Wisler, D. C.; Denton, J. D.; and Strazisar, A. J.: Rotor 37 Blind Test Case. ASME/IGTI International Gas Turbine Conference, The Hague, The Netherlands, 1994.

Zakrajsek, J. J.: An Investigation of Gear Mesh Failure Prediction Techniques. NASA TM–102340, AVSCOM TM 89–C-005, Nov. 1989.

Zakrajsek, J. J.; Townsend, D. P.; and Decker, H. J.: An Analysis of Gear Fault Detection Methods as Applied to Pitting Fatigue Failure Data. Proc. 47th Mtg. Mechanical Failures Prevention Group, Office of Naval Research, Virginia Beach, Va., April 13–15, 1993, pp. 199–208. (Also Nasa TM-105950, AVSCOM TP 92-C-035, April 1993.)

Zakrajsek, J. J.; Handschuh, R. F.; and Decker, H. J.: Application of Fault Detection Techniques to Spiral Bevel Gear Fatigue Data. Proc. 48th Mtg. Mechanical Failures Prevention Group. Office of Naval Research, Wakefield, Mass., April 19–21, 1994, pp. 93–104. (Also Nasa TM-106467, Army RLM-ARL-TR-345, April 1994.)

Zaretsky, E. V. (Editor): Tribology for Aerospace Applications. STLE Publication SP-37, Society of Tribologists and Lubrication Engineers, Park Ridge, Ill., Sept. 1997, p. 851.

Zaretsky, E.V.: Bearing and Gear Steels for Aerospace Applications. In Advanced Materials in Aerospace Applications, ASM International, Materials Park, Ohio, 1990, pp. AIV 1–15.

CHAPTER 8

STRUCTURES AND MATERIALS

Gary D. Roberts,[1] Ramakrishna T. Bhatt,[2] Peter J. Bonacuse,[2] Robert G. Bryant,[3] Michael C. Halbig,[2] Karen E. Jackson,[3] Wade C. Jackson,[3] James C. Johnston,[1] Maria A. Kuczmarski,[1] Robert A. Miller,[1] Thomas K. O'Brien,[3] Ignacy Telesman,[1] and Dongming Zhu[1]

ACRONYMS

ALE	arbitrary Lagrange-Euler
ATD	anthropomorphic test devices
BVI	barely-visible impact
CAI	compression after impact
CARES	Ceramic Analysis and Reliability Evaluation of Structures
CFD	computational fluid dynamics
CMAS	calcium magnesium aluminosilicate
CMC	ceramic matrix composites
CVD	chemical vapor deposition
EA	energy absorber
EBC	environmental barrier coating
EB-PVD	electron beam-physical vapor deposition
EFG	element-free Galerkin
HPBR	High Pressure Burner Rig
LandIR	Landing and Impact Research Facility
PM	powder metallurgy
PS	plasma spray
RF	resorcinol-formaldehyde
SAE	Society of Automotive Engineering
SARAP	Survivable, Affordable, Reparable, Aircraft Program
SFC	specific fuel consumption
SPH	smoothed particle hydrodynamic

[1] NASA Glenn Research Center.
[2] U.S. Army Research Laboratory.
[3] NASA Langley Research Center.

SSEA	specific sustained energy absorption
TBC	thermal barrier coating
TE	thermal etching
UEET	Ultra-Efficient Engine Technology

INTRODUCTION

Current structures and materials research in NASA aeronautics is directed toward advancements in technology that are needed to enable or improve the performance of future subsonic, supersonic, and hypersonic aircraft. Although advancements in structures and materials technology often benefit multiple vehicle types, NASA rotorcraft research is focused on six technology areas that are unique to rotorcraft or are likely to be applied primarily in future rotorcraft. This report describes the state of the art for each of these six areas. Discussions with the rotorcraft industry to identify opportunities for collaboration and to identify additional critical technology areas for future rotorcraft are a continuing process. Interactions with academia are also key in identifying new research that could lead to advanced structures, materials, and analysis methods for rotorcraft. An important goal of NASA is to integrate research from several discipline areas in large-scale technology demonstration tests. Within NASA rotorcraft, the Structures and Materials discipline works closely with the Acoustics discipline for this purpose, with increasing interactions with Propulsion and other disciplines. Opportunities for collaboration with the Department of Defense and industry on demonstration tests are also desirable.

Current research within the NASA rotorcraft Structures and Materials discipline can be divided into the two general areas of propulsion materials and airframe structures and materials. While this division is convenient for this report, there is overlap in some propulsion and airframe technologies. As an example, interior cabin noise is treated as an airframe issue in this report, even though the noise originates in the transmission and propulsion system and then propagates through the airframe structure to the cabin. Cabin noise is therefore affected by how the transmission and propulsion system are integrated with the airframe. Integration is mainly performed by the rotorcraft manufacturer; however, engine manufacturers are increasingly involved in this aspect of system integration. Propulsion-system integration with the airframe will be an important part of future research within the Structures and Materials discipline.

The remainder of this chapter describes research areas within propulsion materials and air frame structures and materials. In each of these major topic areas, current predictive and modeling tools within NASA are discussed. Examples of predictive and testing capabilities are provided in addition to a discussion of planned improvements in capabilities.

PROPULSION MATERIALS

Critical properties for materials used in rotorcraft propulsion systems are determined by the unique rotorcraft mission cycle and operating environment. Rotorcraft perform mostly short-duration flights, resulting in frequent thermal and mechanical cycling of engine components. Maneuvers, hovering, and lifting require frequent high-speed excursions and highly loaded engine conditions that cause high cyclic stresses in rotating components. Takeoff and landing at unimproved sites and operation at low altitude expose the engine to a high concentration of particulates that cause severe erosion of materials and structures in the engine flow path. Resistance to erosion, durability under conditions of severe cyclic loading, and durability under low-cycle fatigue are therefore critical properties for rotorcraft propulsion materials. In addition, lifing methods for rotating components must account for this complex thermal and mechanical loading cycle. Research in the Structures and Materials discipline is focused on development of improved materials and development of improved analysis methods for predicting the life of engine components made with the advanced materials. This research is needed to improve the performance of future rotorcraft engines. The fuel efficiency, power density, and durability of turboshaft engines currently used in rotorcraft propulsion systems are not as advanced as larger fixed-wing aircraft turbofan engines. Rotorcraft turbine engines have been improved in recent years because of advances in propulsion-materials technology. The pressure ratio for state-of-the-art small turboshaft engines has reached approximately 20 to 1 primarily by using integral compressor bladed disks (blisks) made by the powder metallurgy process with nickel-base alloys. An improved machined-ring configuration combustor technology; new materials for the turbine disk, shroud, and blade; and thermal barrier coatings have also been incorporated in the turboshaft engines. As a result, the engine total power has nearly doubled, giving an overall power-to-weight ratio of 5 shaft hp (shp) per pound. Specific fuel consumption (SFC) has also been reduced to approximately 0.45 lb/shp-h. The use of integrally bonded turbine blade and disk rotor technology can further significantly reduce disk weight and improve engine performance. Even with these advancements, only 33 percent of the theoretical Brayton cycle limit has been achieved in modern small turboshaft engines. There remains substantial potential for improvement beyond the state of the art. It is expected that small turboshaft engine efficiency can be further improved by 30 percent within the next decade if the overall pressure ratios can be increased into the range of 25:1 to 30:1 and the turbine inlet temperature can be increased into the range of 2800 to 3000 °F using advanced materials. This process will require a combination of new technologies, including higher temperature (up to 1500 °F capability) high-strength compressor disk materials, improved high-temperature turbine-disk and turbine-blade alloys, and low-conductivity thermal-barrier coatings with significantly higher temperature capability and improved erosion resistance over those at present. Even greater improvements are possible if the technology readiness level can be increased for lightweight, high-temperature Si3N4 monolithic ceramics and SiC/SiC ceramic matrix composites (CMCs) that can be fabricated into engine shrouds, vanes, combustor liners, and other components. In addition to advancements in materials, reliable lifing methods are needed before these advanced materials can be used in commercial engines. Research on propulsion materials in the Structures and Materials discipline is focused on three of these critical propulsion materials technologies: life-prediction methods for powder metallurgy turbine-disk alloys; erosion-resistant thermal-barrier coatings for turbine blades; and ceramic materials, including environmental-barrier coatings for Si3N4 monolithic ceramics and fabrication methods for SiC/SiC CMCs. Research in these technologies is described next.

Life-Prediction Methods for Powder Metallurgy Turbine-Disk Alloys

Although exceedingly rare, inclusion-initiated damage in advanced powder metallurgy (PM) alloys typically exhibit the lowest fatigue lives in specimen tests. A typical alloy characterization (on the order of several hundred fatigue tests) may not be sufficient to fully characterize (or even reveal) this failure mechanism. Therefore, to assess this failure mechanism, some means of characterizing the occurrence rate, size distribution, and effect on fatigue life of inherent inclusions is necessary. Rotorcraft are more susceptible to this type of damage because more partial cycles (throttle excursions) are accumulated in the varied missions and uses compared with fixed-wing aircraft.

Current tools available or in development at NASA

There are no commercially available tools to assess the reliability of turbine-disk components for inclusion-initiated damage. Many, if not all, of the engine manufacturers have at least incipient research efforts in probabilistic modeling of inclusion- and surface-damage-initiated failure mechanisms. These research efforts are proprietary and not widely shared within the industry or with the government and academia. The DARWIN code from Southwest Research Institute is the closest available technology. The code was developed in the wake of the 1989 crash of a United Airlines DC-10 in Sioux City, Iowa. The primary cause of this event was determined to be the catastrophic fatigue failure of a titanium fan disk initiated by a “hard-alpha” inclusion that had avoided detection. Although many of the capabilities of the DARWIN code might be applied to the turbine-disk-inclusion failure mode, numerous aspects require additional research and characterization.

A probabilistic code developed at NASA Glenn Research Center calculates the distribution of expected fatigue lifetimes for fatigue specimens given the stress range, R (minimum stress divided by maximum stress in the loading cycle), the expected inclusion occurrence rate (per unit volume), and the characterized inclusion size distribution. This code has been validated for relatively small samples of “seeded” fatigue specimens. Generally the code does a good job in predicting fatigue lives when cracks are initiated internally or when the surface initiation life is relatively short. However, for conditions that result in surface initiations in a moderate strain range ($\Delta\varepsilon$) or low-R-ratio regime, the model tends to underpredict the fatigue life of the fatigue specimens (fig. 8.1). The effect of surface residual stress from machining, which is currently not accounted for, is the primary suspect for this discrepancy. In summary, this code provides a useful analytical basis for quantifying the effect of inclusion-related failure rate of powder metallurgy superalloy disk materials, but a complete predictive methodology requires quantitative assessment of defect occurrence and morphology, as well as process-related residual stresses.

Examples of current predictive and testing capabilities

The state of the art in testing and validation of inclusion initiation models is the practice of “seeding” the precursor powder with a fully characterized sample of simulated inclusions designed to mimic the morphology and behavior of naturally occurring inclusions.

$\Delta\varepsilon$ = 0.6, R = 0

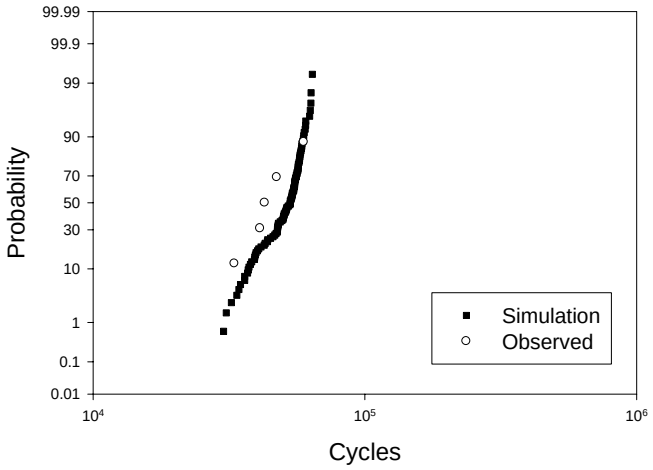

a)

$\Delta\varepsilon$ = 0.6, R = -1

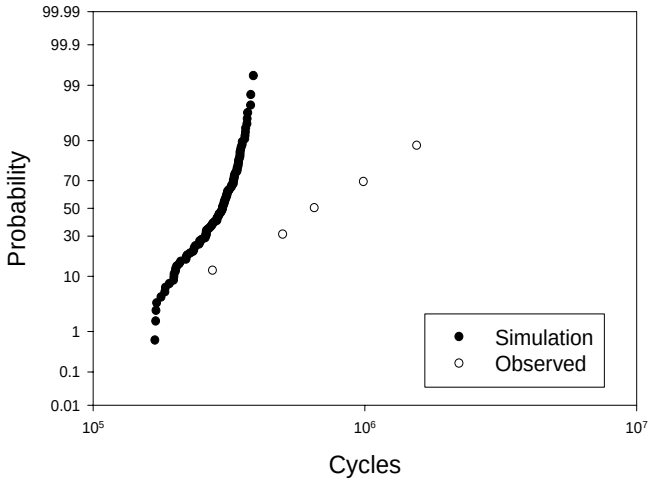

b)

Figure 8.1. Comparison of fatigue life of “seeded” fatigue test bars with the simulated crack propagation lives using the distribution of the simulated largest inclusion in the test bar as the starting crack size.

A significant number of seeded specimens has been tested to investigate the effects of size distribution, inclusion type, and forging strains [Barrie et al., 2005; Bonacuse et al., 2004; Kantzos et al., 2003; Bonacuse et al., 2002; Gabb et al., 2002; and Bonacuse et al., 2001]. Several types and size distributions have been introduced into the model alloy, Udimet 720. Experiments covering a range of strain amplitudes, temperatures, R ratios, and specimen sizes have been performed, including interrupted experiments where the inclusion-initiated crack growth was monitored. The reliability of gas turbine components will be accurately modeled when the fatigue life distribution (central tendency and dispersion) of inclusion-initiated specimen failures can be adequately replicated using an approximated inclusion size distribution and failure-mechanics solutions to simulate the propagation to failure. This replication will require the measurement and modeling of residual stress (from machining, surface processing, overstress, etc.) on crack growth rate, particularly at microstructurally small (on the order of the grain size) crack sizes. When a 90-percent confidence interval, calculated using the simulated fatigue life distribution, captures all of the observed specimen lifetimes, then the life model will adequately represent the failure mechanisms observed.

Plans for improving predictive and testing capabilities

Improvements to the probabilistic modeling code include adapting the current model for prediction of component life distributions given the component geometry and stress distribution from finite-element models. A research code has been developed to display the relative probability of failure in a rotorcraft disk. Code has been incorporated and tested that reads the temperature distribution from the finite-element model as well as a function that takes data from crack growth experiments performed at various temperatures and performs a fit returning a temperature-adjusted crack growth rate. Over the range of temperatures that the disk experiences in service, the crack growth rate for the model alloy varies by a factor of two and a half.

A visualization tool has been incorporated that allows the distribution in the probability of failure in the component to be displayed. Figure 8.2 compares the stress and temperature distribution in a sector model of a second-stage gas generator turbine disk with the relative probability of failure from an inclusion-initiated crack (at 5000 cycles).

Note that, as expected, the probability of failure tends to be high where the stress is highest (at the bolt holes), but the model also identifies the disk bore, the circumferential fillet below the bolt holes, and the base of the fir trees as locations of relatively high failure probability.

The sensitivity of the probability of failure to the crack growth rate and the size and frequency of the inclusions has been probed and found to be highly dependent on these parameters. Because the current incarnation of the probabilistic disk reliability-prediction code uses the volume of the finite elements to calculate the probability of failure, the sensitivity of the probabilistic model to variations in mesh-generation choices will be examined. The code will also be optimized for speed of calculation. The effect of forging strain on inclusion breakup and orientation must also be incorporated into the full disk model. Further model improvement will incorporate the effect of residual stresses on crack growth behavior. These code enhancements are expected to result in substantial improvements in quantified probabilistic predicted lifetimes and predictive confidence levels for powder metallurgy superalloy disks.

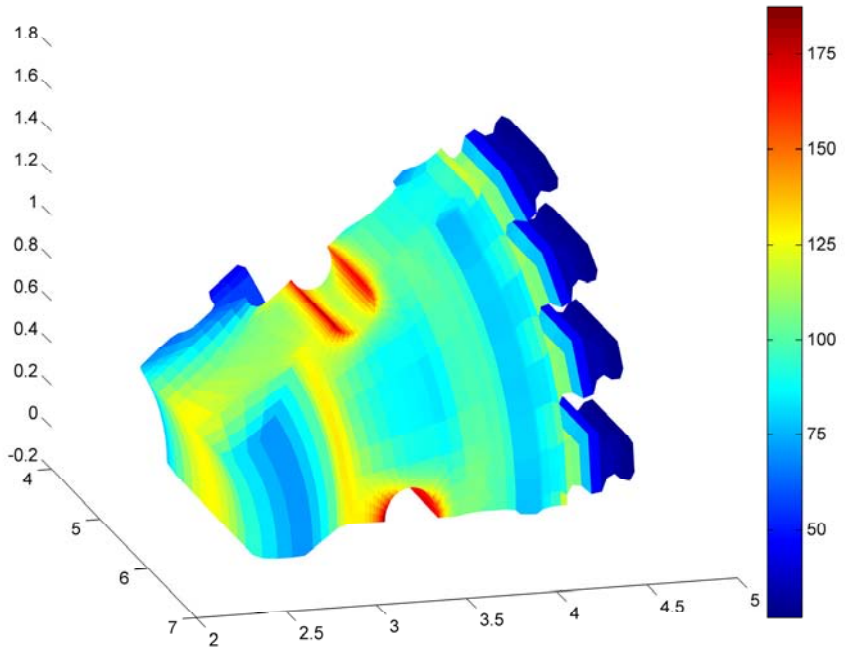

a)

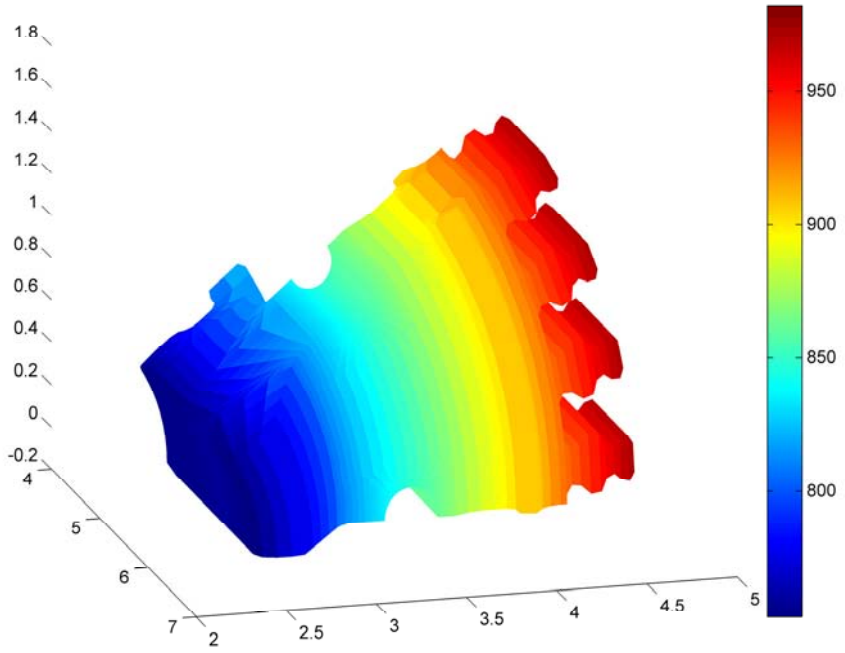

b)

Figure 8.2. Comparison of (a) stress distribution in ksi and (b) temperature profile in °F with (c) probability of failure due to an inclusion-initiated crack, exponential scale—powers of 10, for a turboshaft engine disk.

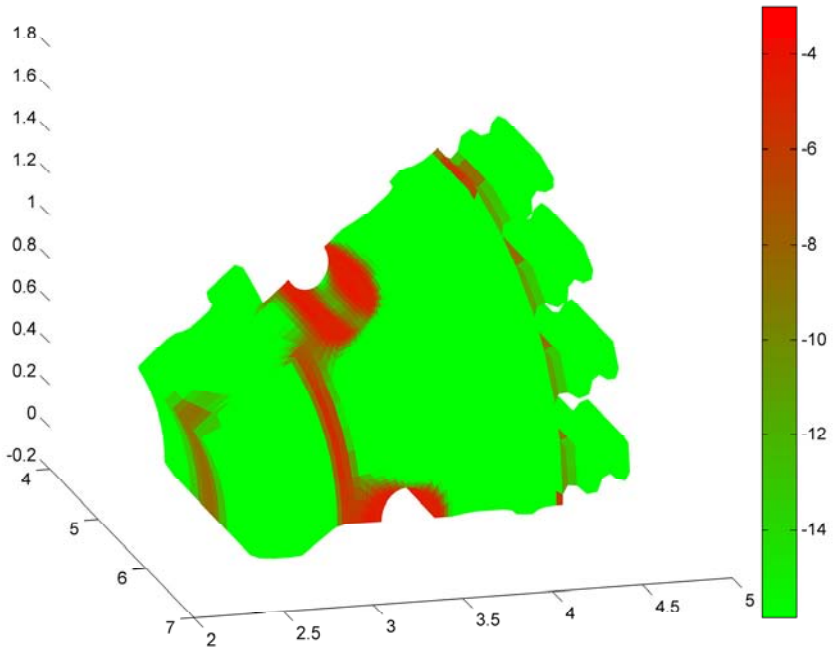

c)

Figure 8.2. Concluded.

Validation data requirements

Testing of full-scale components under realistic operating conditions is necessary to fully validate the models. Coupon testing cannot fully capture the effect of stress gradients and component geometry on crack initiation and propagation. Capturing the effects is typically accomplished by performing cyclic (repeated excursions from 0 to maximum engine operating speed) spin-pit testing of turbine disks. Artificial flaws may be introduced in these tests to facilitate crack propagation validation studies. As NASA does not possess spin-pit capability, other government or contractor facilities will have to be used. In addition, continued testing of seeded coupons will continue to improve our understanding of the effect of various processing parameters on the fatigue life distribution from this failure mechanism.

Cross-cutting technology needs

Machined surfaces have also been identified as a source of premature fatigue crack initiation. Machining practice may synergistically interact with inclusion-initiated cracking. Current plans call for exploration of the effect of machining parameters on the crack initiation behavior of a representative disk alloy. In addition, alloy development continues to improve the crack growth resistance of these materials at elevated temperatures. This development is critical to improving the reliability of these components.

Erosion-Resistant Thermal Barrier Coatings for Turbine Blades

Rotorcraft engines routinely operate in conditions significantly more particle-laden than those usually experienced by other types of engines. For example, they often operate at low altitudes and may take off and land on less-improved landing sites, subjecting them to "self-induced dust storms." The particles reaching the turbine section from the outside environment are generally small in diameter because separators are used to remove larger particles [Hamed et al., 1995; Zedan et al., 1990; and Zedan et al., 1992] and because the compressor tends to further reduce the particle size (as if the particles are traveling through a blender). In extremely dusty environments, such as military applications, the engines may have dust filters in addition to the separator. However, when the filters begin to become clogged, a bypass system is in place that allows an extremely aggressive, particle-laden gas stream to enter the engine. Turbine blade thermal barrier coatings (TBCs) are generally zirconia-yttria ceramics applied over NiCrAlY or PtAl bond coats using an electron beam-physical vapor deposition (EB–PVD) process. They are subject to erosion from particulate matter ingested into engines, as well as from particles coming from the combustor. Erosion generally leads to TBC removal. As with ceramics in general, the rate of erosion is highest from head-on 90-deg impacts to the leading edge of the turbine blade. The trailing edge is also subject to significant erosion damage that may extend below the ceramic TBC layer to the metallic bond coat, where the protective oxide may be removed. TBCs are expected to be such a weak link with respect to erosion resistance that blades often must be designed under the assumption that the coating will be removed from the leading edge and possibly from the trailing edge.

Many of the newer TBCs needed for future engine designs are capable of lower conductivity and higher temperature, but unfortunately, many of them are even less resistant to erosive damage. Turbine blade TBCs in the most demanding first-blade location are generally applied using EB–PVD, producing a columnar structure more erosion-resistant than the alternative splat structure obtained using plasma spray (PS) deposition. EB–PVD coatings also have the advantage of being smoother and less hole-clogging than plasma-sprayed coatings.

A further complication arises because of the higher temperatures made possible by the use of current and future TBCs: at high enough temperatures, the small ingested particles can melt and deposit on the surface of the TBC either as a solid, or more damagingly, as a liquid. If they deposit as a liquid, the molten corrodant will wick into and react with the coating. A model compound for these ingested particles is calcium magnesium aluminosilicate (CMAS), which appears to selectively attack the mechanically desirable t′-ZrO2 phase of the coating, leaving spherical particles of the mechanically unstable m-ZrO2 phase [Borom et al., 1996; and Kramer et al., 2006]. This observation is vitally important in the pursuit of substantially longer-life erosion-resistant turbine blade coatings.

Current tools and materials baseline available or in development at NASA

There are no available codes that designers could use to predict turbine blade TBC damage due to erosion. However, there is active research in this area, which is described in the following section.

In general, the TBCs used today are zirconia-yttria ceramics over NiCrAlY or PtAl bond coats. The TBC compositions still flying today were originally identified by NASA Glenn Research Center in the 1970s [Stecura, 1978]. NASA has also developed low-conductivity TBCs under the Ultra-

Efficient Engine Technology (UEET) program [Zhu, 2004]. These low-conductivity coatings are doped with certain rare Earth oxides—such as gadolinia and ytterbia—resulting in a coating composition capable of lower conductivity and higher operating temperature. However, the compositions having the lowest conductivity suffered from decreased erosion resistance. Towards the end of the UEET program, it was discovered that certain additional dopants could be added to the ceramic "alloy" making the alloy tougher and, therefore, more erosion-resistant, thereby providing valuable physical insight needed to eventually guide the development of substantially improved erosion-resistant coatings.

Examples of current predictive and testing capabilities and coating performance

TBC erosion is generally evaluated in wind tunnel rigs or burner rigs into which particles are injected. In these tests, coating performance is typically ranked against a baseline. The University of Cincinnati [Hamed et al., 2005 and 2006] is the major location nationwide for erosion testing. The university has recently upgraded its facility's upper temperature capability to 2000 °F. This temperature is probably appropriate for the TBC surface temperature under engine cruise conditions; however, it may be lower than the temperature of current engines operating at full throttle, and in the future, temperatures are expected to become even higher. General Electric conducts most of its erosion tests in-house with capabilities for isothermal testing up to 2250 °F using a burner rig [Bruce, 1998]. Tests are run isothermally, typically at somewhat lower temperatures that are more in line with metal alloy capabilities. GE makes no attempt to produce a temperature gradient across the TBC. Under UEET, the company described to NASA typical testing where smaller particles such as 50-μm alumina are used to produce an erosive wear type of failure, while larger particles such as 560-μm alumina are used to assess impact damage to the TBC. A burner-rig-based erosion test has also been developed at Glenn Research Center. This rig is remarkably similar to a rig that ran briefly at NASA Glenn (then called LeRC) in the 1980s [Handschuh, 1984]. Single-specimen tests are run at Glenn Research Center typically at Mach 0.3, where the gradient across the TBC may be about 25 °F. Higher-Mach-number operation is now possible in the rig. Also, a laser-rig-based erosion test has been developed that is capable of testing specimens under realistically high heat-flux conditions where the gradient may be 150 °F.

The burner rig approach has certain disadvantages, but also some advantages, compared with the University of Cincinnati approach. High temperatures and relatively high velocities are attained much more simply in the burner rig than in the long tunnel approach used by the university. Also, the size of a burner rig is much more compact, with much lower construction costs. However, the particle velocities are less well-controlled in the burner rig than in the tunnel. In order to help offset this disadvantage, the Glenn Research Center burner rig task is employing computational-fluid-dynamics (CFD) modeling to help characterize the behavior of particles in the burner rig and to help guide the experimentalists in selecting input parameters. Figure 8.3 shows the results of CFD models of 27-μm alumina particles (intended to represent the larger end of particles passing through a separator and the compressor under nonoverloaded conditions) as they are injected at various velocities into the combustion chamber of the rig. The figure shows particle tracks for three different injection velocities. Figure 8.3 shows: there is a wide range of injection velocities where the particle tracks avoid striking the wall; particle acceleration occurs primarily within the nozzle and the potential core; and these near-center-line particle tracks lead to the highest particle velocity because they remain in the potential core. This CFD modeling is helping to guide rig design.

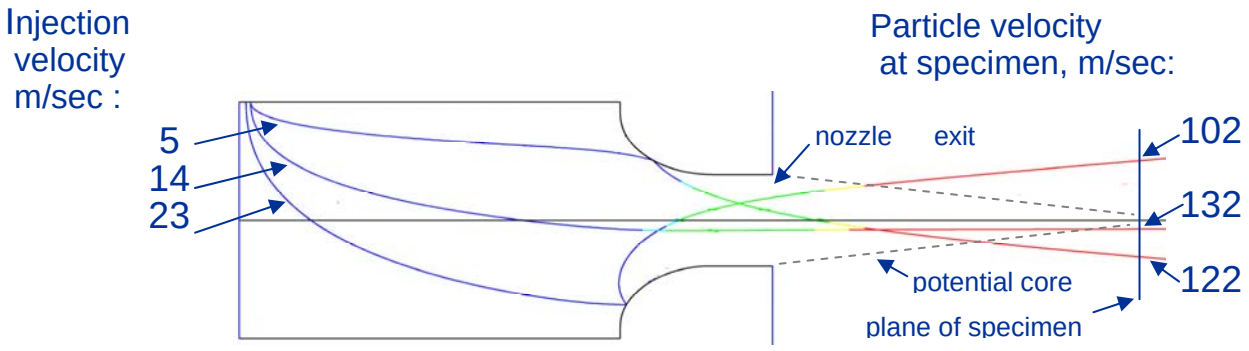

Figure 8.3. CFD model erosion tracks and velocities of 27-μm alumina particles in the NASA erosion burner rig operated at Mach 0.3.

In the cases where CMAS deposits may attack the TBC, this equipment at NASA is quite useful for studying this type of corrosive attack using high-heat-flux laser rigs. In fact, testing has been performed in this area in the past.

Modeling in general has followed three paths. First, at the University of Cincinnati the focus of the modeling has been to characterize the flow of particulates through the turbine section and the interaction of these particles with the turbine-section airfoils [Hamed et al., 2006]. The modeling yields a complete description of frequency of impact, particle velocities, impact angle, and location on the blade. The rate of coating recession as a function of particle velocity and impact angle is obtained from experiment.

Other models are centered at institutions such as University of California, Santa Barbara (UCSB) and Harvard in the United States and Cranfield and Cambridge in the United Kingdom [Evans et al., 2006; Chen et al., 2003 and 2004; Wellman and Nicholls, 2004; and Wellman et al., 2005]. These models are mechanics-based. Generally, they examine the interaction of particulates of various sizes with the columnar TBC, and then seek to develop erosion maps and elucidate the mechanisms for the various failure regimes. These regimes may involve near-surface cracking from small particles, compaction damage from larger particles, and the more significant damage with extensive plastic deformation caused generally by larger particles.

These studies often employ laboratory micro- and nano-indentation tests to complement rig tests. These studies help to illuminate the complexity of the problem. For example, the mechanics-based models show that impact damage is less likely to lead to cracking if the coating is soft. However, this guidance can be counterproductive because a softer coating may then become more subject to a “plowing” type of damage commonly observed with softer materials. Generally, high fracture toughness is always considered to be a desirable coating property.

The prolific group at Cranfield in the United Kingdom, in addition to being a leader in the areas of testing and failure mechanism understanding, has developed an approach that is directly oriented towards lifing. Their approach (which is somewhat related to the University of Cincinnati approach) is a model that employs a Monte Carlo simulation of TBC erosion [Wellman and Nichols, 2004]. With this approach, the model picks a random particle size, and that individual particle is assumed to strike a random column of the coating. The damage is assessed for each event and allowed to accumulate over a great number of such randomly chosen events.

To date, none of these models has evolved to the point where it can be considered to be a lifing model. Coating performance is being improved by compositional variation, which consists of adding additional dopants to the UEET low-conductivity coating. NASA will evaluate 12 new compositions. The composition with the best performance will be determined using the Glenn erosion rig. That composition will then be a candidate for possible further evaluation at the University of Cincinnati.

Plans for improving predictive and testing capabilities

The University of Cincinnati has plans to increase the temperature capability in its facility with a design for a J75-combustor-fired tunnel. At NASA Glenn Research Center we now have the capability to run at Mach 1, a speed that may allow temperature drops across the TBC to reach perhaps 50 °F. Also, rather than quickly eroding the coating in a ranking-type test, the plan is to more slowly erode the coating by limiting the feed rate of particulate used in the test. This limiting will allow the coating to experience longer times at high temperature, a situation that is expected to cause certain changes in the material.

Advanced physics-based erosion models will be developed using combined analytical and finite-element approaches at NASA to predict thermal barrier coating erosion behavior as a function of erodent particulate size, velocity, and impinging angle under simulated turbine engine environments. The erosion models will incorporate multiphysics processes and mechanisms—in particular the sintering, low-cycle fatigue, and molten calcium magnesium aluminosilicate (CMAS) interactions—to describe the observed variable erosion rates during the erosion process under high-heat-flux and thermal-gradient cyclic conditions. The models will be integrated into a coating property and performance database and, along with available CFD modeling results, used to predict the predominant erosion failure locations and mechanisms of engine components with respect to the operating conditions. The comprehensive modeling and high-heat-flux burner and laser erosion rig tests will allow the development of new predictive capabilities for coated rotorcraft engine turbine blades. These new predictive turbine-blade-erosion life models are intended to predict coating life to within 30 percent. The erosion models will be further enhanced to help design advanced coating systems to significantly improve the coated component erosion durability in the engine erosive environments.

To summarize, current erosion modeling efforts tend to focus on the modeling of particle dynamics backed by empirical determination of erosion rates, or they focus on understanding and therefore are not directly aimed at lifing itself. The NASA effort will be the only lifing model that will consider the multiple changes that will occur in the coating because of cyclic high-temperature effects such as coating sintering, low-cycle fatigue, and chemical interactions.

Validation data requirements

The erosion models will be validated in the high-temperature, high-heat-flux erosion rigs under simulated engine temperature and heat-flux conditions. The erosion prediction and subsequent validation of complex-shaped specimens for simulating turbine blade leading- and trailing-edge geometries are especially critical and will be carried out in laboratory testing environments. The validation requirements will also include the simulated component temperature distributions (hot spots), with multiple erodent impinging angles encountered in turbine blades. The coating-erosion-model prediction accuracy will be achieved within 10 percent of the measurements in laboratory controlled environments. Another major emphasis of the validation efforts will be model refinements in accurately predicting the long-term erosion rates in engine-relevant erosive conditions from the laboratory accelerated tests.

Cross-cutting technology needs

There is considerable need to understand the nature of particulate flow through the engine, the effect of the particle separators under light and particle-laden situations, and the effect of the compressor in reducing the size of the particles.

Ceramic Materials

The desire for increased engine performance and efficiency is currently pushing the material capability limits of superalloys. In order to move beyond these constraints, other material systems need to be developed and analyzed. Ceramic materials offer the potential to replace superalloys in rotorcraft engine component applications because of their high corrosion resistance, higher temperature capability, lighter weight, and high strength. Two categories of ceramics, monolithic ceramics and ceramic matrix composites, have the potential for use in rotorcraft engine applications. Applications well-suited for ceramics include vanes, turbine blades, and bearings.

Monolithic ceramics have not typically been used for engine applications because of their limited strain capability, flaw sensitivity, and susceptibility to environmental degradation at engine operating conditions. The feasibility of reducing flaws by an amount sufficient to achieve an acceptable component design is greatest for small components such as those used in rotorcraft engines because smaller components have a lower probability of containing a critical flaw compared with larger components. However, advances are needed in the basic understanding of flaw formation and damage initiation. In addition, environmental degradation of silicon nitride remains a challenge. Environmental protective coatings that address this challenge need further testing and characterization.

CMCs can overcome the limited strain capability and flaw sensitivity of monolithic ceramics. However, reduced design strength (2 to 3 times lower than monolithic ceramics) is a problem with CMCs. Another issue of particular importance for rotary-engine applications is the difficulty of bending and weaving fibers to process fiber preforms for small rotorcraft turbine engine components. Weaving and processing studies are required to fully address this issue. Also, through-thickness properties of CMCs need to be improved, particularly for the interlaminar strength of CMCs compared with their relatively high shear and tensile strengths. Some of the CMC issues are currently being addressed in another NASA project. The progress in this area will be monitored, and a study of the relative merits of CMCs versus monolithic ceramics for rotorcraft engines will be

performed. Input for the study will be sought from engine manufacturers, weavers, and composite fabricators. Recommendations for future work will dictate whether to pursue monolithic ceramics or CMCs for rotorcraft engine components.

The current focus is on monolithic ceramics in the development of new analytical tools and in experimental testing. Ceramics have relatively mature processing methods and lower costs for fabricating rotorcraft engine components compared with that of ceramic matrix composites. Among the monolithic ceramics, silicon nitride is the most promising material for hot-section components of next-generation rotorcraft turbine engines. Silicon nitride offers significant performance benefits over traditional superalloys. Studies have determined that silicon nitride offers 50 percent higher strength at a temperature of 1400 °C; orders of magnitude higher resistance to erosion, creep, and passive oxidation; 20-percent higher conductivity; 60-percent lower density; 50-percent reduction in cooling requirements; and operating temperatures that are 300 °C higher. However, an obstacle that must be overcome is surface recession of silicon nitride that occurs under engine operating conditions. To prevent surface recession, an environmental barrier coating (EBC) that offers high impact resistance is necessary.

EBC compositions that are stable up to 1450 °C have been identified for silicon-based ceramics in the previous NASA UEET program [Lee et al., 2005]. Microstructural stability of one of the EBC systems on SiC/SiC composites has been demonstrated in a moisture environment at 1250 °C for 40,000 hr. In contrast, when the same EBCs were applied to silicon nitride by standard coating methods such as plasma spray, EB–PVD, or chemical vapor deposition (CVD), the silicon nitride substrate showed strength loss up to 50 percent, and the coatings also showed poor impact resistance. The reasons for strength degradation are not clearly understood, but strength degradation could be due to residual tensile stresses in the coating, the coating process damaging the substrate, or lack of crack deflection mechanisms at the coating-substrate interface.

NASA's efforts to advance analytical tools and material development will occur in two major areas: silicon nitride with EBCs and materials joining and integration. Tasks in the first area include: gaining a basic understanding of the chemistry and physics of the degradation process; developing improved coating materials and processes; and developing physics-based models for degradation of silicon nitride coated with the improved EBCs. High impact resistance is of primary importance in the development of an EBC. This resistance is essential so the coating does not spall off during use and expose the underlying silicone nitride, which is susceptible to erosion. The second area focuses on the development and verification of process models for bonding silicon nitride to silicon nitride and silicon nitride to metallic attachments. This development and verification of joining process models will allow for the fabrication of complex shapes and for the integration of ceramic vanes and blades into related component structures.

Current tools available or in development at NASA

A general-purpose series of integrated design software tools has been developed at NASA Glenn Research Center. The Ceramic Analysis and Reliability Evaluation of Structures (CARES) software is used to optimize the design of isotropic brittle material components using probabilistic analysis techniques. Fundamental mechanics theory is incorporated with material-associated computational strategies. CARES can be used with commercially available finite-element analysis software. The CARES software package consists of three distinct programs: CARES/Life, CARES/Creep, and

C/CARES. CARES/Life is used to predict the reliability and life of structures made from advanced ceramics and other brittle materials. CARES/Creep is a program for predicting the lifetime of structural ceramic components subjected to multiaxial creep loads. C/CARES is used to predict the time-dependent reliability of a laminated structural component subjected to multiaxial load conditions [NASA Glenn Research Center, 2005]. Work has also been done on developing a model of impacts to monolithic ceramics. Together, the family of CARES analytical packages provides an important predictive tool for lifetime analyses of and for extending the range of application of ceramic components substantially beyond that of today's metal-based systems.

Examples of current predictive and testing capabilities

The current predictive capabilities focus on the monolithic ceramic silicon nitride. Two areas have been addressed. In the first area two- and three-dimensional finite-element analyses were conducted on uncoated and TBC silicon nitride plates with and without internal cooling by air. The influence of the cooling channels, their shape and size, and the type of coolant on the thermal and stress responses were investigated. The temperature variations observed in the experimental results, with which the finite-element analysis correlated well, are shown in figure 8.4 for different-size circular cooling holes. The analysis showed that air-cooled channels reduced the plate temperature by 204 °C versus the uncooled design. The temperature increased with larger hole sizes for the case without cooling, whereas the temperature decreased for the case with cooling of the same hole size. The shape of the cooling channel significantly affected the temperature level, with an ascending size arrangement giving the lowest temperature at 1077 °C, followed by a rectangular-hole pattern that gave a temperature of 1343 °C, and a similarly sized circular-hole pattern that gave a temperature of 1379 °C. The experimental results show that the cooling hole patterns could be manufactured into silicon nitride plates and that the material was capable of withstanding thermal shock associated with cooling dynamics [Abdul-Aziz et al., 2001].

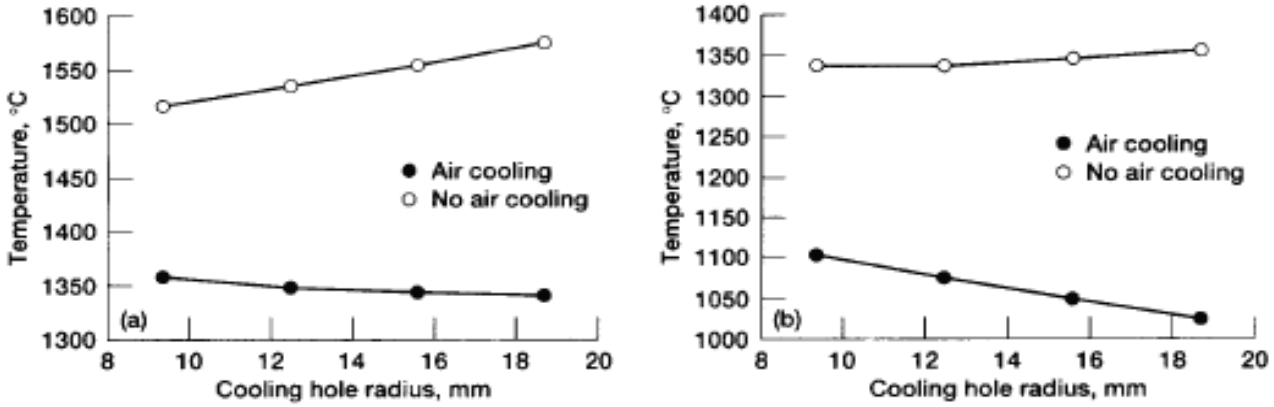

a) Hot-spot temperature b) Cold-spot temperature

Figure 8.4. Temperature variation as a function of hole size. Results are from the experimental analysis of cooled and uncooled silicon nitride plates with machined holes [Abdul-Aziz et al., 2001].

The second area of current predictive capabilities is in impact studies of silicon nitride. The strength degradation of silicon nitride due to ball impact was analyzed in a model. Strength degradation was modeled using Hertzian contact analysis, the principle of energy conservation, and indentation fracture relations. When the post-impact experimental strength data was plotted as a function of impact kinetic energy (fig. 8.5), there was a discrepancy between the model and experimental data. The model predicted a slope of –1/5. The discrepancy could have been due to assumptions in the model that there is an idealized elastic impact, that the impact event was quasi-static, or that cracks were radial or lateral rather than the assumed well-developed cone cracks [Choi et al., 2004].

Two unique combustion rig facilities are examples of current testing capabilities. These rigs are available for experimental testing of materials and subcomponents at NASA Glenn Research Center. The first is the High Pressure Burner Rig (HPBR). This combustion test rig is used to conduct high-temperature environmental durability studies of engine materials. Realistic turbine engine combustion gases are produced at desired chemistries and temperatures by controlling the ratio of burned jet fuel and air. Simulations of the representative pressures and gas velocities are achieved from the test chamber. The second test facility is the Mach 0.3 Burner Rig, which is able to accommodate various geometries of material test articles. The rig allows for materials to be exposed to the high temperatures, high velocities, and thermal cycling of realistic combustion environments. The environment can be oxidative or corrosive, and gas temperatures can range from 370 to 1370 °C. Both facilities provide efficient means for evaluating new material concepts to combustion engine conditions.

Plans for improving predictive and testing capabilities

Theoretical work will initially focus on determining conditions that lead to crack propagation from a coating into the ceramic substrate and crack deflection at the ceramic-EBC interface. The experimental data that are required for developing the model will generate material property data such as elastic and fracture properties of the standalone coating composition under the processing conditions

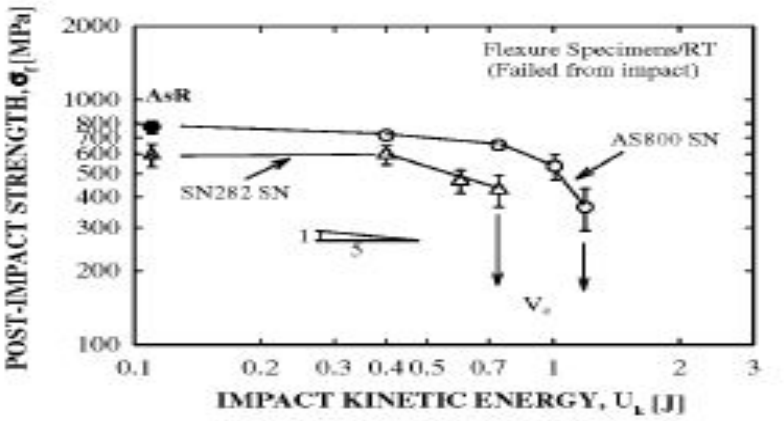

Figure 8.5. Plot of post-impact strength as a function of impact kinetic energy determined for silicon nitrides AS800 and SN 282. The slope (–1/5) indicates the theoretical value. AsR is as-received flexural strength.

of the coating as it will be applied to the substrate. The data will aid in the development of a functionally graded EBC that does not degrade the strength of Si3N4 and deflects cracks at the coating/substrate interface, essential to the development of long-life ceramic components. Coating-induced stresses and flaws will be considered. The experimental tests will be necessary in achieving model predictions within 10 percent of test data. Currently there are no predictions for strength. The shape, size, and distribution of flaws created on the surface of coated Si3N4 must be known in order to predict the strength with current models. This information is currently being generated.

Current efforts are focused on causes of strength degradation in coated silicon nitride due to induced stresses and flaws. A previous study [Lin et al., 2003] has shown that silicon nitride substrates when coated with plasma-sprayed EBC result in a loss in strength of up to 50 percent. This much loss in strength is unacceptable for designing silicon nitride for turbine engine applications. A variety of factors such as tensile residual strength in the coating, the plasma spray (PS) coating method damaging the surface of the substrate during deposition, lack of crack deflection mechanisms at the coating-substrate interface, and nonuniform loading during testing may be responsible for strength degradation. To determine the most dominant strength-degradation mechanisms, a parametric study has been initiated to evaluate the effects of the previously mentioned factors on the strength. In the first stage of the investigation, the strength-limiting flaws in uncoated and PS-coated silicon nitride bars have been identified and cataloged into four groups: edge flaws, unsintered regions in silicon nitride substrate, large pores, and large silicon nitride grain oriented at an angle to the substrate. In general, the uncoated silicon nitride bars failed from the last three types of flaws, but 70 to 80 percent of the PS-coated silicon nitride bars failed from the corner flaws. These results indicate that deposition of PS coating over the beveled edges of the specimen activates edge flaws and that the coating process itself may not degrade the strength of the substrate. Since the coating process itself does not appear to degrade the strength, the current focus is on improving adherence of coatings on the surface of silicon nitride. Surface-preparation studies to reduce flaws have been conducted for silicon nitride. A thermal-etching (TE) process has been developed and practiced on different grades of commercially available silicon nitrides. Preliminary results show that surface microstructure of silicon nitride substrates can be controlled by TE process with minimal loss (<10%) in substrate strength. Currently, silicon nitride specimens thermally etched and coated with an EBC are being thermally cycled at 1300 °C in moisture environment to assess bonding and thermal stability. These analyses for coating application methods, sample preparation, and strength retention will allow for an optimized material system (Si3N4 and EBC) to be characterized and used in development of the model. The efforts will also lead to the demonstration of a bond coat for silicon nitride that extends the life 2 times over uncoated silicon nitride.

Another major effort is in the development of joining-technology and joining-process models, which will allow complex shapes to be fabricated, ceramic vanes to be integrated to a stator, and ceramic turbine blades to be integrated to the hub. For bonding silicon nitride to silicon nitride, the joining approaches of active metal brazing, ceramic adhesives, and transient liquid phase bonding will be investigated. The application conditions, component geometry, and material system (i.e., ceramic to ceramic and ceramic to metal) will determine the joining approach for each case in which the joining technology is to be applied. Initial results have been obtained for the first two approaches:

(1) Active metal brazing was used to successfully join two pieces of Kyocera Si3N4 (SN282) using Morgan Advanced Ceramics's Incusil-ABA brazing foil. Incusil-ABA is 59% Ag, 27.25% Cu, 12.5% In, and 1.25% Ti (in weight percent) and has a liquidus temperature of 715 °C. Initial microscopy analysis shows a good reaction region between the Si3N4 and the Incusil-ABA (fig. 8.6). The interface is composed of large concentrations of Si and Ti, suggesting some form of Ti silicides. Additional samples will be made for mechanical testing. These brazes have working temperatures of less than 1000 °C, possibly limiting their application to joining for engine components targeted for intermediate temperatures. These brazes could find use in joining of silicon nitride to superalloys, which may be at the intermediate temperature range.

(2) In order to increase joint operating temperatures, ceramic adhesives are being developed to form high-temperature ceramic joints. Eight new ceramic adhesive compositions with varying amounts of refractory ceramics and reactive phases have been developed. Eight samples of Kyocera SN281 have been joined using these different compositions. They were cured in an oven at 120 °C and heat-treated in a vacuum furnace at 1450 °C for 15 minutes. After heat treatment all samples remained intact. Microstructural evaluation of joined specimens has been completed, and an example of the microstructure is shown in figure 8.7. All eight samples have shown good interaction between the joining compositions and substrates. Additional formulations and improved processing are under way to reduce porosity within the heat-treated samples. Further process improvements and characterization of joints is under way.

The development of the joining technologies will help lead to the development of predictive models for joining. Such models could be used for predicting the most promising material systems (metals, ceramics, and joining interlayers) that could be used to form robust joints and for developing models that help optimize the joint processing conditions.

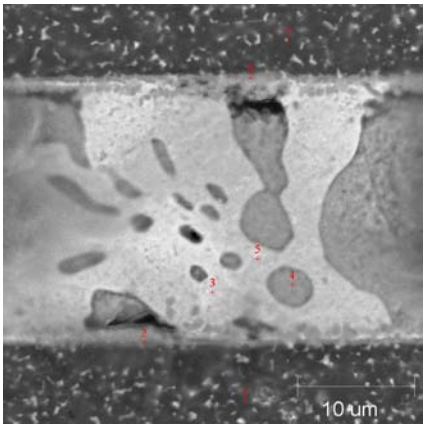

Figure 8.6. Microstructure of a joint from an active metal braze (two-toned central strip) between silicon nitride.

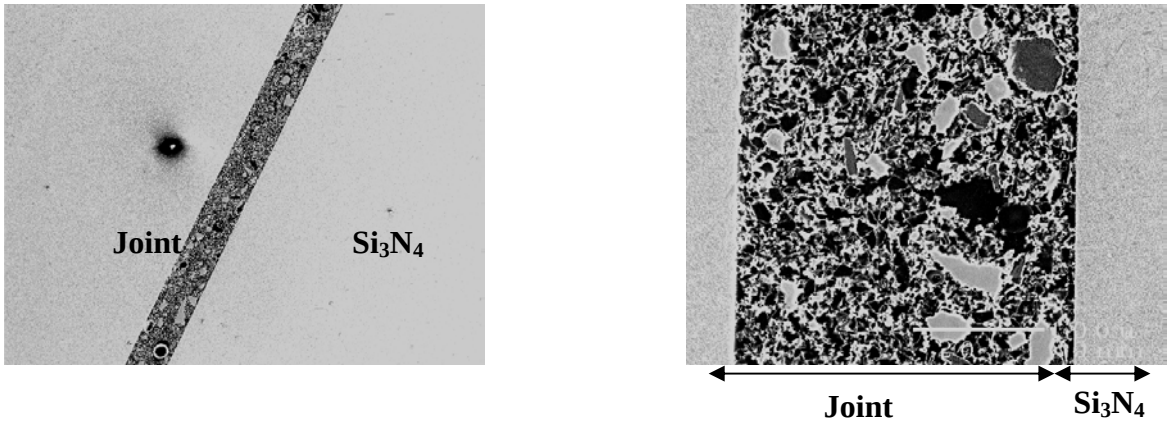

a) Overall view b) Magnified view

Figure 8.7. Optical micrographs showing a ceramic joint formed between two pieces of silicon nitride.

Validation data requirements

In order to identify and demonstrate a bond coat for silicon nitride that extends the life substantially beyond that of uncoated silicon nitride, the EBC system needs to be studied and optimized. The mechanism of strength degradation in the silicon nitride due to the addition of the EBC needs to be understood. The reduction in strength could be due to tensile-induced stresses in the coating, induced flaws from coating processes, or lack of coating deflection mechanisms at the coating-substrate interface. A physics-based strength-degradation model will be developed. The coating deposition parameters and test methodologies will be further optimized.

Impact tests need to be conducted on coated silicon nitride to determine its impact resistance. Based on the experimental data, an analytical model will be developed to predict impact resistance.

The feasibility of fabricating complex-shaped components and integrating a silicon nitride component with a superalloy structure needs to be addressed. Therefore, techniques for joining and bonding ceramics to metals and to other ceramics will be developed. Joining and bonding methods will first be developed using simple shapes. Bonding techniques will include active metal brazing, ceramic adhesives, and transient liquid phase bonding. The best techniques will then be used on real components to get a true indication of performance and reliability. The fabrication of a complex-shaped component that is made of silicon nitride and contains cooling holes needs to be demonstrated.

Cross-cutting technology needs

Several cross-cutting technologies are needed to fully and successfully use ceramics, both monolithic ceramics and ceramic matrix composites, as components in rotorcraft engines. In order to fabricate complex shapes that have vanes integrated into the stator and blades integrated into the turbine disk, joining technologies must be matured and proven. Joining of many material combinations may be required; that is, monolithic to monolithic ceramic, composite ceramic to composite ceramic, and ceramic to superalloy. The joints and interlayer materials must be thermally compatible with the

base materials so that residual stresses are not formed. They must also be chemically compatible with the base material and remain stable and have retained strength at high temperatures.

Another cross-cutting technology needed is for properties that are obtained for flat specimens to be confirmed for more complex and curved shapes. For example, impact tests in the past were performed on flat plates. Impact tests on curved vane and blade shapes should be conducted to confirm that the same performance is achieved. Another area to be validated is the coating durability and strength retention on curved shapes as demonstrated on flat-shaped specimens.

An additional cross-cutting technology need is for advances in fiber preform fabrication for forming small curved shapes, as for blades and vanes in small turbine engines. Preform fabrication will require advances in fibers, fiber architecture designs, and/or weaving and braiding abilities. Currently, the most advanced SiC fibers that offer high-temperature strength and stability are too stiff to be woven into small curved shapes. Stiffness is especially critical for being able to form the sharp curves of blade and vane trailing edges of small rotorcraft engine components. Before ceramic matrix composite material can be fully used for rotorcraft engine components, fiber preform fabrication issues must be addressed.

AIRFRAME STRUCTURES AND MATERIALS

The three research areas related to airframe structures and materials are durability and damage tolerance of composite rotorcraft structure, crashworthiness, and cabin noise reduction. Lightweight airframe structure is important for all aircraft, and significant weight reduction is being achieved in both fixed- and rotary-wing aircraft through the use of composite materials. Lightweight design is achieved by optimizing the fiber architecture in critical load directions. Additional weight reduction and manufacturing efficiency is achieved by combining individual components into a single multifunctional structure. Continued advancements in the use of composite materials will depend on further development of new materials, advancements in design and analysis tools for composite structure, and demonstration of affordable manufacturing approaches. Rotorcraft have unique requirements for combining lightweight design with damage tolerance, durability, and crashworthiness. There are also unique requirements for integration of the transmission and propulsion systems with the airframe. Currently, the lightest weight design approach for a rotorcraft fuselage is a stiffened thin-skin structure that can tolerate occasional shear buckling loads during normal operation. This type of loading can result in a different rate of fatigue damage and possibly different failure modes compared with similar structures that are not allowed to buckle in fixed-wing aircraft. Analysis tools for assessment of the durability of stiffened fuselage structure are being developed within NASA, but not in rotorcraft. Durability and damage tolerance research within NASA rotorcraft focuses on three areas of specific interest to rotorcraft: (1) demonstration of technologies that can mitigate debonding between skins and stiffeners in composite structures subject to loads that are representative of rotorcraft fuselage structure, (2) evaluation of alternative approaches to the stiffened skin design (such as lightweight sandwich structures), and (3) evaluation of the feasibility of using embedded sensors in composite structures. This report focuses on item (2) because new analysis methods developed as part of this research could be widely applicable to a range of new materials and structures, while current research in items (1) and (3) involve a defined set of experiments to evaluate feasibility of specific concepts.

Rotorcraft have unique requirements for crashworthiness because the crash velocity has a large vertical component and because the transmission and engine are mounted on top of the fuselage for many rotorcraft. Structure must be designed to have a controlled progression of damage during a crash in order to absorb energy while also limiting the reduction in cabin volume to an acceptable level to avoid injury to occupants. Proper design and integration of substructures, such as energy-absorbing seats, is important for maximizing occupant survivability and reducing spinal injuries. Use of externally deployed energy absorbers has the potential to contribute significantly to occupant survivability. Research in NASA rotorcraft focuses on the need for efficient and reliable crash analysis tools and on the development of lightweight deployable energy-absorbing structures. Experiments ranging from laboratory-scale materials tests to full-scale helicopter crash tests are being performed for validation of the analysis methods and demonstration of energy-absorbing structures. Crash testing of full-scale rotorcraft fuselages and components are conducted at the Landing and Impact Research Facility (LandIR) at NASA Langley Research Center. A summary of Department of Defense sponsored research conducted at the LandIR is provided in Jackson et al. [2006], which describes military rotorcraft tests from 1975 through 1999.

Rotorcraft have a high level of cabin noise. The primary source of noise is vibrations originating in the gearbox. Vibrations are transmitted through the airframe structure to the cabin area, where sound is radiated into the cabin. The most severe noise issue is large-amplitude multiple tones in the low-frequency range. The sound level in the cabin can be reduced by reducing vibrations near the source, reducing transmitted vibration with damping materials and isolation structures, and attenuating noise with sound-absorbing interior cabin treatment. Only sound-absorbing materials are considered in this chapter. Research here focuses on developing lighter-weight absorbing materials and investigating methods for integrating these materials into multifunctional structures. Methods for achieving lighter weight include development of lower-density open-cell materials, development of processing methods to produce a porosity gradient in the material, and development of hybrid materials. The mechanism for sound absorption in these materials is being investigated, and methods for optimizing materials for sound absorption at multiple tones are being considered.

Durability and Damage Tolerance

Recent and new rotorcraft designs typically include sandwich construction made from thin face-sheets and lightweight cores. This type of structure is very susceptible to damage from out-of-plane loading such as low-velocity impact. These structures must be designed to sustain barely-visible-impact (BVI) damage at ultimate load, which can result in a reduction of 50 percent or more in the design strength relative to an undamaged structure. The failure mechanics in impacted thin-skin sandwich structure are not well-understood, and analytical models are not currently used to predict the compression-after-impact (CAI) strength. Consequently, the design allowables for sandwich structure are normally obtained empirically using coupon and component testing. In order to develop optimized structures, analytical tools that can be used during the design process are needed to predict the performance of impact-damaged sandwich structure.

Impact damage typically consists of a combination of facesheet damage (matrix cracking, delamination, and/or fiber breakage), core debonding, and core crushing. In addition, a residual dent is typically formed around the point of out-of-plane loading. If the damaged facesheet is loaded in compression, two basic failure mechanisms that lead to structural failure have been identified [Cvitkovich and Jackson, 1999]: kink-band propagation and indentation growth. With kink-band propagation (fig. 8.8a), the damage acts as a stress concentration similar to an open hole. As a compressive load Pmax is applied, the tows in the loading direction buckle and break normal to the plane of the facesheet, creating a band of broken fibers that propagates perpendicular to the loading direction. This kink band continues to slowly propagate away from the damaged region with increasing load until a critical length is reached, where the kink band suddenly grows across the width, causing failure. For the indentation-growth failure mode (fig. 8.8b), the residual indentation from the impact begins to buckle and expand as the compressive load increases. The local buckle in the facesheet applies compressive loads to the core, causing additional crushing as well as elastic deflections. When a critical compressive force is reached, the facesheet rapidly buckles across the width and fails.

Current tools available or in development at NASA

There are no commercially available tools to predict the residual compressive strength of impact-damaged sandwich structure. Although critical to the design process, the design of rotorcraft structure is typically based on empirical results and, often, open-hole compression data. During the U.S. Army's Survivable, Affordable, Reparable, Aircraft Program (SARAP), an analysis [Ratcliffe et al., 2004] was developed at NASA to predict the compressive strength of sandwich specimens that fail by kink-band propagation. This analysis was based on an analysis originally developed by Soutis and Fleck [1990] for the compressive strength of solid laminates with open holes. The analysis developed during SARAP has been successfully used to predict the strength of test specimens failing by kink-band propagation. However, this analysis still needs additional validation and possibly refinement.

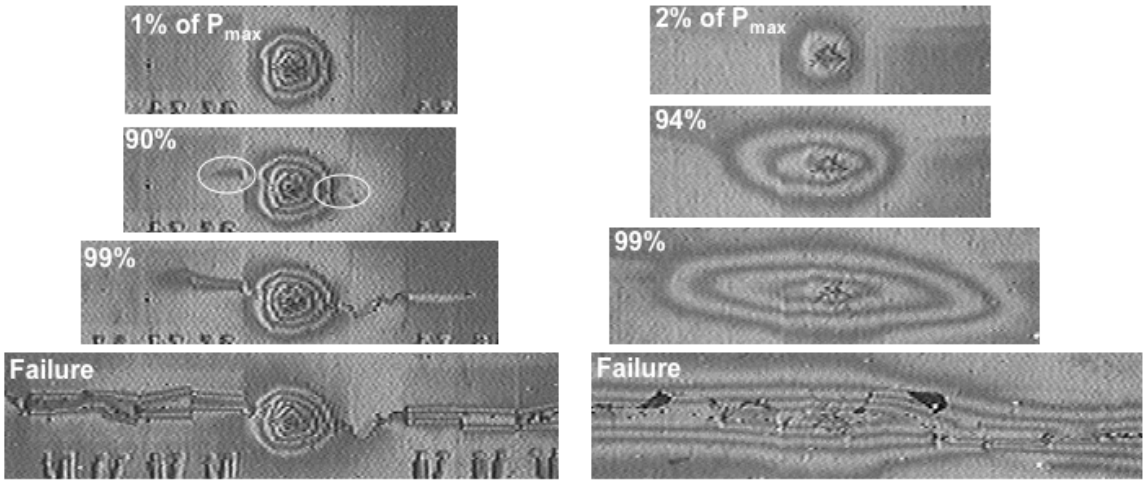

a) Kink-band propagation b) Indentation growth

Figure 8.8. Examples of compressive failure modes.

For specimens failing by indentation growth, a residual compression strength analysis using a finite-element technique is being developed by NASA. An analytical model to understand and predict this type of failure was first developed by Minguet [1991]. Additional researchers have made several improvements to Minguet's analysis since its development [Tsang, 1994; Moody and Vizzini, 2002; and Xie and Vizzini, 2005]. However, this type of analysis is extremely complex, has some significant limitations, and requires an elaborate iterative technique to obtain a solution. Consequently, the analysis is not suitable for use during design. The analysis that is being developed under NASA rotorcraft research uses an array of springs that simulate the behavior of the undamaged and the crushed core. This finite-element-based method is very flexible and can be easily adapted to other configurations, boundary conditions, and core responses. A one-quarter-model mesh with nonlinear springs representing the core is shown in figure 8.9.

Examples of current predictive and testing capabilities

A one-quarter model of a 132-mm square sandwich panel has been generated. The facesheet was represented using layered shell elements. A local indentation with a maximum depth of 1 mm and radius of 6 mm was used to represent the impact-damaged portion of the facesheet. A model containing approximately 54,000 degrees of freedom was selected after conducting a convergence study. As previously described, this analysis used spring elements to represent the core material.

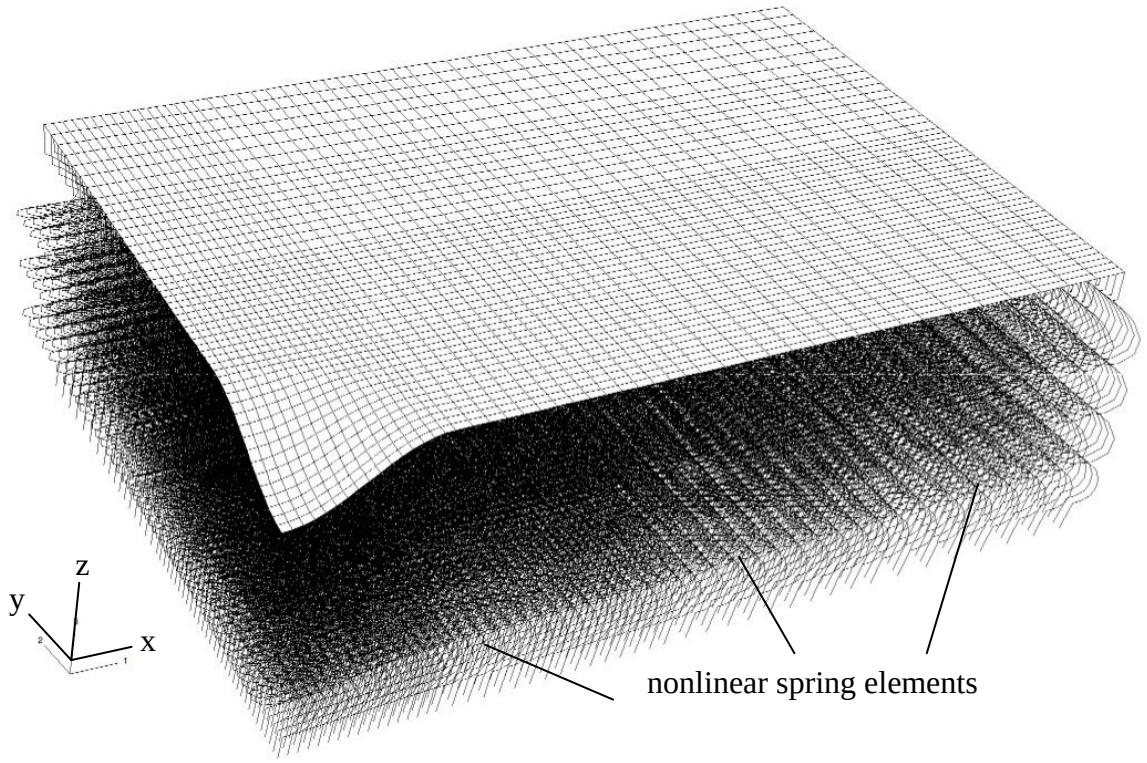

Figure 8.9. One-quarter-model finite-element mesh of impact-damaged compression specimen showing spring elements used to represent the core material.

Empirically based core crush laws were used to assign the nonlinear spring stiffness behavior (in the core thickness direction). During initial analyses, the tension stiffness (referred here as k(tension)) was assumed to be equal to the compression stiffness, k, of the honeycomb. This assumption may not be accurate since the honeycomb configuration may result in a difference between the tension and compression stiffness values. A series of nine analyses was conducted to evaluate the effect of spring-tension stiffness on the force-displacement response. The force-displacement results are given in figure 8.10; they clearly show a significant dependence of the response on k(tension). The residual strength is equivalent to the maximum force of each curve. This finding will be examined in a series of experiments that will be designed to measure differences between the tensile and compressive stiffness of the core material. The data from these measurements will be used to evaluate the value of k(tension) to be used in future analyses.

Plans for improving predictive and testing capabilities

Many improvements over previous analyses have been incorporated during the development of the analysis under NASA. In addition, a series of parametric studies are currently being conducted to determine which properties are the most critical. For example, tensile core properties were not considered important in the core-crushing response. However, a region of tensile stresses that develops in the core during compressive loading has been identified that is critical to the core-crushing response and the corresponding strength of the structure. In addition, the analytical predictions will be compared with a series of experimental measurements of indentation growth as a function of compressive load. If differences with the experimental data are identified, improvements to the analysis will be attempted to obtain better agreement with the experimental results.

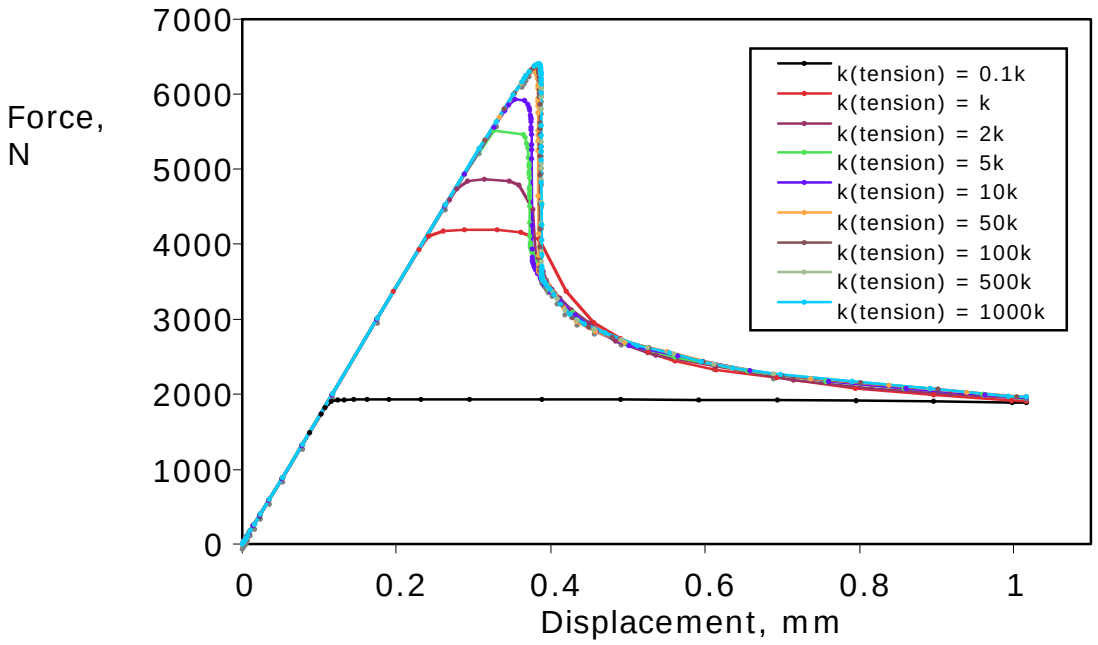

Figure 8.10. Effect of k (tension) on residual strength.

During this program, a body of test data from thin-skin sandwich specimens was identified that was suitable for the development and validation of the residual-strength analysis. To expedite the development, the analysis development has focused on thin-skin sandwich structure rather than sandwich structures with thicker skins. The current residual strength analysis may be suitable for sandwich structure made from thicker skins; however, in-house testing will need to be performed on specimens with the thicker skins to verify the analysis.

Validation data requirements

The analysis that is being developed within NASA rotorcraft will be compared with the results from the analysis developed by Minguet [1991]. An initial comparison of results is shown in figure 8.11 along with an experimental value from Minguet. The residual strength is plotted as a function of the core-crushing properties. Although very different analytical techniques were used, the results are very similar and compare well with the experimental result. In addition, the analysis will be used to predict the strength of test specimens presented by Minguet as well as specimens previously tested at NASA. Additional core testing will be required to obtain properties that are not typically measured.

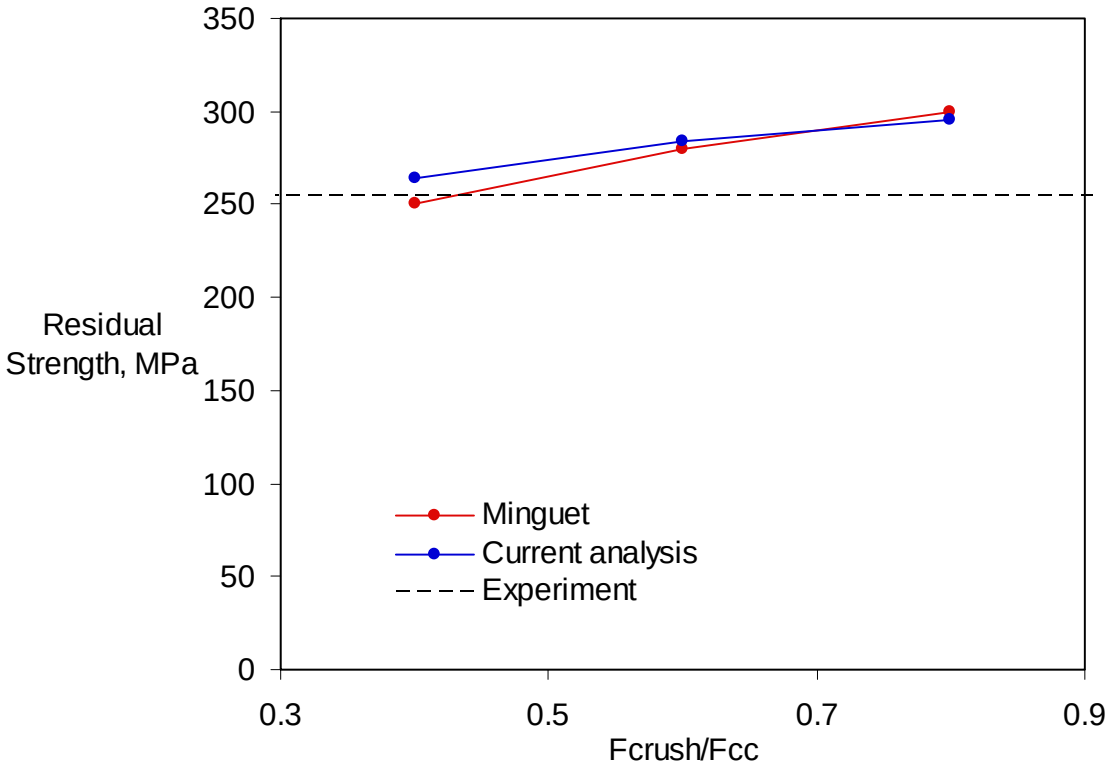

Figure 8.11. Strength comparison between the current and Minguet [1991] analyses.

Crashworthiness

NASA research in rotorcraft crashworthiness focuses on crash modeling and simulation as well as demonstration of advanced concepts for improved energy absorption. Modeling approaches are being developed and validated that include physical representations of human occupants, energy-absorbing subcomponents, composite fuselage structure, and other critical components. These models will be integrated to perform full-scale crash simulations. Testing of materials, subcomponents, and larger components such as fuselage sections will be performed for concept evaluation and to aid in model development. Full-scale helicopter crash tests will be performed for validation. The validated crash simulation models will enable impact evaluations of structural concepts during the preliminary design phase and will enable crash evaluation of future rotorcraft with limited full-scale testing.

The rationale for incorporating crashworthy design features into rotorcraft is to minimize the number of fatalities and serious injuries experienced by the crew and passengers and to reduce the amount of structural damage to the airframe and payload during a severe, but survivable, crash. Crashworthy design of rotorcraft requires a systems approach in which various subcomponents work together to absorb and dissipate the kinetic energy of impact. The crashworthy helicopter is capable of:

- Limiting the loads and decelerations that are transferred to the occupants to humanly tolerable levels, usually through crushable landing gear, energy-absorbing subfloors, and load-limiting seats
- Providing a livable volume for the occupant by preventing structural collapse of fuselage frames and other structural components used to support the overhead rotor and transmission mass
- Providing a secure tiedown for the occupant through seats, restraint systems, seat tracks, and floor attachments
- Eliminating head-strike potential through the use of pretensioned restraint systems and cockpit airbags
- Minimizing post-crash fire hazards
- Providing for emergency egress

The crashworthy helicopter must perform all of these functions while experiencing transitory, multidirectional decelerations associated with impact onto different terrains.

Military Standard MIL–STD–1290A (AV) [1988] defines the certification requirements for crash performance of military helicopters by specifying lateral, vertical, longitudinal, and combined velocity impact conditions that the airframe must withstand with minimal collapse and associated loss of volume (15 percent or less). The requirements in MIL–STD–1290A (AV) are based in part on U.S. Army accident data as summarized in the Aircraft Crash Survival Design Guide [Anon., 1989]. More recently, Aeronautical Design Standard ADS–36 for Rotary Wing Aircraft Crash Resistance [ADS-36, 1987] was developed specifically for qualifying the U.S. Army's new reconnaissance and attack helicopter, the RAH–66, which eventually became the Comanche helicopter. MIL–STD–1290A (AV) encourages the designer to demonstrate compliance with the requirements by using analytical methods. However, the standard also states that "Instrumented full-scale crash test(s) are

desirable to substantiate the capability of the aircraft system to prevent fatalities and minimize injuries during crashes of the severity cited herein. If the system testing is not conducted, then analysis shall be required to show that the individual components and subsystems function together effectively to achieve the specific overall level of crashworthiness." Thus, the military standard establishes both full-scale crash testing and analytical modeling as tools to achieve crash certification. However, the MIL–STD–1290A (AV) does not specify which analytical methods or codes should be used to perform these analyses.

Recent helicopter accident studies show that as improved crashworthy features are incorporated into the modern fleet of military helicopters, the impact velocities for survivable accidents are increasing [Amer, 1991; Burrows, 1993; Shanahan and Shanahan, 1989; and Labun, 2004]. Thus, crew and troop occupants are surviving more severe impact conditions when flying in helicopters with load-limiting seats, improved restraint systems, cockpit airbags, and other crashworthy features. To be effective and minimize cost and weight, a variable design requirement must be written based on helicopter type, mission, weight, and autorotative rate of descent. The military standard defines one set of design criteria for all military helicopters. However, accident data show that it is easier for medium- to large-size helicopters to meet the requirement than it is for small-size helicopters. There is also the issue of weight penalty associated with crash design features. The "one-size-fits-all" approach penalizes the small-size helicopter because a larger percentage of its gross weight is dedicated for crash resistance. Consequently, variable design criteria are needed.

There are no requirements for full-scale crash testing of civil rotorcraft similar to MIL–STD–1290A (AV) or ADS–36. Instead, there are seat requirements described in the Federal Aviation Regulations, Parts 27 and 29, for normal and transport civil rotorcraft [CFR Part 27 and CFR Part 29]. These criteria are summarized in a Society of Automotive Engineering Aerospace Standard [SAE, 1997], and comparisons of military and civil requirements are presented by Bolukbasi [2000] and Coltman et al. [1985]. In general, the findings show that civil helicopters typically crash at consistently lower velocities than do military helicopters. Consequently, applying the military standard to civil helicopters is not appropriate. Optimized energy-absorbing concepts are needed to improve crashworthiness of civil rotorcraft without adding weight. Since full-scale crash testing is not economically feasible for evaluating proposed energy-absorbing concepts, subcomponent testing is needed to both demonstrate the concept and to validate analysis methods. Validated analysis methods can then be used to optimize the design of the energy-absorbing concept and identify how the concept could be integrated into specific rotorcraft designs. Ultimately, full-scale crash testing is needed for validation of energy-absorbing concepts and analysis methods. Both subcomponent and full-scale crash tests are planned in the rotorcraft project. Data from these tests will be used to advance the state of the art in human occupant modeling, modeling of advanced energy-absorbing materials and structures, and modeling of a full-scale helicopter crash. It is anticipated that there will be industry partnerships for the full-scale testing and that the test articles will include fuselage structures made using advanced composite materials.

Current tools available or in development at NASA

Crashworthy design of helicopters requires the capability to predict the dynamic structural and human occupant responses to impact loads. Accurate prediction of these responses necessitates a systems approach to modeling that includes the landing gear, fuselage structure, human occupants,

seats and restraints (including airbags), and fuel-containment systems. Until the late 1990s, most crash simulations were performed using a semiempirical, kinematic code in which the airframe model consisted of a small number of beams, lumped masses, and springs. Typically, the spring properties were derived from component test data. More recently, crash simulations have been performed using nonlinear, explicit transient dynamic finite-element codes. While some progress has been made in validation of these simulations, a general lack of confidence in the accuracy of analytical crash predictions remains, especially for airframes constructed of advanced composite materials.

The military standard for crash resistance, MIL–STD–1290A (AV), clearly states the intent for the designer to demonstrate compliance with the various velocity-change requirements through analytical methods. There were likely two reasons for encouraging the use of analytical methods. First, crash testing of full-scale aircraft, especially prototype aircraft, is relatively expensive. Also, because of the limited availability and high cost of test articles, performing repeated tests or a large number of tests for different impact conditions is generally not feasible. Secondly, the timeframe for the initial publication of the military standard in the mid-1970s corresponded with the initial release of KRASH, a kinematic lumped-spring-mass crash analysis code [Gamon, 1978; and Gamon et al., 1985].

During this same time period, a new code, DYNA3D [Hallquist, 1988], was being developed at Lawrence Livermore National Laboratory under sponsorship by the Department of Energy. DYNA3D was an explicit transient dynamic finite-element code capable of simulating high-speed impacts. Later, the public domain version of DYNA3D was obtained by commercial vendors, who made modifications and now market commercial versions such as MSC.Dytran [Anon., 1997] and LS–DYNA [Anon., 2006], to name two of the many spin-offs. To assess the current state of the art in computational methods for crash analysis, it is important to understand the capabilities of each of the commonly used codes. Since LS–DYNA is used in the NASA crashworthiness research program, a brief description of the code is provided.

LS–DYNA is a general-purpose finite-element code for analyzing the large deformation dynamic response of structures, including structures coupled with fluids. The main solution methodology is based on explicit time integration. An implicit solver is also available. A wide variety of contact definitions is available, including self-contact, surface-to-surface contact, and node-to-surface contact. Spatial discretization is achieved by the use of eight-node solid elements, two-node beam elements, three- and four-node shell elements, truss elements, membrane elements, discrete elements, and rigid bodies. LS–DYNA currently contains approximately 200 different constitutive models and 10 equations of state to cover a wide range of material behavior. Fluid-structure interaction problems are simulated using arbitrary Lagrange–Euler (ALE) coupling. Recently, smoothed particle hydrodynamic (SPH) and element-free Galerkin (EFG) methods were added to provide additional “hydrocode” capabilities. LS–DYNA incorporates human occupant models that are designed to match the inertial and joint stiffness properties of anthropomorphic test devices (ATDs). These models represent the human body using rigid beams surrounded by ellipsoids with kinematic joints. In addition, downloadable models are available that permit designating certain parts as deformable. LS–DYNA is operational on a large number of mainframes, workstations, and personal computers and can be executed using shared memory processors or with multiple parallel processors. As mentioned previously, DYNA3D is a “parent” code to LS–DYNA and to MSC.Dytran. Consequently,

MSC.Dytran is similar to LS–DYNA in many respects. Other commercial explicit transient dynamic codes include PAM–CRASH (ESI Group) and ABAQUS/Explicit (Dassault Systèmes). Each of these codes can be used to predict transient dynamic structural response, and they are potentially suitable analytical tools with which to perform simulated helicopter crash scenarios as well as predict occupant survivability and internal volume reduction.

Examples of Current Predictive and Testing Capabilities

Research performed in rotorcraft crashworthiness includes testing and modeling approaches that incorporate physical representations of human occupants, energy-absorbing subcomponents, composite fuselage structures, and integration of models for all critical components into full-scale helicopter crash simulations. Because of space limitations, this report focuses on development, testing, and modeling of energy-absorbing concepts.

Development and testing of energy-absorbing concepts. A deployable energy absorber (EA) that has been developed at NASA uses an expandable honeycomb-like structure to absorb impact energy by crushing [Kellas and Jackson, 2007]. However, unlike any other cellular energy absorber in use today, the new concept uses a unique and patented flexible hinge at each junction of its cell walls. This feature enables almost any size and strength energy absorber to be fabricated and readily deployed either radially (omnidirectional energy absorption) or linearly (unidirectional energy absorption). Like conventional honeycomb, when expanded the new energy absorber is transformed into an efficient orthotropic cellular structure, with greater strength and stiffness along the cell axis compared with the transverse directions. An example of an isolated cell-wall junction is shown in figure 8.12.

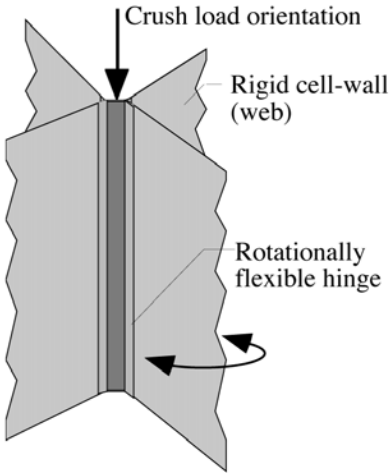

Figure 8.12. Schematic of the junction (hinge) of a square cell deployable structure.

Typically, the hinge consists of a fabric made of relatively strong, stiff, and tough fibers such as Spectra (Honeywell International Inc.), Vectran (Kuraray America, Inc.), Technora (Teijin Techno Products Limited), or aramid fibers. Other flexible materials can also be used for the construction of the hinges; however, advanced fiber-reinforced fabrics are thought to offer some unique opportunities for structural tailoring. Examples of properties that can be optimized, individually or collectively, include minimal deployment force, shear rigidity, shear strength, hinge tearing resistance, and specific energy absorption. The flexible hinge enables various methods of expanding the cellular structure, with the most basic ones shown in figure 8.13.

The linear expansion mode (depicted in fig. 8.13a) represents the simplest mode. When expanded in this fashion the energy absorber produces higher specific energy absorption because of a more efficient volumetric expansion (lower effective expanded density). However, radial deployment (illustrated in fig. 8.13b) produces an energy absorber with better omnidirectional capability. Because most practical applications involve curved rather than flat surfaces, the two basic deployment methods can be combined into a hybrid approach. To minimize the expanded density of the energy absorber, the cells are tapered, as shown in figure 8.13b. For rotorcraft applications, the energy absorber would be stowed under a frangible (or removable) aerodynamic cowling until a command is given to deploy the energy absorbers.

Previous work focused on fabrication studies, material tests, and static and dynamic tests of components to establish a preliminary design. The feasibility of the preliminary EA design has been demonstrated by performing vertical drop tests of a composite fuselage section fitted with the energy-absorbing structure. One of these tests is described as follows:

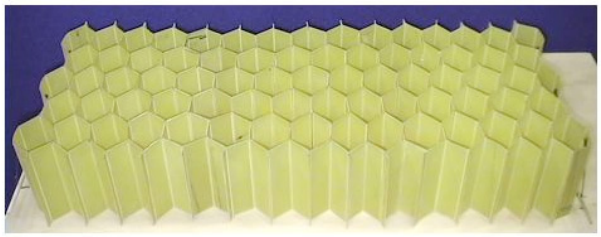

a) Linear deployment

b) Radial deployment

Figure 8.13. Photographs illustrating linear and radial deployment techniques.

A 38.4-ft/sec vertical drop test of a 5-ft-diameter composite fuselage section retrofitted with four blocks of the deployable energy absorbers onto a concrete impact surface was conducted in August 2006. The energy absorbers were made of a single woven ply of Kevlar 129 and weighed 5.6 lb each. Each energy absorber was 20 in. tall, 16.5 in. wide, and 20.5 in. deep. The energy absorbers were sized to provide an average floor-level acceleration of 20g. Vertical accelerations were measured at six locations on the fuselage floor. Acceleration/time histories were used to calculate crush displacements through double integration. The acceleration responses showed that most of the kinetic energy of the fuselage was dissipated effectively through progressive crushing of the energy absorbers, which achieved 70 percent of their 85-percent stroke capability. Pre- and post-test photographs are shown in figure 8.14.

Modeling of energy-absorbing structures. A finite-element model of the composite fuselage section retrofitted with four deployable energy absorbers was developed to simulate the 38.4-ft/sec vertical drop test onto concrete. Details of the modeling approach can be found in Kellas and Jackson [2007]. Eight different material properties were defined in the model. The material properties of the E-glass/epoxy and the graphite/epoxy fabric materials were determined from coupon tests and are represented using a bilinear elastic-plastic material model with strain hardening. The 3- and 8-lb/ft3 polyurethane foam cores, used in the upper cabin and floor, respectively, were modeled as linear elastic solid materials. The laminate stacking sequences of the multilayered face sheets were defined to specify the layer thicknesses and the number of integration points. The energy absorbers were represented using a crushable foam material model with a curve of stress versus strain data input to define the crush response. The stress-strain data were determined from a component test performed at 22.2 ft/sec velocity. A plot of the experimental data and the fitted response that was input to the model is shown in figure 8.15.

a) Pretest photograph b) Post-test photograph

Figure 8.14. Pre- and post-test photographs of the composite fuselage section with energy absorbers.

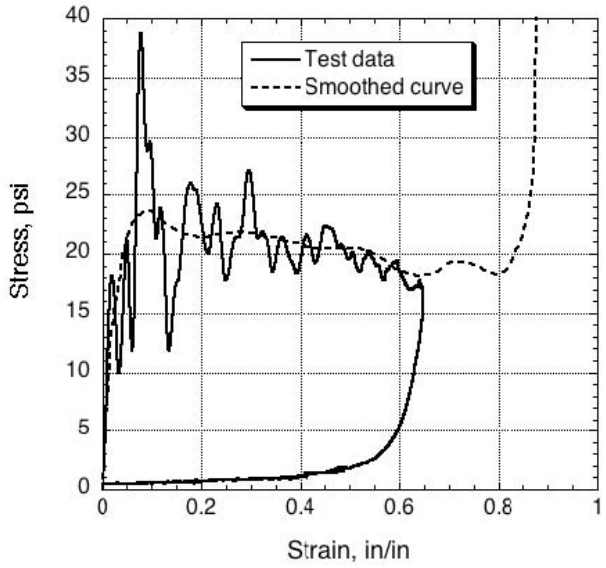

Figure 8.15. Input data for the energy absorber crush response.

An erosion parameter was specified for this material that established the strain (0.85 in./in.) at which an element within the energy-absorbing blocks would be eliminated from the model. Finally, it is worth noting that the unloading curve for this material definition is elastic; that is, the unloading curve is a straight line that initiates at the point of unloading and is parallel to the initial compressive response. However, the experimental data shown in figure 8.15 indicate that the actual unloading curve is hysteretic. The model was executed for 0.15 sec using LS–DYNA v971, which required 7 hr and 30 min of total processing time.

The test-analysis correlation is presented in two parts: a comparison of structural deformation and a comparison of acceleration-, velocity-, and displacement-time history responses. The deformed model and test article are shown in figure 8.16 for two discrete time intervals. At both time steps, the upper cabin of the fuselage section exhibits some elastic deformation evident in both the model and the test article. However, significant differences are observed in how the energy-absorbing blocks behave during impact. For the test, the cell walls within the composite honeycomb structure fold sequentially, forming an accordion-like deformation pattern.

Following the impact event, elastic energy—which is a small portion of the total energy—is released, providing some rebound velocity. Conversely, the energy absorber in the model shows element compression initiating in the area of contact with the impact surface. In addition, some minor crushing is seen at the top of the foam blocks. Early in time, the crushing and compression of the solid elements occurs in a stable manner; however, eventually the blocks buckle as a result of uneven compressive loading. Very little rebound of the model is observed. As expected, the solid-element representation of the energy absorber does not provide the accordion-like deformation pattern observed in the experiment. No damage was predicted or observed in the upper cabin or floor of the fuselage section. Analytical and experimental comparisons of acceleration, velocity, and displacement time histories are plotted in figure 8.17 for the center lead mass on the right side.

Time (s)	Deformed Model	Test Article
0.36		
0.72		

Figure 8.16. Analysis and test comparisons of energy absorber crush.

The analytical acceleration response (fig. 8.17a) shows excellent agreement with the experimental curve for the first 0.03 sec, accurately predicting the magnitude and timing of the peak acceleration (30g). Following the initial peak, the model predicts two additional peaks of lower magnitude (25g) than the first. At 0.06 sec, the predicted acceleration falls off sharply to 0g. Each of the three peaks seen in the predicted response is associated with the collapse of a group of compressed solid elements in the energy absorbers. The experimental acceleration response also exhibits three distinct peaks. The first peak occurs at 0.01 sec and has a magnitude of 30g. The second peak occurs at 0.028 sec with a magnitude of 21g, and the third peak occurs at 0.047 sec with a magnitude of 22g. Following the third peak, the magnitude of the experimental acceleration decreases gradually over the next 0.052 sec to 0g. Because of the sudden drop in the acceleration response and the relatively short pulse duration, the average acceleration of the predicted response is 22.7g. Conversely, the experimental acceleration response has longer pulse duration and an average acceleration of 19.4g. A comparison of the experimental and analytical velocity time histories is shown in figure 8.17b. As expected, a high level of correlation is observed for the first 0.03 sec. After that time, the two curves deviate from one another, with the analytical curve removing velocity more quickly than the test. The analytical velocity response crosses zero at 0.055 sec and exhibits a rebound velocity of 51 in./sec at 0.062 sec. The rebound velocity is reduced nearly to zero by the end of the pulse. Conversely, velocity was removed more slowly for the test and achieves a maximum rebound velocity of 113 in./sec at 0.12 sec. Finally, the velocity responses shown in figure 8.17b were integrated to provide experimental and analytical displacement time histories, which are plotted in figure 8.17c. The displacement curves show excellent agreement up to 0.05 sec. After that time, the predicted displacement curve levels off and achieves a maximum displacement of 13.7 in. at 0.056 sec. Meanwhile, the test curve continues to displace vertically downward to a maximum of 14.25 in. at 0.066 sec. In general, the predictions from LS–DYNA are encouraging. With improvements in the way EA structures are modeled, LS–DYNA can be forged into an effective analytical tool to support helicopter crash simulations and serve as a guide in developing concepts to improve occupant survivability and minimize internal volume reductions.

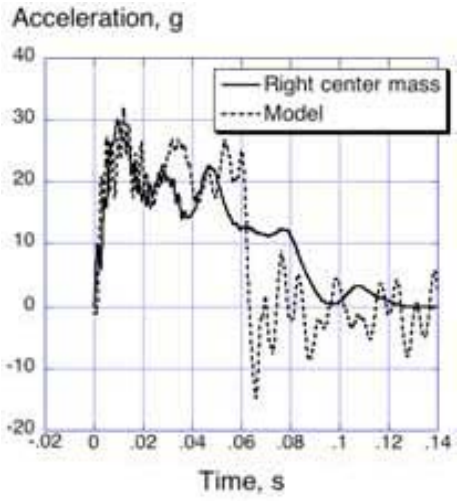

a) Acceleration

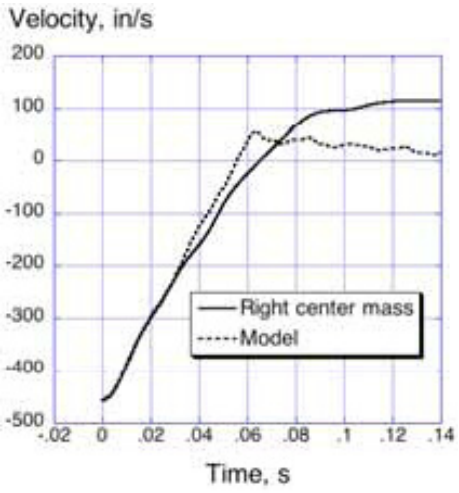

b) Velocity

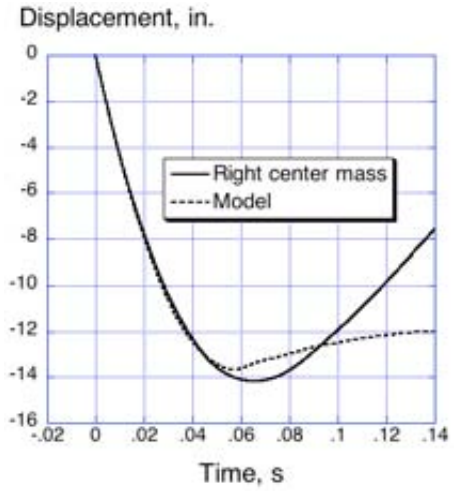

c) Displacement

Figure 8.17. Test-analysis comparisons.

Plans for improving predictive and testing capabilities

Development and testing of energy-absorbing concepts. For cellular structures made of ductile materials such as aluminum, there are three basic modes of energy dissipation: extensional deformation at the center of the deformed element, folding at stationary horizontal hinges, and folding and unfolding due to moving inclined hinges [Wierzbicki and Abramowicz, 1983; Wierzbicki and Bhat, 1987; Hayduk and Wierzbicki, 1982; Abramowitz and Jones, 1986; and Abramowitz and Wierzbicki, 1989]. It has been shown [Kellas, 1995 and 2002; and Kellas and Knight, 2001] that composite cellular structures can be treated using the same theory as long as the cell walls are designed to deform quasi-plastically and energy is absorbed in a similar way to that of metal cellular structures. One obvious difference between the deployable and conventional honeycombs is the flexible hinge. While the effect of the flexible hinge on the energy dissipation cannot be quantified without detailed analysis, it is anticipated that the flexible hinge could lead to lower energy absorption. Differences between conventional and deployable honeycombs can be assessed using the theory of Wierzbicki and Abramowicz [1983] to predict the average crush stress of conventional honeycombs with similar cell-wall properties as those of deployable structures. Such a comparison is depicted in figure 8.18 for three deployable structures of the same cell wall, a single woven ply of Kevlar 129, and different cell widths (W = 0.75 in., 1.0 in., and 1.25 in.).

While similar trends are shown in figure 8.18, there are at least two differences between theory for conventional honeycombs [Wierzbicki and Abramowicz, 1983] and the measured response of the deployable samples chosen for this study: lower measured crush stress and shallower experimental stress/(t/W) slope. Inspection of the folding mechanisms depicted in figure 8.19 shows that the extensional deformation mechanism is not present. Instead, energy is absorbed primarily through the formation of hinge lines and localized delamination to accommodate compatibility. Since extensional deformation is a more efficient mode of energy dissipation, it is anticipated that a better choice of adhesive to minimize delamination and promote stretching and/or tearing can lead to improved energy absorption.

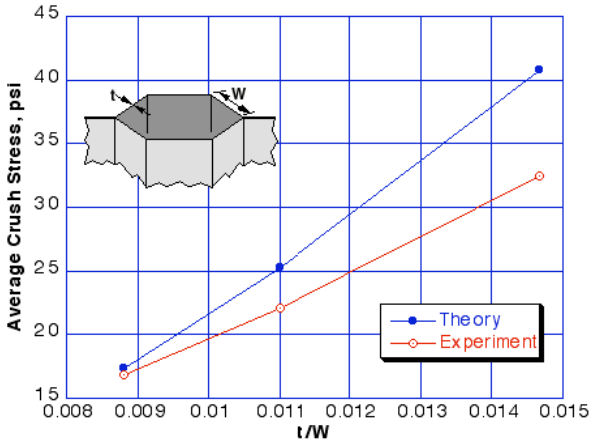

Figure 8.18. Average sustained crush stress versus t/W. Theoretical points were derived using the relationship of stress versus t/W.

Figure 8.19. Postcrush photograph of a deployable honeycomb made of Kevlar.

In addition to the folding differences, other contributing factors to the lower experimental strength compared with theory include the overall size of the energy absorber and cell-wall-perforation effects. Samples used in these tests were of finite width and depth and, as such, are subject to much lower strength because of the weaker cells along the boundary (perimeter). For example, an increase in average crush stress of approximately 20 percent is evident when the cell count of otherwise identical deployable samples was increased from 59 to 104 cells. Guided by the preliminary test results and failure analyses, efforts to improve the energy absorption using alternate materials and cell designs will continue.

Modeling and crash simulation. The level of correlation achieved by the LS–DYNA preliminary simulations of the fuselage section vertical drop test were quite good during the initial part of the honeycomb crush response. However, after 0.03 sec, some significant differences were observed, which are attributed to the fact that the energy absorber was represented using solid elements instead of shells. The model relied on the input stress versus strain properties to mimic the response of the energy absorbers. While this approach worked well initially, the solid-element model could not predict the complex failure mechanisms observed in the test article. For future work, the fuselage section model will be modified to include a shell element representation of the composite honeycomb energy absorbers. An important feature of the shell element model will be the material properties assigned to represent the Kevlar 129 fabric. These properties must accurately represent the material response under multidirectional loading. In addition, it is important that the shell model captures the failure modes seen during the test, including local buckling, tearing, and delamination.

The most appropriate figure of merit for comparing test and analysis of the compressive response of an energy-absorbing structure is the specific sustained energy absorption (SSEA). The SSEA is the energy removed from crushing the energy absorber (area under the load versus deflection curve) divided by the mass of the energy absorber. In order to accurately predict this value, the simulation must capture the initial loading response, the load at which the energy absorber begins to crush, the relative energy associated with each failure mode exhibited by the energy absorber, and the final

compaction response of the energy absorber. These types of correlations have been attempted and have proved mostly unsuccessful except for a few cases where the test specimen was highly constrained [Fleming et al., 2006; and Xiao et al., 2003]. Because of the limited size of this report, the previous discussions focused on only specific issues related to testing and modeling of energy-absorbing structures. A broader list of needs to improve predictive capabilities for rotorcraft crash simulation follows:

- A fundamental materials study is needed to provide a database for accurate material properties for finite-element simulations, including strain-rate effects, composite-material characterization, improved progressive failure models of composite materials, and soil characterization.
- A finite-element-based human occupant model should be developed. The model should incorporate skeletal structure, internal organs, and joints with accurate kinematic properties; also, it should be generated using deformable (not rigid-body) elements. The model would enable more accurate prediction of human soft-tissue injury during crash impact.
- Efficient multiterrain simulation techniques should be developed for modeling structural impact onto water with varying sea states, soft soil, rocks, a mixture of soil and rock, and vegetation. Coupled Lagrange–Euler modeling approaches should be evaluated to predict the fluid-structure interaction.
- Code enhancements are needed to improve contact algorithms, eroding surfaces, efficiency, global-to-local remeshing, portability between codes and platforms, development of higher-order elements with no reduction in efficiency, and coupling of kinematic and finite-element models.
- A code-verification study is needed to establish the boundaries of code accuracy, to provide confidence levels in analytical predictions, to incorporate probabilistic analysis, and to develop accurate methods to assess test-analysis correlation.
- Development of an integrated simulation methodology is needed. The methodology should include the effects of the impact surface, the landing or skid gear, the airframe, the seat and its attachment fittings, the occupant, the restraint system, and any supplemental systems such as external or cockpit airbags.

Validation data requirements

The current approach for model validation is through qualitative test-analysis correlation. For crash simulations, a comparison of acceleration responses is made, and the level of correlation is determined by how well the analysis predicts the acceleration onset rate, the magnitude of the peak, and the pulse duration. However, research should be expanded to consider a more rigorous methodology for test-analysis correlation. Recently, a project was initiated at NASA Langley Research Center to better quantify the accuracy of crash-simulation results. The motivation for the project, as stated by Lyle et al. [2002] was “to document modeling improvements, to evaluate design configurations analytically, and to enable certification or qualification by analysis.” Several important findings are repeated from Lyle et al. [2002], as follows: “It is necessary to quantify and understand experimental variations, channel-to-channel, for symmetric locations, as well as test-analysis variations. Future crash finite element model development could be expedited by correlation with experimental modal analysis results, especially since the modal correlation will depend on the accuracy of the global stiffness and mass distribution of the finite element model. Also, this approach provides a second set of data for correlation, which is important given that most test articles are destroyed during crash

testing." Continued work is needed to automate rigorous test-analysis correlation methodologies to improve and redefine the level of accuracy. Hemez and Doebling [2001] provide an excellent summary of a panel discussion on issues and directions of research in the areas of model updating, predictive quality of computer simulations, model validation, and uncertainty quantification. This paper raises some pertinent questions, such as what model is appropriate for what purpose, and what does it take to be predictive? Hemez and Doebling [2001] question the validity of calling a model predictive when it has been validated through comparison with a single set of test data. Such a model does not guarantee accuracy of predictions for scenarios not represented by the test data. The authors state, "It is our opinion that the focus of the research in model validation should be shifted from validating deterministic models to validating statistically accurate models." Such an approach would account for variability in the operational and testing environment and uncertainties related to manufacturing and fabrication tolerances. Thus, model validation should be strongly coupled with uncertainty quantification. Finally, the authors propose five topic areas that are "critical to the success of model updating, uncertainty quantification, and model validation for linear and nonlinear dynamics." These five topic areas are uncertainty quantification, sampling and fast probability integration, generation of fast-running metamodels, feature extraction, and statistical hypothesis testing. Through addressing these five topic areas, a truly comprehensive prediction model and methodology can be developed, which would substantially enhance helicopter crash simulation and survivability assessment.

Cross-cutting technology needs

Improved material modeling is a continuous ongoing need, especially as new materials are developed and applied. It is also important that existing and updated material models are well-documented. For example, LS-DYNA has approximately 200 hundred different material models available, which the Livermore Software Technology Corp. (LSTC) implements into the code when requested by customers. However, very little documentation exists to guide new users in choosing the correct material model for their application. One shortfall common to explicit transient dynamic finite-element codes is the lack of a rigorous delamination failure capability for composite materials. In general, it is difficult to implement delamination criteria in these codes because of the small mesh size required. A small mesh is needed for accurate prediction; however, such a mesh may result in a reduction in the time step, causing computation time to increase substantially. Also, the dynamic property data needed to predict delamination growth under impact conditions are not easily obtained. A review of several methods to incorporate delamination failure criteria for composites is documented by Fleming et al. [2006].

Cabin Noise Reduction

Lightweight acoustic insulation materials are desired for improving rotorcraft cabin noise without impacting aircraft performance. Traditional acoustic insulators are porous materials with pore diameters much larger than the mean free path of air. Fluid can easily move into and out of the pores. The energy of a sound pressure wave is dissipated by transfer of energy to the solid structure of the insulator through repeated reflections inside the pores. Common examples of such materials are open-cell foams and loosely woven fiber mats that are pressed into place.

The flow resistance and impedance of these materials are often used to evaluate their suitability as acoustics absorbers. They must also be able to absorb sound at various angles of incidence. The range of acceptable flow resistances is determined by their application. A good starting point for internal cabin acoustic insulation for commercial aircraft is Boeing's criteria of a minimum flow resistance of 2.45 rho-c at 105 cm/sec.

Polyimide foams and aerogels are currently being examined to determine their suitability as acoustic absorbers. Both are good thermal insulators and have an extremely low density, possibly resulting in vehicle weight reduction.

Polyimide foams have been around for nearly four decades, mainly serving the military ship industry as a wall-board acoustic panel. One of the earliest polyimide foam patents is credited to E. I. DuPont de Nemours, Inc. (DuPont) in 1966 [Hendrix, 1966]. DuPont's patent describes a foaming process using a chemical blowing agent. Acid mixed into a polyamide acid solution produced bubbles, thus forming the foam. Foam sheets from 0.127 to 254 mm in thickness were produced with densities ranging from 0.04 to 0.4 g/cm^3. A follow-on patent in 1967 [Amborski, et al., 1967] shifted from chemical to physical blowing agents such as nitrogen gas, carbon dioxide (CO2), or mechanically frothed air. Uniform distribution of the blowing agent throughout the polyamide acid resulted in better control of the cell structure.

In 1992, a patent by Lee describes Imi-Tech's foaming technique, which uses a spray-dried polyimide precursor powder combined with water [Lee et al., 1992]. The evolution of water vapor forms the foam. The correlation between weight percent added water and resultant foam density was clearly shown [NASA, 1994]. Imi-Tech then used microwave technology to excite the water molecules and begin the imidization reaction. To better reduce the nonhomogenous cell structure, Imi-Tech used a mixing bar to stir the microwave energy and ensure the even irradiation of the precursor paste. Foam densities of 0.002 to 0.009 g/cm^3 were produced [NASA, 1994]. To date, Imi-Tech's microwave foaming process is the state of the art for low-density polyimide foams.

The late 1990s saw the introduction of TEEK polyimide foams, a new structural foam that could operate at temperatures down to –252.8 °C without cracking or forming frost on the exterior surface. The Boeing Company, Northrop Grumman, and Lockheed Martin conducted a significant amount of research into TEEK as a potential thermal-insulation material for their cryogenic fuel tank concepts for NASA programs such as X-33, Space Launch Initiative (SLI), and Next Generation Launch Technology (NGLT) [Weiser et al., 2000; Williams, et al., 2001; Weiser, 2004; and Williams et al., 2005]. While the TEEK foams performed well for these applications, relatively high cost and difficulty with large-scale manufacture limited their introduction into aeronautics technologies.

Recently, engineers from NASA Langley Research Center and Polyumac TechnoCore, Inc., have developed a novel polyimide foam that may meet the needs of several NASA programs because of its lower cost, excellent performance, and ease of manufacture [Vazquez et al., 2005]. These foams represent the first foams produced at room temperature that are then cured using a microwave. They

have many of the same properties as the TEEK polyimide foam but can be made to very low densities, 0.003 to 0.016 g/cm^3, and used as thermal and acoustic insulation. These foams showed flow-resistance values as low as 1.6 rho-c, surpassing the Boeing goal. More testing will be required to verify the ultimate potential of this material as an acoustic absorber.

Silica aerogels are also being considered for acoustic insulation. They represent silica in its lowest-density form. While chemically identical to silica in bulk form, the nanoscale structure of aerogel provides it with exceptional properties, including extremely low density, extremely low thermal conductivity, and extremely high specific strength. These materials are open-cell materials with void volumes (the fraction of the volume of the apparent solid that is open space) often approaching 95 percent. Pore sizes are extremely small, typically ranging from 1 to 100 nm.

Silica aerogels are formed through a sol-gel process, where primary silica particles approximately 1 nm in diameter form and then agglomerate into porous spheres 10 to 20 nm in diameter. These secondary particles connect to each other, forming tortuous threadlike structures spanning the volume of the growth container. When allowed to dry in ambient air, the structure collapses, forming a material known as a xerogel. As the solvent filling the gel evaporates, the surface tension of the remaining liquid causes it to pull itself into a sphere, and the association between the solvent and the silica skeleton collapses the gel structure. When dried under supercritical conditions, the low density and high void volume are retained and the material is known as an aerogel. Since supercritical drying converts liquid CO2 to gas without an abrupt phase change, collapse of the gel can be avoided. Supercritical drying to from an aerogel was first done by Kistler [1932], using alcohol as the solvent. However, the inherent danger of handling a flammable solvent at high pressure and temperature has prompted the conversion of the process to liquid carbon dioxide. Aerogels are generally dried this way today.

Although the specific strength of silica aerogel is quite high, the extremely low density (~0.1 g/cm^3) means that the strength in absolute terms is very low. The mechanical structure, and therefore the strength, of silica aerogels is dominated by the strength on the “neck” regions where the primary particles intersect. The key to overcoming the extremely fragile nature of conventional silica aerogels lies in strengthening the intersection of the primary particles without compromising the mesoporosity that gives the aerogel its unique properties.

Leventis [Zhang et al., 2003] developed a technique for reinforcing conventional silica aerogel that reacts to the pendant –OH groups on the silica surface with an isocyanide, forming, in effect, a polyurethane coating on the silica backbone, preserving the mesoporosity, and increasing the strength dramatically. Researchers at NASA Glenn Research Center have extended this initial concept, modifying the underlying gel to include a wider range of functional groups on the surface, improving the polyurethane reinforcement, and allowing cross-linking with a range of polymers [Zhang et al., 2004; Meador et al., 2005 and 2007; and Ilhan et al., 2006]. The reinforced aerogel technology allows production of test samples capable of withstanding the forces imposed by handling and practical use.

To date, aerogels have shown some promise as acoustic materials. Several manufacturers offer aerogel-based materials as acoustic insulators. Cabot Corporation (Billerica, Mass.) offers its Nanogel material comprising aerogel particles created without supercritical drying. Cabot cites the low speed of sound in aerogel as one of its advantages, but the company also tailors the panel thickness, particle size, and distribution to adjust the sound-absorption characteristics, suggesting that the acoustic properties of this aerogel material are heavily dependent upon the particle size rather than the aerogel composition, although Cabot does state that the performance can be modified by changes in the material composition.

Aspen Aerogels (Northborough, Mass.) manufactures a series of products with aerogel material applied to fibrous mats that also provide both thermal and acoustic insulation. In this case, the fibrous nature of the aerogel-covered mat is likely to provide a substantial portion of the acoustic-absorbance properties.

A report by Boeing [1996] examines aerogel as an acoustic absorber. The aerogels tested were organic resorcinol-formaldehyde (RF) aerogels, similar in concept to the more familiar silica aerogels, but with a carbon-based framework. These aerogels were unreinforced, and their extreme fragility made them impractical for general use. The report also noted environmental shrinkage, where the samples shrank by about 5 percent over a 2-month period. These samples were subjected to acoustic impedance, flow resistance, and acoustic insertion loss tests. Acoustic impedance tests showed only very small absorption coefficients when compared with polyimide foam or fiberglass. The flow-resistance tests showed essentially no flow through the samples until they broke. Insertion losses were significantly less than those of other materials tested. The conclusion of the report was that aerogels were not suitable acoustic absorbent materials and performed about the same as closed-cell foams.

Comparing the results of the Boeing report and the claims made by Cabot Corp. and others leads to the assumption that when used alone, aerogels of conventional morphology act as if they are closed cell foams—poor absorbers and quite possibly reflectors of acoustic energy. A commonly held theory of acoustic absorbance requires that air penetrate the pores in the material, transferring acoustic energy into the structure. It appears that the Cabot Corp. and Aspen Aerogels materials work as acoustic absorbers because the particle size or fiber mesh provides holes of sufficient size to allow the air to freely enter and transfer energy to the aerogel where the extremely low sound velocity (~100 m/sec) can assist in the dissipation of the acoustic energy.

Calculations made by NASA [Kuczmarki, 2007][4] indicate that even at the upper end of the mesopore size commonly quoted for silica aerogels (~100 nm), the air flow into and out of the pores is in a transition region between bulk and molecular flow. While aerogels are certainly open cell, and gas can pass completely through them, there is a substantial resistance to the free flow of gas through the bulk of the material because of the size of the pores. The mesopore diameter is within about a factor of 2 of the mean free path in air at atmospheric pressure. A calculation was performed that predicts that the minimum pore size necessary for continuum flow in an aerogel is ~ 30 um (30,000 nm.) The

[4] Personal communication. NASA Glenn Research Center, 2007.

flow resistances of the Glenn Research Center-made reinforced aerogels have not yet been determined. It is anticipated that the initial formulations will display high flow resistances because of the extremely small pore sizes and that efforts to increase the pore size will decrease the flow resistance.

Current tools available or in development at NASA

The primary materials used for acoustic insulation in current rotorcraft are fiberglass matting and open-cell foams. A brief description of each of these material types follows:

- Fiberglass matting: Current rotorcraft make extensive use of fiberglass matting for acoustic absorption. Because of the loose nature of fiberglass matting, it is typically compressed on installation as an acoustic absorber to obtain the desired flow resistance and impedance properties.
- Foam: Open-cell foams are also available for acoustic control. They have the advantage of not typically requiring that they be installed and maintained in their compressed form. However, they may exact a weight penalty compared with compressed fiberglass.

A variety of materials is under development as acoustic insulators for rotorcraft:

- Polyimide foam: The current generation of polyimide foams shows low densities (8.4 lb/ft^3, 0.135 g/cm^3) with pore sizes of about 20 pores per inch (ppi). Their normalized flow resistance is approximately 9 at an air velocity of 10 cm/sec, increasing to about 20 at 200 cm/sec. These resistances are higher than recommended for acoustic absorbers, but they show promise of dropping into the desired 0.5-to-3 range with modification of the pore sizes.
- Aerogel: Aerogels, particularly polymer reinforced aerogels, can be formulated at a range of densities, and the mechanical strength of these materials varies with the formulation and density. Pore sizes in aerogels are at least 4 orders of magnitude smaller than in polyimide foams, making them 100 nm or smaller. These extremely small pore sizes are within about a factor of 2 of the length of the mean free path in air, resulting in low-density, open-cell, high-void-volume materials through which air does not easily pass. In fact, these dimensions place the air flow into and out of the pores in the transition region between continuum and molecular flow.
- Hybrids: Hybrid bulk absorbing materials have been suggested in an effort to gain the advantages of both materials used in their composition. Both macro- and microscale hybrids are being considered. Macroscale hybrids combine, for instance, a polyimide foam and an aerogel panel together. A microscale hybrid could consist of intermingled polyimde foam and aerogel.

Among the tools available for acoustic design, there is a collection of design curves that has been developed for fiberglass materials that allow the determination of the acoustic characteristics of the material when used under various conditions (see fig. 8.20) [Beranec and Ver, 1992]. There are no such tools available for either polyimide foams or aerogels. In order to create such design curves, both the flow resistance and the acoustic impedance of the materials must be known. These parameters are currently being measured for polyimide foams at NASA Langley Research Center and will ultimately provide a basis for performance assessment and comparison with state-of-the-art and other developmental acoustic materials.

Examples of current predictive and testing capabilities

The currently accepted tests for determining the suitability of a material as an acoustic absorber are the flow resistance, the acoustic impedance, and the transmission loss. Flow resistance measures the ability of air to move through the material, a prerequisite for acoustic absorption. A typical range for absorbers is from 0.5 to 3.0 rho-c. Materials with flow resistances above 3 rho-c inhibit air flow and begin to reflect, rather than absorb, sound. Materials with resistances below 0.5 rho-c allow so much flow that the ability to interact with the air and thereby absorb sound is reduced.

Acoustic impedance testing measures the frequency-dependent absorption of a material and allows the suitability of a material to be judged based on its performance at frequencies of particular interest. Combined with the flow-resistance measurement, which essentially measures the acoustic impedance at 0 Hz, acoustic impedance testing provides substantial insight into the performance of a material as an acoustic absorber.

Transmission loss measures the ability of a material to measure sound transmitted through the insulation. This property is particularly useful in selecting insulation for use when a noise source can be separated from the people affected by the noise with the insulation.

Current computational acoustics models concentrate on the macroscale. Bulk parameters, such as flow resistivity and porosity, are used to approximate the acoustic absorption behavior of materials. The solid structure is assumed to be rigid in these models [Fahy, 2001]. The relationship between these bulk parameters and absorption performance is often derived. For example, Delany and Bazley [1970] developed relationships that expressed characteristic impedance and propagation coefficient

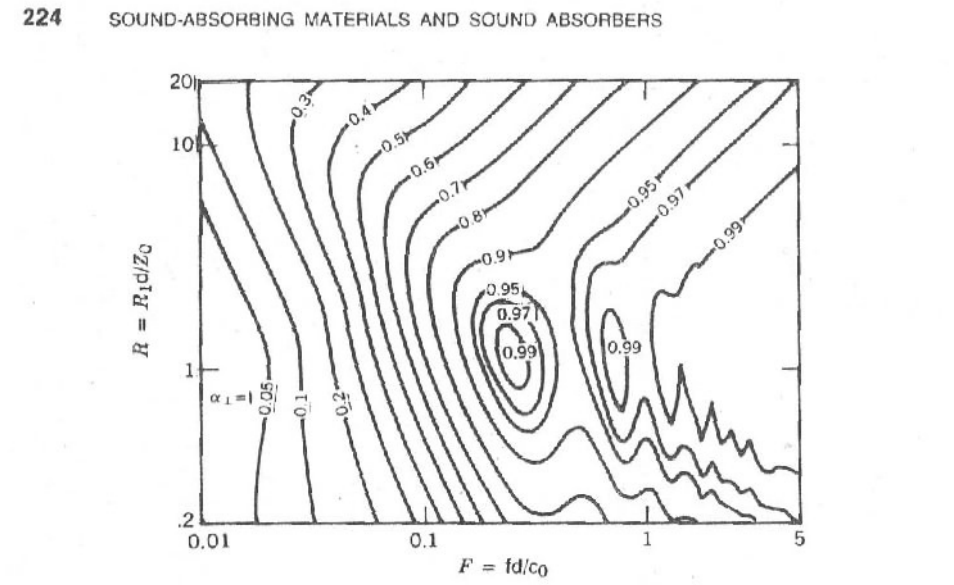

Figure 8.20. Lines of constant absorption at normal-incidence sound; absorption coefficient for fibrous absorbers of thickness, d, and flow resistivity, R_1; no airspace.

as functions of flow resistivity divided by frequency. Poroelastic models seek to describe both the porous and elastic nature of acoustic absorbers by including both fluid flow around the internal solid structure and the motion of the solid structure itself [Allard, 1993; and Kang and Bolton, 1996]. Such models will provide a potential approach to enable the design of advanced material systems that can realize a 5-dB interior noise reduction without unacceptable weight penalties. However, a model that provides a bridge between the physics occurring at the molecular level and the bulk parameters currently used to predict acoustic performance does not exist at this time.

Plans for improving predictive and testing capabilities

Acoustic testing capabilities are being developed at Glenn Research Center for screening materials being investigated for use as acoustic absorbers in rotorcraft. Simple flow-resistance and acoustic-impedance instruments are in development at NASA Glenn Research Center. These instruments are not intended to replace the more sophisticated systems at NASA Langley Research Center, but will be used to rapidly screen new aerogel formulations during the materials development process. In addition, adaptation of these systems to accommodate various sample geometries is being examined. Specifically, an analysis of the experimental apparatus will be performed to predict the capability to adapt them to samples of significantly different shapes or sizes. It is also being proposed that an additional figure of merit be used with these new materials concepts for acoustic absorbers, namely the insertion loss of the material divided by the density. This quantity will be a useful measure of the weight penalty incurred by an insulation concept. Transmission loss measurements will be performed by acoustic researchers at the Langley Research Center.

Computational modeling of the thermal performance of numerous aerogel composite insulation concepts has recently been completed. The possibility of performing acoustic modeling on these concepts is currently being discussed as a way to tailor the properties of the complete panel.

Currently there is no satisfactory understanding of the relationship between morphology and acoustic properties for aerogels in particular. The feasibility of the application of computational modeling of the interaction of the air and the structure of the absorber at the pore level is being examined. For aerogels, the mesopores are on the scale of tens of nanometers. As a result, the flow of air into and out of the pores lies in the transition area between molecular and continuum flow, as the mean free path in air is no more than half the mesopore diameter.

The commercial COMSOL (COMSOL, Inc.) package is currently being evaluated for its ability to address this flow regime. If this package does not work for this particular problem, a truly atomistic approach may have to be taken.

For aerogels, there currently is no adequate understanding of the relationship between processing characteristics and morphology. The processing conditions can have dramatic effects on the morphology of the aerogel, but little is known about the specific effects. These effects become increasingly vital as the acoustic requirements embodied in the 5-dB interior noise reduction push the need to modify the pore sizes in aerogels.

Validation data requirements

Basic acoustic properties (i.e., flow resistivity, acoustic impedance, and transmission loss) must be established for materials being considered for acoustic insulation. Flow resistance, acoustic impedance, and transmission loss data are required for both the polyimide foam and aerogel materials. To date, the polyimide foams have been better characterized than the aerogels, but there will be an ongoing need for this data throughout their development. Interaction with acousticians for higher-level acoustic analysis as the development approaches actual applications is also needed.

Cross-cutting technology needs

Research and development of new materials is necessary as these materials are being considered for acoustic applications. In particular, an optimized morphology is required to bring about low density. Structural integration of these materials must be established for safety, reliability, and durability. There must be manufacturing scale-up for aerogel production for these materials to be useful for engineering components.

REFERENCES

Abdul-Aziz, A.; Baaklini, G. Y.; and Bhatt, R. T.: Design Evaluation Using Finite Element Analysis of Cooled Silicon Nitride Plates for a Turbine Blade Application. NASA/TM–2001-210819, June 2001.

Abramowicz, W. and Jones, N.: Dynamic Progressive Buckling of Circular and Square Tubes. Int. J. Impact Engineering, vol. 4, no. 4, Dec. 1986, pp. 243–270.

Abramowicz, W. and Wierzbicki, T.: Axial Crushing of Multicorner Sheet Metal Columns. J. Applied Mechanics, vol. 56, no. 1, Dec. 1989, pp.113–120.

ADS–36: Aeronautical Design Standard Rotary Wing Aircraft Crash Resistance. U.S. Army Aviation Systems Command, St. Louis, Mo., May 1987.

Allard, J. F.: Propagation of Sound in Porous Media: Modeling Sound Absorbing Materials. Elsevier Applied Science, London, 1993.

Amborski, L. E. et al.: Cellular Polyimide Product. U.S. Patent 3,310,506, Mar. 1968.

Amer, Kenneth, B.: Closing the Loop on Helicopter Crashworthiness Design Requirements. Proc. of the 47th Annual Forum of the AHS, Phoenix, Ariz., May 6–8, 1991, pp. 913–920.

Anon.: Aircraft Crash Survival Design Guide, vols. 1–5, USAAVSCOM TR 89-D-22, Dec. 1989.

Anon.: LS-DYNA Keyword User's Manual, Version 971. Livermore Software Technology Corp., Livermore, Calif., May 2007.

Anon.: MSC/Dytran User's Manual, Version 4.0. The MacNeal-Schwendler Corp., Los Angeles, Calif., Nov. 1997.

Barrie, R. L.; Gabb, T. P.; Telesman, J.; Kantzos, P. T.; Prescenzi, A.; Biles, T.; and Bonacuse, P. J.: Effectiveness of Shot Peening in Suppressing Fatigue Cracking at Non-Metallic Inclusions in Udiment®720. NASA/TM–2005-213577, Mar. 2005.

Beranek, Leo L. and Ver, Istvan L. (eds) : Noise and Vibration Control Engineering: Principles and Applications. John Wiley & Sons, Inc., Hoboken, N.J., 1992.

Boeing Commercial Airplane Group (1996): HSR Interior Noise Technology Development Activities at Boeing during 1995.

Bolukbasi, Akif, O.: Crashworthy Design of Military and Civil Rotorcraft. Proc. of the SAE Advances in Aviation Safety Conf., Daytona Beach, Fla., April 11–13, 2000.

Bonacuse, P.; Telesman, J.; Kantzos, P.; Gabb, T.; Barrie, R.; and Banik, A.: The Effect of Powder Cleanliness on the Fatigue Behavior of Powder Metallurgy Ni-Disk Alloy Udiment®720. Proc. 10th International Symposium on Superalloys – Superalloys 2004, Champion, Penn., Sept. 19–23, 2004, pp. 409–420.

Bonacuse, P. J.; Kantzos, P.; Telesman, I.; Gabb, T.; and Barrie, R. (2002): Modeling Ceramic Inclusions in Powder Metallurgy Alloys. Fatigue 2002, Proc. of the Eighth International Fatigue Congress, Stockholm, Sweden, June 2–7, 2002. Blom, A. F. (ed.), EMAS, West Midlands, U.K., pp. 1339–1346.

Bonacuse, P. J.; Kantzos, P.; and Telesman, J.: Ceramic Inclusions in Powder Metallurgy Disk Alloys: Characterization and Modeling. 5th Annual FAA/Air Force/NASA/Navy Workshop on the Application of Probabilistic Methods for Gas Turbine Engines, Westlake, Ohio, June 11–13, 2001. NASA/CP–2002-211682, Oct. 2002, pp. 359–389.

Borom, M. P.; Johnson, C. A.; and Peluso, L. A.: Role of Environmental Deposits and Operating Surface Temperature in Spallation of Air Plasma Sprayed Thermal Barrier Coatings. Surface Coatings Technology, vol. 86-87, no. 1, 1996, pp. 116–126.

Bruce, R. W.: Development of 1232°C (2250°F), Erosion and Impact Tests for Thermal Barrier Coatings. Tribology Transactions, vol. 41, no. 4, 1998, pp. 399–410.

Burrows, L. T.: Variable Design Criteria for Rotary Wing Aircraft Crash Resistance. Proc. of the 49th Annual Forum of the AHS, St. Louis, Mo., May 19–21, 1993.

Code of Federal Regulations: CFR 14, Title 14, Part 27: Airworthiness Standards: Normal Category Rotorcraft. Vol. 1, Rev. Jan, 2008, pp. 601–683.

Code of Federal Regulations: CFR 14, Title 14, Part 29: Airworthiness Standards: Transport Category Rotorcraft. Vol. 1, Rev. Jan. 2008, pp. 683–799.

Chen, X.; Wang, R.; Yao, N; Evans, A. G.; Hutchinson, J. W.; and Bruce, R. W.: Foreign Object Damage in a Thermal Barrier System: Mechanisms and Simulations. Mat. Sci. Engineering A, vol. 352, no. 1–2, July 2003, pp. 221–231.

Chen, X.; Hutchinson, J. W.; and Evans, A. G.: Simulation of the High Temperature Impression of Thermal Barrier Coatings with Columnar Microstructure. Acta Materialia, vol. 52, 2004, pp. 565–571.

Choi, S. R.; Pereira, J. M.; Janosik, L. A.; and Bhatt, R. T.: Foreign Object Damage in Flexure Bars of Two Gas-Turbine Grade Silicon Nitrides. Mat. Sci. and Engineering A, vol. 379, no. 1–2, Aug. 2004, pp. 411–419.

Coltman, J. W.; Bolukbasi, A. O.; and Laananen, D. H.: Analysis of Rotorcraft Crash Dynamics for Development of Improved Crashworthiness Design Criteria. DOT/FAA/CT-85/11, June 1985.

Cvitkovich, M. K.; and Jackson, W. C.: Compressive Failure Mechanisms in Composite Sandwich Structures, J. Amer. Hel. Soc., vol. 44, no. 4, Oct. 1999, pp. 260–268.

Delany, M. E. and Bazley, E. N.: Acoustical Properties of Fibrous Absorbent Materials. Appl. Acoust., vol. 3, no. 2, April 1970, pp. 105–116.

Evans, A. G.; Fleck, N. A.; Faulhaber, S.; Vermaak, N.; Maloney, M.; and Darolia, R.: Scaling Laws Governing the Erosion and Impact Resistance of Thermal Barrier Coatings. Wear, vol. 260, no. 7–8, 2006, pp. 886–884.

Fahy, F. J.: Foundations of Engineering Acoustics. Elsevier Academic Press, London, England, Sept. 2000.

Fleming, D. C.; Morrow, C.; Ckarke, C. W.; and Bird, C. E.: Finite Element Simulation of Delamination with Application in Crashworthy Design. Proc. of the AHS 62nd Annual Forum, Phoenix, Ariz., May 9–11, 2006.

Gabb, T. P.; Telesman, J.; Kantzos, P. T.; Bonacuse, P. J.; and Barrie, R. L.: Initial Assessment of the Effects of Nonmetallic Inclusions on Fatigue Life of Powder-Metallurgy-Processed Udimet^{TM} 720. NASA/TM–2002-211571, ARL-TR-2804, Aug. 2002.

Gamon, M. A.: General Aviation Airplane Structural Crashworthiness User's Manual. Volume I: Program KRASH Theory. Final Report FAA-RD-77-189-I, Feb. 1978.

Gamon, M. A.; Wittlin, G.; and LaBarge, B.: KRASH 85 User's Guide-Input/Output Format. Final Report DOT/FAA/CT-85/10, Mar. 1986.

Hamed, A.; Jun, Y. D.; and Yeuan, J. J.: Particle Dynamics Simulations in Inlet Separator with an Experimentally Based Bounce Model. J. Propulsion Power, vol. 11, no. 2, March–April, 1995, pp. 230–235.

Hamed, A. A.; Tabakoff, W.; Rivir, R. B.; Das, K.; and Arora, P: Turbine Blade Surface Deterioration by Erosion. J. Turbomachinery, vol. 127, no. 3, 2005, pp. 445–452.

Hamed, A.; Tabakoff, W.; and Wenglarz, R.: Erosion and Deposition in Turbomachinery. J. Prop. Power, vol. 22, no. 2, 2006, pp. 350–360.

Handschuh, R. F.: High-Temperature Erosion of Plasma-sprayed, Yttria-stabilized Zirconia in a Simulated Turbine Environment. AIAA-1985-1219; also NASA/TP-2406, Dec. 1984.

Hallquist, John O.: DYNA3D User's Manual: Nonlinear Dynamic Analysis of Structures in Three Dimensions. University of California Report UCID-19592, Rev. 4, April 1988.

Hayduk, R. J. and Wierzbicki, T.: Extensional Collapse Modes of Structural Members. J. Computers and Structures, vol. 18, no. 3, 1984, pp. 447–458.

Hemez, F. M. and Doebling, S. W.: Model Validation and Uncertainty Quantification. Proc. of the IMAC-XIX, the 19th International Modal Analysis Conf., Kissimmee, Fla., February 5–8, 2001.

Hendrix, W. R.: Forming a Foamed Polyimide Article. U.S. Patent 3,249,561, May 1966.

Housner, J. M., and Noor, A. K. (Compilers): Research in Structural and Solid Mechanics. NASA CP-2245, Oct. 1982.

Ilhan, U. Faysal; Fabrizio, E. F.; McCorkle, Linda; Scheiman, Daniel A.; Dass, Amala; Palczer, Anna; Meador, Mary Ann B.; Johnston, James C.; Leventis, Nicholas: Hydrophobic Monolithic Aerogels by Nanocasting Polystyrene on Amine-modified Silica. J. Mater. Chem., vol. 16, no. 29, 2006, pp. 3046–3054.

Jackson, K. E.; Boitnott, R. L.; Fasanella, E. L.; Jones, L. E.; and Lyle, K. H.: A Summary of DOD-Sponsored Research Performed at NASA Langley's Impact Dynamics Research Facility. J. American Helicopter Society, vol. 51, no. 1, Jan. 2006.

Kang, Y. S. and Bolton, J. S.: Optimal Design of Acoustical Foam Treatments. J. Vibration and Acoustics - Transactions of the ASME, vol. 118, no.3, 1996, pp. 498–504.

Kantzos, P. T.; Barrie, R. L.; Bonacuse, P. J.; Gabb, T.; and Telesman, I.: The Effects of Forging Strain on Ceramic Inclusions in a Disk Superalloy. Proc. of The Minerals, Metals and Materials Society (TMS) Conf. on Advanced Materials and Processes for Gas Turbine Engines, 2003, pp. 245–254.

Kellas, S.: An Experimental Investigation into the Energy Absorption Performance of Composite Beam Web for Aircraft Subfloor Applications. National Technical Specialists' Meeting on Rotorcraft Structures, Design Challenges and Innovative Solutions, sponsored by the AHS, Oct. 1995.

Kellas, S. and Knight, N. F. Jr.: Design, Fabrication and Testing of Composite Energy-Absorbing Keel Beams for General Aviation Type Aircraft. Paper no. AIAA-2001-1529, 42nd AIAA/ASME/ASCE/AHS/ASC Structures, Structural Dynamics, and Materials Conf. and Exhibit, Seattle, Wash., April 16–19, 2001.

Kellas, S.: Design, Fabrication and Testing of a Crushable Energy Absorber for a Passive Earth Entry Vehicle. NASA/CR–2002-211425, April 2002.

Kellas, S. and Jackson, K.: Deployable System for Crash-Load Attenuation. Proc. of the AHS 63rd Forum, Virginia Beach, Va., May 1–3, 2007, pp. 1203–1220.

Kistler, S.S.: Coherent Expanded Aerogels. J. Physical Chem., vol. 36, no. 1, 1932, pp. 52–64.

Kramer, S.; Yang, J.; Levi, Carlos; and Johnson, C. A.: Thermochemical Interaction of Thermal Barrier Coatings with Molten CaO-MgO-Al_2P_3-SiO_2 (CMAS) Deposits. J. Amer. Ceram. Soc., vol. 89, no. 10, 2006, pp. 3167–3175.

Labun, Lance : Final Report on the Survivable, Affordable, Reparable Airframe Program (SARAP) and the Helicopter Kinematic Design Criteria for Crashworthiness. Simula Aerospace and Defense Group, TD-04049, May 2004.

Lee, K. N.; Fox, D. S.; and Bansal, N. P.: Rare Earth Silicate Environmental Barrier Coatings for SiC/SiC Composites and Silicon Nitride Ceramics. J. Eur. Ceram. Soc., vol. 25, no. 10, 2005, pp. 1705–1715.

Lee, R. et al.: Polyimide Foam Products and Methods. U.S. Patent 5,096,932, Mar. 19, 1992.

Lin, H. T.; Ferber, M. K.; Wereszczak, A. A.; and Kirkland, T. P.: Effects of Materials Parameter on Strength of EBC Coated Silicon Nitride. ORNL EBC Workshop, Nashville, Tenn., 2003.

Lyle, K. H.; Bark, L. W.; and Jackson, K. E.: Evaluation of Test/Analysis Correlation Methods for Crash Applications. J. Amer. Hel. Soc., vol. 47, no. 4, Oct. 2002, pp. 233–242.

Meador, M. A. B.; Fabrizio, E. F.; Ilhan, F.; Dass, A.; Zhang, G.; Vassilaras, P.; Johnston, J. C.; and Leventis, N.: Crosslinking Amine-Modified Silica Aerogels with Epoxies: Mechanically Strong Lightweight Porous Materials. Chem. Mater., vol.17, no. 5, 2005, pp. 1085–1098.

Meador, Mary Ann B.; Capadona, Lynn A.; McCorkle, Linda; Papadopoulos, Demetrios S.; Leventis, Nicholas: Structure-Property Relationships in Porous 3-D Nanostructures as a Function of Preparation Conditions: Isocyanate Cross-linked Silica Aerogels. Chem. Mater., vol. 19, no. 9, 2007, pp. 2247–2260.

Military Standard: MIL-STD-1290A (AV), Light Fixed and Rotary-Wing Aircraft Crash Resistance. Department of Defense, Washington, D.C., Sept. 1988.

Minguet, P. J.: A Model for Predicting the Behavior of Impact-Damaged Minimum Gage Sandwich Panels under Compression. AIAA/ASME/ASCE/AHS/ASC 32nd Structures, Structural Dynamics, and Materials Conf., Paper no. AIAA-91-1075-CP, Baltimore, Md. April 8–10, 1991.

Moody, R. C. and Vizzini, A. J.: Test and Analysis of Composite Sandwich Panels with Impact Damage. DOT/FAA/AR-01/124, U.S. Department of Transportation, Federal Aviation Administration, Mar. 2002.

NASA Glenn Research Center, Life Prediction Branch (2005): CARES Software. http://www.grc.nasa.gov/WWW/LPB/cares/ Accessed May 29, 2007.

NASA Contractor Report: NASA Contract No. NASW-4367, Research Triangle Institute, North Carolina, closed material, 1994.

Ratcliffe J.; Jackson, W. C.; and Schaff, J.: Compression Strength Prediction of Impact-Damaged Composite Sandwich Panels. Proc. AHS 60th Annual Forum, Baltimore, Md., June 7–10, 2004.

SAE: Performance Standard for Seats in Civil Rotorcraft, Transport Aircraft, and General Aviation Aircraft. Society of Automotive Engineering Aerospace Standard SAE AS8049 Rev A, Sept. 1, 1997.

Shanahan, Dennis F.; and Shanahan, Maureen O.: Kinematics of U.S. Army Helicopter Crashes: 1979–85. Aviation, Space, and Environmental Medicine, vol. 60, no. 2, Feb. 1989, pp. 112–121.

Soutis, C. and Fleck, N. A.: Static Compression Failure of Carbon Fibre T800/924C Composite Plate with a Single Hole. J. Composite Materials, vol. 24, no. 5, 1990, pp. 536–558.

Stecura, S.: Effects of Compositional Changes on the Performance of a Thermal Barrier Coating System. NASA TM-78976, Aug. 1978.

Tsang, P. H. W.: Impact Resistance and Damage Tolerance of Composite Sandwich Panels. Ph.D. dissertation, Massachusetts Institute of Technology, Cambridge, Mass., vol. 55/05-B, June 1994.

Vazquez, J. M.; Cano, R. J.; Jensen, B. J.; and Weiser, E. S.: Polyimide Foams. U.S. Patent 6,956,066, B2, Oct. 2005.

Weiser, E. S.: Synthesis and Characterization of Polyimide Residuum, Friable Balloons, Microspheres and Foams. Ph.D. Dissertation, The College of William and Mary, Williamsburg, Pa., vol. 65/07-B, June 2004.

Weiser, E. S.; Johnson, T. F.; St. Clair, T. L.; Echigo, Y.; Kaneshiro, H.; and Grimsley, B. W.: Polyimide Foams for Aerospace Vehicles. J. High Performance Polymers, vol. 12, no. 1, Jan. 2000, pp. 1–12.

Wellman R. G. and Nicholis, J. R.: On the effect of aging on the erosion of EB-PVD TBCs. Surface and Coatings Technology, vol. 177–178, Jan. 2004, pp. 80–88.

Wellman, R. G.; Deakin, M. J.; and Nicholis, J. R.: The Effect of TBC Morphology on the Erosion Rate of EB PVD TBCs. Wear, vol. 258, nos. 1–4, Jan. 2005, pp. 349–356.

Wierzbicki, T. and Abramowicz, W.: On The Crushing Mechanics of Thin-Walled Structures. J. Applied Mechanics, vol. 50, no. 4A, 1983, pp.727–734.

Wierzbicki, T. and Bhat, S.: A Note on Shear Effects in Progressive Crushing of Prismatic Tubes. Society of Automotive Engineers, Paper no. 860821, 1987, pp. 304–309.

Williams, M. K.; Nelson, G. L.; Brenner, J. R.; Weiser, E. S.; and St. Clair, T. L.: High Performance Polyimide Foams. Fire and Polymers, Nelson, G. L. and Wilkie, C. A., eds. Ch. 5, Copyright 2001, pp. 49–62.

Williams, M. K.; Holland, D. B.; Melendez, O.; Weiser, E. S.; Brenner, J. R.; and Nelson, G. L.: Aromatic Polyimide Foams: Factors that Lead to High Performance. J. Polymer Degradation and Stability, vol. 88, no. 1, 2005, pp. 20–27.

Xiao, X.; Johnson, N. L.; and Botkin, M.: Challenges in Composite Tube Crush Simulation Proc. of the American Society for Composites (ASC) 18th Technical Conf., Paper 154, 2003.

Xie, Z.; and Vizzini, A. J. (2005): Damage Propagation in a Composite Sandwich Panel Subjected to Increasing Uniaxial Compression after Low-velocity Impact. J. Sandwich Structures and Materials, vol. 7, no. 4, pp. 269–288.

Zedan, M.; Hartman, P.; Mostafa, A.; and Sehra, A.: Viscous Flow Analysis for Advanced Inlet Particle Separators. 26th AIAA/ASME/SAE/ASEE Joint Propulsion Conf., Paper no. AIAA-90-2136, Orlando, Fla., July 16–18, 1990.

Zedan, M.; Mostafa, A.; Hartman, P.; and Sehra, A.: Viscous Flow Analysis of Advanced Particle Separators. J. Propulsion and Power, vol. 8, no. 4, 1992, pp. 843–848.

Zhang, G.; Rawashdeh , A.-M. M.; Sotiriou-Leventis, G.; Leventis, N.: Isocyanate Cross-Linked Silica: Structurally Strong Aerogels. Polymer Preprints, vol. 44, no.1, 2003, pp. 35–36.

Zhang, G.; Dass, A.; Rawashdeh, A.-M. M.; Thomas, J.; Counsil, J. A.; Sotiriou-Leventis, C.; Fabrizio, E. F.; Ilhan, F.; Vassilaras, P.; Scheiman, D. A.; McCorkle, L.; Palczer, A.; Johnston, J. C.; Meador, M. A. B.; and Leventis, N.: Isocyanate Cross-Linked Silica Aerogel Monoliths: Preparation and Characterization. J. Non-Cryst. Solids, vol. 350, 2004, pp. 152–164.

Zhu, Dongming and Miller, Robert A.: Development of Advanced Low Conductivity Thermal Barrier Coatings. International J. Applied Ceramic Technology, vol. 1, 2004, pp. 86–94.

CHAPTER 9

MULTIDISCIPLINARY ANALYSIS AND TECHNOLOGY DEVELOPMENT

Larry A. Young[1]

ACRONYMS

ACES	Airspace Concept Evaluation System
ATM	air traffic management
BADA	Base of Aircraft Data
CD	conceptual design
CTR	civil tiltrotor
HESCOMP	Helicopter Sizing and Performance Computer Program
HPC	high performance computing
MDATD	Multi-Disciplinary Analysis and Technology Development
MDAO	Multi-Disciplinary Analysis and Optimization
NAS	National Airspace System
NextGen	Next-Generation Air Transportation System
NDARC	NASA Design and Analysis of Rotorcraft
PD	preliminary design
PRESTO	Preliminary Rotorcraft Evaluation and Sizing Tool
RC	RotorCraft
RIA	Runway Independent Aircraft
SRW	Subsonic Rotary Wing
STOL	short takeoff and landing
VASCOMP	VSTOL Aircraft Sizing and Performance Computer Program
VMS	Vertical Motion Simulator
VSP	Vehicle Systems Program
VTOL	vertical takeoff and landing

[1] NASA Ames Research Center.

INTRODUCTION

As stated in Chapter 1 of this document, the overarching goal for NASA rotorcraft research is *to radically improve the capabilities and civil benefits of rotary wing vehicles*. The Subsonic Rotary Wing (SRW) project goals for Next-Generation Air Transportation System (NextGen) rotorcraft are: capability for 50% main rotor speed reduction; 100 kt speed increase over present-day rotorcraft; vehicle noise contained in the landing area; and cabin noise < 77dB with no weight penalty.

Most of the research conducted by the SRW project focuses on the development and validation of individual technologies. These technologies, and the promise they hold for rotorcraft, have been documented in the preceding chapters of this report. An integrated system perspective is also required to ensure that the technologies being pursued are coordinated to achieve the project goals. To this end, a SRW multidisciplinary analysis and technology development (MDATD) effort was established to serve as a focus for the underlying technologies pursued within the technical disciplines of the SRW project. The MDATD work includes two primary areas: 1) design and analysis, and 2) integrated system-level demonstrations.

In the area of design and analysis, the MDATD effort draws upon initiatives, not necessarily exclusive to rotorcraft, for systems engineering, systems analysis, design engineering, and higher-performance computing advancements. These efforts are largely focused on developing conceptual design tools with improved modeling fidelity without sacrificing too much computational efficiency. Vehicle reference designs are being developed in parallel with the tool development. The benefits of technology advances are also evaluated as part of the conceptual design work. The MDATD integrated systems technology assessment and validation effort is aimed at four technical challenge areas that support the SRW project goals: integrated aeromechanics/propulsion systems; actively-controlled, efficient rotorcraft; quiet cabin; and NextGen rotorcraft.

The remainder of this chapter further describes the MDATD work, including future plans.

DESIGN AND ANALYSIS

Design paradigms must continuously evolve to encompass new technologies and new analytical tools, theoretical advances, and changing societal needs. For example, Young et al. [2005] and Young [2006a] address some of the challenges of accounting for autonomous-system technologies in systems-analysis studies. Further, new reference design and missions, e.g. Young [2006b and c], can also have a profound influence on conceptual design and systems analysis tools. Recent advances in rotary-wing predictive capability, as a consequence of the general trend towards the use of higher-fidelity physics-based computational tools, have implications for rotorcraft design. The following sections discuss the conceptual design and sizing tools used primarily by NASA rotorcraft researchers, technology benefits assessments, and plans for improving design tools.

Rotorcraft Conceptual Design and Vehicle Sizing Tools

For many years two mainstay conceptual design tools for rotorcraft have been the sizing codes HESCOMP (Helicopter Sizing and Performance Computer Program) and VASCOMP (VSTOL Aircraft Sizing and Performance Computer Program). Originally developed by Boeing in the late 1970s and early 1980s, HESCOMP (Davis et al. [1979]) and VASCOMP (Schoen et al. [1980]) are used within Boeing and the rotary-wing academic community but are generally no longer employed within NASA. Recent examples of design studies using the HESCOMP helicopter sizing code include Crossley et al. [1995], Wells et al. [1999], and Hirsh et al. [2007]. Recent examples of the design studies using the VASCOMP sizing code include Brender et al. [1996], Crossley et al. [1995], Eames [2006], Mavris et al. [2000], Paisley et al. [1989], Stettner et al. [1992 and 1993], and Tai et al. [1996]. In addition to these and other technical papers, many university student design projects are performed using versions of the HESCOMP and VASCOMP software. Within Bell Helicopter, the PRESTO (Preliminary Rotorcraft Evaluation and Sizing Tool) analysis, described in Trept et al. [1995] serves as a primary sizing tool.

In general, HESCOMP and VASCOMP were superceded within NASA by the RC (RotorCraft) sizing code developed by the U.S. Army Aeroflightdynamics Directorate. Johnson [to be published] describes the evolution of the Army codes from the 1970s into the present RC code. Variants of RC were frequently produced to address unique requirements of individual projects (Sinsay [2008]).

NASA is currently developing a new-generation rotorcraft conceptual design tool (Johnson [to be published]): NASA Design and Analysis of Rotorcraft (NDARC). NDARC is an aircraft system tool supporting conceptual design and technology impact evaluations. The development of NDARC benefited greatly from the input of experienced RC users. NDARC makes use of RC's parametric weight equations, component aerodynamic models, and rotor performance model. NDARC, however, is new software with a new architecture that can analyze a wider range of configurations than RC. A single main rotor and tail rotor helicopter, tandem rotor helicopter, coaxial helicopter, and tiltrotors are specific rotorcraft configurations that can be analyzed with NDARC. The modular construction of the software allows higher fidelity models and additional vehicle components to be accommodated. The principal tasks are to design (or size) a rotorcraft to meet specified requirements, including vertical takeoff and landing (VTOL) operation, and then analyze the performance of the aircraft for a set of conditions. The NDARC software is written in Fortran and is intended for public dissemination to support future conceptual design and systems-analysis studies. Within NASA, NDARC will be used to continue the refinement of key reference designs and missions to support the NASA technology research portfolio.

Comprehensive rotorcraft-analysis software packages are frequently used to augment conceptual design sizing codes. Two of the most widely used and powerful tools are CAMRAD II (Johnson, [1994]) and RCAS (Saberi et al. [2004]). Chapter 2 of this report provides examples of the predictive capabilities of these analyses. Studies conducted by Johnson et al. [2005] and Acree et al. [2008], for example, have employed concurrent application of RC and CAMRAD II.

Technology Assessments

Identifying technologies that will enable the NASA goals for advanced civil rotorcraft is a key activity within the MDATD effort. Since the early 2000's, NASA has sponsored and conducted several noteworthy studies.

Under the NASA Runway Independent Aircraft (RIA) project, Smith et al. [2003] describes three RIA configurations analyzed by the rotorcraft industry: the quad tiltrotor (Bell Helicopter), the reverse velocity rotor concept (Sikorsky), and the tiltrotor (Boeing). Figure 9.1 illustrates these industry concepts. The study identified enabling technologies for each of the three RIA aircraft and the potential benefits of the combined technologies.

NASA, with support from the U.S. Army, conducted the design and in-depth analysis of rotorcraft configurations that could satisfy the 2005 NASA Vehicle Systems Program (VSP) technology goals (Johnson et al. [2005]) for a civil heavy-lift rotorcraft. The objective of the investigation was to select a heavy lift rotorcraft system with the best chance of meeting the VSP goals while being econom-ically competitive. The emphasis was on efficient cruise and hover, efficient structures, and low noise. The mission was to carry 120 passengers for 1200 nm, at a speed of 350 knots and 30,000 ft altitude. The configurations (fig. 9.2) investigated were a Large Civil Tiltrotor (LCTR), a Large Civil Tandem Compound (LCTC), and a Large Advancing Blade Concept (LABC). The investigation identified the LCTR as the configuration with the best potential to meet the technology goals. The results of this VSP study and subsequent investigations (van Aken and Sinsay [2006], Johnson et al. [2007]) identified key enabling and enhancing technologies to aid in the development of future advanced rotorcraft configurations. Further analysis and optimization on the LCTR concept has resulted in the LCTR2 concept (fig. 9.3) described in Acree et al. [2008]. The LCTR2 is designed to carry 90 passengers and baggage (19,800 lb payload) for at least 1,000 nautical miles. Vehicle characteristics include a takeoff gross weight of approximately 107,700 lb, two 65-ft rotors near the

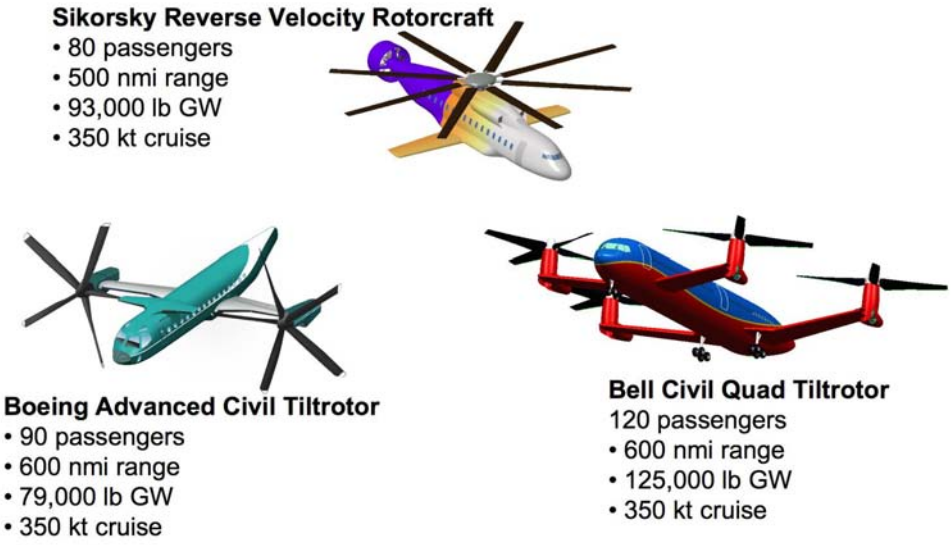

Figure 9.1. Industry concepts for Runway Independent Aircraft (Smith et al. [2003]).

wing tips, with four 7,500 HP turboshaft engines. Although the nominal mission includes takeoff and hover requirements, the climb and cruise segments dominate fuel usage. The cruise condition is 300 knots, 28,000 ft altitude, with an estimated total cruise power requirement of 11,900 HP. To maintain high rotor efficiency and to manage noise levels during takeoff and hover, rotor tip speed was assumed to be 650 ft/s during takeoff/hover and 350 ft/s for the cruise condition; this defines the roughly 50% rotor tip speed variation requirement.

Boeing, under NASA sponsorship, recently completed a systematic technology benefits assessments using a compound single main rotor helicopter and tiltrotor as baseline designs (fig. 9.4). The study by Wilkerson and Smith [2009] used Boeing vehicle-sizing tools and subject-matter expertise to examine a suite of emerging technologies for enabling safe, efficient, and cost-effective large transport rotorcraft.

Planned Improvements to Capability

In the near-term, NASA will continue to enhance NDARC by improving usability, developing models for advanced vehicle components, and validating the analysis for a wider range of configurations.

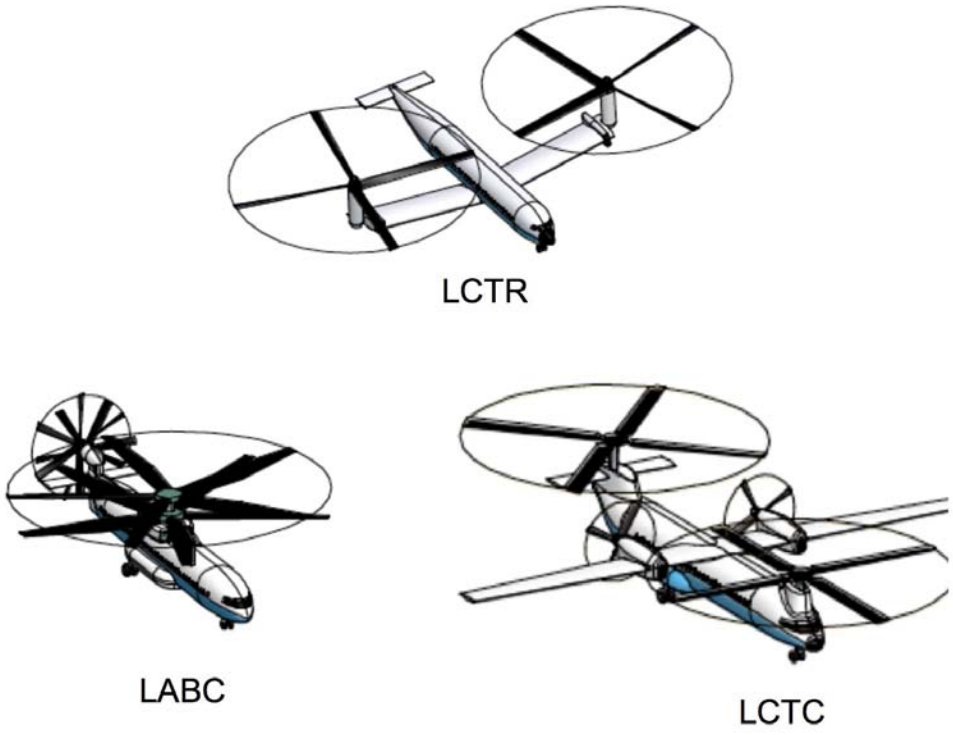

Figure 9.2. NASA Heavy Lift Rotorcraft sizing performed with U.S. Army RC Code (Johnson et al. [2005]).

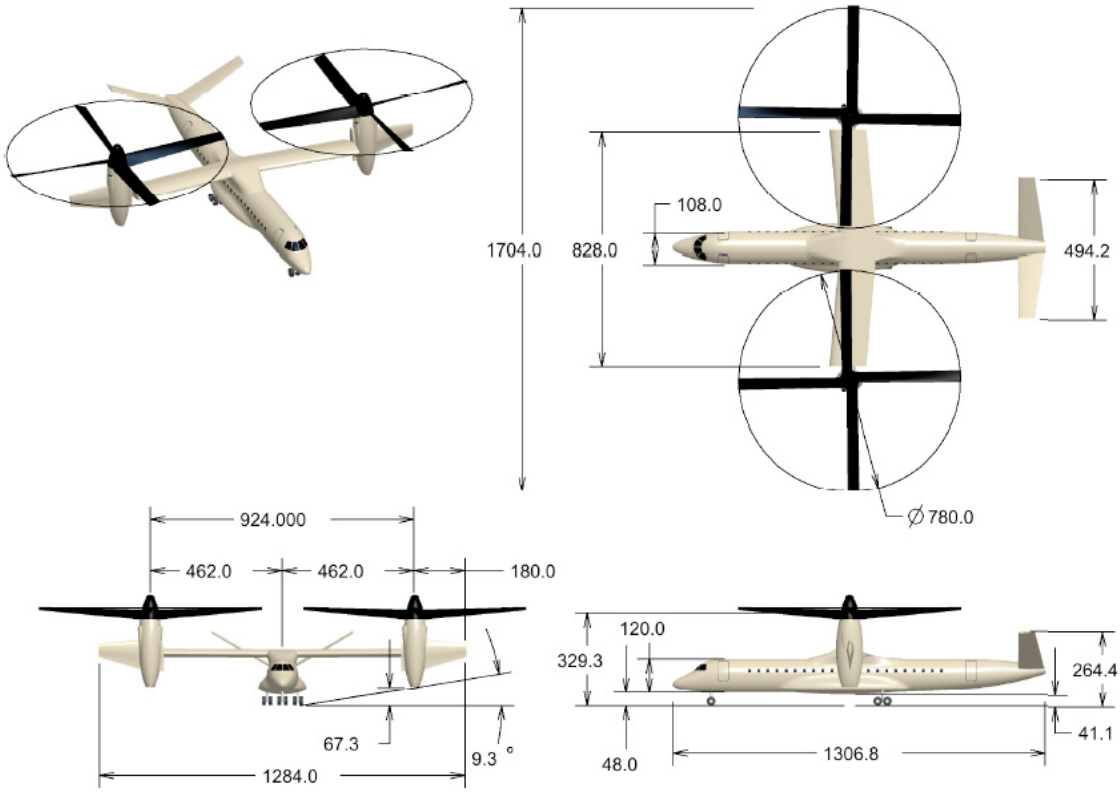

Figure 9.3. LCTR2 vehicle reference design (Acree et al. [2008]).

Higher-fidelity tools are increasingly replacing lower-fidelity analyses as computational power improves. A long-term challenge of the MDATD effort is determining how to interject higher-fidelity analyses and multidisciplinary analysis and optimization (MDAO) earlier into the design cycle, particularly during preliminary design. A robust method is required to significantly improve design confidence and reduce design cycle time for new/advanced vehicles. Just as high-performance computing (HPC) advancements have radically influenced the aerospace research community as a whole, HPC is also significantly affecting rotorcraft design and analysis. Both rotorcraft MDAO and systems-analysis tools can greatly benefit from technical advances made for fixed-wing aircraft, particularly as related to software architectures, user interfaces and database visualization/interrogation, generic modeling techniques, integration of stand-alone engineering analysis tools into a coupled suite of tools, and optimization tools. Datta and Johnson [2008] surveyed the impact of HPC on other aerospace domains and then used the information to identify technology gaps for rotorcraft requirements. In a companion paper, Johnson and Datta [2008] propose a roadmap for developing the multidisciplinary rotorcraft analysis of the future. The analysis is envisioned to be HPC-based, scalable, and modular.

Sheffler et al. [2008] provides an industry perspective and approach for incorporating MDAO framework higher-fidelity analyses in the conceptual design (CD) and preliminary design (PD) phases. Boeing case studies are also discussed illustrating the requirement for higher fidelity

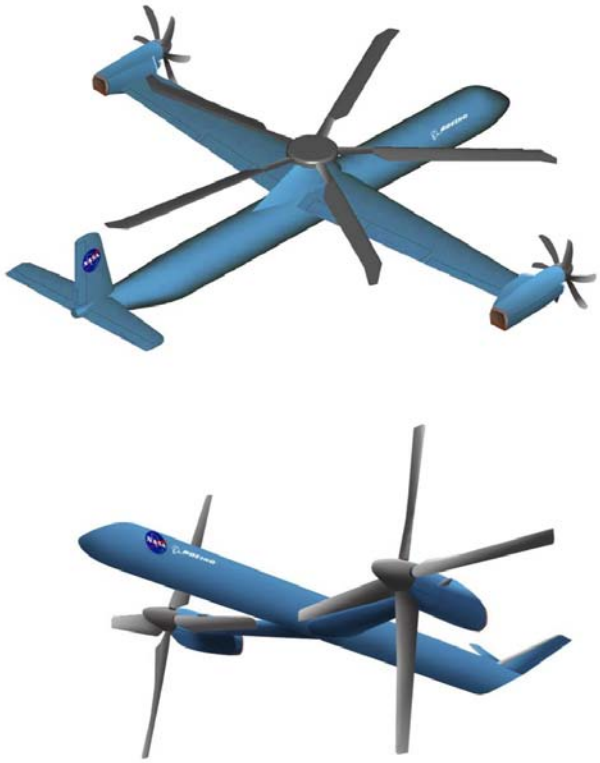

Figure 9.4. Large transport rotorcraft reference designs used for conducting a technology benefits assessment (Wilkerson and Smith [2009]).

analyses in the PD phase. Under NASA sponsorship, Orr and Narducci [2009] examined the technical issues and practices underlying the transition from rotorcraft CD to early- to mid-stage PD and devised a 5-year roadmap by which MDAO could accommodate higher-fidelity analyses (beyond those that are employed in CD) in support of rotorcraft preliminary design. One of their key conclusions is that MDAO is fairly well established for rotorcraft CD but presents many challenges as well as opportunities when applied to PD. Their work also highlights the potential role of MDAO in enabling collaborative design space exploration during the transition from the late stages of conceptual design to the early/mid stages of preliminary design.

Through a NASA Small Business Innovation Research effort, the SRW project is working with Sukra-Helitek, Inc. to develop a CFD tool compatible with the rapid design-cycle turnaround-times required for conceptual design studies. A primary objective of the work is to design and develop a user interface for geometry manipulation and integration with the CFD analysis. Figure 9.5 is an example calculation of the LCTR2.

Establishing the accuracy and range of application for these higher-fidelity tools presents new challenges such as acquisition of new experimental datasets and measurement types for rotorcraft. The planned activities in Chapters 2–8 of this report are aimed at providing some of these new datasets.

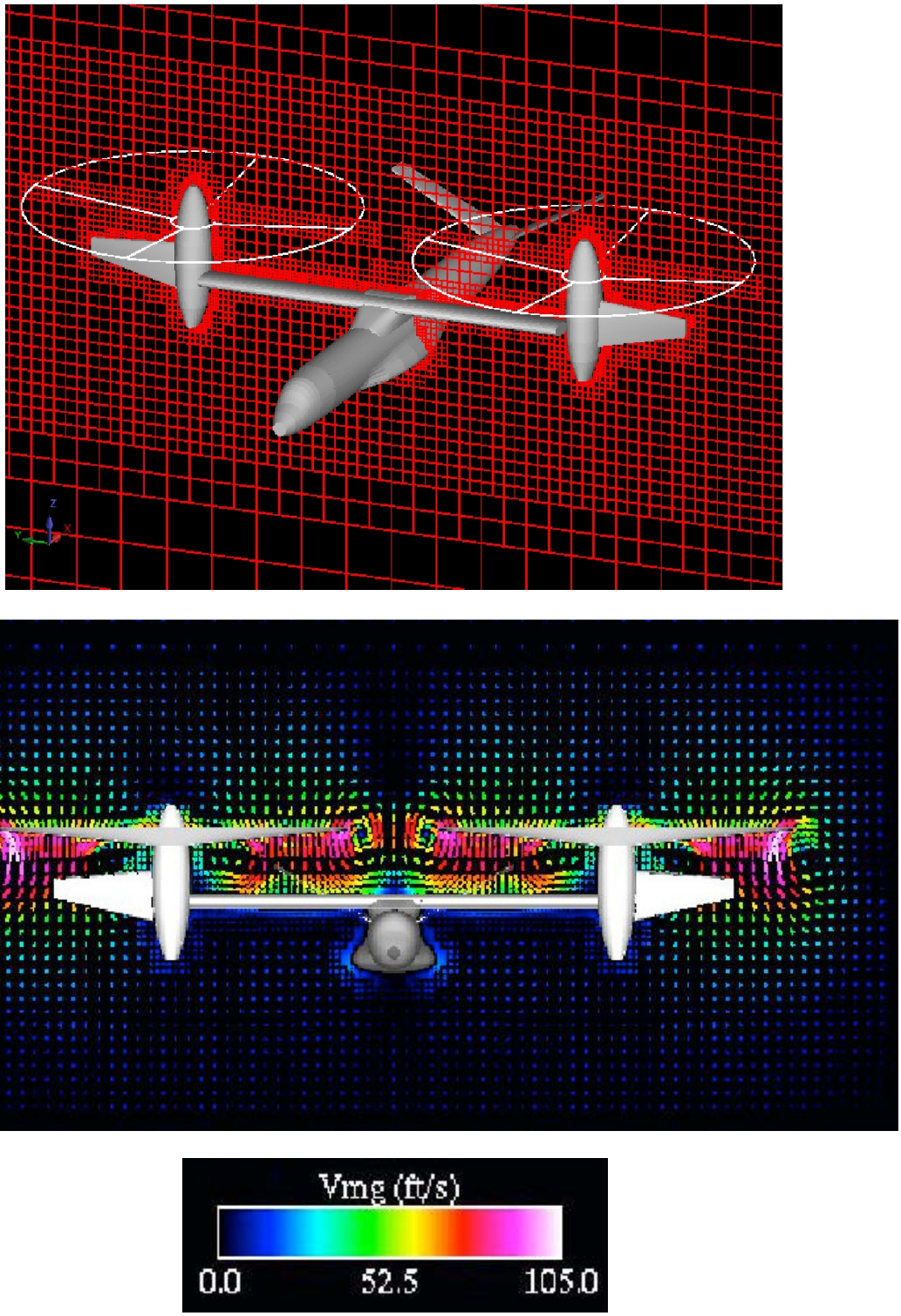

Figure 9.5. Under development: Tools incorporating CFD into the conceptual design process (LCTR2 images courtesy of G. Rajagopalan, Sukra-Helitek, Inc.).

INTEGRATED SYSTEMS TECHNOLOGY ASSESSMENT AND VALIDATION

The technology development described in Chapters 2–8 of this report supports four technical challenges for the NASA Subsonic Rotary Wing (SRW) project: Integrated Aeromechanics/Propulsion System; Actively-Controlled, Efficient Rotorcraft; Quiet Cabin; and NextGen Rotorcraft. These challenges were selected for their relevance to a broad range of industry and government programs, for their inherent requirement to force integration of multiple disciplines to accomplish the tasks, and because current prediction tools are unable to model the problem. For the most part, these challenges represent multi-disciplinary experimental demonstrations. As stated in Chapter 1 and earlier in this Chapter, goals for NextGen rotorcraft are: capability for 50% main rotor speed reduction; 100 kt speed increase over present-day rotorcraft; vehicle noise contained in the landing area; and cabin noise < 77dB with no weight penalty. Progress in each of the 4 challenge areas is intended to advance the state-of-the-art in rotorcraft technology and in particular, will help meet the goals for NextGen rotorcraft.

The following sections describe each of the 4 technical challenges, including recent progress and future plans.

Integrated Aeromechanics/Propulsion System

Identifying the benefits of substantial reductions in rotor tip speed in cruise (versus hover tip speeds) for tiltrotor aircraft and other rotary-wing platforms was a key outcome of NASA conceptual design and systems analysis work (Johnson et al. [2005] and [2007]). The current NASA research portfolio, then, has evolved to reflect technology investments to provide a variable-rotor-speed methodology that can vary rotor tip speed between 100% and 50%, as opposed to current practice in which the rotor speed sees only very modest speed changes (under 20% for current-generation tiltrotor aircraft).

The purpose of the Integrated Aeromechanics/Propulsion System challenge is to develop and demonstrate technologies enabling variable-speed rotor concepts. The goal is to reduce rotor tip speed at high speed cruise by 50% compared to hover tip speeds while maintaining cruise aerodynamic efficiency. Implementing a system to allow large variations in vehicle rotor tip speeds in flight requires substantial progress in transmission and engine technology as well as advances in flight dynamics and control.

For each of the three configurations shown in figure 9.2, Handschuh and Zakrajsek [2006] propose conceptual drive system arrangements that do not require variation in engine speed. In Chapter 6 of this report, the implications of variable rotor speed on flight controls are discussed and a concept of sequential gear-shifting control with two baseline engines (Litt et al. [2007]) is presented. Instead of fixing engine speed, Snyder and Thurman [2009] investigate concepts where all the speed variation is achieved from the engine. Using the LCTR2 (fig. 9.3) as the reference vehicle, Snyder and Thurman [2009] estimate the primary gas turbine engine parameters needed to meet the LCTR2 performance requirements and mission. Analyses for both a one-spool core and two-spool core are performed in their study. NASA is also funding a study with industry to evaluate derivatives of commercial, off-the-shelf engines and a clean-sheet engine design that will meet the LCTR2

reference design requirements. The study will result in the conceptual development of a drive system that will compliment the engine configuration capabilities. Various speed splits between the engine and transmission will be explored to establish the relationship of engine and transmission weight and overall fuel burn with speed variation and technology.

Progressing from the concepts described above to a demonstration test article that integrates a variable-speed propulsion system with a rotor is a major undertaking. As an initial step toward this demonstration article, NASA in partnership with the U.S. Army is investing in a new tiltrotor test stand capable of testing approximately 25-ft diameter rotors. Figure 9.6 shows a conceptual design of the test stand installed in the National Full-Scale Aerodynamics Complex. Variable-speed capability will be introduced in subsequent enhancements to the test stand. In parallel, separate demonstrations of a variable speed transmission and a variable speed engine are planned.

Actively-Controlled, Efficient Rotorcraft

The NASA investigation on heavy-lift rotorcraft systems by Johnson et al. [2005] concluded that active rotor control and active control for reducing hub and fuselage drag were essential features for the advanced rotorcraft configurations studied. The extent to which rotor performance, loads, vibration, and noise can be controlled simultaneously remains unknown.

The objective of the Actively-Controlled, Efficient Rotorcraft (ACER) challenge is to assess multiple active rotorcraft concepts for effectiveness in simultaneously increasing aerodynamic efficiency, controlling dynamic stall for high speed conditions, reducing vibration, and reducing noise. The challenge also includes improving the capability to predict rotorcraft behavior including

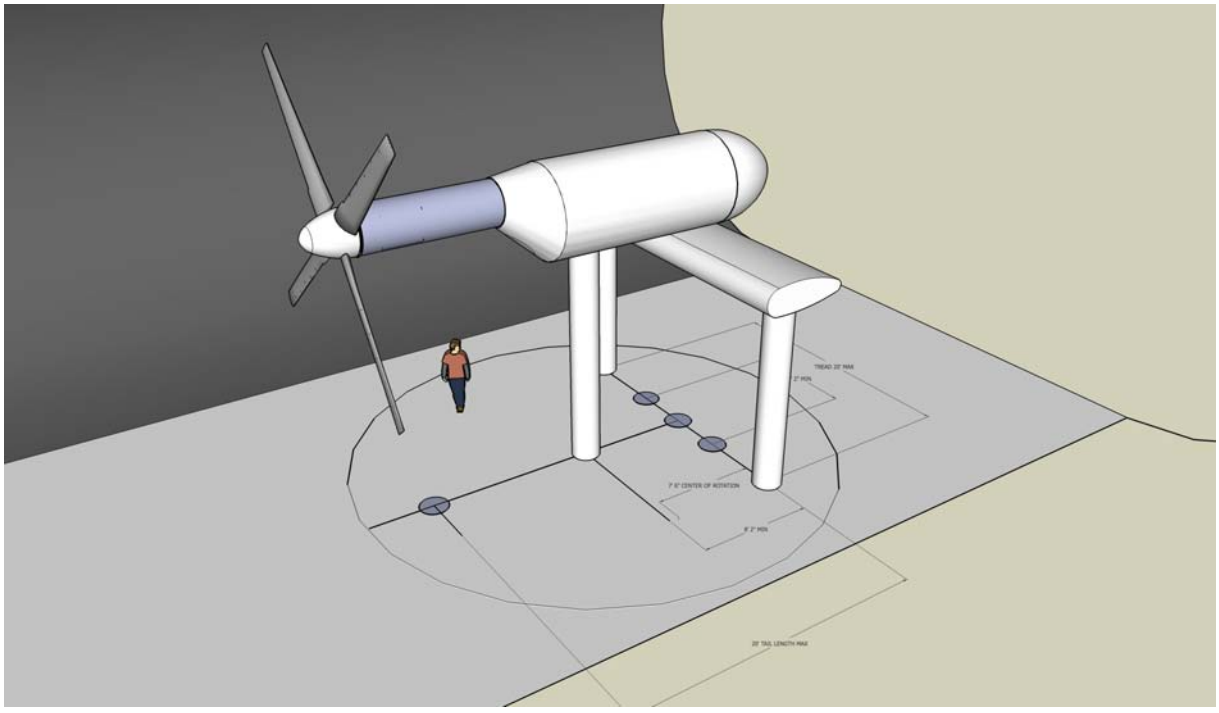

Figure 9.6. Conceptual illustration of a Tiltrotor Test Rig.

performance, airloads, wake, structural loads, and acoustics through collaborative research in CFD and advanced experimental methods. In Chapter 2, recent and planned experiments of active rotors are discussed. Individual blade control, active blade flaps, and on-blade flow control are several types of active rotor control NASA is pursuing. In addition, NASA is investigating fuselage drag reduction using active flow control. Under the ACER challenge, demonstrations will become increasingly comprehensive in terms of measurements, objectives for the active control optimizer, and the number of parameters predicted. The capability to acquire multi-parameter, simultaneous measurements (such as described in Chapter 5) during these demonstrations, whether in the wind tunnel or in flight, to confirm the effects of active control is critical. NASA is planning to participate in two model scale active twist rotor wind tunnel tests and two full-scale active flap wind tunnel tests.

Quiet Cabin

Presently, a predictive capability to correlate changes in drive system noise levels with expected changes in cabin noise levels does not exist. Predicting noise transmission through advanced structures and the resulting impact on interior noise (and consequently, passenger comfort) are required to provide guidance during aircraft design. The objective of the Quiet Cabin challenge is to develop and demonstrate advanced structural concepts and design evaluation methods for interior noise and vibration reduction. Optimized combinations of new acoustic treatment material, new structural designs incorporating acoustic passive and active technology, and reducing transmission gear noise will be considered. NASA is planning a systematic approach to understanding the noise path that includes an integrated analytical model of the structure and an experimental test rig to acquire parametric data. The planned test rig includes a transmission and representative cabin. Using interchangeable gears with interchangeable structural panels, the transmission noise and the noise path can be varied. In parallel, an integrated interior noise prediction capability is planned by combining separate analyses into a comprehensive tool set. The progress in interior noise prediction and advanced structures development described in Chapters 3 and 8, respectively, support the objectives of the Quiet Cabin challenge.

NextGen Rotorcraft

The Joint Planning and Development Office (JPDO) was instituted by the Vision 100 Century of Aviation Reauthorization Act (Public Law 108-176) to address the challenges facing air transportation in the United States by engaging multiple agencies that would collaborate to plan, develop, and implement the Next-Generation Air Transportation System. The JPDO has formulated initial versions of the NextGen Concept of Operation (ConOps) and Enterprise Architecture (see Anon. [2007a] and Anon. [2007b], respectively) and will continue to refine these as progress is made toward implementation of NextGen. These documents define NextGen, as envisioned for operation in 2025. The ConOps provides a broad vision for the air traffic system and the vehicles that operate within NextGen. To realize that vision, the ConOps must be informed with tangible details of the “how” to accomplish NextGen—this “how” is the focus of NASA research in support of NextGen. NASA’s role is discussed in a recent white paper, Anon. [2007c], which states that the greatest impact of NASA’s current research investment will manifest itself in the long term, which represents the fully operational implementation of NextGen in 2025. Critical systems trades and research areas

must be investigated to refine the ConOps and enable implementation by 2025. Advanced rotorcraft must be considered in the NextGen ConOps.

The NextGen Rotorcraft challenge aims to foster, develop and demonstrate technologies that contribute to the commercial viability of large rotary wing transport systems in NextGen. Simulations of simultaneous, non-interfering (SNI) operation of large rotorcraft are planned in the Vertical Motion Simulator (VMS). The Future Flight Central facility at NASA Ames is also being considered for simulating SNI operations. Handling qualities and external noise of large rotorcraft are addressed in Chapters 6 and 3, respectively, and results from these efforts will be combined to develop a low-noise flight path for a NextGen rotorcraft. NASA also intends to address the crashworthiness of future large rotorcraft using analytical techniques described in Chapter 8.

As shown in figures 9.1–9.4, multiple concepts for large rotary wing transports have been studied, though a large tiltrotor has received the most attention. The potential impact of introducing civil tiltrotors (CTRs) into the National Airspace System has been the subject of several comprehensive studies dating back to 1987 (Anon. [1987, 1995a-b], Thompson et al. [1991a-c], and Alexander et al. [1994]). CTRs are expected to successfully compete with fixed-wing aircraft provided a supporting infrastructure (ground facilities and air traffic control) is in place. During 2001–2004, NASA sponsored or co-sponsored several studies (Stouffer et al. [2001], Johnson, et al. [2001], Guilianetti [2003], and Smith et al. [2003]) of the RIA model of operations whereby existing stub runways could be used by vertical takeoff and landing (VTOL) aircraft operating in short takeoff and landing (STOL) mode in addition to operating in VTOL mode from helipads. This operational concept has the potential to increase the capacity of the air transportation system. The increased capacity could then be used to increase throughput or reduce delay significantly throughout the system. Figure 9.7 illustrates a notional integration of a civil tiltrotor in an airport terminal area; the simulation

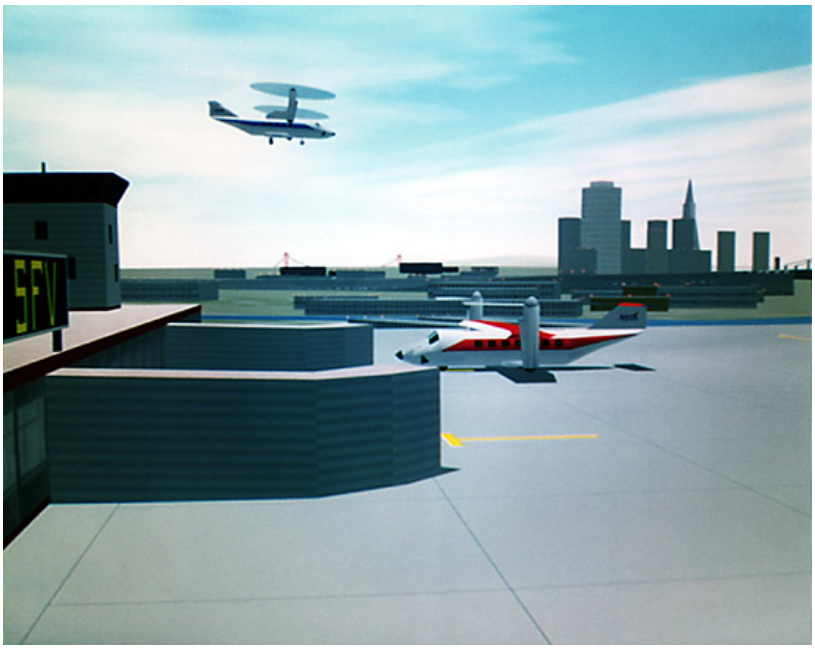

Figure 9.7. CTR and airport/vertiport integration simulation in the Vertical Motion Simulator (VMS).

was developed under the NASA Short Haul Civil Tiltrotor project (Guilianetti [2003]). NASA has conducted several terminal area flight and VMS simulation studies over the past decade and a half; representative results from past studies are given in Hardy [2002]. As discussed previously in this chapter, Johnson et al. [2005] identified a large civil tiltrotor as the configuration with the best potential to meet the technology goals established for a transport rotorcraft. Since the studies of the late-1980s and early 1990s, recent events demonstrating the critical role of rotorcraft in disaster (man-made and natural) relief provide another compelling need for civil transport rotorcraft to be fully incorporated into the next-generation airspace system.

NASA is currently sponsoring a multi-year systems study associated with deploying a fleet of CTRs within NextGen. This notional fleet comprises 10-, 30-, 90-, and 120-passenger CTRs. The study objectives are to understand how CTRs will operate within NextGen and to understand the tradeoffs involved for both vehicles and the air traffic management (ATM) system, including safety considerations, system performance, environmental constraints, and other relevant issues. Figure 9.8 illustrates the conceptual design of the 30-passenger CTR. The CTR fleet study is being defined by the Bell PRESTO conceptual design tool (Trept, et al. [1995]). The estimated performance characteristics of the CTR vehicles will be translated to Eurocontrol-developed BADA (Base of Aircraft DAta) models (Anon. [2009]) that will be used as input for ACES (Airspace Concept Evaluation System) airspace simulations (Kubat et al. [2006] and Santos et al. [2008]). The outcome of this multi-year study is expected to help guide future NASA rotorcraft research related to NextGen.

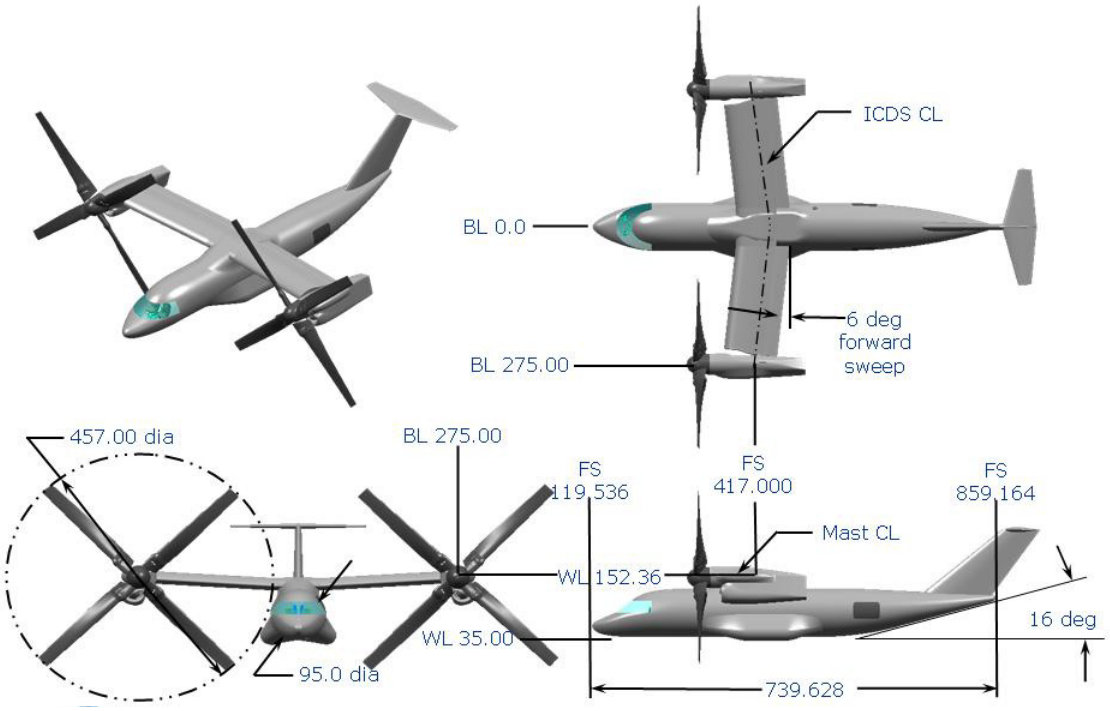

Figure 9.8. Notional 30-passenger CTR for NextGen airspace studies (image courtesy of SAIC and Bell Helicopter Textron).

CONCLUDING REMARKS

A multidisciplinary analysis and technology development (MDATD) effort has been initiated within the NASA Subsonic Rotary Wing (SRW) project. Within the MDATD discipline, progress toward the SRW project-level technical goals and plans is monitored. MDATD embodies elements of traditional work related to rotorcraft conceptual design and systems analysis but also endeavors to integrate discipline-oriented technologies culminating in system-level demonstrations that enable advanced rotorcraft configurations for the NextGen,

This assessment report is a particularly important datum for the MDATD effort. Documenting the NASA rotorcraft research status and predictive capability has been a difficult but valuable exercise. Moving forward, this report will serve as a benchmark against which progress can be measured.

REFERENCES

Acree, Jr., C. W.; Yeo, H.; and Sinsay, J. D.: Performance Optimization of the NASA Large Civil Tiltrotor. Joint AHS/AIAA/ASME/RAeS/SAE International Powered Lift Conf., London, UK, July 22–24, 2008.

Alexander, H. R.; Allen, E. M.; and Bartie, K. M.: Advanced Tiltrotor Transport Technology: Cost/ Benefit/Risk Assessment. Phase I: Final Report. NASA CDCR-20001, Aug. 1994.

Anon.: Civil Tiltrotor Missions and Applications: A Research Study. Supporting Documentation for U. S. Policy Making Decisions. Boeing Commercial Airplane Co., Bell Textron, Inc., Boeing Vertol, NASA CR-177451, Nov. 1987. (Restricted, U. S. Government)

Anon. (U.S. Department of Transportation): Civil Tiltrotor Development Advisory Committee Report to Congress: Vol. 1, Final Report. In accordance with PL102-581, Dec. 1995a.

Anon. (U. S. Department of Transportation): Civil Tiltrotor Development Advisory Committee Report to Congress: Vol. 2, Technical Supplement. In accordance with PL102-581, Dec. 1995b.

Anon. (NextGen Joint Planning and Development Office): Concept of Operations for the Next Generation Air Transportation System, Version 2, June 13, 2007a. http://www.jpdo.gov/library.asp/NextGen_v2.0.pdf. Accessed July 30, 2009.

Anon. (NextGen Joint Planning and Development Office): Enterprise Architecture for the Next Generation Air Transportation System, Version 2, June 22, 2007b. www.jpdo.gov/library/EnterpriseArchitectureV2.zip. Accessed July 30, 2009.

Anon.: NASA & the Next Generation Air Transportation System (NextGen). National Aeronautics and Space Administration, June 26, 2007c. http://www.aeronautics.nasa.gov/nextgen whitepaper.htm. Accessed July 30, 2009.

Anon.: "Base of Aircraft Data" is an Aircraft Performance Model developed and maintained by Eurocontrol Experimental Centre (EEC), Bretigny-Sur-Orge, France. Eurocontrol website: http://www.eurocontrol.int/eec/public/standard_page/proj_BADA.html. Accessed July 30, 2009.

Brender, S.; Mark, H.; and Aguilera, F.: The Attributes of a Variable-Diameter Rotor System Applied to a Civil Tiltrotor Aircraft. NASA CR-203092, 1996.

Crossley, W.; Regulski, J.; Wells, V.; and Laananen, D.: Incorporating Genetic Algorithms and Sizing Codes for Conceptual Design of Rotorcraft. Proc. of AHS Vertical Lift Aircraft Design Conf., San Franciso, Calif., Jan 1995.

Datta, A.; and Johnson, W.: An Assessment of the State-of-the-Art in Multidisciplinary Aeromechanical Analyses. AHS Aeromechanics Specialists Conf., San Francisco, Calif., Jan. 23–25, 2008.

Davis, S. J.; Rosenstein, H.; Stanzione, K. A.; and Wisniewski, J. S.: HESCOMP: The Helicopter Sizing and Performance Computer Program. User's Manual, Rev. 2, Final Report. NASA/CR-168697, Oct. 1979.

Eames, D. J. H.: Short Haul Civil Tiltrotor Contingency Power System Preliminary Design. NASA/CR-2006-214059, Jan. 2006.

Guilianetti, D.: Aviation System Capacity Program: Short Haul Civil Transport Project. Noise Reduction and Terminal Area Operations. NASA/TP-2003-212800, Nov. 2003.

Handschuh, R. F. and Zakrajsek, J. J.: Current Research Activities in Drive System Technology in Support of the NASA Rotorcraft Program. AHS Specialists' Meeting on Vertical Lift Aircraft Design, San Francisco, Calif., Jan. 18–20, 2006; Also NASA/TM-2006-214052, ARL-TR-3707, Jan. 2006.

Hardy, G. H.: Pursuit Display Review and Extension to a Civil Tilt Rotor Flight Director. AIAA Paper 2002-4925, AIAA Guidance, Navigation, and Control Conference, Monterey, Calif., Aug. 5–8, 2002.

Hirsh, J. E.; Wilkerson, J. B.; and Narducci, R. P.: An Integrated Approach to Rotorcraft Conceptual Design. AIAA Paper 2007-1252, 45th AIAA Aerospace Sciences Mtg., Reno, Nev., Jan. 8–11, 2007.

Johnson, J.; Stouffer, V.; Long, D.; and Gribko, J.: Evaluation of the National Throughput Benefits of the Civil Tilt Rotor. NASA/CR-2001-211055, Sept. 2001.

Johnson, W.: Technology Drivers in the Development of CAMRAD II. AHS Aeromechanics Specialists' Meeting, San Francisco, Calif., Jan. 19–21, 1994.

Johnson, W.; Yamauchi, G. K.; and Watts, M. E.: NASA Heavy Lift Rotorcraft Systems Investigation. NASA TP-2005-213467, Dec. 2005.

Johnson, W. R.; Yeo, H.; and Acree, Jr., C. W.: Performance of Advanced Heavy-Lift, High-Speed Rotorcraft Configurations. AHS International Forum on Rotorcraft Multidisciplinary Technology, Seoul, Korea, Oct. 15–17, 2007.

Johnson, W.; and Datta, A.: Requirements for Next Generation Comprehensive Analysis of Rotorcraft. AHS Aeromechanics Specialists Conference, San Francisco, Calif., Jan. 23–25, 2008.

Johnson, W.: NASA Design and Analysis of Rotorcraft (NDARC). To be published as NASA TP.

Kubat, G.; Van Drei, D.; Satapathy, G.; Kumar, A.; and Khanna, M.: Communication, Navigation, and Surveillance Models in ACES for Concept Developers. Proc. 6th Integrated Communications, Navigation and Surveillance (ICNS) Conference & Workshop, 2006, pp. 413–421.

Litt, J. S.; Edwards, J. M.; and DeCastro, J. A.: A Sequential Shifting Algorithm for Variable Rotor Speed Control. NASA/TM-2007-214842, ARL-TR-4086, June 2007.

Mavris, D. N.; Baker, A. P.; and Schrage, D. P.: Technology Infusion and Resource Allocation for a Civil Tiltrotor. AHS Vertical Lift Aircraft Design Conf., San Francisco, Calif., Jan. 19–21, 2000.

Orr, S. A. and Narducci, R. P.: Framework for Multidisciplinary Analysis, Design, and Optimization with High-Fidelity Analysis Tools. NASA/CR 2009-215563, Feb., 2009.

Paisley, D. J.; Blystone, J. R.; and Wichmann, G. R.: The Aerodynamic Assistant. AIAA Paper 1989-3132, 7th AIAA Computers in Aerospace Conf., Monterey, Calif., Oct. 3–5, 1989.

Saberi, H.; Khoshlahjeh, M.; Ormiston, R. A.; and Rutkowski, M. J.: Overview of RCAS and Application to Advanced Rotorcraft Problems. AHS 4th Decennial Specialist's Conference on Aeromechanics, San Francisco, Calif., Jan. 21–23, 2004.

Santos, M.; Manikonda, V.; Feinberg, A.; and Lohr, G.: A Simulation Testbed for Airborne Merging and Spacing. AIAA Paper 2008-6345, AIAA Modeling and Simulation Technologies Conference, Honolulu, Hawaii, Aug. 18–21, 2008.

Schoen, A. H.; Rosenstein, H.; Stanzione, K.; and Wisniewski, J. S.: VASCOMP 2. The VSTOL Aircraft Sizing and Performance Computer Program. Vol. 6 User's Manual, Rev. 3. NASA CR-163639, May 1980.

Sheffler, M.; Streich, E.; Wilkerson, J.; Orr, S.; and Narducci, R.: Bringing Order Out of Chaos: Driving MDA/O and More Accurate Analyses Earlier in the Design. AHS Southwest Specialists' Meeting on Next Generation Vertical Lift Technologies, Dallas, Tex., Oct. 15–17, 2008.

Sinsay, J. D.: The Path to Turboprop Competitive Rotorcraft: Aerodynamic Challenges. AHS Specialists' Conference on Aeromechanics, San Francisco, Calif., Jan. 23–25, 2008.

Smith, D. E.; Wilkerson, J.; Montoro, G. J.; Coy, J.; and Zuk, J.: Technology Development for Runway Independent Aircraft. AHS 59th Annual Forum, Phoenix, Ariz., May 6–8, 2003.

Snyder, C. A. and Thurman, D. R.: Gas turbine characteristics for a Large Civil Tilt-Rotor (LCTR). AHS 65th Annual Forum, Grapevine, Tex., May 27–29, 2009.

Stettner, M. and Schrage, D. P.: An Approach to Tiltrotor Wing Aeroservoelastic Optimization Through Increased Productivity. AIAA Paper 1992-4781.

Stettner, M. and Schrage, D. P.: Tiltrotor Performance Sensitivities for Multidisciplinary Wing Optimization. AHS Specialists' Mtg. on Rotorcraft Multidisciplinary Design Optimization, Atlanta, Ga., April 27–28, 1993.

Stouffer, V.; Johnson, J.; and Gribko, J.: Civil Tiltrotor Feasibility Study for the New York and Washington Terminal Areas. NASA/CR-2001-210659, Jan. 2001.

Tai, J. C.; Mavris, D. N.; and Schrage, D. P.: An Assessment of a Reaction Driven Stopped Rotor/Wing Using Circulation Control in Forward Flight. AIAA Paper 96-5612, 1st World Aviation Congress, Los Angeles, Calif., Oct 21–24, 1996.

Thompson, P.; Neir, R.; Reber, R.; Scholes, R.; Alexander, H.; Sweet, D.; and Berry, D. (Editor): Civil Tiltrotor Missions and Applications. Phase II: The Commercial Passenger Market, Final Report. Boeing Commercial Airplane Group, Bell Helicopter Textron, Inc., Boeing Helicopters, NASA CR-177576, Feb. 1991a.

Thompson, P.; Neir, R.; Reber, R.; Scholes, R.; Alexander, H.; Sweet, D.; and Berry, D. (Editor): Civil Tiltrotor Missions and Applications. Phase II: The Commercial Passenger Market, Final Report, Book Two: Sec. 4 and 5, Proprietary. Boeing Commercial Airplane Group, Bell Helicopter Textron, Inc., Boeing Helicopters, NASA CR-177576, Feb. 1991b. (Restricted, ITAR)

Thompson, R.; Neir, R.; Reber, R.; Scholes, R.; Alexander, H.; Sweet, D.; and Berry, D.: Civil Tiltrotor Missions and Applications, Phase II: The Commercial Passenger Market Final Report, Supporting Documentation for U. S. Policy Making Decisions. NASA CR-177591, Oct. 1991c. (Restricted, U. S. Government)

Trept, T.; Sigl, D.; and Robertson, D.: Development and Application of the PRESTO Air Vehicle Predesign Synthesis Methodology. AHS 51st Annual Forum, Fort Worth, Tex., May 9–11, 1995.

Van Aken, J. M. and Sinsay, J. D.: Preliminary Sizing of 120-Passenger Advanced Civil Rotorcraft Concepts. AHS International Vertical Lift Aircraft Design Conference, San Francisco, Calif., Jan. 18–20, 2006.

Wells, V. L.; Rutherford, J. W.; and Corgiat, A. M.: Mission and Concept Evaluation for a Multirole Mission-Adaptable Air Vehicle. Aircraft Design, vol. 2, no. 1, Pergamon Press, June, 1999, pp. 65–80.

Wilkerson, J. B. and Smith, R.: Aircraft System Analysis of Technology Benefits to Civil Transport Rotorcraft. NASA/CR 2009-214594, June, 2009.

Young, L. A.; Yetter, J. A.; and Guynn, M. D.: System Analysis Applied to Autonomy: Application to High-Altitude Long-Endurance Remotely Operated Aircraft. AIAA Paper 2005-7103, Info-tech@Aerospace Conference, Arlington, Va., Sept. 26–29, 2005.

Young, L. A.: System Analysis Applied to Autonomy: Application to Human-Rated Lunar/Mars Landers. AIAA Paper 2006-7516, AIAA Space Conf. 2006, San Jose, Calif, Sept. 19–21, 2006a.

Young, L. A.: Aerobots as a Ubiquitous Part of Society. AHS International Vertical Lift Aircraft Design Conf., San Francisco, Calif., Jan. 18–20, 2006b.

Young, L. A.: Future Roles for Autonomous Vertical Lift in Disaster Relief and Emergency Response. Heli-Japan 2006: AHS International Specialists Mtg. on Advanced Rotorcraft Technology and Life Saving Activities, Nagoya, Japan, Nov. 15–17, 2006c.

REPORT DOCUMENTATION PAGE

Form Approved
OMB No. 0704-0188

1. REPORT DATE *(DD-MM-YYYY)*	2. REPORT TYPE	3. DATES COVERED *(From - To)*
21/09/2009	Technical Publication	

4. TITLE AND SUBTITLE
A Status of NASA Rotorcraft Research

5a. CONTRACT NUMBER

5b. GRANT NUMBER

5c. PROGRAM ELEMENT NUMBER

6. AUTHOR(S)
Gloria K. Yamauchi and Larry A. Young, Editors

5d. PROJECT NUMBER

5e. TASK NUMBER

5f. WORK UNIT NUMBER
WBS 877868.02.07.01.09.01

7. PERFORMING ORGANIZATION NAME(S) AND ADDRESS(ES)
Ames Research Center, Moffett Field, CA 94035-1000

8. PERFORMING ORGANIZATION REPORT NUMBER
A-090015

9. SPONSORING/MONITORING AGENCY NAME(S) AND ADDRESS(ES)
National Aeronautics and Space Administration
Washington, D.C. 20546-0001

10. SPONSORING/MONITOR'S ACRONYM(S)
NASA

11. SPONSORING/MONITORING REPORT NUMBER
NASA/TP–2009-215369

12. DISTRIBUTION/AVAILABILITY STATEMENT
Unclassified — Unlimited Distribution: Standard
Subject Category: 01
Availability: NASA CASI (301) 621-0390

13. SUPPLEMENTARY NOTES
Point of Contact: Gloria K. Yamauchi, Ames Research Center, MS 243-12, Moffett Field, CA 94035-1000
(650) 604-6719

14. ABSTRACT
In 2006, NASA rotorcraft research was refocused to emphasize high-fidelity, first-principles predictive tool development and validation. As part of this new emphasis, documenting the status of NASA rotorcraft research and defining the state-of-the-art in rotorcraft predictive capability were undertaken. Contributors to this 9-chapter report encompass a wide range of expertise covering the technical disciplines of aeromechanics, acoustics, computational fluid dynamics (CFD), flight dynamics and control, experimental capabilities, propulsion, structures and materials, and multi-disciplinary analysis. Within each chapter, brief descriptions of the discipline and subdisciplines are followed by a discussion of the tools available or in development, examples (where available) of measured versus predicted results, plans for improving predictive capability, required validation data, and possible contributions to other technical areas.

15. SUBJECT TERMS
Rotorcraft research, rotorcraft predictive capability, aeromechanics, acoustics, computational fluid dynamics, flight dynamics and control, experimental capabilities, propulsion, structures and materials, multidisciplinary analysis, conceptual design

16. SECURITY CLASSIFICATION OF:			17. LIMITATION OF ABSTRACT	18. NUMBER OF PAGES	19a. NAME OF RESPONSIBLE PERSON
a. REPORT	b. ABSTRACT	c. THIS PAGE			Gloria K. Yamauchi
Unclassified	Unclassified	Unclassified	Unclassified	416	19b. TELEPHONE *(Include area code)* (650) 604-6719